AD NUMBER

AD410522

NEW LIMITATION CHANGE

TO

Approved for public release, distribution unlimited

FROM

Distribution authorized to U.S. Gov't. agencies and their contractors; Administrative/Operational Use; Jan 1963. Other requests shall be referred to the Ofice of Civil Defense, Washington, DC.

AUTHORITY

OCD D/A ltr, 23 Jun 1969

Volume I

FALLOUT AND RADIOLOGICAL COUNTERMEASURES

Prepared for:

OFFICE OF CIVIL DEFENSE
DEPARTMENT OF DEFENSE
WASHINGTON, D.C.

STANFORD RESEARCH INSTITUTE

MENLO PARK, CALIFORNIA

STANFORD RESEARCH INSTITUTE
MENLO PARK, CALIFORNIA

January 1963

Volume I

FALLOUT AND RADIOLOGICAL COUNTERMEASURES

Prepared for:

OFFICE OF CIVIL DEFENSE
DEPARTMENT OF DEFENSE
WASHINGTON, D.C.

By: Carl F. Miller

SRI Project No. IM-4021

Approved:

Robert A. Harker

ROBERT A. HARKER, DIRECTOR
MANAGEMENT SCIENCES DIVISION

CONTENTS

1 THE NATURE OF FALLOUT 1

1.1 Background 1

1.2 A General Description of Fallout 3

1.3 Characteristic Types of Fallout 4

1.4 Potential Hazards from Fallout 4

1.5 Radioactive Decay 7

1.6 The Standard Intensity and Contour Properties 9

Chapter 1 References 11

2 FORMATION OF FALLOUT PARTICLES 13

2.1 General Definition of the Process 13

2.2 Mass-Chain Yields for the Fission of U-235, U-238 and Pu-239 17

2.3 The Structure and Composition of Individual Fallout Particles 28

2.3.1 Low Yield, Surface Shot, Silicate Soil 28

2.3.2 Low Yield, Underground Shot, Silicate Soil 31

2.3.3 Large Yield, Surface Shot, Coral 31

2.3.4 Tower Shot, Silicate Soil 38

2.3.5 Tower Shot, Coral Soil 41

2.3.6 Surface Shot, Ocean (Sea Water) 45

2.3.7 Inferences on Fallout-Particle Formation Processes 46

2.4 Properties of Small Fallout Particles from Detonations at Weapons Tests 72

2.5 Redistribution of Deposited Fallout 78

2.6 The Collection and Retention of Fallout Particles by Plant Foliage 81

Chapter 2 References 93

CONTENTS

3 A THERMODYNAMIC MODEL OF FALLOUT FORMATION 97

3.1 The Condensation Process 97
3.1.1 Gas-Liquid Phase Condensation 99
3.1.2 Gas-Liquid Phase Material Balance Constraints and Fractionation Numbers 106
3.1.3 Gas-Liquid Phase Condensation--Particle-Size Effects 111

3.2 The Dependence of Fireball Parameters on Weapon Yield and Time After Detonation 115

3.3 Estimates of Fireball Parameters for a Model Surface Burst on a Soil Consisting of Silicate Minerals 133

3.4 Process for Estimating the Concentration of Liquid Soil in the Fireball of a Model Surface Burst and the Fractionation Numbers of the Radionuclides 146

3.5 Computing the Decay Rates of Fission Product Mixtures . . . 177

Chapter 3 References 201

4 DISTRIBUTION OF FALLOUT PARTICLES FOLLOWING A NUCLEAR DETONATION 203

4.1 General Description of the Fallout Distribution Process . . . 203
4.1.1 The Particle Source Geometry 203
4.1.2 The Particle Fall Trajectory 203
4.1.3 Radiological Factors 204

4.2 Mathematical Descriptions of the Fallout Distribution Process 204
4.2.1 Scaling Methods 204
4.2.2 Mathematical Models 204

4.3 Descriptive Features of a Simplified Fallout Scaling System for Land Surface Detonations 206
4.3.1 General Description of the Scaling Method 206
4.3.2 Particles Falling from Cloud Altitudes 207
4.3.3 Particles Falling from Stem Altitudes 211
4.3.4 Methods for Estimating the Dynamics of the Fallout Deposition 220
4.3.5 Estimation of Ionization Rate and Exposure Dose . . . 223

Chapter 4 References 227

CONTENTS

5 CORRELATION OF SCALING MODEL PARAMETERS WITH OBSERVED FALLOUT-PATTERN FEATURES 220

5.1 General Description of Fallout Patterns from Land Surface Detonations 220

5.2 General Conditions to Which the Source Data Apply 231

5.3 Scaling Functions for Fallout Pattern Features of Interest . . 232
5.3.1 Intensity Ridge Near Ground Zero 232
5.3.2 Location of the Downwind Standard Intensity Contour for Fallout from Stem Altitudes 237
5.3.3 Stem Pattern Half-Width 239
5.3.4 The Distance to Fallout Pattern Features for Fallout from Cloud Altitudes 239
5.3.5 The Intensity Levels of Pattern Features for Fallout from Cloud Altitudes 241
5.3.6 The Maximum Pattern Width 243
5.3.7 Areas and Fraction of Total Activity Within Intensity Contours 245

5.4 Summary of Derived Idealized Fallout Pattern Scaling Functions 249

5.5 Illustrative Computations for the Use of the Simplified Fallout Scaling System 255
5.5.1 Construction of Idealized Fallout Patterns 255
5.5.2 Fallout Arrival Rate and Exposure Dose During Fallout Arrival 259
5.5.3 Method for Estimating the Particle Sizes in the Fallout at a Given Location 270

5.6 The Effect of Cross-Wind Shear on the Fallout Pattern Scaling System 288

5.7 Comparison of Several Fallout Pattern Computations 295

Chapter 5 References 299

6 IONIZATION RATE CONTOUR RATIOS AND COMPOSITION OF FALLOUT 301

6.1 Definition and Use of Ionization Rate Contour Ratios 301

6.2 Dependence of the Mass Contour Ratio on Detonation Conditions and Other Parameters 302

CONTENTS

6.2 Continued
- 6.2.1 Dependence on Weapon Type and Yield 302
- 6.2.2 Dependence on Downwind Distance from Shot Point 304
- 6.2.3 Dependence on Height or Depth of Burst 326
- 6.2.4 Mass Contour Ratio for Fallout from a Surface Detonation on Deep Sea Water 327
- 6.2.5 Mass Contour Ratio for Fallout from Detonations in Harbors 330
- 6.2.6 Mass Contour Ratio for Fallout from a 1-MT Detonation at Several Detonation Geometries 335

6.3 Fission-Product and Fraction-of-Device Contour Ratios . . . 338

6.4 Foliage-Contamination Factor Contour Ratio 339
- 6.4.1 Insoluble-Nuclide Fractions 341
- 6.4.2 Soluble-Nuclide Fractions 342
- 6.4.3 Variation of the Foliage-Contamination Factor with Particle Size 342

Chapter 6 References 349

ILLUSTRATIONS

Figure		Page
2.1	Thin Sections and Radiographs of Some Fallout Particles from a Small-Yield Surface Shot at the Nevada Test Site	29
2.2	Thin Section and Radiograph of a Fallout Particle from a Small-Yield Surface Shot at the Nevada Test Site	33
2.3	Thin Section and Radiograph of an Angular Fallout Particle from a Large-Yield Surface Shot at the Eniwetok Proving Ground	34
2.4	Section of a Fallout Particle from a Large-Yield Surface Shot at the Eniwetok Proving Ground	35
2.5	Thin Section and Radiograph of a Spherical Fallout Particle from a Large-Yield Surface Shot at the Eniwetok Proving Ground	37
2.6	Two Fallout Particles from a Tower Shot at the Nevada Test Site	39
2.7	Thin Section and Radiograph of a Fallout Particle from a Moderate-Yield Tower Shot at the Nevada Test Site	40
2.8	Thin Section and Radiograph of a Fallout Particle from a Moderate-Yield Tower Shot at the Eniwetok Proving Ground	43
2.9	Thin Section and Radiograph of a Fallout Particle from a Moderate-Yield Tower Shot at the Eniwetok Proving Ground	44
2.10	Photomicrograph of a Dichromate Reagent Film of an Individual Liquid Fallout Particle from a Large-Yield Barge Shot at the Eniwetok Proving Ground	46

ILLUSTRATIONS

Figure		Page
2.11	Electronmicrograph of the Radioactive Solids in the Liquid Fallout Particles from a Large-Yield Barge Shot at the Eniwetok Proving Ground	47
2.12	Calculated Fraction of Mass Chains 89, 90, 137, and 140 Condensed as a Function of Time after Fission with Indicated Non-condensing Elements	64
2.13	Plot of Calculated r_0 (A) Values for Mass Numbers 90, 137, and 140 against Those of Mass Number 89 for the Assumption that Only the Alkali Metal Elements and Alkaline Earth Elements in the Chain Condense	65
2.14	Reduction in the Ionization Rate at the Center of 10th Street and at the Center of the Plaza, Camp Parks, California	82
2.15	Accumulated Distribution of Number of Particles Having Different Diameters on Foliage	83
2.16	Distribution of Activity as a Function of Particle Diameter for Local Collections of Fallout from Tower-Mounted Detonations	86
3.1	Fraction of Nitrogen Molecules Dissociated as a Function of Temperature and Total Pressure	122
3.2	Fraction of Oxygen Molecules Dissociated as a Function of Temperature and Pressure	123
3.3	The Calculated Variation of n/W, P_s, n_s/n, and n_s/W with Assumed Values of T_s(=) for the Model Surface-Burst Fireball	140
3.4	Comparison of Calculations of the Activity and Photon Emission Rate of the Fission Products from 14-Mev Neutron Fission of U-238 with Those from 8-Mev Neutron Fission of U-238 Given as a Ratio of the Two with Time after Fission	183

ILLUSTRATIONS

Figure		Page
3.5	The Gross Air Ionization Rate Fractionation Number, r_{fp}, Relative to the Ionization Rate of the Fission Products from Thermal Neutron Fission of U-235, for the Fission Product Mixtures from Other Fissile Nuclides and Neutron Energies	185
3.6	The Gross Air Ionization Rate Fractionation Number, r_{fp}, Relative to the Ionization Rate of the Fission Products from Thermal Neutron Fission of U-235, for the Fission Product Mixtures from Other Fissile Nuclides and Neutron Energies	186
3.7	The Number of Photons per Disintegration for the Normal Mixture of Fission Products from 8-Mev Neutron Fission of U-238	188
3.8	The Average Energy of the Photons from the Normal Mixture of Fission Products from 8-Mev Neutron Fission of U-238	189
3.9	The Relative Response of the AN/PDR-39(T1B) Portable Radiac Held by a Man at 3 Feet above an Extended Plane Area Contaminated with Fission Products from Thermal Fission of U-235	191
3.10	Variation of r_{fp} with Time after Fission for the Fractionated Mixture of Fission Products from 8-Mev Neutron Fission of U-238	193
3.11	The Observed Variation of r_{fp} with Time after Fission for Close-in Fallout from a Low Tower Shot at the Nevada Test Site	195
5.1	Schematic Outline for the Intensity Profile Downwind from Ground Zero along the Axis of the Fallout Pattern (y = 0) as Used in the Simplified Fallout Pattern Scaling System	233
5.2	Intensity-Distance Plots for Construction of an Idealized Fallout Pattern for a 1-MT Yield Surface Detonation for a Wind Speed of 15 mph	257

ILLUSTRATIONS

Figure		Page
5.3	Idealized Fallout Pattern for a 1-MT Yield Surface Burst for a Wind Speed of 15 mph and 100 Percent Fission	258
5.4	First Estimate of the Dependence of $K_0(1)\,A_\alpha$ on α for a 1-MT Surface Detonation and Wind Speed of 15 mph	260
5.5	Variation of $K_0(1)A_\alpha(\alpha)$ with α at $X = 1.87 \times 10^5$ ft for $W = 10^3$ KT and a Wind Speed of 15 mph	262
5.6	Time of Arrival of the Various Particle Groups Designated by α For a Wind Speed of 15 mph	267
5.7	Rate of Activity Deposition on the Ground as a Function of α at $X = 1.87 \times 10^5$ ft, for $W = 10^3$ KT and a Wind Speed of 15 mph	268
5.8	Rate of Fallout Arrival as a Function of Time after Detonation at $X = 1.87 \times 10^5$ ft for $W = 10^3$ KT and a Wind Speed of 15 mph	269
5.9	Variation of Ionization Rate with Time after Detonation at $X = 1.87 \times 10^5$ ft for $W = 10^3$ KT and a Wind Speed of 15 mph	270
5.10	Variation of α_{max} and α_{min} with Downwind Distance for a 1-MT Yield Surface Detonation and Wind Speed of 15 mph	273
5.11	First Estimate of $K_R(1)A_\alpha$ as a function of $\bar{a}$ for Fallout from Stem Altitudes for a 10^3 KT Yield Surface Burst and a Wind Speed of 15 mph	275
5.12	Variation of the Ionization Rate with Time after Detonation at $X = 3.36 \times 10^4$ ft for $W = 10^3$ KT and a Wind Speed of 15 mph	278
5.13	Vertical Component of the Velocity for Spherical Particles Falling from Various Altitudes to Sea Level	280

ILLUSTRATIONS

Figure		Page
5.14	Accumulated Activity Distribution as a Function of Particle Size at X = 3.35×10^4 ft and 1.87×10^5 ft Downwind from the 1-MT Yield Surface Burst for a Wind Speed of 15-mph	286
5.15	Comparison of the Gross Activity Distribution on Particles of Various Diameters Derived from the Simplified Fallout Model to Distributions Used in Other Mathematical Fallout Models	287
5.16	Plot of Particle Fall Trajectory Components Relative to Estimated Pattern Center Line for Castle Bravo Winds	292
5.17	Variation of the Calculated Infinite Ideal Plane Standard Intensity with Downwind Distance (Center Line of Pattern) for a 10-MT Yield Surface Detonation (100 percent Fission)	297
6.1	Calculated Ionization Rate as a Function of Time after Detonation for Assumed Condensations up to 60,174 and 406 Seconds after Fission of Fission Products from 8-Mev Neutron Fission of U-238 and an Assumed Surface Burst Total Yield of 14-MT	314
6.2	Estimated Percent of the Fission Product Activity in r/hr at 1 hr from the Fission Products Condensed on Particle Groups with α Values (15-mph Wind Speed) Less than a Stated Value	320
6.3	Proposed Curve for the Variation of $f(\alpha)$ with α for a 15-mph Wind Speed	324
6.4	Proposed Mass Correction Curve to the Mass Contour Ratio as a Function of the Nuclear Scaled Depth of Burst	328
6.5	Proposed Crater Depth Correction Curve for the Mass Contour Ratio as a Function of the Nuclear Scaled Depth	332
6.6	Variation of σ_L with Calculated Values of σ_0	345
6.7	Variation of the Median Particle Diameter of Fallout on Foliage with σ_0 of the Deposited Fallout	347

TABLES

Number		Page
2.1	Fractional Chain Yields for Mass 89 for U-235 Fission	18
2.2	Fractional Chain Yields for Mass 140 for U-235 Fission	19
2.3	Cumulative Mass-Chain Yields of Fission Products	20
2.4	Calculation of Relative Activity Ratios from Kimura's Data on Coral Fallout[28]	51
2.5	Percentage Activities in Ion Exchange Peaks of Different Chemical Groups in Coral Fallout Sample[28]	53
2.6	Summary of Estimated Fractionation Numbers for Beta-Emitting Nuclides in Coral Fallout from No. 5 Fukuryu Maru at D+21 and D+25	54
2.7	Radiochemical Data on Coral Type Fallout Particles from a Large Yield Surface Detonation	57
2.8	Summary of Fractionation Numbers for Mass Numbers 89 and 140 in Coral Fallout Particles	61
2.9	Summary of Fractionation Numbers Relative to Mass Number 89 for Coral and Seawater Fallout Corrected for Appropriate Fission Yields	65
2.10	Comparison of Empirical Fractionation-Correlation Parameters with Those Estimated for Condensation of Alkali and Alkaline Earth Elements of Mass Chains 90, 132, 137, and 140, at Specified Times after Fission	70
2.11	Relative Radioelement Concentrations in Jack Rabbit Bone Tissue at about 20 Days after Detonation of Shot Smoky, Operation Plumbbob, in 1957	75
2.12	Average Fractionation Numbers of Radionuclides in Fallout from Tower- and Balloon-Supported Detonations at the Nevada Test Site	77
2.13	Gross Solubility of Activity from Small Fallout Particles	77

TABLES

Number		Page
2.14	Gross Solubility of Activity from Small Fallout Particles Lodged on Plant Foliage	79
2.15	The Size Distribution and Amount of Fallout Particles Lodged on the Foliage of Different Species of Plants	87
2.16	Collection and Retention of Fallout by Some Forage Crops	88
2.17	The Decontamination of Fallout Particles from Foliage	89
2.18	Summary of Averaged Foliage Contamination Factors for Native Foliage Exposed to Fallout from Tower- and Balloon-Mounted Detonations at the Nevada Test Site	91
3.1	Thermal Properties of Nitrogen and Oxygen as Ideal Gases	124
3.2	The Change in Energy Content and Number of Moles of Gas in Heating 1 Mole of Air as an Ideal Gas from 290°K and 1 Atmospheric Pressure to T°K at Pressures of 1 to 20 Atmospheres	126
3.3	Summary of Values of the Fireball Energy and Gas Content Related to Total Pressure, Volume, and Temperature for Heating Air from 298°K to 8300°K	127
3.4	Summary of Values of n_T/W and p_2 for the Model Air Burst	136
3.5	Thermal Data for Ideal Soil Constituents of Composition $Na_2O \cdot Al_2O_3 \cdot 6SiO_2$	138
3.6	Summary of Calculations for $T_2(s)$ Based on the Assumption of Equal Vapor Densities at the Second Temperature Maximum for the Model Air- and Surface-Burst Fireballs	139
3.7	Summary of Fireball Conditions at the Second Temperature Maximum for the Model Surface Burst of Different Yields Using Eq. 3.132 for $T_2(s)$	141
3.8	Summary of Some Fireball Parameter Values for Various Yields of the Model Surface Burst	147
3.9	Summary of Fireball Parameters and Thermal Data for the 14-MT Yield Model Surface-Burst Fireball	149
3.10	Summary of Estimates of $n(\ell)/V$ for the Model Surface Burst of Different Yields at the Time the Fireball Temperature is 1673°K	153

TABLES

Number		Page
3.11	Summary of Estimates of n(r)/V or n(s)V Based on Fission Content of Fallout	150
3.12	Summary of Empirical Constants for Vaporization Reactions of Fission Products and Other Elements	160
3.13	Summary of Raoult's Law Constants for the Gaseous Species of the Fission Product and Other Elements at 1673° K	166
3.14	Calculated Partial Pressures and Equilibrium Partial Pressures of Some of the More Abundant Fission Product Elements Dispersed Uniformly in the Model Surface-Burst Fireball at 1673° K for a Fission Yield of 14-MT	167
3.15	Summary of r_n(A) Values at 9 and 60 Seconds after Fission for Fission Product Nuclides that Contribute to the Gross Activity at 45.8 Minutes and Longer Times after Fission	169
3.16	Summary of Disintegration Multipliers for the Fission Product and Other Radionuclides[a]	171
3.17	Decay of Normal Fission Products from U-235, U-238, and Pu-239	178
3.18	Summary of H+1 Ionization Rates of Normal Fission Products[a]	187
3.19	Early-Time Ionization Rate, Photon Energy Emission Rate, and Average Photon Energy for Fission Products from Thermal Neutron Fission of U-235	192
3.20	Ionization Rate for Fission Products Condensed on Ideal Soil at 1400°C at 9 Seconds (84-KT) and 60 Seconds (14-MT) after Fission of U-238 (8-Mev Neutrons) and Ratio to That for the Normal Mixture from Fission of U-235 (Thermal Neutrons)	194
3.21	Activity from U-237 for 10^4 Atoms at Zero Time[a]; C(237) = 1	197
3.22	Activity from U-239 for 10^4 Atoms at Zero Time[a]; C(239) = 1	198
3.23	Activity from Np-239 for 10^4 Atoms of U-239 at Zero Time[a]; C(U-239) = 1	199
3.24	Activity from Np-240 for 10^4 Atoms of U-240 at Zero Time[a]; C(U-240) = 1	200

TABLES

Number		Page
4.1	Values of Stem and Fireball-Cloud Geometry Constants for Several Weapon Yields	214
5.1	Equation Parameter Values for the Variation of $\Delta z_{g,n}$ with Wind Speed and Derived Values of $K_{g,n}\bar{A}_f$	237
5.2	Summary of the Relative Wind Speed Shear Factor $S(v_w)$, for the Fallout Pattern Maximum Half-width and Associated Standard Ionization Rate, for Several Wind Speeds	244
5.3	Summary of Fallout Pattern Features and Fallout Scaling System Parameter Values for an Assumed Effective Wind Speed of 15 mph	254
5.4	Comparison of Fallout Pattern Data for a 1-MT Yield Obtained from the Simplified Scaling System Functions and from the ENW Methods	256
5.5	Calculation of Fallout Arrival Rate at $X = 1.87 \times 10^5$ feet, $y = 0$, from a 1-MT Surface Burst for a Wind Speed of 15 mph	261
5.6	Summation of Fallout Rates for α Groups Arriving at the Same Time and Accumulation of Activity and Exposure Dose during the Fallout Period	264
5.7	First Estimate of $K(1)\bar{A}'_\alpha$ as a Function of α for a 1-MT Yield Surface Detonation	274
5.8	Calculated Arrival Times and Dose Rates during the Fallout Period and up to 1.5 hour at the Downwind Distance of 6.3 Miles from a 1-MT Surface Detonation	276
5.9	Diameters of Spherical Particles for Various α Groups Falling at 1.87×10^5 feet and 3.35×10^4 feet Downwind from a 1-MT Yield Surface Detonation Assuming a Wind Speed of 15 mph	284
5.10	Wind Data and Particle Fall Trajectory Components for Jangle "S" Shot	289

TABLES

Number		Page
5.11	Summary of "Equivalent" Uniform Wind Shear from Relative Pattern Spread for the Simple Fallout Scaling System Patterns (Wind Speed of 15 mph)	293
5.12	Ratio of Areas within Stated Standard Intensity Contours for Fallout Patterns Computed	295
6.1	Summary of Fission Product Nuclide $r_i'(A)$ Values for 84-KT and 14-MT Yield Surface Detonations	307
6.2	Equation Constants for Air Ionization Rates from 0.76 to 1.12 Hours after Fission and Fraction of the Total Ionization Rate at H+1 from Fission Products Condensed on Particles at Given Times after Detonation of an 84-KT and a 14-MT Yield Land Surface Burst	311
6.3	Calculated Ionization Rates of Condensed Fission Product Mixtures from U-238 (8-Mev Neutrons) Fission at Selected Condensation Times	313
6.4	Fractionation Numbers for U-238 (8-Mev Neutrons) Fission Products Relative to the Normal Mixture of U-235 (Thermal Neutrons) Fission Products as Calculated for the End of the First Period of Condensation and at 406 Seconds after Detonation	318
6.5	Computation of Particle Size Parameters for Various Condensation Times of the 84-KT and 14-MT Yield Land Surface Detonations	319
6.6	Calculation of $f(\alpha)$ from M_r (1) Data from Operation Jangle Shot "S"	322
6.7	Computation of S_0 for Several Detonation Conditions of a 1-MT Fission Weapon	336
6.8	Computation of $M_{\hat{r}}$ (1) for Several Detonation Conditions of a 1-MT Yield Fission Weapon at Selected Downwind Distances	337
6.9	Summary of Shot Conditions for Estimating the Median Particle-Diameter Designator	343
6.10	Calculation of σ_0 for Some Fallout Locations from Shots Apple II and Smoky	344

Chapter 1

THE NATURE OF FALLOUT

1.1 Background

On the 16th day of August in 1945 the first nuclear explosion, Shot Trinity, was detonated at Alamagordo, New Mexico. The nuclear device was mounted on a tower at a height of about 100 feet and the energy of the explosion was equivalent to that of 19,000 tons of TNT. The explosion, as all nuclear explosions, produced radioactive materials that combined with other materials engulfed by the forces of the explosion. The product of the combination has been given the name fallout.

From most nuclear explosions, fallout is in the physical form of particles. After Shot Trinity some of these particles deposited on pastures and on the backs of cows at some distance from the point of detonation, and the nuclear radiations from the particles caused burn-like injuries on the cows' backs. Other than this the exposure had no ostensible influence on the life of the animals or their offspring.

The incident, however, initiated interest and concern among some scientists and engineers. Both the fate of radioactive substances produced in nuclear explosions and the biological consequences of their interaction with living matter came under study.

In Operation Crossroads, in 1946, ships exposed to the effects of an underwater nuclear detonation, were found to be contaminated with radioactive substances, and military--especially Navy--interest in the fallout phenomenon was aroused. The results of that test initiated the recognition of fallout as one of the primary phenomena of nuclear explosions and one that could have a profound influence on military operations using nuclear weapons.

The recognition and acceptance of the implications of fallout on military operations, however, was at first limited to a rather small group of scientists, engineers, and military people. Additional evidence and data on fallout were obtained in subsequent tests, especially in Operations Greenhouse and Buster-Jangle in 1951 and in Upshot-Knothole in 1953. But it was not until the detonation of Shot Bravo in Operation Castle in 1954 that general recognition of the fallout phenomenon was established.

Two of the better-known incidents that influenced (or forced) such recognition were the exposure of the Marshall Islanders on the Rongelap Atoll and of the Japanese fishermen in their boat at sea to the radiations from fallout. But even after the Shot Bravo experience there remained a few who wanted to believe that a "fluke" had occurred and that fallout was not of military significance.

Now, several years and many test detonations later, there are no remaining doubts about the production of fallout in nuclear explosions. Present studies are directed to quantitative evaluations of the degree to which fallout is significant in the military applications of nuclear explosives. Thus it is no longer of interest simply to note that radioactive atoms are produced in nuclear explosions. The problem is to determine the quantity of the radioactive atoms produced, what physical processes they are subjected to, where they go, and how their disposition may affect the operations and the lives of people.

Because fallout contains radioactive atoms, and because radioactive atoms emit nuclear radiations that can cause damage in the cells of living tissues, the presence of fallout in the environment is usually equated with a potential radiological hazard to living matter. The core of the present-day interest in fallout, therefore, consists of evaluating the biological consequences to humans, animals, and plants of the exposure to nuclear radiations from fallout.

The degree and nature of possible exposures of living matter to nuclear radiation depend upon many physical parameters and these begin with the initial production of the fallout in a nuclear explosion. The nature of the exposure is more fundamentally connected with physical processes than is the degree of the exposure. In terms of degree, it is known that possible radiation exposures would be highest, and therefore the biological consequences most severe, for nuclear explosives used in a large-scale war. This degree of exposure is of concern to many.

After the fallout is in an environment, the degree of this radiological hazard can be measured. But the kind and amount of hazard in a nuclear war situation, at least before the fact, cannot be evaluated without a reasonably detailed description of the history of the radioactive atoms produced in nuclear explosions. Such a history, to be useful, must reveal the essential details of the physical processes in which the radioactive atoms participate, from the instant they are formed up to any desired later time.

The major purpose of this report, therefore, is to outline and discuss these physical processes and the important parameters on which they depend. The data, data analyses, data correlation schemes, and discussions presented here are organized to emphasize basic principles so that an appropriate methodology can be applied in evaluating the radiological consequences of nuclear war.

1.2 A General Description of Fallout

An explosion of any kind, detonated near the surface of the earth, causes material to be thrown up or drawn into a chimney of hot rising gases and raised aloft. In a nuclear explosion, two important processes occur: (1) radioactive elements, which are produced and vaporized in the process, condense into or on this material; and (2) a large amount of non-radioactive material, rises thousands of feet into the air before the small particles begin to fall back. This permits the winds to scatter them over large areas of the earth's surface. Thus, when the particles reach the surface of the earth they are far from their place of origin and contain, within or on their surface, radioactive elements. Whether they are solid particles produced from soil minerals, or liquid (salt-containing) particles produced from sea water, they are called fallout.

The composition of fallout can be described in terms of two or three components. One is the inactive carrier; this consists of the environmental material at the location of the detonation and is the major component in a near-surface detonation. The second component includes all the radioactive elements in the fallout.

These radioactive elements can be subclassified into two groups by source. The first group contains the fission-product elements that are produced in the fission process that initiates the explosion. The second group consists of the elements produced by the capture of neutrons released in both fission and fusion. The kinds and amounts of these neutron-induced radioactive elements in the fallout differ from one detonation to another depending upon the type of weapon used and the chemical elements in the environment at the point of detonation.

Occasionally, a third fallout component group is considered. This consists of the bomb's structural materials and is a major component in air-burst fallout.

The word fallout is occasionally preceded by "close-in" (or "local") and "long-range" (or "world-wide"). These terms have never been precisely defined except for operational purposes. The terms imply some arbitrary differentiation of the fallout, or the radioactivity, on the basis of distance from the point of detonation or time required for the material to fall to the earth's surface. However, as is discussed in the following chapters, the gradual changes in the properties of the fallout with distance make precise definition of these terms impossible, except for the extremes of each fallout classification. Therefore, except for these extreme cases, these descriptions are not used further as definitive terms in discussing the nature and properties of fallout.

1.3 Characteristic Types of Fallout

The characteristic types of fallout are determined by the environment at the point of detonation. They are generally classified as being either land, sea water, harbor, or air fallout.

The major component of the fallout from detonations near the surface of land is the soil particles. In detonations near the surface of the ocean the major component is the sea water residues (salts and water). The fallout from detonations in harbors, rivers, and shallow lakes may contain materials from the bottom as well as water and/or sea water salts; the relative amounts of each depend on the depth of the water, the height or depth of the burst, and the energy released during the explosion.

From an air burst (not near the surface of the earth) the major fallout component is the structural materials, such as iron and aluminum, etc., of the bomb or missile war head. When the mass of these materials is not too large, and when it is all vaporized, only very small fallout particles are formed. The proportion of air burst fallout are those most often associated with the terms long-range or world-wide.

The fallout from the near-surface bursts consists of large particles that fall rapidly to the earth; these fallout types result in much higher deposit densities than those from the air burst. Because of this large difference in fallout deposit density and the associated radiological hazard, only the first three characteristic types of fallout (land, sea, and harbor) are discussed at length in the following chapters.

1.4 Potential Hazards from Fallout

The potential hazards from fallout are mentioned briefly here to identify them, to indicate their relationship with physical quantities that can be measured, and to emphasize the fact that interest in knowledge about fallout has been aroused mainly because of these hazards.

The radioactive elements within or on the surface of the fallout particles emit gamma and X-rays and/or beta or alpha particles. The gamma and X-rays are the same except that the gamma rays are more energetic; they are often termed the penetrating or long-range radiations because gamma and X-rays travel long distances in air and in other low-density materials. The beta and alpha particles are often termed short-range radiations because they do not travel very far even in air and are stopped by small thicknesses of more dense material. Of the two, the alpha particles are the easier to stop.

The potential hazard from the three types of nuclear radiations lies in the capability of the different types of radiation to penetrate material, both living and inanimate, especially when the radioactive source is not in contact with the material irradiated. Thus, from fallout particles deposited on the ground, the gamma rays are the only ones emitted that can penetrate large distances into the human body. The shorter-range beta particles can penetrate a short distance into material when their source is either in contact with its surface or is part of the material (i.e., an internal source). In general, alpha particles are not a fallout hazard because the alpha emitters are so extremely diluted and long-lived.

The gamma rays, then, constitute an external hazard; the beta particles are often termed a contact and an internal hazard; and the alpha rays constitute an internal hazard, if any. But since the major source of alpha particles in fallout is from the decay of unreacted uranium or plutonium, which are very long-lived radionuclides, the alpha-particle hazard is negligible compared with that of the gamma and beta rays derived from other radioactive elements. Hence the alpha-particle hazard is not considered further.

The two radioactive emissions that are of concern in fallout, therefore, are the gamma radiations (including the X-rays) as an external source of hazard, and the beta particles as a contact or internal source of hazard. The significance of this differentiation between the two types of radiations as hazard sources is discussed in later chapters. Both types of radiations cause injury to living organisms by producing ionization along their paths through living tissue. In other words, the rays or particles transfer energy to the electrons of the atoms in the material they penetrate. This causes the electrons to leave their orbits around the nucleus of the atom so that the atom takes on, for a short time, a positive charge.

A specified amount of energy is required to ionize an atom; for every ion pair formed by the passing of a gamma ray or beta particle near an atom, the ray or particle loses an equivalent amount of energy. The amount is not the same for all materials penetrated because the energy required to ionize an atom differs from one chemical element to another. The roentgen is the defined unit for measuring the energy absorbed from gamma and X-rays in air. The value of the r unit is based on the energy required to ionize the nitrogen and oxygen atoms of air to form, in one cubic centimeter of air at standard conditions, one pair of ions. By this definition, the r unit is equivalent to the absorption of about 87 ergs of energy per gram of air.

Since this unit, the r, is defined on the basis of air ionization, it cannot be related to the number of radioactive atoms that emit gamma rays unless both the energy of the rays passing through a given volume of air and the geometric configuration of the emitting sources are known. These

relationships, for a complicated mixture of radionuclides such as would be present in fallout, have only been calculated for a few very simple source geometries. An example is the calculation for the air ionization rate at three feet above an infinite smooth plane covered with a uniform distribution of fission products.[1*]

The air ionization rate, in roentgens per hour, is often called the intensity, or the radiation intensity; when used, these terms always refer to the magnitude of the air ionization rate. Another term often used is dose rate; however, this one is more precisely associated with the rate of energy absorption, from the radiations, in living tissue rather than in air, since dose rate has a biological connotation. In common usage, the three terms (intensity, radiation intensity, and dose rate) are used interchangeably; when their units are r per hour, they are, in fact, air ionization rates.

The total amount of energy absorbed in a volume of air over a period of time is the radiation dose. When the accumulated air ionization rate (i.e., the dose) is associated with biological hazard from an unmodified fallout deposit, the restrictive terms potential dose or exposure dose are often used. Such use actually involves two restrictive concepts or assumptions. The first is that this dose is the total amount of air ionization, per unit volume, that a person or object is exposed to by staying in the specified location for the length of time that the stated energy is being absorbed by the air. The second concept is that the dose, or the energy absorbed by the air, is proportional to the amount of energy absorbed by the person or object.

The terms, dose, potential dose, or exposure dose are used only in reference to the air ionization in the following chapters. While the biological effects of a radiation dose are outside the scope of this discussion, arbitrary values of dose limits are used occasionally; they illustrate the methodology that can be used to solve exposure-control problems.

The dose-limit values used in this report are selected on the basis of assumed relations between air ionization doses and biological effects. These selections, when applicable, include the concept that some biological effects have a threshold dose while others do not, and that, when the dose is absorbed over a long period of time, the biological effect of the dose is decreased due to bodily repair of tissue damaged during the exposure.

*References are listed at the end of each chapter.

The ionization rate and the dose from beta rays are usually defined in terms of the energy absorbed by the ionization of the atoms or molecules in tissue. Since the beta particles do not penetrate very far into the tissue, the dose from beta emitters on the surface of tissue, such as the skin, is absorbed largely in the skin's outer layers. Because of the complicated manner in which the energy of the beta particles is distributed, there is no simple method for estimating the energy absorbed in various thicknesses of a tissue having a deposit of a mixture of radioactive atoms on its surface. Even when the radioactive atoms are uniformly distributed through a tissue, as may be the case for several ingested radio-elements, the methods for estimating the absorbed dose are fairly complicated.[7] In this case, the rates of accumulation in, and elimination from, the tissue must also be considered.

In most of the fallout conditions described in the following chapters, the beta radiation exposure turns out to be the less dominant fallout hazard. However, some times and situations where beta radiation can be a significant hazard are discussed.

The main immediate hazard from fallout when it arrives on the surface on the earth after a nuclear explosion is due to the gamma, or penetrating, radiation. These nuclear radiations can travel long distances, and their summed, or integrated, intensity completely dominates the radiation hazard. This is the case even for persons or objects contaminated with falling particles, since the contribution of the beta particles to the exposure dose is only from those particles that are deposited on exposed tissue.

The ingestion of radionuclides from fallout over a long period of time, however, becomes the predominant hazard after a period of time. The magnitude of this internal hazard depends on the fallout's chemical nature, which uniquely determines both the availability of the radionuclides for ingestion and the period of their retention in living tissue.

1.5 Radioactive Decay

Evaluation of the hazards from fallout so that the necessary degree of protection from the nuclear radiations can be specified requires knowledge of how the air ionization rate decreases with time. The integral, or accumulated, dose is determined from a curve giving the variation of the air ionization rate with time, and, since some value of the dose is known to produce undesirable biological effects, the ratio of the two is used to determine the desired protection factor of either a safety procedure or radiological defense countermeasure, or both.

In a nuclear detonation, the fission process produces about 90 fission-product mass chains, consisting of about 40 different elements. In each mass chain produced in the fission of fissile materials one or more radionuclides are produced. These parent-daughter pairs decay one to the next until finally a single stable nuclide is formed. The decay of this mixture of radionuclides can be calculated from (a) the initial yield of the nuclides in each mass chain, (b) the half-life of each nuclide, and (c) the abundance of the gamma rays produced when each nuclide decays. The details of such calculations as these are discussed in Chapter 2.

In a nuclear detonation, the fission products are initially vaporized; they condense later as the fireball cools. Of the approximately 40 elements present, some are volatile and not usually in a condensed state even at ordinary temperatures. Some elements are refractory and condense at high temperatures. The remainder condense at intermediate temperatures.

Because there is such a large range in the thermal stability of the condensates of the fission-product radionuclides, the normal abundance ratios of the fission-product radionuclides in fallout are altered. It is found that, in the larger fallout particles, the relative concentration of the volatile radionuclides (and their daughters) is low and that the concentration of the more refractory radionuclides is high. Any such alteration in the abundance ratios of the fission products, relative to the original fission-yield abundance ratios, is called fractionation. In most types of fallout, the fission-product radionuclides are found to be fractionated.

Neutron-induced activities are also found in fallout. These induced activities are produced by neutron capture in materials present in the weapon itself and in other environmental materials at the point of detonation. Perhaps the most important of the induced activities are those produced by neutron capture in the elements of the weapon's construction materials. These induced activities result from neutron activation of uranium-238, iron, manganese, and other construction materials. In soil and sea water, manganese and sodium are perhaps the most likely elements to be neutron-activated in highest abundance.

The gross decay, or variation in air ionization rate with time, of the nuclear radiations from fallout is the sum of the contributions of all the radionuclides present in the radiation source. Thus, to specify or even to estimate the gross decay rate of the radioactivity in fallout, both fractionation and neutron-induced activities must be considered.

1.0 The Standard Intensity and Contour Properties

The term standard intensity is defined here as the magnitude of the air ionization rate at three feet above an extended open area covered with fallout, corrected to a stated time after detonation; conventionally the stated time is one hour. This reference-time originated when the "nominal" detonation yield of nuclear weapons was 20 kilotons (KT), and when data on fallout were available only for small-yield weapons, since for such yields the fallout process was essentially complete by one hour after detonation, at least in areas receiving significant amounts of fallout. Of course, the heavy deposition of fallout from megaton (MT) yield explosions is not complete even after several hours. In such cases, the observed radiation intensity at one hour after detonation is not the same as that calculated from a measurement of the intensity after the fallout ceases to arrive and must be decay-corrected to one hour after detonation.

The standard intensity values are used in constructing charts of areas on which fallout has been deposited. A chart showing a fallout pattern consists of a series of isointensity contours. These contours are not lines of equal potential hazard until after the fallout has ceased to arrive at the farthest downwind location on a given contour. The charts are very useful, however, in evaluating the area-coverage of fallout with regard to both the potential radiation hazard and the kinds of protection needed to reduce that hazard to a desired level.

The determination of the standard intensities requires measurements of the intensity, over time, at a series of locations during and after the fallout is deposited, and, in addition, measurements of the ionization rate, over time, on samples collected when the fallout first starts to arrive. A heavily shielded detector is required for the latter. However, for locations where the fallout arrival time is greater than one hour, correcting the obtained data to the conventional time of one hour requires a decay-correction factor for the period between the time of the first measurement and the standard time of one hour. Measurements of the intensity over areas covered with fallout particles, the contaminated areas, have been made, in most cases, with portable ion chambers. The accuracy of the measurements made with most of the presently available portable instruments is not very high; however, if the ion chambers are kept in excellent repair, are carefully handled, and are kept calibrated, accuracies of about 20 percent can be obtained.

The intensity due to the fallout particles depends on (a) the number or mass of the particles deposited, per unit surface area, and (b) the specific activity, or concentration, of the radionuclides in the particles. To reduce the intensity of the fallout from a land detonation by intention, either the particles must be moved away from the location of interest or shielding must be placed between the particles and the location of interest.

Moving the particles efficiently and effectively requires some knowledge of the properties of the particles; also, the removal procedure or decontamination method must be designed to remove fallout particles. Because of these requirements on the performance of decontamination methods, relationships are needed among (a) the mass of the particles, per unit area (b) their specific activity, and (c) their radiation intensity. Such relationships are extremely useful, because intensity measurements, which are easy to make, can then be used to deduce the fallout properties that influence decontamination.

These relationships between the radiation intensity and the related fallout properties are called contour ratios; they are discussed in detail in Chapter 6. The values of these ratios, and the mathematical form of the relationships among these ratios and the other parameters, depend on two major factors. One is the type of chemical system produced under the given conditions of temperature, pressure, and concentrations of various constituent elements in the fireball. The other factor is the manner in which the particles become distributed, both in the forming cloud and in their fall through the atmosphere back to earth.

Definition of the chemical systems formed in these processes, as well as of the chemical systems formed when the fallout particles contaminate surfaces, is important in devising appropriate decontamination procedures. To be useful, such procedures must be designed to operate on any chemical systems that contain radioactive substances.

CHAPTER 1 REFERENCES

1. Miller, C. F., and P. Loeb, Ionization Rate and Photon Pulse Decay of Fission Products from the Slow Neutron Fission of U-235, USNRDL-TR-247 (1958)

2. Morgan, K. Z., and M. R. Ford, Nucleonics, 12, 6, 32 (1954)

Chapter 2

FORMATION OF FALLOUT PARTICLES

2.1 General Definition of the Process

The process of radioactive fallout formation is initiated when fissile material undergoes fission. In each fission event, about 200 million electron volts (Mev) of energy are released; also, two neutron-rich radioactive elements, or particles, plus two to four or five neutrons, and several gamma rays are produced. If the resulting two particles carried all the released energy before colliding with another atom, the average initial energy would correspond to a kinetic temperature of about 10^{12} degrees Kelvin (°K).

The released energy is initially in the form of electromagnetic and kinetic energy whose immediate and rapid transmission to nearby surrounding materials causes the latter to vaporize at high pressure. Thus when many fission events occur in a small volume in a short period of time a high-pressure shock wave forms and a nuclear explosion results.

The two fission-product atoms formed from a heavy-element atom contain more neutrons than do stable elements having the same atomic mass. Therefore, the initial fission-product atoms progress to stability by emitting beta particles and/or neutrons. This beta decay of many of the fission-product radionuclides results in the simultaneous release of gamma rays. Also, the capture of neutrons by nearby atoms results in the release of gamma rays. At detonation, therefore, the gamma ray pulse includes gamma rays from (a) the fission reaction itself, (b) neutron capture by elements in the surrounding media, and (c) the decay of fission products.

In the so-called fusion, or thermonuclear, weapons, the high temperature created by the fission process is utilized to fuse the light elements such as deuterium, tritium, and lithium. In this combining of the lighter elements to form helium or other heavier nuclei, additional energy and neutrons are released. Such neutrons, having higher energies than those produced by fission, are able to cause the fission of uranium-238 or, when captured by the nuclei of other elements near the explosion, to cause the latter elements to become radioactive.

As the thermal and shock waves travel outward from the detonation point, the materials enveloped are also heated to high temperatures; crystal bonds are broken, chemical compounds are decomposed, molecules dissociate, and atoms become thermally ionized. The result is the highly luminous mass of gaseous material called the fireball.

This transfer of energy by the shock wave and radiant processes to these materials and to other substances occurs at the expense of the initial energy of the fission fragments; their kinetic temperature falls extremely fast, by collision with other atoms, as they diffuse outward from the center of the explosion. The rate at which the energy is transferred to the materials being enveloped by the expanding fireball also decreases rapidly as the thermal exhange proceeds, and as the temperature of the materials on the interior of the gas volume decreases. As the temperature decreases, positive ions regain their electrons and become atoms, atoms recombine to form molecules, molecules condense to form liquid droplets, and, finally, when the temperature is low enough, the droplets solidify.

In the cooling of the fireball the important stage in the formation of fallout begins with the time and temperature at which the first liquid drops form. This formation process continues until after the materials involved have cooled to about the temperature of the surrounding air. While the condensing process probably never actually ceases, such a large fraction of the radioactive and other elements have condensed by about five to ten minutes after detonation that the process is essentially complete.

The highest fireball temperature to be considered in the formation of fallout is the boiling point of the most refractory material present in sufficient quantity to form a macroscopic liquid phase. For most materials this temperature is between 3000 and 4000°K.

By the time the fireball temperature cools to 3000 or 4000°K, it has risen some height into the air and, for near-surface bursts, crater materials consisting of liquid and/or solid soil particles have entered the fireball. At first some of these are melted and vaporized; as the gas temperature decreases, fewer and fewer of the crater material particles are melted, until finally those that actually reach the altitude of the rising cloud are only slightly warmed. The melted particles dissolve, aggregate, and occlude the smaller vapor-condensed particles formed by direct vapor condensation even before the mass

of larger particles enters the fireball.* Whether melted or solid, the entering particles present an extremely large amount of surface area upon which the gas atoms or molecules can condense.

There are several basic characterization of the fallout formation process in the developing fireball. The first is that, of the fission products alone, about 40 different radioactive elements are produced in a given yield, or order of abundance, that results in a set of partial pressures of vaporized species whose values are initially ranked in the same order as the abundance values. The second characteristic is that the chemical reactivity and the equilibrium vapor pressure of each element in the fireball differ from those of the other elements; thus the fraction of each element in a condensed state at a given temperature is also different from the fractions of the other elements.

The third characteristic is the presence of inert (nonradioactive) substances; these furnish either (a) an available surface area that the dilute vapors can condense on or interact with, or (b) a dense vapor that condenses to form a macroscopic liquid phase with which the less abundant radioactive elements can interact. The role of the condensation process, both in fallout formation and in fractionation, is discussed in detail later in this chapter. Condensation is one of several causes of observed fractionation in fallout.

An example of the dense-vapor condensation process is a detonation on sea water. In this type of detonation many of the fission-product elements condense, along with the bomb casing materials and the salts, before the water does, but the fission-product elements are occluded or dissolved by the water when it condenses. Such inert materials, that serve to carry the radioactive elements back to earth, are called the carrier or the carrier materials.

The amount of each radioactive element that is actually found in fallout, relative to some standard of measure, depends on five main factors:

1. The original fission yields, that is, the relative abundance of the fission products;

*A more complete general description of the fireball and its behavior is given in The Effects of Nuclear Weapons (designated ENW hereafter). Certain data from that volume are utilized here; generally these are confined to input information required to describe the fallout formation process. Data on the size, temperature, and position of the fireball are important in estimating its energy content, and in establishing an appropriate standard reference time for estimating fireball parameters for different nuclear yields.

2. The capture of neutrons by the fission products themselves;

3. The degree to which each fission product condenses into or onto the carrier particles;

4. The neutron emissions in the decay chain; and

5. The radiochemical standards used in measuring the relative abundances of the fission products.

The relative abundance of each fission product element originally produced at detonation depends on the fissile material used; i.e., whether the material is U-235, U-238, Pu-239, or some other substance. The fission-chain yields also depend on the energy spectrum of the incident neutrons.

In general, in the change of energy of the incident neutrons, the fission yields of the nuclides in the lighter-mass (A = 90 to 100) peak tend to shift more with mass number than do those in the heavier-mass (A = 131 to 144) peak. In the fission of the heavier fissile elements, the center of the lighter-mass group moves toward the higher-mass numbers. As the incident-neutron energy increases, the yields of the mass chains that appear in the valley between the two yield peaks rise, and the yields of the highest- and lowest-mass numbers also rise; also, the neutron yield per fission increases. This increase in neutron yield per fission tends to spread the two peaks farther apart and, again, the lighter-mass group is shifted more than the heavy-mass group.

Neutron capture by the fission-product elements results in a general shift of the whole fission-yield curve to the higher-mass numbers. This causes a decrease in the yields of the elements of both mass groups that have the smaller mass numbers (the left sides of the peaks), and an increase in the yields of the elements of both mass groups that have larger mass numbers. In the yields of the elements in the peaks relatively little change results except for those elements that have extremely high neutron-capture cross-sections. The subject is not discussed further because of insufficient data.

During the decay process, neutron emission results in a product nuclide that has a mass number that is a single unit less than its parent. This chain "shift" can be accounted for if the decay scheme of the radionuclide is known. For many of the short-lived radionuclides, however, there is insufficient data presently available for giving further consideration to decay by neutron emission.

The experimental measure of fractionation is most often given as an "R" factor, or "R" value, that is relative to the fission yields in the thermal-neutron fission of U-235 and of a selected radionuclide. The most commonly

selected radionuclide for comparison is Mo-99. However, a radiochemical assay of a fallout sample that gives an R value different from unity does not necessarily mean that the nuclide in question has, in fact, been fractionated with respect to some other nuclide or element. The true initial fission yields must be known, both to correct the observed assay data and to determine whether fractionation has, in fact, occurred.

2.2 Mass-Chain Yields for the Fission of U-235, U-238, and Pu-239

One major factor that determines the amount of a fission product that condenses with the carrier up to a given time and temperature is the amount of that element present in each of the mass chains. In this section, data on the fission-mass yields are summarized, and estimates of undetermined yields are presented, so that calculations of the fraction of the fission products that condense to form fallout may be made.

The independent yields of all radionuclides, for thermal neutron fission of U-235, have been calculated by Bolles and Ballou[3], according to the theories of independent fission yields of Glendenin[2] and of Present.[4] The fractional chain yields from these calculations, for times from zero to 180 seconds, are given in Table 2.1, for mass 89, and, in Table 2.2, for mass 140. Each chain contains a rare gas (Kr and Xe) element.

The two mass chains selected lie on the outer edge of the two yield peaks. In each case, the independent yield distribution from the Glendenin theory is the broader, and the short-lived, lowest-Z, elements are the more heavily weighted. This difference diminishes as the mass number approaches the value 118.

The fractional yields themselves indicate what might be expected during condensation with respect to the fractionation of the chain members. For example, if only the rare gas member is considered, the maximum loss (minimum amount condensed) should occur between 19 and 28 seconds for mass 89, according to Glendenin; for mass 140, according to both theories of yield, the fraction not condensed should decrease as the time period of the condensation process increases.

Computational estimates of the independent nuclide yields have not yet been made for fission of U-235 and Pu-239 with fission-spectrum neutrons, nor for fission of U-238 with 8-Mev broad-band spectrum neutrons; the latter would be more applicable to nuclear detonations. Moreover, the mass chain yields for even Pu-239 and U-238 fission are not very well known. Available chain yield data and estimates of unmeasured yields are summarized in Table 2.3 for the fission of U-235, U-238 and Pu-239. The bulk of the data are taken from the summary by Katcoff;[5] other references are included in the table.

Table 2.1

FRACTIONAL CHAIN YIELDS FOR MASS 89 FOR U-235 FISSION

τ (sec)	Present[4]					Gleadenin[3]				
	Se	Br	Kr	Rb	Sr	Se	Br	Kr	Rb	Sr
0	0.05	0.372	0.528	0.100	0	0.170	0.420	0.343	0.067	0
1		0.325	0.571	0.104	0	0.121	0.410	0.399	0.070	0
2		0.290	0.602	0.108	0	0.087	0.390	0.452	0.071	0
3		0.345	0.644	0.111	0	0.062	0.362	0.502	0.074	0
4		0.212	0.673	0.115	0	0.044	0.332	0.547	0.077	0
6		0.159	0.720	0.121	0	0.022	0.266	0.629	0.083	0
9		0.102	0.764	0.133	0.0014	0.006	0.183	0.720	0.090	0
13		0.056	0.794	0.147	0.0021	0.002	0.106	0.786	0.105	0.0012
19		0.022	0.809	0.166	0.0030		0.044	0.830	0.124	0.0020
28		0.0054	0.798	0.195	0.0043		0.011	0.832	0.155	0.0032
41			0.764	0.232	0.0064		0.002	0.800	0.192	0.0050
60			0.707	0.283	0.0097			0.744	0.249	0.0076
88			0.638	0.347	0.015			0.670	0.318	0.012
129			0.564	0.436	0.025			0.559	0.419	0.022
199			0.433	0.520	0.047			0.456	0.500	0.044

Table 2.2

FRACTIONAL CHAIN YIELDS FOR MASS 140 FOR U-235 FISSION

t (sec)	Present[4]					Glendenin[3]				
	I	Xe	Cs	Ba	La	I	Xe	Cs	Ba	La
0	0.074	0.493	0.399	0.034	0	0.138	0.408	0.366	0.088	0
1	0.047	0.498	0.416	0.039	0	0.087	0.441	0.380	0.092	0
2	0.029	0.495	0.433	0.043	0	0.055	0.453	0.395	0.097	0
3	0.019	0.485	0.449	0.048	0	0.034	0.454	0.412	0.100	0
4	0.012	0.479	0.466	0.052	0	0.022	0.447	0.426	0.105	0
6	0.005	0.438	0.493	0.064	0	0.009	0.423	0.453	0.115	0
9	0.001	0.389	0.531	0.079	0	0.002	0.377	0.491	0.130	0
13		0.328	0.570	0.102	0		0.316	0.531	0.151	0
19		0.252	0.609	0.139	0		0.246	0.569	0.185	0
28		0.170	0.632	0.198	0		0.167	0.592	0.241	0
41		0.097	0.619	0.284	0		0.095	0.584	0.321	0
60		0.043	0.555	0.402	0		0.041	0.525	0.433	0
88		0.013	0.439	0.548	0		0.012	0.416	0.572	0
129		0.002	0.294	0.704	0		0.002	0.278	0.720	0
189		0.001	0.157	0.842	0			0.149	0.851	0

Table 2.3

CUMULATIVE MASS-CHAIN YIELDS OF FISSION PRODUCTS
(VALUES ARE IN PERCENT OF FISSIONS)

Mass Number	U-235		U-238		Pu-239	
	Thermal Neutrons*	Fission Neutrons	Fission Neutrons	6-Mev Neutrons	Thermal Neutrons	Fission Neutrons
72	1.0×10^{-6}	4.6×10^{-4}	5.0×10^{-6}	-	1.2×10^{-6}*	-
73	1.1×10^{-4}	0.0012	3.7×10^{-5}	-	3.2×10^{-4}	-
74	(3.2×10^{-4})*	0.0034	1.1×10^{-4}	0.001	4.1×10^{-4}	0.0011
75	(8.9×10^{-4})	0.0062	8.3×10^{-4}	0.0040	7.5×10^{-4}	0.0023
76	(0.0029)	0.012	0.0012	0.0078	0.0014	0.0051
77	0.0088	0.023	0.0038*	0.014	0.0026	0.011
78	0.021	0.048	0.0095	0.026	0.0042	0.025
79	(0.041)	0.096	0.019	0.053	0.0090	0.043
80	(0.077)	0.19	0.045	0.096	0.016	0.075
81	0.14	0.21	0.088	0.18	0.030	0.14
82	(0.29)	0.50	0.20	0.35	0.056	0.25
83	0.544	0.80	0.40*	0.66	0.10	0.37
84	1.00	1.3	0.55*	1.02	0.17	0.60
85	1.30	1.85	0.80	1.45	0.28	0.92
86	2.02	2.5	1.35*	1.9	0.45	1.15
87	(2.94)	3.3	1.90	2.35	0.78	1.5
88	(3.92)	4.2	2.45	2.7	1.2	1.9
89	4.79	5.1	2.9*	3.17	1.9*	2.4
90	5.77	5.8	3.2*	3.7	2.4	3.0
91	5.84	5.85	3.6	4.3	3.0	3.7
92	6.00	6.0	4.1	4.8	3.7	4.4
93	6.45	6.4	4.85	5.2	4.6	5.0
94	6.40	6.4	5.3	5.45	5.5	5.4
95	6.27	6.3	5.7*	5.6	5.9*	5.6
96	6.30	6.3	5.8	5.7	5.7	5.3
97	6.00	6.1	5.7	5.64	5.6*	5.2*
98	5.75	5.8	5.7	5.6	5.4	5.4
99	6.06	6.1**	6.0*	6.2**	5.9*	5.9*
100	6.30	6.7	6.1	6.4	6.0	6.4
101	6.0	6.3	6.5	6.5	6.0	6.9

Table 2.3 (continued)

CUMULATIVE-MASS-CHAIN YIELDS OF FISSION PRODUCTS
(VALUES ARE IN PERCENT OF FISSIONS)

Mass Number	U-235		U-238		Pu-239	
	Thermal Neutrons*	Fission Neutrons	Fission Neutrons	8-Mev Neutrons	Thermal Neutrons	Fission Neutrons
102	4.1	2.9	5.0	5.0	5.0	5.0
103	3.0	1.7	0.6	5.0	5.8*	4.0
104	1.8	0.95	5.4	3.2	5.0	0.5
105	0.00	0.54	3.9	2.2	3.9*	3.2
106	0.38	0.30	2.7*	1.5	5.0*	5.0
107	0.19	0.17	1.35	1.0	4.0	3.1
108	(0.085)	0.095	0.67	0.70	3.0	2.0
109	(0.039)	0.058***	0.32*	0.48	1.5*	1.0*
110	(0.020)	0.060	0.15	0.30	0.68	0.81
111	(0.015)	0.022***	0.079	0.29***	0.27*	0.34
112	(0.010)	0.020***	0.046*	0.19	0.10*	0.14*
113	(0.012)	0.018	0.043	0.17	0.055	0.090
114	(0.011)	0.017	0.041	0.16	0.046	0.075
115	0.0104	0.017***	0.040*	0.15***	0.041*	0.060*
116	(0.010)[b]	0.017[b]	0.039	0.14	0.039	0.065
117	(0.010)	0.017	0.039	0.14[b]	0.038	0.065
118	(0.010)	0.017	0.040[b]	0.14	0.038[b]	0.064[b]
119	(0.011)	0.017	0.041	0.14	0.039	0.064
120	(0.011)	0.018	0.042	0.15	0.041	0.065
121	(0.012)	0.020	0.044	0.16	0.044*	0.066
122	(0.015)	0.022	0.040	0.17	0.047	0.069
123	(0.015)	0.030	0.050	0.19	0.052	0.070
124	(0.017)	0.058	0.065	0.20	0.058	0.082
125	0.021	0.095	0.072	0.33	0.072*	0.14
126	(0.058)	0.17	0.175	0.48	0.175	0.35
127	(0.145)	0.30	0.39	0.70	0.39*	0.80
128	0.37	0.54	0.77	1.0	0.77	1.0
129	0.90	0.95	1.45	1.5	1.45	2.5
130	2.0	1.7	2.5	2.2	2.5	3.2
131	(2.88)	2.9	3.2*	3.2	3.8*	3.8

Table 2.3 (continued)

CUMULATIVE MASS-CHAIN YIELDS OF FISSION PRODUCTS
(VALUES ARE IN PERCENT OF FISSIONS)

Mass Number	U-235		U-238		Pu-239	
	Thermal Neutrons*	Fission Neutrons	Fission Neutrons	6-Mev Neutrons	Thermal Neutrons	Fission Neutrons
132	(4.31)	4.5	4.7*	4.4	5.0	4.6
133	(6.45)	6.1	5.5*	5.4	5.27*	4.9
134	(7.80)	7.5	6.6*	6.5	5.69*	5.2
135	(6.40)	6.3	6.0*	5.9	5.53*	5.1
136	(6.36)	6.4	5.9*	5.8	5.00*	5.3
137	(6.05)	6.0	6.2	5.85	5.24*	6.4*
138	5.74	5.7	6.4	5.9	5.5	5.4
139	(6.34)	6.4	6.3	6.0	5.7*	5.2
140	6.44	6.4	5.7*	5.6	5.68*	5.0*
141	(6.30)	6.3	5.7	5.5	5.2*	4.7
142	(5.85)	5.9	5.7	5.4	6.69*	4.9
143	(5.87)	5.8	5.5	4.07	5.4*	5.0
144	5.07	5.1**	4.0*	4.3**	5.29*	4.8
145	3.95	4.2	3.7	3.7	4.24*	4.4
146	3.07	3.3	3.1	3.17	3.53*	3.7
147	2.38	2.5**	2.6**	2.7**	2.92*	3.0
148	1.70	1.85	2.0	2.27	2.38*	2.36
149	1.13	1.3**	1.45	1.5**	1.75	1.86
150	0.67	0.80	1.05	1.45	1.38*	1.48
151	0.45	0.50	0.74	1.02	1.08	1.16
152	0.285	0.31	0.50	0.66	0.80*	0.92
153	0.15	0.19**	0.32	0.41**	0.52	0.60
154	0.077	0.090	0.19	0.25	0.32*	0.37
155	0.033	0.048	0.11	0.15	0.20	0.23

Table 2.3 (concluded)

CUMULATIVE MASS-CHAIN YIELDS OF FISSION PRODUCTS
(VALUES ARE IN PERCENT OF FISSIONS)

Mass Number	U-235		U-238		Pu-239	
	Thermal Neutrons*	Fission Neutrons	Fission Neutrons	8-Mev Neutrons	Thermal Neutrons	Fission Neutrons
156	0.014	0.023**	0.066*	0.092**	0.12*	0.14
157	0.0078	0.012	0.034	0.057	0.064	0.075
158	0.002	0.0062	0.016	0.032	0.034	0.043
159	0.00107	0.0034**	0.0090**	0.017**	0.020****	0.025
160	8.5×10^{-4}	0.0012	0.0036	0.0085	0.0092	0.011
161	7.6×10^{-5}	4.6×10^{-4}**	9.4×10^{-4}	0.0044**	0.0038****	0.0051

*Seymour Katcoff, Fission-Product Yields From U, Th and Pu, Nucleonics, Vol. 16, No. 4, p. 78-85 (1958).

**L.R. Bunney, E. M. Scadden, J. O. Abriam, and N. E. Ballou, Radiochemical Studies of the Fast Neutron Fission of U-235 and U-238, Second UN International Conference on the Peaceful Uses of Atomic Energy, A/Conf. 15/P/643, USA, June 1958.

***G. P. Ford, J. S. Gilmore, et al., Fission Yields, LADC-8088, 1958.

****L. R. Bunney, E. M. Scadden, J. O. Abriam, and N. E. Ballou, Fission Yields in Neutron Fission of Pu-239, USNRDL-TR-268, 1958, Unol.

a. Parentheses indicate estimated values or where Katcoff's value was altered in order to adjust the yields to a gross sum of 100 in each peak.

b. Line indicates division of two peaks that was used for individual peak sums.

The yield curve for thermal neutron fission of U-235 gives an average value of 2.5 neutrons per fission. For fission-spectrum neutron fission of U-238, an average value of 3.1 neutrons per fission is obtained. These two values, together with the referenced data in Table 2.8, are used to derive a set of stylized yield curves for the fission-neutron fission of U-235 and Pu-239 and for the 8-Mev neutron fission of U-238.

In each case, the fission by fission neutrons is assumed to yield about 3 neutrons per fission and the 8-Mev fission to yield 4 neutrons per fission. For such a variation with neutron energy in the neutron yield per fission, 14-Mev neutron fission gives about 4.5 neutrons per fission. At a given mass chain yield, the increase in the neutron energy from thermal to fission-spectrum energies shifts the right side of the heavy-element peak to the heavier masses by about a 1/4-mass unit. Where there are no data to indicate any possible changes in the fine-structure shape of the yield curve at the peak, the general shape of the thermal-neutron yield curves is retained, but is adjusted in height so that the total yield in each peak is reasonably near 100.

The large discrepancy between Katcoff's values and those given by Bunney (see Table 2.8) in the rare earth yields for thermal-neutron fission of Pu-239 may be due to persistent errors in the counter calibration. The yield values given by Bunney are lower by a factor of 1.5 at mass number 144 and approach Katcoff's values as the mass increases; at mass number 156, Bunney's value is only about 20 percent lower. Katcoff's values give a peak sum nearer 100; therefore are used in Table 2.8.

Comparison of the cumulative chain yields at the two peaks (A = 90 to 100 and A = 131 to 144) for these types of fission indicates that no very large differences in the gross decay rates of the fission products from the three fissile nuclides should be expected. The mass-chain yields for fission-neutron fission of Pu-239 appear to differ most from the yields of the thermal-neutron fission of U-235. For mass numbers such as 140 and 95, whose radioisotopes may contribute more than 50 percent of the total gamma radiation at specific times after fission, the largest difference is 28 percent for mass number 140 and 11 percent for mass number 95. The yield of mass number 90, however is significantly lower for U-238 (8-Mev neutrons) and Pu-239 (fission neutrons); the differences are 36 and 48 percent, respectively.

The yields of mass number 137 are all more nearly alike. The largest chain yield differences occur between the peaks and the yields that appear at the highest and lowest mass numbers. But even for U-238 fission (8-Mev neutrons), where the yields of the mass numbers near 115 are more than a factor of ten larger than the yield for U-235 fission (thermal neutrons), the contribution of these "valley" elements is a small fraction of the total radioactivity of the fission products.

To use the mass chain-yield values in computations of the amount of each element that is condensed to form fallout and in calculating the gross decay rate of the mixture requires some estimate of the independent yield of each chain member. Partly for convenience, the independent yields calculated by Bolles and Ballou[8] for thermal-neutron fission of U-235 are converted to fractional chain yields so that they may be applied directly to all the cumulative mass-chain yields for each type of fission.

Although it appears that Glendenin's symmetrical charge-distribution curve is generally applicable for all fissile nuclides in low energy neutron fission, it has been shown[9] that the most probable charge, Z_p, (for a given mass distribution) shifts toward stability with increasing neutron energy. That is, the higher fractional yields appear farther to the right (toward a higher Z number) in any decay chain. Pappas[7] used a discontinuous function for Z_p and considered the primary fragments before neutron boil-off; however, Wahl[9] has shown empirically that the Z_p function in thermal fission of U-235 is continuous, as was originally postulated by Glendenin et al.[6] Herrington[10] proposes two charge-distribution curves, one for the even-neutron nuclides and another, showing a lower yield, for the odd-neutron nuclides.

It is clear that there is no unequivocal choice among methods for estimating the independent yields of the chain members, even for thermal-neutron fission of U-235. For the independent yields of higher-energy fission, the experimental data are rarer yet. It is therefore assumed that the fractional independent yields for thermal fission of U-235 calculated by Bolles and Ballou on Glendenin's postulate are not too inappropriate for any kind of fission with low-energy neutrons. When more data become available on the total chain yields and on the independent yields for each fissile nuclide, the indicated corrections can be easily applied to the computations.

The total energy released in the fission process can be calculated by using the mass packing-fraction curves, for the final stable nuclide in each mass chain, for the fissile nuclide involved, and for the fractional mass-chain yields. The calculated energy releases are:

199 Mev per fission for fission-neutron U-235 fission,

204 Mev per fission for 5-Mev neutron fission of U-238, and

209 Mev per fission for fission-neutron fission of Pu-239.

By use of the value 1.10×10^{12} calories per kiloton of TNT, and the value 3.827×10^{-14} calories per Mev, the number of fissions that release the same energy as 1 kiloton of TNT can be obtained. These are:

1 KT = 1.44×10^{30} fissions (U-235, fission-neutrons)

1 KT = 1.41×10^{30} fissions (U-238, 8-Mev neutrons)

1 KT = 1.38×10^{30} fissions (Pu-239, fission-neutrons).

All of the original computations in which this number-of-fissions conversion factor is used are made by using the value 1.45×10^{30} fissions per KT, without reference to the type of fissile material the computation applies to.[11] The excess neutrons, produced by the fission process only, are: 0.48 moles per KT for U-235 (fission neutrons), 0.47 moles per KT for U-238 (Mev-neutrons), and 0.46 moles per KT for Pu-239 (fission neutrons).

The energy and neutron yields that are possible for some thermonuclear reactions can be estimated from the reactions given in ENW (p. 16). These include, for deuterium combinations:

$$2\,{}_1H^2 = {}_2He^3 + n + 3.2 \text{ Mev}$$

$$2\,{}_1H^2 = {}_1H^3 + {}_1H^0 + 4.0 \text{ Mev}$$

$${}_1H^3 + {}_1H^2 = {}_2He^4 + {}_0n^1 + 17.0 \text{ Mev}$$

and

$${}_1H^1 + {}_0n^1 = {}_1H^2 + 2.2 \text{ Mev}.$$

The sum of these reactions is

$$4\,{}_1H^2 = {}_2He^3 + {}_2He^4 + {}_0n^1 + 23.6 \text{ Mev}.$$

The indicated energy release is 0.80 KT per mole of deuterium molecules; the neutron yield is 1.7 moles per KT.

For the tritium reaction,

$$2\,{}_1H^3 = {}_2He^4 + 2\,{}_0n^1 + 11 \text{ Mev}.$$

The energy release for this reaction is 0.28 KT per mole of tritium molecules; the neutron yield is 5.4 moles per KT.

For the combination of light elements, such as lithium and deuterium, a reaction such as

$$_3Li^7 + {}_1H^2 \rightarrow 2\,{}_2He^4 + {}_0n^1 + 15.1\ \text{Mev}$$

can occur. In this reaction, the energy released is 0.32 KT per mole of lithium deuteride, with a neutron yield of 3.1 moles per KT. Several other reactions can be formulated for the fusion of these light elements; most of them give reaction energies in the range of 10 to 25 Mev, and neutron yields of between zero and 2 for each reaction. Thus, for the energy-release and the neutron yields of thermonuclear reactions, a reasonable estimate seems to be that about 0.8 KT of energy per mole of reactant is released, and about 2.5 moles of neutrons per KT are produced.

In all thermonuclear weapons, the total yield of the explosion is the sum of the energy released by both the fission and the fusion processes. However, the amount of radioactive fission products produced depends only on the fission yield. Thus, in considering fallout, the ratio of fission to total yield is an important quantity; the concentration of the fission products is directly proportional to the ratio of the fission yield to the total weapon yield. For example, if the fission and fusion yields of a thermonuclear weapon are equal, the radiation from the fallout would be about half that of a pure fission weapon of the same yield.

The number of neutrons produced is also of interest in fallout. Since all the neutrons released are captured by some nearby atom, a considerable amount of additional radioactivity may result. It may be noted that in the fission of U-238 the amount of radioactive fission-product elements produced is 0.47 moles/KT. If all of the excess neutrons were captured by some substance to produce a radioactive product, the total initial radioactive yield would be 1.17 moles/KT. In the same situation, but for a pure thermonuclear yield, the neutron activations alone would amount to 2.5 moles/KT. Thus, in a sense, a pure thermonuclear, or so-called "clean", weapon could have a radiological capability twice that of a pure fission weapon.

But, it would be a rare occurrence that this capability would be realized, because many of the naturally occurring elements that are in large abundance (such as hydrogen, silicon, oxygen, and aluminum) can capture neutrons to produce either another stable nuclide or a very short-lived radionuclide. On the other hand, if a thermonuclear explosion took place where such elements as sodium (salt), manganese, cobalt, and so on, were concentrated in large quantities, the radioactive yield of these elements could be expected to be high.

2.3 The Structure and Composition of Individual Fallout Particles

Information on the structure and composition of individual fallout particles is obtained mainly from two types of observations: (1) petrographic and radiographic analyses of thin sections of fallout particles and (2) radiochemical and chemical analyses of fallout particles. The results of analyses of single fallout particles contribute more to the understanding of the fallout formation process than any other type of analysis. The major limitation in the analyses of single particles is that the methods are not applicable to the study of particles of less than about 100 microns in diameter (and usually larger) for the petrographic methods, and of particles with less than a given radioactive content for the radiochemical methods. The pertinent results from the petrographic and radiographic studies are summarized here, and a description of the experimental techniques follows the summary.

2.3.1 Low Yield, Surface Shot, Silicate Soil

Particles from Operation Jangle in 1951 were analyzed by Adams, Poppoff, and Wallace[12] of the U.S. Naval Radiological Defense Laboratory (NRDL) and by others.[13,14,15] The results of these analyses are the only ones available on fallout from a detonation on the surface of a silicate soil. The particles studied ranged in size from 500 to 10,000 microns in diameter and were selected on the basis of activity content. Thus the results apply to the larger and most highly radioactive of the fallout particles. The observations were made on thin sections about 30 microns thick taken from the central region of the particles (see Figure 2.1).

The findings are summarized as follows:

1. In thin section, almost all of the fallout particles consisted throughout of a transparent glass (i.e., a fused silicate mass). Many contained fragments of unmelted mineral grains and air bubbles inside the glass. The mineral grains composed perhaps a few percent of the volume of a particle and the bubbles or voids composed something like two to four times the volume of the mineral grains. Some particles, in the glass phase, contained neither mineral grains nor air bubbles and no radioactivity was found in the unmelted mineral grains.

2. Most of the mineral grains in the glass particles were too small to be easily identified with the petrographic

Figure 2.1
THIN SECTIONS AND RADIOGRAPHS OF SOME FALLOUT PARTICLES FROM A SMALL-YIELD SURFACE SHOT AT THE NEVADA TEST SITE. THE PARTICLES ARE A TRANSPARENT, GREEN-YELLOW GLASS WITH THE RADIOACTIVITY DISTRIBUTED MORE OR LESS UNIFORMLY THROUGHOUT THEIR VOLUMES

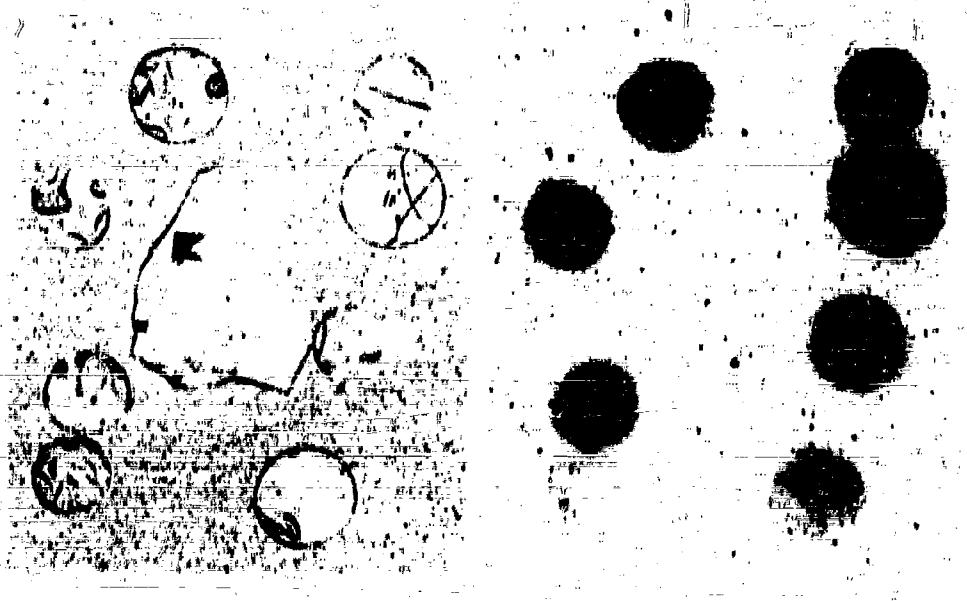

microscope. Those that were large enough were identified as quartz or feldspar; about 75 percent of the soil at the shot point consisted of these two minerals. Most of the grains were smaller than that of the native soil, appeared to be shattered, generally gave no appearance of being melted, and generally were found scattered at random throughout the glass phase.

3. A fairly large fraction of the particles were spherical or spheroidal; some were true spheres of about 500 microns diameter. The smaller of the particle sizes studied contained fewer mineral grains and voids than the larger irregularly-shaped particles.

4. The exterior appearance of the spherical particles varied from a transparent yellow-green color to a light brown color, and the radioactivity was distributed more or less homogeneously throughout their volume. Many of the spheres had smaller spheres attached or partially fused to their surfaces.

5. The exterior appearance of the irregular particles was the same as that of the native soil mineral grains, but in the glass phase the radioactivity was distributed in an irregular manner throughout the irregular particle.

The study indicated that the large glass particles containing significant amounts of radioactivity could not have been formed by direct vapor condensation of the silicate glass. Electron micrographs of fallout collected on air filters revealed the presence of spheres having diameters of the order of 0.1 micron. Theoretical calculations such as those of Stewart[18] on the condensation of such materials as iron and fission products (in air) in the cooling fireball give particle diameters of the order 0.1 micron. In his calculation, Stewart assumed a fireball containing 20 tons of iron in a radius of 500 feet and that the growth of the particles was a combination of condensation and coagulation. Stewart obtained a modal diameter of 0.2 micron for the iron oxide particles.

Simple kinetic theory equations that describe the growth of particles by collision processes give particle-diameter values, for the formation of particles of a given size in the vapor condensation process, that range from about 0.001 to 0.1 micron, depending on various assumed values of the initial vapor density. Thus the small spherical particles in the NRDL study, with diameters of the order 0.1 micron, probably resulted from direct vapor condensation plus some growth by particle impaction in the liquid state.

The larger spherical particles (containing radioactivity but very few or no mineral grains and no voids) were most likely either mineral grains heated to temperatures near the boiling point of the glass so that the glass became very fluid, or were from a layer of liquid soil, at a point nearest the initial fireball gases, that formed particles when the crater material was violently pulled upward as the fireball rose in the air. The more irregular particles containing the shattered but unmelted mineral grains could have been formed by the violent mixing of the molten glass with the grains of soil minerals that were originally outside the melted zone. The voids also could have been produced in this violent mixing process, as well as by the partial vaporization of volatile constituents in the melted soil that was not sufficiently hot and fluid to permit the escape of these gases.

2.3.2 Low Yield, Underground Shot, Silicate Soil

Particles from a low-yield underground shot were also examined by Adams, Poppoff, and Wallace. None of the larger particles were spherical. However, fused glass spheres in the small size range (less than 100 microns in diameter) were observed. Superficially most of the radioactive particles looked like the original soil minerals of the detonation area. They were usually a light brown in color, and opaque. In thin section they were transparent and colorless, had the glass structure found for the surface-shot fallout, but contained a much higher concentration of unmelted mineral grains and voids.

2.3.3 Large Yield, Surface Shot, Coral

Particles available for analysis from detonations of large-yield weapons on the surface of land areas are restricted to those of the fallout produced from coral atolls. The coral reefs are, of course, composed largely of calcium carbonate in the form of aragonite.[17] The findings of C. E. Adams,[18] from analyses of particles obtained from the Mike shot of Operation Ivy, the first large thermonuclear detonation, are summarized as follows:

1. The particles available for study were grains of a solid white material whose diameters range from about 3,000 microns to less than 25 microns. (Those selected for petrographic and radiographic analyses had diameters between about 750 and 1,500 microns.)

2. The principal constituents, as determined from X-ray diffraction patterns of powders prepared from a group

of particles, were calcium carbonate, in both the calcite and aragonite forms, and calcium hydroxide. Sodium chloride and magnesium oxide were also present but the calcium carbonate and hydroxide compounds were in highest abundance. Small amounts of calcium nitrate were also found on the exterior of some particles.

3. Most of the particles were composed of calcium hydroxide, with a surface layer of calcium carbonate of the calcite structure. The thickness of the surface calcium carbonate layer, on particles exposed to the open air, increased with time. These particles were generally angular in shape.

4. A few particles consisted of only calcium carbonate (aragonite structure).

5. The radiographs of the thin sections of the particles showed that the radioactivity was usually concentrated in a band near the outer surface of the particle (see Figure 2.2). However, a significant fraction of the particles studied had radioactivity distributed more or less uniformly throughout their volumes. These distributions were not found to be related to the chemical or physical structure of the particles.

This information on fallout from detonations on coral was later added to; analyses were made of particles collected from other thermonuclear detonations and by improved sampling methods and coverage. A general discussion of all the results was given by Adams, Farlow, and Schell.[19] The findings pertinent to fallout from large detonations on coral are:

1. The angular particles found predominating in the Operation Ivy Mike shot fallout were always observed. Variations in this general type of angular particles included some particles containing a core of unaltered calcium carbonate and others with many small reddish-orange-to-black spheres adhering to the particle surface.

2. Occasionally, unaltered coral particles were found that had small black spheres attached to their surfaces (see Figure 2.4). The size of the small spheres generally ranged from submicroscopic up to about 10 microns in diameter.

Figure 2.2
THIN SECTION AND RADIOGRAPH OF A FALLOUT PARTICLE FROM A SMALL-YIELD SURFACE SHOT AT THE NEVADA TEST SITE. THE PARTICLE IS A TRANSPARENT YELLOW-BROWN GLASS WITH MANY INCLUSIONS OF GAS BUBBLES AND UNMELTED MINERAL GRAINS. THE RADIOACTIVITY IS DISTRIBUTED IRREGULARLY THROUGHOUT THE GLASS PHASE OF THE PARTICLE

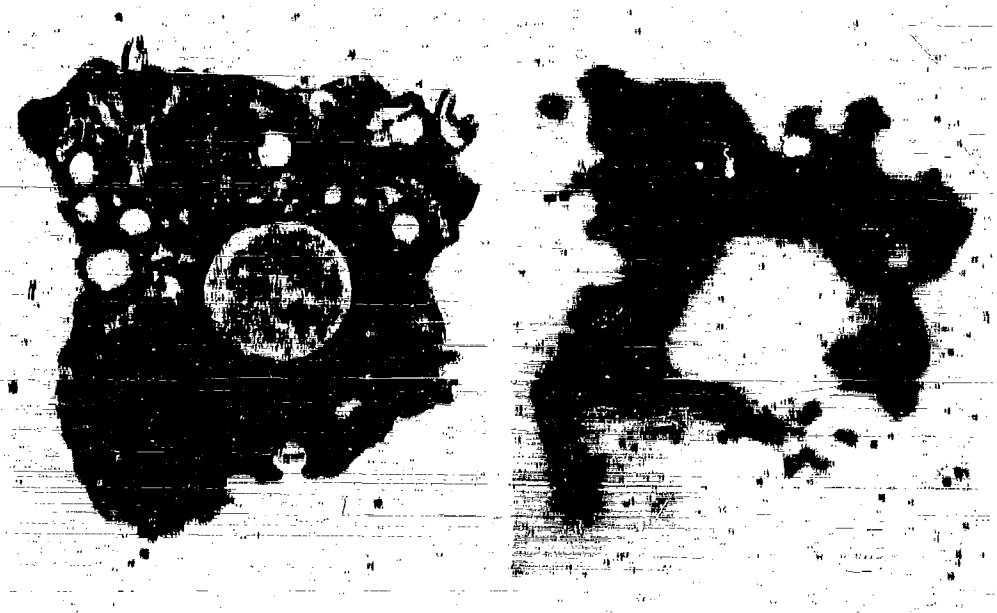

Figure 2.3
THIN SECTION AND RADIOGRAPH OF AN ANGULAR FALLOUT PARTICLE FROM A LARGE-YIELD SURFACE SHOT AT THE ENIWETOK PROVING GROUNDS. THIS PARTICLE IS COMPOSED ALMOST ENTIRELY OF CALCIUM HYDROXIDE WITH A THIN OUTER LAYER OF CALCIUM CARBONATE. THE RADIOACTIVITY HAS COLLECTED ON THE SURFACE AND HAS DIFFUSED A SHORT DISTANCE INTO THE PARTICLE

Figure 2.4
SECTION OF A FALLOUT PARTICLE FROM A LARGE-YIELD SURFACE SHOT AT THE ENIWETOK PROVING GROUND. THE SMALL, BLACK, RADIOACTIVE SPHERES SHOWN ADHERING TO THE SURFACE OF A CORAL SAND GRAIN ARE FORMED BY VAPOR CONDENSATION, WITH SUBSEQUENT GROWTH BY COAGULATION, OF MATERIALS VAPORIZED IN THE FIREBALL

3. The third general type of particle found was spherical; it was composed of calcium oxide that, by the time of analysis, had partially hydrated to calcium hydroxide. The surface was covered with a thin layer of calcium carbonate in the calcite form. In these spherical forms the radioactivity was usually distributed more or less uniformly throughout the particle (see Figure 2.5).

4. The fourth general type of particle found was a very fragile fluffy particle similar to a snow-flake. (Most of these apparently broke easily, either on landing in the collectors or in the handling and shipping of the samples.)

The angular particles, the ones having the irregular shape of fractured coral grains, must have been heated to temperatures higher than 800 to 900°C, since this range of temperatures decarbonates the calcium carbonate. However, the angular particles did not reach the temperature of 2590°C required to melt the calcium oxide. The microporous calcium oxide was hydrated by atmospheric water after it cooled and during its fall to the earth. The calcium carbonate layer in the calcite form must have been formed from the carbon dioxide of the atmosphere after the particle had cooled, since calcite is the stable structure formed by this reaction at temperatures less than 30°C.

The small orange-red-to-black spheres were vapor-condensed particles consisting of a mixture of calcium, iron, and fission-produced oxides. Since it was later found that a large fraction of the activity was in ionic form and could be leached from the angular particles leaking the spheres on their surfaces, it is likely that these radioactive fission products were present in molecular or ionic form in the structure of the particle. The band of activity around the edge of the particle indicates that some inward diffusion must have occurred.

The small particles on the surfaces of the larger ones, however, did not lose activity by diffusion. Hence, some of the activity in these irregular particles must have been collected by the vapor condensation of fission-product elements in their molecular form and some from collisions with vapor-condensed solid (or liquid) particles ranging from molecular size to 10 microns in diameter. The solid calcium oxide, in the presence of carbon dioxide, can exist between 900°C and 2590°C, and many of the fission-product oxides can condense from a vapor phase in this temperature range. The iron, for production of the vapor-condensed spheres, came from the structures around the test device, and the calcium oxide from the vaporized coral at shot point.

Figure 2.5
THIN SECTION AND RADIOGRAPH OF A SPHERICAL FALLOUT PARTICLE FROM A LARGE-YIELD SURFACE SHOT AT THE ENIWETOK PROVING GROUND. THIS PARTICLE IS COMPOSED ALMOST ENTIRELY OF CALCIUM OXIDE WITH A THIN SURFACE LAYER OF CALCIUM HYDROXIDE AND CALCIUM CARBONATE. THE RADIOACTIVITY IS DISTRIBUTED MORE OR LESS UNIFORMLY THROUGHOUT THE VOLUME OF THE PARTICLE

The spherical particles were formed from coral particles heated to temperatures between 2500°C, the melting point of calcium oxide, and about 3500°C, its boiling point (in the presence of about one atmosphere of oxygen). Since this temperature range is not large and would be of short duration, spherical particles were neither formed nor found in great abundance or in large size ranges in coral fallout. Also, melting would destroy the porous structure of the calcium oxide, so that the hydration process would be much slower, hence in these spherical coral particles a large fraction of the oxide would not be converted to hydroxide until after a long exposure to humid atmospheric conditions.

Hydration of the fused calcium oxide involves an increase by a factor of 2 in the volume of the solid, resulting in a rupture of the crystal to the crumbly, fluffy structure. Hence the fragile fluffy particles may have formed from small vapor-condensed calcium oxide particles that hydrated as they fell and agglomerated with other similar particles. Some of these particles may have been formed from larger melted particles that collided with water drops in their fall and thus completely hydrated to the observed structure.

2.8.4 Tower Shot, Silicate Soil

Fallout particles from tower shots over both coral and silicate soils have been collected and analyzed. The results of analyses on particles from a tower detonation over silicate soils by C.E. Adams and J.P. Wittman[90] are summarized as follows:

1. The particle size used in the study ranged from 140 to 1750 microns in diameter. Most of the particles were brown-to-black spheres or spheroids, but some were irregular in shape (see Figure 2.6). Most of them were magnetic. The surface luster was between dull metallic and a brilliant gloss. Their measured densities were between 1.4 and 2.9 gm/cm^3. Many of the particles had smaller spheres fused onto their surfaces.

2. In thin section the central core of the particles was transparent glass with a color ranging from light brown to colorless (see Figure 2.7). The core was surrounded by an irregular thickness of dark brown (or black) opaque glass.

3. The glass occasionally had flow lines and in many cases a fairly large number of voids; the latter were responsible for the extreme variation in the observed densities. A few mineral grains were observed in the glass matrix.

Figure 2.6
TWO FALLOUT PARTICLES FROM A TOWER SHOT AT THE NEVADA TEST SITE. THE PARTICLE ON THE LEFT IS A PERFECT SPHERE WITH A HIGHLY GLOSSY SURFACE; THE ONE ON THE RIGHT HAS MANY PARTIALLY-ASSIMILATED SMALLER SPHERES ATTACHED TO ITS SURFACE. BOTH PARTICLES ARE BLACK AND MAGNETIC AND HAVE A SUPERFICIAL METALLIC APPEARANCE. THE INTERIOR STRUCTURE OF THIS TYPE OF PARTICLE IS SHOWN IN FIGURE 2.7

Figure 2.7
THIN SECTION AND RADIOGRAPH OF A FALLOUT PARTICLE FROM A MODERATE-YIELD TOWER SHOT AT THE NEVADA TEST SITE. THIS PARTICLE IS COMPOSED OF A TRANSPARENT GLASS CORE WITH A DARKLY COLORED IRON OXIDE GLASS OUTER ZONE. MOST OF THE RADIOACTIVITY IS CONCENTRATED IN THE OUTER ZONE

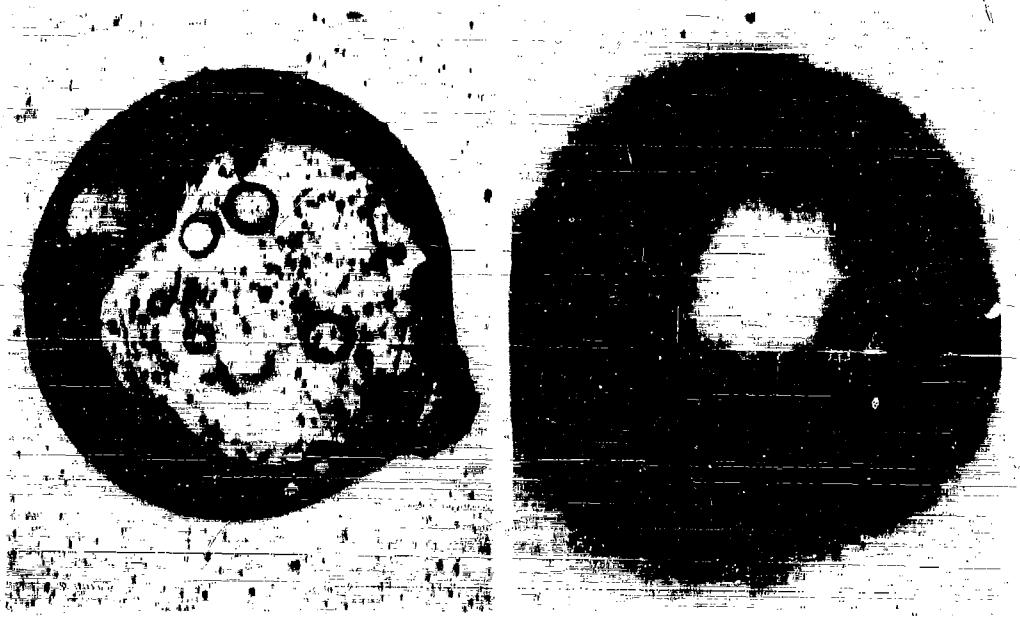

4. The radiographs showed that the radioactivity was usually more highly concentrated in the opaque glass around the core. In some particles the core was inactive; in others the radioactivity was distributed in a more or less random manner throughout the particle.

The strong magnetic property of these particles was due to the iron oxide (opaque) glass around the central core. The smaller particles tended to be more opaque throughout their volumes; i.e., without the transparent central core. The amount of iron oxide glass varied somewhat with weapon yield and with the tower's size or mass; the heavier tower types resulted in particles containing as much as an average of 5 percent iron by weight.

2.3.5 Tower Shot, Coral Soil

The results of analyses of particles from a tower detonation over coral soils by C.E. Adams and J.D. O'Connor[11] are summarized as follows:

1. Three general types of radioactive particles were found.

2. The most abundant type was dull black, spheroidal, weakly magnetic, and cracked and veined with white crystalline material. The sizes analyzed had diameters from about 500 to 1000 microns. The thin sections (see Figure 2.8) showed that these particles had a central core--originally calcium oxide but partially converted to calcium hydroxide and calcium carbonate by the time of sectioning--that was surrounded by a thick layer of black opaque material identified as dicalcium ferrite ($2CaO \cdot Fe_2O_3$). The white material in the veins was found to be a mixture of calcite and vaterite, the two low-temperature crystal forms of calcium carbonate. The radioactivity was always concentrated in the dicalcium ferrite phase.

3. The second most abundant type was a magnetic black spherical particle with a glossy luster. The particles in the samples analyzed were between 250 and 500 microns in diameter, and were composed mostly of magnetite (Fe_3O_4) along with some hematite (Fe_2O_3). The radioactivity was found to be more or less uniformly distributed throughout the particle volume (see Figure 2.9).

4. The third type, not very abundant, was white and irregular in shape and looked much like grains of the original coral. The

thin sections showed these particles to be composed either of unaltered coral or of calcium hydroxide with a thin coating of calcium carbonate. Many small black spheres with diameters about 10 microns or less were found attached to the surface of these least abundant particles. The radioactivity, as shown by radiographs, was concentrated in these attached small black spheres.

The most abundant type of particles contained dicalcium ferrite; these could only have been formed either by the reaction between liquid calcium oxide particles and iron vapor in the presence of oxygen or by the impaction and solution of small drops of liquid iron oxide to form the dicalcium ferrite. Since the calcium oxide has a two-fold volume increase on hydration to the hydroxide, the veins must have formed after the particles solidified under internal pressure resulting from the hydration of the inner core of calcium oxide. In this process, some of the hydroxide apparently diffused into the fissures where it was carbonated by atmospheric carbon dioxide.

The second most abundant type, the iron oxide particles, were probably formed during the cooling of the fireball by the oxidation of liquid iron drops (from the steel tower). Both the vaporized iron and some of the fission-product elements apparently condensed more or less simultaneously to form these particles; apparently they solidified without colliding with molten calcium oxide particles.

Since the melting temperature of magnetite is 1600°C and that of the calcium oxide is 2590°C, the two would not be present in liquid form in the temperature range 1600°C to 2590°C. In fact, the more stable liquid iron oxide (in the presence of about one atmosphere of oxygen at temperatures above the melting point) is FeO; under these conditions, its boiling point is about 3300°C. Thus the temperature range over which both liquid calcium oxide and iron oxide may exist is between about 2600°C and 3300°C. The iron came from the tower, it was located nearer to the center of the detonation than the calcium oxide that was originally coral at the base of the tower; the presence of the pure iron oxide particles indicates that the two materials did not mix homogeneously in the fireball by the time it cooled to 2600°C. The absence of calcium in the particles also indicates that the amount of calcium oxide vaporized was very small.

The third type of particle was apparently formed by collisions between the small vapor-condensed iron oxide particles and grains of coral not heated to 2590°C. Thus these least-abundant particles must have formed at later times than the other two types. The fact that the small attached particles were as large as 10 microns indicates that the initial vapor condensation process continued long enough to permit considerable coagulation.

Figure 2.8
THIN SECTION AND RADIOGRAPH OF A FALLOUT PARTICLE FROM A MODERATE-YIELD TOWER SHOT AT THE ENIWETOK PROVING GROUND. THE GRAY CENTRAL AREA AND VEINS ARE REMNANTS OF THE ORIGINAL INACTIVE MELTED CALCIUM OXIDE PARTICLE. THE DARK AREAS ARE THE DICALCIUM FERRITE IN WHICH THE RADIOACTIVITY IS CONCENTRATED

Figure 2.9
THIN SECTION AND RADIOGRAPH OF A FALLOUT PARTICLE FROM A MODERATE-YIELD TOWER SHOT AT THE ENIWETOK PROVING GROUND. THIS PARTICLE IS COMPOSED ENTIRELY OF MAGNETITE AND THE RADIOACTIVITY IS DISTRIBUTED UNIFORMLY THROUGHOUT ITS VOLUME

That the pure iron oxide particles were not observed in the fallout from tower shots over silicate soil does not prove their nonexistence, but that, if produced, their abundance in the fallout was very low. This is best explained by the fact that the glass from silicate minerals can exist in a liquid (i.e., fluid) state at temperatures even lower than those at which the pure iron oxide solidifies. This would permit more time for mixing in the fireball and for coagulation of the liquid drops of iron oxide and the silicate minerals. Since many of the silicate glass particles had small spheres attached or fused onto their surfaces, the process of coagulation must have continued until the surface of the particles was very viscous.

Weapon yield, the height and mass of the tower, and the boiling temperatures of the various substances are all factors in determining whether ground-surface materials are vaporized, and, if they are vaporized, in determining the quantities that enter the fireball in vapor form. Most of the fallout particles from tower shots are undoubtedly derived from grains of original soil. However, in one or two cases, where the surface soil contained an appreciable amount of substances that melt at low temperatures, such as sodium carbonate, that could act as a fluxing agent, evidence of liquid puddling on the surface of the soil under the tower was observed.

2.8.6 Surface Shot, Ocean (Sea Water)

Only a few fallout particles or liquid drops from detonations on or near the surface of the ocean have been analyzed, mainly due to the fact that special analytical techniques not available early in the weapons test series had to be developed. However, special reagent films developed by Farlow[22] for analyzing liquid drops were used on a few collected samples (see Figure 2.10). The particles, collected at a single location from a detonation on a barge anchored in the lagoon at Bikini Atoll, consisted of a saturated solution of sea water salts, some suspended crystals of sodium chloride, and some insoluble solids.

Most of the insoluble solid materials were found to be agglomerates of small reddish-orange-to-black spheres. Some of these were as large as 30 microns in diameter (see Figure 2.11). From their X-ray diffraction pattern, the spheres were identified as being composed of dicalcium ferrite. In these particular samples, only about 15 percent of the activity diffused into the reagent films; the remainder was associated with the solids. The iron came from the large steel barge and the calcium came from the coral sand used as ballast in the barge.

Figure 2.10
PHOTOMICROGRAPH OF A DICHROMATE REAGENT FILM OF AN INDIVIDUAL LIQUID FALLOUT PARTICLE FROM A LARGE-YIELD BARGE SHOT AT THE ENIWETOK PROVING GROUND. THE SOLUBLE CHLORIDE IN THE DROP HAS REACTED WITH THE REAGENT FILM, FORMING A WHITE CIRCULAR AREA INDICATING THE AMOUNT OF CHLORIDE IN THE DROP. THE AREA OF THE CENTRAL ELLIPTICAL TRACE COVERED BY SMALL SOLID PARTICLES IS A MEASURE OF THE WATER CONTENT OF THE DROP. THE SOLIDS IN THE CENTER ARE SMALL SPHERES FORMED BY THE CONDENSATION OF THE VAPORIZED BARGE AND BALLAST MATERIALS

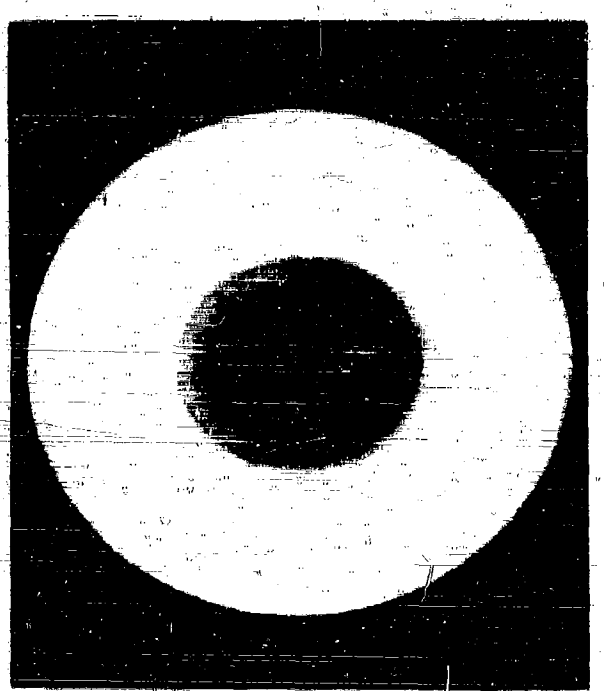

Figure 2.11
ELECTRONMICROGRAPH OF THE RADIOACTIVE SOLIDS IN THE LIQUID FALLOUT PARTICLES FROM A LARGE-YIELD BARGE SHOT AT THE ENIWETOK PROVING GROUND. THIS AGGLOMERATION OF VERY SMALL SPHERES, EACH FORMED FROM THE CONDENSATION OF THE VAPORIZED BARGE AND BALLAST MATERIALS, IS COMPOSED LARGELY OF DICALCIUM FERRITE

For these sea water fallout particles, the association of the results of the analyses with possible high-temperature reactions is not quite as straightforward as for the completely solid particles from the other types of detonations. Because of the presence of water, the droplet or particle can change in size. Perhaps changes in the relative amounts of various chemical constituents also occur during the fall of the droplet through the atmosphere. These changes are due to evaporation of water in the drop or to the condensation of atmospheric water vapor, as well as to a continual process of accretion of neighboring particles.

Certainly a large amount of sea water would be vaporized initially along with the fission-product elements and the solid materials of the bomb structure (including the barge and ballast in the test shots). The iron and calcium oxide vapors condense, to form the small calcium ferrite particles, in much the same way as was observed in the fallout from the coral surface and tower detonations. These oxides and some of the more refractory fission-product oxides would condense first, at the higher temperatures. The next substances to condense are the sodium chloride and the less refractory fission products (oxides, hydroxides, or chlorides). And finally, at temperatures around 100°C, the water vapor condenses. It is likely that the first particles to be formed serve as nuclei or surfaces upon which the remaining vapor condenses, although this may not be the only process involved. The same final particle could be formed by separate condensation of the various substances, and by particle growth by impaction, especially when the water drops are present in liquid form and in high concentration.

The water content of the final particle would depend on the humidity and temperature conditions of the atmosphere through which it falls. While the final water content of the particle would be determined to a large degree by these conditions in the latest part of their fall trajectory near the earth, the particles carried to great altitudes would fall through air layers at temperatures less than 0°C. In these layers the particles would be solid, and the time that they would remain in the solid state from a large yield detonation would be a large fraction of their total fall time. The loss and/or gain in water content during the fall would result in corresponding changes in particle size and density as well as in fall velocity of the particle.

2.3.7 Inferences on Fallout Particle Formation Processes

The consistent inferences of the data, with regard to the formation of the fallout particles in the cooling fireball, are:

1. The vapor-condensation of small particles begins at the highest temperature at which a macroscopic liquid phase can exist in equilibrium with its saturated vapor. The

substance forming this initial liquid phase is always a non-radioactive material, such as the metal oxides from the structural components of the weapon and/or the decomposition products of the soils. These substances are the ones, nearest the point of detonation, whose vapors are intimately mixed with the fission-product gas atoms. Some of the fission product atoms or molecules condense to form a dilute solution in these particles.

2. Heated soil (and tower) materials are drawn into the fireball as it rises; some of these form particles from the disintegration of a bulky layer of liquid material or are otherwise melted before they enter the cooling fireball. Certain other particles are melted after they enter the fireball, some are only partially melted, and some are not melted at all. The degree of heat treatment received by the various types of particles depends upon the time the particle entered the fireball, its trajectory through the hot gases, the temperatures along that trajectory, and the particle's velocity.

3. The larger of the melted particles collide with and dissolve the small vapor-condensed particles, thus acquiring the radioactive elements they contain.

4. Radioactive elements that remain in the gaseous state during the time these melted particles exist--that is, when the fireball temperature is between the melting and boiling points of the particles--vapor-condense directly onto the particle surfaces to form dilute solutions of the mutually-soluble oxides or compounds. The elements may solidify as separate phases in the particles if the concentration is sufficiently large, or remain essentially as an impurity site in the crystal or glass phase of the larger melted particles.

5. The latest solid particles to arrive in the fireball collide with and scavenge some of the remaining small particles, which then remain on the surface of the larger (unmelted) particles. Since these solid particles collect on their surfaces other particles as large as 10 microns in diameter, they can also vapor-condense on their surfaces the more volatile of the radioactive atoms not previously condensed into the liquid particles. And, since some of the fission products are rare gas elements, this latter type of condensation proceeds as long as the particles and gas atoms remain together.

The particle thin-section analyses, although giving much information on the structures of fallout particles and on the way they are formed, give no quantitative data on the radio-chemical composition of the particles, and only a limited amount of unclassified information is available from radio-chemical analyses of fallout particles. The first information of this kind was reported by Kimura[35] et al, who presented analyses of the fallout from Shot Bravo, detonated on March 1, 1954. The fallout for these analyses contaminated the Japanese boat No. 5 Fukuryu Maru. Some of the particles, called ashes or dust because of the white color of calcium carbonate or hydroxide, were collected by the crew of the ship who carried the material back to the Japanese mainland where the analyses were made.

In the report, Kimura chose to refer his data to the thermal-neutron fission of Pu-239. The data were reanalyzed on the basis of 8-Mev neutron fission of U-238 because of the reported high abundance of the nuclide, U-237, presumably produced by a (n, 2n) reaction on U-238. In this instance, the Pu-239 was presumably produced by a (n,γ) reaction on U-238 in which the initial product, U-239, had, to a great degree, decayed to Np-239 and then to Pu-239 by the time of the analyses. Kimura's data are compared with the calculated activities for U-238 fission at D + 25 (25 days after detonation) and summarized in Table 2.4. The ratios of the observed percentages to those calculated for the rare earth nuclides, Y-91 and Nb-95, are greater than one. It is clear that the percentage of fission product activity missing is greater than the 17.45 percent unaccounted for in the sample analyses. To check the reality of the high yield for Nd-147 and the low yield for Ce-141, the two ion-exchange elution curves given by Kimura for the rare earth nuclides at D + 40 were integrated, giving the following percentages: Y-91, 18-21 percent; Pm-147, Nd-147, 8-12 percent; Pr-143, 15-30 percent; and Ce-141, Ce-144, Pr-144, 40-50 percent. These values agree with the calculated percentages of Y-91, 21 percent; Nd-147, 10 percent; Pr-143, 25 percent; and Ce-141, Ce-144, Pr-144, 45 percent, at D + 40. Thus it was concluded that the ratios 0.85 and 2.06 in Table 2.4, for Ce-141 and Nd-147 respectively, do not indicate a depletion of Ce-141 and an enrichment of Nd-147.

Assuming that the rare earth elements, yttrium, zirconium, and niobium are in the correct ratios for U-238 fission, their gross contribution to the activity may be used as a basis for estimating the relative depletion or enrichment of other fission-product nuclides. The data of Bolles and Ballou[36] for U-235 fission products (with adjustment to the fission yields of Table 2.3) were used to calculate the percentage of activity at D + 25 for U-238 fission with 8-Mev neutrons. The indicated unfractionated nuclides contribute 46.9 percent of the beta activity, whereas the observed percentage was 65.0 percent; hence only 72 percent of the normal fission-product mixture activity must have been present in the sample. The remaining 28 percent was then either with another group of particles or did not condense on any large fallout particles.

Table 2.4

CALCULATION OF RELATIVE ACTIVITY RATIOS FROM KIMURA'S DATA ON CORAL FALLOUT[25]

Nuclide	Half-Life	Percent Of Total Activity On D+25	Percent Of Fission Product Activity On D+25	Percent Of Activity For U-238 Fission On D+25	Ratio $\left(\frac{\% \text{ Observed}}{\% \text{ For U-238}}\right)$	Adjusted Percent Of Fission Products In Fallout	Fractionation Number r_n (A)
Sr-89	53d	1±0.5	1.25	4.01	0.31	0.90	0.22
Sr-90	28y	0.02±0.01	0.025	0.053	0.47	0.018	0.24
Y-90	61h	0.02±0.01	0.025	0.053	0.47	0.018	0.24
Y-91	57d	8±3	10.0	5.89	1.70*	7.22	(1.0)
Z-95	65d	5±2	6.25	6.94	0.90*	4.51	(1.0)
Nb-95	35d	3±1	3.75	3.06	1.23*	2.71	(1.0)
Ba-140	12.8d	5±1	6.25	11.92	0.52	4.51	0.35
La-140	40h	6±1	7.50	13.69	0.55	5.41	0.40
Ce-141	33d	7±5	8.75	10.55	0.83*	6.31	(1.0)
Ce-144	282d	2±1	2.50	1.49	1.68*	1.80	(1.0)
Pr-143	13.7d	16±5	20.0	12.02	1.66*	14.4	(1.0)
Pr-144	17.5m	2±1	2.5	1.49	1.68*	1.80	(1.0)
Nd-147	11.3d	9±4	11.25	5.46	2.06*	8.12	(1.0)
U-237	6.75d	20±10	–	–	–	–	–
Pu-239	24,360y	(4±2)x10^{-4}	–	–	–	–	–
		Sum	82.55				
		Missing	17.45				

* Nuclides with these ratios are assumed to be in correct relative abundance; the ratio of their sums (65.0% of FP activity observed, 46.3% of FP activity for Normal U-238 mixture) is 0.72. The values of r_n (A) are calculated from the ratios of the values of Column 6 to those of Column 4, except for the elements which are assumed to have r_n (A) values of unity.

The ion exchange elution curves reported by Kimura for a gross sample on D + 20 to 22 were also integrated and adjusted to the percentages of the total activity lying under the curve at D + 21. The results are given in Table 2.5, along with the data from Table 2.4 for comparison. In this case, the observed percentage for the rare earth (yttrium, zirconium, and niobium) nuclides is 65.4 percent and the calculated fraction is 45.4 percent; this indicates that, at D + 21, 66 percent of the total activity of the normal mixture was present in the sample. The percentages at the two times differ a little; they would, of course, be expected to change with time.

The estimated fractionation numbers, $r_0(A)$, given in Table 2.6 for various nuclides in the fallout were compiled from the data of Tables 2.4 and 2.5 and other sources as noted. In addition to the rare gas elements and their daughter products, the important elements in the fallout that were depleted include Ru, Te, and I. Other elements undoubtedly were also fractionated but are not listed because they would not contribute significant amounts of activity at D + 21 and D + 25. The summed beta activity for the unfractionated mixture of activities at D + 25 is 7.61×10^{-6} disintegrations per second (d/s) per fission. Since only 72 percent at this amount is present in the fallout sample, the equivalent beta activity at D + 25 is 5.49×10^{-6} d/s per fission.

Pu-239, with a 24,360-year half-life and formed from the decay of U-239 and Np-239, has a decay rate ($1/\lambda$) value of 1.11×10^{16} atoms of Pu-239 per d/s. At D + 25, the reported ratio of the Pu-239 activity to the fission product activity is 5.0×10^{-6}. The product of these values gives 0.8 atoms Pu-239 per fission. This is essentially equal to the number of U-239 atoms formed at zero time.

The ratio of the activity of the U-237 to the fission products at D + 25 is given as 20/80. For the 6.75-day half-life, $1/\lambda$ is 8.42×10^5 atoms U-237 per d/s; hence the relative capture number, C, is

$$C(237) = (20/80) \times 8.42 \times 10^5 \times 5.49 \times 10^{-6} / \exp\left[\frac{-0.693 \times 25}{6.75}\right] \qquad (2.1)$$

$$= 0.15 \text{ atoms/fission}$$

Since the alpha-counting technique and separation methods might result in low values of Pu-239 activity relative to the total, the yield of U-239 (or Pu-239) in the sample could well have been larger than 0.8 atoms per fission. For a broad energy band of neutrons centering at about 8-Mev, the yield from a (n,γ) reaction on U-238 could be as much as 5 times the yield of the (n, 2n) reaction.

Table 2.5

PERCENTAGE ACTIVITIES IN ION EXCHANGE PEAKS OF DIFFERENT CHEMICAL GROUPS IN CORAL FALLOUT SAMPLE[23]

Peak No.	Elements	Percent Of Total Activity At D+21	Percent Of FP Activity At D+21	Percent Of U-238 FP Activity At D+21	Adjusted Percent Of FP Activity At D+21	Adjusted Percent Of FP Activity At D+25
1	Sb, Te, I, Ru, Rh, Mo	13.5	17.2	19.8	11.4	12.6
2	Zr, Nb	8.3	10.6	8.25	7.0	7.2
3	U	21.3	–	–	–	–
4	Y, Ce, La, Pr, Nd, Pm	49.4	62.7(54.8)*	35.2	36.4	39.7
5	Sr (Y)	1.3	1.6	3.61**	1.06	0.92
6	Ba (La)	6.2	7.9(15.8)*	26.1	16.5	9.9

*7.9% for La-140 is added to Peak 6 and subtracted from Peak 4 for calculating the fraction of normal fission-product activity present.

**Includes Sm and Eu as contributing to Sr fraction.

Table 2.6

SUMMARY OF ESTIMATED FRACTIONATION NUMBERS FOR BETA-EMITTING NUCLIDES IN CORAL FALLOUT FROM NO. 5 FUKURYU MARU AT D-21 AND D-25

Nuclide	Note	Fractionation Number, $r_n(A)$ D-21 data	D-25 data	Selected Value
Kr-85	1	(0)	(0)	0
Sr-89		0.27	0.22	0.22
Sr-90		0.27	0.34	0.34
Y-90		0.27	0.34	0.34
Y-91		1.6	1.0	1.0
Zr-95		1.0	1.0	1.0
Nb-95		1.0	1.0	1.0
Mo-99	1	(1.0)	(1.0)	1.0
Ru-103	1	(1.0)	(1.0)	1.0
Ru-106	2	0.14	0.41	0.41
Rh-106	2	0.14	0.41	0.41
Ag-111	1	(1.0)	(1.0)	1.0
Cd_i-115	1	(1.0)	(1.0)	1.0
Cd_g-115	1	(1.0)	(1.0)	1.0
In-118	1	(1.0)	(1.0)	1.0
Sn-120	1	(1.0)	(1.0)	1.0
Sn-125	1	(1.0)	(1.0)	1.0
Sb-125	1	(1.0)	(1.0)	1.0
Sb-127	1	(1.0)	(1.0)	1.0
Te-127	1	(1.0)	(1.0)	1.0
Te-129	2	0.00	0.27	0.27
Te-132	2	0.06	0.19	0.19
I-131	2	0.08	0.24	0.24
I-132	2	0.00	0.10	0.10
Xe-133	1	(0)	(0)	0
Cs-137	3	--	0.20	0.20
Ba-140		0.40	0.30	0.40
La-140		0.40	0.39	0.40
Ce-141		1.0	1.0	1.0
Ce-144		1.0	1.0	1.0
Pr-143		1.0	1.0	1.0

Table 2.0 (concluded)

SUMMARY OF ESTIMATED FRACTIONATION NUMBERS FOR BETA-EMITTING NUCLIDES IN CORAL FALLOUT FROM NO. 5 FUKURYU MARU AT D+21 AND D+25

Fractionation Number, r_0 (A)				
Nuclide	Note	D+21 data	D+25 data	Selected Value
Nd-147		1.0	1.0	1.0
Pm-147		1.0	1.0	1.0
Sm-151		1.0	1.0	1.0
Sm-153		1.0	1.0	1.0
Eu-155		1.0	1.0	1.0
Eu-150		1.0	1.0	1.0

Note 1: Estimated

Note 2: Estimated from ion exchange elution peak activity percentage and from data of Section 2.8, giving the relative fractions condensed of mass numbers 132, 131, 129, and 100, considered to be in the ratio of 1 : 1.3 : 1.4 : 2.2.

Note 3: From a plot of r_0 (A) versus the half-life of rare-gas precursors.

It may be noted that, at D + 25, the relative activity of 50 hour Np-239 is 2.00×10^{-9} d/s per atom of U-239 produced initially, and for 0.75 day U-237 it is 0.13×10^{-8} d/s per atom of U-237. Thus, even at a 5 to 1 yield ratio, the activity of the Np-239 at D + 25 would be only 1/8 of the U-237 activity and would be difficult to detect. The factor of 5 would give a capture number, C(239), value of 0.75 atoms per fission.

The second set of unclassified data on the radiochemical content of radioactive particles was reported by Mnokin and coworkers at NRDL.[24] The sample particles were obtained from detonations on coral islands at the Eniwetok Proving Grounds in 1956. In this case, analyses are made for only a few radionuclides: Mo-99, Sr-89, Ba-140, and Np-239. However, no Np-239 data are reported. In addition, the gross activity of the particles is measured by using a well-crystal (WC) NaI(Tl) scintillation counter and a 4π high-pressure argon gas (at a pressure of 600 psig) gamma ionization chamber.[25]

Many of the particles were weighed so that specific activities could be determined, and some data on gross samples were obtained. The Mo-99 radionuclide was utilized as the "fission" tracer with the assumed yield of 6.1 percent; this yield value is sufficiently close to the yield for the 8-Mev neutron fission of U-238 that no adjustment of the reported values was required. Some of the data are summarized in Table 2.7. The particle type designations "altered" and "unaltered" used by the authors have been changed to "fused" particles and "irregular" particles as the first classification of the particles as the first classification of the particle type since the thin-section analyses showed that most of the irregular particles have been calcined.

Because of analytical requirements, only the more highly radioactive particles were used in the reported analyses. This means that the results are applicable only to a description of the larger particles. However, even with this bias, the results are useful in illustrating the possible range in values of all the measured quantities.

The counting-rate and ion-current measurements were corrected to 1470 hours before the apparent average ionization rates, WC-rates per fission, ion current per fission, and the specific ionization rate were computed. The decay corrections for the WC measurements were obtained from the reported decay curves for the two types of particles; the ionization rate decay corrections were obtained from unpublished data on particles from the same set of samples. It is quite likely that each particle had its own decay rate, differing to some degree from other particles of the same general type. Therefore, with a single type of decay curve, the corrections to a common time are only approximate.

The variability of the ratio of the ion current to the WC count-rate of the set of particles is the first indication of a gross difference in the relative abundances of the emitted gamma rays of different energies, hence of a

Table II.7

RADIOCHEMICAL DATA ON CORAL TYPE FALLOUT PARTICLES FROM A LARGE YIELD SURFACE DETONATION

Collecting Station	Particle Description	t (H + hour)	Crystal Well Counter: Activity (cpm x 10^{-9})	Crystal Well Counter: Decay Corrections to H + 70	Gamma Ion Chamber: GIC Assay (mr x 10^{11})	Gamma Ion Chamber: Decay Corrections to H + 70 hr	I (neutrons x 10^{-10})	Particle Weight (mg)	Apparent Average Ionization Energy, H + 70 (mev-equiv x 10^{17})	WCC at H + 70 (cpm/D x 10^{3})	GIC (at H + 70 mm Hg x 10^{10})	Specific Ionization Ratio at H + 70 (mm Hg x 10^{11})
A. Fused Particles												
Ship	WI	70	0.017	1.00	26	1.00	0.07		1307	0.004	18.8	
	WW	70	0.0067	1.00	7	1.00		0.0004	1817			740
	YW	70	0.001	1.00	55	1.00	0.75		80	0.404	54.7	
	YW	70	0.047	1.00	41	1.00	1.4		74	0.070	28.3	
	YI	71	0.066	1.01	30	1.01	0.80		102	0.038	38.8	
	WI	73	0.007	1.03	10	1.03	0.43		81	0.410	40.7	
	YW	73	0.010	1.03	10	1.03	0.70		97	0.071	28.9	
	WW	74	0.178	1.04	15	1.07			66			
Island	YI	100	5.50	1.30	407	1.58	30.0	0.106	62	0.666	38.0	351
	YW	104	1.17	1.48	158	1.84			104			
	W	105	10.0	1.48	1,020	1.68	75.0	0.046	77	0.076	30.0	870
	WW	114	0.75	1.68	311	1.98	17.0	0.009	88	0.007	38.0	302
Large	YW	300	37.5	4.20	1,000	5.00		0.90	70			304
	YW	350	87.5	4.60	3,500	5.60		17.5	108			3,070
	YW	350	50.5	4.60	2,720	5.60		9.70	90			1,780
	W	300	6.00	4.00	344	5.00			472			
	W	350	16.7	4.60	900	5.60			65			
	W	350	24.5	4.60	1,400	5.60		7.10	70			1,100
	W	350	9.05	4.60	405	5.60		5.60	68			1,100
	W	350	2.65	4.60	164	5.60	48.0	1.75	75	0.047	18.8	887
	YW	300	5.75	4.00	435	5.00		0.10	84			310
	YI	350	28.0	4.60	1,720	5.60		28.8	75			970
	YW	600,401	0.70	11.8	360	14.8	180.0	0.76	85	0.011	30.0	1,800
	WW	600,401	1.04	11.8	100	14.8	180.0	1.78	81	0.008	18.8	1,610
B. Irregular Particles												
Ship	WI	70	0.088	1.00	80	1.00	0.07		140	0.034	14.6	
	WI	70,71	0.0411	1.02	8	1.02			497			
	WI	70,74	0.008	1.04	26	1.04	0.34		109	0.013	38.8	
	WI	70,74	0.0178	1.04	8	1.04			178			
Island	GI	98	0.01	1.30	433	1.58	0.4	18,440	137	0.738	63.1	30.3
	I	99	1.71	1.31	168	1.59		0.110	174			41.0
	WI	99	0.08	1.31	178	1.59	1.0	0.600	889	0.482	18.	87.8
	WI	100	0.48	1.33	810	1.60	8.7	0.170	138	0.088	120	64.9
	WI	100	0.0001	1.33	8	1.60		0.000	382			1.30x
	I	103	0.33	1.36	257	1.64	5.6	0.305	882	1.74	143	118
	WI	104,105	1.18	1.38	141	1.66	1.0	4.180	181	1.84	808	42.0
	I	104	0.0242	1.38	4	1.66		0.171	124			24.1
	GI	105	0.701	1.39	98	1.67	0.64	0.080	134	1.68	818	182
	GI	108	0.108	1.39	24	1.67		1.085	188			18.7
	WI	108	0.080	1.36	110	1.67	0.87	0.072	148	1.88	180	106
	WI	110	0.114	1.38	18	1.67		0.388	148			88.0
	WI	110	0.110	1.38	18	1.67		0.004	110			80.0
	GI	110	0.0048	1.38	10	1.67		2.728	118			8.10x
	GI	110	0.480	1.38	84	1.67		1.078	141			64.0
	GI	110	0.007	1.38	20	1.67		1.187	188			28.8
Large	I	300	0.45	3.95	800	5.00		40.1	787			20.0
	I	300	0.101	3.93	--	5.00		11.0	(188)			4.40x
	WI	300	1.04	3.93	220	5.00	18	68.8	188	0.477	78.7	36.1
	I	300	0.68	3.93	200	5.00		11.4	138			102
	GI	300	0.444	3.93	81	5.00		48.8	114			4.08x
	I	300	1.70	3.93	180	5.00		300.0	107			1.90x
	I	300	1.71	3.93	180	5.00		487.6	116			1.70x
	I	300	0.071	3.93	--	5.00		0.0	(188)			4.00x
	WI	600,401	1.07	14.6	100	18.7	44	11.84	188	0.088	84.8	218

† Questionable type designation or experimental error
x Bulgium particles, presumably formed by collision of small active particle and large inactive particle.
YW - yellowish sphere
WW - white sphere
YI - yellowish irregular
GI - greyish irregular
WI - white irregular

	Fused Particles	Irregular Particles (I)	Irregular Particles (II)
Average mm equiv	88 x 10^{-17}	138 x 10^{-17}	--
Mean cpm/ f	0.363 x 10^{-4} (± 38%)	0.363 x 10^{-4} (± 78%)	--
Mean mm f	30.0 x 10^{-21} (± 38%)	115.6 x 10^{-21} (± 57%)	--
Mean mm mg	803 x 10^{-21} (± 85%)	84.4 x 10^{-21} (± 105%)	2.01 x 10^{-21} (± 83%)
Mean Particle Mass, mg		3.30	86.4
Specific Activity, f mg	26.0 x 10^{19}	0.471 x 10^{19}	0.0261 x 10^{19}

variation in the constituent radionuclides. Although the ratios of the two measurements of the gross activity in the fused particles (i.e., spheres or broken spheres) and the irregular particles have values that average 83×10^{-17} ma/cpm and 132×10^{-17} ma/cpm, respectively, there are overlapping values in each particle group. Perhaps if the number of particles analyzed had been doubled, this ratio, as a second particle-type classification or distinction between the two groups, might be less marked. In any case, at H+70 the activity on or in the irregular particles emitted more high-energy gamma rays than the activity emitted by the fused particles.

The third type of classification of the two types of particles is the comparison count per minute (cpm) per fission of the WC values or the ma per fission ratios. Of the two, the ion current per fission gives the larger differentiation, since it is a more sensitive measure of the total photon energy emitted from the mixture. The unfractionated fission-product mixture from the thermal-neutron fission of U-235 gives an ion current of 39.1×10^{-21} ma/fission[20] at H+70. This should be within a few percent of the ion current per fission for the unfractionated fission products from 8-Mev neutron fission of U-238. The value, 50.8×10^{-21} ma/fission for the fused particles indicates that if Mo-99 is a good fission indicator the relative abundance of many other nuclides in these particles is low. The value, 115.6×10^{-21} ma/fission for the irregular particles indicates that the relative abundance of the other nuclides is high. The fact that the two values do not have a mean value near 39.1×10^{-21} ma/fission must be due, in part, to the presence of induced activities.

Assuming that the two types of particles together condensed essentially all of the gamma-emitting radionuclides that contribute at H+70, and that all the excess ionization is due to Np-239, the capture number, C(239), for U-239 can be estimated from

$$r_{ip}(70)\,39.1 \times 10^{-21} + 27.4 \times 10^{-21}\,C(239) = 50.8 \times 10^{-21} \qquad (2.2)$$

where $r_{ip}(70)$ is the gross fission-product ionization-rate fractionation number at H+70, which for the combination of both particle sets is approximately equal to one; 27.4×10^{-21} is the ion current at H+70 per atom of U-239 at zero time; and 50.8×10^{-21} ma per fission is the geometric mean value for the two types of particles.

Setting $r_{ip}(70)$ equal to one gives C(239) equal to 0.70. Since the authors indicate that C(239) is about the same for both particle types, $r_{ip}(70)$ can be back-computed for each type. For the fused particles $r_{ip}(70)$ is 0.20 and for the irregular particles it is 2.45. The fission-product nuclides in the irregular particles, therefore, emit about 0.3 times more gamma energy per fission (relative to Mo-99) than the spherical particles at H+70. When calculated

per unit fission, the reported decay curves of the two types of particles tend to approach each other at about 6000 hours after fission. At these times most of the ionization is due to Zr and Nb nuclides. Hence, these two elements cannot be fractionated with respect to Mo-99; and, further, at about 6000 hours after fission there are no differences in the radiations emitted from the two types of particles.

The fourth comparison between the spherical and irregular types of particles is by their specific activity. At 1470, the ion current per milligram (mg) of the fused particles is about 15 times larger than that of the irregular particles. In this classification, the sample set of irregular particles is given an additional arbitrary subclassification by selection; the particles with a very low specific activity are separated out. The particles so selected for elimination are of the type found in the thin-section analyses where a small active particle is observed to be attached to a larger inactive coral grain. It is also possible that, had more particles been analyzed, the number distribution in specific activities could have filled in the intermediate values to give a broader single distribution.

The specific activity of the fused particles in terms of fissions per gram, based on Mo-99 yields, is about 55 times that of the irregular particles. Since the ion current per fission of the two types of particles becomes equal at about 6000 hours after fission, the ion current from the fused particles is, on the average, 55 times larger than that of the irregular particles.

In a sense, the comparisons given should be taken with some reservation because of the small sampling. On the other hand, the large errors indicated by the standard deviations do not in themselves influence the validity of the conclusions from the data. These deviations rather indicate the breadth of the distributions in the radioactive content of the fallout particles or any other parameter of concern. Thus, the single-particle data of this type are very useful; they provide detailed information on the likely nature of large-sample distributions.

The fractionation numbers for mass numbers 89 and 140, for some of the coral particles, are given in Table 2.8. The values given by Meskin and coworkers[44] are corrected to correspond to the yields from U-238 fission with 8-Mev neutrons. The original R_{99}^{A} values are defined by

$$R_{99}^{A}\,(\text{U-235 fission}) = \frac{(\text{Content of Mass A in Sample})/(\text{Content of Mass 99 in Sample})}{(\text{Yield of Mass A in U-235 fission})/(\text{Yield of Mass 99 in U-235 fission})} \qquad (2.3)$$

Table 2.8

SUMMARY OF FRACTIONATION NUMBERS* FOR MASS NUMBERS 89 AND 140 IN CORAL FALLOUT PARTICLES

Particle Description	GIC/f at H+70 (ma/f)x10^{9}	R_{99}^{89}	R_{99}^{140}	R_{99}^{140}/R_{99}^{89}
A. Fused Particles				
WS	18.8	0.024	0.015?	0.625
S	18.8	0.012	0.030	2.50
YS	25.2	0.20	-	-
YS	26.9	0.026	0.028	1.08
S	29.0	0.0058?	0.018?	3.14
YI	32.8	0.046	0.14	3.04
YS	34.7	0.023	-	-
YI	35.0	0.041	0.14	3.41
WI	38.8	0.114	0.32	2.81
WI	40.7	0.23	-	-
WS	58.0	0.040	0.20	5.00
Geometric Mean	-	0.050(±180%)	0.10(±180%)	-
B. Irregular Particles				
WI	54.9	1.81	0.82	0.453
WI	78.7	0.64	1.8	2.81
WI	88.6	0.36	-	-
GI	93.1	0.82	2.7	3.29
WI	120	1.0	4.0	4.00
WI	126	1.7	2.6	1.53
I	142	0.52	0.89	1.71
WI	208	2.3	3.6	1.56
GI	218	2.3	4.0	1.74
Geometric Mean	-	1.05(±98%)	2.19(±94%)	-

R_{99}^{89} (U-238 fission) = 1.54xR_{99}^{89} (U-235 fission)

R_{99}^{140} (U-238 fission) = 1.17R_{99}^{140} (U-235 fission)

? Questionable values, not used to calculate means.

where the content and yields are given in terms of activity at a given time or of number of atoms at zero time, or, in terms of a count rate, from a calibrated analytical procedure in which a foil of U-235 is bombarded with thermal neutrons. The values in the table show that, relative to mass 99, mass 89 was very much depleted in the fused particles and was enriched in some of the irregular particles. For mass 140, the enrichments in the irregular particles were as high as a factor of 4.

The corrected fractionation numbers for the gross-fallout sample collected near the barge-sample particles are 0.061 for mass 89 and 0.12 for mass 140. These values indicate that most of the activity in the gross sample was from the fused (spherical) particles. Because most of the reported data was obtained from large particles, it is not known whether the high fractionation numbers are applicable to small irregular particles and hence to locations further away from ground zero. At least, in the samples further from ground zero, the relative abundance of the fused particles was decreased.

In the irregular particles, the relative amounts of Sr-89 and Ba-140 were higher by factors of 21.0 and 21.9, respectively, than they were in the fused particles. These ratios are not comparable to the ratio of the r_{f_p} (70) values for the two types of particles, since the latter refers to the relative ionization rate at H+70 hours only, and, of course, the r_{f_p} values change with time. The fractionation numbers for the irregular particles appear to decrease with particle mass (or size); no comment can be made on the dependence of the fractionation numbers on particle mass for the fused particles because of the small range (1.7 to 3.8 mg) of particle sizes used.

Correlations of fractionation numbers for fallout from relatively high-yield detonations on the surface of coral islands and on sea water are reported by Freiling[7]. In the report, Freiling mentions the identification of the induced activities of Na-24, S-35, Ca-45, Sr-92, U-237, U-240, and Np-239 although no yields are given. The presence of the last three nuclides suggests that much of the fission yield was due to the fission of U-238. The correlations indicate some relationship among the fractionation numbers namely, that relative to the refractory elements, the fractionation numbers of the volatile elements increase or decrease more or less as a group. This could be due to the relative composition of the gross samples with respect to the two types of particles, as suggested by the data of Maskin for the coral fallout. It could also result from a time, concentration, and temperature dependence of the condensation process for each particle or particle group. The correlations, therefore should depend on weapon yield and on type of environmental carrier material in forming the particles.

Freiling's treatment in correlating all the data, irrespective of yield or carrier material, neglects these effects. The methods of using the ratio of the fractionation numbers to a highly fractionated nuclide in the correlations is an artifact to spread out the data on a graph but, unfortunately, the technique does not give reliable statistical data. Converted to fractionation numbers relative to mass numbers 95 or 99 and corrected to U-238 fission yields, the data are reproduced in Table 2.6. The mass number 99 is used as the reference nuclide. For the samples in which the relative yields of the other refractory elements (Zr, Ce, U) are appreciably different from unity, indicating possible error in the data for mass number 99, one of the other refractory elements could be the chosen reference nuclide.

With corrections, the data indicate that:

1. Within experimental error, the mass numbers 95, 99, 144, 237, and 239 are present in their original ratios in all samples.

2. Only mass numbers with rare gas elements in the chain are fractionated in sea water fallout.

3. For the large yield detonation on the surface of deep sea water, the mass numbers with rare gas elements in the chain are not fractionated to a significant degree.

4. The fractionation numbers increase with (downwind) distance from shot point and therefore must decrease with the mean particle size, and

5. The mass number 132 with the elements Sn, Sb, Te, and I in the decay chain has fractionation numbers in the coral fallout that are nearly equal to those for mass number 99.

Some idea of what occurred in the fallout formation process for mass numbers 89, 99, 137, and 140 can be deduced from the curves of Figure 2.12; these show the fraction of each chain that could have condensed at a given time after fission with the exception of the indicated elements. For the loss of rare gas members only, the minimum fractionation numbers for the four mass numbers are: 89, 0.10; 99, 0.36; 137, 0.24; and 140, 0.55. In this treatment the fractionation numbers are relative to the independent yields of the chain, and not to another mass chain yield; therefore values larger than 1 are not possible. However, these minima occur at different times; therefore they do not all occur for a given group of particles.

Figure 2.12
CALCULATED FRACTION OF MASS CHAINS 89, 90, 137, AND 140 CONDENSED AS A FUNCTION OF TIME AFTER FISSION WITH INDICATED NON-CONDENSING ELEMENTS.
(Based on Glendenen's Postulate of Independent Yields.)

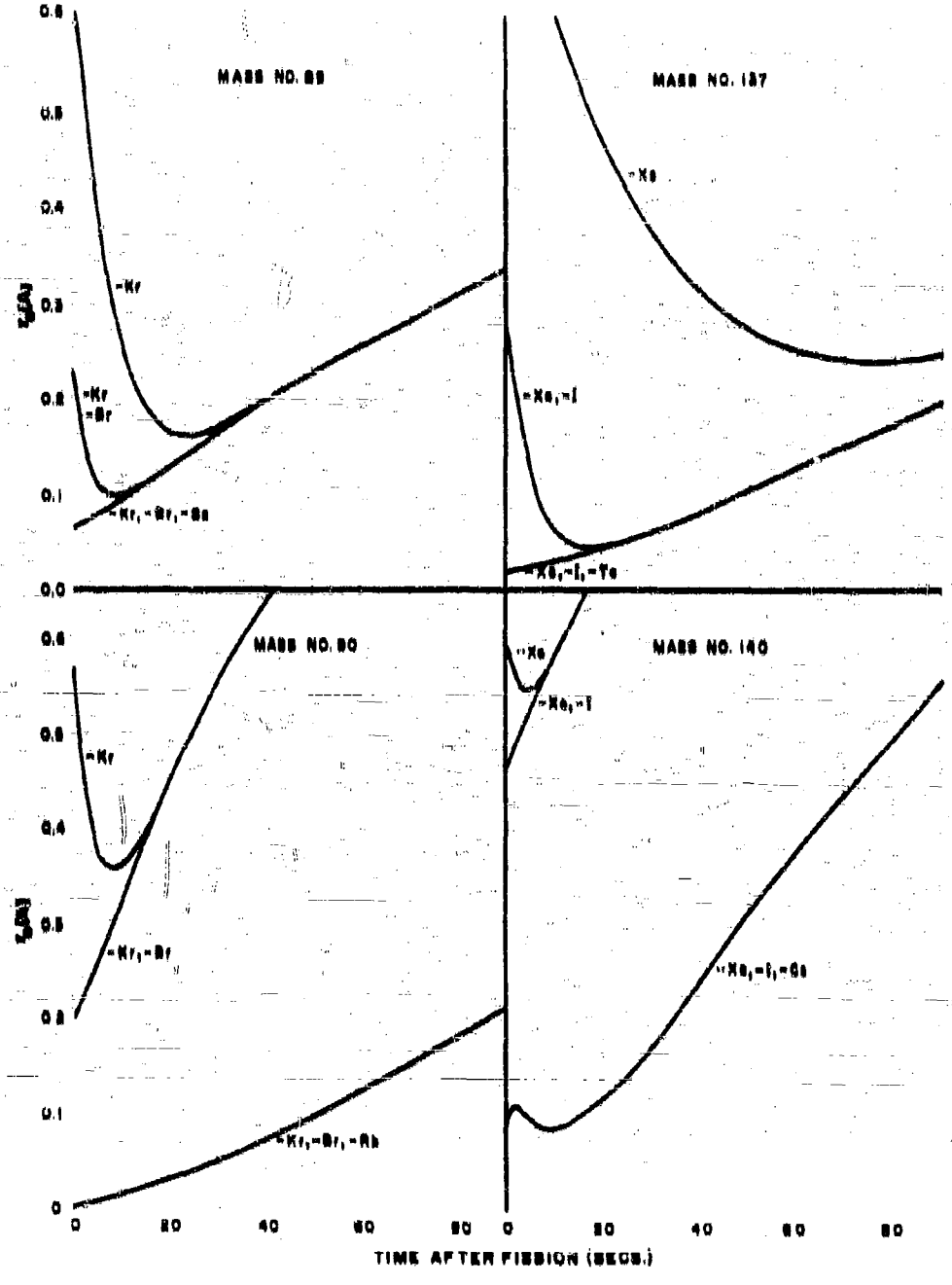

Table 2.9

SUMMARY OF FRACTIONATION NUMBERS RELATIVE TO MASS NUMBER 90 FOR CORAL AND SEAWATER FALLOUT CORRECTED FOR APPROPRIATE FISSION YIELDS

	Relative Sample Location	Mass Number									
		89	90	95	99	132	137	140	144	237[a]	239[a]
		A. Larger Yield (MT Range) Coral Surface Detonation									
Increasing Distance from Shot Point	Cloud Sample	5.1	4.0	2.1	(1.0)	2.5	3.3	4.2	2.0	1.2	1.2
	A	0.83	0.97	1.6	(1.0)	1.3	–	–	1.5	0.91	0.99
		0.38	0.44	1.0	(1.0)	0.69	0.22	0.88	0.96	0.78	0.87
		0.031	0.079	0.94	(1.0)	0.12	0.020	0.14	0.95	0.71	0.75
		0.13	0.24	0.82	(1.0)	0.45	0.046	–	0.88	0.73	0.78
		0.056	0.093	1.0	(1.0)	0.15	0.013	–	0.65	0.74	0.81
		B. Large Yield (MT Range) Shallow Water Surface Detonation (Coral Bottom)									
Increasing Distance from Shot Point	Cloud Sample	2.1	2.1	1.4	(1.0)	1.5	1.7	2.2	1.2	1.0	1.0
	A	0.42	0.57	1.1	(1.0)	0.94	0.37	–	1.2	0.87	0.92
		0.65	0.74	1.5	(1.0)	1.3	0.20	–	1.6	1.0	1.1
		0.38	0.49	0.92	(1.0)	0.81	0.13	0.86	0.89	0.77	0.82
		0.082	–	0.51	(1.0)	0.27	–	–	0.60	0.56	0.63
		0.24	0.36	0.84	(1.0)	0.48	0.13	–	0.81	0.70	0.76
		0.12	0.18	0.84	(1.0)	0.34	0.052	0.42	0.70	0.72	0.71

a. Values for 237 and 239 are not corrected for yields.

Table 2.9 (concluded)

	Relative Sample Location	Mass Number									
		89	90	95	99	132	137	140	144	237[a]	239[a]
	C. Medium Yield (KT Range) Surface Detonation on Deep Water										
Increasing Distance from Shot Point	Cloud Sample	2.6	1.7	0.90	(1.0)	1.0	2.5	1.6	0.96	1.0	0.98
	↓	0.73	–	1.0	(1.0)	1.1	0.42	–	1.1	1.0	0.97
		0.79	0.78	0.94	(1.0)	0.97	0.38	–	0.90	0.99	0.94
		0.46	0.47	1.3	(1.0)	0.98	–	0.70	1.1	1.1	0.98
		0.51	0.51	1.0	(1.0)	1.0	0.20	0.90	0.94	1.0	1.1
		0.30	0.57	1.1	(1.0)	0.99	–	–	1.0	1.1	0.96
	D. Large Yield (MT Range) Surface Detonation on Deep Water										
Increasing Distance from Shot Point	Cloud Sample	1.1	–	1.2	(1.0)	0.77	–	1.0	1.0	0.98	1.0
	↓	1.2	0.99	1.1	(1.0)	1.0	–	–	1.3	0.94	0.97
		0.96	0.93	1.1	(1.0)	0.95	0.41	–	0.92	0.96	0.96
		0.90	0.94	0.92	(1.0)	1.0	1.0	–	1.0	1.1	1.1
		0.53	0.89	1.5	(1.0)	1.0	1.2	–	1.1	0.64	0.71
		0.90	1.2	1.3	(1.0)	1.1	–	–	1.4	0.72	0.74
		1.6	1.2	0.95	(1.0)	1.1	–	–	0.94	0.72	0.74

Figure 2.13
PLOT OF CALCULATED $r_g(A)$ VALUES FOR MASS NUMBERS 90, 137, AND 140 AGAINST THOSE OF MASS NUMBER 89 FOR THE ASSUMPTION THAT ONLY THE ALKALI METAL ELEMENTS AND ALKALINE EARTH ELEMENTS IN THE CHAIN CONDENSE

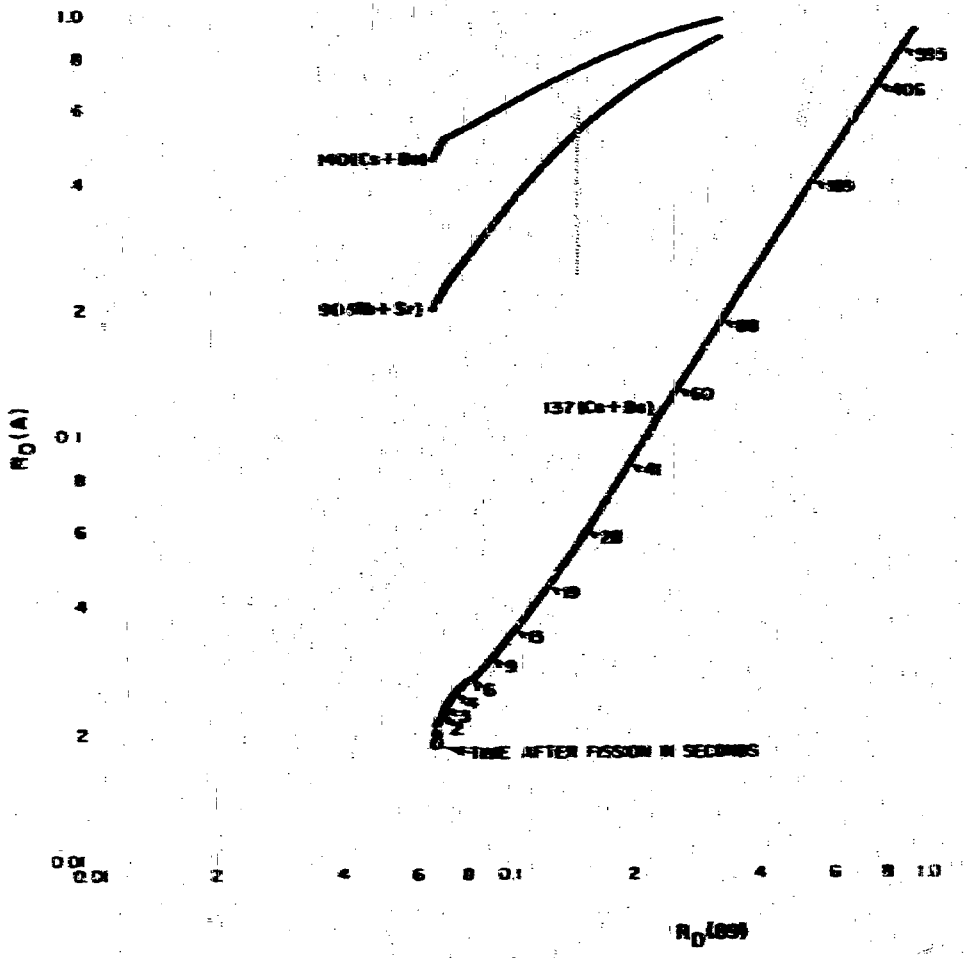

If the independent yields from Glendenin's postulate for U-235 fission are reasonably accurate estimates for the yields from a nuclear weapon, then, for condensation times up to 60 seconds, it appears from the data that only the alkaline earth members of the chains (Sr, Ba) and a fraction of the alkali metal elements (Rb, Cs) condensed in the coral particles falling nearest to shot point. For the condensation of like fractions of each element at any time up to 60 seconds after fission, the curves indicate that the fractionation number for mass number 90 should be larger than for mass number 89, and that its value for mass number 140 should be larger than for mass number 137.

The effect of increasing weapon yield on the condensation is to extend both the time and time-period over which the condensation occurs, since the rate of decrease of the fireball temperature decreases as the yield increases. On the average, the fallout from larger yield weapons, therefore, is less fractionated in mass numbers 89, 90, and 140 and even perhaps in mass number 137. The maximum amount of fractionation of these mass numbers results from condensations occurring between about 10 and 20 seconds after fission.

A plot of calculated $r_0(A)$ values for mass numbers 90, 137, and 140, based on the independent yields of the chain members and the complete condensation of the alkali and alkaline earth nuclides, as a function of the $r_0(A)$ value for mass number 89, is shown in Figure 2.18. The shape of the curves suggests possible correlations among the fractionation numbers, especially if the condensation period is short. For times longer than about 60 seconds after fission, the curves for mass numbers 90 and 140 represent the case for noncondensation of only the rare gas chain members. If the condensation takes place over a relatively short time interval, the fractionation numbers are related according to

$$r_0(A) = r_0^{\beta}(A) \left[r_0(89)\right]^n \qquad (2.8)$$

where $r_0^{\beta}(A)$ and n are constants; the constant n is the slope of the curve for a short period of time.

The empirical correlation constants for Eq. 2.8 are given in Table 2.10, along with the mean values of the condensation times taken from a plot of $r_0^{\beta}(A)$ and n as derived from the tangents to the $r_0(A)$ curves in Figure 2.18, with time after fission; $r_0^{\beta}(A)$ is the coefficient for the observed data. The mean times of condensation range from about 25 to 50 seconds after fission and agree reasonably well considering the scatter in the data. More precise data would permit estimating the fractionational condensation of the alkali metal elements and even perhaps of iodine in the case of mass

number 137. However, the results of the treatment give reasonable values of the times at which the condensation occurred.

The main feature of this type of data correlation is the notion that the fractionation numbers of the volatile elements vary in some uniform manner, so that if one element is fractionated all other elements are also fractionated to a degree specified by the empirical correlations. Unfortunately, the method requires the fractionation number of at least one mass number in addition to the analysis of a reference nuclide before it can be utilized to make estimates of the fractionation number of other radionuclides. In addition, a sufficient number of mass numbers correlations are not reported from which to estimate the gross decay and the potential dose from fallout.

The chief interest in fractionation in fallout concerns the mixture of radioelements in fallout from silicate soil rather than from coral soil detonations. Since the silicate monomers melt at lower temperatures than calcium oxide, the elements condensed into the fused particles should, for the same weapon yield, have a different composition. Therefore the radioactive mixture in silicate fallout should exhibit a different combination rate decay than that in coral fallout.

The petrographic and radiochemical analyses described in this section, as well as other analyses of fallout, were made on samples of fallout collected from test weapons detonated at the Nevada Test Site and the Eniwetok Proving Grounds. The collection methods and devices varied considerably. The more crude methods used a shovel and pail or a pie can to scoop up a surface layer of contaminated soil. Others used sheets of canvas spread on the ground, a sweeper and vent tube, pans, pans, pails (with or without plastic liners), trays, and gummed paper. The more elaborate methods consisted of collectors that opened and closed automatically by use of radio signals and timing devices and were sealed against the weather when not open for fallout collection. Others were designed to collect a large number of fallout samples serially and automatically, for a pre-set short time, on greased trays or on special films. Still others were designed to collect the particles directly from the air by drawing them into filters. The analyses described here were made on fallout samples collected by a variety of these methods.

Since each method has its own peculiar collection bias with respect to the surrounding terrain, probably none gave a more representative sample than the shovel. However, the shovel and the exposed devices gave samples that contained much non-fallout debris. These samples were not useful, except for certain types of analyses, since it is obviously impossible to separate cleanly the fallout from the terrestrial material in a reasonable period of time.

Table 2.10

COMPARISON OF EMPIRICAL FRACTIONATION-CORRELATION PARAMETERS WITH THOSE ESTIMATED FOR CONDENSATION OF ALKALI AND ALKALINE EARTH ELEMENTS OF MASS CHAINS 90, 133, AND 140, AT SPECIFIED TIMES AFTER FISSION

Mass Number	Data Source	$r_0^*(A)$	n	t(sec)	$r_0'(A)$
90	Shot A	1.12	0.77	34[a]	2.25
	Shot B	1.[illegible]	0.82	31[a]	2.43
	Shot C	0.91	0.66	47[a]	1.83
133	Shot A	1.81	0.90	-	-
	Shot B	1.76	0.75	-	-
137	Shot A	0.90	1.46	35[a], 35[b]	0.90, 0.88
	Shot B	0.71	1.19	25[b]	0.71
	Shot C	0.87	1.66	39[a]	1.05
140	Shot A	1.60	0.82	39[b]	1.60
	Shot B	1.44	0.38	52[b]	1.44
	Shot C	1.98	0.42	38[a]	1.68

a. From n vs t (t is the estimated time of condensation)
b. From $r_0'(A)$ vs t

The single particle analyses, as mentioned previously, were made on samples further biased with regard to minimum particle size, minimum radioactivity content, and [illegible] numbers. These analyses were also biased as to the limitations of the extensibility of the procedure as well as because of lack of time.

Two methods were used to identify and select the radioactive particles from among inactive particles mixed with soil materials. One method was to subdivide the sample and check each fraction with a portable survey meter or gamma scintillation counter until the subdivided fractions containing the radioactive particles could be viewed easily under a low-power binocular microscope. The radioactive particle or particles could then be identified by their distinctive appearance and manually removed and surveyed for activity.

The second method, better for very small particles, involved distributing the particles on the backs of photographic sheet film sprayed with liquid plastic. After allowing an appropriate exposure time, the film was developed and fixed by brushing the developing and fixing solutions on the emulsion side of the film without disturbing the particles on the reverse side. The radioactive particles then were located with a low-power binocular microscope by the dark areas of the exposed film. Both stripping film and single-coated X-ray film were found suitable for this method.

The thin sections of individual fallout particles were made by casting the particles in plastic cylinders, using paraffin molds, and bake-hardened at 60°C. One end of the cylinder was then ground down with a motor driven iron wheel using carborundum abrasive until the center portion of the particle was exposed. The exposed surface was then polished on a glass plate and cemented with Canada Balsam to a glass microscope slide. Then the other end of the cylinder was ground down until the thin section of particle and plastic remaining was about 30 microns thick. The thickness of the thin section was estimated by observing, with the petrographic microscope, the birefringence of grains of quartz placed in the plastic along with the fallout particles. At the required thickness, the quartz shows a grayish-white or grey interference color.

The distribution of the radioactivity within the thin section was determined by radiograph techniques using Eastman NTE stripping films. For this, the thin section was cemented with a gelatin-alum cement or taped to the back of the film during exposure.

The petrographic microscope with and without polarized light was used to give information on the crystal structure and, in some cases, the chemical composition of the particles. The crystal structures were also identified by X-ray diffraction analysis.

The size and composition of sea water fallout particles, was determined by use of a special reagent film developed by Farlow[21] which served both as a collecting surface and analytical device. One of its advantages was that the particles could be analyzed *in situ* and involved no sample recovery problems. In order to keep the film from being saturated with water drops, pieces of the film were usually exposed by use of a cycling collector and each piece of fim surface was exposed serially for a pre-set time; these collectors used a circular piece of film about 3-in. in diameter.

The reagent film for determing the amount of soluble chloride present in a liquid particle was prepared by impregnating one side of a commercial gelatin-coated film (such as Eastman Type K-509) with rod silver dichromate. The film area over which the reaction occurs was easily measured with a microscope. Since the reaction area for a given film preparation was found to be proportional to the amount of soluble chloride present in a drop

of fallout, it was possible to determine a calibration curve for each film preparation and thus to determine the amount of chloride in other drops. The method was useful in the determination of 1 to 10^{-6} micrograms (μg) of sodium chloride.

The chloride-sensitive reagent film was also useful in determining the water content of the drops. The measurement depends upon the presence of some very small insoluble particles, suspended in the drop. Each drop spreads over an area of the film related to its volume and, when dry, the solid residues remaining (called an "artifact") forms an outline of the maximum spread of the drop such as that shown in Figure 2.10. The film can be calibrated by suspending some insoluble solid particles in standard chloride solutions and aspirating the mixture on the film. The chloride-reaction area determines the water content of the drop; the area of the artifact is then measured. This technique measures water volumes as small as 0.1 micromicroliter ($\mu\mu l$). Comparative visual standards use aluminum oxide suspensions prepared for estimating the amount of solids present in the residue.

2.4 Properties of Small Fallout Particles from Detonations at Weapons Tests

Several properties of fallout particles can be inferred from the interactions of the radioelements with biological systems such as the uptake of certain fission-product elements by plants and animals. Data on these biological reactions, the physical properties of the fallout particles, and ground distribution of the smaller fallout particles from nuclear detonations (mainly from tower and balloon-supported test devices) have been summarized by Larson and Neal[28] and Nishita, Romney, and Larson.[29] The basic information was derived from data such as those reported by Bellamy,[30] Rainey,[31] and Lindberg.[32] (See References 28 and 29 for a more complete bibliography of workers contributing to the data on these subjects.)

The physicochemical properties of the fallout particles inferred from these data that are of main interest here are those that describe the fallout formation process with respect to the disposition of individual radioelements in the fallout particles for different conditions of detonation. Data describing the contamination processes are also very important in understanding the entire fallout process, including the major factors that determine the fate of the radioelements. Radioelements which are condensed on the surface of fallout particles (i.e., are not fused in the interiors of the particles) are available for uptake by plants and animals; thus information and data on uptake processes also provide information about the fallout formation process and the contamination process.

There are three major paths by which a radioelement carried by fallout particles becomes incorporated into animal tissue. One involves dissolution in water, transfer to the root zone of plants, uptake through the root system to the plant tops, and thence into the animal that eats any part of the plant. The second path involves the direct assimilation of the radioelement by the plant leaves which are then eaten by an animal. The third path is the direct intake, when eaten by the animal, of the fallout particles that remain on the surface of plant leaves or other parts of the plant.

In general, the dissolution process for the incorporation of a radioelement into the parts of plants occurs in neutral (or at most slightly acidic) water systems. The possible exception to this process is radioiodine, which, in air, tends to volatilize as rapidly as it is formed by the decay of the tellurium parent. In the vapor state radioiodine can react with any nearby organic material, especially by addition to unsaturated hydrocarbons such as a leaf surface or decayed organic matter. This behavior should dilute the radioiodine concentrations in the plants (relative to the other elements) and spread it by transfer through the air.

By contrast, the dissolution process for the uptake path involving direct intake into an animal that eats the plant parts on which the fallout particles are deposited proceeds in acidic water systems of the animal's digestive tract. Because the stomach fluids are acidic, this direct path should result in a maximum transfer of radioelements from a fallout particle (or group of particles) into the body tissues of the animal.

The gross fission-product uptake by radishes from a subsurface detonation at the Nevada Test Site, is found by Nishita, Romney, and Larsen[30] to vary from 0.005 to 0.050 percent (based on beta activity measurements). These authors also report the uptake by red clover grown in soil contaminated by fallout from a 500-foot tower detonation; the uptake varied from about 0.001 to 0.01 percent. In the latter case, the red clover uptake was greater from the soil contaminated at the larger distance from ground zero (i.e., where the smaller fallout particles landed). As might be expected, the amount of uptake was found to be dependent on the plant species and the soil type.

In the areas on and adjacent to the Nevada Test Site, vegetation retained predominately particles with diameters less than 44 microns. Also, the gross solubility of the fission products carried by these particles from tower-mounted detonations was found to vary from 5 to 55 percent in 0.1 normal HCl (0.1 normal HCl is approximately the acidity of digestive fluids).[30,31] On this basis, the uptake in animals foraging on clover whose leaves were contaminated by fallout, as compared to foraging on new clover grown on contaminated ground (Nevada Test Site tower detonation), would range from about 2,500/1 to 5000/1 if the clover covered 100 percent of the ground and the particles were 44 microns or less in diameter.

The value of the relative uptake would vary with (a) the time after detonation and period of exposure, (b) the particle sizes, (c) the fraction of area covered by foliage, and (d) the weather conditions prevailing during the period under consideration. The data on particle retention by foliage are discussed more fully in Section 2.6. Although the data apply only to a tower-type detonation, the magnitude of the relative uptake, even as a maximum, suggests that the direct-uptake path would also predominate for fallout from large-yield surface detonations.

The major contributing radioelements found in the tissue of rabbits and rodents taken from areas near the Nevada Test Site on which small fallout particles deposited within the first day after a test detonation include iodine, strontium, yttrium, ruthenium, cesium, barium, and cerium.[40] The tissue concentrations increased with distance from shot point up to a maximum and then decreased again.[41] The maximum tissue concentrations generally occurred at locations where the fallout arrival time was about 2 to 3 hours after detonation. These data indicate that the fraction of the radioelements on the exterior of the particles available for uptake increased with decreasing particle size more rapidly than the total amount of fallout deposited decreased with distance, up to some distance. At farther distances, the decrease in the deposit level predominated, and the amount of uptake also decreased with downwind distance.

Radioiodine was found to be 80 to 90 percent of the activity in the thyroid tissue of native rodents.[38] The radioelements found in the bone tissue of jack rabbits at about 20 days after a tower shot are listed in Table 2.11 in which a few of the data given by Larson and Neel[28] have been converted to number of atoms and approximate fission equivalents taken up and deposited in the bone tissue. The relatively low uptake factor of yttrium, ruthenium, and cerium (last column of the table) is probably due to both a lower solubility in the rabbit digestive tract (especially if the r_s (A) values are assumed to be correct) and a lower retention of these elements in the bone tissue of rabbits.

The main point of the data is that the listed radioelements were dissolved by the acidic digestive tract fluids from small fallout particles that pass through the gut. Other radioelements in fallout, but not listed, presumably were not dissolved in appreciable or significant amounts. The listed elements are those expected to be depleted in the larger fallout particles, and enriched in the smaller fallout particles, relative to the other refractory type fission product elements.

The effects of detonation conditions on the properties of fallout can be illustrated by comparisons between the data on fallout from balloon-supported devices (i.e., low air bursts) and tower-mounted devices (i.e., near-surface bursts).[28] The total amount of local fallout deposited, up to about 200 miles from ground zero at the Nevada Test Site, from tower detonations, has been observed to be 30 to over 100 times the amount observed for air bursts. Those

Table 2.11

RELATIVE RADIOELEMENT CONCENTRATIONS IN JACK RABBIT BONE TISSUE AT ABOUT 20 DAYS AFTER DETONATION OF SHOT SMOKY, OPERATION PLUMBBOB, IN 1957

Radionuclide	A(20 days) (d/m/gm bone)	N(20 days) (atoms/gm bone)	Y_i (21 days)[c] (atoms/fission)	$1-r_o$ (A)[d] (availability factor)	A_o (fissions/gm bone)	U_i[e] uptake factor)
Sr-89	200	$2.3x10^7$	0.0349	0.99	$7.2x10^8$	1.0
Sr-90	(1.7)[b]	($3.6x10^7$)	0.0516	0.97	($7.2x10^8$)	1.0
(Sr-91)Y-91	35	$4.1x10^6$	0.0420	0.89	$1.1x10^8$	0.1
Ru-103(Ru-106)[a]	4.5	$3.7x10^5$	0.0235	0.65	$0.24x10^8$	0.03
Cs-137[a]	1.7	$4.8x10^7$	0.0577	0.99	$8.33x10^8$	1.0
Ba-140	700	$1.9x10^7$	0.0195	0.86	$11.1x10^8$	1.0
Ce-141(Ce-144)[a]	4.0	$2.7x10^5$	0.0384	0.42	$0.17x10^8$	0.02

a. Possible partial elimination prior to 20 days

b. Estimated from assumption of $7.2x10^8$ fissions/gm bone and $U_i = 1.0$

c. For fission products from thermal fission of U-235 (see reference 2)

d. r_o (A) taken from Table 2.23 for 31 KT surface burst without correction for yield and type of detonation

e. Relative uptake factor assuming value of 1.0 for Sr, Cs, and Ba

lower fallout depositions from the air bursts reflect the fact that the sizes of the fallout particles formed in the air burst are very small compared to those formed in the near-surface burst. For example, in some fallout samples from tower detonations, about 80 percent of the sample activity is found on particles with diameters less than 44 microns, and as much as 15 percent on particles with diameters less than 5 microns. In samples from a balloon-supported detonation, of similar yield and burst height, about 70 percent of the activity is found on particles with diameters less than 44 microns, and as much as 58 percent on particles with diameters less than 5 microns.

The average fractionation numbers of some radionuclides in fallout from some tower and balloon-supported detonations are given in Table 2.12, relative to the refractory Zr-95 nuclide and to the mass chain yields for thermal neutron fission of U-235. The values were derived from the data of Larson and Neel[98] and presumably apply to particles with diameters less than about 100 or 200 microns having mean diameters of about 50 microns. The values of the fractionation numbers for the fallout from the tower-mounted explosions suggest that the Zr-95 condensed more completely than the other nuclides on the larger particles, and that the nuclides Sr-89, Sr-90 and Ru-103(106) did not condense completely on the particle-size groups in the observed samples. The fractions of these three elements not condensed would then be concentrated on the very small particles and carried to much greater distances away.

The same general statement applies to the fractionation numbers for the fallout from the balloon-supported detonations, except that the mean diameters of the particles in the samples must have been smaller and that the Zr-95 is more depleted. Thus there may be even a higher degree of separation between the very refractory and the volatile fission product elements in the fallout particles from an air burst than in the near-surface burst fallout particles. Possible causes of this separation are (1) a lower concentration of available liquid or solid surfaces in the air-burst fireball, and (2) a corresponding delay, due to lower vapor pressures, in the selective condensation.

The gross solubility data in terms of gross beta count-rate measurements of the radioactivity in some gross fallout samples under several different detonation conditions, from the data of Larson and Neel[98] are given in Table 2.13. Although the time of measurement was not given, but is presumed to be about 2 weeks or so after detonation, the general magnitudes of the fraction of the activity which was soluble clearly show that the nuclides in the fallout from the air-burst detonation were the more soluble. The higher solubility of the activity in water, for the air-burst fallout, suggests that many more of the fission-product radionuclides were condensed on the surfaces of the particles

Table 2.12

AVERAGE FRACTIONATION NUMBERS OF RADIONUCLIDES IN FALLOUT FROM TOWER AND BALLOON-SUPPORTED DETONATIONS AT THE NEVADA TEST SITE

Nuclide	R(95)[a]	
	Tower	Balloon
Sr-89	0.32	1.5
Sr-90	0.05	-
Y-91	1.4	2.8
Zr-95	1.0	1.0
Ru-103(106)	0.45	3.2
Ba-140	1.4	3.5
Ce-141(144)	1.4	2.8

a. Relative to the yields for thermal neutron fission of U-235.

Table 2.13

GROSS SOLUBILITY OF ACTIVITY FROM SMALL FALLOUT PARTICLES

Type of Detonation	Percent Activity Soluble[a]		Particle Size (microns)
	in H_2O	in 0.1N HCl	
Underground	5.4	85	0-44
Tower-Mounted	2	14 to 30	0-44
	1	5	44-ca 100
Balloon-Supported	14	60	0-44
	31	80	44-ca 100

a. Based on beta count-rate measurements (presumably at about 2 weeks after detonation).

than were condensed in this manner in the tower detonation. The higher solubility of the activity in acid, especially for the air burst fallout, may be partially due to dissolution of the primary iron oxide or alumina particles. However, the very high solubility in both water and acid of the radioactivity on the larger particles from the air burst suggests almost complete surface

condensation of the radionuclides on these larger particles at late times, since a significant fraction of these particles were grains of soil, of which some had been melted. The solubility of the activity on the particles from the tower mounted detonations, on the other hand, decreased with increasing particle size. Fallout particles with diameters of 200 to 2000 microns from low tower detonations often have negligible solubilities, in water or even in strong acids.[55]

The gross solubility data on the radioactivity from small fallout particles lodged on foliage after some tower detonations, as taken from Romney and coworkers,[56] are given in Table 2.14. The solubility was measured by suspending 0.5 gm samples of dry plant material in 10 ml of 0.1 normal HCl after the samples have been radioassayed. The suspension was then shaken for 30 minutes, centrifuged for 15 minutes, and the supernatant solution separated by filtration.

Since the data do not indicate a consistent trend in solubility with distance from ground zero, averages were calculated. The average fraction of the activity dissolved was the same (24 percent) for the Apple shots detonated on 500-foot towers; it was smaller (16 percent) for the Met shot detonated on a 400-foot tower. The data suggest that the particle size retained by the different plants was about the same; that is, the type of foliage was not a dominant factor in either the gross solubility or biological uptake potential of the retained fallout.

2.5 Redistribution of Deposited Fallout

The redistribution of deposited fallout should depend on (1) the type of surface on which the particles land, (2) the size of the particles, (3) the amount and frequency of rainfall, and (4) the surface wind conditions. The combined effect is often called "weathering." On land areas, the combined effects of weathering processes are found to be rather small, even for the small fallout particles from which a larger fraction of the radionuclides are soluble. After nine years on undisturbed soil, fallout from the Trinity Shot (New Mexico) was still confined to the surface two inches of soil.[28]

Resurvey data from the surface and underground shots at Operation Jangle (Nevada Test Site), after exposure to winter winds, snow, and spring rains, indicated no significant change other than that due to radioactive decay.[58] Radiation measurements taken during Operation Castle (Eniwetok Proving Grounds) in 1954 on the islands of several atolls (before and during heavy rains for several months) show no decrease that could not be accounted for on the basis of radioactive decay.[59] Dunning[17] and Lapp[18] erroneously attribute the rapid decrease in the gamma radiations during the first year to a

Table 2.14

GROSS SOLUBILITY OF ACTIVITY FROM SMALL FALLOUT PARTICLES LODGED ON PLANT FOLIAGE

Plant Type	Distance From Ground Zero (miles)	Fraction Dissolved[a] in 0.1N HCL
1. Shot Apple I (14 KT on 500 ft. Tower)		
Artemisia (Sagebrush)	12	0.30
Ephedra (Mormon tea bush)	40	0.27
Ephedra (Mormon tea bush)	80	0.15
Juniperus (Juniper)	165	0.32
	Average:	0.24
2. Shot Met (22 KT on 400 ft. Tower)		
Larrea (Creosote bush)	30	0.26
Larrea (Creosote bush)	58	0.06
Medicago (Alfalfa)	140	0.14
	Average:	0.16
3. Shot Apple II (29 KT on 500 ft. Tower)		
Triticum (wheat)	7	0.10
Triticum (wheat)	40	0.17
Triticum (wheat)	106	0.35
	Average:	0.24

a. Based on beta count-rate measurements.

weathering factor of 0.4 due to the first heavy rains 10 to 20 days after the first detonation, apparently by comparison with an inappropriate decay curve. This misinterpretation has also been noted by Knapp[39] in discussions of this subject.

Experimental measurements reported by Miller and Bottomley[40] on soluble radionuclides deposited on soils through which water has passed gave an average leaching depth, for Sr-89, of 0.75 inch after passing 30 inches of water, and 1.5 inches after passing 300 inches of water. The movement of Cs-137 is found to be only 0.25 inch after passage of 300 inches of water, even in sandy soil. Larson and Neel[28] report penetrations up to 0.5 inch after the passage of 84 inches of water; the source of the activity used in the experiments was not specified.

These data show that the soluble radionuclides, in almost all cases, would be absorbed by the top inch or two of soil particles and remain there unless the whole layer eroded away in heavy rains. But even in this case the nuclides would remain attached to the particles; the fraction of the nuclide soluble in water in such conditions would be negligibly small. The studies of Thornthwaite, Mather, and Nakamura[41] show that many rain cycles would be needed to transport the activity farther than about two inches below the surface of the soil. Since most of the radioactivity on the larger fallout particles would be fused into the particles, the only way it could move into the soil is by mechanical mixing, as occurs in the plowing or disking of agricultural lands.

The translocation of fallout particles on land areas by wind occurs to a small degree. The experience in the Nevada Test Site, (under dry conditions) where excursions in the fallout area were made by experimental crews to recover fallout samples, was that, for entries during the first day after a detonation, clothes became contaminated with small fallout particles due to the stirring up of surface dusts and brushing against desert plants, but that, for entries after the second day or so, only the bottom parts of shoes (or booties) picked up fallout particles. Apparently the small particles become adsorbed or physically attached to larger particles, or otherwise become mechanically trapped by the surface soil grains.

Movement of large particles by the wind is usually small because the larger gravity force retards such movement. However, particles in the size range of about 100 to 500 microns drift more easily than particles of other diameters if the surface wind speed is in excess of about 10 mph. These particles, if dislocated, may carry with them small attached fallout particles. Data from experiments at Camp Parks, California, reported by Sartor and Owens[42] in which particles with diameters from 150 to 300 microns (tagged with Ba(La)-140) were deposited on various types of surfaces showed that the movement of the particles on unpaved areas and on tar and gravel roofs is insignificant, even for wind speeds up to 20 mph. The movement of the particles on and from paved

areas is found to be quite large; the particles apparently moved in the wind by hopping and by rolling over the smooth surfaces, although very few particles were raised higher than 3 or 4 inches. They did not jump over curbs but were deposited along the gutters and in depressions and behind low obstructions.

The fraction of the original ionization rate remaining, as measured in the center of a street and in the center of a rather large area of asphaltic concrete, is plotted in Figure 2.14 as a function of the total wind vector (including only winds in excess of 10 mph) that occurred over a ten-day period. Further data of this kind on other particle sizes are needed to establish whether the data of Figure 2.14 are representative of the reductions that could occur generally in the ionization rate at locations of interest. The reduction in the ionization rate for both areas in the first four days (wind vector of 200 miles) was equivalent to a decontamination of about 50 percent; some of this, of course, was due to shielding, since the particles concentrated in surface depressions and along barriers.

2.6 The Collection and Retention of Fallout Particles by Plant Foliage

Some of the data obtained at weapons' tests on the collection and retention of fallout particles by foliage are reported by Romney, Lindberg, Hawthorne, Bystrom, and Larson.[55] Their stated findings, with respect to the ability of the outer surface of leaves to trap and retain fallout particles, were that the size-range of particles lodged on the foliage was predominately less than 100 microns in diameter and that the best correlations of the amount of activity (beta count-rate) on the foliage was with the fraction of the total activity carried by particles having diameters less than 44 microns that landed at the same location. These two findings suggest that the foliage of most plants is selective in trapping only the smaller sizes of fallout particles. Some of the reported data are given in Table 2.16, as converted from curie units at H+12 to the equivalent number of fissions by use of the factor, 5.67×10^9 fissions/microcurie.[55] The median particle diameters are taken from the plotted particle-size distributions in Figure 2.15.

It is interesting that the median particle diameter increased with fallout arrival time up to arrival times of 4 to 5 hours after detonation. However, since the data are for different plant species, part of this increase also may be due to the plant species selected for analysis. The spread of the distributions, however, tend to decrease with time of fallout arrival or with decreasing particle size of the arriving fallout. The upper-limit particle diameter cut-off is fairly sharp at diameters larger than 88 microns, excepting for the bushmallow foliage sample. The higher retention levels and larger particles on the bushmallow foliage is probable due to the high density of stellate hairs on the leaves which would serve to trap and hold particles onto the surface.

Figure 2.14
REDUCTION IN THE IONIZATION RATE AT THE CENTER OF 10TH STREET AND AT THE CENTER OF THE PLAZA, CAMP PARKS, CALIFORNIA, AS A FUNCTION OF THE WIND VECTOR (sum of the products of wind speed · time) FOR WINDS IN EXCESS OF 10 MPH OVER A 10-DAY PERIOD. THE TAGGED PARTICLES WERE 150 TO 300 MICRONS IN DIAMETER

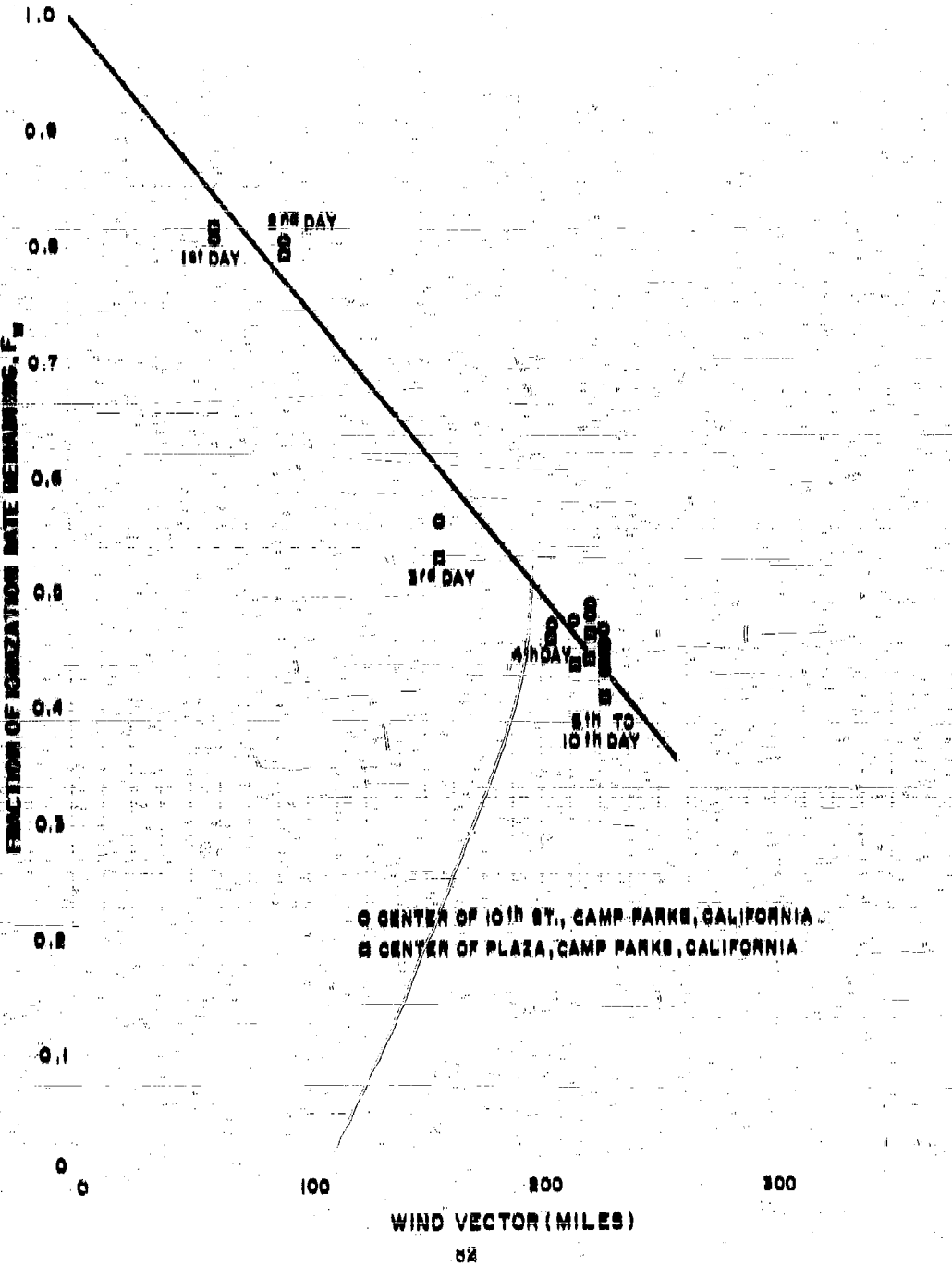

Figure 2.15
ACCUMULATED DISTRIBUTION OF THE NUMBER OF PARTICLES WITH DIFFERENT DIAMETERS ON FOLIAGE

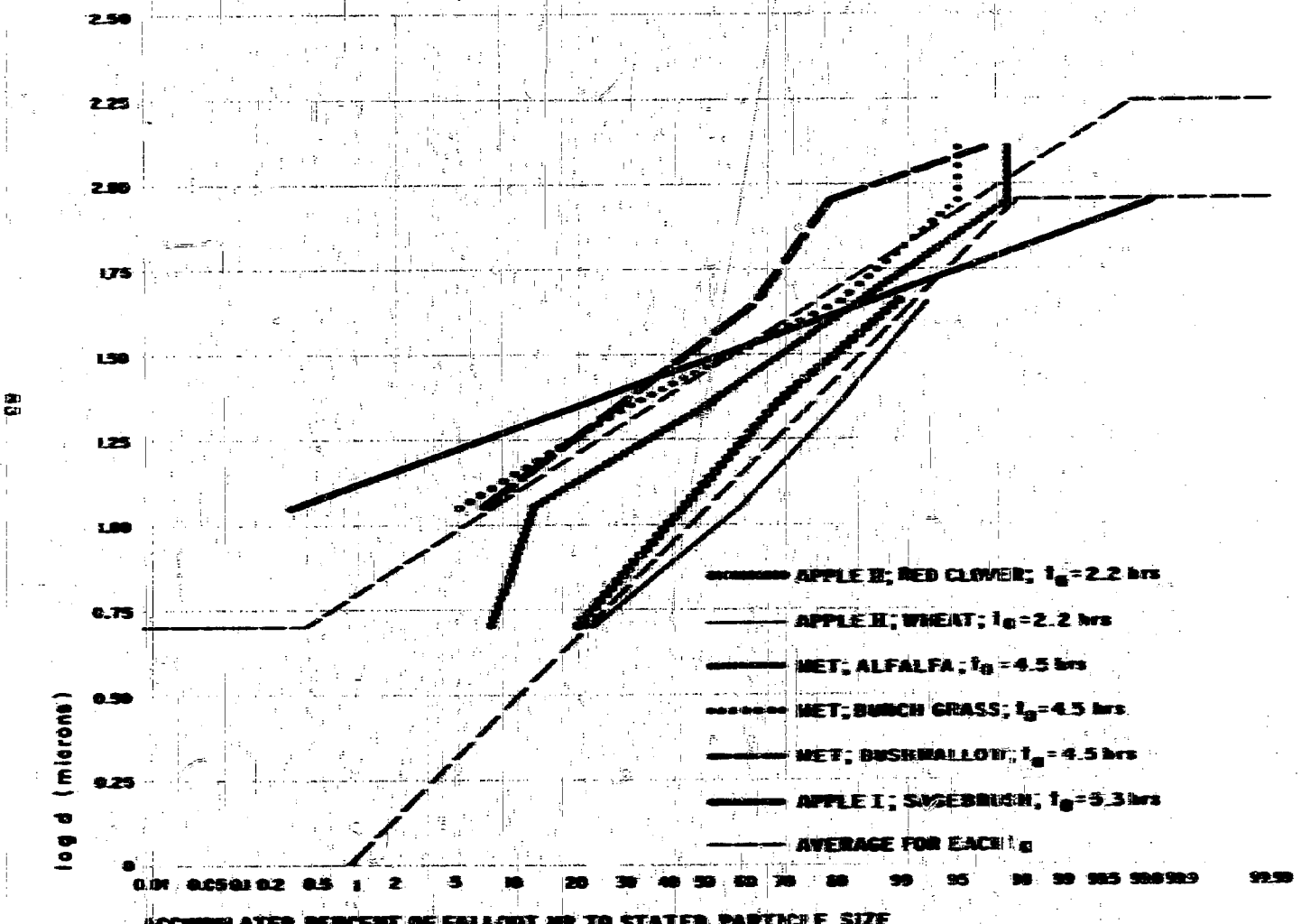

Data on the collection of the fallout from Apple II shot and Smoky shot tower detonations by some forage crops are given in Table 2.16. The fractions of the deposited fallout retained by red clover (in flats) increased with time of fallout arrival from about 0.1 percent at 7 miles downwind from the Apple II shot to about 1 percent at 100 miles away. For wheat, the fractions retained increased from about 0.2 percent to about 6 percent over the same range in distance. The highest fraction retained, of these data, was for alfalfa foliage at 250 miles away from shot Smoky. The distributions of the activity on the fallout particles that were deposited at several of the locations are plotted in Figure 2.10. The values of the median diameters decrease with time of arrival as would be expected but the spread of the various activity-size distributions appears to be roughly the same, in logarithmic units, in all the collected samples.

The major conclusion from the data of Romney and coworkers is that the fraction of the deposited fallout collected and retained by foliage is rather small even when the diameters of the arriving particles are small enough to be trapped by the hairs and resins on the leaves. Thus large trees and shrubs cannot be considered as significant sources of radiation where heavy fallout deposits from land surface detonations occur and where the particle diameters are in excess of about 50 microns.

There are no good data on the decontamination of fallout particles from foliage (neglecting data on the very fine material of world-wide fallout). Romney and coworkers,[50] however, do report data on the decontamination of fallout particles from foliage; these can be used to indicate at least the upper limit of a decontamination by a heavy rain. The results of the experiments, using the decontamination reagents water, 0.1 normal HCl and 5 percent EDTA, are summarized in Table 2.17. The water decontamination data would be most representative of the decontamination that could result in a heavy rain. The desert foliage decontaminated generally to levels between about 30 and 40 percent of the initial deposit. However, the smooth-leaf annual was decontaminated to 9 percent and growing wheat was decontaminated to about 20 percent of the initial level. The latter value should be representative of most grass-type foliage.

The foliage contamination data appear to show that all the leaves on a plant retain about the same level of contamination on all the foliage. If exceptions to this rather uniform distribution on plant foliage can occur, they conceivably would be most predominant in foliage growths such as a very dense tall growth of grass. This interpretation of the contamination process at least agrees better with the observations than a process in which only the exposed surfaces of the exterior or upper leaves are assumed to be the only collecting surfaces. The use of the assumption of uniform contamination of all the foliage on a plant allows correlation of the fallout particle retention data in terms of the mass of the collecting foliage on a plant. The correlation of the fallout retained per unit

of dry plant (leaf) mass with the total amount of fallout deposited at a location can then be used to evaluate the internal radiological hazard from the intake of radionuclides in the fallout retained on foliage. To make the correlations, a foliage contamination factor, n_L, is defined as the ratio of the number of fissions per gram of dry plant (foliage) to the number of fissions of total fallout per sq. ft. of soil surface. If the plant or foliage surface density is defined as w_L in grams of dry foliage per sq. ft. of soil surface, the fraction of the fallout retained by foliage is

$$F_L = n_L w_L \frac{(\text{fissions/ft}^2 \text{ on foliage})}{(\text{fissions/ft}^2 \text{ on soil})} \qquad (2.5)$$

The denominator quantity, fissions/ft^2 on soil is the total fallout deposit uncorrected for the amount on the foliage. The value of w_L is a measure of the density of plants growing on the land. The values of n_L and n^*_L (for only particles with diameters less than 44 microns) reported by Romney and co-workers[11] are given in Table 2.18 for native desert-type foliage. The independence of the values of n^*_L on distance from ground zero is further evidence of the selectivity of the foliage in retaining only the smaller particles. The high values of n^*_L for the fallout from Shots Met, Diablo, and Shasta could be due either to higher humidity conditions and early post-shot plant collections or to the fact that the fallout from these detonations contained a fairly large fraction of the activity on particles with diameters between 44 and 88 microns which were retained by the foliage.

For general use, the value of n_L is a more important quantity than n^*_L. The dependence of the values of n_L on several detonation parameters and further analysis of the data presented in this section are given in Chapter 6 in the form of fallout contour ratio scaling functions. In most of the data of Table 2.18, the values of n_L increase with distance from ground zero.

It was previously mentioned that, for 100 percent retention of the fallout on clover, the predominance of the direct uptake path for animals eating contaminated clover might be on the order of 3500 to 5000 times greater than that of eating new clover on contaminated soil. However, for foliage conditions where the value of n_L is 1.0×10^{-6} and w_L is 10, the factor of predominance for the direct-uptake path is reduced to the order of 35 to 50. Thus the direct-uptake path, at least for exposure times of about a year, can be expected to be the predominating source of an internal hazard to animals and humans after a nuclear war in which land-surface explosions take place.

Figure 2.16
DISTRIBUTION OF ACTIVITY AS A FUNCTION OF PARTICLE DIAMETER FOR LOCAL COLLECTIONS OF FALLOUT FROM TOWER-MOUNTED DETONATIONS

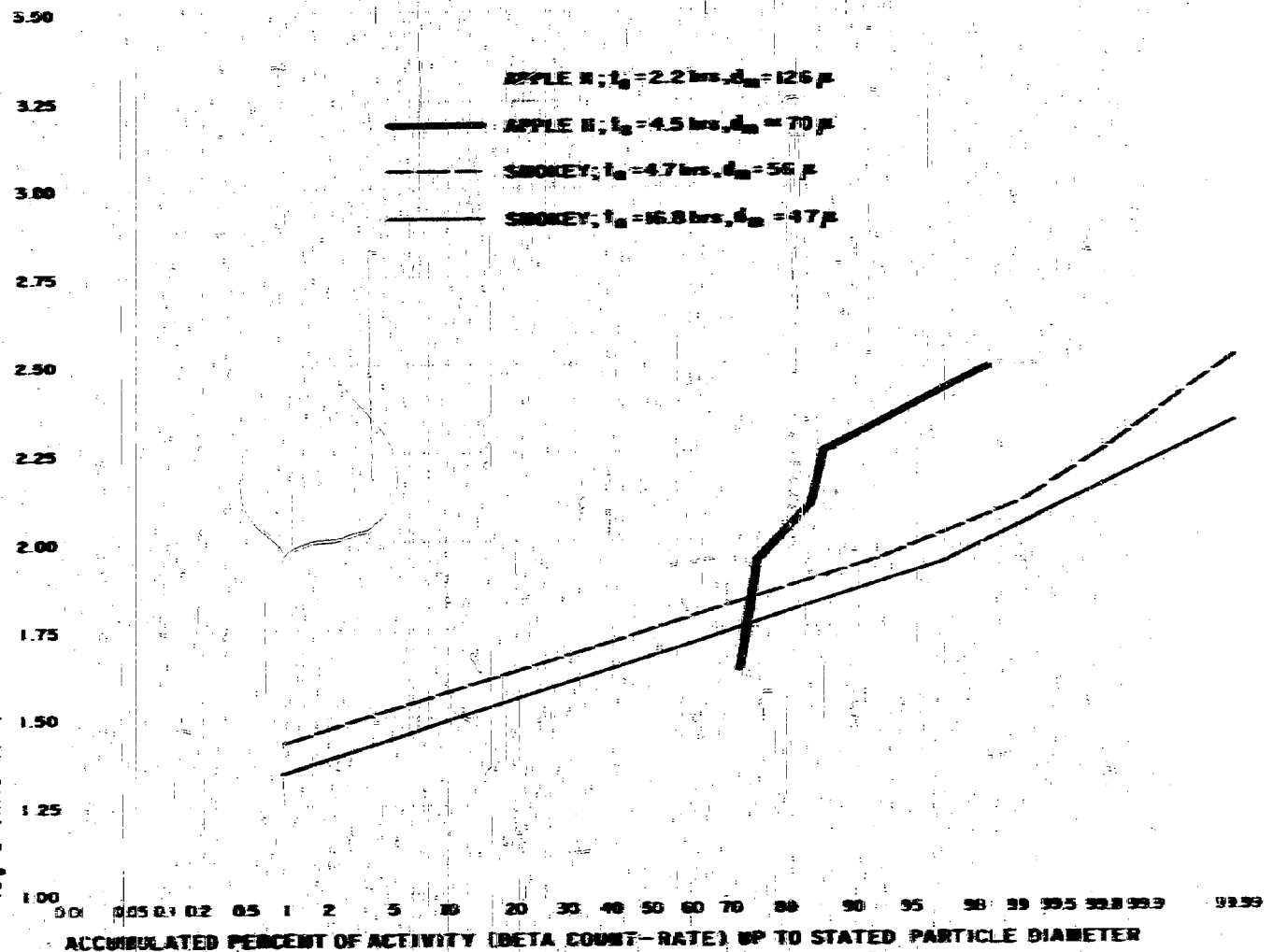

Table 2.15

SIZE DISTRIBUTION AND AMOUNT OF FALLOUT PARTICLES LODGED ON THE FOLIAGE OF DIFFERENT SPECIES OF PLANTS

Quantity	Quantity Value for Designated Plant					
Description of Plant	Artemisia (Sagebrush)	Sphaeralcea (Bushmallow)	Oryzopsis (Bunch Grass)	Alfalfa	Red Clover	Wheat
Nuclear Shot	Apple I	Met	Met	Met	Apple II	Apple II
Yield (KT)	14	22	22	22	29	29
Type of Shot	Tower	Tower	Tower	Tower	Tower	Tower
Height of Burst (ft)	500	400	400	400	500	500
Mid-Height of Cloud (ft)	37,000	35,500	35,500	35,000	36,520	35,500
t_2 (H + hrs)	5.2	4.5	4.5	4.5	2.2	2.2
Particles/cm² of Leaf Surface	10.	34	6.8	5.4	3.6	2.3
Fissions/ft² of Leaf Surface	0.75×10^9	30×10^9	1.1×10^9	1.6×10^9	1.2×10^9	0.75×10^9
Fissions/particle (Average)	0.80×10^5	13×10^5	1.8×10^5	3.3×10^5	3.6×10^5	3.7×10^5
Median Particle Diameter	30μ	35μ	25μ	22μ	33μ	9.4μ
Particle Diameter (μ)	Accumulated Distribution of Particle Size on Foliage (Percent)					
0 to 5	0	0	0	7.5(2.5)[a]	19.6	22.5(21)
0 to 11	0	5.9	5.0	12.5(8)	42.5	57.5(59)
0 to 22	13.2	27.6	30.0	50.0(35)	67.4	80.0(75)
0 to 44	94.6	62.0	80.0	82.5(75)	90.1	92.5(91)
0 to 88	100.0	79.2	95.0	97.5(91)	100.0	100.0(100)
0 to 125		96.4	95.0	97.5(96.3)		
0 to 177		100.0	100.0	100.0(100)		
0 to 250						

a. Numbers in parentheses are average values for all types of foliage at the location

Table 3.15

COLLECTION AND RETENTION OF FALLOUT BY SOME FORAGE CROPS

Quantity	Apple II Shot			Smoky Shot		
Yield (KT)	29			44		
Type of Shot	Tower			Tower		
Height of Burst (ft)	300			700		
Mid-Height of Cloud (ft)	38,500			32,000		
t_a (H + hrs)	0.3	2.2	4.5	4.7	11.8	11.5
X (miles) from ground zero	7	48	106	132	293	329
Y (miles) from lat line	0.6	8.8	24	2.5	8	3.5
Fallout Deposit (fissions/ft^2)	1.07×10^{13}	3.60×10^{12}	1.33×10^{11}	4.25×10^{13}	7.54×10^{11}	4.73×10^{11}
	Fallout Lodged on Plant Foliage (fissions on foliage/ft^2 of soil surface)					
Red Clover[a]	1.33×10^{10}	2.38×10^{10}	1.42×10^{9}	–	–	–
Wheat[a]	2.35×10^{10}	8.55×10^{10}	6.58×10^{9}	–	–	–
Alfalfa[b]	–	–	–	2.10×10^{10}	–	5.61×10^{10}
Mixed Grasses[b]	–	–	–	–	2.83×10^{10}	2.55×10^{10}
	Fraction of Activity (Beta-Count-Rate) Lodged on Foliage					
Red Clover	1.3×10^{-3}	6.6×10^{-3}	1.25×10^{-2}	–	–	–
Wheat	2.2×10^{-3}	2.37×10^{-2}	5.80×10^{-2}	–	–	–
Alfalfa	–	–	–	4.93×10^{-2}	–	0.117
Mixed Grasses	–	–	–	–	3.75×10^{-2}	5.35×10^{-2}
	Surface Density of Foliage (gm. dry plant/ft^2 of soil surface)					
Red Clover	19.6	15.6	15.1	–	–	–
Wheat	33.8	28.6	32.4	–	–	–
Alfalfa	–	–	–	19.2	–	27.9
Mixed Grasses	–	–	–	–	–	16.5
	Accumulated Percent of Activity (Beta-Count-Rate) Up to Stated Particle Diameter For the Fallout Deposited at The Location					
Particle Diameter (μ)						
0 to 44	0.15	15.26	71.67	31.31	71.52	No
0 to 88	0.21	17.42	75.74	92.23	96.36	Fallout
0 to 125	0.29	82.48	94.58	99.87	98.36	Sample
0 to 179	0.39	98.72	98.84	99.81	98.36	
0 to 254	0.45	98.51	98.22	99.96	100.00	
254	100.00	100.00	100.00	100.00		

a. Plants were grown in flats of soil and placed at location 1 day before detonation.

b. Plants were collected from farms in the fallout area.

Table 2.17

THE DECONTAMINATION OF FALLOUT PARTICLES FROM FOLIAGE

Plant	Distance From Ground Zero (miles)	Fraction of Gross Activity Remaining on the Foliage After Decontamination*		
		Reagent		
		Water	0.1N HCL	5% EDTA
1. Shot Met (22 KT on a 400 ft. Tower)				
Larrea (Creosote bush)	29	0.52	0.34	0.33
Lepidium (Peppergrass)	58	0.19	0.10	0.05
Artemisia (Sagebrush)	140	0.64	0.51	0.46
2. Shot Apple II (29 KT on a 500 ft. Tower)				
Broad-leaf annual	7	0.022	0.18	0.28
Coleogyne (Black brush)	7	0.38	0.18	0.58
Triticum (wheat)	45	0.18	0.10	0.19
Artemisia Spinescens (Sagebrush)	45	0.32	0.16	0.17
Artemisia Tridentata (Sagebrush)	48	0.33	0.20	0.14
Chrysothamnus (Rabbit brush)	48	0.38	0.29	0.10
Atriplex (Shadscale)	105	0.26	0.26	0.21
Chrysothamnus (Rabbit brush)	105	0.40	0.26	0.11

a. Based on beta count-rate measurements

Table 2.17 (concluded)

Leaf Surface Properties
Larrea – very-resinous Lepidium – glabrous and glaucous Artemisia – dense, matted, unbranched hairs and glands Broad-leaf annual – smooth, veined, sparse hairs Coleogyne – dense, fine hairs Triticum – rows of short hairs, parallel to veins Chrysothamnus – dense, soft, wooly hairs Atriplex – scurfy surface Ephedra – scale-like, muricated branches Juniperus – scale-like, imbricated Oryzopsis – sparse, barb-like hairs Sphaeralcea – dense, stellate hairs Trifolium (clover) – rough, with scattered, unbranched hairs

Table 2.18

SUMMARY OF AVERAGED FOLIAGE CONTAMINATION FACTORS FOR NATIVE FOLIAGE EXPOSED TO FALLOUT FROM TOWER- AND BALLOON-MOUNTED DETONATIONS AT THE NEVADA TEST SITE

Shot	Distance from Ground Zero (miles)	$10^n \frac{*}{L}$ (fissions/gm of dry plant / fissions/ft^2 of total fallout)	$10^n \frac{*}{L}$ (fissions/gm of dry plant / fissions/ft^2 of ≈44μ fallout)
Tesla, 1955	12	0.008	2.20
	60	0.418	2.21
	79	0.459	2.20
	96	0.524	2.09
Apple I, 1955	12	0.365	2.78
	40	0.522	2.36
	80	0.405	2.02
Met, 1955	20	0.026	18.04
	80	2.07	18.00
	140	2.05	18.28
Apple II, 1955	7	0.002	2.30
	48	0.720	2.32
	106	0.07	2.00
Priscilla, 1957[a]	7	4.80	5.00
	84	2.28	7.27
	129	5.12	6.42
	154	5.20	6.46
	190	4.80	6.16
Diablo, 1957	12	1.91	23.8
	15	1.70	30.0
	30	1.03	17.8
	40	0.25	12.2
	62	12.0	10.5
Shasta, 1957	15	1.52	11.6
	44	1.87	7.72
	76	2.81	5.68
	172	5.10	0.42
Smoky, 1957	48	0.460	2.08
	80	0.070	2.52
	100	0.250	2.85

Table 2.18 (concluded)

Shot	Distance from Ground Zero (miles)	$10^{n}\,a_{T_i}$ (fissions/gm of dry plant / fissions/ft² of total fallout)	$10^{n}\,a'^{k}_{L_i}$ (fissions/gm of dry plant / fissions/ft² of ≈44μ fallout)
	150	0.529	2.70
	158	1.40	3.12
	175	1.20	2.00
	206	0.002	3.28

a. Balloon-mounted detonation

CHAPTER 2 REFERENCES

1. The Effects of Nuclear Weapons, U.S. Government Printing Office, Washington 25, D.C.(1957)

2. Bolles, R. C., and N. E. Ballou, Calculated Abundances of U-235 Fission Products, USNRDL-456, 1956

3. Glendenin, L. E., Technical Report No. 85, Massachusetts Institute of Technology, Cambridge, Mass., 1949

4. Present, R. D., Phys. Rev., 72, 7 (1947)

5. Katcoff, Seymour, Nucleonics, 16, 4, 78 (1958)

6. Steinberg, E. P., L. E. Glendenin, International Conference on The Peaceful Uses of Atomic Energy, 7, 3 (1956)

7. Pappas, A. C., International Conference on The Peaceful Uses of Atomic Energy, Vol. 15, 558 (1958)

8. Wahl, A. C., J. Inorg. Nucl. Chem. 6, 263 (1958)

9. Glendenin, L. E., C. D. Coryell, and R. R. Edwards, Radiochemical Studies: The Fission Products, NNES, Plutonium Project Record, Div. IV, 9, 489, McGraw Hill, New York, N.Y., 1951

10. Herrington, A. C., Massachusetts Institute of Technology, Laboratory for Nuclear Science, Annual Progress Report, p. 87, June 1957-June 1958

11. Miller, C. F., A Theory of Formation of Fallout, USNRDL-TR-425, 1960

12. Adams, C. E., I. G. Popoff, and N. R. Wallace, The Nature of Individual Radioactive Particles, I. Surface and Underground ABD Particles from Operation Jangle, USNRDL-374, 1952

13. Maxwell, Ray D., Project 2.5a-3 Report, Operation Jangle, 1952

14. Schorr, M. G., and E. S. Gilfillan, Project 2.0 Report, Operation Jangle, 1952

15. Alexander, L. T., J. M. Blume, and M. E. Jefferson, Project 2.8 Report, Operation Jangle, 1952

16. Stewart, K., Trans. Faraday Soc. 52, 161 (1956)

17. Pettijohn, F. J., Sedimentary Rocks, Harper Brothers, New York, N.Y., 1949

18. Adams, C. E., The Nature of Individual Radioactive Particles, II. Fallout Particles from M-Shot, Operation Ivy, USNRDL-408, 1955

19. Adams, C. E., N. H. Farlow, and W. R. Schell, Geochimica et Cosmochimia, 18, 18 (1960)

20. Adams, C. E., and J. P. Wittman, The Nature of Individual Radioactive Particles from An ABD of Operation Upshot-Knothole, USNRDL-440, 1954

21. Adams, C. E., and J. D. O'Connor, The Nature of Individual Radioactive Particles. VI. Fallout Particles from a Tower Shot, Operation Redwing, USNRDL-TR-208, 1956

22. Farlow, N. H., Analyt. Chem. 29, 883 (1957)

23. Konjiro Kimura, Geneva Conference on The Peaceful Uses of Atomic Energy, 7, 196 (1956)

24. Mackin, J., P. Zigman, D. Love, D. McDonald, and D. Sam, J. Inorg, Nucl. Chem., 15, 20 (1960)

25. Jones, J. W., and R. T. Overman, AECD-2867, 1948

26. Miller, C. F., and P. Loeb, Ionization Rate and Photon Pulse Decay of Fission Products from The Slow Neutron Fission of U-235, USNRDL-TR-247, 1958

27. Freiling, E. C., Fractionation Correlations, USNRDL-TR-365, 1959

28. Larson, K. H., J. W. Neel, et al., Summary Statement of Findings to the Distribution, Characteristics, and Biological Availability of Fallout Debris Originating from Testing Programs at the Nevada Test Site, UCLA-488, 1960

29. Nishita, Hideo, E. M. Romney, and K. H. Larson, Agricultural and Food Chemistry, 9, 2, 101 (1961)

30. Bellamy, A. W., et al., The 1948 Radiological and Biological Survey of Areas in New Mexico Affected by the First Atomic Bomb Detonation, UCLA-32, 1949.

31. Rainey, C. T., et al., Distribution and Characterization of Fallout at Distances Greater Than Ten Miles from Ground Zero, March and April, 1953, Operation Upshot/Knothole, WT-811, 1954.

32. Lindberg, R. G., et al., The Factors Influencing the Biological Fate and Persistence of Radioactive Fallout, Operation Teapot, WT-1177, 1960.

33. Romney, R. G. Lindberg, H. A. Hawthorne, B. G. Bystrom, and K. H. Larson, Health Physics (to be published).

34. Fuller, R. K., unpublished data, USNRDL, 1960.

35. Heiman, W. T., and R. L. Stetson, unpublished data, USNRDL, 1952.

36. Miller, C. F., Analysis of Fallout Data, II. Radioactive Decay, USNRDL-TR-221, Del. 1958.

37. Dunning, Gordon M., Ed., Radioactive Contamination of Certain Areas in the Pacific Ocean from Nuclear Test Washington, D.C. Atomic Energy Commission, August 1957.

38. Lapp, Ralph E., Local Fallout Radioactivity, Bulletin Atomic Scientists, XV, 5, 191, 1959.

39. Knapp, H. A., External Gamma Doses and Dose Rates from the Fallout from Nuclear Detonations, Civil Defense, Hearings before a Subcommittee of the Committee on Government Operations, U.S. Congress, 1960.

40. Miller, J. R., and R. F. Reitemeier, Rate of Leaching through Soils by Simulated Rain and Irrigation Waters, ARS Report No. 300, 1957.

41. Thornthwaite, C. W., J. R. Mather, and J. K. Nakamura, Science, 131, 1015 (1960).

42. Sartor, J. D., and W. L. Owens, Radiological Recovery of Land Target Components, Complex I and II, USNRDL-TR (in preparation), 1961.

Chapter 3

A THERMODYNAMIC MODEL OF FALLOUT FORMATION

3.1 The Condensation Process

The essential features of the fallout formation process deduced from the final structures, compositions, and general properties of fallout particles as described in Sections 2.3 and 2.4 are that:

1. Some portion of the radioactive elements condenses into liquid particles.

2. Some portion condenses onto the surface of solid particles.

3. If a time limit is placed on the process, some fraction of some of the radioactive elements will be still in the vapor phase.

Even in the case where the bulk carrier is sea water, the first two statements are valid for the fallout from a moderately high-yield detonation near the sea surface, since the temperature of the drops, at the altitude of the cloud, will at some time fall below freezing.

The general condensation process can be divided into two general time periods. The first period of the process is characterized by the presence of gas and liquid phases and the second period by the existence of gas and solid phases. The first period of condensation ends when the bulk carrier particles solidify. There is probably no real precise instant at which this occurs in the fireball since temperature gradients must certainly exist; the different-sized particles cool and solidify at different rates and times.

One most important aspect of the condensation of the radioactive fission products into the liquid phase is that the fission-product elements and compounds are dissolved to form a very dilute solution. Because of this dilution, the solution process can be treated with neglect of (a) surface saturation effects and (b) interactions among the various radioactive elements in the formation of the solution.

In a glassy matrix, i.e., after solidification, the dissolved or compounded fission products should not be able to escape. With concentrations of the order

of 10^{-10} moles of fission products per mole of glass, the vapor pressure would be extremely low and the diffusion of the elements through the solid glass would be very slow.

The fraction of each fission product that is condensed into the liquid carrier particles when they solidify will be determined by (a) the melting point of the carrier and (b) the time after fission at which the solidification occurs. If the melting point of the carrier is high, the fractions that are condensed will be smaller than those in carrier materials having low melting points. For some of the larger particles, the fractions that are condensed will be determined by the time at which solidification of the particle occurs. In the case where the carrier can exist in the liquid state over a relatively large temperature range, and the yield is reasonably large so that fireball does not cool too rapidly, the larger particles can not only enter but can leave the fireball volume before the interior gases cool to the temperature at which the particles solidify.

The fraction of each fission product that is not condensed into the liquid phase of the carrier can still condense on or react with the surface of the solid particles. The solid particles available could consist of (a) the smaller of the melted particles (since these do not fall out of the cloud volume as soon or as rapidly as the larger particles) or (b) of unmelted particles that enter the gas volume at later times.

The best illustration of the latter type of particle is the irregular particles found in the coral fallout. Because of the high melting point of calcium oxide, the number of the more active (fused, spherical) particles found was usually, but not always, smaller than the number of irregular unmelted particles. Even though the fused particles had higher specific activities, they carried a fraction of the total radioactivity produced that was much smaller than the fraction carried by the irregular unmelted particles.

The reverse was true for the particles of the lower-melting silicate glasses. There is no doubt that both unfused and sintered grains of soil and the smaller fused spheres carried radioactivity on their surfaces; various amounts of activity were leached from the samples of these particles in water and dilute acids. However, in the presence of the larger fused spheres in heavy-fallout regions the irregular soil grains contributed only a rather small fraction of the total radioactive content of the fallout deposit.

In the second period of condensation, i.e., after the particles solidify, the fission-product elements may condense by (a) sublimation on the surface of solid particles or (b) they may react directly with the carrier substance. In the case of a more or less open or porous crystal structure, the fission products could diffuse well into the body of the particle. This process was evidenced by the layer of activity in the irregular coral particles.

The previously mentioned vapor-condensation computations using simple kinetic theory, or the more complicated method used by Stewart[1], both indicate that condensation-vaporization equilibrium can be established within a fraction of a second at temperatures around 2000°K. The finding of the small spheres confirms the nature of this early direct vapor-condensation. When equilibrium is established the gaseous species of each fission product element can either (a) react with the vapor or liquid products of the bulk carrier, or (b) dissolve into the liquid phase according to Henry's law of dilute solutions. These solutions of fission product elements or compounds in the liquid phase should be (a) sufficiently dilute to result in no change in the free energy of the liquid carrier, and (b) so dilute that the free energy of solution of each element is independent of the concentration of all other fission-product elements.

3.1.1 Gas-Liquid Phase Condensation

Because of the extreme dilution of the fission product elements in the fallout particles, it is possible to consider the gas-liquid phase condensation and the solubility of each fission product element in the carrier as an independent two-component system. Moreover, there should be no appreciable surface loading (due to large excess surface concentrations during the condensation process) if the temperature range over which the liquid carrier exists exceeds 200 or 300°C. Concentration gradients in particles may occur, however; particles that are not heated very much above the softening temperature and are not very fluid, or larger particles that may not have been melted in their center by the time the surface temperature falls below the melting point, would each contain concentration gradients when solidified.

Two general types of gas-liquid phase condensation processes may be considered. One is Henry's law of dilute solution; the other is compound formation with carrier material. Henry's law of dilute solution is given by

$$p_j = k_j N_j \qquad (3.1)$$

in which N_j is the mole fraction of element j in the liquid phase, k_j is the Henry's law constant, and p_j is the partial pressure of the gaseous species of element j. For a mixture of gases,

$$p_j = N_j^v P \qquad (3.2)$$

in which N_j^v is the mole fraction of the gaseous species of element j in the vapor and P is the total pressure. Combining Eq. 3.1 and 3.2 gives

$$N_j^v / N_j = k_j / P \qquad (3.3)$$

In the thermodynamic treatment, the dependence of k_j on P will be assumed too small for all elements. The dependence of k_j on temperature is described by $k_j^\circ e^{-\Delta H_v/RT}$ where k_j° is a constant and ΔH_v is given by

$$\Delta H_v = \bar{L}_j^\circ - \bar{L}_j \tag{3.4}$$

where $\bar{L}_j^\circ$ is the relative partial molar heat content of element j in the gas phase and $\bar{L}_j$ is its relative partial molar heat content in the liquid phase. For an ideal gas and an ideal solution, ΔH_v is the heat of vaporization of the condensing species of element j.

It may be noted from Eq. 3.3 that a decrease in the total pressure, P, results in an increase in the ratio, N_j°/N_j, or a decrease in the mole fraction of the minor constituent, j, in the liquid phase relative to its mole fraction in the gas phase. Because of this, N_j°/N_j depends on the vapor pressures of the various major constituents in the fireball.

For early time condensations (as would occur with a high-melting-temperature carrier and when the temperature is high and gas volume not fully expanded) the total pressure should also be high. The high pressure would tend to decrease the value of N_j°/N_j. However, the high temperature would tend to increase the value of N_j°/N_j by the term $e^{-\Delta H_v/RT}$. Since both the pressure and temperature decrease with time, the one should tend to cancel or balance the effect of the other on producing changes in N_j°/N_j with time, although over a long period of time the effect of the temperature decrease will generally prevail in the cooling of the fireball.

If the liquid soil particles are assumed to be more or less uniformly distributed throughout the fireball volume, and the temperature is also assumed to be somewhat uniform, then all the liquid particles may be considered as a single liquid phase in contact with the gas at a given temperature and time. Although a given pair of values of P and T at a given time would be valid only for some small increment of the fireball volume, it is obvious that these cannot be given a uniform or average value for the whole volume is assumed in the treatment.

Without specifying the number or size of particles, the mole fraction of element j in the liquid phase is given by

$$N_j = n_j/n(t) \tag{3.5}$$

where n_j is the number of moles of element j dissolved in $n(t)$ moles of liquid carrier where $n_j \ll n(t)$. The mole fraction of element j in the vapor phase is given by

$$N_j^\circ = n_j^\circ/n \tag{3.6}$$

where n_j^o is the number of moles of element j mixed with n moles of vapor and $n_j^o \ll n$.

If the perfect-gas law is assumed for all the gaseous species comprising the n moles of gas, then Eq. 3.6 can be written as

$$N_j^o = n_j^o RT/PV \tag{3.7}$$

Substituting Eqs. 3.5 and 3.7 into Eq. 3.3 gives

$$n_j^o = \frac{n_j k_j}{[n(\ell)/V]\,RT} \tag{3.8}$$

The ratio, n_j^o/n_j, in Eq. 3.8 depends on the values of k_j, T, and $n(\ell)$ per unit volume in the fireball at the time.

Because the mole fractions are small, the value of n_j^o/n_j is independent of the total amount of the element present. Therefore the same fraction of an element should be condensed at a given time and temperature for a 100 percent fission weapon as for a "clean" thermonuclear weapon of the same total yield. The value of $n(\ell)/V$ depends on the total yield and time after detonation, since the amount of carrier material liquefied depends on (a) how the total energy is utilized in the process and (b) the rate of the in-flow and spatial distribution of the carrier material passing through the fireball volume.

Compound formation of an element with the carrier in the gas phase, followed by condensation of the heavier gas molecule into a liquid solution with the melted carrier material, can also be described by use of Henry's Law for the dilute solution. However, when the compound is formed with the (bulk) liquid carrier, then the free energy of formation of the compound and its heat of vaporization must be considered. The over-all reaction for a direct combination of fission product element A with carrier material B to form the compound AB may be written as follows:

$$A(g) + B(\ell) \rightarrow AB(\ell), \text{ dilute solution in } B(\ell) .$$

This reaction may be written as a sum of three or four separate reactions depending on whether the combination of A and B occurs as A condenses or when B is in the vapor phase prior to condensation.

There should be no difference in the two processes with regard to the total change in free energy between the same initial and final thermodynamic

states. The difference, if any, would be in the kinetics of the process. In the first process, the separate reactions and the standard free-energy changes are:

$$1.\quad A(g) \rightarrow A(l) \tag{3.9}$$

$$\Delta F_1^\circ = RT \ln p_A$$

$$2.\quad A(l) + B(l) \rightarrow AB(l) \tag{3.10}$$

$$\Delta F_2^\circ = -RT \ln K_{AB}$$

where K_{AB} is the equilibrium constant for the formation of $AB(l)$ from $A(l)$ and $B(l)$ at the temperature, T. The solution reaction is

$$3.\quad AB(l) \rightarrow AB(l),\ \text{dilute solution in } B(l) \tag{3.11}$$

$$\Delta F_3^\circ = -RT \ln a_{AB}$$

where a_{AB} is the thermodynamic activity of $AB(l)$ in $B(l)$ and is equal to $N_{AB} k_{AB}$ if N_{AB} is the mole fraction and k_{AB} is the Henry's law constant or activity coefficient. The sum of the standard free-energy changes for the three reactions, or the free energy of the over-all reaction, is

$$\Delta F^\circ = RT \ln \frac{p_A}{N_{AB} k_{AB} K_{AB}} \tag{3.12}$$

In the second process, the separate reactions and the standard free-energy changes are:

$$1.\quad A(g) + B(g) \rightarrow AB(g)$$

$$\Delta F_1^\circ = -RT \ln \frac{p_{AB}}{p_A p_B} \tag{3.13}$$

$$2.\quad B(l) \rightarrow B(g)$$

$$\Delta F^\circ = -RT \ln p_B \tag{3.14}$$

$$3.\quad AB(g) \rightarrow AB(l)$$

$$\Delta F^\circ = RT \ln p_{AB} \tag{3.15}$$

$$4.\quad AB(l) \rightarrow AB(l),\ \text{dilute solution in } B(l)$$

$$\Delta F^\circ = -RT \ln N_{AB} k_{AB} \tag{3.16}$$

The sum of the standard free-energy changes for these four reactions is

$$\Delta F^{\circ} \qquad RT \ln \frac{p_A}{N_{AB} k_{AB}} \tag{3.17}$$

The free-energy changes given by Eqs. 3.12 and 3.17 would be equal if $p_A/N_{AB}K_{AB}$ of Eq. 3.12 is equal to p_A/N_{AB} of Eq. 3.17, or if K_{AB} is unity. If the perfect-gas law is used to estimate the number of moles of A, n_A in the gas volume from p_A in Eqs. 3.12 or 3.17 and if N_{AB} is replaced by $n_{AB}/n(\ell)$, the two equations become

$$n_A = \frac{n_{AB} k_{AB} K_{AB} e^{\Delta F^{\circ}/RT}}{[n(\ell)/V]\,RT} \tag{3.18}$$

and

$$n_A = \frac{n_{AB} k_{AB} e^{\Delta F^{\circ}/RT}}{[n(\ell)/V]\,RT} \tag{3.19}$$

respectively. Replacing either $k_{AB}K_{AB}e^{\Delta F^{\circ}/RT}$ (Eq. 3.18) or $k_{AB}e^{\Delta F^{\circ}/RT}$ (Eq. 3.19) by k'_{AB} reduces the two equations to the same form as Eq. 3.8. The same computational treatment would therefore apply except that the standard free-energy functions, when available, could be used to calculate the free-energy change for the compound-formation reactions.

The first compound-formation reaction described above did not include any reaction between the atmospheric oxygen and the element A in the condensation process. Of course, even in the presence of oxygen many of the fission-product oxides are partially or completely dissociated in the vapor phase. For those that are completely dissociated at the temperatures where the carrier material exists as a liquid, the above reaction(s) is applicable. Also, if the oxides are completely associated, A(g) may be taken to represent the oxide molecule, and Eq., 3.18 or 3.19 can be applied. However, for the elements in which the oxide molecule is partially dissociated in the vapor state and associates further with oxygen in the condensed state, the oxygen partial pressure will influence the relative amounts of the element in the liquid and the gas phases.

The over-all reaction for this condensation process is

$$A(g) + xO_2(g) + B(\ell) \rightarrow AO_{2x}B(\ell), \text{ dilute solution in } B(\ell)$$

in which x is the number of oxygen molecules that combine with each atom of

element A. Separate reactions for this over all reaction can be set up in the same way as above, but for this over all reaction to be different from the one above (or competing with it), the gas atoms of A and O_2 must be in equilibrium with the oxide of element A in the vapor state. The oxide molecules then either (a) react with B(ℓ) as they condense or (b) they react with B(g) in the vapor before the larger oxide molecules condense to form the dilute solution. In the first of these two processes, the separate reactions and the standard free-energy changes are:

$$1.\quad A(g) + xO_2(g) \rightarrow AO_{2x}(g) \tag{3.20}$$

$$\Delta F^\circ = -RT\ln p_{AO}/p_A p_O^x$$

$$2.\quad AO_{2x}(g) \rightarrow AO_{2x}(\ell) \tag{3.21}$$

$$\Delta F^\circ = RT\ln p_{AO}$$

$$3.\quad AO_{2x}(\ell) + B(\ell) \rightarrow AO_{2x}B(\ell) \tag{3.22}$$

$$\Delta F^\circ = -RT\ln K_{AOB}$$

where K_{AOB} is the equilibrium constant for the formation of $AO_{2x}B(\ell)$ from the two liquid compounds at the temperature, T.

$$4.\quad AO_{2x}B(\ell) \rightarrow AO_{2x}B(\ell) \text{ dilute solution in } B(\ell) \tag{3.23}$$

$$\Delta F^\circ = RT\ln N_{AOB}\,k_{AOB}$$

The sum of these reactions and their standard free-energy changes give

$$\Delta F^\circ = RT\ln \frac{p_A p_O^x}{N_{AOB}\,k_{AOB}\,K_{AOB}} \tag{3.24}$$

In the second process, the separate reactions and the standard free-energy changes are:

$$1.\quad A(g) + xO_2(g) \rightarrow AO_{2x}(g) \tag{3.25}$$

$$\Delta F^\circ = -RT\ln p_{AO}/p_A p_O^x$$

$$2.\quad AO_{2x}(g) + B(g) \rightarrow AO_{2x}B(g) \tag{3.26}$$

$$\Delta F^\circ = -RT\ln p_{AOB}/p_{AO}p_B$$

3. $$B(\ell) \rightarrow B(g) \qquad (3.27)$$

$$\Delta F^{\circ} = -RT \ln p_B$$

4. $$AO_{x} B(g) \rightarrow AO_{x} B(\ell) \qquad (3.28)$$

$$\Delta F^{\circ} = RT \ln p_{AOB}$$

5. $$AO_{x} B(\ell) \rightarrow AO_{x} B(\ell), \text{ dilute solution in } B(\ell) \qquad (3.29)$$

$$\Delta F^{\circ} = -RT \ln N_{AOB} k_{AOB}$$

The sum of the five standard free-energy changes is

$$\Delta F^{\circ} = RT \ln \frac{p_A p_O^x}{N_{AOB} k_{AOB}} \qquad (3.30)$$

Equations 3.24 and 3.30, when solved for n_A by use of the perfect-gas law, give

$$n_A = \frac{n_{AOB} k_{AOB} K_{AOB} e^{\Delta F^{\circ}/RT}}{[n(\ell)/V] RT p_O^x} \qquad (3.31)$$

and

$$n_A = \frac{n_{AOB} k_{AOB} e^{\Delta F^{\circ}/RT}}{[n(\ell)/V] RT p_O^x} \qquad (3.32)$$

respectively.

The values of n_A in Eqs. 3.31 and 3.32 are sensitive to the oxygen partial-pressure. If p_O is greater than 1 atmosphere, the value of n_A will be decreased (most with largest x value) and the amount of element A condensed is increased. If p_O is less than 1 atmosphere, the value of n_A will be increased (most with largest x value) and the amount of element A condensed is decreased. If p_O^x is incorporated into the k_{AOB} in the same way as was done for the factors of Eqs. 3.18 and 3.19, then Eqs. 3.31 and 3.32 can also be reduced to the same form as Eq. 3.8 for material balance and other general summation formulas.

Equations 3.0 to 3.32 are perhaps more rigorous in the definition of the condensation process than that given by Eq. 3.8 which describes the process only in terms of Henry's law. In a real case, the carrier material is not an inert substance but is capable of forming compounds with many of the fission product elements. Also, the Eqs. 3.0 to 3.32 will be applicable for elements that react with the carrier in the solid state for these, the notations only need be changed from (ℓ) to (s) to refer to the solid rather than the liquid state.

Before considering the second period of condensation, the material-balance equations (in terms of fission yields and fractionation numbers) for the first period of condensation are presented. Although the form of Eq. 3.8 for Henry's law of dilute solution is used in the treatment, the final material balance equations would be identical for the compound-formation processes.

3.1.2 Gas-Liquid Phase Material Balance Constraints and Fractionation Numbers

Since the condensing elements are radioactive, the number of moles of each is constantly changing; therefore the material balance of a given element also changes with time. On the other hand, the fission yield of a given mass chain (except for neutron emitters) is constant. If the amount of a radionuclide of element j and mass number A present at the time, t, after fission is given by $y_{jA}(t)$, then the total amount of element j present at time t is

$$Y_j(t) = \sum_A y_{jA}(t) \text{ atoms or moles} \qquad (3.33)$$

The corresponding sum for the chain yield of mass number A is

$$Y_A = \sum_j y_{jA}(t) \text{ atoms or moles} \qquad (3.34)$$

in which Y_A is constant except for the mass chains containing neutron emitters. The material balance for the amounts element j in the gas and liquid phases is

$$Y_j(t) = n_j^g(t) + n_j(t) \qquad (3.35)$$

where the time dependence of n_j^g and n_j of Eq. 3.8 is indicated.

If n_{jA}^g and n_{jA} are taken for the amounts of each nuclide in the gas and liquid phases, respectively, the material balance for each element is

$$\sum_A y_{jA}(t) = \sum_A n_{jA}^g(t) + \sum_A n_{jA}(t) \qquad (3.36)$$

If k_j^n is used for $k_j / \left[(n(\ell)/V)RT\right]$, substitution of Eq. 3.8 in Eq. 3.36 gives

$$\Sigma_A Y_{jA}(t) \quad (1 + k_j^n)\, \Sigma_A n_{jA}(t) \tag{3.37}$$

and, since $(1 + K_j^n)$ is the multiplier for each of the $n_{jA}(t)$ terms, the terms for each nuclide can be separated out. The separated terms then give the amount of each nuclide condensed, which is

$$n_{jA}(t) = \frac{Y_{jA}(t)}{1 + k_j^n} \tag{3.38}$$

The fraction of the mass chain that is condensed, or the absolute fractionation number (i.e., referred to the fission yield rather than to another nuclide), $r_n(A,t)$, for the end chain-members, is defined by

$$r_n(A,t) = \frac{1}{Y_A} \Sigma_j n_{jA}(t) \tag{3.39}$$

Substitution of Eq. 3.38 and replacing the $Y_{jA}(t)/Y_A$ ratios by $y_j(A,t)$ in Eq. 3.39 gives, for the fractionation number of each mass number,

$$r_n(A,t) = \Sigma_j \frac{y_j(A,t)}{1 + k_j^n} \tag{3.40}$$

in which $y_j(A,t)$ is the fraction of the chain yield of element j having mass number A. According to Eq. 3.40, the fraction of the chain that is condensed in the liquid phase depends only on k_j^n and the fractions of the chain yield of the elements present. The use of this equation, therefore, requires values of the independent yields of each member element of the chain at times from a few seconds after fission, or at least for the time of the end of the first period of condensation that may be applicable to the first group of particles that leave the fireball in the liquid state.

The experimental radiochemical fractionation number for a given sample of fallout (or quantity of mixed fission products) is usually defined as the ratio of the number of atoms of a given mass number that are present to the number of atoms of mass number 99 that are present, divided by the expected value of the ratio for thermal neutron fission of U-235. In mathematical notation, this is

$$R^{99}(A) = \frac{n(a)}{K_n(A)\, n(99)} \tag{3.41}$$

Ordinarily, count-rate ratios are used, along with the appropriate decay corrections from the time of analysis to zero time, with a corresponding value of $K_n(A)$ that has been previously determined from an analysis of a sample of U-235 bombarded with thermal neutrons. For analyses made more than several days after fission, only the last or last two members of a decay chain of most mass numbers will be present in appreciable amount.

Since the observed "R" factors give an over-all measure of variation from U-235 thermal-neutron fission, another factor is needed to account only for that part of the variation that is due to the first period of the condensation process. For this, let

$$r^{99}(A) = \frac{n(A)}{K(A)\, n(99)} \tag{8.42}$$

in which K(A) is the true yield ratio, Y_A/Y_{99}, of mass number A to that of mass number 99, which varies with the kind of fissioning nuclide and incident neutron spectrum (the same definition holds if some mass number other than 99 is selected as the reference nuclide).

The value of the ratio, n(A)/n(99), should be the same as the ratio of the sum over j of the respective $n_{jA}(t)$ terms. The fractionation number from the material balance equations referred to a standard nuclide (in this case mass number 99) becomes

$$r^{99}(A) = \frac{\sum_j y_j(A,t)/(1+k_j')}{\sum_j y_j(99,t)/(1+k_j')} \tag{8.43}$$

when K(A) is replaced with Y_A/Y_{99}. It is possible for $r^{99}(A)$ to have values greater than one; the values of $r_0(A)$ cannot be greater than one.

In the second period of condensation, the fraction of each element not condensed from the gas phase (when the fireball temperature has fallen below the melting point of the carrier material) can begin plating out on the surface of solid particles. The available particles for this period of condensation can be the smaller solidified particles that have not settled out of the radioactive gas volume plus the unmelted soil grains that entered the fireball late and were not heated to their melting temperature.

Although it is possible that a variety of gas-solid state reactions may occur for the different elements, depending on the physical and chemical properties of the carrier particles, only one simple and idealized process is considered here. This is that the fraction of each element that is condensed, up

to some stated time after fission, is related to that element's total sublimation pressure. Further, it is assumed that the carrier surface acts as if it were the pure solid compound of the condensing species. Under these conditions, the computational values of the amounts condensed reflects the relative volatility of the (assumed) constituent gaseous molecules at all temperatures at which this kind of condensation can occur.

If an excess of solid-surface area is presented to the condensing molecules, the number of molecules condensed by the process (assuming the process to be reversible) at any time after the solidification of the carrier is defined by

$$n_j' = n_j^0 - n_j'' \tag{3.44}$$

where n_j' is the amount of element j condensed on the surface of the solid particles, n_j^0 is the amount of the element remaining in the gas phase when the carrier particles solidified, and n_j'' is the amount in the vapor phase at any later time. Because of radioactive decay, all three amounts depend on the time after fission.

If the perfect-gas law is assumed for each gaseous species, then

$$n_j'' = \frac{p_j^s V}{RT} \tag{3.45}$$

where V is the gas volume containing the n_j'' moles and p_j^s is the equilibrium sublimation pressure which, in turn, is given by

$$p_j^s = e^{-\Delta F_s / RT} \tag{3.46}$$

in which ΔF_s is the free energy of sublimation. If uniform mixing in the fireball volume is assumed for the particles and gaseous species at all times, then V is the fireball (or cloud) volume. The time-dependent material balance for element j is

$$Y_j(t) = n_j(t) + n_j'(t) + n_j''(t) \tag{3.47}$$

where n_j is the number of moles condensed in the liquid phase.

Use of Eq. 3.8 for n_j' and Eq. 3.45 for n_j'', combined with Eq. 3.47, gives

$$n_j' = \frac{k_j^0 Y_j}{1 + k_j^0} - \frac{V p_j^s}{RT} \tag{3.48}$$

or, for all mass numbers of a given element,

$$\sum_{\Lambda} n'_{j\Lambda} = \frac{k''_j}{1 + k''_j} \sum_{\Lambda} y_{j\Lambda} = \frac{V}{RT} \sum_{\Lambda} p''_{j\Lambda} \qquad (3.49)$$

Separating out the terms for each nuclide results in

$$n'_{j\Lambda} = \frac{k''_j y_{j\Lambda}}{1 + k''_j} = \frac{V p''_{j\Lambda}}{RT} \qquad (3.50)$$

In this case the partial pressure of each nuclide is proportional to its abundance at the time and is given by

$$p''_{j\Lambda} = (y_{j\Lambda}/Y_j) p''_j \qquad (3.51)$$

The fractionation number of the end-chain member of each mass chain, or, the fraction of the chain that is condensed up to a given time in the second period of condensation, $r'_0(\Lambda,t)$, is defined by

$$r'_0(\Lambda,t) = \sum_j \frac{y_j(\Lambda,t) k''_j}{1 + k''_j} = \frac{V}{RT} \sum_j p''_j(\Lambda,t) \qquad (3.52)$$

in which

$$p''_j(\Lambda,t) = \frac{p''_{j\Lambda}}{0.241 y_\Lambda \beta W} \qquad (3.53)$$

where y_Λ is the fractional chain yield in atoms per fission, β is the ratio of fission to total yield, and W is the total yield in kilotons; the total chain yield is $0.241 y_\Lambda \beta W$ moles.

In Eq. 3.52, the k''_j values are, as in Eq. 3.40, evaluated at the temperature of the end of the first period of condensation; this is different from the temperature, T, in the second term. Thus the fractions of each element not condensed during the first period of condensation (given by the first term of Eq. 3.52) must be decay-corrected to the time of interest to determine $y_{j\Lambda}$ and Y_j applicable to Eq. 3.51.

In assuming the condensation to be independent of the nature of the particle surface, and in neglecting solid-solution-compound or formation with the carrier material, the components and equations for each element have to be reduced by one. Therefore the fractional partial-pressures become yield

dependent, as shown in Eq. 3.53. The dependence of $r_0'(A,t)$ on weapon yield, however, will be determined by the variation of V/W with yield.

In summary, the over-all fallout particle formation process, from the above treatment, may be described as follows. In the first period of condensation, when the liquid and gas phases predominate in the fireball, the more refractory elements are dissolved into the liquid phase of the carrier material. The larger fallout particles, which fall away from the fireball while they are in the liquid state, will contain only these more refractory radionuclides. These particles will land nearest to the point of detonation.

The smaller particles, that stay with the rising fireball for a longer time, may condense out radioelements during both periods of condensation. These, as well as the particles that enter the fireball late, should carry radioelements that were condensed on their surfaces. The smallest of the particles would make up the world-wide fallout or would be deposited at large distances from ground zero.*

The intermediate size particles, that deposit at intermediate distances from ground zero, should contain radioelements that were condensed during both periods of condensation. In fallout of a given particle size in which a fraction of a mass chain had condensed during the first period of condensation and the remainder of the mass chain during the second period, the gross fractionation number of the fallout sample would be given by

$$R_0(A) = x(t') \left[1 - \frac{V}{RT} \sum_i p_i^0(A,t')\right] \qquad (3.54)$$

in which $x(t')$ is the fraction of the element not carried out of the fireball by larger particles prior to t'. No single value of $r_0(A)$ or $r_0'(A)$ would apply to all the particles since the fraction condensed depends on the time period that each particle spends in the gas volume.

3.1.3 Gas-Liquid Phase Condensation--Particle-Size Effects

In the discussion of the condensation processes, some attention must be given to the effect of particle size on the amount of the element condensed. The vapor pressure over the liquid drops can depend on the size of the drop, especially at the higher temperatures. The relationship between

*The world-wide fallout from air, sea water, tower, and surface bursts also contains vapor-condensed particles which have activity more or less uniformly distributed through their volumes.

drop size and vapor pressure is given by

$$RT\ln p/p_0 = 4\gamma M/\rho d \qquad (3.55)$$

in which p_0 is the vapor pressure of the carrier material over the liquid with a flat surface; p is the pressure over the drop of diameter, d; γ is the surface tension of the drop (assumed independent of T); M is the molecular weight of the carrier; and ρ is the density of the liquid. For Al_2O_3 at 2050°C and SiO_2 at 1800°C, the value of γ is 600 dynes/cm and 307 dynes/cm, respectively.[10]

The value of the ratio, p/p_0, for these values of γ is not very different from unity for particles having diameters larger than a few tenths of a micron. Hence, unless the carrier material has a surface tension that is larger than that of these two oxides by more than two orders of magnitude, the increased vapor pressure of the carrier material over the larger drops should not be enough to influence the condensation process.

If the surface tension of the carrier material were extremely large, the fission product elements most likely to be preferentially condensed on the smaller particles are those elements whose volatilities are the same as, or lower than, that of the carrier itself. These would co-condense with the volatilized carrier molecules as soon as the temperature dropped to the carrier boiling point, since at this time the vapor pressure of the carrier material should be a significant fraction of the total pressure. At the melting point of the carrier, its own vapor pressure would be so small a fraction of the total pressure that it could not influence the mole-fraction ratio even if the surface tension were extremely large.

Thus the variations with distance, or with particle size, that are found in the fractionation numbers in the data (see Sections 2.3 and 2.4) must arise from two causes. The first cause is the gradual shift with downwind distance in the mixing of the melted with the irregular particles or of the particles present during both periods of condensation. The second cause is the difference in the period of time that the different-sized particles stay in the gas volume.

For particles with a fairly large range in sizes, the mole fraction, N_i, needs to be precisely defined (see p. 99). Carrier materials such as silicate soils containing metal oxides are refractory materials with low heat conductance. But a particle need not be completely melted throughout its volume in order to condense and dissolve gaseous molecules; only a thin liquid layer on its exterior is required for the process. Because of its low thermal conductivity, some maximum-size carrier particle or group of particles should exist that melts completely when exposed to a given thermal cycle. This partial melting

of the larger particles would limit the penetration of the condensing elements and of those collected through collision with the very small liquid particles.

The penetration of the condensates into the liquid drop, and the rate of distribution of these condensates throughout the volume of the drop, would be more rapid if caused by turbulence and convection rather than by simple diffusion, especially in penetrating or distributing through the peripheral regions of the liquid particles. The general uniformity of the radioactive concentration in the silicate fallout particles--especially from the low-tower shots--indicates that diffusion is not the controlling process. The condensates are often found deposited more or less to a given depth from the surface of the very largest particles and in a more or less uniform concentration throughout the medium-size and smaller particles. Although there are no data for verification, the more volatile elements may form solutions in particles with the larger-surface concentration excesses by condensing in relatively large amounts just as the particles are solidifying.

If the average depth of the surface layer containing the condensates is designated as h and is assumed to be the same for all particles, then the number of moles of carrier per (spherical) particle involved in forming the dilute solution is given by

$$n(r,p) = \frac{\pi\rho h}{M}\left|d(d-2h) + (4/3)h^2\right|, \quad d > 2h \qquad (8.56)$$

in which $n(r,p)$ is the number of moles of the carrier (that was melted) in the surface layer of the particle and d is the particle diameter. For dilute solutions, $n_j(p)$, the number of moles of element j in the particle is given by

$$n_j(p) = N_j \frac{\pi\rho h}{M}\left|d(d-2h) + (4/3)h^2\right|, \quad d > 2h \qquad (8.57)$$

If $n_0(p)$ is taken as the total number of moles of the carrier in the particle, then

$$n_j(p)/n_0(p) = 6.00\, N_j h \frac{\left|d(d-2h) + (4/3)h^2\right|}{d^3}, \quad d > 2h \qquad (8.58)$$

or

$$n_j(p)/n_0(p) = N_j, \quad d \gg 2h \qquad (8.59)$$

The mole fraction in Eq. 3.50 is for the particles that had been completely melted. The relative concentration of the solute, $n_i(p)/n_o(p)N_i$, becomes proportional to $1/d$ for $d > 2h$; this occurrence would be equivalent to the condensation of amounts of activity in proportion to the surface area of the particle.

There are two additional factors that could have some bearing on the relative amount of an element that condenses into the liquid particles. First, the larger particles may fall out of the gaseous volume before they solidify and, second, they may be melted only on one side (not sufficiently melted to form a spherical particle). Both of these two groups of particles would condense smaller amounts of all elements per particle than would be estimated from Eq. 3.58.

The origins of the melted particles in the fireball may be several in number. The small vapor-condensed particles originating from vaporized soil have been mentioned. Others are the particles that were originally lying on the ground out to some distance from shot point, some of which probably are warmed and perhaps melted by the heat absorbed from the radiant energy emitted at detonation. These particles are then drawn into the fireball as it rises.

In low air bursts, where a very small crater is formed, the latter mechanism probably is the dominant process by which particles enter the fireball. In this case the size distribution of the fallout particles that are produced should be the same as the original size distribution of the surface soil. In the detonation, the blast wave would powder the surface layer of soil to some depth and the resulting dust particles, like the surface-melted particles, would retain their size in the formation process. However, these particles would not be melted until after they entered the fireball.

For surface detonations, two other major mechanisms may occur that cause particles to enter the fireball. One is the "jetting" of the soil where the blast or shock wave hits the soil surface; this should occur at very early times after detonation. The soil grains in the jets may be partially heated or even melted by absorption of energy from the blast wave and then vaporized as they penetrate into the hot fireball gases at high velocity. Following this ejection of the surface-layers of soil material, new exposed but thin layers of soil may be melted. It seems reasonable that such a liquid layer of soil would intervene between the vapor in the fireball and the layer of shock-powdered earth as long as the fireball remained in contact with the earth's surface. If enough "fluxing" material (such as the carbonates) is present, a rather large amount of fluid material could be formed. The other major mechanism takes place as the fireball lifts; the liquid is broken up into drops that enter the fireball, followed by

the powdered soil. The mechanical break-up of the fluid mass should produce about the same size distribution of particles from all liquids that have about the same surface tension.

8.2 The Dependence of Fireball Parameters on Weapon Yield and Time After Detonation

A descriptive mathematical model of the fireball--giving its size, temperature, rate of rise, energy content, and other characteristics--is needed to specify the boundary conditions for use in the condensation equations. Specifically, the mathematical description of the fireball should be designed to yield estimates of the quantity, $n(t)/V$, in addition to the others.

The descriptive models presented here, although crude and much oversimplified, are organized to bring together the major parameters that are involved. It should be understood that improvements in the model can be made when more details of the basic data are declassified.

The basic reference data from ENW used here deals mainly with the description of air and/or tower detonations. To develop the model presented in this report for the surface detonation the parameters describing the air burst case were organized first. Then the major differences and similarities in the parameters, for the two types of detonations, were noted or assumed. From these, new parameter values for the surface burst case were established. The air-burst fireball model is identified for a detonation at sea level without an air-soil interface. For the surface burst model presented here, the interface is added.

Condensation reactions occur during the cooling of the fireball; therefore the highest temperature observed in the final cooling curve of the fireball is used as a reference point in temperature and time. This reference point is the time of the second-maximum in the observed (exterior) fireball temperature, which occurs just after the blast wave breaks away from the fireball. At this point the energy of the shock wave has decreased to a level at which it is no longer able to cause incandescence of the air molecules.

The descriptive models are developed according to the following format:

1. At the starting reference time, the fraction of the released energy is specified for:
   a. The fireball
   b. The blast wave
   c. The amount of energy lost by thermal radiation

2. The original state of the materials in the fireball is taken as their standard thermodynamic state at 298°K and 1 atmosphere.

3. Where materials are heated sufficiently to cause dissociation, the energies are calculated as if dissociation occurred at 298°K and as if the dissociated atoms had been heated as ideal gases.

4. The internal energy of the gas atoms in the fireball is utilized or released during cooling by

   a. The heating of inflowing air and/or soil material

   b. The expanding of the gases against the external atmosphere (at 1 atmos)

   c. The radiating of energy into the atmosphere

5. The second reference point for establishing a thermal balance is taken at the time at which the solidification temperature of the carrier occurs.

A more refined treatment would consider these parameters for the whole temperature range over which the liquid carrier material can exist. Also, except for energy lost through radiation, ionization energies are not considered.

The distribution of the released energy for the air burst, according to ENW, p.6, is 15 percent for nuclear radiation, 35 percent for thermal radiation (ENW occasionally terms this thermal energy), and 50 percent for blast and shock. The time or time period after the detonation at which these values apply is not given, nor is energy allotted for the processes enumerated above. Certainly the distribution of the total energy among its various forms is time dependent, and eventually all of the released energy does become thermal or heat energy. But for the purposes of the descriptive model used here, the initial specification of the energy distribution is required for the time of the second temperature maximum. Therefore, of the energy distribution values given by ENW, only the 15 percent for nuclear radiation is assumed to be unavailable for use in other processes. The remaining 85 percent, then, is to be distributed among

1. The energy lost by radiance
2. The energy carried beyond the fireball perimeter by the blast wave
3. The energy content of the fireball.

In making the estimates of the energy distribution among these three quantities, data for the 20-KT air burst from ENW is used. The energy conversion factor, 1.11×10^{19} ergs/KT (calories per kiloton), is adopted so that a 20-KT yield is equal to an energy release of 2.22×10^{19} calories. Of this, 1.80×10^{19} calories is available for division into three parts.

In the following treatment it is assumed that the air molecules in the blast wave as it leaves the fireball move outward at least as fast as the fireball expands; they are not enveloped by the fireball prior to the second temperature maximum. Since these molecules absorb some of the energy in the blast wave, envelopment of a good fraction of them would increase the energy content of the fireball relative to that carried away by the blast wave.

The energy lost from the fireball by radiance prior to the time of the second temperature maximum is estimated to be 8 percent of the total energy (see below). For a 20-KT air burst, the radiant energy lost up to this time is then 1.8×10^{18} calories. This leaves 1.71×10^{19} calories for both formation of the fireball and dispersal by the blast wave.

The energy carried away by the blast wave as it separates from the fireball should consist of

a. The internal energy content of the air molecules expressed as a temperature rise,

b. The compression energy (i.e., the dynamic pressure of the pulse), and

c. The potential energy or work expressed in terms of the outward velocity of the wave. For a 20-KT yield weapon the measured fireball temperature decrease prior to the second maximum (see ENW, p. 60) is taken to be the decrease of the air temperature within the blast wave itself.

The temperature curve in this period of time, expressed as an increase in the air temperature from that of the ambient atmosphere can be represented by

$$\Delta T = 2041 t^{-0.423} \qquad (8.60)$$

for t in seconds and T in °K. For an apparent breakaway time (i.e., the time the blast wave is no longer incandescent) of 0.015 seconds, ΔT is 7800°K. For this temperature rise, the change in internal energy, ΔE, for air is 10,800 calories per molecule.

The peak over-pressures from ENW, p. 100), for a 20 KT air burst can be represented in part, by

$$p = 1.20\times10^{18}\ r^{-2.31}\ ,\ r = 2.4\times10^{4}\ \text{to}\ 5.0\times10^{4} \qquad (3.01)$$

where r is the fireball radius in cm and p is the over-pressure in psi. The variation of the fireball radius with time up to the breakaway (from ENW, p. 65) can be represented by

$$r_{a0} = 1.98\times10^{4}\ t^{0.372}\ ,\ t = 10^{-4}\ \text{to}\ 0.015 \qquad (3.02)$$

for r in cm and t in seconds. At 0.015 second r is 1.04×10^{4} cm, and, extrapolating Eq. 3.01 to 1.04×10^{4} cm, p is 620 psi (42 atmospheres). The corresponding value of the peak dynamic pressures is 1380 psi, which is equal to 2.19 cal/cm^3 (1 psi = 1.65×10^{-3} cal/cm^3). For a temperature of 2100°K (1800°C), the number of moles of gas atoms per cm^3 at a pressure of 42 atmospheres, by use of the perfect gas law, is 2.4×10^{-4}. The energy absorbed by the gas due to the compression is then 9.1×10^{3} cals/mole.

The outward velocity of the blast wave is obtained by differentiating Eq. 3.02 to give

$$v_r = 1.85\times10^{4}t^{-0.628} \qquad (3.03)$$

Using the gross kinetic energy, $1/2\ mv_r^2$, as a measure of the potential work of the wave in moving the air molecules outward, and converting this measure to number of moles of air and to calorie units, the energy content at 0.015 second is

$$q_r = 2.28\times10^{4}n_1 \qquad (3.04)$$

Where n_1 is number of moles of air in the blast wave at the breakaway. The total energy in the blast wave is then approximately

$$Q_1 = 1.09\times10^{4}n_a + 0.91\times10^{4}n_a + 2.28\times10^{4}n_a \qquad (3.05)$$

$$= 4.28\times10^{4}n_a$$

The energy content of the fireball at the second maximum should be equal to the energy utilized in its formation. That is, it consists of

a. The internal energy for a temperature rise to 8000°K (for 20-KT, see ENW, p. 60)

b. The dissociation of a certain number of air molecules

c. The work of expanding the gases to the fireball volume at the second maximum

The thermodynamic first law energy balance for this process, assuming ideal behavior of the gases, is

$$Q_s = (\Delta E_T + \frac{n'}{n} \Delta E_D) n_0 + P_0 V_s = n_0 R T_0 \qquad (3.06)$$

in which n_0 is the number of moles of undissociated air molecules, n' is the number of moles of dissociated atoms, ΔE_T is the change in internal energy, $E_{max} - E_{sea}$, per mole of air molecules for the final mixture of gases, ΔE_D is the average dissociation energy per mole of dissociated atoms, V_s is the fireball volume at the second maximum, $n_0 R T_0$ is a substitution for $P_0 V_0$ where V_0 is the original volume of the heated air molecules, T_0 is taken as 298°K, and P_0 is taken as 1 atmosphere.

From the curve given in ENW, p. 65, for the 20-KT burst, the fireball radius at the second temperature maximum at 0.15 seconds is 620 feet or 1.89×10^4 cm. The volume, V_s, is then 2.83×10^{13} cm^3 and hence $P_0 V_s$ is 6.8×10^{11} cals (1 cal = 41.29 cm-atmos).

The values of ΔE_T, ΔE_D, n_0 and n' depend upon the internal pressure because the degree of dissociation of the oxygen and nitrogen are pressure sensitive. For example, with pure nitrogen where the dissociation reaction is defined by

$$N_2(g) \rightarrow 2N(g) \qquad (3.07)$$

the fraction of the $N_2(g)$ molecules dissociated is

$$x/n_0(N_2) = \frac{K_p^{1/2}}{\sqrt{4P + K_p}}$$

where K_p is the dissociation constant in terms of the partial pressures, $n_0(N_2)$ is the total amount of nitrogen in terms of $N_2(g)$ and x is the amount of $N_2(g)$ dissociated.

The relationship between the fraction of the molecules dissociated in a mixture of gases and the total pressure is more complicated than that given by Eq. 3.67. The equilibrium distribution equations for air, using a mixture of $0.8n_0$ of $N_2(g)$ and $0.2n_0$ of $O_2(g)$, are

$$K_N = \frac{4P^2x^2}{(n_0+x+y)(0.8n_0-x)} \tag{3.68}$$

and

$$K_O = \frac{4P^2y^2}{(n_0+x+y)(0.2n_0-y)} \tag{3.69}$$

in which K_N and K_O are the K_p for nitrogen and oxygen, respectively; x and y are the respective amounts dissociated, and P is the total pressure.

The solution for x and y can be simplified over much of the temperature range of interest from inspection of the thermal data on the two gases shown in Table 3.1. The values of $\bar{H}_T - \bar{H}_{298}$ and K_p were derived mainly from the data of K.K. Kelley[9] and Stull and Sinke.[8] Conversion from the heat content data was made using the relation

$$\bar{H}_T - \bar{H}_{298} = H_T - H_{298} = R(T-298) \tag{3.70}$$

The dissociation constant values indicate that oxygen is almost completely dissociated at 6000°K and above for pressures up to 30 atmospheres. Also, at temperatures below 4000°K, nitrogen is dissociated to a negligible degree. For these two temperature ranges Eqs. 3.68 and 3.69 can be solved to give

$$x/n_0(N_2) = \frac{1.25K_N}{(4P^2+K_N)}\left[\sqrt{1 + 1.6P^2/K_N} - 0.20\right], \quad T \geq 6000°K \tag{3.71}$$

and

$$y/n_0(O_2) = \frac{1.1K_O}{(4P^2+K_O)}\left[\sqrt{1 + 2.2P^2/K_O} - 2/3\right], \quad T \geq 4000°K \tag{3.72}$$

Approximate solutions for the temperature range 4000 to 6000°K and for cases where other gases besides nitrogen and oxygen are present are

$$x = \frac{n_T K_N}{4P} \left[\sqrt{1 + \frac{12.8 P n_o}{n_T K_N}} - 1 \right] \tag{3.73}$$

and

$$y = \frac{n_T K_o}{4P} \left[\sqrt{1 + \frac{3.2 P n_o}{n_T K_o}} - 1 \right] \tag{3.74}$$

where n_T is the total number of moles of gas present. These equations can be solved by a series of approximations. The change in energy content (including dissociation energy and number of moles of gas in heating air as an ideal gas) from the above equations are given in Table 3.2; the E_T-E_{298} values are to be identified with $\Delta E_T - \frac{R}{n} \Delta E_D$ of Eq. 3.66. The fractions of the nitrogen and oxygen molecules dissociated as a function of temperature and pressure are shown in Figures 3.1 and 3.2.

At the temperature of the second maximum of the 20-KT fireball, 8300°K, the curves show, as previously stated, that the oxygen molecules are 100 percent dissociated at pressures up to 20 atmospheres or greater. However, the nitrogen molecules are not; at 20 atmospheres, less than 50 percent are dissociated. And, since the dissociation energy is large, compared to the $C_v dT$ contributions, an estimate of the internal gas pressure (at the second maximum) is needed to obtain a reasonable value of the total change in energy.

Since the fireball volume and temperature at the second maximum are specified, the ratio of the number of moles of gas to the pressure, by assuming the perfect gas law, is

$$n_T / P = 4.15 \times 10^7 \tag{3.75}$$

Figure 3.1
FRACTION OF NITROGEN MOLECULES DISSOCIATED AS A FUNCTION OF TEMPERATURE AND TOTAL PRESSURE

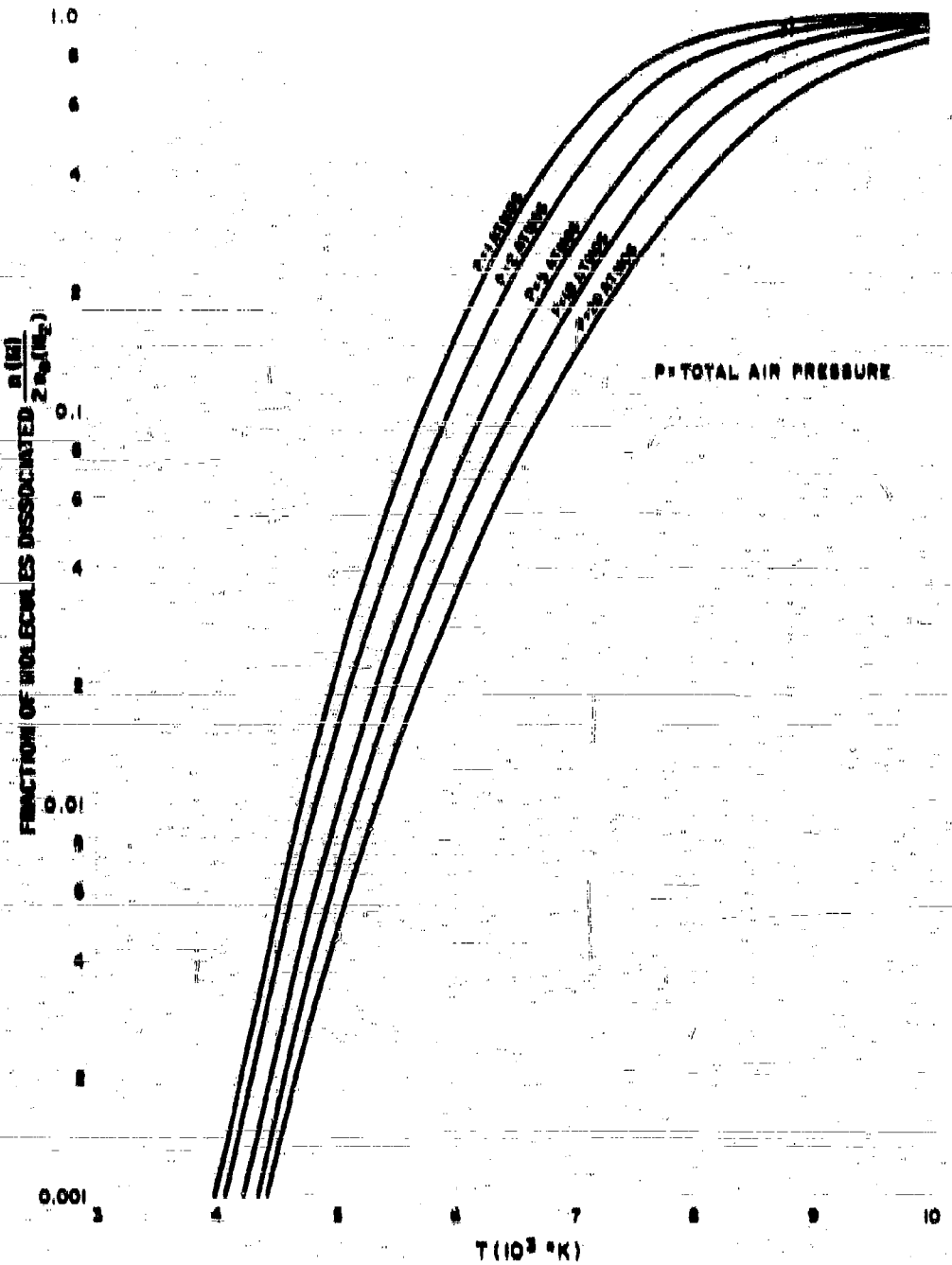

Figure 3.2
FRACTION OF OXYGEN MOLECULES DISSOCIATED AS A FUNCTION OF TEMPERATURE AND PRESSURE

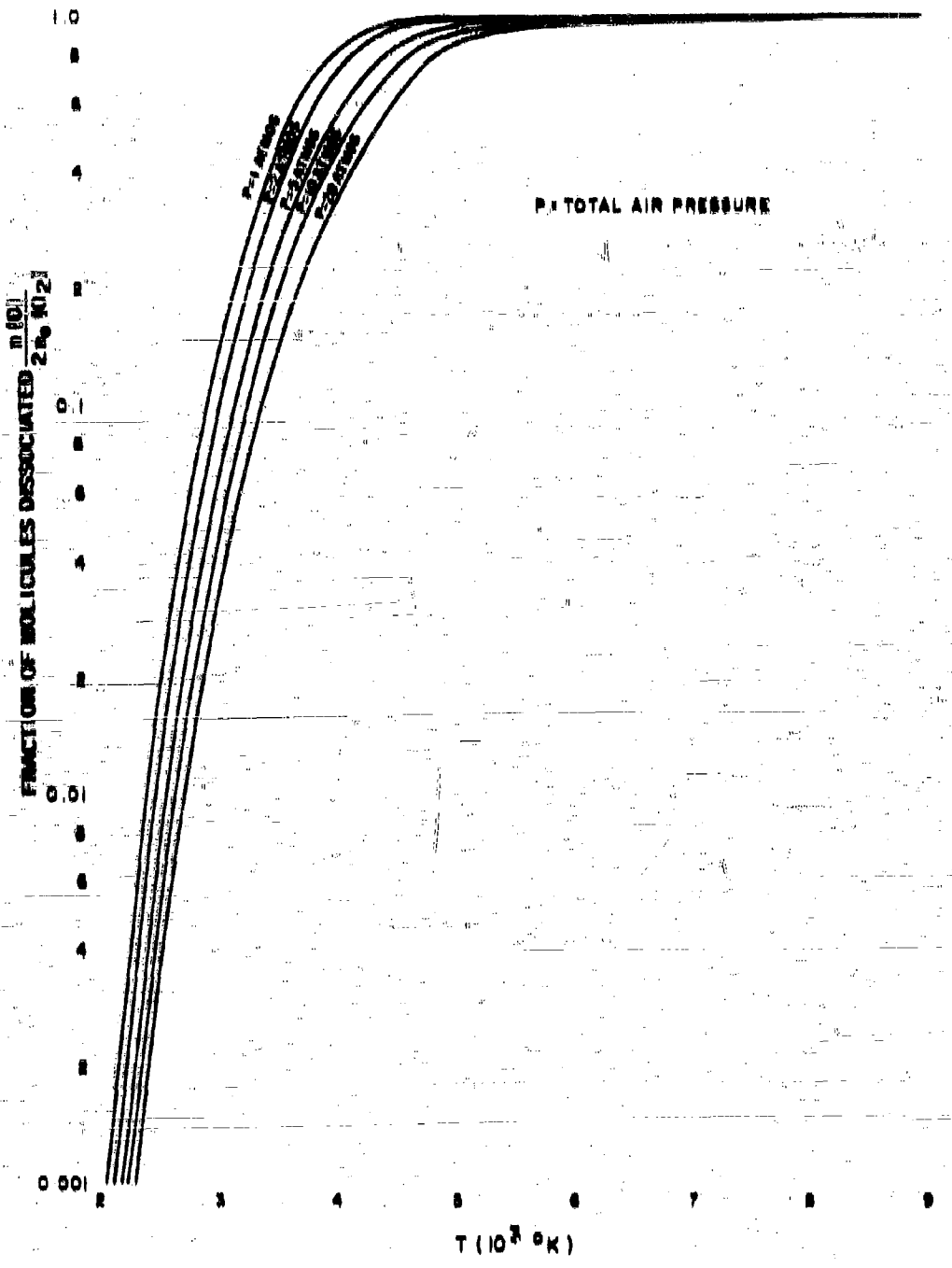

Table 8.1

THERMAL PROPERTIES OF NITROGEN AND OXYGEN AS IDEAL GASES

T°K	N_2 (g)	N(g)	O_2(g)	O(g)	Dissociation Constant, K_p* Nitrogen	Oxygen
298	0	0	0	0	-	-
500	1,001	602	1,055	737	-	-
1,000	3,734	2,092	4,052	2,156	-	-
1,673	7,902	4,101	8,490	4,179	-	-
2,000	10,050	5,085	10,780	5,168	7.94×10^{-20}	4.40×10^{-7}
2,500	13,390	6,568	14,350	6,652	8.35×10^{-14}	2.07×10^{-4}
3,000	16,800	8,069	18,070	8,159	1.66×10^{-10}	1.26×10^{-3}
4,000	23,750	11,190	25,350	11,220	3.10×10^{-6}	2.17
5,000	30,810	14,000	33,010	14,380	1.09×10^{-3}	4.88×10^{1}
6,000	37,850	16,440	42,060	17,650	5.58×10^{-2}	3.84×10^{2}
7,000	44,950	22,510	50,250	21,040	0.970	1.71×10^{3}
8,000	52,250	27,590	58,360	24,000	8.47	5.25×10^{3}
9,000	59,680	32,640	67,350	28,000	4.72×10^{1}	1.24×10^{4}
10,000	67,350	37,390	76,570	31,540	1.85×10^{2}	2.51×10^{4}

a. For reactions $N_2(g) \rightarrow 2N(g)$; $O_2(g) \rightarrow 2O(g)$. Values of ΔH_f° used were 113,240 cal/mole for the heat of formation of N(g) and 58,985 cal/mole for the heat of formation of O(g). The values of ΔE_{298} of formation are 112,085 cal/mole of N(g) and 59,360 cal/mole of O(g).

The other facts seem apparent. First, the fireball is still expanding at the second maximum; therefore, the internal pressure must be greater than 1 atmosphere. Second, the blast wave separated at a pressure of around 40 atmospheres at 0.015 second; therefore the internal pressure of the fireball must be less than this and would have decreased considerably, by both cooling and expanding, up to 0.15 second. For example, the gas volume at the breakaway, from r_{po}, is 4.7×10^{42} cm^3; thus the fireball volume increased by a factor of 8 between 0.015 and 0.15 second so that, on volume expansion alone, the pressure would have decreased from 42 to 6 atmospheres.

The values of the ratio of the total number of gas molecules (associated plus dissociated air molecules) to the number of original (associated) gas molecules, n_g/n_{g_0}, for heating air ($0.8N_2 + 0.2O_2$) from 298 to 8000°K, and the energy change per molecule of the original air molecules along with the compatible values of P and n_p from Eq. 3.75 are shown in Table 3.8.

The total energy required for heating and dissociating the air, $n_g(E_p - E_{298})$, for each value of P shows that all the available energy for both the blast wave and the fireball would be required if the internal pressure were as much as 3.9 atmospheres. In this case, the original volume of the air, according to the perfect-gas law, would be about 2.5×10^{18} cm^3, or about half the volume enclosed by the blast wave at the time of breakaway (4.7×10^{18} cm^3). Since it seems reasonable to assume that the original air molecules at a given location would not be subject to forces tending to move them away from the center of the explosion prior to the arrival of the blast wave, a reasonably good estimate of the original air molecules involved in both the formation of the fireball and in the blast wave packet is that they are those enclosed within the volume of the latter at breakaway. The perfect gas law estimate, for air at 298°K and 1 atmosphere ($V = 4.7 \times 10^{18}$ cm^3), gives the number of air molecules for n_1, the number of air molecules in the blast wave, and n_2, the number of air molecules in the fireball, to be

$$n_1 + n_2 = 1.92 \times 10^{19} \qquad (3.76)$$

The calculated values of n_g are shown in the last column of Table 3.8. A plot of n_p and n_g against the compatible values of P give an intercept at $n_g = 4.37 \times 10^{19}$ moles of air and P = 1.00 atmospheres. At this pressure, $E_p - E_{298}$ is 220,000 cal/mole of air molecules, so that the energy absorbed by the air for the 20-KT yield fireball is 1.01×10^{18} calories. Hence, Q_0 is 1.08×10^{18} calories or 40 percent of the total energy, and Q_1 is 0.80×10^{18} calories or 28 percent of the total energy.

The yield-dependent functions (scaling relationships) for the fireball temperature, radius, and other parameters can be derived from the information given in ENW, pp. 66, 69 and 800-803. In the treatment here some adjustment is made to obtain consistency among the various functions.

The thermal power of the fireball, assuming black-body conditions, is given by

$$P = 1.73 \times 10^{-11}\ T^4\ R^2 \qquad (3.77)$$

for P in calories per second, T in °K, and R, the fireball radius, in cm. The

Table 3.9

THE CHANGE IN ENERGY CONTENT AND NUMBER OF MOLES OF GAS IN HEATING 1 MOLE OF AIR AS AN IDEAL GAS FROM 298°K AND 1 ATMOSPHERIC PRESSURE TO T°K AT PRESSURES OF 1 TO 20 ATMOSPHERES

1. $(E_T - E_{298})$ cal/mole of air*

	Total Pressure, Atmospheres				
T°K	1	2	5	10	20
500	1020	1020	1020	1020	1020
1000	3800	3800	3800	3800	3800
2000	10,210	10,210	10,200	10,200	10,200
2500	15,040	15,030	15,750	15,650	13,650
3000	19,800	19,070	18,340	17,970	17,710
4000	42,700	40,210	36,400	33,770	31,400
5000	67,400	60,110	54,310	52,740	50,000
6000	80,210	79,030	72,520	69,100	66,820
7000	157,500	136,200	113,700	101,100	91,700
8000	231,400	214,000	184,000	161,200	140,000
9000	291,500	256,000	242,000	220,000	204,500
10,000	275,000	274,000	269,700	265,200	251,800
	2. n_n/n_o moles gas/mole air				
2000	1.000	1.000	1.000	1.000	1.000
2500	1.003	1.002	1.001	1.001	1.001
3000	1.021	1.017	1.011	1.008	1.006
4000	1.160	1.150	1.100	1.083	1.065
5000	1.313	1.208	1.195	1.155	1.166
6000	1.512	1.280	1.261	1.230	1.220
7000	1.590	1.501	1.402	1.340	1.305
8000	1.884	1.807	1.070	1.576	1.485
9000	1.974	1.901	1.800	1.721	1.720
10,000	1.993	1.980	1.968	1.940	1.891

*n_o = 0.8n (N_2) 0.2n(O_2); E_T includes energy of dissociation.

Table 3.3

SUMMARY OF VALUES OF THE FIREBALL ENERGY AND GAS CONTENT RELATED TO TOTAL PRESSURE, VOLUME, AND TEMPERATURE FOR HEATING AIR FROM 298°K TO 5301°K

P (atmos)	n_T/n_o (moles gas / mole air)	$E_T - E_{298}$ (cal/mole air)	n_T* (moles gas)	n_o* (moles air)	$n_o(E_T - E_{298})$ (cal)	$n_o(E_T - E_{298})/Q_{1,2}$**	n_2*** (moles air)
1	1.928	242,500	4.15×10^{7}	2.16×10^{7}	5.24×10^{12}	0.319	4.11×10^{7}
2	1.864	229,600	8.30×10^{7}	4.45×10^{7}	1.02×10^{13}	0.622	4.39×10^{7}
5	1.760	205,800	2.08×10^{8}	1.18×10^{8}	2.43×10^{13}	1.48	5.03×10^{7}
10	1.656	182,000	4.15×10^{8}	2.51×10^{8}	4.57×10^{13}	2.79	5.89×10^{7}
20	1.564	159,100	8.30×10^{8}	5.33×10^{8}	8.48×10^{13}	5.17	7.05×10^{7}

* for $n_T = 4.15 \times 10^{7}\ P$

** $Q_{1,2} = 1.64 \times 10^{13} = (Q_1 + Q_2 - 6.5 \times 10^{11})$; $n_o\ (E_T - E_{298})/Q_{1,2} = 1.0$ at 3.33 atmos, where $n_T = 1.38 \times 10^{8}$, $n_o = 7.62 \times 10^{7}$

*** from $n_2 = 8.2 \times 10^{12}\ /\ (E_T - E_{298} - 42,800)$

radiant energy emitted is convenient to use to adjust the desired scaling relationships since experimental measurements indicate that the total amount of energy radiated is, at least approximately, proportional to the released energy. The radiant energy lost up to the time of the second temperature maximum, t_s, is

$$q_l(s) = \int_0^{t_s} P dt \qquad (8.78)$$

A similar expression can be written for $q_s(s)$, the energy radiated from t_s to some later time, t.

Integration to times when incandescence no longer occurs should be equivalent to the total measured amount of radiated energy. Integration of the P/P_s curve given in ENW, p. 330, gives $q_s(s)$ equal to $0.67\ P_s\ t_s$ calories. The value of $q_s(s)$ is found to be given by

$$q_s(s) = P_s t_s \left[0.345 + 1.28 \int_{1.4}^{10} (t/t_s)^{-1.590}\, d(t/t_s) + 10 q_s^{\infty} \right] \qquad (8.79)$$

where P_s is the thermal power at the second maximum, t_s is the time of the second maximum, and $10\ q_s^{\infty}$ is the energy radiated after $t/t_s = 10$. The second term of Eq. 8.79 was derived from the curve of ENW and gives a fairly precise representation of the P/P_s curve between the t/t_s values of 1.4 and 10. By use of Eq. 8.77, it can be written

$$T^4 R^2 = 1.28 T_s^4 R_s^2 (t/t_s)^{-1.590}, \quad 1.4 \leq t/t_s \leq 10 \qquad (8.80)$$

If R is assumed to be constant in this interval of time and equal to the maximum fireball radius, R_m, then we have that

$$R_m = 1.13 R_s \quad , \quad 1.4 \leq t/t_s \leq 10 \qquad (8.81)$$

and

$$T = T_s (t/t_s)^{-0.398} \quad , \quad 1.4 \leq t/t_s \leq 10 \qquad (8.82)$$

However, the curve of temperature with time given in ENW (p. 69) is represented only approximately by Eq. 3.82 in this relative time period when plotted against t/t_q using 0.15 seconds for t_q.

On the other hand, for t/t_q values greater than 10 the temperature curve is well represented by a function of the form $T_o \exp(-kt/t_q)$, (T_o and k being constants) which joins smoothly to the curve from earlier times. This suggests that, for times greater than t/t_q of 10, an exponential temperature-time function should give a better representation of the temperature variation with time than Eq. 3.82. The function, fitted to join Eq. 3.82 smoothly at $t/t_q = 10$ is

$$T = 0.595T_q' e^{-0.0398t/t_q} \quad , \quad t/t_q \geq 10 \tag{3.83}$$

The value of $10q_q'$ can be evaluated by use of either temperature equation by noting that, experimentally, q is not measurable at temperatures lower than about $0.1T_q$ (i.e., between 600 and 1000°K) when the assumption is made that the fireball radius remains constant for a very long period of time. When $0.1T_q$ is substituted for T in Eq. 3.82, t/t_q is 326 and with Eq. 3.83, it is 45. The times for the temperature to drop to $0.1T_q$ for a t_q of 0.15 seconds (20-KT) are 49 seconds and 7 seconds, respectively. Because of the obvious overestimate, from use of Eq. 3.82, of the time for the temperature to fall to $0.1T_q$ a high value of $10q_q'$ would result from its use even without considering an increase in the fireball radius after $10t_q$.

However, in proceeding further with these assumptions, it is found that the two respective values of $10q_q'$ are $0.48P_q t_q$ for Eq. 3.82 and $0.51P_q t_q$ for Eq. 3.83, indicating that Eq. 3.82 would give about twice as much radiant energy emitted after $10t_q$ as would Eq. 3.83. The total energy radiated is then

$$q_T(a) = 2.61P_q t_q \tag{3.84}$$

by use of Eq. 3.82 for T from $t/t_q = 10$ to 326 or

$$q_T(a) = 2.36P_q t_q \tag{3.85}$$

by use of Eq. 3.83 to T from $t/t_q = 10$ to 45.

If the information of ENW (p.331) is used to solve for the coefficient of $P_g t_g$, with q_T equal to W/3, a coefficient of 2.60 is obtained; this corresponds to the result of Eq. 3.84 with the excessively large value of $10q_n$". The coefficient of $P_g t_g$ can be solved with respect to the total available energy by $q_T(a)$ equal to $1.11\times10^{12} f_\eta W$ in calories, where f_η is the fraction of the total energy released. For P_g in terms of R_g and T_g, the above equations can be rearranged to give

$$f_\eta = 1.56\times10^{-28}\ T_g^4 R_g^2 t_g a W^{-1} \qquad (3.86)$$

where a is the coefficient of $P_g t_g$ in Eqs. 3.84 and 3.85. If the previously used values, $R_g = 1.89\times10^4$ cm, $T_g = 8800$°K, $t_g = 0.15$ seconds, and W = 20-KT, are substituted, f_η is then 0.198 a so that for an a value of 2.65, f_η is 0.52 and for the value of 2.36 it is 0.47. The value of a, 2.60, calculated from the ENW data by using an f_η value of 0.888 to begin with, gives back the value, 0.515, for a. It may be concluded from this value that the curves for R and T for the 20-KT yield and the information on q_T, P_g, and t_g as given in ENW are not consistent.

The dependence of T_g on yield can be evaluated by rearranging Eq. 3.86 to give

$$T_g^4 R_g^2 t_g = 6.41\times10^{27} f_\eta\ W/a \qquad (3.87)$$

If the values of R_g (= $R_m/1.15$), t_g, T_g, and a obtained from ENW are substituted, the value of T_g is found to be 8800 $W^{-0.075}$. This function gives a T_g value of 8800°K for a 20-KT yield and of 4250°K for a 1-MT yield. Thus, T_g, as derived from the ENW scaling functions, is 1900° lower than the "observed" curve in ENW for the 20-KT yield and decreases much too rapidly with yield.

To obtain more reasonable and more internally consistent information for use in the idealized air burst fireball model, the various parameter functions from ENW were adjusted to a set that was consistent with respect to their functional form and numerical values. The resulting set of functions was derived from the energy utilizations given by

$$q_T(a) = 0.50\ W\ KT \qquad (3.88)$$

$$q_1(a) = 0.08\ W\ KT \qquad (3.89)$$

$$q_2(a) = 0.42\ W\ KT \qquad (3.90)$$

$$Q_2 = 0.49\ W\ KT \qquad (3.91)$$

The utilization of the fractions of the total energy (0.25 for blast, 0.15 for nuclear radiation, and 0.57 in the fireball up to the second maximum, including the 0.08 lost by radiation up to that time) leaves, from the above separations, 0.07 of the total energy for such processes as heating and mixing of air that enters the fireball after the second maximum and for expansion of the heated gas against the atmosphere.

The expansion of the fireball from t_s to time of maximum expansion, t_m, is represented by the ratio

$$R_m/R_s = 1.24 \tag{3.92}$$

This ratio is the value obtained from the data for the 20-KT yield in ENW and replaces the value derived from the P/P_s function.

The radiant energy from Eq. 3.88 in terms of $P_s t_s$, is given by

$$q_T(a) = 2.52\, P_s t_s \tag{3.93}$$

in which

$$q_1(a) = 0.40\, P_s t_s \tag{3.94}$$

$$1.0q_1^{10}(a) = 1.68\, P_s t_s \tag{3.95}$$

$$10q_1^{\infty}(a) = 0.44\, P_s t_s \tag{3.96}$$

The $P_s t_s$ multiplier for $q_1(a)$ was reduced from 0.57 to 0.40 so as to retain about the same ratio between $q_1(a)/q_T(a)$ as that given in ENW. The value of $1.0q_1^{10}(t/t_s = 1$ to 10) was increased by a factor of 1.2 due to the change to the R_m/R_s ratio given in Eq. 3.92. The remainder of the 2.52 is the multiplier for $10q_1^{\infty}$. Since the temperature decrease after about $10t_s$ is probably better described by Eq. 3.88 than Eq. 3.82, the larger multiplier for $10q_1^{\infty}(a)$ can only be obtained by accounting for an increase in the fireball radius with t/t_s after $10t_s$. A suitable function for such a variation of the fireball radius with t/t_s, when selected for convenience of integration as well as for expressing an appropriate acceleration of volume expansion, is

$$R = 0.71\, R_m\, e^{0.035t/t_s}, \quad 10 \leq t/t_s < 45 \tag{3.97}$$

when the constants are evaluated. A function of this form must be restricted as an estimate of the fireball radius for t/t_s values less than 45. In this time period, T will decrease to the order of $0.1T_s$ and the increase in R is about a factor of 3.5.

The increase in the mean cloud radius to essentially full expansion at 6 to 8 minutes is between 8000 to 10,000 times R_m. In the model air burst, the fireball radius increases from R_0 at t_0 to R_m at $1.4t_y$, remains constant from $1.4t_y$ to $10t_y$ and then begins to increase again to form the large cloud about the time the incandescence disappears.

The relation among T_y, R_y, t_y and W, using 0.50 W for q_T (a), is

$$T_y^4 R_y^2 t_y = 1.27 \times 10^{20} W \qquad (3.98)$$

in which

$$T_y = 10^4 W^{-0.020} \ ^\circ K \qquad (3.99)$$

$$t_y = 0.050 W^{0.413} \text{ sec} \qquad (3.100)$$

and

$$R_y = 5.04 \times 10^4 W^{0.333} \text{ cm} \qquad (3.101)$$

In obtaining the above functions, the first assumption is that the 50 percent of the energy lost by radiation is independent of yield. The corollary assumption is that the fireball volume is proportional to the yield, or that simple geometric scaling applies. The remaining residual difference in the exponent on W, namely 0.167, was distributed in equal parts to t_y and T_y^4 (using the ENW dependence of t_y as being proportional to $W^{0.5}$ to start with) and that, for Q_y and $q_T(a)$ to be directly proportional to the yield, T_y should be almost independent of yield.

The coefficient for T_y was taken from a logarithmic extrapolation of the temperature curve in ENW for the 20-KT yield along a line with the slope, -0.4, and using the temperatures from the curve between the t/t_y values of 3 and 8. The coefficient for t_y was obtained by adjusting the values of t_y from the ENW curve to give the same percentage difference at yields of 20-KT and 1-MT. In doing this, t_y for 20-KT is increased from 0.15 to 0.17 second and for 1-MT it is decreased from 1.0 to 0.80 second. The coefficient of R_y was finally derived from Eq. 3.98.

The corresponding values of the fireball parameters of interest are:

$$T = 10^4 W^{-0.020} (t/t_y)^{-0.398} \ ^\circ K, \quad t_y \leq t \leq 10t_y \qquad (3.102)$$

$$T = 4.04 \times 10^3 W^{0.144} t^{-0.398} \ ^\circ K, \quad t_y \leq t \leq 10t_y \qquad (3.103)$$

$$T = 5.95\times10^{3}W^{-0.020}\exp(-0.0398t/t_{\mu})\ ^{\circ}K\ ,\ t \geq 10t_{\mu} \qquad (3.104)$$

$$= 5.95\times10^{3}W^{-0.020}\exp(-0.79^{n}W^{-0.413t})\ ^{\circ}K\ ,\ t \geq 10t_{\mu} \qquad (3.105)$$

$$t_m = 0.070W^{0.413}\ \text{sec} \qquad (3.106)$$

$$R_m = 6.28\times10^{3}W^{0.333}\ \text{cm}\ ,\ t_m \leq t \leq 10t_{\mu} \qquad (3.107)$$

and

$$R = 4.41\times10^{3}W^{0.333}\exp(0.70W^{-0.413t})\ \text{cm}\ ,\ 10t_{\mu} \leq t < 45t_{\mu} \qquad (3.108)$$

The adjustments, in general, result in a displacement or shifting of the parameter values between 10 and 25 percent from those given in ENW, except for the fireball radius. For example, the adjusted values of the radius R_m are 10 percent less at 1-KT and 44 percent less at 1-MT than those given by the ENW functions. This decrease in the radius from that of ENW is in agreement with the observations of other authors. Lapple[4], for example, writes that the true fireball radius may actually be as small as half of that given in ENW.

3.3 Estimates of Fireball Parameters for a Model Surface Burst on a Soil Consisting of Silicate Minerals

The fireball parameter scaling functions for the model surface detonation are derived on the basis of assumed differences or similarities with the fireball from the model air burst. In this model, the soil-air interface is introduced.

The main assumptions used in the derivation of the parameter scaling functions are:

1. In the model surface burst, half the energy in the fireball at the second maximum is used to heat, dissociate, and expand the gas molecules from the air and half the energy is used to vaporize, dissociate, and expand the gaseous products from the soil;

2. The vapor density of the fireball at the time of the second temperature maximum is the same for both air and surface types of bursts;

3. The blast and shock wave carry away 28 percent of the released energy (as for the air burst), and 15 percent of the fission yield goes into nuclear radiation;

4. The fireball volume at the second maximum for the surface burst is the same as that of the air burst except that it has a hemispherical rather than spherical shape.

Taking the last assumption first,

$$R_s(s)/R_a(a) = 2^{1/3} = 1.26 \qquad (3.109)$$

where R_s (s) is the fireball radius for the surface burst and R_a (a) is that for the air burst. The ratio of the energies radiated into the air space around the two fireballs at the time of the second maximum is

$$q_s(s)/q_a(a) = 0.794 \left[T_s(s)/T_a(a)\right]^4 \qquad (3.110)$$

where q_a (a) is the radiated energy and T_a (a) is the temperature at the second maximum for the surface burst, and q_a (a) and T_a (a) are for the air burst. But since much of the energy is lost before the second maximum occurs and at much higher temperatures, before the blast wave breaks away, the amount lost by radiation up to this time should be insensitive to the ratio of the two values of T_a. Therefore, the fraction of energy radiated into the air space is taken to be 0.8x8 percent, or 6 percent.

The total surface area of the surface burst fireball under the equal volume assumption is 1.19 times that of the air burst, so that the amount radiated through all surfaces would be nearly 10 percent of the total energy with 4 percent of this amount being radiated into the ground surface. However, since the whole bottom of the fireball is in direct thermal contact with the ground, some additional energy would be absorbed by the latter. An additional 5 percent is therefore assumed to be lost, or not contained within the gaseous phase of the fireball at the second maximum. With these assumptions, the model surface burst fireball contains 49 percent of the released energy at the time of the second temperature maximum.

The assumption of equal vapor densities and fireball volumes leads to the equality of the number of gas molecules heated to the respective values of T_a per unit of yield, since the fireball volume scaling function is proportional to the yield. The combination of all the assumptions permits the estimation of T_s (s) for the surface burst.

The first law of thermodynamics for the utilization of 49 percent of the released energy in heating air as an ideal gas, in the model air burst, is

$$Q_a = n_a(E_T - E_{298}) + p_a(V_a - V_s) \qquad (3.111)$$

in which n_a is the number of moles of air heated to T_1 (a), $E_T - E_{298}$ is the change in energy, including dissociation, of the air molecules in cal/mole of air, p_a is the external pressure (1 atmos.), V_1 is the volume of the fireball at second maximum, V_a is the original volume of the air molecules, and t_2 is 5.44×10^{11} W cals (for W in KT). For a spherical fireball, V_1 from Eq. 3.111 is

$$V_1 = 5.36 \times 10^{11} \text{ W cm}^3 \qquad (3.112)$$

With the ideal-gas law, $p_a V_a$ is replaced by $n_a RT_a$ or 592 n_a cals. Also, $p_a V_1$ is equal to 1.3×10^{11} W cals. Replacing the appropriate equalities in Eq. 3.111 results in

$$n_a/W = \frac{5.31 \times 10^{11}}{(E_T - E_{298} - 592)} \text{ moles air/KT} \qquad (3.113)$$

Assuming the perfect gas law to estimate the number of moles of gas in the fireball results in

$$n_T/W = 6.53 \times 10^3 W^{0.02} p_2 \text{ moles/KT} \qquad (3.114)$$

when Eqs. 3.00 and 3.112 are substituted for T_1 and V_1, respectively; p_2 is the total internal pressure at t_2. Combination of Eqs. 3.113 and 3.114 gives

$$n_T/n_a = 1.23 \times 10^{-8} W^{0.02} p_2 (E_T - E_{298} - 592) \qquad (3.115)$$

in which the compatible values of n_T/n_a, p_2, and $(E_T - E_{298} - 592)$ are obtained from the thermal data on air at a given temperature and can be determined by calculating p_2 of Eq. 3.115 and then plotting the calculated values as a function of p; the equation is satisfied at the point where $p = p_2$. A single value of p results for each selected value of W. The solutions of Eq. 3.115 for different values of W are shown in Table 3.4 along with the corresponding values of n_T/W.

In order to make a similar computation for the model surface burst, the thermal properties of an "ideal" soil must be specified. For this, the thermal properties of the mineral albite or anorthoclase ($Na_2O \cdot Al_2O_3 \cdot 6SiO_2$), with a selected melting point of 1400°C, are assumed. One mole of the soil, upon complete dissociation, produces 26 moles of gas atoms; the molecular weight of the compound is 524 and its heat of formation at 298°K is 1,800 kcal/mole.

Table 3.4

SUMMARY OF VALUES OF n_g/W AND p_g FOR THE MODEL AIR BURST

W(KT)	T_g (°K)	P_g (atmos)	n_g/W (moles/KT)
1	10,000	5.90	3.80×10^{0}
10	9,550	5.85	4.00×10^{0}
10^{2}	9,120	5.79	4.14×10^{0}
10^{3}	8,710	5.76	4.32×10^{0}
10^{4}	8,320	5.80	4.00×10^{0}
10^{5}	7,940	6.11	5.03×10^{0}

The data of K.K. Kelly[8] and Stull and Sinke[9] were used to calculate the energy changes of the following reactions at 298°K:

$Na_2O{\cdot}Al_2O_3{\cdot}6SiO_2(c) \rightarrow 2Na(c) + 2Al(c) + 6Si(c) + 8O_2(g)$, $\Delta E = 1{,}798{,}000$ cal/mole

$2Na(c) \rightarrow 2Na(g)$ $\Delta E = 50{,}520$ cal/mole

$2Al(c) \rightarrow 2Al(g)$ $\Delta E = 150{,}820$ cal/mole

$6Si(c) \rightarrow 6Si(g)$ $\Delta E = 926{,}400$ cal/mole

$8O_2(g) \rightarrow 16O(g)$ $\Delta E = 948{,}080$ cal/mole

$Na_2O{\cdot}Al_2O_3{\cdot}6SiO_2(c) \rightarrow 2Na(g) + 2Al(g) + 6Si(g) + 16O(g)$ $\Delta E = 3{,}577{,}000$ cal/mole

$= 157{,}700$ cal/mole of gas atoms

Where appropriate, the heat content data were corrected to ΔE by subtraction of the quantity ΔnRT, Δn being the change in the number of moles for the gaseous species. The values of $E_T - E_{298}$ for the ideal soil, and some of its decomposition products at higher temperatures, are given in Table 3.5. The values for the soil composition assume complete dissociation of all the oxide products and of the oxygen molecule.

The first law of thermodynamics for the conversion of 42 percent of the released energy, for the model surface burst at the second temperature maximum, is

$$4.66\times10^{11}\ \text{W} = n_0\,(\Delta E_a - 592) + n_s \Delta E_s + 1.30\times10^{10}\ \text{W} \qquad (5.116)$$

In which ΔE_a and ΔE_s are the $E_p - E_{298}$ values, including dissociation, for the air and soil, respectively; n_s is the number of gas atoms from the soil, and 1.30×10^{10} W is the $p_0 V_0$ term as before. According to the definition of the ideal surface burst, the equal portions of the energy for heating soil and air that remain after subtraction of $p_0 V_0$ are

$$2.266\times10^{11}\ \text{W} = n_0\,(\Delta E_a - 592) \qquad (5.117)$$

and

$$2.266\times10^{11}\ \text{W} = n_s \Delta E_s \qquad (5.118)$$

Since the oxygen molecules are essentially all dissociated at the temperatures of interest, n_0 and ΔE_a can be determined for given temperatures, as they were in the case of the air burst, by estimating $n_s(g)$, the number of moles of gas from the air, on assumption of the perfect gas law. In this case

$$n_s = \frac{p_s V_0}{R T_s(s)} = 6.53\times10^{9}\ \text{W}\, p_s / T_s(s) \qquad (5.119)$$

where p_s is the sum of the partial pressures of $N_2(g)$, $N(g)$, $O_2(g)$, and $O(g)$ from the original air, and $T_s(s)$ is the temperature at the second maximum. Combining Eqs. 5.117 and 5.119 gives

$$n_s/n_0 = 2.88\times10^{-2}\ p_s(E_a - 592)/T_s(s) \qquad (5.120)$$

The values of n/W, given by

$$n/W = n_s/W + n_a/W \qquad (5.121)$$

were determined at several assumed values of $T_s(s)$. The values of $T_s(s)$ for different values of W were then determined, from a smoothed plot of n/W vs $T_s(s)$, by reading off $T_s(s)$ at the corresponding n/W values for the air burst for each yield. The results of these calculations are summarized in Table 5.6.

Table 3.5

THERMAL DATA FOR IDEAL SOIL CONSTITUENTS OF COMPOSITION $Na_2O{\cdot}Al_2O_3{\cdot}6SiO_2$, cal/mole

$E_T - E_{298}$, cal/mole

T(°K)	Na (g)	Al (g)	Si (g)	Soil Composite[b]	Soil Composite[c]	Soil (c)	Soil (g)
298	0	0	0	0	0	0	0
300						22,780	23,160
1,000						92,440	94,440
1,100						107,440	110,100
1,200	2,085	2,720	2,770			122,080	126,700
1,300						136,120	143,300
1,400	3,285	3,920	3,985			150,720	160,180
1,500						160,440	177,460
1,600	3,880	5,015	4,005			185,240	195,100
1,700						201,080	213,300
1,800	4,475	4,515	4,040				
2,000	5,080	5,110	5,285				
3,000	8,000	8,100	8,050				
4,000	11,410	11,080	12,100				
5,000	15,080	14,150	15,700	14,770	152,500		
6,000	22,420	17,450	19,240	18,360	180,100		
7,000	30,500	21,020	22,780	22,420	100,100		
8,000	40,000	20,130	26,500	27,040	104,700		
9,000	72,910[a]	32,010[a]	30,510[a]	32,020[a]	179,100[a]		
10,000	100,700[a]	41,700[a]	36,100[a]	38,080[a]	170,400[a]		

a. Estimated from extrapolation of heat capacity data

b. Cal/mole gas atoms basis, gas at 298°K

c. Cal/mole gas atoms basis, $Na_2O{\cdot}Al_2O_3{\cdot}6SiO_2$ (g) at 298°K

Table 3.6

SUMMARY OF CALCULATIONS FOR $T_s(s)$ BASED ON THE ASSUMPTION OF EQUAL VAPOR DENSITIES AT THE SECOND TEMPERATURE MAXIMUM FOR THE MODEL AIR AND SURFACE-BURST FIREBALLS

$T_s(s)$ (°K)	p_s (atmos)	n_s/W (10^{11} moles/KT)	n_s/W (10^6 moles/KT)	n/W (10^5 moles/KT)	W (KT)
6000	3.54	3.60	1.462	5.31	--
6300	3.35	3.40	1.441	4.90	--
6600	3.14	3.11	1.430	4.54	--
6900	2.96	2.74	1.419	4.16	--
7200	2.07	2.42	1.407	3.85	--
7140	2.72	2.48	1.41	3.80	1
7080	2.81	2.58	1.42	4.00	10
6910	2.80	2.72	1.42	4.14	10^2
6770	3.00	2.89	1.43	4.32	10^3
6550	3.17	3.17	1.40	4.60	10^4
6220	3.40	3.58	1.44	5.02	10^5

The derived $T_s(s)$ values are represented quite well from 10^2- to 10^4-KT by the scaling function

$$T_s(s) = 7200\ W^{-0.010}\ °K \qquad (3.122)$$

for W in KT. It should be noted that this equation is used in estimating $T_s(s)$ in all following computations rather than the values given in Table 3.6; this is done to maintain consistency among the various parameters derived from use of the $T_s(s)$ value. The model surface-burst fireball conditions, using the smoothed values of $T_s(s)$, are summarized in Table 3.7. The parameter values are tabulated with more significant numbers than are warranted by the assumptions merely to aid in interpolation to other values of W. Interpolations to other yields can be made by plotting the parameters against $T_s(s)$, which is related to W by Eq. 3.122 as is shown in Figure 3.3. The values of ΔE_s and ΔE_s-500 can be then calculated by use of Eqs. 3.116 and 3.117. It should be mentioned that the recalculated values of n/W do not quite conform to the assumption of equal vapor densities in the model air and surface bursts at all yields.

Figure 3.3
CALCULATED VARIATION OF n W, P_{max}, n_0 n, AND n_0 W WITH ASSUMED VALUES OF $T_g(s)$ FOR THE MODEL SURFACE-BURST FIREBALL

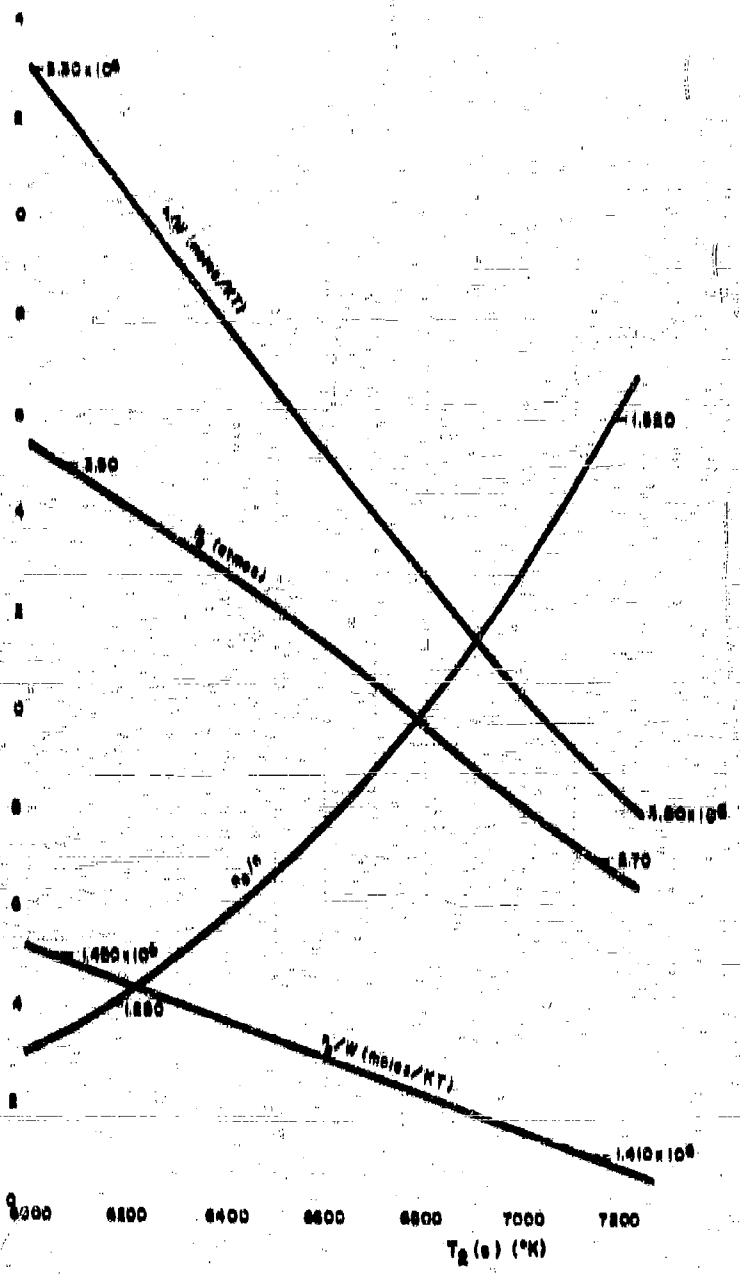

Table 3.7

SUMMARY OF FIREBALL CONDITIONS AT THE SECOND TEMPERATURE MAXIMUM FOR THE MODEL SURFACE BURST OF DIFFERENT YIELDS USING EQ. 3.122 FOR T_s (s)

Quantity	W(KT)					
	1	10	10^2	10^3	10^4	10^5
T_s (s), °K	7,200	7,040	6,880	6,720	6,570	6,420
p_s, atmos	2.667	2.781	2.905	3.037	3.158	3.264
p_0, atmos	4.218	4.301	4.390	4.479	4.568	4.666
n_s/n_0	1.525	1.479	1.422	1.381	1.347	1.320
n_s/W, 10^6 moles/KT	1.407	1.414	1.420	1.428	1.431	1.436
n_0/W, 10^6 moles/KT	2.420	2.576	2.762	2.951	3.140	3.319
n/w, 10^6 moles/KT	3.827	3.990	4.182	4.376	4.571	4.755
ΔE_s, cal/mole gas atoms	161,050	160,280	159,010	158,090	158,380	157,700
(ΔE_s -592) cal/mole air	148,100	139,320	116,060	106,050	97,200	90,110

The assumptions that given fractions of the released energy are contained in the fireball, carried away by the blast wave, and lost by thermal radiation, and the corollary assumption that the time dependence of the various parameters can be given in terms of the time relative to t_s, as was done for the model air burst, leads to the mathematical requirement that, for the model surface burst, t_s must vary as $W^{0.375}$. By adjusting the t_s values for the model air burst to give the same percentage deviation at 20-KT and 1-MT, the model surface burst scaling function for t_s that results is

$$t_s = 0.61\ W^{0.375}\ \text{sec}, \qquad (3.125)$$

This gives 0.10 seconds for 20-KT and 0.80 seconds for the 1-MT yield. The lower values of T_s (s) and t_s (higher yields) for the surface burst would indicate that the surface burst fireball either cools more rapidly than the air burst fireball at the very early times or that it never was as hot, or both.

At t_s the model surface-burst fireball is in the shape of a hemisphere centered at the point of detonation; in the model it remains in this position and shape until it reaches full expansion at t_m. After t_m, it begins to rise and in doing so takes on the shape of a sphere as it separates from the earth's surface at t_s. During this time, the volume remains constant; as in the case of the air burst, the fireball volume is assumed to remain essentially constant from

$t = 1.4t_g$ to $t = 10t_g$. Since the same fireball volumes are assumed for both types of bursts, the same type of equation for the increase in radius after $10t_g$ is used. The fallout particles enter the fireball some time after t_g and, presumably to a larger degree, even after $10t_g$.

From the assumption of equal fireball volumes, the fireball radius for the model surface burst is

$$R_g = 6.35 \times 10^4 W^{0.333} \text{ cm} \quad (3.124)$$

$$R_m = 7.88 \times 10^4 W^{0.333} \text{ cm} \quad (3.125)$$

and

$$R_s = 6.25 \times 10^4 W^{0.333} \text{ cm} \quad (3.126)$$

In order to estimate the energy radiated to the atmosphere between t_m and t_s, the value of R_e, the effective radius for the surface of the fireball exposed to the atmosphere, is assumed to vary as $(t/t_g)^m$, where m is a constant that is independent of yield, so that the form of the integral of Pdt during this period is the same as for the period between t_s and $10t_g$. (The value of m can be evaluated from the height of the cloud for a 1-MT yield as given in ENW, p. 23.)

The curve can be represented, with a fair degree of precision, by

$$h_t = 4.24 \times 10^4 t^{0.704} \text{ cm} \quad , \quad t = t_m \text{ to } 60 \text{ sec} \quad (3.127)$$

and

$$h_t = 6.46 \times 10^4 t^{0.600} \text{ cm} \quad , \quad t = 60 \text{ to } 390 \text{ sec} \quad (3.128)$$

For the model surface-burst fireball, h_t is equal to $2R_s$ at t_s.

For the 1-MT yield, $2R_s$ is 1.28×10^5 cm; t_s is then 4.66 seconds. Since t_g for this yield is 0.80 second, t_s/t_g is 5.80. Using the values of 0.70 R_m^g and R_s^g at t_m and t_s, respectively, the variation of R_e, the effective "spherical" radius, with t/t_g, during t_m to t_s is

$$R_e = 5.42 \times 10^4 W^{0.333} (t/t_g)^{0.081} \text{ cm} \quad , \quad t/t_g = 1.4 \text{ to } 5.8 . \quad (3.129)$$

The estimates of t_m and t_s are given by

$$t_m = 0.085W^{0.373} \text{ sec} \qquad (3.130)$$

$$t_s = 0.154W^{0.373} \text{ sec} \qquad (3.131)$$

The fireball radius from $t/t_g = 5.8$ to $t/t_g = 10$ is assumed to be the same as R_m for the model air burst which is $6.25 \times 10^5 W^{0.333}$ cm as given by Eq. 3.120 for R_s.

The variation of the temperature with t/t_g for the model surface burst is assumed to follow the same pattern of decrease with time as in the air burst. That is, it varies as $(t/t_g)^{-n}$ up to $t/t_g = 10$ and thereafter varies as $\exp(-k(t/t_g))$ where n and k are yield-independent parameters. Since $T_g(s)$ is much lower than $T_g(a)$, it would appear that the temperature should be decreasing at a somewhat slower rate, at this time, for the surface burst. That is, the constant n should be less than 0.4.

A likely value of n can be determined from evaluation of the integrals for the radiant energy lost to the surrounding atmosphere, as was done for the air burst. Although the total amount of energy radiated to the atmosphere should be less than for the air burst (50 percent), the lower limit would certainly be about 20 percent, with an upper limit of around 40 percent. Allowing the estimate of 6 percent for the amount of energy lost up to T_g and $0.30 \times 0.81 P_g t_g$ (or 4 percent) from t_g to t_m, as in the case of the air burst (but corrected for geometry and temperature), and assuming the same variation of n with t/t_g after $10t_g$ as for the air burst case (as a first approximation), the integrals give 25 percent of the energy radiated to the atmosphere for $n = 0.35$ and about 40 percent lost for $n = 0.30$. On this basis, n was taken as 1/3. The estimate of the fireball temperature for the surface burst then is

$$T = 7.2 \times 10^3 W^{-0.010} (t/t_g)^{-1/3} \text{ °K}, \qquad t/t_g = 1 \text{ to } 10 \qquad (3.132)$$

$$T = 2.83 \times 10^3 W^{0.114} t^{-1/3} \text{ °K}, \qquad t = t_g \text{ to } 10t_g \qquad (3.133)$$

$$T = 4.66 \times 10^3 W^{-0.010} \exp(-0.0334 t/t_g) \text{ °K}, \quad t/t_g = 10 \text{ to } 50 \qquad (3.134)$$

$$T = 4.66 \times 10^3 W^{-0.010} \exp(-0546 W^{-0.373} t) \text{ °K}, \quad t = 10t_g \text{ to } 50t_g \qquad (3.135)$$

Because the main concern is with the surface burst, it is desirable to have a better estimate of the fireball radius and volume after $t/t_g = 10$ than was obtained for the air-burst fireball. To do this, the work done in the expansion of the fireball against the atmosphere and in the heating of inflowing air, as well as thermal radiation losses, are taken into account in estimating the rate of expansion of the fireball after its initial rapid expansion to V_m or V_s. To a first

approximation. In these estimates, the presence of the soil need not be taken into account if the end point of the calculation for the energy balance for the expansion is taken at a sufficiently low temperature. In its solid form, the soil would not contribute to the volume, and, because of the high relative abundance of air molecules, the proportion of the fireball energy that is absorbed by the soil should be small.

First, the energy radiated to the air between $t/t_q = 1$ and $t/t_q = 10$ must be subtracted from the 4.50×10^{11} W cals in the fireball at t_q. The energy radiated to the air up to $t/t_q = 10$ is summarized by

$$q^1 = 6.66 \times 10^{10} \text{ W cals} \quad (6.0\%) \tag{3.136}$$

$$1q^{1.4} = 4.44 \times 10^{10} \text{ W cals} \quad (4.0\%) \tag{3.137}$$

$$1.4q^{5.8} = 9.92 \times 10^{10} \text{ W cals} \quad (8.9\%) \tag{3.138}$$

$$5.8q^{10} = 3.06^{10} \text{ W cals} \quad (2.8\%) \tag{3.139}$$

The energy remaining, after subtracting the last three above quantities, is 2.70×10^{11} W cals; it is available for the processes mentioned above. The mathematical form of the increase of the fireball radius after $t/t_q = 10$ is assumed, as in the case of the air burst, to be

$$R = R_q \exp \alpha(t/t_q - 10) \tag{3.140}$$

in which the constant is yield-independent.

According to the variation of the temperature with t/t_q (from Eqs. 3.132 to 3.135) a temperature between 800 and 900°K is reached at $t/t_q = 50$, for all yields from 1 - to 10^5-KT. Since this is about the time the fireball as such should disappear, it was selected as the end point for evaluating the constant of Eq. 3.141 by means of an energy balance.

The work of expansion against the atmosphere is

$$q(\Delta V) = P(V_{50t_q} - V_q) = 2.48 \times 10^{10} \text{ W} \exp(120\alpha) = 1.16 \times 10^{10} \text{ W cals} \tag{3.141}$$

The number of moles of gas molecules present at the end point can be estimated by use of the perfect-gas law plus the assumption that the internal pressure of the gases, at $t = 50t_q$, is the same as the external pressure (1 atmosphere). The number of moles of air molecules present, at t_q, ranges from 1.0×10^6 W (for 1-KT) to 2.5×10^6 W (for 10^5-KT). The value 2.12×10^6 W for 10^3-KT is used as an average value to estimate the number of moles of air that have entered the fireball between t_q and $50t_q$.

The estimate of the energy used in heating additional air to 800°K, with these provisions, is

$$\Delta E = \Delta n(E_{800} - E_{298}) = 4.74\times10^{10} W \exp(120a) - 6.44\times10^{8} W \text{ cals} \quad (3.142)$$

in which Δn is the increase in number of moles of air between t_s and $50t_s$ and $E_{800} - E_{298}$ is 8040 cal/mole.

The radiant energy lost is approximately

$$10 q_s^{-} = 1.73\times10^{-11} t_s \int_{10}^{\infty} T^4 R^2 d(t/t_s) = \frac{5.12\times10^{9} W}{(0.133-2a)} \text{ cals} \quad (3.143)$$

Summing these energies and equating to $2.79\times10^{11} W$ cals gives

$$4.13 = \exp(120a) + \frac{0.071}{(0.133-2a)} \quad (3.144)$$

The equation is satisfied for $a = 0.0104$; this value of the constant is about a third of that obtained for the air burst where thermal radiation only was considered.

The estimated radius is now given by

$$R = 5.69\times10^{3} W^{0.333} \exp(0.0104\, t/t_s) \text{ cm}, \; t/t_s = 10 \text{ to } 50 \quad (3.145)$$

or

$$= 5.69\times10^{3} W^{0.333} \exp(0.170 W^{-0.333} t) \text{ cm}, \; t = 10t_s \text{ to } 50t_s \quad (3.146)$$

The radiant energy lost is

$$10 q_s^{-} = 4.65\times10^{10} W \text{ cals} \; (4.2\%) \quad (3.147)$$

Therefore the radiant energy lost to the atmosphere (surrounding air) is 25.9 percent of the total released.

The thermal power functions for the model surface burst from $1.4t_s$ to about $50t_s$ are

$$P = 5.13\times10^{10} W^{1.062} t^{-1.171} \text{ cals/sec}, \; t = 1.4t_s \text{ to } 5.8t_s \quad (3.148)$$

$$P = 4.33\times10^{10} W^{1.123} t^{-1.333} \text{ cals/sec}, \; t = 5.8t_s \text{ to } 10t_s \quad (3.149)$$

$$P = 2.64\times10^{11} W^{0.627} \exp(-1.84 W^{-0.373} t) \text{ cals/sec}, \; t = 10t_s \text{ to } 50t_s \quad (3.150)$$

In the evaluation of the constant, n, it would be preferable to integrate the energies to the time at which the gases reach ambient temperature. In such a case, the only energy lost would be in the work of expansion and in the radiant energy. In the real case, the cloud would have formed at higher altitudes by this time. In addition, the observed value for the increase in fireball volume would be required for the calculation. Even further, the additional energy released by the cooling of the original gas to lower temperatures than 208°K would have to be considered, as well as the decrease in the external pressure to below 1 atmosphere.

The times after burst of chief interest in the fallout formation are those when the temperature of the fireball has fallen below about 2500°K. For the ideal soil, the end of the first period of condensation should occur at the soil-melting temperature, 1673°K.

Some of the fireball temperatures and times, for yields between 1- and 10^5-KT, as calculated from the above scaling functions are summarized in Table 3.8. For most yields, the temperature range of interest occurs between $20t_s$ and $30t_s$. The times at which the temperature is estimated to decrease to 1673°K varies from about 2 seconds for 1-KT to about 122 seconds for 10^5-KT. In scaled time, the change is only from $31t_s$ to $27t_s$ from 1 - to 10^5-KT, respectively.

Because of the many assumptions involved in deriving the descriptive equations for the surface burst fireball, no reliability can be attached to the numerical values derived from them. However, the general trends in those values, as given by the functions with respect to time and yield, and with respect to the model air burst, are consistent with observations. Except on the point of accuracy, the descriptive value that can be placed on the development of the functions, and therefore their presentation here, is associated with pointing out what the important fireball parameters are, with respect to fallout formation, and how they are related to each other. When more data are made available, appropriate adjustments in the scaling function parameters can be made.

3.4 Process for Estimating the Concentration of Liquid Soil in the Fireball of a Model Surface Burst and the Fractionation Numbers of the Radionuclides

The use of the fireball scaling functions for estimating the value of $n(r)/V$ which is required in Eqs. 3.8, 3.10, or 3.32 in the evaluation of the $r_0(A)$ of each mass chain, is illustrated in this section. In the illustrative calculation, the

Table 3.8

SUMMARY OF SOME FIREBALL PARAMETER VALUES FOR VARIOUS YIELDS OF THE MODEL SURFACE BURST

Parameter	Weapon Yield					
	1	10	10^2	10^3	10^4	10^5
t_g (sec)	0.001	0.14	0.84	0.80	1.89	4.47
T at $10t_g$ (°K)	3340	3200	3100	3120	3050	2980
T at $20t_g$ (°K)	2000	2040	2280	2280	2180	2130
T at $30t_g$ (°K)	1720	1680	1040	1600	1570	1530
T at $40t_g$ (°K)	1250	1200	1170	1150	1120	1100
T at $50t_g$ (°K)	880	860	840	820	800	785
t/t_g at 1673°K	30.8	30.1	29.4	28.7	28.0	27.4
t at 1673°K (sec)	4.88	4.54	10.0	23.1	53.1	122

value of $n(\ell)/V$ is estimated at only one temperature for each of several weapon yields, and the temperature at which the ideal soil solidifies is selected so that fractions of each element condensed may be calculated to apply at the time of the end of the first period of condensation.

Two times are selected for a complete computation of the $r_0(A)$ values. The first time, 60 seconds after burst, was selected so as to minimize, to a degree, any possible errors in the relative abundances of the short-lived fission products, and so as to make the computations apply to a land-surface burst in the megaton yield range. The second time, of 0 seconds, was used to determine the sensitivity of the results of the computation to the changes in relative abundance of the different nuclides due to decay and to the changes in the weapon yield.

The use of single values for temperature and time neglects both the possible variation of $n(\ell)/V$ with time and the possible losses of some of the fission products and soil from the fireball at earlier times. The computation of the liquid soil concentration at a given time and fireball temperature by means of energy balances is not an optimum method because of the approximations used in the fireball scaling functions and because the calculations involve the determination of small differences in rather large numbers which themselves cannot be computed with accuracy.

The selection of the fireball temperature and its time of occurrence determines the yield, by use of Eqs. 3.133 or 3.135. Substitution of 1073°K and 60 seconds and solving for W gives a yield of 14,000-KT (14-MT); the yield for 0 seconds is 84-KT. The method of computing the necessary quantities is discussed below for the 14-MT yield detonation.

To estimate, by means of energy balances, the molar concentration of the soil in the fireball requires estimates of the disposition of the energy contained in the fireball between the time of the second temperature maximum and 60 seconds. In this time period, the following processes must be considered:

1. Cooling to 1073°K, and recombination of the gases at $T_g(s)$ including liquefaction of the vaporized soil.

2. Loss of energy due to radiation from the fireball.

3. Loss of energy due to expansion of the fireball gases against the atmosphere.

4. Loss of energy in heating the additional air that enters the fireball.

5. Loss of energy in heating and melting a given amount of additional soil.

An estimate of the energy exchanged among the first four processes is required, in order to calculate the amount of soil that is both present and melted in the fireball at 1073°K.

The thermal data and parameters describing the 14-MT yield fireball, for use in the calculations, are summarized in Table 3.0. The values of n/W were taken from Figure 3.1, the other data were calculated from the scaling functions or from the interpolation of data in the tables and graphs of Section 3.0. In using the plotted data at odd values of $T_g(s)$, a check computation is required to assure that the energy sum at t_p is 42 percent of the yield. The data are interpolated from the curves plotted against temperature, after calculation of $T_g(s)$, rather than against yield, because the initial computations were made from such curves. The amount of soil vaporized and present at t_p would form, upon complete condensation at 60 seconds, 5.51×10^4 W moles in accounting for the 28 atoms per molecule.

Table 8.9

SUMMARY OF FIREBALL PARAMETERS AND THERMAL DATA FOR THE 14-MT YIELD MODEL SURFACE-BURST FIREBALL

Parameter	Value
t_B	2.14 sec
T_B	6,545°K
n/W	4.000×10^{6} moles/KT
n_a/W	1.482×10^{6} moles/KT
n_s/W	3.166×10^{6} moles/KT
V_B	5.80×10^{11} W cm^3
p_a	4.61 atmos
p_s	3.18 atmos
n_s/n_a	1.842
n_a/W	2.301×10^{6} moles/KT
ΔE_a -592	95,950 cals/mole air
ΔE_s	158,240 cals/mole soil/gas atmos
$60/t_B$	28.04
$10q_B^{87}$ w	8.68%

The energy released on cooling the gases from 6560°K to 1675°K, including association of the gas molecules, is calculated by the process of cooling to 298°K and reheating to 1675°K. Thus, for the air,

Air, 298°K→Air, 1675°K, ΔE = 8,020 cal/mole

Air, 6545°K→Air, 298°K, ΔE = -95,950 cal/mole

Air, 6545°K→Air, 1675°K, ΔE = -87,930 cal/mole

Therefore the heat released on cooling and recombining the air is

$$Q_1 = -2.14 \times 10^{11} \text{ W cals} \qquad (8.151)$$

For the soil, including melting at 1073°K,

Soil (c), 298°K→Soil (ℓ), 1073°K, ΔE = 227,700 cal/mole

Soil (g), 6545°K→Soil (c), 298°K, ΔE = -4,114,200 cal/mole

Soil (g), 6545°K→Soil (ℓ), 1073°K, ΔE = -3,886,500 cal/mole

Therefore the heat released on cooling, recombining, and liquifying the soil is

$$Q_1'' = -2.14\times10^{11} \text{ W cals} \tag{3.152}$$

Thus, the release of energy on cooling and recombining the fireball gasses is

$$Q_1 = -4.22\times10^{11} \text{ W cals} \tag{3.153}$$

The radiant energy lost from the fireball from t_g to $10t_g$ is 15.7 percent; the additional amount from $10t_g$ to $28.0t_g$ is 3.6 percent for a total of 19.3 percent. Hence the total energy lost by radiation from t_g to $28.0t_g$ is

$$Q_2 = 2.14\times10^{11} \text{ W cals} \tag{3.154}$$

The spherical fireball volume, from Eq. 3.146 is

$$V = 7.72\times10^{11} \text{ W } \exp(0.510W^{-0.373}t) \text{ cm}^3, \quad t = 10t_g \text{ to } 50t_g \tag{3.155}$$

Therefore the volume at 60 seconds, for 14-MT, is

$$V = 1.85\times10^{12} \text{ W cm}^3 \tag{3.156}$$

The change in volume from V_g is therefore

$$\Delta V = V - V_g = 1.31\times10^{12} \text{ W cm}^3 \tag{3.157}$$

The work energy used in expanding all the gases from V_g to V against the external pressure of 1 atmosphere (1 cal = 41.25 cm^3-atoms) is

$$Q_3 = 3.17\times10^{10} \text{ W cals} \tag{3.158}$$

In order to estimate the number of additional moles of air that have entered the fireball between t_2 and $28.0t_2$, it is assumed that the internal pressure of the fireball at $28.0t_2$ is very close to 1 atmosphere. With this assumption and that of the perfect-gas law, the number of moles of gas in the 14-MT fireball at 60 seconds is

$$n_T = 1.35 \times 10^7 W \text{ moles} \tag{3.159}$$

The net gain in air molecules, neglecting the small amount of other gases, is

$$\Delta n = n_T - n_0 = 1.11 \times 10^7 W \text{ moles} \tag{3.160}$$

On this basis, about 80 percent of the fireball gas molecules at 60 seconds is from the air that entered after t_2. The energy required to heat this air from 298°K to 1673°K is

$$Q_4 = 8.90 \times 10^{10} W \text{ cals} \tag{3.161}$$

Since the energy changes for all processes must equal zero, the remaining amount not accounted for is

$$Q_5 = 8.73 \times 10^{10} W \text{ cals} \tag{3.162}$$

Assuming that this remainder is utilized to heat and melt soil, the amount of soil that could be liquified (at the melting temperature) plus that condensed from the vapor is

$$\begin{aligned} n(\ell) &= 3.83 \times 10^5 W + 5.51 \times 10^4 W \text{ moles} \\ &= 4.38 \times 10^5 W \text{ moles} \end{aligned} \tag{3.163}$$

Therefore at 1673°K, or 60 seconds after detonation of the 14-MT model surface burst, the gross concentration of the liquid soil is

$$n(\ell)/V = 2.37 \times 10^{-7} \text{ moles/cm}^3 \tag{3.164}$$

The results of similar computations of $n(\ell)/V$ at 1673°K for values of W from 1- to 10^3-KT are summarized in Table 3.10. Over this large range in yields, the $n(\ell)/V$ values for the model surface burst vary only from about 1.8×10^{-7} to 2.5×10^{-7} moles of soil/cm^3. The fractions of the energy required to melt these amounts of soil range from 7.5 to 9.2 percent of the total. For a low yield tower shot, Adams[5] estimated that about 9 percent of the energy was used in heating the soil and tower materials. Since it is expected that a larger fraction of the energy would be utilized in a surface burst, the two estimates are in relative agreement.

In regard to the energy balance, it may appear during the development of the equations that 9 percent of the energy initially absorbed by the soil at t_g has been discarded from the calculations. But some of the soil heated by this energy is certainly part of the $n(t)$ moles that are melted. This readdition of energy is partially, and arbitrarily, compensated for by not accounting for further losses to the underlying soil surface between t_α and t_g.

If these energy losses are considered to occur over the bottom of the fireball, and the readditions are considered to occur only for soil from the crater area, the fractional error in the neglect of the readditions can be estimated from the relative areas involved. The crater radius, from ENW, is $62.5W^{1/3}$ feet (for W in KT), or,

$$R_g = 1.90 \times 10^3 \ W^{1/3} \ \text{cm} \qquad (3.165)$$

The ratio of the surface area of the crater to the surface area covered by the fireball should give the fraction of energy recovered, assuming uniform losses from the surface of the fireball that is in contact with the earth. The ratio of R_g^2/R_1^2 is 0.09; hence the amount of energy recovered from this area only would be 0.81 percent of the total.

While it is possible that a large part of the energy losses to the soil could be near the center of the area covered by the fireball, these losses were not considered to occur before t_g. Because of the low thermal conductance of the soil minerals and the high temperatures of the liquid layer or boundary, if any, between the gases and the solid soil should be very thin. The final computation of $n(t)$ does not stipulate whether the energy losses to the soil after t_g result in the formation of a liquid layer or puddle in the crater which is thereafter disrupted and sucked up into the fireball or liquid particles by the direct melting of individual soil grains. Therefore, except for the averaging of the energy losses over the fireball surface up to t_g, no specification of the fate of the 9 percent of the energy lost to the soil can be given.

The final major assumption for the calculation of $n(t)/V$ is that the internal pressure of the fireball is 1 atmosphere. There is apparently no data to substantiate this assumption except the inference from the fact that the early expansion of the fireball then stops at t_α, so that even at this early time the internal pressure cannot be very much larger than the external pressure. At the time the temperature has reached 1673°K, the fireball is quite high. For example, at 23 seconds the top of the fireball (or forming cloud) for the 1-MT yield, from Eq. 3.127 would be at an altitude of about 12,000 feet. At this altitude, the actual external pressure is considerably less than 1 atmosphere. The number of moles of air, as estimated by the use of the assumption, is about twice the original number of air atoms in the same volume at 1 atmosphere and

Table 3.10

SUMMARY OF ESTIMATES OF $n(r)/V$ FOR THE MODEL SURFACE BURST OF DIFFERENT YIELDS AT THE TIME THE FIREBALL TEMPERATURE IS 1673°K

Quantity	Units	Yield (KT)					
		1	10	10^2	10^3	10^4	10^5
n_o	10^6 W moles orig air	1.584	1.749	1.942	2.137	2.331	2.514
$\Delta E(T_2$ (s) to 1673°K)	cal/mole air	−135,080	−121,300	−108,640	− 98,030	− 89,130	− 82,090
$\Delta E(T_1$ (s) to 1673°K)	cal/mole soil atoms	−152,260	−151,520	−150,850	−150,230	−149,620	−149,030
Q_1	10^{11} W cals	− 2.140	− 2.122	− 2.110	− 2.095	− 2.079	− 2.064
Q_1'	10^{11} W cals	− 2.142	− 2.142	− 2.142	− 2.141	− 2.141	− 2.140
Q_1	10^{11} W cals	− 4.282	− 4.264	− 4.252	− 4.236	− 4.220	− 4.204
Q_2	10^{11} W cals	2.162	2.159	2.156	2.151	2.147	2.141
V, 1673°K	10^{12} W cm^3	2.017	1.974	1.932	1.892	1.851	1.811
ΔV	10^{12} W cm^3	1.481	1.438	1.396	1.356	1.315	1.275
Q_3	10^{11} W cals	0.359	0.348	0.338	0.328	0.318	0.309
n_T, 1673°K	10^7 W moles air	1.469	1.438	1.407	1.378	1.348	1.319
Δn	10^7 W moles air	1.311	1.263	1.312	1.164	1.115	1.068
Q_4	10^{11} W cals	1.051	1.013	0.973	0.934	0.894	0.857
Q_5	10^{11} W cals	0.710	0.744	0.785	0.823	0.861	0.897
$n(r)$	10^8 W moles soil	3.659	3.811	3.993	4.162	1.331	1.491
$n(r)/V$, 1673°K	10^{-4} moles soil/cm^3	1.81	1.93	2.07	2.20	2.34	2.45
$n(r)/V$, 1673°K	10^{-4} gm soil/cm^2	0.951	1.01	1.08	1.15	1.23	1.30

208°K and, of course, the energy balance equations do not specify the origin of the gas atoms. Some of the additional air certainly comes from the volume swept out above the fireball as it rises; also, some must enter from the bottom along with the column of soil particles that is formed by the updrafts. The latter is particularly noticeable on the periphery of the columns of the larger yield detonations.

Some estimate of the amount of the crater material that is involved in the formation of $n(\ell)$ can be made, using the crater radius given above and the crater depth, $25W^{1/3}$ feet, as given in ENW. For the crater volume, a cone shape is used, which is somewhat more typical of the shape of craters from the larger yield nuclear weapons than the ellipsoid of revolution of ENW. Taking 110 lb/cu. ft for the soil density gives

$$M_0 = 5.11 \times 10^{11} W^{0.917} gm \qquad (3.166)$$

for the amount of soil removed from the crater (yields in the MT range leave no crater lip). The range in the mass of $n(\ell)$ from 1-KT to 10^3-KT according to the model surface burst fireball (mol. wt. 524) is $1.93 \times 10^{11} W$ gms to $2.35 \times 10^{11} W$ gms; with the crater mass of Eq. 3.166, the corresponding range in the percentage of the crater mass that forms $n(\ell)$ is from 3.8 percent to 12 percent, respectively. In terms of the model, those are the fractions of the crater mass that have entered the fireball up to 1.0 and 122 seconds after detonation, providing no significant amounts of melted soil have fallen out of the fireball volume during this period.

It is clear that the $n(\ell)/V$ ratios, as calculated, assume that many soil particles have entered the fireball and that none have left. If a large number of particles have been ejected from the fireball during the period when the liquid soil can exist, then the computed values of $n(\ell)/V$ are too large. However, the assumption that only an insignificant fraction of the particles leave the fireball during the period when the more refractory fission products condense should be valid because of the short times involved. If it is further assumed that the mixing in the volume is rather uniform and that equilibrium conditions exist between the liquid particles and vapor, then estimates can be made of $n(\ell)$ (or of $n(s)$ if complete condensation of all the elements does not occur at temperatures above the melting point of the carrier) from observed values of the concentration of fission product elements in fallout.

The condensation of the more refractory fission-product elements occurs independently of the state of the carrier material. All that is required is the presence of a macroscopic condensed phase, liquid or solid, on which the vapor can condense. When complete condensation of one or more of the fission product

elements occurs, the ratio of the total amount of soil present in the fireball to the total amount of the element present in the fireball volume is equal to the ratio found in the fallout particles formed. In the more general case, this ratio is given by

$$n(\ell) = \frac{Y_A}{N_A} \sum_j \frac{y_j(A,t)}{\left(1 + \frac{k_j'}{(n(\ell)/V)RT}\right)} \qquad (3.107)$$

in which Y_A is the total weapon yield of mass number A (in moles or fission equivalents), and N_A is the mole fraction or concentration of mass number A in the fallout particles in (moles or fissions)/(mole or gm of soil). For mass chains containing only elements whose gaseous species are less volatile than the carrier, the summation term is equal to one.

For investigating possible times and temperatures at which a given element condenses, radiochemical data on the fractionated mass chains are required. In this case, the better estimate of $n(\ell)/V$ would result when the summed term has values between 0.2 and 0.8. Unfortunately, no unclassified data are available on fractionated chains for use in solving Eq. 3.107. Some data, based on Mo-99 analyses in terms of fissions and other measurements, are available for making rough estimates of $n(\ell)$ or $n(s)$, assuming the mass 99 chain had completely condensed while all the fallout forming particles were present; these data are summarized in Table 3.11.

The fireball volumes used to calculate the fission concentrations of Table 3.7 was the 1078°K volume for the model surface burst. The only data directly applicable for comparison with model surface burst calculations are those of the operation Jangle "S" shot. Some error is involved in the estimates of the factors used to convert the $M_s(i)$ values to $1/N_{fi}$ values applicable to the refractory elements; also, some bias is introduced because the samples from which the $M_s(i)$ values were derived were known to contain some unknown fraction of background soil, not fallout, which would tend to make the calculated values of $n(\ell)$ or $n(s)$ high. The factor-of-two difference between the "data" and the model values could be reconciled on this basis alone. The data from the other shots were included only to exhibit differences; no fireball model has been developed for them as yet.

For the underground shot, the fireball volume from the model surface burst is certainly larger than the actual gas volume was at 1078°K. Therefore the true value of $n(\ell)/V$ or $n(s)/V$ for an underground detonation would be even larger than that of Table 3.11. On the other hand, the samples from which the $M_s(i)$ values were determined contained more background soil, not fallout, than those from the surface shot. However, the excess was probably not a factor of two greater, so the larger value of $n(\ell)/V$ or $n(s)/V$ calculated for the underground shot represents a real excess over that of the surface shot fallout, and it could be even larger.

Table 3.11

SUMMARY OF ESTIMATES OF n(i)/Y OR n(s)/Y BASED ON FISSION CONTENT OF FALLOUT

Type of Shot	Fission Yield (10^{23} fissions)	Total Yield (MT)	$1/N_{f_p}$ (10^{-15} gm/fission)		n(i) or n(s) (10^{8} gms)	n(i)/Y or n(s)/Y (10^{-4} gm cm^{-2})
			Mean	Range		
Jangle "S" - Land Surface[a]	1.58	1.1	3.1	1.5 - 5.9	4.9	2.2
Jangle "U" - Underground[a]	1.73	1.2	10	2 - 25	17	7.9
Low Tower Shot Over Soil[b]	34.5	17	0.87	0.8 - 1.0	21	0.63
Surface Coral Detonation[c]	3,000	5,000	5.8	3 - 12	12,000	1.3
Surface Coral Detonation[c]	11,000	15,000	3.2	- -	24,000	0.87

---

a. From Reference 6 values of $M_f(1)$. The $1/N_{f_p}$ values are estimated by assuming a terraine factor of 0.75, a gross fractionation number of 0.3, and 5.49×10^{-13} (r/hr at 1 hr) / (fission/sq ft) for the ionization rate at 3 ft above a smooth uniformly contaminated plane including an instrument response factor of 0.75.

b. Based on data from fused silicate particles containing about 5 percent Fe in the silicate glass. The $1/N_{f_p}$ are average for gross sample of mixed particle sizes.

c. Yields estimated; sample weights are corrected to original coral composition based on sample analysis of CaO and MgO; data from References 7 and 8.

The fireball volume of the low tower shot should be reasonably near that of the surface burst. The lower value of $n(\ell)/V$ (i.e., fused particles) in this case is mainly due to height of burst; a true air burst at the same height would be expected to have even lower soil concentrations. Even with these differences, the calculated value of $n(\ell)/V$ is less than a factor of two from that of the model.

In the case of the coral detonations, the samples contained both fused and irregular particles, hence a large fraction of the fission product elements present had condensed on the solid CaO particles. The model values of $n(\ell)/V$ again agree with the observed data (in this case $n(s)/V$) within a factor of two. All the observed data for the fallout from a near surface detonation where more than one sample or datum point is available, show the derived $n(\ell)/V$ or $n(s)/V$ values to have a spread of about a factor of two. Since the values calculated for the ideal surface burst fireball model lie within this range one concludes that these concentrations can be estimated from the model with about the same reliability as they are known from the available data.

If the Henry's law constants for all the radionuclides in equilibrium with a silicate soil were available, the fractions of each that have condensed at a given temperature could be calculated by using the estimated values of $(n(\ell)/V)RT$. But while there are some thermal data on silicate compounds, they are not sufficiently extensive to include many fission-product elements. No comprehensive study has been made to correlate all the available thermal data on silicate materials at high temperatures, as has been made of other compounds. If this latter data were carefully studied, perhaps they and other data could be utilized to make reasonable estimates of the vapor pressures of many of the important fission-product elements over a molten soil mineral.

In order to test the model of the condensation process, and to estimate on a relative basis of the fractions that condensed, the following compromises with reality were made:

(1) The fission product, its oxide or other compound, forms an ideal solution in the molten silicate glass during the first period of condensation;

(2) The carrier material is non-reactive, so that no compound-formation with the fission product elements or oxides occurs; and

(3) The gaseous species of each fission-product element (with a few exceptions) is, in the presence of oxygen, the same as that which is in equilibrium with its own liquid or solid oxide.

For many of the fission product elements, the first compromise, or specification, is perhaps reasonable, because many oxides do form solutions in silicate glasses and, in this case, the solution is very dilute. The second and third compromises merely state the premise on which concentrations, in the liquid and vapor state, respectively, are computed. The simplification of the liquid-vapor phase system to a set of ideal solutions means that the solution behavior is defined by Raoult's law, rather than Henry's law, and that the vapor pressure of the gaseous species, i, of element j is given by

$$p_{ij} = N_i p^0_{ij} \qquad (3.158)$$

where p^0_{ij} is the vapor pressure of the gaseous atom or molecule over the pure compound in the liquid or solid state at the same temperature, and N_i is the mole fraction of the pure compound in the molten soil.

In the real chemical system, many of the fission-product oxides or other compounds would certainly exhibit significant deviation from ideal behavior, even at low concentrations. In the case of the liquid silicate as a condensing surface, it might be expected that those elements whose ionic character differs most from that of Si^{+4} would probably deviate most from ideal behavior. The elements expected to deviate most would therefore be those of the alkali metals. However, similar oxides should give similar deviations, so that the relative values of p_{ij} for similar oxides should be in the same numerical order as the Henry's law constants.

There is one additional factor that eliminates, to some degree, the requirement for knowing the vapor pressures of all the elements over the condensed phase to a high degree of accuracy. In the condensation equations, the value of $F_0(A)$ varies inversely with $1 + p_{ij}/((n(t)/V)RT)$, where k_j is replaced by p_{ij}. The value of the sum of a series of these terms depends on the value of p_{ij} relative to the value of $(n(t)/V)RT$. If the ratio, given by the second term, is less than 0.001, then the element is essentially 100 percent condensed, and if the second term is more than about 500, the fraction condensed will be negligible (i.e., its contribution to the sum activity will be negligible). In the cases where the value of the second terms is outside these limits, no accuracy in the actual value of p_{ij} is required. The greatest accuracy in the p_{ij} value is desired when the value of the ratio is near unity.

The vapor pressure data for the assumed vaporization, or condensation, reactions for the many elements considered are given, in Table 3.12, in terms of empirical constants for the equation

$$\log p^0_{ij} = \frac{A}{T} + B + C \qquad (3.160)$$

where p_j^o is in atmosphere, A and B are empirically-fitted constants, and

$$C = (x_{ij}z-w) \log P(O_2) \tag{3.170}$$

based on the volatilization reaction of the condensed oxide, $M_y O_x$, according to

$$x_{ij} M_y O_x (c, \ell, gf) \rightarrow M_{x_{ij}y} O_w(g) + \frac{(x_{ij}z-w)}{2} O_2(g) \tag{3.171}$$

where $P(O_2)$ is the oxygen pressure in atmosphere and the x_{ij}, y, x, and w are numbers. The designation (c) is for crystal, (ℓ) is for liquid, and (gf) for glass. The constant, C, determines the effect of oxygen pressure on the amount of the gaseous species that condenses. In all but a very few cases, the free energy data for the condensed phases of the oxides as reported by Coughlin[9] were used in the evaluation of the constants of Eq. 3.169. The free energy data used for the elements was that of Stull and Sinke[8]. The other data sources used, mainly those of Brewer and coworkers, are given in the table.

The empirical constants were evaluated from the free-energy data as near 1700°K as was feasible. Where tabulated data were available, the free-energy changes from the linear equation were calculated for comparison; in most cases the deviation of the values given by the equation from the tabulated data at extremes of the given temperature ranges were less than 500 cal/mole. The estimated equation constants were usually obtained from estimates of the free-energy functions of the gaseous molecules and from estimates of the heat capacities for the condensed phase.

Taking into account the effects of the oxygen pressure and of the dissociation and/or polymerization of the gas molecules requires some adjustment of the material balance equations that were developed for the application of Henry's law. From the generalized vaporization equation, the following quantities are defined:

$$N_j = n_j / \text{yn}(\ell) \tag{3.172}$$

for the mole fraction of the condensed oxide in solution and in equilibrium with one or more gaseous species, i;

$$N_{ij}^o = n_{ij}^o / \text{xyn} \tag{3.173}$$

for the mole fraction of the gaseous species, and

$$p_{ij} = N_{ij}^o P \tag{3.174}$$

Table 3.12

SUMMARY OF EMPIRICAL CONSTANTS[a] FOR VAPORIZATION REACTIONS OF FISSION PRODUCTS AND OTHER ELEMENTS

Reaction	Temperature Range (°K)	A[b]	B[b]	C[b]	M.P. (°K)
$1/2\ Na_2O(c) \rightarrow Na(g) + 1/4\ O_2(g)$	700–1,100	−10,300	8.242	$-1/4 \log P(O_2)$	1,190
$1/2\ Na_2O(\ell) \rightarrow Na(g) + 1/4\ O_2(g)$	1,100–2,000	−14,740	9.977	$-1/4 \log P(O_2)$	
$1/2\ K_2O(c) \rightarrow K(g) + 1/2\ O_2(g)$	700–1,033	−18,850	8.193	$-1/4 \log P(O_2)$	1078
$1/2\ K_2O(c) \rightarrow K(g) + 1/4\ O_2(g)$	1,033–1,500	−32,280	7.985	$-1/4 \log P(O_2)$	
$1/2\ Rb_2O(c) \rightarrow Rb(g) + 1/4\ O_2(g)$	700–974	−18,090	7.180	$-1/4 \log P(O_2)$	750
$1/2\ Rb_2O(\ell) \rightarrow Rb(g) + 1/4\ O_2(g)$	974–1,500	−33,070	6.886	$-1/4 \log P(O_2)$	
$1/2\ Cs_2O(c) \rightarrow Cs(g) + 1/4\ O_2(g)$	700–938	−16,540	7.470	$-1/4 \log P(O_2)$	708
$1/2\ Cs_2O(\ell) \rightarrow Cs(g) + 1/4\ O_2(g)$	938–1,500	−31,130	7.049	$-1/4 \log P(O_2)$	
$MgO(c) \rightarrow Mg(g) + 1/2\ O_2(g)$	923–1,093	−98,780	11.108	$-1/2 \log P(O_2)$	3,075
$MgO(c) \rightarrow Mg(g) + 1/2\ O_2(g)$	1,093–2,000	−98,470	10.891	$-1/2 \log P(O_2)$	
$MgO(\ell) \rightarrow Mg(g) + 1/2\ O_2(g)$	2,075–2,400	−88,580	7.977	$-1/2 \log P(O_2)$	
$CaO(c) \rightarrow Ca(g) + 1/2\ O_2(g)$	1,123–1,740	−91,800	10.108	$-1/2 \log P(O_2)$	2,860
$CaO(c) \rightarrow Ca(g) + 1/2\ O_2(g)$	1,740–2,000	−91,080	10.008	$-1/2 \log P(O_2)$	
$CaO(\ell) \rightarrow Ca(g) + 1/2\ O_2(g)$	2,800–3,000	−87,150	9.708	$-1/2 \log P(O_2)$	
$SrO(c) \rightarrow Sr(g) + 1/2\ O_2(g)$	1,023–1,040	−98,200	9.909	$-1/2 \log P(O_2)$	2,750
$SrO(c) \rightarrow Sr(g) + 1/2\ O_2(g)$	1,040–2,000	−97,010	9.828	$-1/2 \log P(O_2)$	
$SrO(c) \rightarrow SrO(g)$	1,000–2,000	−92,920	7.538	-	
$SrO(\ell) \rightarrow Sr(g) + 1/2\ O_2(g)$	2,700–3,000	−80,800	8.538	$-1/2 \log P(O_2)$	
$BaO(c) \rightarrow Ba(g) + 1/2\ O_2(g)$	1,000–2,196	−90,700	8.981	$-1/2 \log P(O_2)$	2,190
$BaO(c) \rightarrow BaO(g)$	1,000–2,196	−80,880	6.760	-	
$BaO(\ell) \rightarrow Ba(g) + 1/2\ O_2(g)$	2,196–3,000	−87,800	9.188	$-1/2 \log P(O_2)$	
$BaO(\ell) \rightarrow BaO(g)$	2,196–3,000	−80,980	6.988	-	
$ZnO(c) \rightarrow Zn(g) + 1/2\ O_2(g)$	998–2,000	−84,070	10.947	$-1/2 \log P(O_2)$	(2,000)
$ZnO(c) \rightarrow ZnO(g)$	1,000–2,000	(−84,080)[c]	(8.175)[c]	-	
$CdO(c) \rightarrow Cd(g) + 1/2\ O_2(g)$	1,088–2,000	−48,770	10.000	$-1/2 \log P(O_2)$	(d)
$1.000\ Fe_{0.947}O(c) \rightarrow Fe(g) + 0.894\ O_2(g)$	1,000–1,650	−85,550	10.042	$-0.894 \log P(O_2)$	1,650
$1.000\ Fe_{0.947}O(\ell) \rightarrow Fe(g) + 0.894\ O_2(g)$	1,650–2,000	−83,240	9.204	$-0.894 \log P(O_2)$	
$1/3\ Fe_3O_4(c) \rightarrow Fe(g) + 1/2\ O_2(g)$	1,000–1,870	−80,870	12.100	$-1/2 \log P(O_2)$	1,870
$1/3\ Fe_3O_4(\ell) \rightarrow Fe(g) + 1/2\ O_2(g)$	1,870–2,000	−67,240	10.082	$-1/2 \log P(O_2)$	
$1/2\ Y_2O_3(c) \rightarrow YO(g) + 1/4\ O_2(g)$	1,000–2,000	−44,850	11.005	$-1/4 \log P(O_2)$	2,000
$1/2\ La_2O_3(c) \rightarrow LaO(g) + 1/4\ O_2(g)$	1,000–2,500	−40,470	10.864	$-1/4 \log P(O_2)$	2,500
$1/2\ Pr_2O_3(c) \rightarrow PrO(g) + 1/4\ O_2(g)$	1,000–2,400	(−38,000)	(9.700)	$-1/4 \log P(O_2)$	(2,400)
$1/2\ Nd_2O_3(c) \rightarrow NdO(g) + 1/4\ O_2(g)$	1,000–2,350	(−34,810)	(10.047)	$-1/4 \log P(O_2)$	(2,350)

Table 3.12 (continued)

Reaction	Temperature Range (K)	A[b]	B[b]	C[b]	M.P.(K)
$1/3\ Pm_2O_3(c) \rightarrow PmO(g) + 1/4\ O_2(g)$	1,000-2,000	(-81,270)	(9.915)	-1/4 log P(O_2)	(2,000)
$1/3\ Nm_2O_3(c) \rightarrow NmO(g) + 1/4\ O_2(g)$	1,000-2,000	(-27,850)	(9.818)	-1/4 log P(O_2)	(2,000)
$1/3\ Al_2O_3(c) \rightarrow AlO(g) + 1/4\ O_2(g)$	1,000-2,200	-47,115	11.507	-1/4 log P(O_2)	2,300
$Al_2O_3(c) \rightarrow Al_2O(g) + O_2(g)$	1,000-2,000	-76,020	19.055	-log P(O_2)	
$1/3\ Al_2O_3(c) \rightarrow Al(g) + 3/4\ O_2(g)$	1,000-2,300	-99,750	14.545	-3/4 log P(O_2)	
$Al_2O_3(c) \rightarrow Al_2O(g) + 1/2\ O_2(g)$	1,500-2,300	-64,050	14.705	-1/2 log P(O_2)	
$1/3\ Al_2O_3(\ell) \rightarrow AlO(g) + 1/4\ O_2(g)$	2,300-3,500	(-47,940)	(11.500)	-1/4 log P(O_2)	
$Al_2O_3(\ell) \rightarrow Al_2O(g) + O_2(g)$	2,300-3,500	(-70,680)	(19.760)	-log P(O_2)	
$1/3\ Al_2O_3(\ell) \rightarrow Al(g) + 3/4\ O_2(g)$	2,300-3,500	(-90,560)	(14.708)	-3/4 log P(O_2)	
$1/3\ Ga_2O_3(c) \rightarrow GaO(g) + 1/4\ O_2(g)$	1,000-1,998	-41,860	11.928	-1/4 log P(O_2)	1,998
$Ga_2O_3(c) \rightarrow 2\ Ga(g) + 3/2\ O_2(g)$	1,000-1,998	-42,150	14.609	-3/4 log P(O_2)	
$1/3\ In_2O_3(c) \rightarrow InO(g) + 1/4\ O_2(g)$	1,000-2,000	-43,390	11.405	-1/4 log P(O_2)	1,500
$1/3\ In_2O_3(c) \rightarrow In(g) + 3/4\ O_2(g)$	1,000-2,000	-26,370	13.940	-3/4 log P(O_2)	
$2\ As_2O_3(\ell) \rightarrow As_4O_6(g)$	750-1,000	-3,675	5.025	-	586
$1/3\ As_2O_3(\ell) \rightarrow AsO(g) + 1/4\ O_2(g)$	1,000-2,000	(-16,670)	(7.948)	-1/4 log P(O_2)	
$2\ Sb_2O_3(\ell) \rightarrow As_4O_6(g)$	925-2,000	-3,894	5.298	-	928
$1/3\ Sb_2O_3(\ell) \rightarrow SbO(g) + 1/4\ O_2(g)$	1,000-2,000	(-25,720)	(8.716)	-1/4 log P(O_2)	
$ZrO_2(c) \rightarrow ZrO(g) + 1/2\ O_2(g)$	1,500-2,300	-60,900	13.468	-1/2 log P(O_2)	2,990
$ZrO_2(c) \rightarrow ZrO_2(g)$	1,500-2,500	-40,150	5.656	-	
$CeO_2(c) \rightarrow CeO(g) + 1/2\ O_2(g)$	1,500-2,870	(-45,610)	(14.501)	-1/2 log P(O_2)	2,870
$CeO_2(c) \rightarrow CeO_2(g)$	1,500-2,870	(-25,000)	(9.224)	-	
$UO_2(c) \rightarrow UO(g) + 1/2\ O_2(g)$	1,500-2,680	-58,670	12.048	-1/2 log P(O_2)	2,680
$UO_2(c) \rightarrow UO_2(g)$	1,500-2,680	-32,010	5.594	-	
$UO_2(c) + 1/2\ O_2 \rightarrow UO_3(g)$	1,500-2,680	-11,280	4.968	-1/2 log P(O_2)	
$SiO_2(c) \rightarrow SiO(g) + 1/2\ O_2(g)$	1,000-1,950	-40,180	12.090	-1/2 log P(O_2)	1,950
$SiO_2(c) \rightarrow SiO_2(g)$	1,000-1,950	-28,980	8.905	-	
$SiO_2(\ell) \rightarrow SiO(g) + 1/2\ O_2(g)$	1,950-2,500	-38,780	12.268	-1/2 log P(O_2)	
$SiO_2(\ell) \rightarrow SiO_2(g)$	1,950-2,500	-27,810	8.289	-	
$GeO_2(g\ell) \rightarrow GeO(g) + 1/2\ O_2(g)$	800-1,890	-39,250	12.020	-1/2 log P(O_2)	1,890
$GeO_2(\ell) \rightarrow GeO(g) + 1/2\ O_2(g)$	1,890-2,000	-31,920	10.892	-1/2 log P(O_2)	
$SnO_2(c) \rightarrow SnO(g) + 1/2\ O_2(g)$	1,500-1,898	-38,480	12.720	-1/2 log P(O_2)	1,898
$SnO_2(\ell) \rightarrow SnO(g) + 1/2\ O_2(g)$	1,898-2,500	-25,940	11.400	-1/2 log P(O_2)	
$RuO_2(c) \rightarrow RuO(g) + 1/2\ O_2(g)$	1,000-2,500	(-25,610)	(13.997)	-1/2 log P(O_2)	
$RuO_2(c) \rightarrow Ru(g) + O_2(g)$	1,000-2,000	-45,300	16.509	-log P(O_2)	
$1/2\ Rh_2O(c) + 1/4\ O_2(g) \rightarrow RhO(g)$	1,000-2,000	(-15,000)	(6.010)	-1/4 log P(O_2)	
$1/2\ Rh_2O(c) + 3/4\ O_2(g) \rightarrow RhO_2(g)$	1,000-1,500	-12,060	1.890	-3/4 log P(O_2)	
$ReO_3(c) \rightarrow ReO_2(g)$	500-1,000	-4,550	7.044	-	444 sub
$ReO_3(c) \rightarrow Re(g) + 1/2\ O_2(g)$	500-1,000	-13,714	10.704	-1/2 log P(O_2)	
$ReO_3(c) \rightarrow Re(g) + 1/2\ O_2(g)$	1,000-2,000	(-16,330)	(12.227)	-1/2 log P(O_2)	

Table 3.12 (concluded)

Reaction	Temperature Range (°K)	A[b]	B[b]	C[b]	M.P. (°K)
$TeO_2(c) \rightarrow TeO(g) + 1/2\ O_2(g)$	723–1,000	+28,870	12.880	+1/2 log P(O_2)	1,000
$TeO_2(\ell) \rightarrow TeO_2(g)$	1,000–2,000	(+10,150)	(6.606)	"	
$2\ TeO_2(\ell) \rightarrow Te_2(g) + 2\ O_2(g)$	1,000–2,000	(+88,000)	(18.278)	+ 2 log P(O_2)	
$TeO_2(\ell) \rightarrow TeO(g) + 1/2\ O_2(g)$	1,000–2,500	(+28,180)	(9.860)	+1/2 log P(O_2)	
$1/2\ Nb_2O_5(c) \rightarrow NbO(g) + 5/4\ O_2(g)$	1,000–1,785	+40,810	10.202	+5/4 log P(O_2)	1,785
$1/2\ Nb_2O_5(s) \rightarrow NbO_2(g) + 1/4\ O_2(g)$	1,000–1,785	+30,470	11.700	+1/4 log P(O_2)	
$1/2\ Nb_2O_5(\ell) \rightarrow NbO(g) + 5/4\ O_2(g)$	1,785–2,500	+40,800	14.225	+5/4 log P(O_2)	
$1/2\ Nb_2O_5(\ell) \rightarrow NbO_2(g) + 1/4\ O_2(g)$	1,785–2,500	+26,000	9.793	+1/4 log P(O_2)	
$3\ MoO_3(c) \rightarrow Mo_3O_9(g)$	800–1,068	+17,500	14.027	"	1,068
$4\ MoO_3(c) \rightarrow Mo_4O_{12}(g)$	800–1,068	+20,450	17.045	"	
$5\ MoO_3(c) \rightarrow Mo_5O_{15}(g)$	800–1,068	+23,077	18.647	"	
$MoO_3(\ell) \rightarrow MoO(g) + O_2(g)$	1,068–2,000	+51,590	13.888	+ log P(O_2)	
$MoO_3(\ell) \rightarrow MoO_2(g) + 1/2\ O_2(g)$	1,068–2,000	+34,780	10.140	+1/2 log P(O_2)	
$MoO_3(\ell) \rightarrow MoO_3(g)$	1,068–2,000	+17,810	7.570	"	
$2\ MoO_3(\ell) \rightarrow Mo_2O_6(g)$	1,068–2,000	+11,650	5.948	"	
$3\ MoO_3(\ell) \rightarrow Mo_3O_9(g)$	1,068–2,000	+ 4,705	3.089	"	
$4\ MoO_3(\ell) \rightarrow Mo_4O_{12}(g)$	1,068–2,000	+ 1,168	0.490	"	
$5\ MoO_3(\ell) \rightarrow Mo_5O_{15}(g)$	1,068–2,000	+ 1,081	-2.048	"	
$MoO_3(c) \rightarrow MoO_3(g)$	1,068–2,000	+29,210	8.990	"	
$MoO_3(c) + 1/2\ O_2(g) \rightarrow MoO_3(g)$	1,068–2,000	+12,340	6.418	+1/2 log P(O_2)	
$2\ MoO_3(c) + O_2(g) \rightarrow Mo_2O_8(g)$	1,068–2,000	+ 406.6	3.647	+ log P(O_2)	
$5\ MoO_3(c) + 5/2\ O_2(g) \rightarrow Mo_5O_{15}(g)$	1,068–2,000	+11,046	-0.061	+5/2 log P(O_2)	
$4\ MoO_3(c) + 2\ O_2(g) \rightarrow Mo_4O_{16}(g)$	1,068–2,000	+21,110	-4.108	+2 log P(O_2)	
$5\ MoO_3(c) + 5/2\ O_2(g) \rightarrow Mo_5O_{20}(g)$	1,068–2,000	+28,880	-7.798	+5/2 log P(O_2)	
$TeO_2(c,\ell) \rightarrow TeO(g) + 1/2\ O_2(g)$	1,000–2,000	(+45,980)	(12.607)	+1/2 log P(O_2)	
$TeO_2(c,\ell) \rightarrow TeO_2(g)$	1,000–2,000	(+25,670)	(9.004)	"	
$Te_2O_7(\ell) \rightarrow Te_2O_7(g)$	898– 988	+ 8,089	5.228	"	898
$Cu(c) \rightarrow Cu(g)$	800–1,356	+17,419	6.814	"	1,356
$Cu(\ell) \rightarrow Cu(g)$	1,356–2,000	+16,558	6.881	"	
$Ag(s) \rightarrow Ag(g)$	800–1,234	+14,689	6.844	"	1,234
$Ag(\ell) \rightarrow Ag(g)$	1,234–2,000	+13,788	6.078	"	
$Pd(c) \rightarrow Pd(g)$	1,000–1,828	+20,010	6.106	"	1,828
$Pd(\ell) \rightarrow Pd(g)$	1,828–2,500	+19,140	6.040	"	
$Kr(\ell) \rightarrow Kr(g)$	"	"	"	"	
$Xe(\ell) \rightarrow Xe(g)$	"	"	"	"	
$NaBr(\ell) \rightarrow NaBr(g)$	1,026–2,000	+8,010	5.046	"	1,026
$NaI(\ell) \rightarrow NaI(g)$	982–2,000	+8,840	5.050	"	982

a. Values in parentheses are estimated values.
b. See text.

Bibliography for Table 3.13

1. Coughlin, James P., Bureau of Mines, Bulletin 542, 1954.

2. Stull, D. R., and G. C. Sinke, The Thermodynamic Properties of the Elements, Am. Chem. Soc., Washington, D.C. 1956.

3. Kelley, K. K., Bureau of Mines, Bulletin 584, 1960.

4. Brewer, Leo, Chem. Revs., 52, 1 (1953).

5. Brewer, Leo, UCRL-2854 (rev.), 1955.

6. Brewer, Leo, UCRL-8856, 1958.

7. Brewer, Leo, and J. Drowart, UCRL-8686, 1959.

8. Chandrasekharaiah, M. S., and L. Brewer, UCRL-8736, 1959.

9. Brewer, L., and M. S. Chandrasekharaiah, UCRL-8713 (rev.), 1960.

10. Chupka, W. A., and J. Berkowitz, J. Chem. Physics, 26, 1207 (1957).

11. Burns, R. P., G. De Maria, J. Drowart, and R. T. Grimley, J. Chem. Physics, 32, 1668 (1960).

12. Drowart, J., G. De Maria, R. P. Burns, and M. G. Inghram, J. Chem. Physics, 32, 1366 (1960).

13. Chupka, W. A., M. G. Inghram, R. F. Porter, J. Chem. Physics, 24 702 (1956).

14. De Maria, G., R. P. Burns, J. Drowart, and M. G. Inghram, J. Chem. Physics, 32, 1378 (1960).

15. Alcock, C. B., and G. W. Hooper, Proc. Royal Society (London), A254, 551 (1960).

16. Soulen, J. R., P. Shapiianonda, and J. L. Margrave, J. Chem. Physics, 50, 182 (1955).

Combining these with Eq. 3.8 gives

$$n_{ij}^{n} \quad s_{ij} k_{ij}^{n} \tag{3.175}$$

where k_{ij}^{n} is substituted for $p_{ij}^{n} / \left[(n(\ell)/V) RT \right]$

These definitions, together with use of Raoult's law and the material balance requirements, result in the value of k_{j}^{n} defined for Eq. 3.37 to be given by

$$k_{j}^{n} \quad \sum_{i} s_{ij} k_{ij}^{n} \tag{3.176}$$

The values of s_{ij} are given by the individual reactions in Table 3.12.

At the temperature of the soil melting point i.e., at the end of first period of condensation, the gases that determine the total pressure are the nitrogen and oxygen of the air. The partial pressures of all the other materials are relatively small. In the model surface burst, relatively large amounts of soil are considered to be vaporized so that the vapor products of Al_2O_3, Na_2O, and SiO_2 are introduced into the fireball. The Al_2O_3, with a boiling point of about 3000°K (in 1 atmosphere of oxygen) could start vapor-condensing at this, or lower, temperature into liquid drops. In doing so the Al_2O_3 would co-condense some of the less volatile fission products which could not vapor-condense otherwise because their individual vapor pressure would be lower than that calculated from the data of Table 3.12. These small vapor-condensed Al_2O_3 drops may solidify, when they cool to about 2300°K, or they may combine with the SiO_2 liquid drops, that are forming at about this temperature, to form alumino-silicate liquid drops.

Also, at these lower temperatures, larger soil particles entering the fireball can exist in the liquid state and would dissolve any of these small particles they collide with. In a very short time the majority of these small particles disappear. In the meantime, the more volatile fission-product elements are condensing into all the liquid particles present according to their vapor pressure equilibria with the liquid phase.

If one is interested in the equilibria conditions at the higher temperatures when the partial pressures from the soil constituents are high, then these constituents must be considered and added to the partial pressures of N_2, O_2, and possibly O. However, if it is assumed that no particles leave the fireball before the end of the first period of condensation, then it suffices to compute the fractions of each radioelement condensed at that instant. At this time or temperature even the partial pressure of the Na_2O (or Na) can be neglected. This assumption was followed in the foregoing computations.

The weighted values of the Raoult's law constants, or vapor pressures, of all the elements of interest at 1073°K are summarized in Table 3.13; an oxygen pressure of 0.2 atmosphere was used in the calculation. The two rare gas elements have been assigned infinity values because it is expected that the fractions of those elements condensing in the molten glass would be negligible. The other elements that are indicated as not fully condensed in the ideal solution are Cl, As, Se, Br, Rb, Mo, Ru, Cd, Sb, Te, I, and Cs.

If no carrier material were present in the fireball with the fission product elements and if all were in the vapor state at 1073°K, their partial pressures could be estimated from use of the perfect gas law using the calculated volume of the model surface burst fireball and the yield factor of 0.5 moles of fission products per KT. The calculated partial pressures for a 14-MT yield surface burst fireball are shown in Table 3.14 for some of the more abundant fission product elements. The atom percent abundances were taken from the tabulations of Bolles and Ballou[10]. Of all the elements listed, only Sr, La, and Zr would have condensed to a solid state at the indicated temperature and time.

In order to test the effect of weapon yield on the fractions of each fission product nuclide condensed in the ideal solution as previously stated, end-period times of 0 and 60 seconds were selected; these correspond to yields of about 84 and 14,000 KT, respectively. The $r_0(A)$ calculations were made by rearranging Eq. 3.40 for the independent nuclide yields in terms of 10^4 fissions so that the data of Bolles and Ballou[10] could be used without conversion to fractions of the chain yield. The chain yields derived from Glendenin's postulate were used. The calculations were made from the chain summations according to

$$r_0(A,t) = \frac{\sum_j N_j(A,t)/(1+k_j^0)}{\sum_j N_j(A,t)} \qquad (3.177)$$

where $N_j(A,t)$ is the number of atoms of element, j, of mass number, A, per 10^4 fissions present at time, t, after fission. The values of $(n(\ell)/V)RT$, from the data of Table 3.23 are 2.84×10^{-4} atmosphere for the 84-KT yield and 3.25×10^{-4} atmosphere for the 14-MT yield. The calculated values of $r_0(A)$ for each nuclide contributing to the gross activity at 45.8 minutes after fission are given in Table 3.15. It may be noted that the fractions of the Kr and Xe isotopes condensed are not zero. This is because it was assumed that these, as decay products of Br and I, do not readily escape from the glass after it has solidified.

Table 3.13

SUMMARY OF RAOULT'S LAW CONSTANTS FOR THE GASEOUS SPECIES OF THE FISSION PRODUCT AND OTHER ELEMENTS AT 1073°K

Element	p_j^0(atmos)[a]	Element	p_j^0(atmos)
Cu	9.04×10^{-5}	Ag	2.70×10^{-3}
Zn	2.05×10^{-1}	Cd	0.302
Ga	9.75×10^{-11}	In	2.60×10^{-9}
Ge	0.420	Sn	1.22×10^{-4}
As	1.35×10^{5}	Sb	1.84
Se	1.01×10^{6}	Te	4.04
Br	1.04	I	2.25
Kr	(∞)[b]	Xe	(∞)[b]
Rb	0.605	Cs	1.88
Sr	4.61×10^{-16}	Ba	2.04×10^{-9}
Y	8.75×10^{-16}	La	3.53×10^{-14}
Zr	4.54×10^{-16}	Ce	4.08×10^{-8}
Nb	2.97×10^{-7}	Pr	8.30×10^{-14}
Mo	13.32	Nd	5.20×10^{-11}
Tc	5.26×10^{-5}	Pm	1.24×10^{-10}
Ru	1.14	Sm	1.31×10^{-7}
Rh	1.08×10^{-3}	U	8.50×10^{-4}
Pd	1.39×10^{-6}		

a. $p_j^0 = \Sigma_i x_i p_{ij}^0$

b. Taken to be large so that the fraction condensed is negligible.

Table 3.14

CALCULATED PARTIAL PRESSURES AND EQUILIBRIUM PARTIAL PRESSURES OF SOME OF THE MORE ABUNDANT FISSION PRODUCT ELEMENTS DISPERSED UNIFORMLY IN THE MODEL SURFACE-BURST FIREBALL AT 1078°K FOR A FISSION YIELD OF 14-MT

Element	Percent Number of Atoms at 1 min.	Partial Pressure in Volume (10^{-9} atmos)	Partial Pressure Over Oxide (atmos)
Rb	5	1.0	1.2
Cs	5	1.0	3.8
Sr*	8	3.0	4.0×10^{-13}
Ba	7	2.6	2.0×10^{-6}
La*	4	1.7	3.5×10^{-14}
Ce	6	2.2	4.4×10^{-5}
Sb	4	1.5	0.02
Zr*	8	3.0	4.5×10^{-15}
Nb	6	2.2	5.0×10^{-7}
Mo	8	3.0	4.2
Te	6	2.2	1.0

*Elements that would have formed a condensed phase from the vapor at 1078°K

The most exact method of computing the amount of each radionuclide present (and its activity) for a given number of fissions would be to use the value of $y_j(A)/(11k)'$ for each and the appropriate decay formula for the production of the daughter products. But to simplify the computation process, the calculations were made by direct multiplication of the $r_n(A)$ values and the single nuclide d/m values per 10^4 fissions and the disintegration multipliers as given in Table 3.16. Although this procedure gives higher values for the daughter products in each chain, the error decreases with time. Compared to other possible errors involved in the computation, the error due to this approximation is rather insignificant.

For example, at 60 seconds the initial fraction for Sr-89 is 0.010 which increases, after Rb-89 decays out, to 0.0206, in the exact method of computation, the latter value is reached by 2.5 hours. The r_n (60) value for Sr-90 is valid from 31.2 minutes and the $r_n(140)$ value for Ba-140 is essentially valid at 60 seconds. The multipliers of Table 3.16 are from decay scheme data available up to about 1959 as indicated by the references given in the table.

Table 8.15

Summary Of r_{ij} (A) Values At 0 and 60 Seconds After Fission For Fission Product Nuclides That Contribute To The Gross Activity At 45.8 Minutes And Longer Times After Fission

Nuclide	r_{ij} (A)	
	(0 sec)	(60 sec)
Zn-72	0.004	0.004
Zn-74	0.004	0.004
Ga-72	0.006	0.004
Ga-73	0.006	0.006
Ga-74	0.007	0.004
Ge-75	0.042	0.005
Ge_g-77	0.074	0.146
Ge-78	0.424	0.0758
As-77	0.062	0.114
As-78	0.414	0.0788
As-79	0.276	0.0150
Se_1-81	0.0050	0.000801
Se_1-83	0.0028	0.000158
Se_1-83	0.00100	0.0
Br-83	0.00175	0.00702
Br-84	0.002210	0.00080
Kr-83	0.00175	0.00702
Kr_1-85	0.0122	0.0258
Kr_g-85	0.0122	0.0240
Kr-87	0.0190	0.0167
Kr-88	0.0125	0.00152
Rb-88	0.0180	0.00226
Rb-89	0.00804	0.0128
Rb_g-91	0.0280	0.0504
Sr-89	0.00804	0.0201
Sr-90	0.0021	0.101
Sr-91	0.107	0.200
Sr-92	0.205	0.024
Sr-93	0.708	0.008
Y-90	0.0021	0.101
Y-91	0.107	0.200
Y_g-91	0.107	0.200
Y-92	0.308	0.025
Y-93	0.724	0.008
Y-94	0.040	1.00
Zr-95	0.080	1.00
Zr-97	1.00	1.00
Nb_1-95	0.080	1.00
Nb_g-95	0.080	1.00
Nb-97	1.00	1.00
Nb_1-97	1.00	1.00
Nb-98	1.00	1.00
Mo-99	0.057	0.764
Mo-101	0.011	0.0237
Mo-102	0.009	0.00507
Tc-99	0.057	0.764
Tc-101	0.013	0.0036
Tc-102	0.044	0.0804
Ru-103	0.050	0.536
Ru-105	0.025	0.110
Ru-106	0.450	0.0270
Rh-103	0.050	0.536
Rh_1-105	0.025	0.111
Rh_g-105	0.025	0.112
Rh-106	0.450	0.0270
Rh-107	0.048	0.167
Pd-109	0.409	0.009
Pd-111	0.801	0.008
Pd-112	0.018	1.00
Ag-109	0.409	0.009
Ag-111	0.801	0.006
Ag-112	0.014	1.00
Ag-113	0.008	0.001
Ag-115	0.004	0.026
Cd_1-115	0.008	0.005
Cd_g-115	0.008	0.005
Cd-117	0.847	0.468
Cd-118	0.740	0.258
Cd-120	0.564	0.0000
In-115	0.004	
In-117	0.847	
In-118	0.740	
In-119	0.020	
In-120	0.008	
Sn-121	0.384	
Sn-123	0.020	
Sn-125	0.008	
Sn-126	0.050	
Sn-127	0.003	
Sb-125	0.860	
Sb-126	0.045	
Sb-127	0.044	
Sb-128	0.050	
Sb-129	0.200	
Sb-131	0.0807	
Te_1-125	0.860	
Te_1-127	0.044	
Te_1-127	0.044	
Te_g-129	0.200	
Te_g-129	0.202	
Te_1-131	0.0807	
Te_1-131	0.0764	
Te_g-132	0.0357	
Te_1-133	0.0120	
Te_g-133	0.0113	
Te-134	0.00803	
I-131	0.0752	
I-132	0.0852	
I-133	0.0110	
I-134	0.00800	
I-135	0.0103	
Xe_1-131	0.0702	
Xe_1-133	0.0110	
Xe_1-133	0.0110	
Xe_g-135	0.0101	
Xe_1-135	0.00954	
Xe_g-138	0.00280	
Cs-137	0.00720	
Cs-138	0.00300	
Cs-139	0.0116	

Table 3.16

Summary Of r_0 (A) Values At 0 and 60 Seconds After Fission For Fission Product Nuclides That Contribute To The Gross Activity At 46.8 Minutes And Longer Times After Fission

Nuclide	r_0 (A)	
	(0 sec)	(60 sec)
Zr-96	0.080	1.00
Zr-97	1.00	1.00
Nb^1-95	0.080	1.00
Nb^2-95	0.080	1.00
Nb^1-97	1.00	1.00
Nb^1-97	1.00	1.00
Nb^2-98	1.00	1.00
Mo-99	0.057	0.704
Mo-101	0.511	0.0207
Mo-102	0.000	0.00507
Tc-99	0.057	0.704
Tc-101	0.513	0.0086
Tc-102	0.044	0.0804
Ru-103	0.355	0.550
Ru-105	0.525	0.110
Ru-106	0.450	0.0270
Rh-103	0.000	0.506
Rh^1-105	0.525	0.111
Rh^2-105	0.525	0.112
Rh-106	0.450	0.0270
Rh-107	0.940	0.107
Pd-109	0.409	0.009
Pd-111	0.801	0.008
Pd-112	0.010	1.00
Ag-109	0.409	0.009
Ag-111	0.801	0.008
Ag-112	0.014	1.00
Ag-113	0.008	0.001
Ag-115	0.004	0.000
Cd^1-115	0.008	0.006
Cd^2-115	0.008	0.005
Cd-117	0.847	0.408
Cd-118	0.748	0.250
Cd-120	0.884	0.0000

Nuclide	r_0 (A)	
	(0 sec)	(60 sec)
In^1-115	0.004	0.020
In-117	0.847	0.400
In-118	0.748	0.253
In-119	0.020	0.285
In-120	0.052	0.144
Sn-121	0.004	0.815
Sn-123	0.020	0.080
Sn-125	0.863	0.000
Sn-126	0.050	0.000
Sn-127	0.003	0.096
Sb-125	0.860	0.000
Sb-126	0.048	0.071
Sb-127	0.044	0.041
Sb-128	0.550	0.0882
Sb-129	0.296	0.0178
Sb-131	0.0807	0.0174
Te^1-125	0.860	0.000
Te^1-127	0.044	0.041
Te^2-127	0.044	0.041
Te^1-129	0.296	0.0177
Te^2-129	0.292	0.0170
Te^1-131	0.0807	0.0165
Te^2-131	0.0754	0.0150
Te^2-132	0.0057	0.0124
Te_1-133	0.0126	0.0135
Te^2-133	0.0112	0.0124
Te-134	0.00801	0.00061
I-131	0.0752	0.0150
I-132	0.0052	0.0124
I-133	0.0110	0.0110
I-134	0.00080	0.00081
I-135	0.0100	0.0141
Xe^1-131	0.0752	0.0150
Xe^1-133	0.0113	0.0110
Xe^2-133	0.0113	0.0110
Xe^2-135	0.0101	0.0108
Xe^1-135	0.00084	0.0134
Xe-138	0.00286	0.0
Cs-137	0.00726	0.00303
Cs-138	0.00086	0.00201
Cs-139	0.0110	0.0170

Nuclide	r_0 (A)	
	(0 sec)	(60 sec)
Ba-137	0.00726	0.00303
Ba-139	0.0320	0.0010
Ba-140	0.107	0.442
Ba-141	0.870	0.001
Ba-142	0.850	1.00
La-140	0.107	0.442
La-141	0.882	0.001
La-142	0.870	1.00
La-143	0.085	1.00
Ce-141	0.882	0.001
Ce-143	0.080	1.00
Ce-144	1.00	1.00
Ce-145	1.00	1.00
Ce-146	1.00	1.00
Pr-143	0.080	1.00
Pr-144	1.00	1.00
Pr-145	1.00	1.00
Pr-146	1.00	1.00
Nd-147	1.00	1.00
Nd-149	1.00	1.00
Nd-151	1.00	1.00
Pm-147	1.00	1.00
Pm-149	1.00	1.00
Pm-150	1.00	1.00
Pm-151	1.00	1.00
Pm-152	1.00	1.00
Pm-153	1.00	1.00
Sm-151	1.00	1.00
Sm-153	1.00	1.00
Sm-155	1.00	1.00
Sm-156	1.00	1.00
Sm-158	1.00	1.00
Eu-155	1.00	1.00
Eu-156	1.00	1.00
Eu-157	1.00	1.00
Eu-158	1.00	1.00
Gd-159	1.00	1.00
Tb-161	1.00	1.00

Table 3.16

SUMMARY OF DISINTEGRATION MULTIPLIERS
FOR THE FISSION PRODUCT AND OTHER RADIONUCLIDES[a]

Nuclide	Betas (Betas /dis)	Photons (Photons /dis)	Photon Energy (Mev/dis)	Air Ionization $\left(\frac{10^{-9}\ r/hr\text{-}ft^2}{dis/sec}\right)$	Meter Response $\left(\frac{10^{-9}\ r/hr\text{-}ft^2}{dis/sec}\right)$
Zn-72	1.00	0.95	1.24	6.75	5.18
Zn-74	1.00	1.00	0.70	4.22	3.28
Ga-72	1.00	2.07	2.81	14.3	10.7
Ga-73	1.00	3.02	0.350	2.11	1.30
Ga-74	1.00	1.80	2.57	12.4	9.07
Ge-75	1.00	0.136	0.0356	0.216	0.170
Ge-77	1.00	2.80	2.38	13.1	10.1
Ge-78	1.00	1.00	0.445	2.74	2.14
As-77	1.00	0.042	0.0109	0.0735	0.0520
As-78	1.00	0.555	0.436	2.51	1.78
As-79	1.00	0.0	0.0	0.0	0.0
Se_I-81m	0.0	1.00	0.0206	0.117	0.0446
Se_{II}-81	1.00	0.0	0.0	0.0	0.0
Se-83	1.00	3.04	2.26	12.8	10.2
Br-83	1.00	0.15	0.0029	0.0174	0.00426
Br-84	1.00	1.05	1.68	8.12	6.26
Kr-83m	0.0	2.00	0.0160	0.0959	0.0
Kr_I-85m	0.77	1.00	0.161	0.975	0.681
Kr_{II}-85	1.00	0.010	0.0052	0.0316	0.0247
Kr-87	1.00	1.38	1.41	7.03	5.20
Kr-88	1.00	1.60	1.50	7.40	5.42
Rb-88	1.00	0.533	0.861	4.30	3.23
Rb-89	1.00	1.71	2.30	12.0	9.03
Rb-91	1.00	1.00	1.20	6.67	5.11

Table 3.16 (continued)

Nuclide	Betas (Betas /dis)	Photons (Photons /dis)	Photon Energy (Mev/dis)	Air Ionization $\left(\frac{10^{-6}\ r/hr\text{-}ft^2}{dis/sec}\right)$	Meter Response $\left(\frac{10^{-6}\ r/hr\text{-}ft^2}{dis/sec}\right)$
Sr-89	1.00	0.0	0.0	0.0	0.0
Sr-90	1.00	0.0	0.0	0.0	0.0
Sr-91	1.00	0.08	0.806	5.08	3.66
Sr-92	1.00	1.02	1.28	6.08	5.48
Sr-93	1.00	1.00	0.2	1.20	0.964
Y-90	1.00	0.0002	0.0001	0.008	0.006
Y_1-91m	0.0	1.00	0.526	3.24	2.52
Y_2-91	1.00	0.002	0.0024	0.0135	0.0102
Y-92	1.00	1.44	1.17	6.50	5.05
Y-93	1.00	0.196	0.150	0.817	0.633
Y-94	1.00	1.00	1.2	6.07	5.11
Zr-95	1.00	0.97	0.719	4.32	3.35
Zr-97	1.00	0.076	0.0301	0.346	0.268
Nb_1-95m	0.0	1.00	0.233	1.41	1.12
Nb_2-95	1.00	1.00	0.702	4.56	3.54
Nb_1-97m	0.0	1.00	0.736	4.42	3.42
Nb_2-97	1.00	1.00	0.665	4.02	3.13
Nb-98	1.00	1.00	2.7	11.7	8.10
Mo-99	1.00	0.415	0.100	0.772	0.597
Mo-101	1.00	1.70	0.814	6.85	3.07
Mo-102	1.00	0.0	0.0	0.0	0.0
Tc-99m	0.0	1.00	0.150	0.782	0.614
Tc-101	1.00	1.05	0.334	2.00	1.56
Tc-102	1.00	1.00	0.4	2.45	1.88
Ru-103	1.00	0.991	0.487	2.90	2.30
Ru-105	1.00	1.00	0.720	4.30	3.39
Ru-106	1.00	0.0	0.0	0.0	0.0

Table 3.10 (continued)

Nuclide	Betas (Betas /dis)	Photons (Photons /dis)	Photon Energy (Mev/dis)	Air Ionization $\left(\frac{10^{-9}\ r/hr\text{-}ft^2}{dis/sec}\right)$	Meter Response $\left(\frac{10^{-9}\ r/hr\text{-}ft^2}{dis/sec}\right)$
Rh-106m	0.0	1.00	0.0207	0.150	0.0192
Rh_1-105m	0.0	1.00	0.0472	0.388	0.154
Rh_2-105	1.00	0.30	0.0015	0.550	0.467
Rh-106	1.00	0.488	0.304	1.81	1.41
Rh-107	1.00	3.00	0.829	5.08	3.90
Pd-109	1.00	0.0	0.0	0.0	0.0
Pd-111	1.00	1.20	0.88	5.00	3.90
Pd-112	1.00	1.00	0.0037	0.0225	0.0
Ag-109m	0.0	1.00	0.0288	0.172	0.0302
Ag-111	1.00	0.11	0.0286	0.175	0.134
Ag-112	1.00	0.85	0.843	4.59	3.50
Ag-110	1.00	0.090	0.0268	0.158	0.0950
Ag-115	1.00	1.09	0.211	1.26	0.960
Cd_2-115	1.00	0.030	0.0328	0.187	0.144
Cd_2-115	1.00	0.088	0.180	1.11	0.863
Cd-117m	0.0	2.00	1.40	8.11	6.08
Cd-116	1.00	0.0	0.0	0.0	0.0
Cd-120	1.00	1.00	0.5	3.08	2.40
In-115	1.00	0.045	0.184	1.12	0.851
In-117	1.00	0.89	0.224	1.00	1.00
In-116	1.00	1.00	3.3	19.5	8.25
In-110	1.00	1.00	0.092	0.0371	0.0
Sn-121	1.00	0.0	0.0	0.0	0.0
Sn-120	1.00	0.0	0.0	0.0	0.0
Sn-125	1.00	1.71	1.05	6.19	4.82
Sn-120	1.00	0.0	0.0	0.0	0.0
Sn-127	1.00	1.00	0.5	3.08	2.40
Sb-125	1.00	1.55	0.455	2.78	2.08
Sb-120	1.00	3.00	2.82	16.1	12.4
Sb-127	1.00	1.20	0.446	2.70	2.05
Sb-128	1.00	2.00	2.4	13.0	9.95
Sb-120	1.00	2.55	1.00	6.10	4.75
Sb-131	1.00	1.00	0.6	3.66	2.80

Table 3.16 (continued)

Nuclide	Betas (Betas /dis)	Photons (Photons /dis)	Photon Energy (Mev/dis)	Air Ionization $\left(\frac{10^{-9}\ r/hr\text{-}ft^2}{dis/sec}\right)$	Meter Response $\left(\frac{10^{-9}\ r/hr\text{-}ft^2}{dis/sec}\right)$
Te_I-125m	0.0	2.0	0.0502	0.0525	0.0054
Te_I-127	0.015	0.995	0.0276	0.151	0.0
Te_{II}-127	1.00	0.0120	0.0040	0.0240	0.0192
Te_I-129m	0.0	1.00	0.0670	0.396	0.230
Te_{II}-129	1.00	1.50	0.262	1.52	1.00
Te_I-131	0.785	3.12	1.48	8.42	6.48
Te_{II}-131	1.00	1.20	0.347	2.08	1.62
Te-132	1.00	2.00	0.253	1.52	1.15
Te_I-133m	0.0	1.00	0.128	0.790	0.544
Te_{II}-133	1.00	1.70	1.57	9.12	7.04
Te-134	1.00	1.00	1.50	7.89	6.00
I-131	1.00	1.05	0.390	2.35	1.85
I-132	1.00	2.77	2.22	13.0	10.0
I-133	1.00	1.05	0.590	3.50	2.80
I-134	1.00	1.70	1.66	9.63	7.42
I-135	1.00	1.40	1.76	9.60	7.17
Xe_I-131	0.0	1.00	0.0344	0.207	0.0273
Xe_I-133m	0.0	1.00	0.0682	0.413	0.211
Xe_{II}-133	1.00	1.00	0.0510	0.304	0.121
Xe_I-135m	0.0	1.00	0.427	2.60	2.07
Xe_{II}-135	1.00	1.00	0.254	1.55	1.21
Xe-138	1.00	1.00	1.5	7.80	6.00
Cs-137	1.00	0.0	0.0	0.0	0.0
Cs-136	1.00	1.71	2.15	11.2	8.47
Cs-138	1.00	2.00	0.787	4.75	3.72
Ba-139m	0.0	1.00	0.007	0.65	2.88
Ba-137	1.00	0.37	0.143	0.886	0.690
Ba-140	1.00	1.14	0.183	1.10	0.846
Ba-141	1.00	1.00	0.7	4.22	3.28
Ba-142	1.00	1.00	1.0	5.70	4.44

Tabel 3.10 (continued)

Nuclide	Betas (Betas /dis)	Photons (Photons /dis)	Photon Energy (Mev/dis)	Air Ionization $\left(\frac{10^{-9}\ r/hr\text{-}ft^2}{dis/sec}\right)$	Meter Response $\left(\frac{10^{-9}\ r/hr\text{-}ft^2}{dis/sec}\right)$
La-140	1.00	2.66	2.42	13.0	8.93
La-141	1.00	0.05	0.0765	0.400	0.304
La-142	1.00	1.70	2.33	11.6	8.87
La-143	1.00	1.0	1.2	6.07	5.11
Ce-141	1.00	0.708	0.0778	0.470	0.353
Ce-143	1.00	1.66	0.890	2.54	1.73
Ce-144	1.00	0.481	0.0512	0.188	0.117
Ce-145	1.00	1.00	0.7	4.22	3.26
Ce-146	1.00	1.30	0.265	1.60	1.24
Pr-143	1.00	0.0	0.0	0.0	0.0
Pr-144	1.00	0.0255	0.0315	0.163	0.125
Pr-145	1.00	0.0	0.0	0.0	0.0
Pr-146	1.00	1.55	1.12	6.42	4.94
Nd-147	1.00	1.05	0.157	0.968	0.683
Nd-149	1.00	2.35	0.383	2.31	1.74
Nd-151	1.00	2.25	1.10	6.44	4.91
Pm-147	1.00	0.0	0.0	0.0	0.0
Pm-149	1.00	1.80	1.26	7.25	5.67
Pm-150	1.00	1.61	0.844	4.09	3.55
Pm-151	1.00	1.50	0.366	2.21	1.68
Pm-152	1.00	2.00	0.62	3.79	2.96
Pm-153	1.00	1.0	0.8	4.76	3.69
Sm-151	1.00	1.00	0.0000	0.0544	0.0
Sm-153	1.00	1.20	0.0756	0.455	0.271
Sm-155	1.00	2.00	0.001	1.80	1.36
Sm-156	1.00	1.0	0.2	1.20	0.964
Sm-158	1.00	1.0	0.5	3.08	2.40
Eu-155	1.00	1.44	0.0560	0.314	0.178
Eu-156	1.00	0.00	1.14	5.55	4.17
Eu-157	1.00	1.75	0.028	3.78	2.00
Eu-158	1.00	2.00	1.2	7.21	5.60

Table 3.10 (concluded)

Nuclide	Betas (Betas /dis)	Photons (Photons /dis)	Photon Energy (Mev/dis)	Air Ionization $\left(\frac{10^{-9}\ r/hr\text{-}ft^2}{dis/sec}\right)$	Meter Response $\left(\frac{10^{-9}\ r/hr\text{-}ft^2}{dis/sec}\right)$
Gd-159	1.00	0.288	0.0721	0.430	0.328
Tb-161	1.00	0.50	0.0207	0.123	0.0570
U-237	1.00	2.77	0.200	1.13	0.808
U-239	1.00	1.00	0.0641	0.388	0.215
U-240	1.00	0.0	0.0	0.0	0.0
Np-239	1.00	2.07	0.185	1.11	0.790
Np-240	1.00	0.46	0.852	2.07	1.60
Mn-56	1.00	1.47	1.76	9.40	7.17

a. References: (1) C. F. Miller, Response Curves for USNRDL 4-pi Ionization Chamber, USNRDL-TR-155 (1957)
(2) C. F. Miller, Proposed Decay Schemes for Some Fission-Product and Other Radionuclides, USNRDL-TR-160 (1957)
(3) C. F. Miller and P. Loeb (Ref. 12)
(4) P. D. La Riviere, private communication, (July 1959)

3.5 Computing the Decay Rates of Fission Product Mixtures

In making the decay rate computations, the data of Bolles and Ballou[10] based on Glendenin's postulate of independent yields for the slow neutron fission of U-235 were used as the basic input data. As discussed in Section 3.4, it is assumed that the fractional chain yields are the same for all fissile nuclides so that the disintegration rate per fission of a given nuclide from each type of fission differs only by a constant. This constant is the ratio of the mass chain yield in a given type of fission to the mass chain yield in the slow neutron fission of U-235, this constant is here called the chain-yield multiplier.

Where the decay schemes of fission products are known, gamma ray characteristics can be calculated. In this case it is convenient to give multipliers in terms of the characteristic emissions per disintegration of each nuclide. The multipliers for the gamma ray energy emitted, in terms of Mev/dis and r/hr at 3 feet above an ideal plane per dis/sec per sq ft., given in Table 3.16, are ones of chief interest for use in these calculations.

The results of the computations of the disintegration rates, photon emission rates, photon energy emission rates, and air ionization rates, for times extending from 45.8 minutes to 25.7 years after fission for the fissile nuclides U-235, U-238, and Pu-239, are given in Table 3.17. The use of Katcoff's yields[11] (adjusted) for thermal fission give disintegration rates that are almost identical with those of Bolles and Ballou. The air ionization rate (U-235, thermal) is also very close to that of Reference 12; at 2.4 hours, it is about 5 percent higher and at 2.6 years it is about 10 percent lower (maximum fluctuation).

Dolan[13,14] calculated the disintegration rates and photon emission rates for 14-Mev neutron fission of U-235. The ratios of the calculations for 2-Mev neutron fission of U-235 in Table 3.17 to Dolan's values for 14-Mev neutrons are given in Figure 3.4. It may be noted that the disintegration rates are within 5 percent of each other from 1 to about 350 hours; the agreement in the photon emission rates is not quite as good, with Dolan's values being more than 10 percent lower after 40 hours. The maximum spread is +8 percent at (75 hours) to -12 percent at (2,500 hours) for the disintegrations-per-second computations, and +6 percent at (7.5 hours) to -17 percent at (1,200 hours) for the photons-per-second computations. A few more photons were counted in the method by which the data in Table 3.17 were obtained than by the method used by Dolan; these photons were chiefly in the energy range 0 to 20 Kev.

Table 3.17

DECAY OF NORMAL FISSION PRODUCTS FROM U-235, U-238 AND Pu-239

1. In dis/sec for 10^4 fission (Glendenin)

Age			U-235		U-238	Pu-239	
Years	Days	Hours	Thermal	Fission	(8 Mev)	Thermal	Fission
		0.766	1.615	1.615	1.598	1.556	1.536
		1.12	1.072	1.076	1.048	1.008	1.001
		1.64	0.6800	0.6933	0.6578	0.6259	0.6269
		2.40	0.4361	0.4454	0.4152	0.3867	0.3936
		3.52	0.2818	0.2908	0.2691	0.2473	0.2568
		5.16	0.1847	0.1916	0.1780	0.1640	0.1734
		7.56	0.1228	0.1271	0.1195	0.1117	0.1186
		11.1	(1)8171	(1)8393	(1)8000	(1)7601	(1)8036
		16.2	(1)5260	(1)5373	(1)5201	(1)5107	(1)5245
		23.8	(1)3511	(1)3541	(1)3291	(1)3304	(1)3318
	1.45	34.8	(1)2087	(1)2042	(1)2049	(1)2092	(1)2062
	2.13	51.1	(1)1323	(1)1219	(1)1250	(1)1297	(1)1260
	3.12	74.9	(2)7417	(2)7881	(2)7698	(2)8062	(2)7751
	4.57	109.7	(2)4737	(2)4775	(2)4078	(2)5205	(2)4982
	6.70	161	(2)3239	(2)3236	(2)3223	(2)3448	(2)3290
	9.82	236	(2)2227	(2)2222	(2)2247	(2)2318	(2)2198
	14.4	345.7	(2)1528	(2)1502	(2)1501	(2)1548	(2)1458
	21.1	506	(2)1025	(2)1001	(2)1002	(2)1038	(2)9685
	30.9	742	(2)6823	(3)6603	(3)6662	(3)6910	(3)6385
	45.3	1,087	(3)4456	(3)4277	(3)4365	(3)4544	(3)4191
	66.4	1,594	(3)2872	(3)2743	(3)2814	(3)2951	(3)2738
	97.3	2,335	(3)1838	(3)1764	(3)1790	(3)1925	(3)1780
	143	3,430	(3)1117	(3)1088	(3)1082	(3)1170	(3)1080
	208	4,990	(4)6162	(4)6078	(4)5988	(4)7188	(4)6507
	301	7,220	(4)3192	(4)3174	(4)3140	(4)4175	(4)3722
1.2	438	10,520	(4)1676	(4)1666	(4)1710	(4)2506	(4)2185
1.75	650	15,600	(5)9864	(5)9766	(4)1025	(4)1538	(4)1341
2.60	948	22,760	(5)6010	(5)5978	(5)6286	(5)8855	(5)7926
3.60	1387	33,300	(5)3715	(5)3732	(5)3740	(5)4617	(5)4400
5.58	2037		(5)2479	(5)2556	(5)2339	(5)2332	(5)2479
8.18			(5)1915	(5)1987	(5)1751	(5)1449	(5)1688
12.0			(5)1509	(5)1589	(5)1323	(5)1036	(5)1253
17.6			(5)1189	(5)1201	(5)1027	(6)7922	(6)9719
25.7			(6)9079	(6)9624	(6)7814	(6)6061	(6)7465

Table 3.17 (continued)

2. In betas/sec for 10^4 fissions (Glendenin)

Age			U-235		U-238	Pu-239	
Years	Days	Hours	Thermal	Fission	(8 Mev)	Thermal	Fission
		0.765	1.544	1.548	1.527	1.482	1.466
		1.12	1.009	1.015	0.9810	0.9432	0.9308
		1.64	0.6358	0.6444	0.6070	0.5724	0.5707
		2.40	0.3988	0.4081	0.3703	0.3457	0.3542
		3.52	0.2547	0.2687	0.2402	0.2170	0.2272
		5.16	0.1655	0.1722	0.1571	0.1420	0.1515
		7.56	0.1088	0.1150	0.1042	(1)9550	0.1025
		11.1	(1)7159	(1)7577	(1)6982	(1)6518	(1)6892
		16.2	(1)4581	(1)4850	(1)4496	(1)4346	(1)4484
		23.8	(1)2860	(1)2905	(1)2860	(1)2840	(1)2859
	1.45	34.8	(1)1781	(1)1897	(1)1804	(1)1831	(1)1802
	2.13	51.1	(1)1093	(1)1095	(1)1125	(1)1165	(1)1180
	3.12	74.9	(2)6697	(2)7117	(2)6847	(2)7450	(2)7166
	4.57		(2)4532	(2)4658	(2)4698	(2)4911	(2)4709
	6.70		(2)3102	(2)3180	(2)3155	(2)3268	(2)3125
	9.82		(2)2143	(2)2158	(2)2121	(2)2150	(2)2076
	14.4		(2)1455	(2)1480	(2)1404	(2)1440	(2)1380
	21.1		(3)9707	(3)9701	(3)9216	(3)9454	(3)9256
	30.9		(3)6373	(3)6550	(3)5999	(3)6158	(3)5740
	45.3		(3)4108	(3)4085	(3)3852	(3)3968	(3)3694
	66.4		(3)2682	(3)2608	(3)2459	(3)2559	(3)2390
	97.3		(3)1697	(3)1684	(3)1581	(3)1690	(3)1579
	143		(3)1025	(3)1025	(4)9610	(3)1075	(4)9900
	208		(4)5919	(4)5920	(4)5587	(4)6756	(4)6167
	301		(4)3118	(4)3110	(4)3038	(4)4070	(4)3610
1.2	438		(4)1639	(4)1629	(4)1666	(4)2469	(4)2140
1.78	650		(5)9542	(5)9455	(5)9923	(4)1511	(4)1307
2.60			(5)5708	(5)5680	(5)5921	(5)8595	(5)7605
3.80			(5)3419	(5)3442	(5)3444	(5)4364	(5)7605
5.56			(5)2194	(5)2257	(5)2080	(5)2089	(5)2181
8.18			(5)1648	(5)1723	(5)1469	(5)1216	(5)1401
12.0			(5)1255	(5)1348	(5)1062	(6)8220	(6)9019
17.6			(6)9621	(5)1041	(6)8124	(6)6002	(6)7878
25.7			(6)7129	(6)7787	(6)6974	(6)4412	(6)5456

Table 8.17 (continued)

B. In photons/sec for 10^4 fissions (Glendenin)

Age			U-235		U-238	Pu-239	
Years	Days	Hours	Thermal	Fission	(5 Mev)	Thermal	Fission
		0.768	1.937	1.984	1.928	1.905	1.921
		1.12	1.280	1.278	1.259	1.269	1.250
		1.64	0.8049	0.8068	0.7821	0.7888	0.7858
		2.40	0.4908	0.4977	0.4751	0.4495	0.4581
		3.52	0.2971	0.3060	0.2904	0.2654	0.2708
		5.16	0.1815	0.1893	0.1810	0.1628	0.1776
		7.56	0.1149	0.1204	0.1165	0.1052	0.1166
		11.1	(1)7584	(1)7901	(1)7741	(1)7150	(1)7808
		16.2	(1)4989	(1)5146	(1)5080	(1)4666	(1)5183
		23.8	(1)3289	(1)3310	(1)3307	(1)3268	(1)3320
	1.45	34.8	(1)2106	(1)2140	(1)2151	(1)2160	(1)2157
	2.13	51.1	(1)1355	(1)1372	(1)1355	(1)1444	(1)1398
	3.12	74.9	(2)8799	(2)8907	(2)9118	(2)9597	(2)9145
	4.57		(2)5556	(2)5968	(2)6115	(2)6461	(2)6097
	6.70		(2)3927	(2)3974	(2)4050	(2)4267	(2)3994
	9.82		(2)2562	(2)2590	(2)2626	(2)2758	(2)2551
	14.4		(2)1644	(2)1629	(2)1648	(2)1720	(2)1577
	21.1		(2)1020	(3)9949	(2)1019	(2)1064	(3)9640
	30.9		(3)6166	(3)5995	(3)6212	(3)6526	(3)5849
	45.3		(3)3573	(3)3894	(3)3965	(3)3995	(3)3467
	66.4		(3)2014	(3)2100	(3)1992	(3)2268	(3)2015
	97.3		(3)1165	(3)1058	(3)1213	(3)1330	(3)1188
	143		(4)6400	(4)5880	(4)6540	(4)7810	(4)6540
	208		(4)3542	(4)3179	(4)3535	(4)3810	(4)3460
	301		(4)1421	(4)1893	(4)1481	(4)1725	(4)1508
1.2	435		(5)5158	(5)5175	(5)5581	(5)7512	(5)6714
1.75	650		(5)2117	(5)2158	(5)2647	(5)2752	(5)3004
2.60			(5)1109	(5)1145	(5)1384	(5)2058	(5)1884
3.80			(6)6058	(6)6348	(6)9011	(5)1040	(5)1024
5.58			(6)3762	(6)3948	(6)5505	(6)5079	(6)5644
8.18			(6)3014	(6)3080	(6)3893	(6)3190	(6)3861
12.0			(6)2709	(6)2690	(6)3088	(6)2583	(6)3158
17.6			(6)2413	(6)2357	(6)2559	(6)2256	(6)2700
27.7			(6)2074	(6)2016	(6)2141	(6)1919	(6)2310

Table 3.17 (continued)

4. In photon Mev/sec for 10^{6} fissions

Age			U-235		U-238	Pu-239	
Years	Days	Hours	Thermal	Fission	(8 Mev)	Thermal	Fission
		0.708	1.850	1.850	1.720	1.693	1.005
		1.42	1.240	1.240	1.147	1.084	1.005
		1.64	0.7757	0.7770	0.7137	0.6850	0.6550
		2.40	0.4510	0.4604	0.4170	0.3983	0.3795
		3.72	0.2584	0.2604	0.2379	0.2283	0.2170
		5.06	0.1403	0.1529	0.1364	0.1300	0.1271
		7.50	(-1)8549	(-1)8988	(-1)8172	(-1)7964	(-1)7786
		11.3	(-1)5202	(-1)5456	(-1)5006	(-1)4869	(-1)4840
		16.2	(-1)3120	(-1)3259	(-1)3013	(-1)2911	(-1)2958
		23.8	(-1)1807	(-1)1864	(-1)1744	(-1)1730	(-1)1756
	1.05	34.8	(-1)1008	(-1)1000	(-1)1001	(-1)1003	(-1)1046
	2.10	50.1	(-2)6128	(-2)6311	(-2)6521	(-2)6693	(-2)6975
	3.12	74.9	(-2)3807	(-2)3974	(-2)4004	(-2)4254	(-2)4464
	4.37		(-2)2370	(-2)2498	(-2)2665	(-2)2845	(-2)3060
	6.70		(-2)1750	(-2)1840	(-2)1917	(-2)1998	(-2)2178
	9.82		(-2)1100	(-2)1256	(-2)1286	(-2)1375	(-2)1570
	14.4		(-3)8000	(-3)8309	(-3)7126	(-3)8247	(-3)7484
	21.1		(-3)5722	(-3)5977	(-3)5009	(-3)5259	(-3)4780
	30.9		(-3)3220	(-3)3329	(-3)3125	(-3)3293	(-3)3011
	45.3		(-3)1962	(-3)1881	(-3)1909	(-3)1906	(-3)1706
	66.4		(-3)1088	(-4)9996	(-3)1011	(-3)1086	(-4)9784
	97.3		(-4)6070	(-4)5890	(-4)5976	(-4)6387	(-4)5946
	143		(-4)3540	(-4)3400	(-4)3490	(-4)3700	(-4)3500
	208		(-4)1995	(-4)1945	(-4)1894	(-4)2170	(-4)1972
	303		(-5)8961	(-5)8924	(-5)7951	(-5)9507	(-5)8671
1.2	444		(-5)3197	(-5)3040	(-5)2891	(-5)3001	(-5)3150
1.78	650		(-6)1038	(-6)1025	(-6)9031	(-5)1542	(-5)1312
2.60			(-6)5460	(-6)5188	(-6)4724	(-6)5450	(-6)4618
3.80			(-6)2445	(-6)2485	(-6)2050	(-6)2553	(-6)2469
5.58			(-6)1042	(-6)1057	(-6)8494	(-6)1077	(-6)1000
8.18			(-6)4724	(-6)4720	(-6)3881	(-6)4700	(-6)4028
12.0			(-6)1979	(-6)1902	(-6)1600	(-6)1944	(-6)1820
17.6			(-6)8405	(-6)8177	(-6)6820	(-6)8258	(-6)7867
25.7			(-6)3408	(-6)3468	(-6)2889	(-6)3040	(-6)3207

Table 3.15 (concluded)

5. In air 3 ft above an infinite plane for 10^6 fissions per sq ft

Age			U-235		U-238	Pu-239	
Years	Days	Hours	Thermal	Fission	(8 Mev)	Thermal	Fission
		0.763	(8)9977	(8)9970	(8)9329	(8)8007	(8)8750
		1.12	(8)6648	(8)6632	(8)6172	(8)5806	(8)5761
		1.64	(8)4140	(8)4153	(8)3827	(8)3592	(8)3537
		2.40	(8)2453	(8)2444	(8)2256	(8)2071	(8)2085
		3.52	(8)1410	(8)1450	(8)1303	(8)1180	(8)1193
		5.16	(9)8079	(9)8418	(9)7582	(9)6642	(9)7098
		7.56	(9)4786	(9)5014	(9)4587	(9)3986	(9)4308
		11.1	(9)2964	(9)3094	(9)2807	(9)2555	(9)2821
		16.2	(9)1804	(9)1860	(9)1792	(9)1626	(9)1761
		23.8	(10)9716	(9)1094	(9)1073	(9)1010	(9)1065
	1.45	34.8	(10)6305	(10)6428	(10)6303	(10)6235	(10)6300
	2.13	51.1	(10)3730	(10)3786	(10)3817	(10)3855	(10)3811
	3.12	74.9	(10)2276	(10)2319	(10)2365	(10)2470	(10)2302
	4.57		(10)1483	(10)1524	(10)1556	(10)1645	(10)1546
	6.70		(11)9986	(10)1031	(10)1039	(10)1090	(10)1021
	9.82		(11)6774	(11)6972	(11)6899	(11)7244	(11)6655
	14.4		(11)4490	(11)4587	(11)4462	(11)4650	(11)4226
	21.1		(11)2910	(11)2940	(11)2845	(11)2953	(11)2660
	30.9		(11)[illegible]	(11)[illegible]	(11)[illegible]	(11)[illegible]	[illegible]
	45.3		(11)1061	(11)1039	(11)1034	(11)1092	(12)9777
	66.4		(12)6655	(12)5807	(12)5910	(12)6360	(12)5728
	97.5		(12)3676	(12)3497	(12)3559	(12)3896	(12)3543
	143		(12)2170	(12)2096	(12)2079	(12)2320	(12)2200
	208		(12)1194	(12)1164	(12)1153	(12)1287	(12)1180
	301		(13)4974	(13)4790	(13)4733	(13)5707	(13)5170
1.2	438		(13)1399	(13)1373	(13)1525	(13)2135	(13)1864
1.78	650		(14)3604	(14)3758	(14)5517	(14)6083	(14)7090
2.60			(14)2031	(14)1975	(14)3166	(14)4094	(14)4252
3.80			(14)1444	(14)1432	(14)2213	(14)2692	(14)2594
5.58			(14)1154	(14)1158	(14)1603	(14)1442	(14)1611
8.18			(14)1026	(14)1021	(14)1201	(15)9971	(14)1225
12.0			(15)9432	(15)9293	(14)1094	(15)8452	(14)1057
17.6			(15)8310	(15)8211	(15)9164	(15)7377	(15)9160
27.7			(15)7183	(15)7431	(15)7431	(15)6216	(15)7668

a. Number in parenthesis indicates number of zeros between decimal and first digit.

Figure 3.4
COMPARISON OF CALCULATIONS OF THE ACTIVITY AND PHOTON EMISSION RATE OF THE FISSION PRODUCTS FROM 14-Mev NEUTRON FISSION OF U-238 (Dolan[47,48]) WITH THOSE FROM 8-Mev NEUTRON FISSION OF U-238 (Miller[13]) GIVEN AS A RATIO OF THE TWO WITH TIME AFTER FISSION

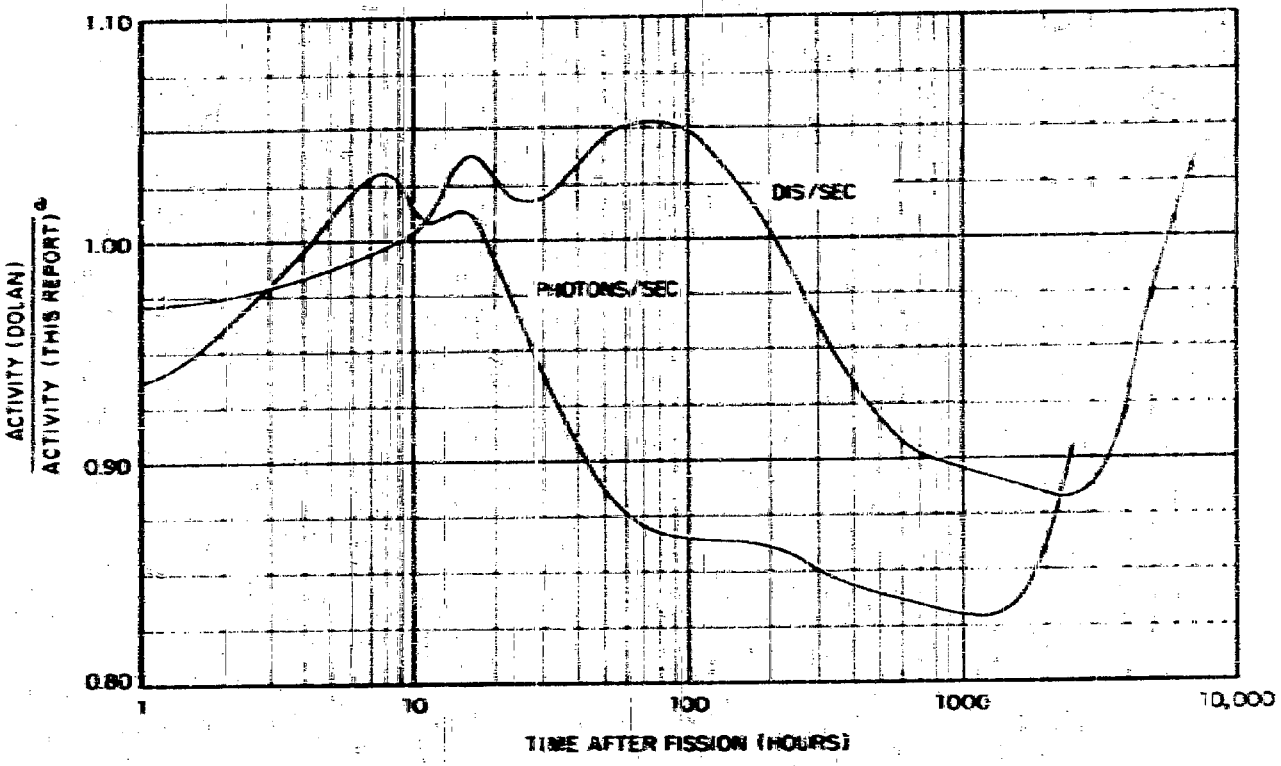

The air ionization rate curves from each type of fission are of chief interest; these are compared in Figures 3.5 and 3.6 in terms of an air ionization rate "R" factor. The factor, r_{fp}, is the ratio of the air ionization rate from one type of fission to the rate from thermal neutron fission of U-235. The fluctuation in the curves of Figures 3.3 and 3.4 reflects the relative prominence of the important gamma emitters in each mixture.

The deviation in r_{fp} from the value 1 is a measure of the difference in the ionization rate from that of the U-235 thermal fission reference curve. The order in the r_{fp} deviations, from least to most, is:

1. fission neutron fission of U-235,
2. 8-Mev neutron fission of U-238,
3. fission-neutron fission of Pu-239, and
4. thermal-neutron fission of Pu-239.

The maximum relative deviation for the first three (combined), between 1 and 7000 hours after fission, is from -16 percent at 2.5 hours to +5.5 percent at 110 hours. However, between 2 and 3 years after fission the U-238 (8-Mev neutrons) r_{fp} value is almost 1.6 and the Pu-239 (fission neutrons) r_{fp} value is almost 2.8 because of the higher yields for the rare earth elements (heavy mass peak) in the fission products from the heavier fissile nuclides and larger neutron energy.

The two main factors that determine the gross decay of the normal product mixtures (besides the half-lives and the individual nuclide-decay schematics) are the mass chain yields and the independent yields of the isotopes in the chain. For times after fission of about 1 hour and greater, the Bolles-Ballou calculations[10] show that the difference in the total disintegration rates, based on Present's yield theory, from those based on Glendenin's postulate is insignificant. This is due to the fact that, at these times after fission, most of the chains have decayed from the short-lived early members to the last one or two active members. The displacement from 1.00 in the curves of Figures 3.2, 3.3, and 3.4 therefore are due to differences in the chain yields. The curves show that, for times between about 1 hour and 1 year, the maximum error in the ionization rate by use of the data for thermal neutron fission of U-235 would be about 15 percent.

Figure 3.5
GROSS AIR IONIZATION RATE FRACTIONATION NUMBER, $r_{f,p}$, RELATIVE TO THE IONIZATION RATE (in hours) OF THE FISSION PRODUCTS FROM THERMAL NEUTRON FISSION OF U-235, FOR THE FISSION PRODUCT MIXTURES FROM OTHER FISSILE NUCLIDES AND NEUTRON ENERGIES

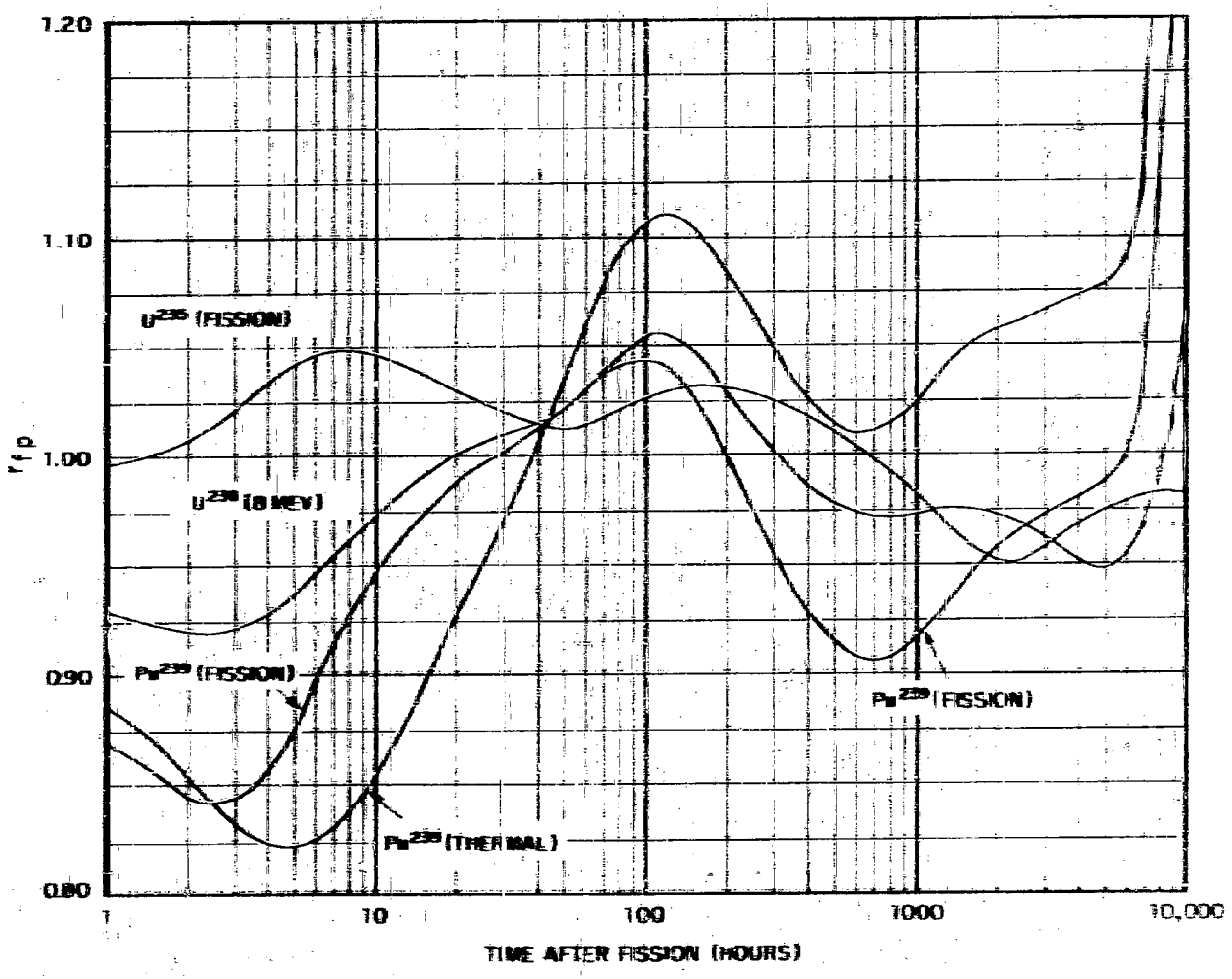

Figure 3.6
GROSS AIR IONIZATION RATE FRACTIONATION NUMBER, r_{fp}, RELATIVE TO THE IONIZATION RATE (In years) OF THE FISSION PRODUCTS FROM THERMAL NEUTRON FISSION OF U-235, FOR THE FISSION PRODUCT MIXTURES FROM OTHER FISSILE NUCLIDES AND NEUTRON ENERGIES

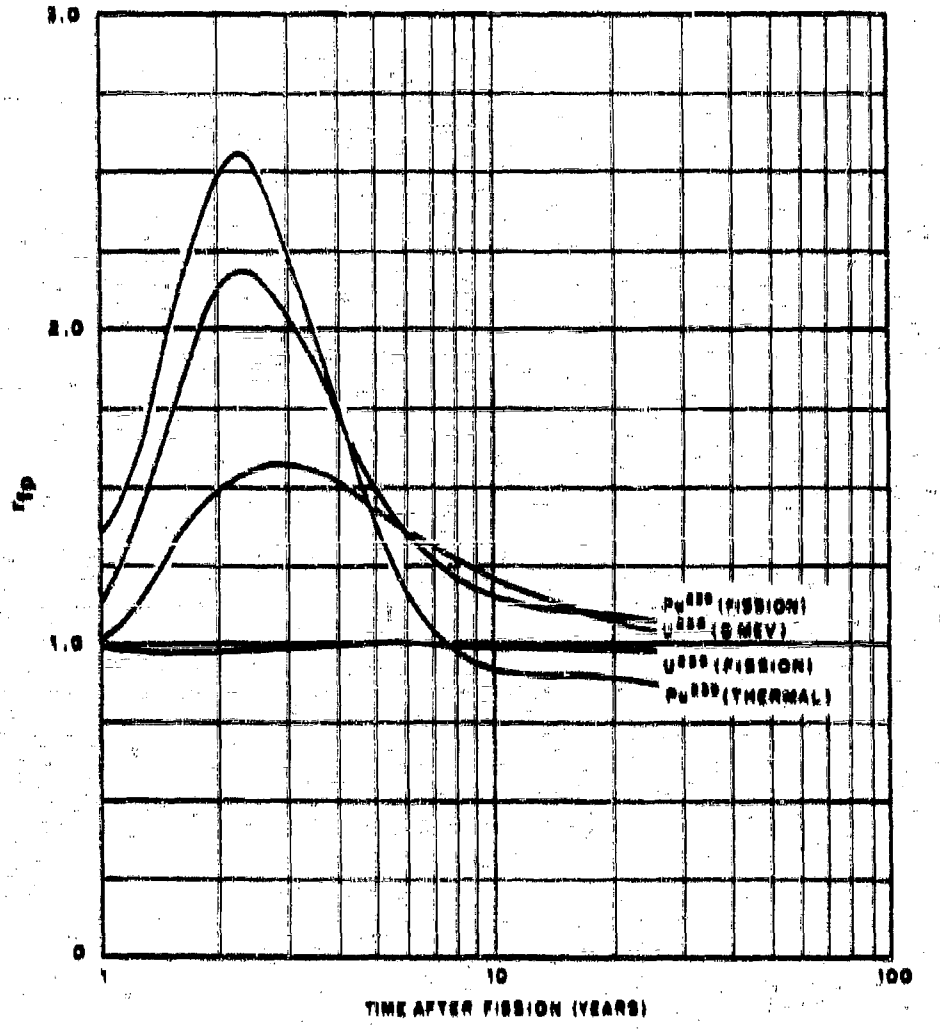

The H+1 ionization rates at 3 feet above an infinite smooth contaminated plane for a unit yield distribution of fission products per unit area are summarized in Table 3.18. The highest value is for the thermal neutron fission of U-235; the lowest is for fission-neutron fission of Pu-239.

Table 3.18

SUMMARY OF H+1 IONIZATION RATES OF NORMAL FISSION PRODUCTS[a]

Type of Fission	(H+1 Ionization Rate) / (unit yield/unit area)	
	(r/hr at 1 hr) / (fiss/sq ft)	(r/hr at 1 hr) / (KT/sq mi)
U-235 (thermal)	7.60×10^{-13}	3050
U-235 (fission)	7.58×10^{-13}	3040
U-238 (2-Mev)	6.04×10^{-13}	3010
Pu-239 (thermal)	6.70×10^{-13}	3480
Pu-239 (fission)	6.54×10^{-13}	3400

a. Per unit yield per unit area, for 3 feet above an infinite smooth contaminated plane.

The same value, 1.46×10^{23} fissions/KT, was used to convert all the ratios from fissions to kilotons. The corresponding ionization rate factor derived from ENW is (1240 r/hr a 1 hr)/(KT/sq mi.) or about a factor of 3 lower than the values of Table 3.18. Other authors[15,16,17,18] have made similar calculations and comparisons of these factors and of the decay curves for the thermal neutron fission of U-235.

The number of photons per disintegration and the average energy of the photons for the normal mixture of fission products from 8-Mev-neutron fission of U-238 are shown as a function of time after fission in Figures 3.7 and 3.8, respectively.

Figure 3.7
NUMBER OF PHOTONS PER DISINTEGRATION FOR THE NORMAL MIXTURE OF FISSION PRODUCTS FROM 8-Mev NEUTRON FISSION OF U-238

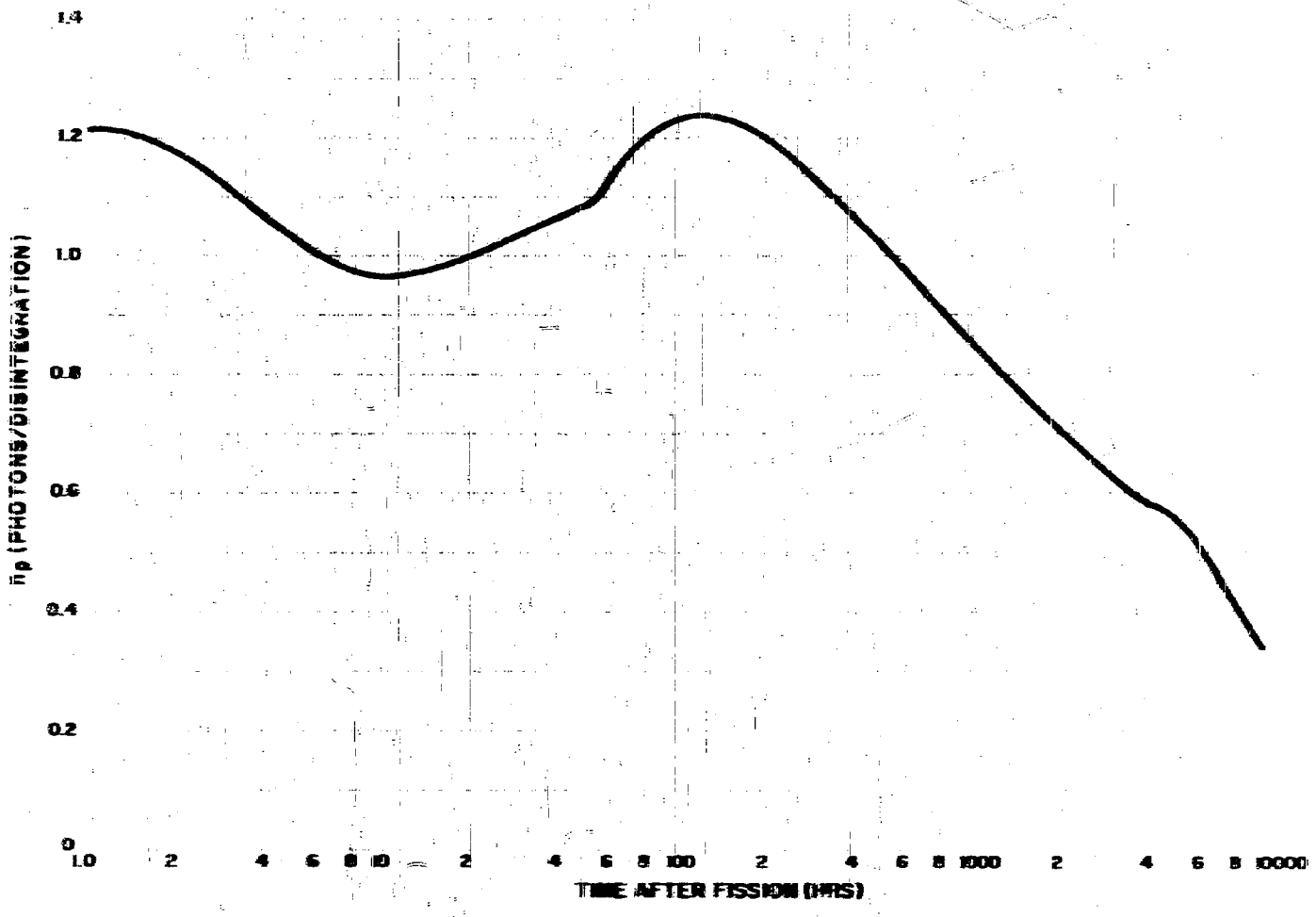

Figure 3.8
AVERAGE ENERGY OF THE PHOTONS FROM THE NORMAL MIXTURE OF FISSION PRODUCTS FROM 8-Mev NEUTRON FISSION OF U-238

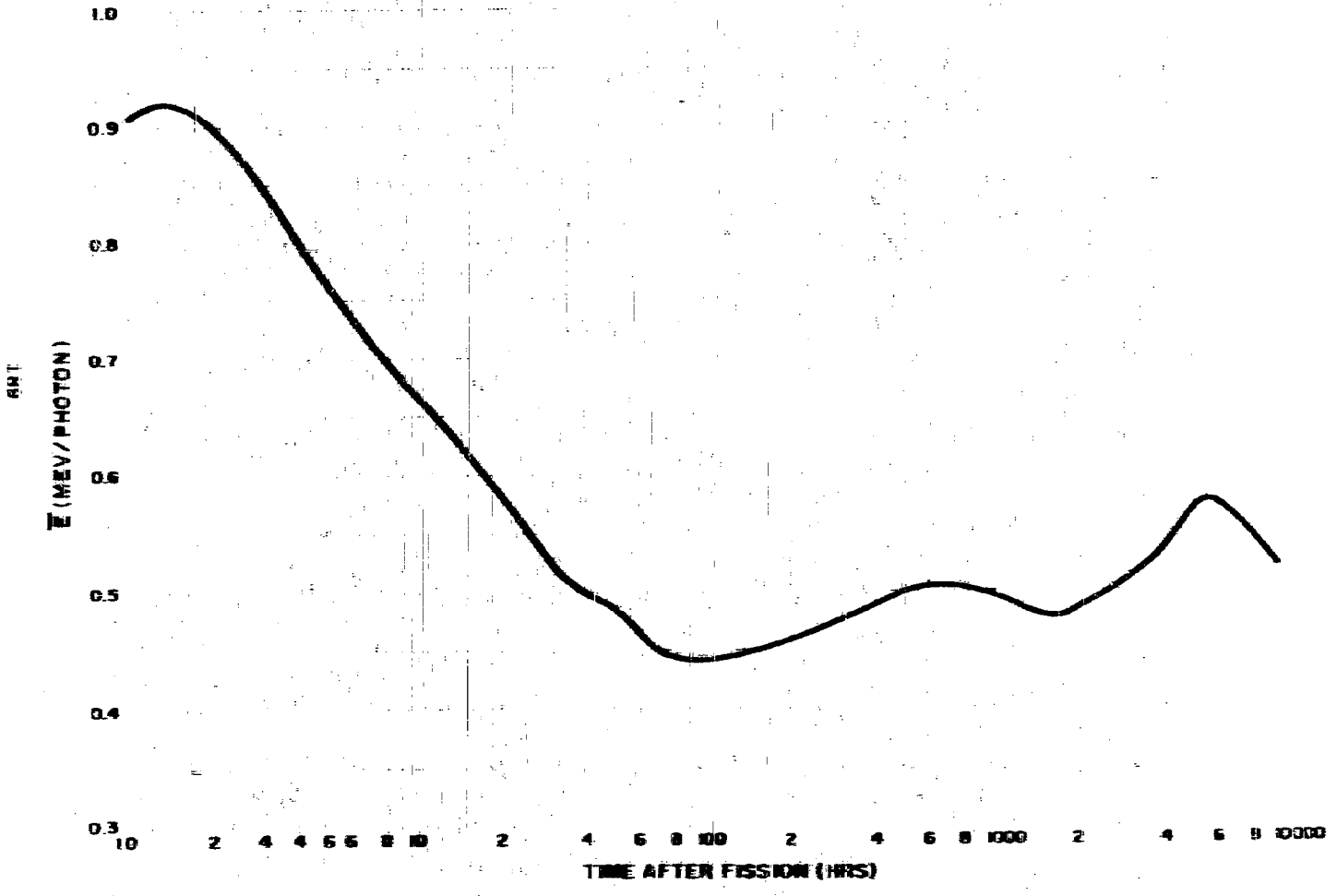

The ratio of the response of an AN/PDR 39(TIB) radiac held by a man at about 3 feet above a uniform distribution of fission products over a plane area to the calculated air ionization rate is shown in Figure 3.9 as a function of time after fission. The instrument, for the indicated response, is held by a man and is calibrated with a Co-60 standard source.[9] The ratio varies from about 73 to 77 percent; most of the reduction in the ionization rate measured is due to attenuation of the gamma rays by the person holding the instrument and by the batteries and other dense materials near the ion chamber of the instrument.

The only estimates of the ionization rate of mixed fission products at early times after fission available are those for the products of the thermal neutron fission of U-235. The data, and calculations of the gamma energy release, from these fission products at early times, after fission have been summarized by Zigman and Mackin.[10] This summary of the gamma ray abundances is converted to the ionization rates, photon energy emission rate, and average photon energies given in Table 3.19. To adjust the ionization rate values calculated from the data of Zigman and Mackin to those of Table 3.17 at 45.5 minutes, the former were increased by 22.5 percent; this adjustment provides a smooth join of the ionization rate decay curve from the early to the later times.

The computed ionization rates for the fission product elements condensed in the liquid of the ideal soil when it solidifies at 1400°C (end of the first period of condensation) for times of 9 seconds (84-KT) and 60 seconds (14-MT) are given in Table 3.20 for 5-Mev neutron fission of U-238. Also given are the F_{t_0} values, with respect to the normal fission-product mixture from thermal neutron fission of U-235. The variation in Figure 3.10 of the computed values of F_{t_0} with time after fission shows that the dependence of the fractionation on times of condensation of 9 seconds and 60 seconds (84-KT and 14-MT, respectively) is not large, but that between about 2 hours and 4000 hours after fission the mixture from the lower yield is more highly fractionated.

The minimum in the curve at 2 hours is due to major depletions in Cs and Te, whereas the minimum at about 200 hours is due to depletions in I-131 and Ba-140 - La-140. The maximum in the curve, at 3000 hours, results from the high abundance of Zr-95 - Nb-95, and the peaks at times longer than 10,000 hours are due to the high yields of the rare earth elements from U-238 fission products with respect to the U-235 fission products.

The observed variation in F_{t_0} with time after fission as measured with a standard ionization chamber, is shown in Figure 3.11 for the fallout from a low tower shot.[10] The observed F_{t_0} value at 1 hour after detonation is very close to the values computed for the larger yields and with the exception of some details in the curve that may be due in part to the response characteristics of the ion chamber and, in part, to the type of fission, the calculated curves follow the trend of the observed curve quite well.

Figure 3.9
RELATIVE RESPONSE OF THE AN/PDR-39(T1B) PORTABLE RADIAC HELD BY A MAN AT 3 FEET ABOVE AN EXTENDED PLANE AREA CONTAMINATED WITH FISSION PRODUCTS FROM THERMAL NEUTRON FISSION OF U-235

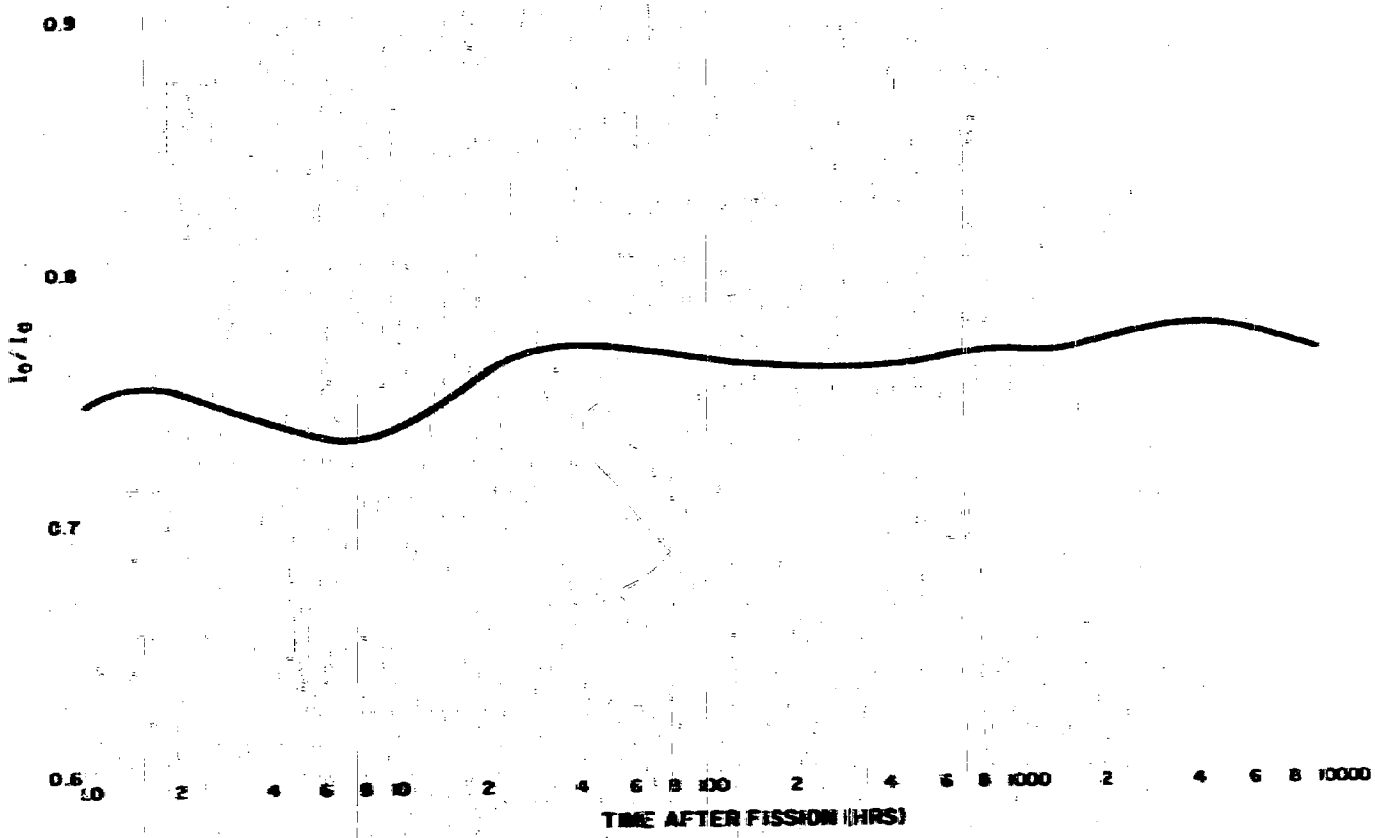

Table 3.10

EARLY-TIME IONIZATION RATE, PHOTON ENERGY EMISSION RATE, AND AVERAGE PHOTON ENERGY FOR FISSION PRODUCTS FROM THERMAL NEUTRON FISSION OF U-235

Time After Fission (secs)	Air Ionization Rate $(10^{-15}$ r/hr)/(fission/sq ft)	Photon Energy Emission Rate (Mev/sec)/(10^{4} fissions)	Average Photon Energy (Mev/photon)
1	25,600	5,020	1.150
1.5	19,600	3,940	1.178
2	16,600	3,300	1.200
3	12,700	2,550	1.235
4	10,300	2,060	1.262
6	7,530	1,510	1.296
9	5,660	1,060	1.328
13	3,820	768	1.345
19	2,650	541	1.363
28	1,840	368	1.375
41	1,250	252	1.384
60	840	168	1.390
88	560	112	1.393
129	373	74.3	1.390
189	250	49.1	1.376
277	166	32.0	1.355
406	109	20.6	1.308
595	70.2	13.5	1.245
870	45.5	8.65	1.170
1280	28.5	5.42	1.074
1870	17.9	3.29	0.992
2750	10.5	1.92	0.958
4050	6.05	1.24	0.970
5900	4.15	0.776	0.964

Figure 3.10
VARIATION OF γ_{fp} WITH TIME AFTER FISSION FOR THE FRACTIONATED MIXTURE OF FISSION PRODUCTS FROM 8-Mev NEUTRON FISSION OF U-238

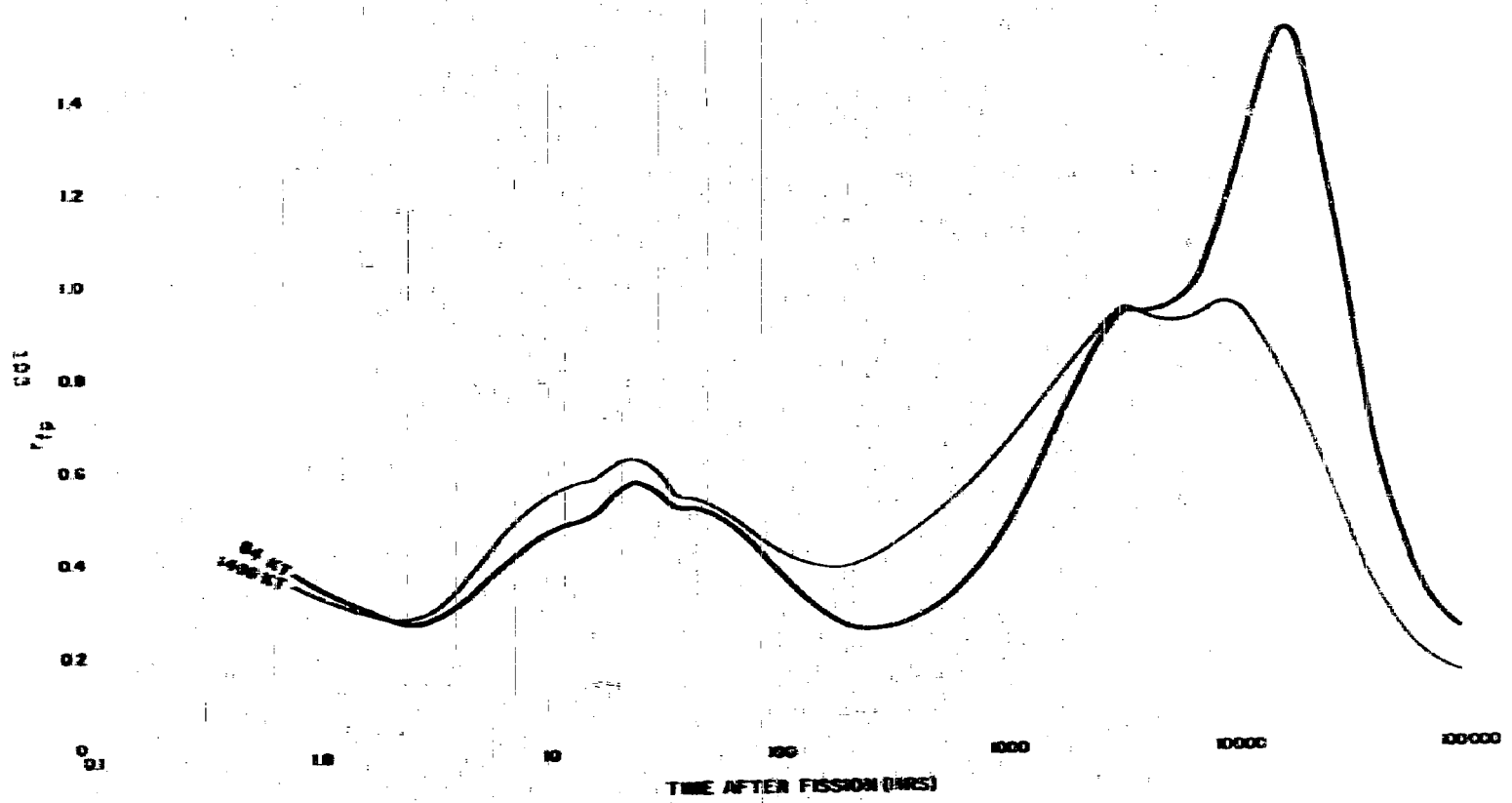

Table 3.30

IONIZATION RATE FOR FISSION PRODUCTS CONDENSED ON IDEAL SOIL AT 1400 C AT 8 SECONDS (84 KT) AND 60 SECONDS (14 MT) AFTER FISSION OF U-238 (8 MEV NEUTRONS) AND RATIO TO THAT FOR THE NORMAL MIXTURE FROM FISSION OF U-235 (THERMAL NEUTRONS)

Time After Detonation			I_{fp}[a]		F_{fp}	
Years	Days	Hours	84-KT	14-MT	84-KT	14-MT
		0.768	(8)371[b]	(8)345	0.372	0.346
		1.12	(8)210	(8)220	0.331	0.316
		1.64	(8)119	(8)118	0.287	0.284
		2.40	(9)642	(9)667	0.262	0.272
		3.52	(9)393	(9)429	0.279	0.304
		5.16	(9)274	(9)313	0.339	0.388
		7.56	(9)197	(9)231	0.412	0.483
		11.1	(9)137	(9)161	0.462	0.543
		16.2	(10)990	(9)102	0.498	0.565
		23.8	(10)644	(10)689	0.560	0.607
	1.45	34.8	(10)423	(10)457	0.513	0.555
	2.18	51.1	(10)188	(10)189	0.481	0.507
	3.12	74.9	(11)965	(10)105	0.434	0.455
	4.57	110.	(11)608	(11)591	0.330	0.395
	6.70	161.	(11)269	(11)268	0.269	0.368
	9.82	236.	(11)162	(11)259	0.289	0.382
	14.4	346.	(11)110	(11)191	0.245	0.426
	21.1	506.	(12)823	(11)141	0.258	0.485
	30.9	742.	(12)559	(11)100	0.352	0.551
	45.3	1,087.	(12)498	(12)678	0.469	0.689
	66.4	1,594.	(12)287	(12)455	0.689	0.752
	97.3	2,335.	(12)298	(12)311	0.798	0.846
	143.	3,430.	(12)195	(12)200	0.915	0.922
	209.	4,990.	(13)110	(12)107	0.921	0.896
	301.	7,220.	(13)479	(13)458	0.962	0.895
1.50	438.	10,520.	(13)170	(13)180	1.215	0.922
1.78	650.	15,600.	(14)577	(14)619	1.486	0.921
2.60	949.	22,760.	(14)279	(14)126	1.575	0.680
3.80	1,387.	33,300.	(14)153	(15)599	0.921	0.415
5.58	2,037.	48,900.	(15)875	(15)264	0.498	0.246
8.18	2,986.	71,700.	(15)292	(15)161	0.255	0.157
12.0			(15)194	(15)111	0.206	0.119
17.6			(15)138	(16)807	0.166	0.097
25.7			(16)986	(16)607	0.130	0.085

a. r/hr at 3 ft above an infinite smooth plane for 10^8 fissions per sq ft.

b. Number in parenthesis is number of decimal points between decimal point and first digit (see Figure 3.21).

Figure 3.11
OBSERVED VARIATION OF r_{1a} WITH TIME AFTER FISSION FOR CLOSE-IN FALLOUT FROM A LOW TOWER SHOT AT THE NEVADA TEST SITE

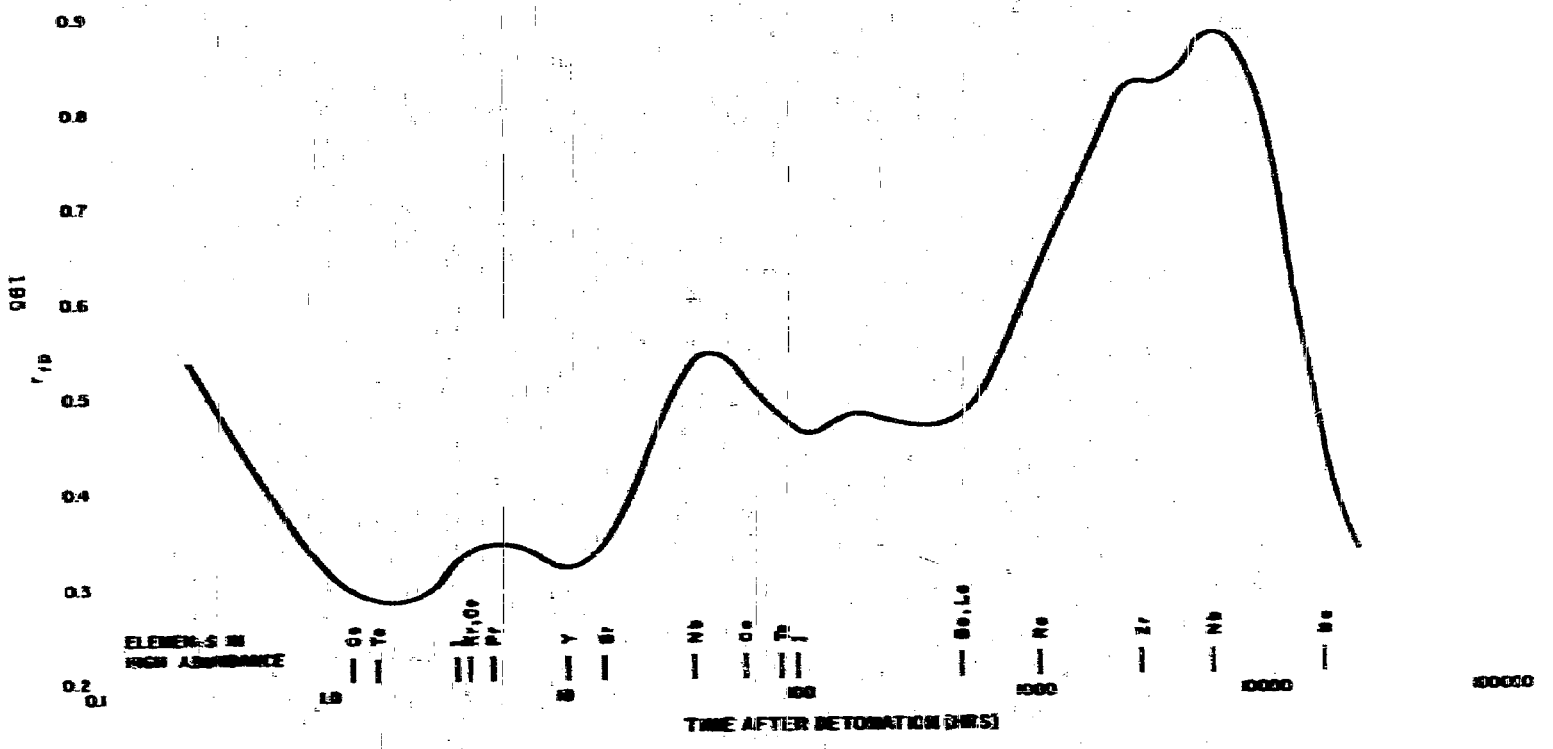

For an r_{ip} of 38 percent at H+1, the ionization rate at 1 hour per KT per sq mi, would be 1100 for the mixture of fission products condensed up to the indicated times. If the fallout also contained neutron-induced activities that contribute at H+1, the ratio would be higher. The important likely (or possible) induced activities are those produced from neutron captures by U-238 as was found by Kimura[7], Maskin[8], Freiling[32] and also reported by Stewart, Crooks and Fischer[31].

The activities and ionization rates of the possible product nuclides, for a yield of 10^4 atoms at zero time and up to 100 days later, are summarized in Tables 8.21 to 8.24. For the case in which the tabulated activities are associated with the activities from 10^4 fissions, they are equivalent to a yield of one product-nuclide for each fission. Thus, for the case where one of the neutrons from each fission event results in a (n, γ) reaction with U-238, the ionization rate from the products U-239 and Np-239 at H+1 would be 0.557×10^{-12} r/hr per fission or about 180 r/hr per KT/sq mi. The ratio for the gross mixture is then 1070 r/hr at 1 hour per KT/sq mi.

If the relative yield of U-237 was that found by Kimura[7], namely 0.15 atoms per fission, the additional activity at H+1 would be 0.0020×10^{-12} r/hr per fission or about 1 r/hr per KT/sq mi. A yield of 0.15 atoms per fission of U-240, however, would give a contribution at H+1 of about 20 r/hr per KT/sq mi. If this occurred, the ratio for the mixture would be 1300 r/hr at 1 hour per KT/sq mi. The observed ratio for this mixture of radionuclides in fallout particles on an open real terrain would be less than this value, due to both the instrument response mentioned above and to shielding by the roughness of the terrain. If it is assumed that the instrument response to the final mixture is about the same as it is for the normal mixture of fission products, then a value of about 75 percent (see Figure 2.9) would be appropriate for the AN/PDR-39(TIB) or similar radiac instrument. An effective terrain attenuation of 75 percent with respect to the ideal smooth plane would give an observed value for the ratio of about 780 r/hr at 1 hour per KT/sq mi. This is lower than the value, 1240, obtained from the data of the ENW.

Additional discussions of how the condensation process may proceed at times longer than the end of the first period of condensation, and of how the radioactive composition can vary with particle size and downwind distance, are given in Chapter 6.

Table 3.21

ACTIVITY FROM U-237 FOR 10^4 ATOMS AT ZERO TIME[a];
G(U-237) = 1

Time After Fission	A (d/s)	I_a (r/hr x 10^6)	I_o (r/hr x 10^6)	$D_a(1)$ (r x 10^6)
1h	(1)1183[b]	(1)1330[b]	(2)967[b]	0
1.5h	(1)1181	(1)1330	(2)965	(2)000[b]
2h	(1)1178	(1)1333	(2)962	(1)138
3h	(1)1173	(1)1328	(2)948	(1)207
4h	(1)1168	(1)1322	(2)944	(1)400
6h	(1)1158	(1)1310	(2)936	(1)844
8h	(1)1148	(1)1299	(2)928	(1)992
10h	(1)1138	(1)1288	(2)920	0.1160
12h	(1)1129	(1)1278	(2)913	0.1488
15h	(1)1114	(1)1261	(2)901	0.182
18h	(1)1100	(1)1245	(2)889	0.210
24h	(1)1072	(1)1213	(2)867	0.260
1.5d	(1)1018	(1)1152	(2)831	0.436
2d	(2)968	(1)1095	(2)783	0.570
3d	(2)873	(2)988	(2)706	0.821
4d	(2)789	(2)893	(2)638	1.040
6d	(2)640	(2)724	(2)518	1.450
8d	(2)520	(2)592	(2)423	1.740
10d	(2)426	(2)481	(2)344	2.005
15d	(2)264	(2)297	(2)205	2.457
20d	(2)152	(2)173	(2)120	2.725
30d	(3)547	(3)610	(3)442	2.957
40d	(3)196	(3)221	(3)160	3.080
60d	(4)252	(4)285	(4)204	3.125
80d	(5)928	(5)805	(5)201	3.130
100d	(6)414	(4)468	(6)335	3.132

a. I_a, I_o, and $D_a(1)$ are for the distribution of 10^4 atoms per square foot over an infinite plane at zero time. I_a is in air ionization rates, I_o is in instrument response units.

b. Number in parenthesis is number of zeros between decimal point and first digit.

Table 3.32

ACTIVITY FROM U-239 FOR 10^4 ATOMS AT ZERO TIME[a] (U-239)

Time After Fission	A (d/s)	I_α (r/hr x 10^0)	I_n (r/hr x 10^0)	$D_\alpha(1)$ (e x 10^0)
1h	0.8365	0.3246	0.1760	0
1.5h	0.3485	0.10252	(1)749	0.1080
2h	0.1420	(1)5533	(1)317	0.1527
3h	(1)240	(2)042	(2)522	0.1775
4h	(2)413	(2)160	(3)888	0.1830
6h	(3)122	(4)473	(4)202	0.1839
8h	(5)004	(5)120	(6)718	0.1839
10h	(6)161	(7)502	(7)217	0.1839
12h				0.1839
15h				0.1839
18h				0.1839
24h				0.1839
1.5d				0.1839
2d				0.1839
3d				0.1839
4d				0.1839
6d				0.1839
8d				0.1839
10d				0.1839
15d				0.1839
20d				0.1839
30d				0.1839
40d				0.1839
60d				0.1839
80d				0.1839
100d				0.1839

a. I_α, I_n, $D_\alpha(1)$ are for the distribution of 10 atoms per square foot over an infinite plane at zero time

b. Number in parenthesis is number of zeros between decimal point and first digit.

Table 3.23

ACTIVITY FROM Np-239 FOR 10^4 ATOMS OF U-239 AT ZERO TIME[a]
C(U-239) 1

Time After Fission	A (d/s)	I_β (r/hr x 10^{11})	I_α (r/hr x 10^{11})	D_β (1) (r x 10^9)
1h	(1)2870[b]	(1)3107[b]	(1)2270[b]	0[b]
1.5h	(1)3182	(1)3541	(1)2513	(1)108
2h	(1)3288	(1)3659	(1)2597	(1)349
3h	(1)3323	(1)3698	(1)2626	(1)714
4h	(1)3302	(1)3644	(1)2600	0.1084
6h	(1)3216	(1)3570	(1)2540	0.1808
8h	(1)3137	(1)3491	(1)2477	0.2512
10h	(1)3060	(1)3406	(1)2417	0.320
12h	(1)2984	(1)3321	(1)2357	0.387
15h	(1)2877	(1)3202	(1)2278	0.485
18h	(1)2769	(1)3081	(1)2187	0.579
24h	(1)2572	(1)2862	(1)2032	0.757
1.5d	(1)2215	(1)2465	(1)1750	1.077
2d	(1)1910	(1)2125	(1)1509	1.351
3d	(1)1419	(1)1579	(1)1121	1.791
4d	(1)1055	(1)1174	(2)833	2.122
6d	(2)583	(2)648	(2)460	2.545
8d	(2)322	(2)358	(2)254	2.787
10d	(2)178	(2)198	(2)141	2.910
15d	(3)402	(3)447	(3)318	3.082
20d	(4)911	(3)101	(4)719	3.002
30d	(5)467	(5)519	(5)369	3.007
40d	(6)240	(6)267	(6)190	3.008
60d				3.008
80d				3.008
100d				3.008

a. I_β, I_α, and D_β (1) are for the distribution of 10^4 atoms per square foot over an infinite plane at zero time.

b. Number in parenthesis is number of zeros between decimal point and first digit.

Table 3.34

ACTIVITY FROM Np^{240} FOR 10^4 ATOMS OF U^{240} AT ZERO TIME[a]
(U^{240}) $\frac{1}{}$

Time After Fission	A (d/s)	I_a (r/hr s 10^9)	I_0 (r/hr s 10^9)	$D_0(1)$ (r s 10^9)
1h	0.1307	0.2705	0.2007	0
1.5h	0.1270	0.2647	0.2052	0.104
2h	0.1248	0.2588	0.2002	0.205
3h	0.1180	0.2401	0.1907	0.518
4h	0.1131	0.2241	0.1815	0.788
6h	0.1026	0.2124	0.1645	1.212
8h	(1)928[b]	0.1921	0.1489	1.611
10h	(1)843	0.1744	0.1352	1.975
12h	(1)760	0.1570	0.1224	2.312
15h	(1)658	0.1362	0.1055	2.754
18h	(1)569	0.1177	(1)913[b]	3.150
24h	(1)424	(1)878[b]	(1)680	3.750
1.5d	(1)255	(1)486	(1)377	4.547
2d	(1)180	(1)260	(1)209	4.980
3d	(2)400	(2)828	(2)642	5.572
4d	(2)123	(2)254	(2)197	5.484
6d	(3)116	(3)240	(3)186	5.580
8d	(4)110	(4)227	(4)176	5.600
10d	(5)104	(5)215	(5)167	5.598
15d	(8)286	(8)592	(8)459	5.598
20d				5.598
30d				5.598
40d				5.598
60d				5.598
80d				5.598
100d				5.598

a. I_a, I_0, and $D_0(1)$ are for the distribution of 10^4 atoms per square foot over an infinite plane at zero time.

b. Number in parentheses is number of zeros between decimal point and first digit.

CHAPTER 3 REFERENCES

1. Stewart, K., Trans. Faraday Soc., 52, 161 (1956).

2. Kelley, K. K., Contributions to the Data on Theoretical Metallurgy, XIII. High Temperature Heat-Content, Heat-Capacity, and Entropy Data for the Elements and Inorganic Compounds, U.S. Bureau of Mines, Bulletin 584, 1960.

3. Stull, D. R., and G. C. Sinke, The Thermodynamic Properties of the Elements, Am. Chem. Soc., Washington, D.C., 1956.

4. Lapple, C. E., Fallout Control, Stanford Research Institute, SRIA-3, 1958.

5. Adams, C. E., N. H. Farlow, W. R. Schell, The Compositions, Structures, and Origins of Radioactive Fallout Particles, USNRDL-TR-209, 1958.

6. Miller, C. F., Analysis of Fallout Data, I. The Jangle "S" and "U" Shot Fallout Patterns, USNRDL-TR-220, Del, 1958.

7. Kimura, Kenjiro, Geneva Conference on the Peaceful Uses of Atomic Energy, 7, 196 (1956).

8. Mackin, J., P. Zigman, D. Love, D. McDonald, and D. Sam, J. Inorg, Nucl. Chem., 15, 20 (1960).

9. Coughlin, J. P., U.S. Bureau of Mines, Bulletin 542, 1954.

10. Bolles, R. C., and N. E. Ballou, Calculated Abundances of U-235 Fission Products, USNRDL-456, 1956.

11. Kateoff, Seymour, Nucleonics, 10, 4, 78 (1958).

12. Miller, C. F., and P. Loeb, Ionization Rate and Photon Pulse Decay of Fission Products from the Slow Neutron Fission of U-235, USNRDL-TR-247, 1958.

13. Dolan, P. T., Calculated Abundances and Activities of the High Energy Neutron Fission of Uranium-238, DASA-525, 1956.

14. Dolan, P. T., Gamma Spectra of Uranium-238 Fission Products at Various Times after Fission, DASA-526, 1956.

15. Knapp, H. A., Civil Defense Hearings before a Subcommittee of the Committee on Government Operations, U.S. Congress, External Gamma Doses and Dose Rates from the Fallout from Nuclear Detonations, 1960.

16. Lapp, Ralph E., Local Fallout Radioactivity, Bulletin Atomic Scientists, XV, 5, 181, 1959.

17. Perkins, J. F., and R. W. King, Energy Release from the Decay of Fission Products, Nuclear Sci. and Eng., 9, 746, 1961.

18. Knabe, W. E., and G. E. Putnam, The Activity of the Fission Products of U-235, General Electric Co., APEX-448, 1958.

19. Zigman, P., and J. Mackin, Early Time Decay of Fission Products, Health Physics, 5, 79, 1961.

20. Strope, W. E., Evaluation of Countermeasure System Components and Operational Plumbbob, WT-1464, 1958.

21. Stewart, N. G., R. N. Crooks, E. M. R. Fischer, Hearings of the Joint Committee on Atomic Energy, U.S. Congress, The Nature of Radioactive Fallout and Its Effects on Man, p.1690, June 1957.

22. Freiling, E. C., Fractionation Correlations, USNRDL-TR-385, 1959.

Chapter 4

DISTRIBUTION OF FALLOUT PARTICLES FOLLOWING A NUCLEAR DETONATION

4.1 General Description of The Fallout Distribution Process

4.1.1 The Particle Source Geometry

A very simple descriptive statement of the fallout process might be that a cloud of particles is formed rapidly as the result of an explosion and that this cloud is then dispersed by the wind and by the force of gravity acting on the particles to return them to the earth. Most investigators concerned with the distribution of fallout assume that the visible volume occupied by the nuclear cloud and stem above the point of detonation within a few minutes after explosion more or less defines the volume source of the fallout particles[1].

Anderson[2], however, considers a moving source volume which might be described as the air volume swept through by the rising fireball and stem. In either case the source volumes for the particles depend on total yield and, if other than surface detonations are considered, on the height or depth of burst. The yield dependent parameters which are used to define the particle source geometry include the cloud height, cloud thickness and radius, and, occasionally, the stem geometry. Anderson's studies include consideration of the time dependence of these parameters.

One important additional factor that is usually considered is the distribution, or spatial concentration, of the particles in the volume, and qualitative considerations have been given to internal circulations of the particles by several investigators.[3]

4.1.2 The Particle Fall Trajectory

The fall trajectory of a particle depends on its own properties and on meteorological factors. The various aspects of these factors have been discussed by Schuert,[4] Anderson[2] and others[1]. The major properties that influence a particle's fall rate through the atmosphere are its density, diameter or size, and shape. The major meteorological factors are the wind speed and direction, and the air density and viscosity.

The two air properties, of course, are dependent on the air pressure and temperature and these, in turn, change with altitude. The wind speed and direction are also highly variable quantities since each has both spatial and time variations. The vertical motions of the air and particle-group diffusion can influence the fall trajectory of particles, but are usually not taken into account in the study of the fallout distribution process.

4.1.3 Radiological Factors

The major radiological factors in the fallout distribution process are the fission yield and the variation with particle size of the gross radioactivity carried by particles of a given size. The first essentially determines the total radioactivity available for distribution on the particles; the second involves the distribution of that radioactivity among particles of different sizes.

Additional factors, such as neutron induced radioactivity, fractionation, and the biological availability of single fission-product elements, have not yet been incorporated into studies of the fallout distribution process in a systematic way by most investigators and fallout model designers.

4.2 Mathematical Descriptions of the Fallout Distribution Process

4.2.1 Scaling Methods

The original attempt to describe and/or predict the end result of the fallout distribution process--the fallout pattern--was made by C.F. Kaanda and coworkers in 1953[5]. The original scaling method was based on the work of Laurino and Poppoff[6] which described some fallout patterns from Operation Jangle in 1951 from low yield devices. The original scaling method was intended for predictions or estimates of fallout patterns from yields possibly as high as 10-KT. In 1955[7] the method was expanded to include yields in the megaton range, without adequate explicit experimental documentation. This method was subsequently included in ENW.[8] In some studies of fallout effects a scaling system is to be preferred over a complex mathematical model. Therefore, a scaling method for estimating fallout patterns is described in Section 4.3.

4.2.2 Mathematical Models

Mathematical models attempt to establish quantitative values for the several factors mentioned in Section 4.1 and to compute the activity deposited on the ground at various locations usually with use of electronic computers. The general approach used and the organizations and investigators involved in the

development and testing of these models up to 1957 is described in some detail by Kellogg.[1] Later developments include the work by Anderson,[8,9] by Pugh and Galiano,[10] by Callahan, et al[11] and by Rapp,[12] to mention a few of the unclassified reported studies. A general comment on the results might be that none of the models agree with each other in several details, and that none of the models reproduce very accurately all of the few data in the yield range of 1-KT to 15-MT that are experimentally available.

The exact causes of the differences among the various models are difficult to isolate for at least two reasons: 1. Each model is different from any other in several of its assumptions about parameter values or in its manner of handling the many variables mathematically. 2. The reports describing the models generally do not include sufficient detailed information regarding the minor assumptions and the methods used in making the computations. If the input data in the mathematical models were all more reliably established experimentally, many of the differences among them would disappear. Whether better agreement with observations resulted would still have to be established.

Nonetheless, many of the features of the mathematical models are used in Section 4.3 which describes the derivation of a simplified scaling method. A few of the parameter values used in several of the mathematical models are discussed there to better describe the over-all process of fallout distribution as it might take place. In Chapter 6 some general concepts are described that could be utilized to derive a more refined mathematical model of fallout than is presently available. Some possible improvements in the treatment of the problem are also touched upon in this chapter.

In most mathematical models, after selecting the values of the source geometry, trajectory, and radiological factors, the computation is carried out by dividing the source geometry for each of several particle size ranges into horizontal discs of finite thickness. The location on the ground where these "particle discs" land, under the influence of the ascribed meteorological conditions, is then calculated. All the activity at each of a series of coordinate points is then summed, according to the number of different discs that land at the point and the amount of activity assigned to each disc.

So short a summary of the work on the mathematical models should not be interpreted to mean that the efforts in the development of the mathematical models have been small and unfruitful. On the contrary, much has been learned about the fallout process through them, and most of the concepts employed by many of the mathematical model developments are covered in the remainder of this chapter. But to describe all the work and all the details of each model currently in use is not considered to be within the scope of this discussion.

4.3 Descriptive Features of a Simplified Fallout Scaling System for Land Surface Detonations

4.3.1 General Description of the Scaling Method

The fallout scaling system described here was developed for estimating standard intensities, potential exposure doses, and other radiological quantities by use of both manual and machine computational techniques. The system is based on corrected experimental data, on empirical relationships among the geometrical arrangement of the cloud and stem as the source of fallout particles, and on several of the observed features of the fallout pattern of radiation intensities on the ground. In the system, the cloud and stem dimensions are stylized as simple solid geometric configurations to facilitate the use of algebraic relationships among the model parameters and the dependence of the parameter values on weapon yield.

In making estimates of the hazards from fallout, for the purpose of establishing the nature and required degree of protection against these hazards, two major quantities requiring evaluation are (1) the exposure dose levels that can result at different distances from the detonation, and (2) the land surface area in which the exposure dose is greater than a stated amount. To make these evaluations requires estimates of the amount of fallout that deposits at various locations, the time at which the fallout arrives, and the rate of its arrival.

Such general evaluations of hazard levels, and of the protection requirements for radiological countermeasures in defense planning, must first consider the possible levels of effect (or hazard) and, in a generalized manner, the feasibility of methods for protecting against these levels of possible hazard. For these purposes a rather simplified fallout scaling system can serve because no precise or accurate prediction of fallout under specified detonation and wind conditions is possible even with the most complicated fallout models at their present stage of development. Therefore in the following discussion the presentation is limited to the description of a simplified version of the fallout distribution process.

The mathematical derivations of the simplified fallout scaling system attempt to depict the fall of particles of different size-groups from a volume source in the air; the boundaries of that source are assumed to depend only on weapon yield. The problem is to describe mathematically the dependence of the fallout pattern features, in space and time, on (a) the cloud and stem geometry, (b) the particle fall velocities, (c) the wind velocity, (d) the radioactivity-particle size distributions, and (e) the weapon yield.

The geometrical configuration of the cloud is taken to be an oblate spheroid, and the configuration of the stem as the frustum of an exponential cone or horn whose larger base is approximately adjacent to the bottom of the spheroid. The fall of particles from each of these source volumes is considered separately

4.3.2 Particles Falling from Cloud Altitudes

The descriptive equations for fallout from cloud altitudes are based on the following premises:

1. The cloud source of the particles (at about H+6 minutes to H+8 minutes after detonation) has the shape of an oblate spheroid where a is the major axis (parallel to the earth's surface) and b is the minor axis.

2. The particles of a given size-parameter, α, fall with a constant terminal velocity vector, v_t, from their position in the cloud to the ground.

3. The wind velocity, v_w, is constant with time and space through all altitudes from the ground to the top of the cloud.

4. The initial distribution of the particles of each size-parameter inside the cloud is uniform.

5. The fractional distribution of the total activity on each particle group can be determined from fallout pattern data as a function of that group's fall velocity parameter.

The outer dimensions of the cloud, according to the first premise, are defined by

$$\frac{x^2 + y^2}{a^2} + \frac{z^2}{b^2} = 1 \qquad (4.1)$$

where the origin of the x, y, z coordinate system is directly over ground zero at the altitude, h, at the center of the cloud.

A particle originating at the point x, y, z in the cloud moves along a line of slope, v_t/v_w, and lands on the ground at the downwind distance, X, given by

$$X = \alpha(h + z) + x \tag{4.2}$$

where α is equal to v_w/v_t (v_w is independent of v_t).

The number of particles with a given value of α that fall at the downwind distance, X, from ground zero, for a uniform distribution in the cloud, are proportional to the length of the line given by Eq. 4.2 contained within the cloud. The total number of particles having size-parameter α is $n_v L \Delta f^2$, where n_v is the number per unit volume, L is the length along the line of fall in the cloud, and Δf^2 is the cross-sectional area along the line.

The area on the earth's surface intercepted by Δf^2 is $\Delta f \Delta X$ (Δf in y direction) such that

$$\Delta X = \sqrt{(1 + \alpha^2)}\ \Delta f \tag{4.3}$$

The number of particles per unit area at X is then

$$N_x = \frac{n_v L}{\sqrt{1 + \alpha^2}} \tag{4.4}$$

Similarly, A_v is the activity per unit volume of cloud carried by the particles having the inverse fall velocity, or size-parameter, α. The amount of activity per unit area at X contained in the group is

$$A_x(\alpha) = \frac{A_v L}{\sqrt{1 + \alpha^2}} \tag{4.5}$$

where $A_x(\alpha)$ is the activity per unit area on the ground at the distance, X, that is carried by the particles having the size-parameter α.

The value of L is determined from the two intercepts of the line given by Eq. 4.2 with the spheroid described by Eq. 4.1 by use of

$$L^2 = \Delta x^2 + \Delta z^2 \tag{4.6}$$

Solving Eq. 4.6 for Δx and Δz gives

$$L^2 = \frac{4a^2b^2(1 + \alpha^2)\left[(a^2 + \alpha^2 b^2)(1 - \alpha^2/\alpha^2) - (X - \alpha h)^2\right]}{(a^2 + \alpha^2 b^2)^2} \tag{4.7}$$

The activity per unit area on the ground, $A_s(\alpha)$, is then

$$A_s(\alpha) = \frac{2A_\alpha ab\sqrt{(a^2 + \alpha^2 b^2)(1 - y^2/a^2) - (X - \alpha h)^2}}{(a^2 + \alpha^2 b^2)} \tag{4.8}$$

The activity contours on the ground surface for a given value of α therefore are ellipses; Eq. 4.8, in standard elliptical form, is

$$\frac{(X - \alpha h)^2}{(a^2 + \alpha^2 b^2)\left[1 - \frac{A_s^2(\alpha)(a^2 + \alpha^2 b^2)}{4A_\alpha^2 a^2 b^2}\right]} + \frac{y^2}{a^2\left[1 - \frac{A_s^2(\alpha)(a^2 + \alpha^2 b^2)}{4A_\alpha^2 a^2 b^2}\right]} = 1 \tag{4.9}$$

The centers of the ellipse are at X equal to αh and at y equal to 0.

The total activity per unit area deposited at the location X, y (y is taken as the same lateral dimension on the ground as it is in the cloud) is determined by summing the contributions from all possible values of α; it is given by

$$A_s = \int_{\alpha(\min)}^{\alpha(\max)} A_s(\alpha)\, d\alpha \tag{4.10}$$

where α(max) and α(min) are given by the two respective values of

$$\alpha_m = \frac{hX \pm \sqrt{X^2 b^2(1 - y^2/a^2) + (a^2 - y^2)h^2 - b^2(1 - y^2/a^2)}}{h^2 - b^2(1 - y^2/a^2)} \tag{4.11}$$

Equation 4.10 can be integrated graphically if the values of A_α and the other parameters are provided. From the data given by Pugh and Galinno[16] and by Schuert[4], the following empirical scaling functions were derived for the yield-dependent parameters of the above equations:

$$a = 2.34\times10^3\ W^{0.431}\ \text{ft}, \quad W = 1\text{-KT to } 10^5\text{-KT} \tag{4.12}$$

$$b = 1.40\times10^3\ W^{0.300}\ \text{ft}, \quad W = 1\text{-KT to } 10^5\text{-KT} \tag{4.13}$$

$$h = 0.66\times10^4\ W^{0.445}\ \text{ft}, \quad W = 1\text{-KT to } 28\text{-KT} \tag{4.14}$$

$$h = 1.68\times10^4\ W^{0.164}\ \text{ft}, \quad W = 28\text{-KT to } 10^5\text{-KT} \tag{4.15}$$

An approximation method for estimating A_α can be derived from information on the final fallout pattern itself. From Eqs. 4.12 and 4.13, the cloud volume for the ellipsoid of revolution about the minor axis is

$$V_\alpha = 3.21\times10^{10}\ W^{1.109}\ \text{cu. ft.},\quad W = 1\text{-KT to } 10^8\text{-KT} \tag{4.16}$$

If the fraction of the total activity associated with the particles having the inverse falling velocity α is f_α and these particles are uniformly distributed throughout the volume, then A_α is equal to $f_\alpha A_s / V_\alpha$, where A_s is equal to $1.4\times10^{20} g_s$ BW fissions (B here is the ratio of the fission to total yield; g_s is the fraction of the total activity produced that is contained in the cloud; and W is the total yield in KT). The value of A_α is then given by

$$A_\alpha = 4.36\times10^{10}\ f_\alpha g_s\ \text{BW}^{0.109},\quad W = 1\text{-KT to } 10^8\text{-KT} \tag{4.17}$$

where the dependence of g_s and f_α on W is unspecified.

From arbitrary distributions of A_α and from evaluations of $A_x(\alpha)$ and the difference, $\alpha_{max} - \alpha_{min}$, from Eq. 4.11, it was noted that (1) the difference, $\alpha_{max} - \alpha_{min}$, generally is not large, and (2) the maximum value of $A_x(\alpha)$ generally occurs near the value of α that is equal to X/h (designated here as α_0). The first estimate of the A_α values is obtained from experimental knowledge (or estimates) of A_x along the line y = 0 from field test data, and from the assumption of a constant value of $A_x(\alpha)$ evaluated at α_0 as a rectangular step function between α_{min} and α_{max}. With this approximation Eq. 4.10 becomes

$$A_x = A_x(\alpha_0)(\alpha_{max} - \alpha_{min}) \tag{4.18}$$

Substituting X/h for α in Eqs. 4.8 and 4.11 gives

$$A_x(\alpha_0) = \frac{2ab\,A_\alpha}{\sqrt{a^2h^2 + b^2X^2}} \tag{4.19}$$

and

$$\alpha_{max} - \alpha_{min} = \frac{2\sqrt{b^2X^2 + a^2(h^2 - b^2)}}{(h^2 - b^2)} \tag{4.20}$$

so that Eq. 4.18 becomes, when solved for A_α,

$$A_\alpha = \frac{(h^2 - b^2)A_x}{4ab\sqrt{1 - \dfrac{1}{h^2/b^2 + X^2/a^2}}} \tag{4.21}$$

For all values of the constants, and for reasonable values of X, the value of the radical in Eq. 4.21 is between 0.95 and 1.00, so that, within less than 5 percent,

$$A_{\pi} = \frac{(h - b)(h + b)}{4ab} A_s \qquad (4.22)$$

The relationship between A_s and the observed intensity, $I_s(1)$, is discussed in Section 4.8.5.

4.8.3 Particles Falling from Stem Altitudes

The source volume for particles falling from the stem is described, in outline, by a figure that is circular in the plane parallel to the ground but whose radius increases exponentially with altitude. The lower radius is equal to that of the fireball (R_s) at the time the fireball leaves the ground; the height at this point is also R_s. The stem radius at the height, h, is the same as that of the cloud at full expansion. This geometry portrays a particle source volume that expands laterally, with increasing altitude as well as with fireball rise and expansion, until it forms the characteristic cloud. The entire volume or space through which the fireball (or cloud) passes in its rise is considered to be the source volume of the fallout particles from the stem.

The assumptions used for the model are listed below; some discussion of these assumptions is given in the following text. Many fundamental difficulties in the fallout models and in the basic understanding of fallout formation and its distribution could be removed if more information were available on the processes that actually occur during the cloud rise.

The descriptive equations for the fallout from the stem altitudes are based on the following assumptions:

1. The stem source of particles has the shape of an inverted exponential horn.

2. The spherical exponential horn-shaped volume has a radius, R_s, at the height R_s, and a radius, a, equal to the cloud radius at the height h.

3. The particle fall velocity vector, v_f, wind velocity, v_w, and their ratio, the particle size-parameter, σ, are the same as for particles falling from cloud altitudes.

4. The volume and shape of the cloud, as it rises, are specified by the major radius (defined in 2 above) and a minor radius that also increases exponentially with altitude from R_s at the height R_a to the cloud half-thickness, b, at the height h.

5. To make hand computations feasible, the particles having a given value of σ in the cloud volume at a given altitude are assumed to be concentrated on a horizontal plane through the center of the cloud volume.

6. The particles rise with a velocity that is equal to or greater than the rate of rise of the center of the cloud; they begin to fall earthward from the altitude at which their fall velocity (due to gravity forces) equals the rate of rise of the mass of air surrounding the particles. This altitude is assumed to be located in the region near or below the bottom of the rising cloud. Together with assumption 5, this assumption specifies that particle groups with a given value of σ fall only from one altitude or altitude increment. Therefore the size- segregation with altitude, as described, is somewhat similar to that of an ideal fluidized bed of particles.

7. Particles having the same value of σ fall in the downwind direction along the length of a high-intensity ridge near ground zero. The diameter of the stem at the altitude of origin of this group of particles is then equal to the length of the ridge.

The mathematical model for the shape of the volume of air that is swept out by the rising cloud is based on thermodynamic equations for the adiabatic expansion of an ideal gas, including a term for the change in free energy with altitude, and assuming that the external pressure is proportional to $\exp(-mgz/kT)$. In this stem-model approximation for the rising cloud (in which the number of moles of gas in the volume is increasing) only the exponential form of the equation is retained for empirical fit to the data. The volume of the stem is then represented by

$$V_z = V_o e^{k_v z} \tag{4.23}$$

where V_o and k_v are determined from a known volume at a minimum of two altitudes.

Since the stem volume must have the same shape as the cloud volume at full expansion, namely an elliptical spheroid of revolution about the z axis, the major semi-axis of the stem volume may be written as

$$a_s = a_0 e^{k_s z} \tag{4.24}$$

and its minor semi-axis as

$$b_s = b_0 e^{k_b z} \tag{4.25}$$

where V_0 is equal to $(4/3)\pi a_0^2 b_0$ and k_v is equal to $2k_s + k_b$.

The values of a_0, k_s, b_0, and k_b, are determined from

$$\log a_0 = \log a - \frac{h \log a/R_s}{h - R_s} \tag{4.26}$$

$$k_s/2.303 = \frac{\log a/R_s}{h - R_s} \tag{4.27}$$

$$\log b_0 = \log b - \frac{h \log b/R_s}{h - R_s} \tag{4.28}$$

and

$$k_b/2.303 = \frac{\log b/R_s}{h - R_s} \tag{4.29}$$

Values of the stem and fireball-cloud geometry constants for several yields are listed in Table 4.1. The outer dimensions of the stem are defined by

$$x^2 + y^2 = a_s^2 \tag{4.30}$$

for which the center of the coordinate system is at surface zero.

The particle fall and accumulation equations for the stationary cloud could be used for the rising cloud in estimating the σ groups arriving at a given downwind location. However, such computations would require the use of an electronic computer, and the more complicated treatment would not necessarily improve the accuracy of estimates made by using the simpler computation. These mathematical complications are eliminated when it is assumed that all the particles falling from the rising fireball or cloud are concentrated at the horizontal plane through its center. This assumption also eliminates specification, except for the height, of the point of origin whithin the stem for any σ group arriving at a particular point on the ground surface. If the σ values for

Table 4.1

VALUES OF STEM AND FIREBALL-CLOUD GEOMETRY CONSTANTS FOR SEVERAL WEAPON YIELDS

Yield (KT)	a_0 (ft)	$k_a/2.303$ (ft^{-1})	b_0 (ft)	$k_b/2.303$ (ft^{-1})
1	1.92×10^{3}	1.07×10^{-4}	1.00×10^{3}	1.20×10^{-4}
10	4.20×10^{3}	6.51×10^{-5}	4.28×10^{3}	4.40×10^{-5}
10^{2}	9.01×10^{3}	3.64×10^{-5}	9.20×10^{3}	2.19×10^{-5}
10^{3}	1.88×10^{4}	2.72×10^{-5}	1.04×10^{4}	1.45×10^{-5}
10^{4}	3.68×10^{4}	2.04×10^{-5}	4.05×10^{4}	9.71×10^{-6}
10^{5}	6.85×10^{5}	1.54×10^{-5}	5.04×10^{5}	6.58×10^{-6}

the particle groups falling from the downwind edge of the stem α_{min}, and, those from the upwind edge of the stem, α_{max}, at a given downwind distance can be determined, then it is possible to sum up the activity deposited at that location. The simplest case is at the y = 0 plane; the solution can then be generalized by replacing a_x with $\sqrt{a_x^2 - y^2}$.

To determine α_{min} and α_{max}, three equations are required in order to eliminate a_x and z from the stem model equations with equation constants and yield-dependent parameters. Two of the three equations are

$$a_x = a a_0 e^{k_a z} \tag{4.31}$$

and

$$a_x = X - \alpha z \tag{4.32}$$

where α is either α_{min} or α_{max} depending on the sign of a_x.

The third required equation must give the α value of the particle group falling from a given altitude. An equation for this description was derived from the data of Anderson[8] by the following technique. The altitude, z, is first defined as the mean altitude of location for the particles that have entered the fireball or cloud and have collected condensing radioactive elements at time, t, after detonation. The altitudes z_b, z_t, and z_c are the heights of the bottom, top, and center of the visible fireball or cloud at time, t, after detonation.

From a plot of Anderson's data on the rate of rise of the cloud for the 1.3-KT yield it is found that rates of rise, $\dot{z}_b$ and $\dot{z}_t$, could be represented quite accurately by a function of the form: constant times (exp - kt) over a given period of time. The integration of the rates of rise with time should give the cloud height as a function of time. The function for z_b thus determined is

$$z_b = (h-b)(1 - e^{-0.0123t}), \quad t = 10 \text{ to } 250 \text{ sec} \tag{4.33}$$

where h is the height of the cloud and b its half-thickness at 8 to 10 minutes after detonation. The multiplier (h-b) is 6 percent larger than that obtained directly from Anderson's data.

In the case of z_t, Anderson's data give values that are about 4000 feet greater at 5 minutes after detonation than can be obtained from Schuert's data[4] for the 10-minute cloud expansion. Since Anderson's data give larger values, it is assumed that he either used uncorrected observed data or that his values were adjusted to the heights at the Nevada Test Site. Anderson's values, accordingly, were reduced by 30 percent to agree with the values of h+b that would be obtained from Eqs. 4.13, 4.14, and 4.15, giving

$$z_t = 0.331(h+b)(1 - e^{-0.0626t}), \quad t = 5 \text{ to } 20 \text{ sec} \tag{4.34}$$

and

$$z_t = 0.893(h+b)(1.120 - e^{-0.00784t}), \quad t = 20 \text{ to } 200 \text{ sec}. \tag{4.35}$$

To test whether the only yield dependence of the equation is that in the parameters h and b, the rates of rise, $\dot{z}_t$, are computed for the 1-MT yield for comparison with the values given in ENW (p. 21). The calculated values of $\dot{z}_t$ are found to be from 0 to 15 percent lower, up to 1.8 minutes; but, by 3.8 minutes, the ENW rates of rise are 3 times larger. Also, the larger rates from the ENW data give integrated cloud heights that are larger than h+b when the cloud rise-rates are integrated over the rise-time. Therefore, the rate of rise must decrease more rapidly at the longer times than is indicated by the cloud rise-rate data of ENW.

The height of the center of the cloud, z_c, as determined from the average of z_b and z_t, is approximated by

$$z_c = 0.915h\,(1.093 - e^{-0.00905t}), \quad t = 20 \text{ to } 200 \text{ sec}. \tag{4.36}$$

If v_x If the falling rate of a particle at the height, x (v_f is its average fall velocity, x/t, from x to the ground), and $\dot{x}$ is the rate of rise at x of the air around the particle, the particle starts to fall earthward immediately after its normal fall rate equals the rate of rise of the surrounding air mass, or after

$$v_x = \dot{x} \tag{4.37}$$

From Anderson's particle falling-rate data for spherical particles[5], the following relations between v_x and v_f were determined:

$$v_x / v_f = 0.95 + 1.02 \times 10^{-5}\, x$$

$$x = 5000 \text{ to } 50,000 \text{ ft,} \tag{4.38}$$

$$d = 200 \text{ to } 1200 \text{ microns}$$

and

$$v_x / v_f = 0.58 + 1.74 \times 10^{-5}\, x$$

$$x = 50,000 \text{ to } 110,000 \text{ ft,} \tag{4.39}$$

$$d = 300 \text{ to } 1000 \text{ microns}$$

Equation 4.38, which is applicable to most of the altitude region of possible stem fallout, fits the plotted data extremely well in the altitude and particle-size range indicated. Even when applied to altitudes of 1000 and 60,000 feet and to particle diameters up to 2000 microns, the difference between the ratios calculated from the tabulated fall-rates and from the equation are less than 20 percent.

When the cloud rates of rise, $\dot{h}_0$, $\dot{h}_t$, or $\dot{h}_1$, and the particle-fall rates are used to compute the time of arrival of particles at locations very close to ground zero where fallout from stem altitudes should predominate, the calculated arrival times are quite consistently longer than the observed times when compared with the few available observed arrival times in which the particle sizes are also known. Actually, the same discrepancy is often observed for cloud fallout at larger distances.

This result, i.e., the longer arrival time computed for particles falling near ground zero, is not as general or comprehensive as might be desired because of the shortage of data for complete verification. But it suggests two deductions about the fallout process from stem altitudes, provided it is assumed that, at a given time, the values of the particle-fall rates are more accurately

known than is the rate of rise of the air surrounding the particles (this assumption is without doubt a good one). The first deduction is that the change in rate of rise of the cloud, with time, as given by the exponential terms in the equations for w_0, k_0, and z_0, represents the change in rate of rise of the air around the particles more accurately than the rate of rise of the air itself is represented because of inaccuracies in the equation multipliers. If this were not the case, the discrepancies in the calculated and observed arrival times would not be consistently of the same sign.

The second deduction is that, when the rising cloud takes on a toroidal motion, the larger particles are involved in such a way that they experience downward accelerations for some rather extended period of time. Because the calculated fall rates include only accelerations due to gravity, the computed time of fall (neglecting downward accelerations) from the height of the cloud would always be longer than the true time. Conversely, when the fall rates are used, in order to estimate the height of origin of a particle from the time of its arrival on the ground (including its rise time), the computed height of origin is less than the cloud height.

This interpretation of the above-mentioned observations of particle-arrival time may be used to describe, in qualitative terms, the process of stem fallout. The rising cloud takes on toroidal circulation when the internal pressures and temperatures of the fireball approach those of the ambient air and a large-scale air circulation is established. Air and soil particles rise from directly below the cloud in a narrow visible stem or chimney, and the surrounding air is entrained over the whole length of this stem. This rising material flows into the bottom center of the cloud, and the countercurrent air flow, around the periphery of the cloud, is downward. The observable effect, upon occasion, is that the mass of particles appears to flow out from the top portion of the cloud and then downward.

When the toroidal circulation starts, a particle (or liquid drop) in the central region of the cloud could, by centrifugal force, be moved to the outer periphery of the cloud and then be accelerated downward at speeds greater than the particle's normal fall velocity; it would then be at a lower altitude than the cloud when its terminal fall velocity is reached. However, even if this centrifugal motion and movement to the exterior of the rising cloud did not occur for the majority of the particles, they could still fall from lower altitudes, by virtue of the downward circulation around the periphery of the cloud, than would be calculated on the basis that gravity-pull alone was overcoming the gross rise-rate of the visible cloud.

However, even with toroidal motion the separation of fallout particles by their sizes because of gravity forces is still a valid concept. The smaller particles will not move outward by centrifugal forces as far as the

larger ones in the circulation and they could be swept back upward through the cloud as long as the velocity of the rising air is sufficiently large. To use this concept in a mathematical treatment requires a method of estimating the upward velocity of the air directly below the cloud, or a particle-altitude function for estimating the apparent origin of particles having a given value of v_t.

Assumption 7 and a few observed data were used to derive a particle-altitude function whose use gives a good representation of the input data on the particle arrival times and particle sizes used in its derivation. The best representation of the data is

$$z = z_0 (1 - e^{-k_z t}) \tag{4.40}$$

where k_z is 0.011 sec^{-1}, and z_0 is a yield-dependent multiplier whose evaluation by means of Assumption 7 is discussed later. The obtained value of k_z is between the values found for the z_a and z_b time-dependent functions. For use in the scaling system, the lower limit of application of Eq. 4.40 is assumed to be about 20 seconds and the upper limit about 8 minutes. The rate of rise of the air layer from which the particles fall, represented by the coordinate z, is

$$\dot{z} = z_0 k_z e^{-k_z t} \tag{4.41}$$

or

$$\dot{z} = k_z (z_0 - z). \tag{4.42}$$

The particle size parameter α, for the particle groups falling from the apparent altitude, z, as defined by the ratio v_w/v_t, is obtained from the combination of Eqs. 4.37, 4.38 or 4.39, and 4.42, and is

$$\alpha = \frac{v_w(v_0 + w_0 z)}{k_z(z_0 - z)} \tag{4.43}$$

where v_0 and w_0 are the constants of Eqs. 4.38 and 4.39.

In the functions for the simplified fallout scaling system, the standard conditions adopted are that z is 5000 to 50,000 feet and that v_w is 15 mph or 22 feet/second. For these conditions $v_w v_0/k_z$ is 1900 feet and $v_w w_0/k_z$ is 0.020. In cases where z_0 and z are greater than 50,000 feet, these parameters are 1160 feet and 0.035, respectively; where appropriate, they are substituted for the standard values in making computations.

Having found a suitable relationship between σ and z, the values of σ_{min} and σ_{max} arriving at a given downwind distance along the center of the pattern can be determined from

$$\frac{k_s(u_0\sigma_{min} - 1900)}{2.303(\sigma_{min} + 0.020)} = \log\left[X - \frac{\sigma_{min}(u_0\sigma_{min} - 1900)}{(\sigma_{max} + 0.020)}\right] - \log u_0 \tag{4.44}$$

and

$$\frac{k_s(u_0\sigma_{max} - 1900)}{2.303(\sigma_{max} + 0.020)} = \log\left[\frac{\sigma_{max}(u_0\sigma_{max} - 1900)}{(\sigma_{max} + 0.020)} - X\right] - \log u_0 \tag{4.45}$$

The particle group arriving at the distance X from the center of the stem, σ^*, under the same range of altitudes and wind speed as in Eqs. 4.44 and 4.45, can be estimated from

$$\sigma^* = \frac{(X + 1900) + \sqrt{(X + 1900)^2 + 0.0816u_0X}}{2u_0} \tag{4.46}$$

The height from which the group falls is

$$z^* = \frac{\sqrt{(X + 1900)^2 + 0.0816u_0X} - (X + 1900)}{0.0408} \tag{4.47}$$

(For altitudes greater than 50,000, the constants 0.0816 and 0.0408 are 0.130 and 0.0800, respectively.)

Because the equations for σ_{min} and σ_{max} are not solved explicitly in terms of the equation constants and X, it is simpler to obtain σ_{min} and σ_{max} graphically computing u_z and σ at selected values of z, calculating X from Eq. 4.39, and then plotting the two values of σ as a function of X.

Since the stem fallout scaling system has been simplified to designate a spatial distribution of the σ groups that are uniformly distributed in a horizontal plane at a given value of z, it is convenient to define the activity concentration of each group in terms of the number of fissions per unit cross-sectional area of the stem. If this concentration is designated as A'_{σ}, then the total activity carried by each group is

$$A_\sigma(\sigma) = \pi A'_\sigma R_\sigma^2 \tag{4.48}$$

The total activity per unit area accumulated on the ground at the downwind distance, X, is given by the sum of the A_{α} from α_{min} to α_{max}, or:

$$A_x = \int_{\alpha_{min}}^{\alpha_{max}} A_{\alpha} d\alpha \tag{4.49}$$

The procedure for estimating A_{α} for stem fallout is essentially the same as that for estimating A_{α} for cloud fallout. The method is based on the use of observed or estimated values of A_x, given as a function of X, to determine by successive approximations A_{α} as a function of α. The first approximation is obtained by calculating an average value of A_{α}, for the value of α at each of a series of selected values of X along the center of the pattern (y = 0), by use of

$$A_{\alpha} = \frac{A_x}{\alpha_{max} - \alpha_{min}} \tag{4.50}$$

The appropriate values of α_{min}, α, α_{max}, and A_x, for a given yield, can be read from a plot of each with the downwind distance, X.

4.3.4 Methods for Estimating the Dynamics of the Fallout Deposition

The time of fallout arrival, time of fallout cessation, rate of deposition during fallout, variation of the dose-rate, and potential dose during the fallout period, can all be estimated by use of the simplified fallout scaling system. Association of particle sizes with the average fall rates from different altitudes will give the particle size ranges that fall at any location.

The assumption of a uniform distribution in the cloud of the particles having a given value of α implies that, at the location X, y, the first particles of the arriving group fell from the height of the bottom boundary of the cloud, h_1, and that the particles (or activity) from each α group will accumulate on the ground at a constant rate until the last ones falling from the height of the top boundary of the cloud, h_2, arrive.

For a constant value of the wind speed, or wind velocity vector from cloud to ground,

$$v_f = \frac{v_w}{\alpha} \tag{4.51}$$

so that the time of arrival, $t_a(r)$, for the group is given by

$$t_a(r) = \frac{r h_1}{v_w} \tag{4.52}$$

where

$$h_1 = h + z_a \tag{4.53}$$

and the time of cessation, $t_c(r)$, for the group is given by

$$t_c(r) = \frac{r h_2}{v_w} \tag{4.54}$$

where

$$h_2 = h + z_c \ , \tag{4.55}$$

In these equations, z_c is the positive, or largest, value of z, and z_a is the negative, or smallest, value of the intercepts of the particle group trajectory with the cloud boundary. The intercepts are given by

$$z = \frac{a(X - rh)b^2 \pm ab\sqrt{(a^2 + r^2b^2)(1 - y^2/a^2)\ (X - rh)^2}}{a^2 + r^2b^2} \tag{4.56}$$

The time period over which the group arrives is

$$\Delta t(r) = \frac{r \Delta z(r)}{v_w} \tag{4.57}$$

where

$$\Delta z(r) = z_c - z_a \ , \tag{4.58}$$

Since the total amount of particles or activity per unit area that arrives at X, y is given by $A_z(r)$, the rate of arrival of the group is given by

$$A_z(r)/\Delta t = \frac{v_w A_z(r)}{r \Delta z(r)} \ , \tag{4.59}$$

The total rate of arrival of fallout at any time after the first particles start arriving can be determined by summing the individual rates for all the σ groups arriving at a given time. This sum is given by

$$(A_s/\Delta t)_t = \int_{\sigma_{min,t}}^{\sigma_{max,t}} \frac{A_s(\sigma)\, d\sigma}{\Delta t(\sigma)} \qquad (4.60)$$

The $(\sigma_{min,t})$ and $(\sigma_{max,t})$ values are obtained from a plot of $t_a(\sigma)$ and $t_p(\sigma)$ as a function of σ. The integration indicated by Eq. 4.60 can be carried out graphically from a plot of $A_s(\sigma)/\Delta t(\sigma)$ as a function of σ.

The gross activity, or number of radioactive atoms per unit area, accumulated on the ground at any time after the first particles arrive is given by

$$A_s(t) = \int_{t_a(1)}^{t} (A_s/\Delta t)_t\, dt \qquad (4.61)$$

where $t_a(1)$ is the time of arrival of the first group. When t is t_a of the last group to arrive, Eq. 4.61 is equal to the A_s of Eq. 4.10. For close-in locations, 8 minutes should be added to these times to account for the cloud-formation time.

The time of arrival of each particle group falling from the stem altitudes at a given downwind location is the sum of its rise time and fall time. The rise time of each group may be estimated from a combination of Eqs. 4.41, 4.42 and 4.48 which is

$$t_r(sec) = 209\left[\log(\sigma + 0.020) - \log(1900/u_0 + 0.020)\right], \qquad (4.62)$$

When t_a is greater than 20 seconds the time required for the group to fall to the ground is

$$t_f = u/v_f = \sigma u/v_w \qquad (4.63)$$

or, with Eq. 4.48, the time of fall under the same conditions of wind speed and height of origin as in Eq. 4.62 is

$$t_f(sec) = \frac{\sigma(\sigma u_0 - 1900)}{22(\sigma + 0.020)} \qquad (4.64)$$

The activity accumulated to any time can be determined from a plot of the integral (or sum),

$$A_x(t) = \int_{\alpha_{min}}^{\alpha} A_\alpha d\alpha \qquad (4.65)$$

against the time of arrival of the α group as given by $t_x + t_f$. The rate of arrival of the α groups, if desired, can be determined for various times by taking slopes from the curve. The delay time due to particle circulation, as is discussed in Chapter 4, would increase the arrival times given by $t_x + t_f$.

4.8.5 Estimation of Ionization Rate and Exposure Dose

In order to estimate the air ionization rate and exposure dose from A_x (t), both a conversion from fissions per unit area to r/hr and a decay curve for the gross radioactive mixture are needed. The conversion factor from fissions/sq.ft to r/hr is defined by

$$I_x(t) = K_x(t)A_x \qquad (4.66)$$

and

$$K_x(t) = Dq_x \left[r_x(t)I_{fp}(t) + I_i(t)\right] \qquad (4.67)$$

in which I_{fp} (t) is the air ionization rate per fiss/ft at 3 feet above an infinite ideal plane for a uniform distribution of the normal fission product mixture, I_i (t) is the same unit for neutron-induced activities, r_x (t) is the gross fission product fractionation number, q_x is the terrain shielding factor, D is an instrument response factor, and t is the time after fission. The true air ionization rate, I_x^0 (t), is obtained when D is set equal to one.

Since most fallout data have been corrected to a standard time of H + 1 hr and reported in values as of this time (even though the fallout had not yet arrived at 1 hour), it is convenient to refer to the common-time data in r/hr by means of a decay correction factor, d(t,1), defined by

$$I_x(t) = d(t,1)I_x(1) \qquad (4.68)$$

where $I_s(t)$ is the air ionization rate corrected to H + 1. It is seen that

$$I_s(t) = K_s(t)A_s \tag{4.69}$$

and

$$I_s(t) = K_s(t)d(t,1)A_s \tag{4.70}$$

The potential (exposure) dose from deposited fallout during fallout arrival is

$$D_s = \int_{t_s}^{t_c} I_s^o(t)\,dt \tag{4.71}$$

where t_s and t_c are the arrival and cessation times, respectively, for all values of σ arriving at X. Equation 4.71 can be integrated from a plot of $I_s^o(t)$ as a function of time.

In order to estimate the dose rate contribution from the activity in the air as it falls, the air concentrations of all the particle groups are needed. Since a uniform volume distribution of the particle groups was assumed and a single velocity for the wind speed was taken, the concentration of particles for each value of σ remains the same at all altitudes and is given by A_{σ}.

From calculations made by Laumetzy[18] the air ionization rate at three feet inside a plane boundary of a semi-infinite volume containing a uniformly-distributed radiation source is given by

$$I_s(t) = 0.950\times10^{-9} A_t A_{\sigma} E_t \text{ in r/hr} \tag{4.72}$$

in which A_t is the activity in dis/sec per fission at the time, t, after fission, A_{σ} is the concentration in fissions/ft^3, and E_t is the total gamma ray energy in Mev/dis.

At a given time, A_t and E_t are constant, so that the contributions from the particle groups of all σ values arriving at a given time can be summed as in the case of the deposited material. Multiplication by the appropriate values of A_t and E_t for the designated time will convert the sum to r/hr. The sum for fallout from cloud altitudes is given by

$$I_s(t) = 0.950\times10^{-9} A_t E_t \int_{\sigma_1}^{\sigma_2} A_{\sigma}\,d\sigma \tag{4.73}$$

Values for A_c and E_c can be derived from the data of Bolles and Ballou[14] Lalibriere,[15] and Zigman and Mackin.[16]

The method of estimation for the ionization rate from the airborne particles arriving from the stem altitudes is the same as for those from cloud altitudes, except that the value of A_α in Eq. 4.72 must be estimated from

$$A_\alpha = \frac{1}{v_f} \frac{dA_s}{dt} \tag{4.74}$$

where $v_f = v_w/\alpha$. In Eq. 4.74, the v_f applies to the α group arriving at the time as given by Eqs. 4.63 and 4.64. The ionization rate is given directly by Eq. 4.72 because the simple stem fallout scaling system gives only one particle-size group as arriving at a given instant.

CHAPTER 4 REFERENCES

1. Kellogg, W.W., Hearings before the Special Subcommittee on Radiation of the Joint Committee on Atomic Energy, U.S. Congress, The Nature of Radioactive Fallout And Its Effects on Man, Part I, p. 104-41, 1957.

2. Anderson, A.D., A Theory for Close In Fallout, USNRDL-TR-249, 1958.

3. Kellogg, W.W., R.R. Rapp, and S.M. Greenfield, J. Meteor. 14, 1, 1-8 1957.

4. Schuert, E.A., A Fallout Forecasting Technique With Results Obtained at the Eniwetok Proving Ground, USNRDL-TR-139, 1957.

5. Kaauda, C.F., L. Minvielle, and A. Moskin, Scaling of Contamination Patterns, Surface and Underground Detonations, USNRDL-TR-1, 1958 (Classified).

6. Laurino, R.K., and I.G. Poppoff, Contamination Patterns at Operation Jangle, USNRDL-899, 1958.

7. Capabilities of Atomic Weapons, Armed Forces Special Weapons Project, TM23-200, 1958 (Classified).

8. The Effects of Nuclear Weapons, U.S. Government Printing Office, Washington, D.C., 1957.

9. Anderson, A.D., Application of "Theory for Close-In Fallout" To Low-Yield Land Surface and Underground Nuclear Detonations, USNRDL-TR-289, 1959.

10. Pugh, G.E., and R.J. Galiano, An Analytic Model of Close-In Deposition of Fallout for Use in Operational-Type Studies. Research Memorandum No. 10, Weapons Systems Evaluations Group, 1959.

11. Callahan, E.D., L. Rosenblum, J.D. Kaplan, and D.R. Batten, The Probable Fallout Threat over the Continental United States, TO-B60-18, 1960.

12. Rapp, R.R., Summary Report of RAND Work on the AFSWP Fallout Project, RM-2334, 1959 (Classified).

13. Laumetz, E., Private Communication, USNRDL, 1960.

14. Bolles, R.C., and N.E. Ballou, Calculated Abundances of U-235 Fission Products, USNRDL-456, 1956.

15. LaRiviere, P.D., Early-Time Gamma Ray Properties of U-235 Gross Fission Products, USNRDL-TM-89, 1955.

16. Zigman, P., and J. Mackin, Early Time Decay of Fission Product Mixtures --II Health Physics 5, 79 1961.

Chapter 5

CORRELATION OF SCALING MODEL PARAMETERS WITH OBSERVED FALLOUT PATTERN FEATURES

5.1 General Description of Fallout Patterns from Land Surface Detonations

Although observed data on fallout patterns from land surface shots of various yields are very meager, the processed data give indication in a qualitative way of a number of persistent characteristics. For example, the general shape of the fallout standard intensity contours (in r/hr at 1 hr) from shots where the wind structures were rather simple, resembles a shadow of the mushroom cloud and its stem on the ground.

Because of the shortage of reliable data on the fallout patterns from land surface detonations, any systematic method for scaling fallout patterns--i.e., methods for interpolating and/or extrapolating data from one weapon yield to another--must take full advantage of all such apparently persistent qualitative characteristics of the available patterns. In devising methods that can convert the qualitative characteristics to quantitative ones, the methods must, of course, be capable of at least reproducing the observed data that was used in obtaining the original scaling relationships, which are given as functions of weapon yield.

Some of the apparently persistent characteristics of the fallout patterns from surface detonations are:

1. In the region near ground zero, the intensity gradient in the upwind and crosswind directions is very steep
2. The high intensities near ground zero appear as an intensity ridge (rather than as a circular peak) displaced in the downwind direction
3. The length of this high intensity ridge appears to be proportional to the width of the lower portion of the stem
4. The peak intensity of the ridge increases with yield in the 1- to 10-KT yield range and decreases in the 100-KT to 10-MT yield range

5. The best simple empirical relationship for the variation of the intensity with upwind and crosswind distance from ground zero, from graphical plots of the data, is that of the form, $I_0 e^{-kx}$, where I_0 is the ridge peak intensity, k is a constant for a given yield, and x is the upwind and/or crosswind distance from the upwind shoulder of the ridge peak

9. The contours downwind from ground zero appear to be parallel to the intensity ridge for its entire length

7. At distances greater than the length of the ridge, the intensity contours directly downwind decrease with distance from ground zero

8. At some distance downwind (or perhaps even upwind for very large yields), the low-valued intensity contours fan out and the intensities directly downwind from ground zero rise sharply with distance and then more slowly with distance to a peak value

9. The distance from ground zero to this downwind peak intensity increases with weapon yield

10. The magnitude of the peak intensity also appears to increase continuously with yield

11. The distance between the lower-valued contours appears to be related to the width of the cloud (not considering wind shear differences) and the maximum width seems to occur farther downwind than the peak intensity

12. The variation of the intensity with downwind distance from this outer pattern peak can be approximated within reasonable limits of error if the wind shear is not large by a function of the form $I_0 e^{-mx}$, where I_0 is the peak intensity, m is a yield dependent parameter and x is the downwind distance from the peak.

The above listed fallout pattern characterizations are based on a combination of experimental observations and analyses of field test data. The most reliable of the group appear to be those numbered 1, 2, 4, 6, 7, 8, and 9.

5.2 General Conditions to Which the Source Data Apply

In deriving the empirical constants for the scaling functions of the fallout patterns, the available data were converted to the reference of 100 percent fission yield (B = 1), including 0.8 neutron captures per fission by U 238 to give the appropriate value of $I_\gamma(1)$ in roentgens per hour at 1 hour.

Also, the $I_\gamma(1)$ values (or standard intensities) correspond to radiac measurements taken at three feet above an extended open area contaminated with fallout as it existed when the measurements were taken. The reference radiac instrument for the $I_\gamma(1)$ values is the AN/PDR-39(T1B) portable radiac; it has a geometric and photon energy response of very nearly 75 percent of the true air ionization rate at three feet above a plane source of fission products uniformly distributed on the area. Therefore to obtain the true air ionization, in calculating exposure doses, the $I_\gamma(1)$ values should be multiplied by 1.33.

The average value of the terrain shielding factor, which is automatically contained in the source data, is about 0.75. The data, in general, apply to U-238 fission, for which the $I_{fp}(1)$ of Eq. 4.07 is 0.94×10^{-10} r/hr at 1 hr per fission/sq ft. The value of $I_\gamma(1)$ for the indicated induced activities is 0.10×10^{-10} r/hr at 1 hr per fission/sq ft. With these numbers, Eq. 4.07 becomes

$$K_\gamma(1) = 3.90 \times 10^{-10} \left[r_\gamma(1) + 0.019 \right] \frac{\text{r/hr at 1 hr}}{\text{fission/sq. ft.}} \qquad (5.1)$$

The numerical coefficient is 5.40×10^{10} in r/hr at 1 hr per KT/sq ft and 1980 in r/hr at 1 hr per KT/sq mi. However, $r_\gamma(1)$ is also included in the observed data to some degree; just how much is unknown because most of these data were decay-corrected to H+1 by a single decay curve. The exact value and dependence of $r_\gamma(1)$ on distance is not needed for developing the scaling functions since it is unnecessary to separate the product $K_\gamma(1)A_\gamma$ in the derivations. An average value of $r_\gamma(1)$ is defined at the end of this section to account for the fraction of the total activity produced that falls within a given area on the ground.

The average wind speed, for the source data used, was between 12 and 15 mph. It may be assumed, therefore, that the scaling functions are for an average or effective wind speed of 15 mph.

5.3 Scaling Functions for Fallout Pattern Features of Interest

Some of the pattern features of interest along the downwind axis (y = 0) of the idealized fallout pattern are shown in Figure 5.1 as a schematic intensity profile. The numbers shown in the figure correspond to the number subscripts of the scaling functions. The evaluated scaling functions for these and other quantities are given in Section 5.4. The procedures and assumptions used in obtaining the numerical values are described below.

5.3.1 Intensity Ridge Near Ground Zero

This ridge is assumed to result from the deposition of particles from stem altitudes. Because (1) more data are available on the fallout deposited in the vicinity of ground-zero for surface land shots than for other downwind areas and (2) the simplified fallout scaling system for the stem geometry could not be utilized in a straightforward manner to reproduce the observed intensities upwind from ground zero, the scaling function for $-X_1$, the upwind distance to the 1 r/hr at 1 hr intensity, was derived directly from the observed data.

According to observation 5 in Section 5.4.1, the peak intensity near ground zero is given by

$$I_{u,\beta} = \exp k_{I,\beta} (X_u - X_1) \qquad (5.3)$$

where $k_{I,\beta}$ is a yield-dependent parameter evaluated empirically from observed data. The parameter designated by X_u is the distance to the upwind shoulder of the intensity ridge; this location generally does not coincide with that of the crater at $X = 0$.

The length of the intensity ridge, $X_\beta - X_u$, is assumed to be equal to the diameter of the stem, $2a_\beta$, for the particle groups falling from a characteristic altitude, z_β. One possible explanation for the observation of the intensity ridge is that a large number of fallout particles having a rather narrow size-range fall from a given small range of altitude after the fireball rises some distance from the ground because a basic change in the internal circulation has occurred. The onset of toroidal motion, for example, might result in the rapid ejection of the larger particles in a short period of time. The dumping or ejection of a rather large number of big particles might also coincide with the time it takes the larger particles to make one pass through the rising fireball prior to their mass migration to the peripheral regions where the air currents can accelerate their fall downward.

Figure 5.1
SCHEMATIC OUTLINE FOR THE INTENSITY PROFILE DOWNWIND FROM GROUND ZERO ALONG THE AXIS OF THE FALLOUT PATTERN ($y = 0$) AS USED IN THE SIMPLIFIED FALLOUT PATTERN SCALING SYSTEM

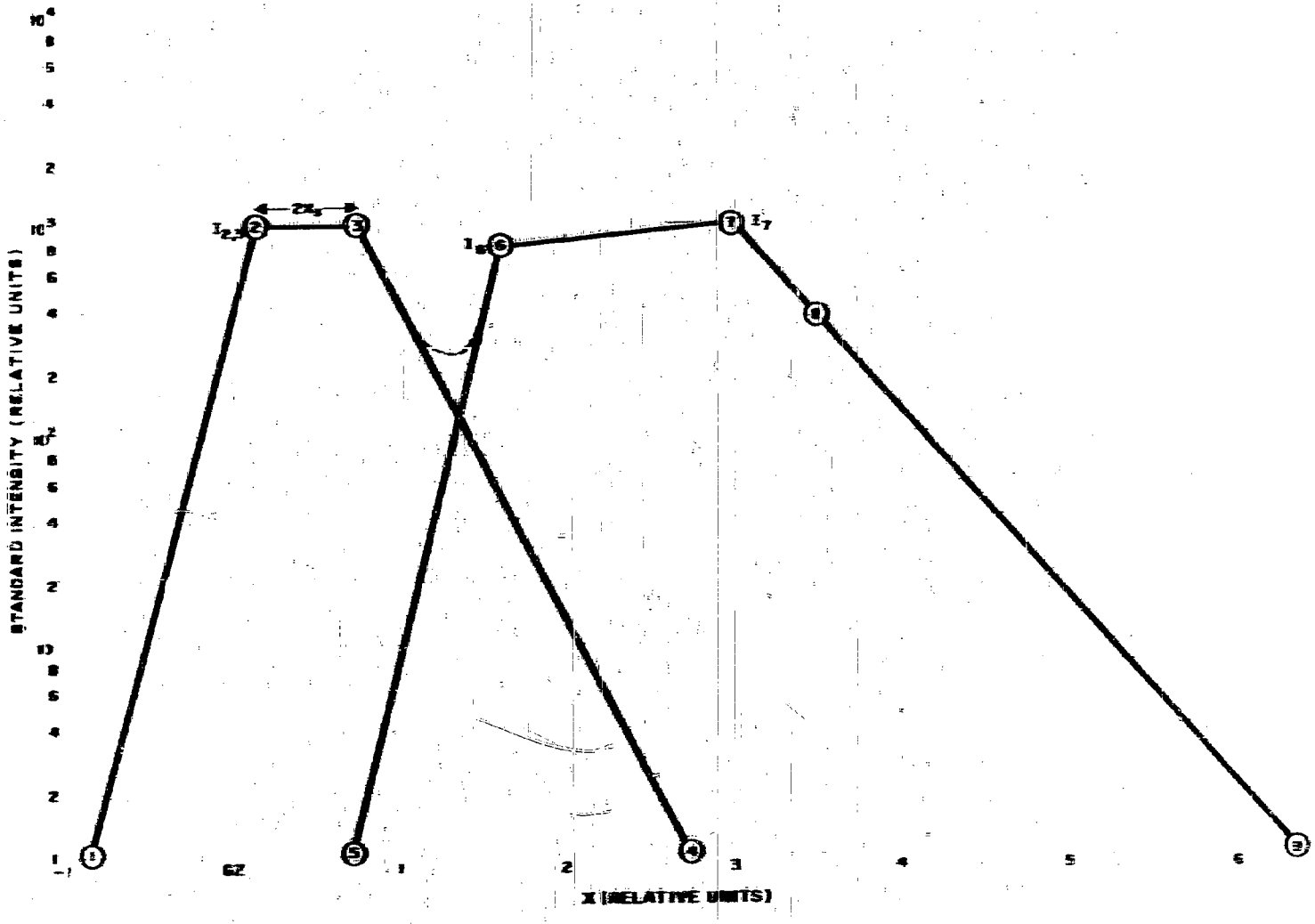

Since both R_n and $\underline{g}$ are proportional to W^n, where n is near 1/3, the same type of dependence on yield is assumed for $(X_\mu - X_\eta)/\sigma$, or $\sigma_{\mu,\eta}$. Because the assumption requires that the particle groups falling from $\sigma_{\mu,\eta}$ are the minimum σ group that arrive at X_μ and the maximum σ group that will at X_η, the particles that fall from the center of the storm must land near $X_\mu + (X_\eta - X_\mu)/2$. The particle-size parameter indicator for these particles, therefore, can be defined by

$$\sigma_{\mu,\eta} = \frac{X_\mu + X_\eta}{2R_n} \tag{5.3}$$

where

$$R_n = \frac{2.303(\log a_n - \log t_0)}{k_n} \tag{5.4}$$

Once the yield-dependence of $\sigma_{\mu,\eta}$ is determined, the value can be calculated. It is then available to give an estimation of X_μ and X_η for any yields, by use of the relations

$$X_\mu = \sigma_{\mu,\eta} R_n - R_n \tag{5.5}$$

and

$$X_\eta = \sigma_{\mu,\eta} R_n + R_n \tag{5.6}$$

The additional use of $\sigma_{\mu,\eta}$ is to evaluate the parameter n_n that defines the rate-of-rise functions, $(\ldots)^{n_n}$ of Eq. 5.43 to make the evaluation results in

$$R_n = \frac{v_w v_n}{\sigma_{\mu,\eta} k_n} + \frac{(\sigma_{\mu,\eta} + v_w v_n/k_n)t_0}{\sigma_{\mu,\eta}} \tag{5.7}$$

which, for the 22 ft/sec wind speed, 50,000 to 60,000 ft altitudes, and rise times of 20 to 500 sec, is given by

$$R_n = \frac{1000 + (\ldots + 0.020)t_0}{\sigma_{\mu,\eta}} \tag{5.8}$$

and, for use with z values greater than 50,000 ft, is given by

$$z_a = \frac{1160 + (\alpha_{y,s} + 0.015)z_s}{\alpha_{y,s}} \qquad (5.9)$$

These evaluations of z_a assume that at z_s the same upward force is acting on the particles that may go higher than 50,000 feet as is acting on those that fall back from lower altitudes. In a general way, the equation constants for the higher altitudes should not apply to yields for which z_a itself is less than 50,000 feet. For the empirically-evaluated constants, the yields for which the high-altitude equations apply is actually near 10^3 -KT. The upper limit of z_a is (h-b). This limit is exceeded for yields less than about 8- or 9-KT; therefore, for the lower yields, z_a is replaced by (h-b).

In estimating the change in the relationship between $I_{g,s}$, X_2, and X_1 with change in wind speed, $k_{1,2}$ is assumed to remain constant. This means that the intensity levels in the upwind and crosswind directions increase or decrease with $I_{g,s}$ as the wind speed decreases or increases. In the model for fallout from stem altitudes, only one particle-size group is described as falling from a given altitude.

The inverse of the fall velocity of the group, from Eqs. 4.38 and 4.43, is

$$1/v_f = \frac{86.4 + 9.27 \times 10^{-4} z}{z_a - z} \qquad (5.10)$$

The downwind distance at which the particle group falls from either edge of the stem is defined by

$$X = v_w z/v_f \pm s_z \qquad (5.11)$$

where s_z is the stem radius at z, as given by Eq. 4.31, and v_w is the wind speed. By calculating the values of $1/v_f$, X, and s_z for a series of selected values of z, it is possible to construct a plot of the maximum and minimum values of $1/v_f$ against X for a selected wind velocity. When this is done, the two values of $1/v_f$ approach a central value as the wind speed increases and diverge as the wind speed decreases.

If the location $X_{g,s}$ at the center of the downwind intensity ridge is selected as the location at which the variation of $I_{g,s}$ with wind speed is to be estimated, and if it is assumed that an average value of the activity per unit volume can be assigned to a central particle group, then $I_{g,s}$ can be estimated

from

$$I_{g,s} \quad K_{g,s}(1)\overline{\Lambda}_f(z_g - z_s) \tag{5.13}$$

where $\overline{\Lambda}_f$ is the average value of the concentration, in fissions per cu ft; $K_{g,s}(1)$ is a constant for conversion to r/hr at 1 hr, z_g is the altitude of origin of the largest particle size group arriving at $X_{g,s}$, and z_s is taken as the lowest altitude from which particles fall at $X_{g,s}$. In the yield range of from 100 to 50,000 KT, and for wind speeds from 7.5 to 45 mph, the dependence of $z_g - z_s$, or $\Delta z_{g,s}$, on wind speed can be represented by

$$\Delta_{g,s} \quad \Delta z^{s}_{g,s} v_w^{n} \tag{5.18}$$

where $\Delta z^{s}_{g,s}$ and n are yield-dependent parameters. The values of these two parameters and the derived values of $K_{g,s}(1)\overline{\Lambda}_f$ are given in Table 5.1 at several values of weapon yield. In making the calculation, $X_{g,s}$ is estimated from

$$X_{g,s} = \sigma_{g,s} z_s \tag{5.14}$$

Thus $X_{g,s}$ varies directly with wind speed, since $\sigma_{g,s}$ is equal to $v_w/v_{g,s}$ where $v_{g,s}$ is the fall velocity of the central particle-size group that arrives at $X_{g,s}$.

The scaling system described above is designed to reproduce roughly, by means of the assumed particle source geometry, (1) the fall behavior of a given particle-size group, and (2) the variation in size-spread of the group as a function of wind speed and weapon yield. This general approach is repeated for other fallout pattern features in the following sections.

The variation of X_p and X_0 with wind speed is estimated by multiplying $\sigma_{g,s}$ by $v_w/15$; a_1 is assumed to be independent of wind. The indicated change of X_1 with wind speed, from the assumption of a constant value of $k_{1,s}$, is

$$X_1 = X_g - \frac{2.303 \log I_{g,s}}{k_{1,s}} \tag{5.15}$$

where $I_{g,s}$ is given by Eq. 5.12. For X_p computed for the same value of v_w as $I_{g,s}$, the value of X_1 in Eq. 5.15 is for $I_1 = 1$ r/hr at 1 hr.

Table 5.1

EQUATION PARAMETER VALUES FOR THE VARIATION OF $\Delta s_{g,0}$ WITH WIND SPEED[a] AND DERIVED VALUES OF $K_{g,0}\bar{A}_f$

W (KT)	$\Delta s^0_{g,0}$ (ft)	n	$K_{g,0}(1)\bar{A}_f$ (r/hr at 1 hr/ft)	$K_{g,0}(1)\bar{A}_f\,\Delta s^0_{g,0}$ (r/hr at 1 hr)
100	12,200	-0.78	23.0	202,000
200	12,700	-0.78	15.2	105,000
500	13,400	-0.77	8.50	112,000
1,000	13,800	-0.765	5.60	76,700
2,000	13,000	-0.76	3.04	54,500
5,000	14,000	-0.75	2.60	36,400
10,000	15,500	-0.74	1.92	26,500
20,000	18,100	-0.71	1.39	18,200
50,000	11,100	-0.63	0.933	10,200

a. Wind speed in mph.

5.3.2 Location of the Downwind Standard Intensity Contour for Fallout from Stem Altitudes

The particle-size group designator, α_4, for particles falling at X_4 is assigned to the group that originated from the center of the stem. This group, from Eq. 4.46 is specified by

$$\alpha_4 = \frac{(X_4 + 1900) + \sqrt{(X_4 + 1900)^2 + 0.0816\, s_0 X_4}}{s_0} \qquad (5.16)$$

and, given the yield-dependence of α_4, X_4 can be estimated from

$$X_4 = \frac{\alpha_4(\alpha_4 s_0 - 1900)}{(\alpha_4 + 0.020)} \qquad (5.17)$$

If s_4, given by X_4/α_4, is greater than 50,000 feet, the indicated equation constants are replaced by those previously given for the higher altitudes.

For wind speeds other than 10 mph, X_4 is directly proportional to the wind speed. If the fall velocity of the center particle-size group is designated v_4, then Eq. 5.17 is

$$X_4 = \frac{v_w(v_0 / v_4 - 86.36)}{(1 + 9.273\times10^{-4} v_4)} . \tag{5.18}$$

The variation of the ionization rate at X_4 due to the narrowing of the particle size with wind speed is given by

$$I_4 = K_4(1)\bar{A}_f \Delta z_4 \tag{5.19}$$

where Δz_4 is the span in altitude from which the particles fall to X_4. The value of Δz_4 is given by

$$\Delta z_4 = \frac{(v_1 - v_2)(86.36 + 9.273\times10^{-4} v_0)}{(1 + 9.273\times10^{-4} v_1)(1 + 9.273\times10^{-4} v_2)} \tag{5.20}$$

in which v_1 and v_2 are the respective values of the largest and smallest particle fall rates for the groups that arrive at X_4. Their values are determined by the method described for estimating the variation of $I_{2,3}$ with wind speed. Calculations of Δz_4 for yields from 500 to 50,000 KT, and for wind speeds from 5 to 50 mph, give

$$\Delta z_4 = 1720 W^{0.046} / v_w \tag{5.21}$$

Also, it was determined that

$$K_4(1)\bar{A}_f = 8.72\times10^{-3} W^{-0.046} \tag{5.22}$$

so that, as might be expected, I_4 is inversely proportional to wind speed and is given by

$$I_4 = 15.0 / v_w \tag{5.23}$$

for v_w in mph. This result occurs because the span in altitude of origin for the particles arriving at X_4 is very narrow.

5.3.3 Stem Pattern Half-Width

The half-width of the stem fallout, designated Y_s, is the lateral distance from the center-line of the stem pattern (y = 0) to the 1 r/hr at 1 hr contour. Because of the geometry used for the stem, where the diameter of the upper portion of the stem becomes proportional to the cloud diameter, the ratio Y_s/a is assumed to vary uniformly with yield according to a function of the form: constant times W^n. The constants were evaluated empirically from observed data.

For wind speeds other than 15 mph, the r/hr at 1 hr contours may be estimated from

$$Y_s = \frac{Y_s^0 \log I_{s,s}}{\log I_{s,s}^0} \qquad (5.24)$$

where Y_s^0 is the half-width and $I_{s,s}^0$ is the ridge intensity for the 15 mph wind speed. This relationship assumes that the logarithmic slope from the intensity ridge in the y, or cross-wind, direction is independent of wind speed. The logarithmic slope, and $k_{1,s}$ assumed constant for a given yield of detonation, results in a slight reduction in the fraction of the total activity that is accounted for in the stem pattern with increasing wind velocity, since the decrease in the total activity that is due to the decrease in $I_{s,s}$ with wind speed is not quite compensated for by the increase in the distance $X_4 - X_3$.

An additional contributing factor is the neglect of any spread in $X_3 - X_2$ with wind speed. The over-all error in the areas enclosed by given contours, or in the total activity in a pattern, by this simplified treatment of the variation of Y_s with wind speed, however, is not large; the error should decrease with yield since the fraction of the total activity in the fallout pattern that comes from stem altitudes (according to the scaling system) decreases with increasing weapon yield. The shape of the so-called ground zero circular contours should tend to flatten on the sides and the radius should decrease toward the value of Y_s as the wind speed increases.

5.3.4 The Distance to Fallout Pattern Features for Fallout from Cloud Altitudes

The basic assumption in the scaling of the cloud fallout pattern features is that the distances from ground zero to various points in the pattern are approximately proportional to the height of the particle cloud source geometry. The second assumption is that all variations from a direct proportionality to cloud height for triangular scaling of distances, for example, involves a gradual

change, with weapon yield, in the particle size groups that arrive at a location of interest.

The assumed form of the gradual change of the inverse fall-velocity designator, α_0, is $\alpha_0^0 W^n$, where α_0^0 and n are yield-independent parameters. In the central area of fallout from cloud altitudes, the above assumptions result in a distance-scaling function given by

$$X = 6.60 \times 10^3 W^{0.445} \alpha_0, \quad W = 1 \text{ to } 28\text{KT} \tag{5.25}$$

or

$$X = 1.68 \times 10^4 W^{0.164} \alpha_0, \quad W = 28\text{KT to } 10^3\text{KT} \tag{5.26}$$

where α_0 is the particle-size designator for particles falling along a line from the center of the cloud to X since α_0 is equal to X/h. The distances designated X_6, X_7, X_8, and X_9 are scaled by use of these functions.

For locations underneath the cloud and near the upwind limit of the fallout from cloud altitudes, the distances are better determined by α_{max} because the peak value of $A_n(\alpha)$ tends to shift towards α_{max} as X becomes small. The location of interest in this case is the upwind point of the 1 r/hr at 1 hr standard intensity designated as X_5. The distance-scaling function for this location is

$$X_5 = 6.60 \times 10^3 W^{0.445} \alpha_0 - 1.40 \times 10^3 W^{0.300} \sqrt{1.06 W^{0.262} + \alpha_0^2}, \quad W = 1 \text{ to } 28\text{KT} \tag{5.27}$$

or

$$X_5 = 1.68 \times 10^4 W^{0.164} \alpha_0 - 1.40 \times 10^3 W^{0.300} \sqrt{1.06 W^{0.262} + \alpha_0^2}, \quad W = 28 \text{ to } 10^3\text{KT}. \tag{5.28}$$

The scaling function for α_0 is assumed to be of the form, $\alpha_0^0 W^n$. For lower weapon yields, X_5 is larger than $\alpha_0 h$; at the yields and wind speeds where this occurs, the variation of X_5 with yield is given by Eq. 5.25 or 5.26.

5.3.5 The Intensity Levels of Pattern Features for Fallout from Cloud Altitudes

Functions for estimating the variation of the standard ionization rate, or the radiation intensity, at the selected downwind locations are derived from the assumption that an average value of Λ_{σ} can be assigned to the particle groups centering at σ_0 where the values of $X-\sigma h$ are small. The average value of $\Lambda_x(\sigma)$ for these conditions is

$$\overline{\Lambda}_x(\sigma) = \frac{2\overline{\Lambda}_{\sigma} a h}{\sqrt{a^2 + \sigma^2 b^2}} \qquad (5.29)$$

The integral of $\overline{\Lambda}_x(\sigma)d\sigma$ is then given by

$$A_x = 2\overline{\Lambda}_{\sigma} a \ln \left\{ \frac{\sigma_{max} + \sqrt{a^2/b^2 + \sigma^2_{max}}}{\sigma_{min} + \sqrt{a^2/b^2 + \sigma^2_{min}}} \right\} \qquad (5.30)$$

where A_x is the total activity in the same units as A_0. Actually, the approximate integral of $\overline{\Lambda}_x(\sigma)d\sigma$ may be applied to the levels at locations where both X and σ are small, as well as at locations where the mid-range value of σ is near σ_0. This application is for locations underneath the cloud where X is smaller than the cloud radius.

Although the values of σ_{max} and σ_{min} can be evaluated from Eq. 4.11 in terms of σ_0, it is more convenient, for hand computations, to evaluate the logarithmic term by approximating σ_{max} and σ_{min} from

$$\sigma_{max} \approx \frac{X + a}{b} \qquad (5.31)$$

or

$$\sigma_{max} \approx \sigma_0 + a/b \qquad (5.32)$$

and

$$\sigma_{min} \approx \frac{X - a}{b} \qquad (5.33)$$

or

$$\sigma_{min} \approx \sigma_0 - a/b \qquad (5.34)$$

variation of the three parameters with weapon yield or by the variation in σ_n with wind speed. Since the lower limit of σ from the storm model is $\sigma_{y,n}$, and the lower limits of σ for the cloud model are not specified without complete evaluation of A_{σ}, the value of σ_{min} for locations at which $\sigma_n > nh$ is taken to be

$$\sigma_{min} = \sigma_{y,n} \tag{5.35}$$

Although the scaling functions for the different characteristic standard intensities at locations underneath the cloud where $\sigma_n > nh(X > n)$ are evaluated in Eq. 5.8 by using $\sigma_{y,n}$ for σ_{min}, better first estimates of A_{σ} as a function of σ are obtained when the quantity $X_1/(h-b)$ is substituted for σ_{min}, providing X_1 is less than X_η. The true values of σ_{min} for different weapon yields have not yet been determined.

With the above limits on σ_n, the scaling equations for the intensity levels at the selected locations are

$$I_1 = K_1(1)\,\bar{A}_{\sigma n} - 4.606 \log \phi_1 \quad , \quad \sigma_1 \geq n/h \tag{5.36}$$

and

$$I_1 = K_1'(1)\,\bar{A}_{\sigma n} - 4.606 \log \phi_1' \quad , \quad \sigma_1 \leq n/h \tag{5.37}$$

where

$$\phi_1 = \frac{(\sigma_1 + n/h) + \sqrt{n^2/b^2 + (\sigma_1 + n/h)^2}}{(\sigma_1 + n/h) + \sqrt{n^2/b^2 + (\sigma_1 + n/h)^2}} \quad , \quad \sigma_1 \geq n/h \tag{5.38}$$

and

$$\phi_1' = \frac{(\sigma_1 + n/h) + \sqrt{n^2/b^2 + (\sigma_1 + n/h)^2}}{\sigma_{y,n} + \sqrt{n^2/b^2 + \sigma_{y,n}^2}} \quad , \quad \sigma_1 \leq n/h \tag{5.39}$$

and σ_1 is σ_n for the distance X_1. In the case of X_n, however, σ_n' is the same as σ_{max}. At X_0 where $\sigma_0 + n/h$ is much larger than n/b, ϕ_0 reduces to

$$\phi_0 = \frac{\sigma_0 + n/h}{\sigma_0 - n/h} \tag{5.40}$$

The parameters $K_i(1)A_{\sigma_i}$ and $K_i'(1)A_{\sigma_i}$ are assumed to be dependent on only the weapon yield and to have a yield-dependence of the form: constant times W^n. The effect of the wind speed on I_i is determined by the change in $\log \eta_i$ caused by the increase or decrease in σ_i with wind speed, which is determined from

$$\sigma_i(v_w) = (v_w/15)\,\sigma_i(15) \qquad (5.41)$$

for v_w in mph. The scaling functions of σ_i with weapon yield were evaluated from data for a presumed effective wind speed of 15 mph.

The scaling functions presented here could be used to evaluate A_σ as a function of σ as well as for the approximations that are given by Eqs. 4.32 and /or 4.50. Use of either set would require a series of recomputations of A_i to obtain a reasonably good fit to the general shape of the fallout pattern downwind intensity profile and to other pattern features.

5.3.6 The Maximum Pattern Width

The scaling function for the downwind distance, X_g, to the maximum pattern half-width, Y_g, is taken to be similar to those for X_s and X_y. The particle-group designator for this distance, σ_g, is taken to represent the case in which the maximum pattern width is measured between the 1 r/hr at 1 hr contours when the average wind speed is 15 mph. For some of the data used to determine scaling function parameters, the maximum half-width was found to be roughly proportional to the cloud radius as of 5 to 10 minutes after detonation.

The crosswind distances to given contours in the fallout area depend, first, on the lateral displacement of the particles during the rise of the cloud; second, on the wind directions at all altitudes from the bottom to the top of the cloud; and third, on the wind speeds. Thus, the observed half-widths result from the combination of the three.

The wind speed has two effects on the lateral displacement of an intensity contour. One is the displacement of particles, because of the relative horizontal distance traveled in a given period of time. The other is the decrease in surface density of a given size group with wind speed, because of the change in the angle of the particle trajectory. Hence, even for the case in which the wind direction is the same at all altitudes, a change in wind speed results in a change in the maximum cross-wind distance of a given intensity contour.

In general, the difference in direction of the horizontal components of particle-fall trajectories, because of the differences in direction and speed of the air flow from the bottom to the top of the fallout particle source volume,

is called the wind shear. Because of the difficulties in correcting fallout-pattern data, and because some of the available data have maximum pattern-widths roughly proportional to the cloud diameters for about the same wind speeds, the overall effect of the wind shear is assumed to be the same as for that group of data. The data, together with derived restrictions on the fraction of the total activity that is carried by fallout particles within a stated low intensity contour, were used to determine the variations of Y_s with weapon yield. The method used is given in Section 5.3.7.

The variation of Y_s with wind speed (for a given wind direction) is determined relative to Y_s for a wind speed of 15 mph. The representation for this variation is

$$Y_s(v_w) = Y_s(15)\, S(v_w) \tag{5.42}$$

in which $S(v_w)$ is the relative shear factor due to wind speed only.

The values of $S(v_w)$ determined from the fallout scaling system parameters for different wind speeds are essentially independent of yield. The indicated value of $Y_s(v_w)$ is for the particle groups falling at the downwind distance; the associated intensity contour, that passes through the location at $Y_s(v_w)$, X_s, is the same as that at X_s for the same wind speed. The intensity at the location is thus 1 r/hr at 1 hr when the wind speed is 15 mph. Values of $S(v_w)$ at several wind speeds, and the associated intensities, are given in Table 5.2.

Table 5.2

SUMMARY OF THE RELATIVE WIND SPEED SHEAR FACTOR, $S(v_w)$, FOR THE FALLOUT PATTERN MAXIMUM HALF-WIDTH AND ASSOCIATED STANDARD IONIZATION RATE, FOR SEVERAL WIND SPEEDS

Wind Speed (mph)	$S(v_w)$	I_w (r/hr at 1 hr)
7.5	1.675	2
15	1	1
20	0.840	0.75
30	0.694	0.50
45	0.604	0.33

The value of Y_B for the 1 r/hr at 1 hr contour can be estimated from

$$Y_B(1) = \frac{Y_B(v_w) \log I_\gamma}{\log I_\gamma / I_B} \tag{5.43}$$

where I_γ and I_B are the intensities at X_γ and X_B ($y = 0$) for a given value of v_w.

5.3.7 Areas and Fraction of Total Activity within Intensity Contours

With the simplified fallout scaling system and the stylized downwind intensity profile it is convenient to construct contours by using simple geometric forms which approximate to some degree the true shapes of the contours, and, within reasonable limits, account for the fraction of the activity produced that falls back to earth within their areas.

The assumed shape of the intensity contours for fallout from stem altitudes is a partial circle having its center at X_B and an elliptical contour about the intensity ridge whose major axis is down the length of the ridge and whose minor axis is crosswind. The center of the ellipse is at the intersection of the circle, centered about X_B with the major axis of the ellipse. Thus, the area within the 1 r/hr at 1 hr contour (15 mph wind speed) may be approximated by

$$SA(1) = 3.14(X_B - X_1)^2 + 1.571\, Y_\gamma(1)(X_4 - 2X_B + X_1) \tag{5.44}$$

This approximation gives an underestimate of the enclosed area because the ellipse is actually centered at a downwind distance of $X_B - X_1$; at that point the minor axis of the half-ellipse is tangent to the circle. The error in the area estimate is largest for the lower-valued contours and for the larger weapon yields. The maximum underestimate possible, for yields less than about 10MT, is 7 to 8 percent of the total area of the stem pattern contour, based on the assumed geometric shape; the true error involved is unknown.

For the stem-fallout pattern, the area within contours other than the 1 r/hr at 1 hr contour can be estimated from the following functions. These are derived from the definitions of the idealized three-dimensional intensity surface. The functions are:

$$SA(1) = 3.14\,(X_B - X')^2 + 1.57\, Y_\gamma\,(X + X' - 2X_B) \tag{5.45}$$

where

$$X' = X_B - (2.303/k_{I,B}) \log (I_{B,B}/I) \tag{5.46}$$

$$X = X_B + \frac{(X_A - X_B) \log (I_{B,B}/I)}{\log (I_{B,B}/I_A)} \tag{5.47}$$

$$Y_B = (2.303/k_B) \log (I_{B,B}/I) \tag{5.48}$$

and

$$2.303/k_B = Y_B^0/\log I_{B,B}^0 \tag{5.49}$$

where X' is the upwind distance between X_I and X_B, X is the downwind distance between X_B and X_A, and Y_B is the crosswind distance for the contour of intensity, I_I, for I values between I_I and $I_{B,B}$. The values of Y_B^0 and $I_{B,B}^0$ are those for a wind speed of 15 mph.

The shape of the 1 r/hr at 1 hr contour (15 mph wind speed) for fallout from cloud altitudes is described by the smooth join of two ellipses at X_B, Y_B and centered at the point X_0 on the pattern center line. The upwind half-ellipse for the 1 r/hr at 1 hr contour (15 mph wind speed) has a major axis of Y_B and a minor axis of $X_0 - X_B$; the downwind half-ellipse has a major axis of $X_0 - X_A$ and a minor axis of Y_B. Thus the area within this contour can be estimated from

$$CA(1) = 1.57\ Y_B(1)\ (X_0 - X_B)\ , \tag{5.50}$$

For other contours, the areas can be estimated from

$$CA(I) = 1.57\ Y\ (X - X') \tag{5.51}$$

where

$$Y = \frac{Y_B \log (I_\gamma/I)}{\log (I_\gamma/I_B)} \tag{5.52}$$

$$X = X_\gamma + \frac{(X_0 - X_\gamma) \log (I_\gamma/I)}{\log (I_\gamma/I_B)} \tag{5.53}$$

and

$$X' = X_A + \frac{(X_0 - X_A)\log(I/I_0)}{\log(I_0/I_A)}, \quad I \le I_0, \tag{5.54}$$

or

$$X' = X_B + \frac{(X_T - X_0)\log(I/I_0)}{\log(I_T/I_0)}, \quad I_0 \le I \le I_T \tag{5.55}$$

In the above equations, X is the distance to the intensity I farther downwind than X_T, X' is the downwind distance between X_A and X_T, and Y is the cross-wind distance. The variation of the distance Y with intensity is calculated from the assumption that log I decreases linearly with the distance between the points $(X_T,0)$ and (X_B,Y_B), and I is I_T and I_B, respectively, at the two locations. The total area within some of the lower-valued contours for the combined fallout from both stem and cloud altitudes is less than the sum of SA(I) and CA(I) when the two overlap. The joint center of the ellipses moves from X_B toward X_T as I is increased from I_B. For wind speeds other than 15 mph, I_A and I_B (at X_A and X_B) are not 1 r/hr at 1 hr.

The activity produced by a detonation is about 1.4×10^{23} fW fissions where W is the total yield in KT and f is the ratio of fission to total yield. Some fraction of this total activity is contained within the fallout pattern. If the activity in a pattern is summed over the fallout area from the central high intensities down to a stated low-valued intensity contour enclosing the largest area, the fraction accounted for increases with yield. An ionization rate or intensity sum of a fallout pattern made in this way does not account for the activity deposited on the ground at lower intensities than the selected "lowest" contour, nor does it account for the fraction carried away on very small particles as world-wide fallout. The sum or integration of the activity over the fallout area can be used, however, to determine the fraction of the activity that is accounted for, in the fallout pattern, out to a stated low-level contour.

This fraction is defined by

$$C(1)\overline{K(1)}\,1.4\times10^{23}\,fW = \int_0^{A_n} I_A(1)\,da \tag{5.56}$$

in which C(1) is the true fraction of the number of fissions accounted for, and K(1) is the average value of the ratio of r/hr at 1 hr to the number of fissions per unit area for all the activity within the area, A_n. The average or accumulated fractionation number, for the radioactive elements accounted for, may be

defined through $\overline{K(1)}$ by

$$\overline{K(1)} = \overline{Dq}\left[\overline{r(1)}k_{\beta}^{n}(1) + k_{\gamma}^{n}(1)\right] \tag{5.57}$$

When the standard values of D, q, $k_{\beta}^{n}(1)$ and $k_{\gamma}^{n}(1)$, from Eq. 5.1 are substituted, the activity integral is

$$\int_{a}^{\infty} I_{a}(1)\,da = 5.46\times10^{10}\left[\overline{r(1)} + 0.19\right]\,C(1)BW \tag{5.58}$$

For observed fallout patterns, the integration is carried out by replacing the integral with a sum, such as

$$\int_{a}^{\infty} I_{a}(1)\,da = \Sigma_{j} I_{j}\,\Delta a_{j} \tag{5.59}$$

where $\overline{r}_{j}$ is determined from

$$\overline{r}_{j} = \frac{I_{j} - I_{j+1}}{2.303\log I_{j}/I_{j+1}} \tag{5.60}$$

in which the designation j is for the successive decreasing values of $I_{a}(1)$ used in carrying out the summation, and Δa_{j} is the area between the contours I_{j} and I_{j+1}. This particular value of $\overline{r}_{j}$ results from the semilogarithmic approximation of the variation with distance of the intensity profile.

The activity integrals over the fallout areas obtained from the scaling system can be carried out, using the assumed shapes of the contours for the patterns from the stem and cloud fallout. The activity integral for the stem fallout pattern, designated A_{s}, for the sum out to I_{4}, can be estimated from

$$A_{s} = I_{s,s}\left\{\frac{6.28}{k_{\beta,s}^{2}} + \frac{1.57}{k_{0}}\left[\frac{2(X_{4} - X_{3})}{2.303\log(I_{s,s}/I_{4})} + X_{3} - X_{s} - \frac{2}{k_{1,s}}\right]\right\} \tag{5.61}$$

for the case where $I_{s,s} \gg I_{4}$.

The activity integral for the cloud fallout pattern, designated A_c, can be estimated from

$$A_c = \frac{1.364\,Y_8}{\log I_7}\left\{\frac{(X_6 - X_7)}{\log(I_7/I_6)} + \frac{(X_7 - X_8)}{\log(I_7/I_8)}\right\} * \left\{0.434(I_7 - I_8) - I_8 \log (I_7/I_8)\right\}$$

$$+ \frac{0.6822\,Y_8 I_8}{\log I_7}\left\{\frac{(X_6 - X_7)}{\log(I_7/I_6)}\left[2\log (I_7/I_8) + 0.868\right]\right. \qquad (5.62)$$

$$\left. + \frac{(X_6 - X_8)}{\log (I_6/I_8)}\left[\log (I_7/I_6) - \log (I_6/I_8) + 0.868\right] + X_7 - X_8\right\}$$

for the case where $I_8 >> I_9$.

The dependence of Y_8 on wind speed is determined from these equations by computing the values of the various distances and intensities at several weapon yields and wind speeds and then solving for Y_8 by keeping the sum of A_8 and A_c constant for a given weapon yield. This procedure keeps constant, at least approximately, the fraction of the total activity that is carried by particle groups of a given minimum size. The integration is carried out to the low intensities, I_4 and I_8, whose dependence on wind speed is the same, so that the limit of integration is, in fact, changed with wind speed. The lower intensity limit used is the 1 r/hr at 1 hr for a wind speed of 15 mph; this defines the particle groups that are involved in the integrals for other wind speeds.

5.4 Summary of Derived Idealized Fallout Pattern Scaling Functions

The scaling functions given below contain constants evaluated from observed fallout pattern data. The number subscripts correspond to the notations given in Figure 5.1 on the descriptive plot of the standard intensity profile for the line directly downwind from ground zero. The functions apply to an effective wind speed of 15 mph and for a surface burst of 100 percent fission yield. All distances are in feet; all intensities are in r/hr at 1 hr; and the yield is in KT.

The scaling functions for the α values are:

$$\log \alpha_{8,8} = -0.509 + 0.076 \log W \quad , \quad W = 1 \text{ to } 10^5 \text{ KT}$$
$$\log \alpha_4 = 0.270 + 0.080 \log W \quad , \quad W = 1 \text{ to } 10^5 \text{ KT}$$
$$\log \alpha_8 = -0.170 + 0.022 \log W \quad , \quad W = 1 \text{ to } 10^5 \text{ KT}$$

$$\log \sigma_R' = -0.054 + 0.006 \log W \quad , \quad W = 1 \text{ to } 10^8 \text{KT}$$
$$\log \sigma_0 = 0.030 + 0.090 \log W \quad , \quad W = 1 \text{ to } 10^8 \text{KT}$$
$$\log \sigma_7 = 0.043 + 0.141 \log W \quad , \quad W = 1 \text{ to } 10^8 \text{KT}$$
$$\log \sigma_8 = 0.185 + 0.151 \log W \quad , \quad W = 1 \text{ to } 10^8 \text{KT}$$
$$\log \sigma_9 = 1.071 - 0.124 \log W \quad , \quad W = 1 \text{ to } 28 \text{ KT}$$
$$\log \sigma_9 = 0.080 + 0.140 \log W \quad , \quad W = 28 \text{ to } 10^8 \text{KT}$$

The scaling functions for the distances are:

$$\log(-X_1) = 0.398 + 0.400 \log W \quad , \quad W = 1 \text{ to } 28\text{-KT}$$
$$= 0.504 + 0.310 \log W \quad , \quad W = 28 \text{ to } 10^8\text{-KT}$$
$$X_2 = \sigma_{2,3} z_R - a_R$$
$$X_3 = \sigma_{2,3} z_R + a_R$$

$$X_4 = \frac{\sigma_4(\sigma_4 z_0 - 1000)}{\sigma_4 + 0.020}$$

where

$$\log a_R = 2.880 + 0.048 \log W \quad , \quad W = 1 \text{ to } 10^8\text{-KT}$$

$$z_R = \frac{2.303(\log a_R - \log a_0)}{k_R}$$

$$\log a_0 = \log a - (h \log a/R_a)/(h - R_a)$$
$$\log a = 3.380 + 0.481 \log W \quad , \quad W = 1 \text{ to } 10^8\text{-KT}$$
$$\log h = 3.820 + 0.445 \log W \quad , \quad W = 1 \text{ to } 28\text{-KT}$$
$$\log h = 4.226 + 0.104 \log W \quad , \quad W = 28 \text{ to } 10^8\text{-KT}$$
$$\log a/R_a = 1.070 + 0.098 \log W \quad , \quad W = 1 \text{ to } 10^8\text{-KT}$$
$$\log R_a = 2.810 + 0.383 \log W \quad , \quad W = 1 \text{ to } 10^8\text{-KT}$$
$$k_R = (\log a/R_a)/(h - R_a)$$

and

$$z_0 = \frac{1000 + (\sigma_{2,3} + 0.020) z_R}{\sigma_{2,3}} \quad , \quad W \geq 0\text{-KT} \quad , \quad v_w = 15 \text{ mph}$$

or

$$z_0 = (h - b) \quad , \quad W \geq 0\text{-KT}$$

For z or z_0 greater than 50,000 feet, the constants 1000 and 0.020 are 1100 and 0.035, respectively. The parameters a_R, z_R, and z_0 are assumed to be independent of the wind speed.

$$\log X_0 = 3.044 + 0.467 \log W, \quad W = 1 \text{ to } 28\text{KT}, \quad \sigma_0 \approx \text{n/h}$$
$$= 4.049 + 0.180 \log W, \quad W = 28 \text{ to } 10^5\text{KT}, \quad \sigma_0 \approx \text{n/h}$$

$$X_8 = 5.88\times10^1 W^{0.540} - 1.24\times10^1 W^{0.305} \sqrt{1 + 0.303\, W^{0.305}}, \quad W = 1 \text{ to } 28 \text{ KT}, \quad \sigma'_8 \approx \text{n/h}$$

$$X_8 = 1.464\times10^1 W^{0.250} - 1.24\times10^1 W^{0.305} \sqrt{1 + 0.303\, W^{0.305}}, \quad W = 28 \text{ to } 10^5\text{KT}, \quad \sigma'_8 \approx \text{n/h}$$

$$\log X_6 = 3.850 + 0.481 \log W, \quad W = 1 \text{ to } 28\text{KT}$$
$$= 4.255 + 0.200 \log W, \quad W = 28 \text{ to } 10^5\text{KT}$$

$$\log X_7 = 3.802 + 0.586 \log W, \quad W = 1 \text{ to } 28\text{KT}$$
$$= 4.268 + 0.305 \log W, \quad W = 28 \text{ to } 10^5\text{KT}$$

$$\log X_8 = 4.005 + 0.506 \log W, \quad W = 1 \text{ to } 28\text{KT}$$
$$= 4.410 + 0.315 \log W, \quad W = 28 \text{ to } 10^5\text{KT}$$

$$\log X_9 = 5.190 + 0.319 \log W, \quad W = 1 \text{ to } 28\text{KT}$$
$$= 5.202 + 0.311 \log W, \quad W = 28 \text{ to } 10^5\text{KT}$$

$$\log Y_8 = 3.228 + 0.400 \log W, \quad W = 1 \text{ to } 10^5\text{KT}$$

Values of Y_8 for yields other than those given can be obtained from a plot of the listed values against yield.*

The scaling functions for the high intensity ridge near ground zero, the intensities at the shoulder in the cloud pattern, and the intensities of the downwind pattern features, are:

$$\log I_{y-1} = k_{1,8}(X_8 - X_1)/2.303$$

where

$$\log k_{1,8} = 2.503 - 0.404 \log W, \quad W = 1 \text{ to } 28\text{-KT}$$
$$= 2.600 - 0.337 \log W, \quad W = 28 \text{ to } 10^5\text{-KT}$$

* See Tables 5.2 above and 5.3 below.

or

$$\log I_{n,s} = \log k_{n,s}(1)\bar{A}_f + \log \Delta r_{n,s}$$

and

$$\log I_i = \log k_i(1)\bar{A}_f + \log \Delta r_i$$

where

$$\log \Delta r_{n,s} = \log \Delta r^0_{n,s} + n \log v_w \quad \text{(see Table 5.1)}$$

and

$$\log \Delta r_i = 3.230 + 0.046 \log W - \log v_w \;, \quad W = 10^3 \text{ to } 10^9$$

also,

$$\log K_{n,s}\bar{A}_f = 2.088 - 0.402 \log W \;, \quad W = 10^3 \text{ to } 10^9 KT$$
$$\log K_i\bar{A}_f = 3.050 - 0.046 \log W \;, \quad W = 10^3 \text{ to } 10^9 KT$$

For $i = 5$ through 9:

$$I_i = 4.606n\, K_i\bar{A}_f \log \phi_i \;, \quad \alpha_i \geq n/h$$
$$= 4.606n\, K_i'\bar{A}_f \log \phi_i' \;, \quad \alpha_i < n/h$$

where

$$\log n/h = -0.481 - 0.014 \log W \;, \quad W = 1 \text{ to } 28KT$$
$$= -0.887 + 0.267 \log W \;, \quad W = 28 \text{ to } 10^9 KT$$

and

$$\phi_i = \frac{(\alpha_i + n/h) + \sqrt{(n/h)^2 + (\alpha_i + n/h)^2}}{(\alpha_i - n/h) + \sqrt{(n/h)^2 + (\alpha_i - n/h)^2}} \;, \quad \alpha_i \geq n/h$$

$$\phi_i' = \frac{(\alpha_i + n/h) + \sqrt{(n/h)^2 + (\alpha_i + n/h)^2}}{\alpha_{n,s} + \sqrt{(n/h)^2 + \alpha_{n,s}^2}} \;, \quad \alpha_i < n/h$$

where

$$\log (n/h)^2 = 0.486 + 0.262 \log W$$
$$\log n = 3.389 + 0.481 \log W$$

and where

$$\log K_0\overline{A}_\alpha = -0.286 - 0.808 \log W \text{ , } W = 1 \text{ to } 28 \text{ Kt} \text{ , } \alpha_0 \geq \text{ n/h}$$
$$= -2.880 - 0.572 \log W \text{ , } W = 28 \text{ to } 10^5 \text{KT, } \alpha_0 \geq \text{ n/h}$$

$$\log K_0'\overline{A}_\alpha = -0.185 - 0.406 \log W \text{ , } W = 28 \text{ to } 10^5 \text{Kt, } \alpha_0' < \text{ n/h}$$

$$\log K_0\overline{A}_\alpha = -1.134 - 0.074 \log W \text{ , } W = 1 \text{ to } 10^5 \text{KT, } \alpha_0 \geq \text{ n/h}$$
$$\log K_0'\overline{A}_\alpha = -1.225 - 0.022 \log W \text{ , } W = 1 \text{ to } 10^5 \text{KT, } \alpha_0' < \text{ n/h}$$

$$\log K_7\overline{A}_\alpha = -0.969 - 0.037 \log W \text{ , } W = 1 \text{ to } 10^5 \text{KT, } \alpha_7 \geq \text{ n/h}$$
$$\log K_7'\overline{A}_\alpha = -1.079 - 0.020 \log W \text{ , } W = 1 \text{ to } 10^5 \text{KT, } \alpha_7' < \text{ n/h}$$

$$\log K_0\overline{A}_\alpha = -2.166 - 0.552 \log W \text{ , } W = 1 \text{ to } 10^5 \text{KT, } \alpha_0' \geq \text{ n/h}$$

The values of the fallout pattern features from the above scaling functions are given in Table 5.3 for several weapon yields.

The scaling functions for α_1 and $K_1(1)A_\alpha$ derived from the scaling system suggest that (1) the distribution of the activity in the different particle-size groups tends to broaden with yield, and (2) the distribution shifts to smaller particle sizes with increasing weapon yield. Because the highest intensities are near X_7, the particle-size groups having the highest value of A_α are those of the size group designated by α_7. None of the more complicated fallout models in use at the present time considers a change with yield in either the activity particle size or the activity fall-velocity distributions, as this result suggests.

The product $(\overline{r(1)} + 0.02)C(1)$ for the scaling system varies from about 0.4 to 0.8 between 1-KT and 10^5-KT (for integrations out to the 1 r/hr at 1 hr contour). These results indicate, at least for the larger yields where the fraction of the activity on the ground but outside the 1 r/hr at 1 hr contour is very small, that both the over-all fractionation and the fraction contributed to world-wide fallout decrease with increasing yield. These indications are in accord with (1) the shift of the activity particle size distribution mentioned above, and (2) the slower cooling of the fireball with yield. Both factors should contribute to a more complete scavenging of the vaporized fission products by soil particles. For comparison with similar values in PNW and other publications, the values of $C(1)\overline{K}(1)$ in terms of r/hr at 1 hr per KT/sq mi for the six selected yields, 1 to 10^5-KT, are 850, 1140, 1290, 1380, 1480, and 1560, respectively.

Table 5.3

SUMMARY OF FALLOUT PATTERN FEATURES AND FALLOUT SCALING SYSTEM PARAMETER VALUES FOR AN ASSUMED EFFECTIVE WIND SPEED OF 15 MPH[a]

Pattern Feature or Parameter	Weapon Yield					
	1KT	10KT	100KT	1MT	10MT	100MT
X_1	-2,030	-6,370	-15,900	-33,100	-69,200	-144,000
X_2	306	1,750	3,750	4,150	3,360	3,520
X_3	1,860	5,120	11,300	21,300	40,300	79,600
X_4	7,730	32,600	60,200	97,100	162,000	252,000
X_5	4,300	13,000	26,400	37,000	23,300	-76,100
X_6	7,600	21,400	45,300	71,600	114,000	190,000
X_7	7,290	28,900	75,500	152,000	306,000	621,000
X_8	10,100	39,500	130,000	236,000	468,000	915,000
X_9	155,000	323,000	667,000	1,360,000	2,790,000	5,719,000
Y_5	1,670	4,200	10,500	25,500	56,700	167,000
Y_8	6,600	12,200	43,200	167,000	342,000	634,000
$I_{2,3}$	1,730	22,900	35,300	9,500	3,550	1,440
I_6	130	212	585	1,730	5,350	15,500
I_7	180	317	883	2,712	9,670	30,530
z_a	5,200	14,900	22,300	28,900	39,000	74,900
k(1)=0.02C(1)	0.43	0.58	0.63	0.68	0.73	0.79
[b]C(1)	1.95×10^{-13}	2.17×10^{-13}	2.45×10^{-13}	2.64×10^{-13}	2.84×10^{-13}	3.19×10^{-13}

a. Distances are in feet. Intensities are in r/hr at 1 hr (observed).
b. In r/hr at 1 hr per kiloton/sq ft.

5.5 Illustrative Computations for the Use of the Simplified Fallout Scaling System

5.5.1 Construction of Idealized Fallout Patterns

The use of the scaling functions and of the simplified fallout scaling system is illustrated in this section by some calculations for a 1-MT yield surface detonation. The first step in constructing the idealized contours is to plot (or compute) the intensity profiles along the center line of the pattern as log I (1) against distance. The second step is to compute or read off the distances from surface zero to a pre-selected set of contour values. The third step is to plot or compute the semilogarithmic line from $(I_{g,s}, 0)$ to $(1, Y_s)$ for the lateral locations of the contours for the stem fallout (see Eqs. 5.46 to 5.49).

The fourth step is to construct the stem-fallout pattern by marking on a rectangular grid the noted distances to each contour along the line $y = 0$. The "ground-zero" circular portion of the pattern is then drawn in, by first drawing the appropriate circles centered at X_s and then closing them to the lateral distances taken from the $I_{g,s}$-Y_s plot. At this point, the contours are drawn parallel to the X-axis and closed (with an elliptical shape) if a common point occurs on the X-axis. The remainder are extended to about the distance to the lowest-valued closed contour.

The fifth step is to draw or compute the semilogarithmic line from $(I_{g}, 0)$ to $(1, \sqrt{Y_s^2 + (X_s - X_g)^2})$ to determine the contour locations between $(X_t, 0)$ and (X_g, Y_g). If the distance between these two locations is designated D, and the distances from $(X_g, 0)$ to the selected contours are D', then the lateral distance to each one, Y, is determined from $D'Y_g/D$ or directly from Eq. 5.53. The corresponding downwind location, X_g, is $X_g + D'(X_s - X_g)/D$ or $X_g + (X_s - X_g)(Y/Y_g)$. These are the points through which the elliptical contours of the cloud fallout pass.

The farthest upwind locations at X', 0 are read from the intensity profile between X_s and X_g or computed from Eqs. 5.54 or 5.55. The upwind half-ellipse is given by the equation

$$\frac{(X_s - x)^2}{(X_s - X')^2} + \frac{y^2}{Y^2} = 1 \qquad (5.63)$$

The downwind half-ellipse is

$$\frac{(x - X_s)^2}{(X - X_s)^2} + \frac{y^2}{Y^2} = 1 \qquad (5.64)$$

in which X is the downwind distance to the contour between X_u and X_y (see Eq. 5.53). The various intensity-distance lines and profiles for the 1-MT yield are shown in Figure 5.2; the contours derived from them are shown in Figure 5.3, with the distances converted to statute miles.

The pattern of Figure 5.3 is in many respects quite different from those described in ENW. Table 5.4 gives a few comparisons of the two derivations for the 1-MT yield.

Table 5.4

COMPARISON OF FALLOUT PATTERN DATA FOR A 1-MT YIELD OBTAINED FROM THE SIMPLIFIED SCALING SYSTEM FUNCTIONS AND FROM THE ENW METHODS

	Distance in Miles[a]	
	Simplified System	ENW Method
Upwind Distance to 1 r/hr contour	6.2	17.4
Downwind Distance to 1000 r/hr contour	55	28
Downwind Distance to 100 r/hr contour	122	98
Downwind Distance to 10 r/hr contour	190	270
Maximum Half-Width, 1 r/hr contour	32	89

a. Wind speed of 15 mph.

The major pattern features not recognized in the ENW scaling method are the observed presence of the major downwind peak and the corresponding rapid broadening of the pattern in the region of this peak. Also, the huge ground-zero circle obtained by the ENW method does not agree with observations for yields greater than a few KT; these two scaling systems should give patterns most nearly alike for yields in the region of 1-KT. Comparisons of the fallout pattern features calculated from the simple scaling system presented here with those from other fallout models, are discussed further in Section 5.6.

Figure 5.2
INTENSITY-DISTANCE PLOTS FOR CONSTRUCTION OF AN IDEALIZED FALLOUT PATTERN FOR A 1-MT YIELD SURFACE DETONATION FOR A WIND SPEED OF 15 MPH

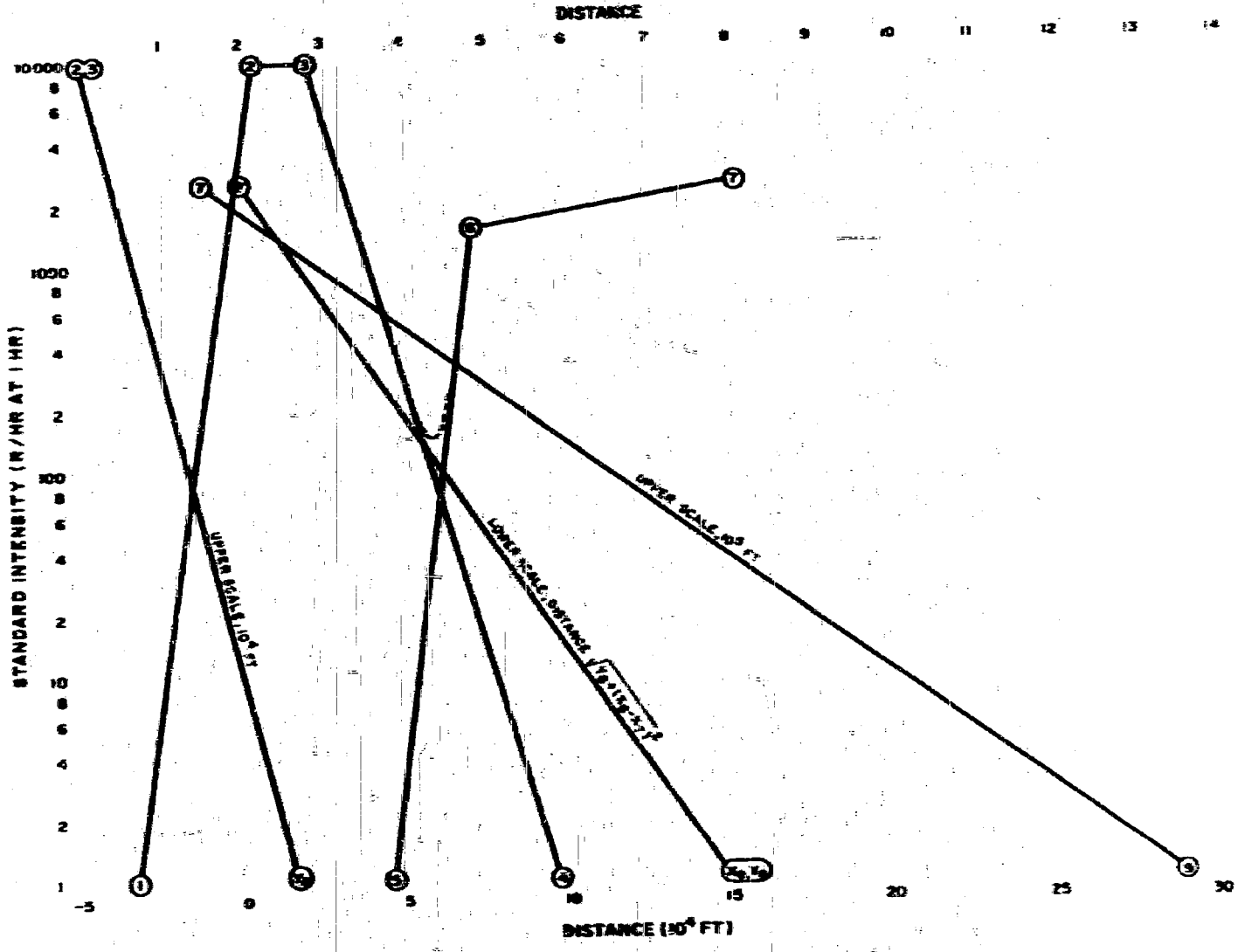

Figure 5.3
IDEALIZED FALLOUT PATTERN FOR A 1-MT YIELD SURFACE BURST FOR A WIND SPEED OF 15 MPH AND 100 PERCENT FISSION

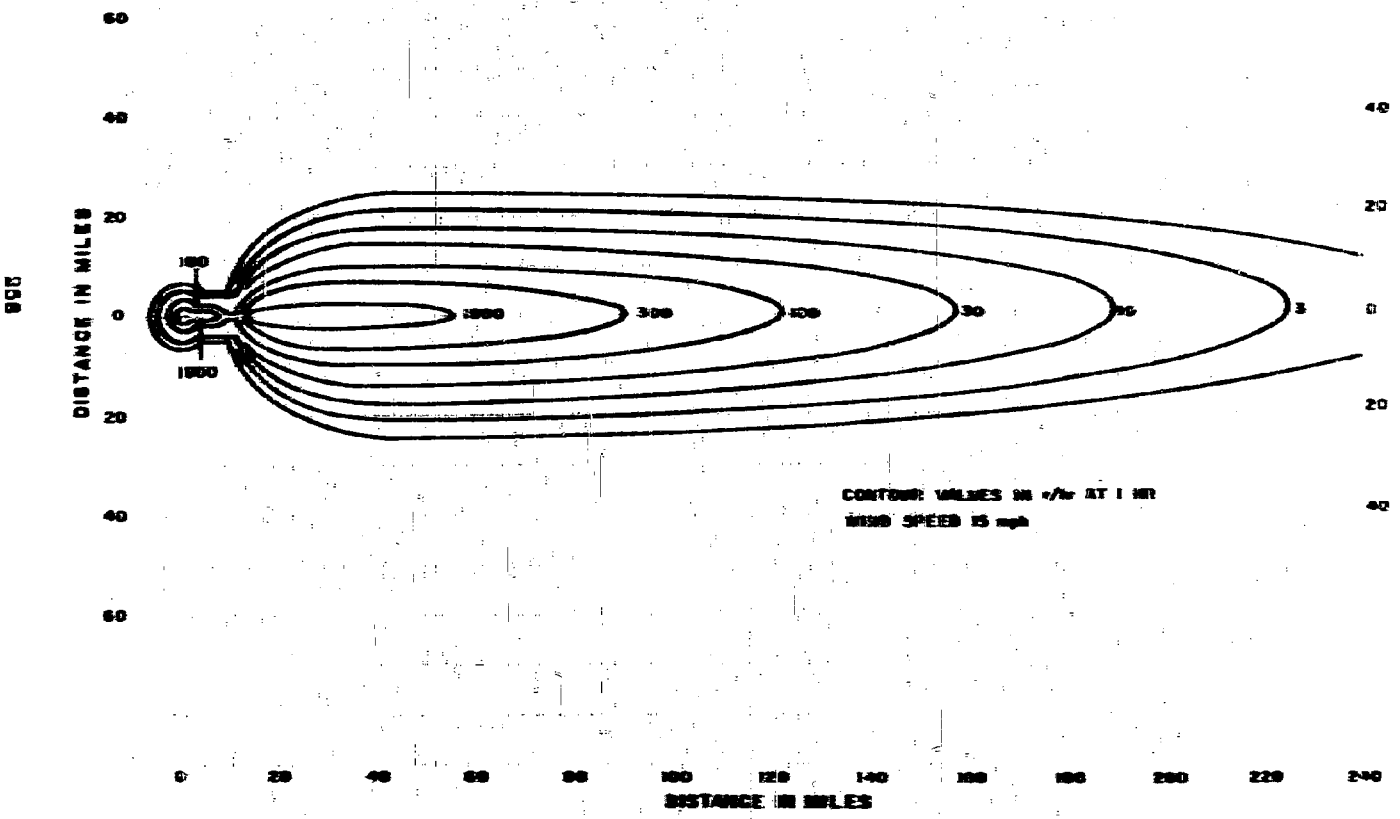

5.5.2 Fallout Arrival Rate and Exposure Dose during Fallout Arrival

The method of estimating the times, rates, and duration of fallout arrival, and the resulting exposure dose, is illustrated by calculations for the 1-MT yield. Two locations are selected, one at the downwind distance of 5.35×10^4 ft (8.8 miles) and the other at 1.87×10^5 ft (35.4 miles); both are on the center line of the idealized pattern. The standard intensity at both these locations is 2000 r/hr at 1 hr. At the shorter distance, essentially all the fallout comes from stem altitudes; at the greater distance it all arrives from cloud altitudes. Different methods are applicable to the two cases; the one for the fallout from cloud altitudes is described first.

To make these calculations, estimates of A_α as a function of α are required in order to evaluate the integral of $A_\alpha(\alpha)$ as indicated by Eqs. 4.8 to 4.11. From Eqs. 4.22, 4.66, and 4.75, the first estimate of A_α is given by

$$A_\alpha \approx \frac{6.17 \times 10^7 I_\alpha(1)}{\left[r_\alpha(1) + 0.019\right]} \quad . \tag{5.65}$$

However, since $r_\alpha(1)$ is not known, and since the term $(r_\alpha(1) + 0.019)$ will cancel out in adjusting the integral of $A_\alpha(\alpha)\,d\alpha$ to 2000 r/hr at 1 hr, it is convenient to replace the multiplier of $I_\alpha(1)$ with the constant, $1/K_0(1)$, so that

$$K_0(1) = 1.62 \times 10^{-8} \left[r_\alpha(1) + 0.019\right] \frac{\text{r/hr at 1 hr}}{\text{fission/sq ft}} \quad . \tag{5.66}$$

In the first estimate of the distribution of $K_0(1)A_\alpha$ with α, the α for a given value of $I_\alpha(1)$ is taken to be equal to $\bar{X}/h$. The distribution curve for $K_0(1)A_\alpha$ is shown in Figure 5.4.

The computations for α_{min}, α_{max}, h_0, h_1, t_0, $K_0(1)A_\alpha(\alpha)$, and $K_0(1)A_\alpha(\alpha)/\Delta t$ are summarized in Table 5.5. The values of $K_0(1)A_\alpha(\alpha)$ are plotted in Figure 5.5. The peak value is noted to occur at an α of about 3.1, which is less than the value of $\alpha_{\bar{x}} = 3.556$ for this distance. The integral under the curve is $K_0(1)A_\alpha = 6.36 \times 10^7$ r/hr at 1 hr-ft, and A_α is $3.93 \times 10^{12} / \left[r_\alpha(1) + 0.019\right]$ fissions/sq ft.

The calculated standard intensity, from

$$I_\alpha(1) = 3.90 \times 10^{-13} \left[r_\alpha(1) + 0.019\right] A_\alpha \tag{5.67}$$

Figure 5.4
FIRST ESTIMATE OF THE DEPENDENCE OF $K_\beta(\Omega)A_x$ ON x FOR A 1-MT SURFACE DETONATION AND WIND SPEED OF 15 MPH

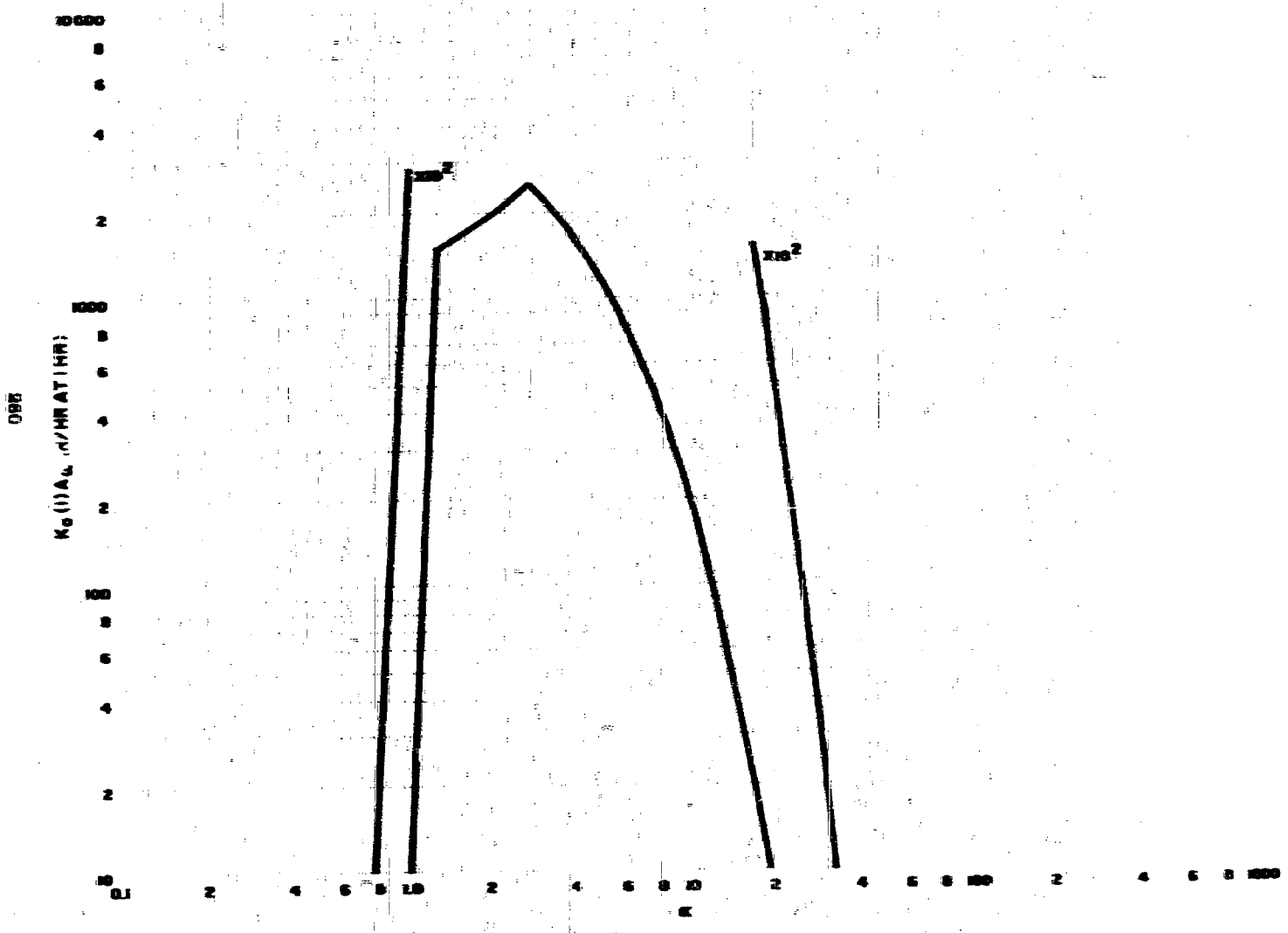

Table 5.5

CALCULATION OF FALLOUT ARRIVAL RATE AT X = 1.87×10^5 ft, y = 0
FROM A 1-MT SURFACE BURST FOR A WIND SPEED OF 15 MPH

n	h_2 (10^5 ft)	h_1 (10^5 ft)	t_a (hr)	t_c (hr)	Δt (hr)	$K_n(1)A_{n-1}(\sigma)$ (10^7 r/hr at 1 hr-ft)	$K_n(1)A_{n-1}(\sigma)/t$ (10^7 r/hr at 1 hr-ft/hr)
2.538	5.38	5.38	1.97	1.97	0	0	0
2.6	5.36	6.12	1.89	2.14	0.25	1.79	6.80
2.8	4.99	6.39	1.90	2.36	0.46	3.16	6.87
3.0	4.77	6.32	1.94	2.53	0.59	3.62	6.17
3.2	4.60	6.28	1.99	2.67	0.68	3.83	5.63
3.4	4.46	6.19	2.05	2.79	0.74	3.68	4.97
3.6	4.35	6.06	2.11	2.89	0.78	3.40	4.36
3.8	4.25	5.91	2.18	2.97	0.79	3.06	3.78
4.0	4.18	5.74	2.25	3.03	0.78	2.70	3.46
4.2	4.14	5.55	2.33	3.07	0.74	2.28	3.08
4.4	4.11	5.34	2.42	3.10	0.68	1.86	2.73
4.6	4.10	5.10	2.51	3.10	0.59	1.42	2.41
4.8	4.11	4.84	2.61	3.06	0.42	0.957	2.28
4.986	4.27	4.27	2.99	2.99	0	0	0

---

a = 4.52×10^5 ft

b = 1.11×10^5 ft

h = 5.22×10^5 ft

$I_n(1)$ = 2000 r/hr at 1 hr

t_a and t_c = time of fall plus 0.13 hr. (8 min.)

Figure 5.5
VARIATION OF $K_0(1)A_x(\alpha)$ WITH α AT $x = 1.87 \times 10^5$ FT FOR W = 10^3 KT
AND A WIND SPEED OF 15 MPH

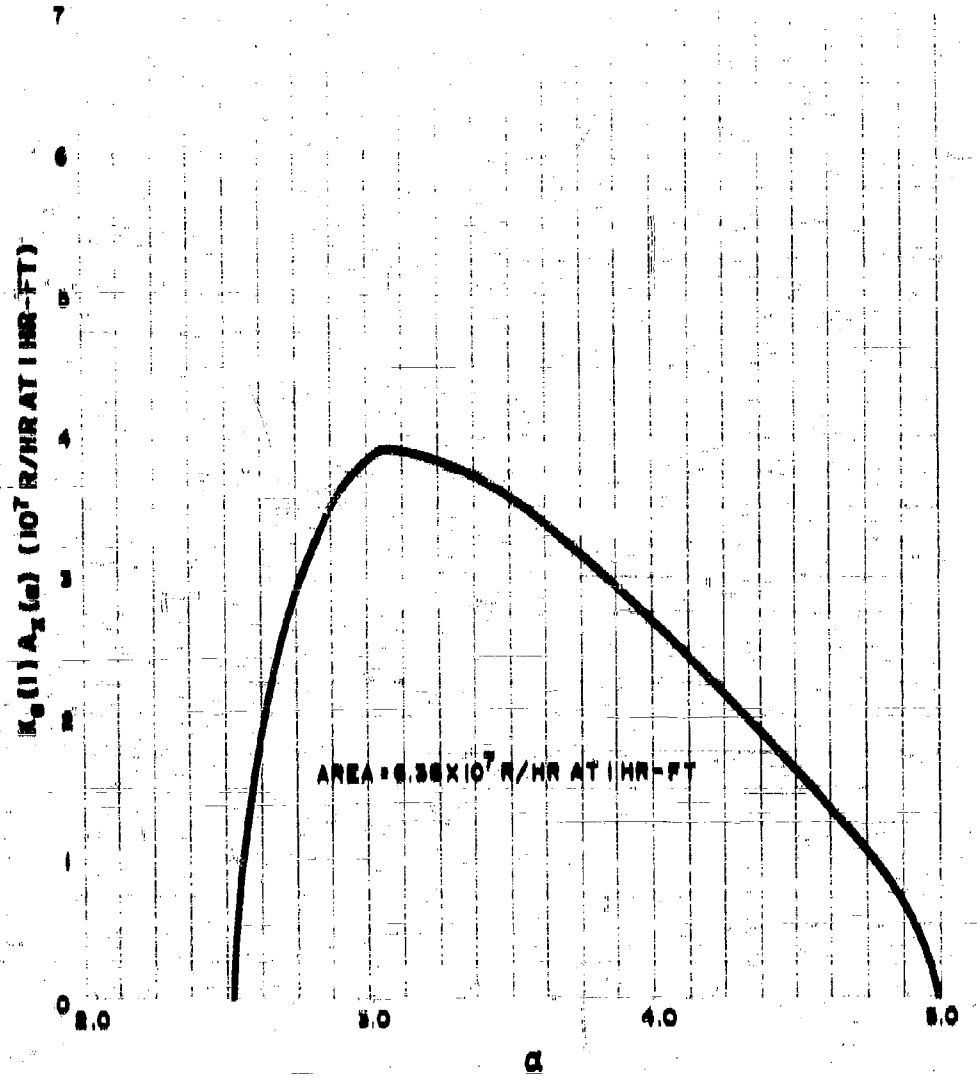

is 1530 r/hr at 1 hr. This value is about 76 percent of the pattern value, 2000 r/hr at 1 hr. In order to make the calculation more exact, the distribution curve of $K_n(1)A_\alpha$ should be increased about 31 percent for α values between 2.5 and 5.0. However, since similar calculations at several additional locations would be required to make a complete second estimate of $K_n(1)A_\alpha$ and since these have not yet been done, no correction is made in $K_n(1)A_\alpha$ for this illustration. Instead, the correction was applied as a single multiplier to the final values of $I_n(1)$.

The times of fallout arrival, t_a, and of cessation, t_c, were increased by 0.13 hour (8 minutes) to account for the time of cloud formation. The time of arrival intervals, shown in Figure 5.6 as a function of α, form a closed loop; this curve is used to provide the range of α groups that are landing at any given time. The rate of arrival of the radioactivity carried by each α group in Figure 5.7 shows the highest rate of accumulation for the larger particles (those having the lower α values).

The activity arriving at any given time is the sum of that being deposited by all the α groups that are landing. The indicated summation is shown in part of Table 5.6. First, the sum under the curve of Figure 5.7 was obtained by summing the areas of rectangles. This was done by reading the midpoints of each 0.05 increment of α and accumulating 0.05 times the values directly on an adding machine. The α ranges for selected values of the time were taken from Figure 5.6 and the differences in the summation to the respective values of α_{max} and α_{min} arriving at each time were then calculated by direct interpolation of the summation.

The total rate of arrival shown in Figure 5.8 reaches its maximum at about 2.3 hours after detonation. The summation of the activity under this curve is 5.51×10^7 r/hr at 1 hr-ft, which is in agreement with the summation of $K_n(1)A_n(\alpha)$. The $I_n(1)$ values were obtained by adjusting the total to 2000 r/hr at 1 hr and adjusting all the other values by the same factor. The decay correction factors, d(t,1), were calculated from the data of Figure 11.2 (see Volume II, Chapter 11), which includes the contributions of about 0.8 atoms of U-239 produced at zero time for each fission event. The product, $I_n(1)d(t,1)$, is the value of $I_n(t)$ at each time after fission.

The maximum observed intensity indicated is 433 r/hr, occurring at 8 hours after detonation. The shape of the intensity-time curve is shown in Figure 5.9. The exposure dose, D_{en}, is the summation under this curve times 1.33; this factor corrects for the instrument response contained in the values of $I_n(t)$.

The dose accumulation (true air ionization) over terrain such as existed at the test sites is 444 roentgens up to time of cessation (3.11 hours).

Table 5.6

SUMMATION OF ARRIVAL RATES FOR α GROUPS ARRIVING AT THE SAME TIME AND ACCUMULATION OF ACTIVITY AND EXPOSURE DOSE DURING THE FALLOUT PERIOD

α	$0.05\Sigma K_\alpha(1)A_\alpha(\alpha)/\Delta t$ (10^7 r/hr at 1 hr-ft/hr)	t (hr)	α Range	$\alpha=\alpha_{max}$ Σ $\alpha=2.5$	$\alpha=c_{min}$ Σ $\alpha=2.5$	$K_\alpha(1)A_\alpha/\Delta t$ (10^7 r/hr at 1 hr-ft/hr)
				(10^7 r/hr at 1 hr-ft/hr)		
2.5	0.0	1.88	–	–	–	0.0
	0.175	1.9	2.56-2.80	1.884	0.242	1.642
2.6	0.508	2.0	2.52-3.22	4.538	0.070	4.468
	0.848	2.1	2.55-3.55	6.188	0.175	6.013
2.7	1.194	2.2	2.63-3.83	7.344	0.712	6.632
	1.539	2.3	2.74-4.13	8.398	1.470	6.928
2.8	1.884	2.4	2.86-4.37	9.104	2.294	6.810
	2.226	2.5	2.97-4.58	9.651	3.031	6.620
2.9	2.566	2.6	3.12-4.73	10.004	3.966	6.038
	2.900	2.7	3.26-4.87	10.315	4.757	5.558
3.0	3.228	2.8	3.43-4.96	10.494	5.626	4.868
	3.543	2.9	3.63-5.00	10.532	6.536	3.996
3.1	3.848	3.0	3.88-4.93	10.442	7.530	2.912
	4.143	3.1	4.40-4.60	9.700	9.187	0.513
3.2	4.428	3.11	–	–	–	0.0
	4.704					
3.3	4.970					
	5.229					

Table 5.6 (continued)

α	$0.852K_\gamma(1)A_{ir}(\alpha)/\Delta t$ (10^7 r/hr at 1 hr-ft/hr)	t (hr)	$K_\gamma(1)A_{ir}$ (10^7 r/hr at 1 hr-ft)	$I_\gamma(1)$ (r/hr at 1 hr)	d (t, 1)	I_γ (t) (r/hr)	D_{ir}[a] (r)
3.4	5.400						
	5.723						
3.5	5.959	1.88	0.0	0.0	0.416	0.0	0.0
	6.188	1.9	0.016	5.1	0.497	2.1	0.03
3.6	6.408		0.144	46.	0.394	18	0.63
	6.622	2.0	0.338	107.	0.380	41	2.58
3.7	6.830		0.591	187.	0.365	68	6.23
	7.033	2.1	0.879	279.	0.353	98	11.58
3.8	7.229		1.192	378.	0.342	129	19.48
	7.420	2.2	1.518	481	0.330	159	29.23
3.9	7.604		1.854	587	0.321	188	40.93
	7.784	2.3	2.198	696	0.311	216	54.58
4.0	7.958		2.544	806	0.303	244	70.06
	8.128	2.4	2.886	915	0.294	269	87.23
4.1	8.294		3.226	1,022	0.285	291	105.83
	8.454	2.5	3.560	1,128	0.278	314	125.96
4.2	8.609		3.886	1,231	0.271	334	147.53
	8.760	2.6	4.196	1,330	0.264	351	170.28
4.3	8.906		4.492	1,423	0.257	365	194.13
	9.045	2.7	4.776	1,513	0.250	378	218.95
4.4	9.187		5.047	1,599	0.245	392	244.63
	9.321	2.8	5.301	1,680	0.239	401	271.08
4.5	9.451		5.536	1,754	0.233	409	298.13
	9.577	2.9	5.750	1,822	0.228	415	325.63

Table 5.6 (concluded)

	$0.052K_o(1)A_x(\sigma)/\Delta t$ (10^7 r/hr at 1 hr-ft/hr)	t (hr)	$K_o(1)A_x$ (10^7 r/hr at 1 hr-ft)	$I_x(1)$ (r/hr at 1 hr)	d (t, 1)	$I_x(t)$ (r/hr)	D_{ex}[a] (r)
4.6	9.700		5.939	1,882	0.224	422	353.48
	9.819	3.0	6.102	1,933	0.219	423	381.63
4.7	9.936		6.231	1,974	0.214	422	409.53
	10.050	3.1	6.309	1,999	0.211	421	438.63
4.8	10.162	3.11	6.312	2,000	0.210	420	443.65
	10.272	4.			0.155	310	
4.9	10.380	5.			0.125	250	
	10.484	6.			0.0990	198	
5.0	10.532	8.			0.0726	145	
		10.			0.0573	115	

a. Summation of I(t)x1.33

Figure 5.6
TIME OF ARRIVAL OF THE VARIOUS PARTICLE GROUPS DESIGNATED BY α
FOR A WIND SPEED OF 15 MPH

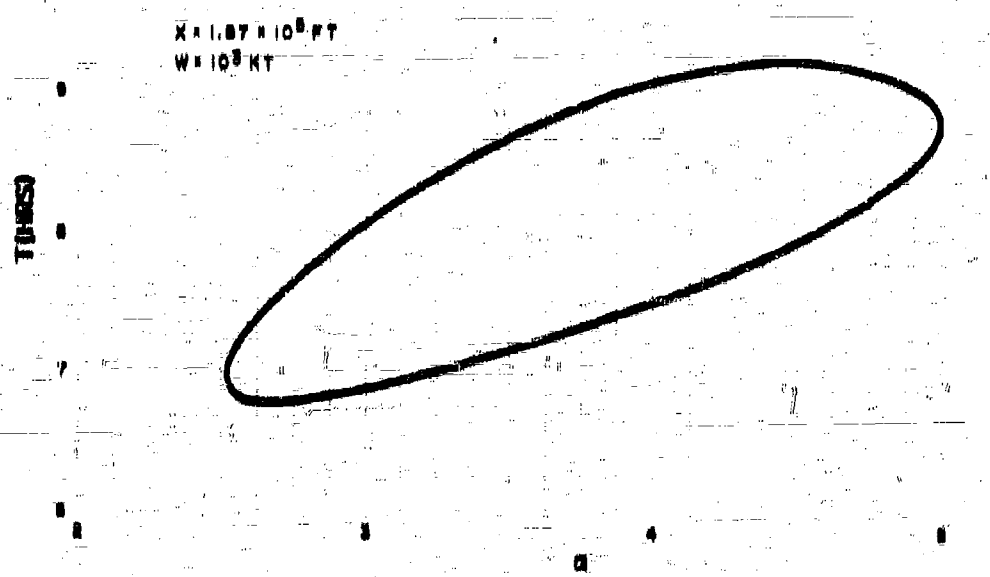

Figure 5.7
RATE OF ACTIVITY DEPOSITION ON THE GROUND AS A FUNCTION OF α AT $X = 1.87 \times 10^5$ FT, FOR $W = 10^3$ KT AND A WIND SPEED OF 15 MPH

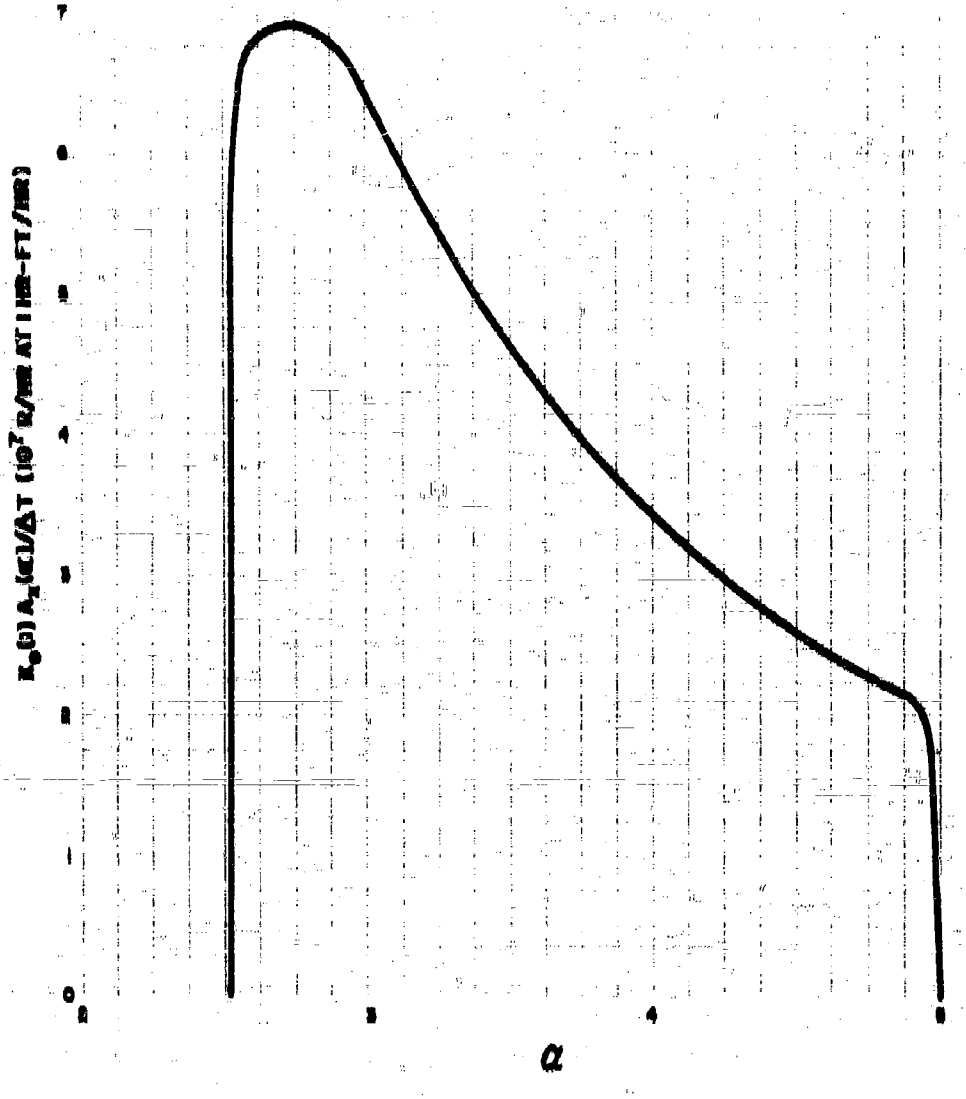

Figure 5.8
RATE OF FALLOUT ARRIVAL AS A FUNCTION OF TIME AFTER DETONATION AT
$X = 1.87 \times 10^5$ FT FOR $W = 10^3$ KT AND A WIND SPEED OF 15 MPH

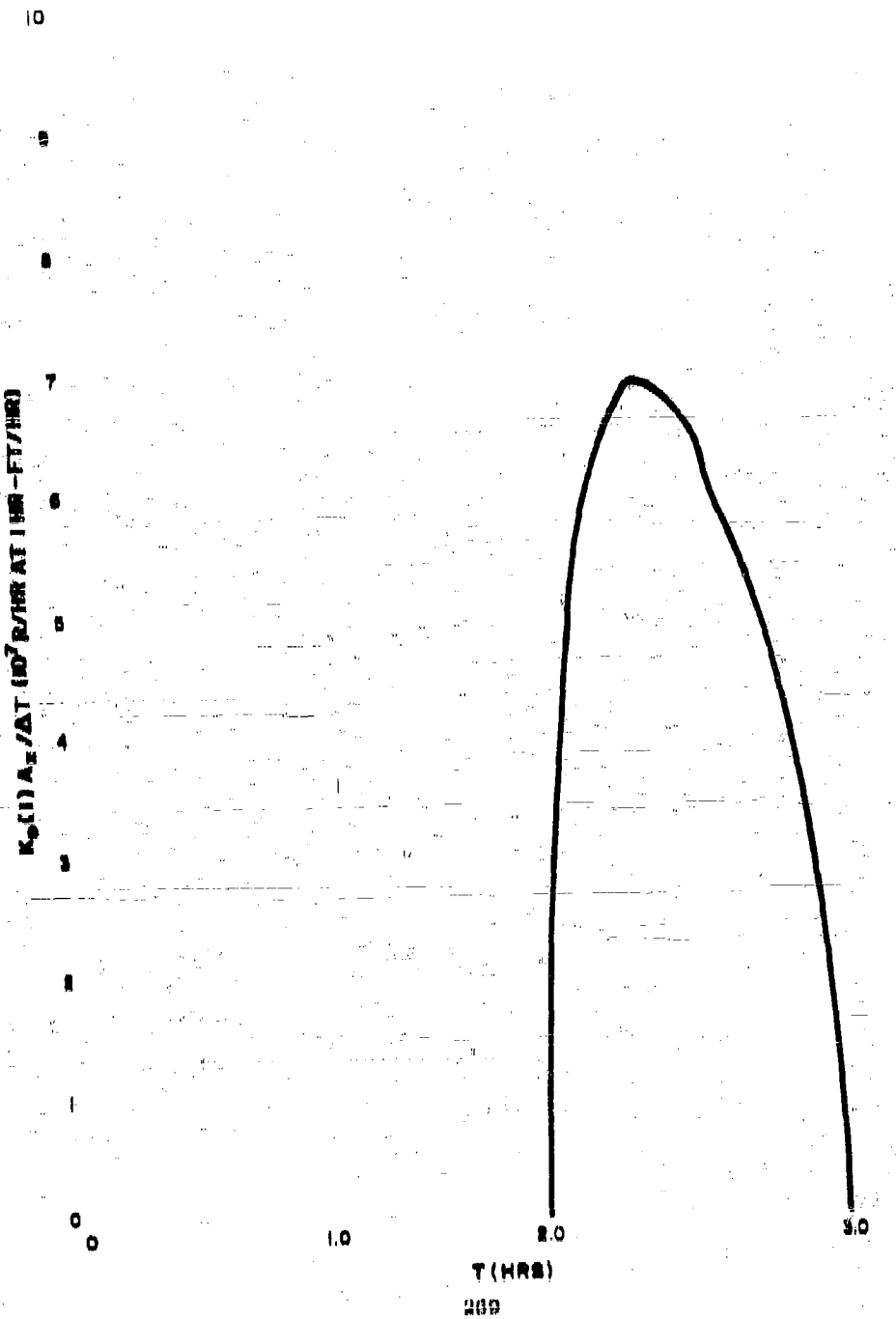

Figure 5.9
VARIATION OF IONIZATION RATE WITH TIME AFTER DETONATION AT X = 1.87 × 10^5 FT FOR W = 10^3 KT AND A WIND SPEED OF 15 MPH

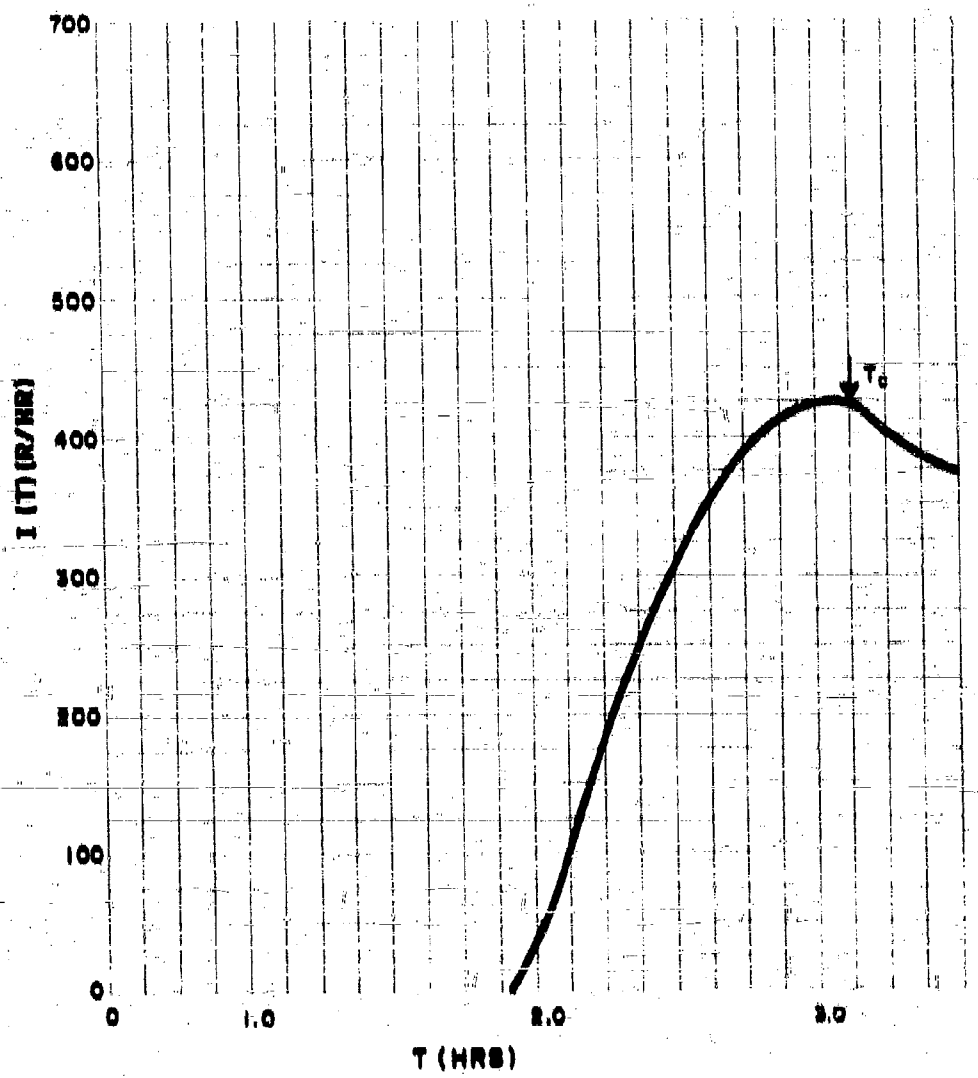

From the decay curve of Figure 11.2 (see Volume II, Chapter 11) the total exposure dose is 4540 roentgens at 48 hours, 6080 roentgens at 1 week, and 8470 roentgens at 2.3 years (this is the so-called infinity dose).

The contribution to the dose rate from airborne activity can be estimated if it is assumed that the fractionation effect on A_i cancels that in A_α. The dose rate from the airborne material should be proportional to the rate of deposition of the activity, so that if it is computed for one time the contribution at other times should be proportional to $K_\gamma(1)A_\gamma/\Delta t$. The time selected for the calculation was 2.3 hours, the time of maximum fallout deposition.

At this time the arriving particle groups have α values between 2.74 and 4.13 (see Table 5.6). From Figure 5.4, the integral, or summation of $K_\gamma(1)A_\alpha d\alpha$, between these α values is 2.92×10^{6} r/hr at 1 hr; increasing this by 31 percent to correspond to the adjusted deposit level gives 3.86×10^{6} r/hr at 1 hr (observed). If $(r_\gamma(1) + 0.019)$ is assumed to equal unity, and the value of $A_i E_i$ is taken as that for unfractionated fission products, then the integral of $A_\alpha d\alpha$ in Eq. 4.73 is 2.38×10^{11} fissions/cu ft, and $A_i E_i$ is 4.4×10^{-5} Mev/sec/fission. These values give a dose rate of 9.9 r/hr at 2.3 hours.

The contribution to the ionization rate at 3 feet above the surface from the deposited material at this time of 2.3 hours is 216 r/hr, giving a total ionization rate of 226 r/hr. The airborne contribution at 2.3 hours is, therefore, about 4 percent of the total ionization rate. However, at 1.9 hours, just as the fallout is beginning to deposit, the airborne ionization rate is about 2.4 r/hr or just over 50 percent of the total. It is seen from Table 5.6 that, at 2.3 hours, the summation of $K_\gamma(1)A_\gamma/\Delta t$ is slightly less than this value and, since the same summation would apply to the ionization rate from airborne material, the total exposure dose from this source would be less than 9.9 roentgens. This is about 2 percent of the total exposure dose. Therefore, at this selected location, the airborne material is not an important contributor to the total exposure dose.

The first step in making estimates of the arrival times of the various particle groups and the resulting dose rate from stem fallout is to compute the values of α_{min} and α_{max} at several downwind distances. The α values are plotted against distance and read off at selected distances as required to make the first estimate of the distribution of A'_α as a function of α. To make this estimate, Eq. 4.50 is used, in the form

$$K_\gamma(1)A'_\alpha = I_\gamma(1)/(\alpha_{max} - \alpha_{min}) \qquad (5.68)$$

where $K_\gamma(1)$ is assumed to be constant in lieu of information on the dependence of $r_\gamma(1)A'_\alpha$ on α. The average particle-size group at a given downwind distance, α, is calculated from $(\alpha_{min} + \alpha_{max})/2$.

The values of σ_{min} and σ_{max} at various downwind distances are most easily determined by calculating the values of R_x and σ for different values of x by use of Eqs. 4.31 and 4.48 and then from Eq. 4.32, computing the distance. These equations, for a 1-MT yield detonation, are

$$\log R_x = 3.261 + 2.72 \times 10^{-5} x, \tag{5.69}$$

$$\sigma = \frac{1900 + 0.020\, x}{28{,}900 - x}, \tag{5.70}$$

and

$$X = \sigma x + R_x . \tag{5.71}$$

The values of σ_{min} and σ_{max} obtained from these three equations are plotted in Figure 5.10. The computation of the first estimate of $K_x(1)A'_{\bar{\sigma}}$ as a function of $\bar{\sigma}$, which is shown in Table 5.7 and is plotted in Figure 5.11, was made by use of the $I_x(1)$ values of Figure 5.2. The odd shape of the distribution near its maximum is due to the assumption in the scaling system, that the top of the activity ridge is flat from X_β to X_α.

The time of fallout arrival and the distribution function of $K_x(1)A'_{\bar{\sigma}}$ should not be applied to distances less than R_x, which is about 2000 feet for the 1-MT yield; however, $K_x(1)A'_{\bar{\sigma}}$ should approach zero as σ or $\bar{\sigma}$ approaches zero. These distances will not be of much interest for estimating fallout arrival times, since R_x is approximately equal to the crater radius.

For the illustrative computation of the arrival rate of fallout from stem altitudes, the standard intensity of 2000 r/hr at 1 hr was again selected. For the stem fallout, this intensity occurs at $X = 3.30 \times 10^5$ feet, or 6.3 miles, and $y = 0$. The time of arrival of each particle group, selecting 15 mph for the wind speed, can be estimated from Eqs. 4.62 and 4.64. For the 1-MT yield, these arrival times are

$$t_x = 0.0581 \left[\log (\sigma + 0.020) + 1.182\right] \tag{5.72}$$

and

$$t_f = \frac{1.26 \times 10^{-5}\, \sigma (28{,}900\, \sigma - 1900)}{(\sigma + 0.020)} \tag{5.73}$$

for the time in hours. The group arrival time is the sum of t_x and t_f (neglecting the delay-time due to circulation in the fireball). From Figure 5.10, at the selected distance of 6.3 miles, σ_{min} is 0.80, and σ_{max} is 1.60. The arrival times for these groups and for particle groups with intermediate values of σ, the calculated activity sums, and the calculated ionization rates, are shown in Table 5.8.

Figure 5.10
VARIATION OF α_{max} AND α_{min} WITH DOWNWIND DISTANCE FOR A 1-MT YIELD SURFACE DETONATION AND WIND SPEED OF 15 MPH

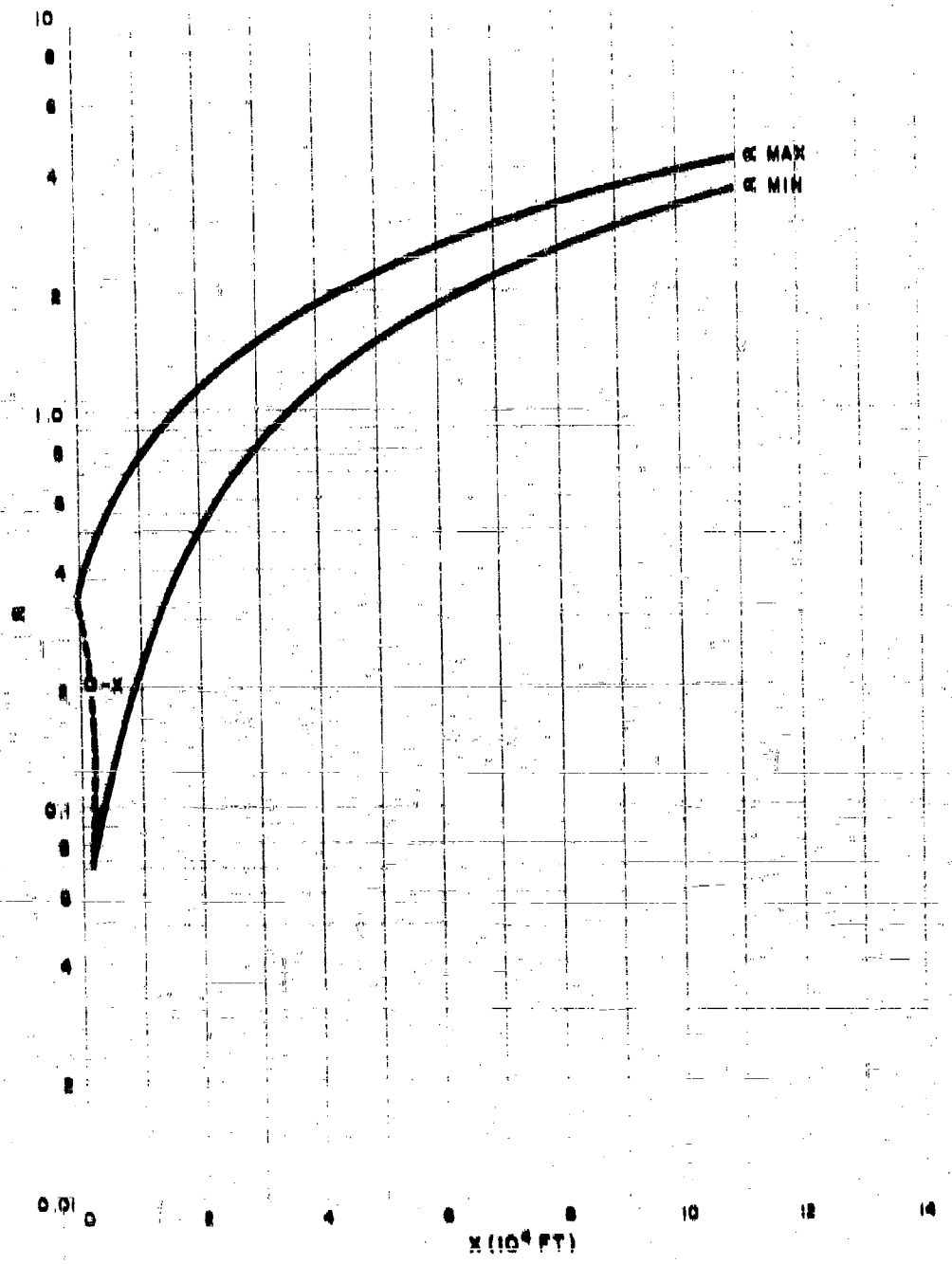

Table 5.7

FIRST ESTIMATE OF $K_\gamma(1)A_\sigma$ AS A FUNCTION OF σ FOR A 1-MT YIELD SURFACE DETONATION

X (10^4 ft)	σ_{max}	σ_{min}	$\Delta\sigma_m$	$I_\gamma(1)$ (r/hr at 1 hr)	$K_\gamma(1)A_\sigma$ (r/hr at 1 hr)	σ
0	0.32	0	0.32	3500	1.00×10^4	0.16
0.20	0.48	0.07	0.36	0000	1.01×10^4	0.25
0.455	0.53	0.11	0.42	9800	2.30×10^4	0.32
1.0	0.75	0.22	0.53	9800	1.86×10^4	0.48
2.0	1.10	0.40	0.61	9800	1.04×10^4	0.80
2.19	1.15	0.52	0.63	9800	1.59×10^4	0.84
2.5	1.20	0.64	0.65	9700	8.77×10^3	0.96
3.0	1.48	0.80	0.68	9100	4.05×10^3	1.14
4.0	1.84	1.13	0.71	940	1.52×10^3	1.48
5.0	2.19	1.47	0.72	285	390	1.83
6.0	2.53	1.80	0.73	85	116	2.16
7.0	2.90	2.17	0.73	25.5	35	2.54
8.0	3.28	2.51	0.72	7.7	10.7	2.87
9.0	3.56	2.85	0.71	2.30	3.28	3.20
9.7	3.79	3.08	0.71	1.0	1.41	3.44

Figure 5.11
FIRST ESTIMATE OF $K_2(1)A'$ AS A FUNCTION OF α FOR FALLOUT FROM STEM ALTITUDES FOR A 10^3 KT YIELD SURFACE BURST AND A WIND SPEED OF 15 MPH

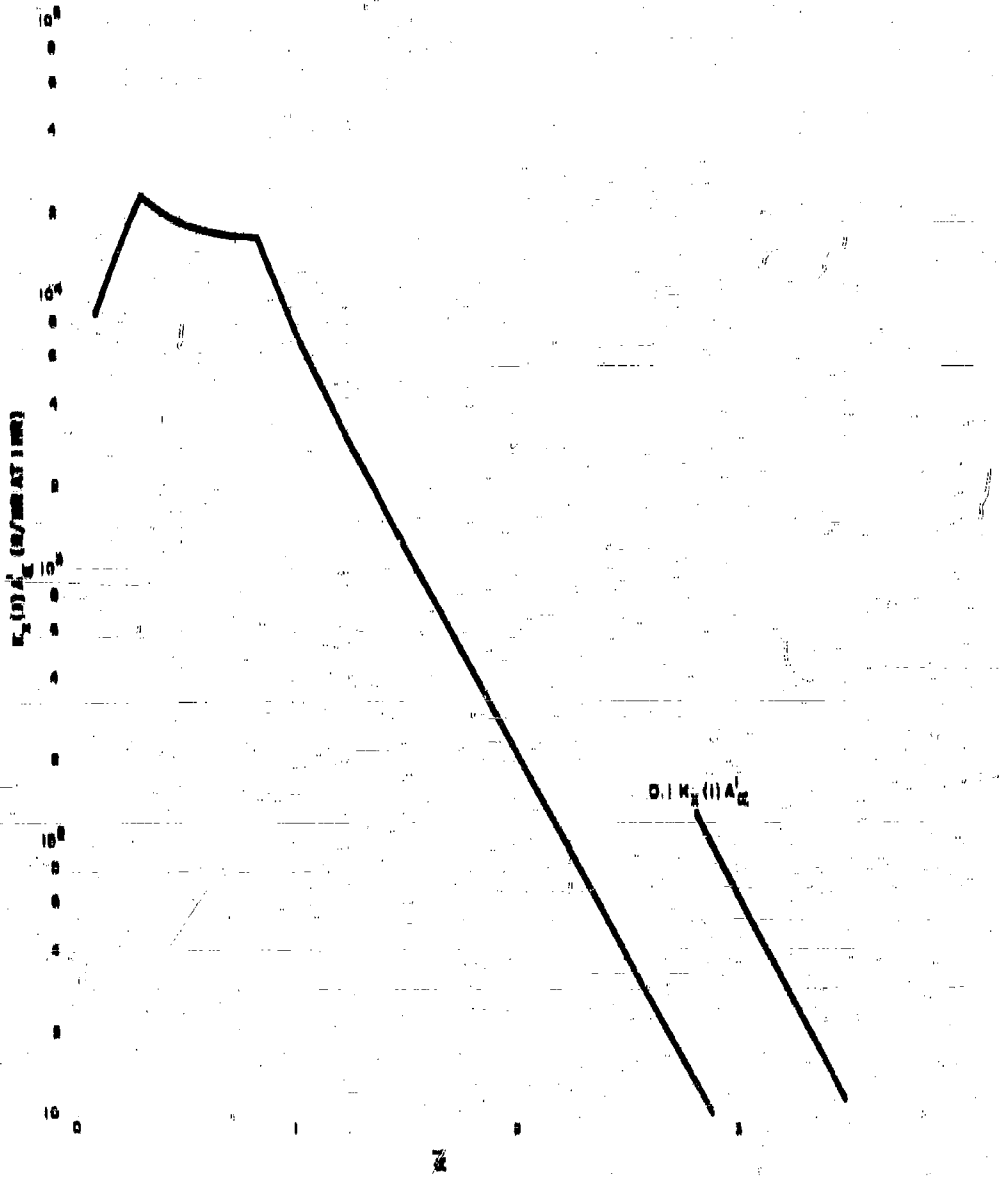

Table 5.8

CALCULATED ARRIVAL TIMES AND DOSE RATES DURING THE FALLOUT PERIOD AND UP TO 1.8 HR AT THE DOWNWIND DISTANCE OF 0.9 MILES FROM A 1-MT YIELD SURFACE DETONATION

r	t_a (hr)	t_f (hr)	t (hr)	$K_\gamma(1)A'_{Cl}$ (r/hr at 1 hr)	$K_\gamma(1)A_\gamma$ (r/hr at 1 hr)	$I_\gamma(1)$ (r/hr at 1 hr)	$d(t,1)$	$I_\gamma(t)$ r/hr
0.90	0.067	0.208	0.305	1.20×10^4	0	0	2.80	0
0.95	0.068	0.310	0.384	9.7×10^3	550	000	2.08	1,040
1.00	0.060	0.004	0.408	7.9	000	700	2.50	1,700
1.05	0.070	0.358	0.428	6.4	1,540	950	2.42	2,300
1.10	0.072	0.371	0.448	5.2	1,080	1,160	2.34	2,710
1.15	0.073	0.385	0.462	4.3	1,805	1,325	2.25	3,080
1.20	0.074	0.407	0.481	3.6	2,000	1,460	2.17	3,170
1.25	0.075	0.425	0.500	2.95	2,222	1,580	2.09	3,300
1.30	0.076	0.444	0.520	2.48	2,358	1,675	2.01	3,370
1.35	0.077	0.462	0.539	2.08	2,471	1,770	1.94	3,430
1.40	0.078	0.480	0.558	1.78	2,565	1,820	1.80	3,440
1.45	0.078	0.498	0.576	1.47	2,645	1,880	1.825	3,430
1.50	0.070	0.517	0.596	1.28	2,712	1,925	1.760	3,390
1.55	0.080	0.534	0.614	1.05	2,768	1,970	1.700	3,350
1.60	0.081	0.552	0.633	8.7×10^2	2,816	2,000	1.640	3,280
			0.80				1.200	2,580
			1.0				1.000	2,000
			1.2				0.704	1,500
			1.4				0.636	1,280
			1.6				0.520	1,000
			1.8				0.442	884

In the computation, $K_\gamma(1)A_\gamma$ is the summation of $K_\gamma(1)A_\alpha$ over the α increments. The summation is made by reading off the midpoint values of $K_\gamma(1)A_\alpha$ for each 0.05α increment, multiplying by 0.05, and summing. Since the model is set up for the arrival of only one α group at a time, the summation can be made by using either α or the arrival time as the independent variable. This procedure actually utilizes α as a designator for a group of particles of a finite particle size range in which α may be considered to be the designator for the average or median size of the particles in that group.

The summation, $K_\gamma(1)A_\gamma$, up to the time of fallout cessation (0.63 hours), gives a value of 2,816 r/hr at 1 hr rather than the scaled value of 2,000 r/hr at 1 hr; hence the second estimate of $K_\gamma(1)A_\alpha$ for α values between 0.90 and 1.00 would be 71 percent of the values of $K_\gamma(1)A_\gamma$ shown in Figure 5.11. Since the other calculations necessary for adjusting the whole distribution curve have not yet been made, all the $K_\gamma(1)A_\gamma$ values were multiplied by 0.71 to obtain the appropriate values of $I_\gamma(1)$. The decay correction factors were obtained, as before, from Figure 11.9.

The variation of the dose rate with time after detonation, at the 0.8 mile distance, is shown in Figure 5.12. Since in this case fallout has stopped before H+1, the curve passes through the 2,000 r/hr at 1 hr point at 1 hour after detonation. Because of the rapid rate of arrival of the larger particles and the rapid decay rate, the intensity rises very rapidly to a peak of about 3,400 r/hr at about 0.56 hours. In the cloud fallout case, by contrast, the peak intensity is relatively nearer the time of fallout cessation and the rate of build-up is not nearly as rapid.

The summation of the area under the $I_\gamma(t)$ curve was made by using 0.02 hour increments. The sum to 0.63 hour is 775 roentgens; the exposure dose itself, therefore, is 1,080 roentgens. At 1 hour the exposure dose would be 2,200 roentgens; at 48 hours it would increase to 8,550 roentgens; at 2 weeks the exposure dose would be 11,000 roentgens; and at about 2 years (the infinity dose) it would increase to 12,800 roentgens.

The most rapid arrival rate occurs at the beginning of fallout. The contribution of the airborne activity to the dose rate at this time should be at a maximum. It can be estimated by use of Eqs. 4.73 and 4.72, if the fractionation is assumed to cancel between $A_i \bar{m}_i$ and $K_i(1)A_\gamma$ and if $(r_\gamma(1) + 0.010)$ is not equal to unity. The average value of dI_γ/dt (i.e., for the corrected values of $K_\gamma(1)A_\gamma$) from 0.365 to 0.384 hours is about 2.05×10^4 r/hr at 1 hr per hour. Using 3.9×10^{-13} r/hr at 1 hr per fission/sq ft for $K_\gamma(1)$, the value of dA_γ/dt is 5.26×10^{16} fissions/sq ft-hr. At the mid-time of the time interval, particles with an α value of 0.925 are arriving, so that, with a 15 mph wind speed, the value of A_α of Eq. 4.73 for these particles is 0.14×10^{11} fissions/cu ft.

Figure 5.12
VARIATION OF THE IONIZATION RATE WITH TIME AFTER DETONATION AT
X = 3.35 · 10^4 FT FOR W = 10^3 KT AND A WIND SPEED OF 15 MPH

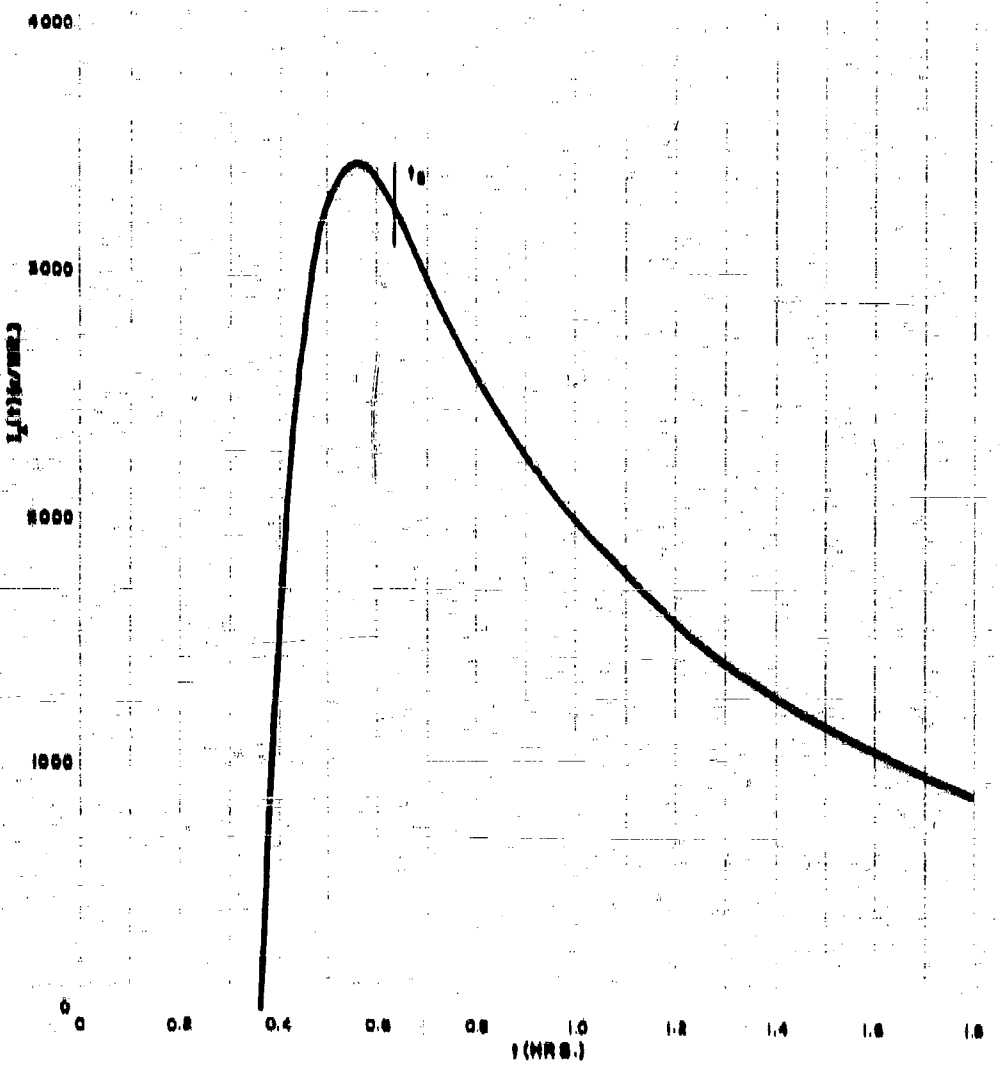

The calculations of LaRiviere[1] give $A_i E_i$ at 0.374 hours as 2.5×10^{-4} Mev/sec-fission. Use of these values in Eq. 4.72 gives 2.0 r/hr at 0.374 hours. Since this is about the maximum airborne contribution to the ionization rate because of the rapid rate of fall and of accumulation of particles on the ground, the contribution of the airborne activity to the total dose during fallout at this location is negligible.

5.5.3 Method for Estimating the Particle Sizes in K e Fallout at a Given Location

The particle-size range of the fallout at a given location or locations is an important consideration in the design of fallout shelter ventilation systems as well as in the planning and execution of decontamination operations. For purposes of conducting realistic and meaningful experiments in decontamination and in shelter design, methods for estimating likely particle sizes are necessary for the preparation and use of fallout simulants.

The simplified fallout-system scaling functions, together with particle fall-rate data, can be used to estimate the particle-size groups that fall at any given downwind location. Further, they can be used to make estimates of the fraction of the activity that is carried by the different sizes of particles that fall from both stem and cloud altitudes. This information could also be used in the more sophisticated computer programs for estimating fallout depositions under meteorological conditions other than those of uniform wind speed and direction.

Because the fall velocity of a particle of a given size varies with altitude in falling through the atmosphere, the designator, α, of a given fall vector represents a group of particles, with a spread in diameters that depends on both the thickness of the cloud and the altitude from which the group falls. In Figure 5.13 the size of spherical particles falling through a standard atmosphere from various altitudes is plotted as a function of vector velocity. These curves were prepared by D. E. Clark from data provided by A. D. Anderson.[3] The estimated diameters of the particles falling at $X = 1.87 \times 10^4$ feet and at $X = 3.35 \times 10^4$ feet for the 1-MT yield detonation used in Section 5.4 are shown in Table 5.9. For $v_w = 15$ mph,

$$v_f = 22/\alpha \text{ ft/sec}, \tag{5.74}$$

The height of fall for the particles falling from stem altitudes is

$$z = \frac{(28,900\alpha - 1900)}{(\alpha + 0.020)} \text{ ft}. \tag{5.75}$$

Figure 5.13
VERTICAL COMPONENT OF THE VELOCITY FOR SPHERICAL PARTICLES FALLING FROM VARIOUS ALTITUDES TO SEA LEVEL

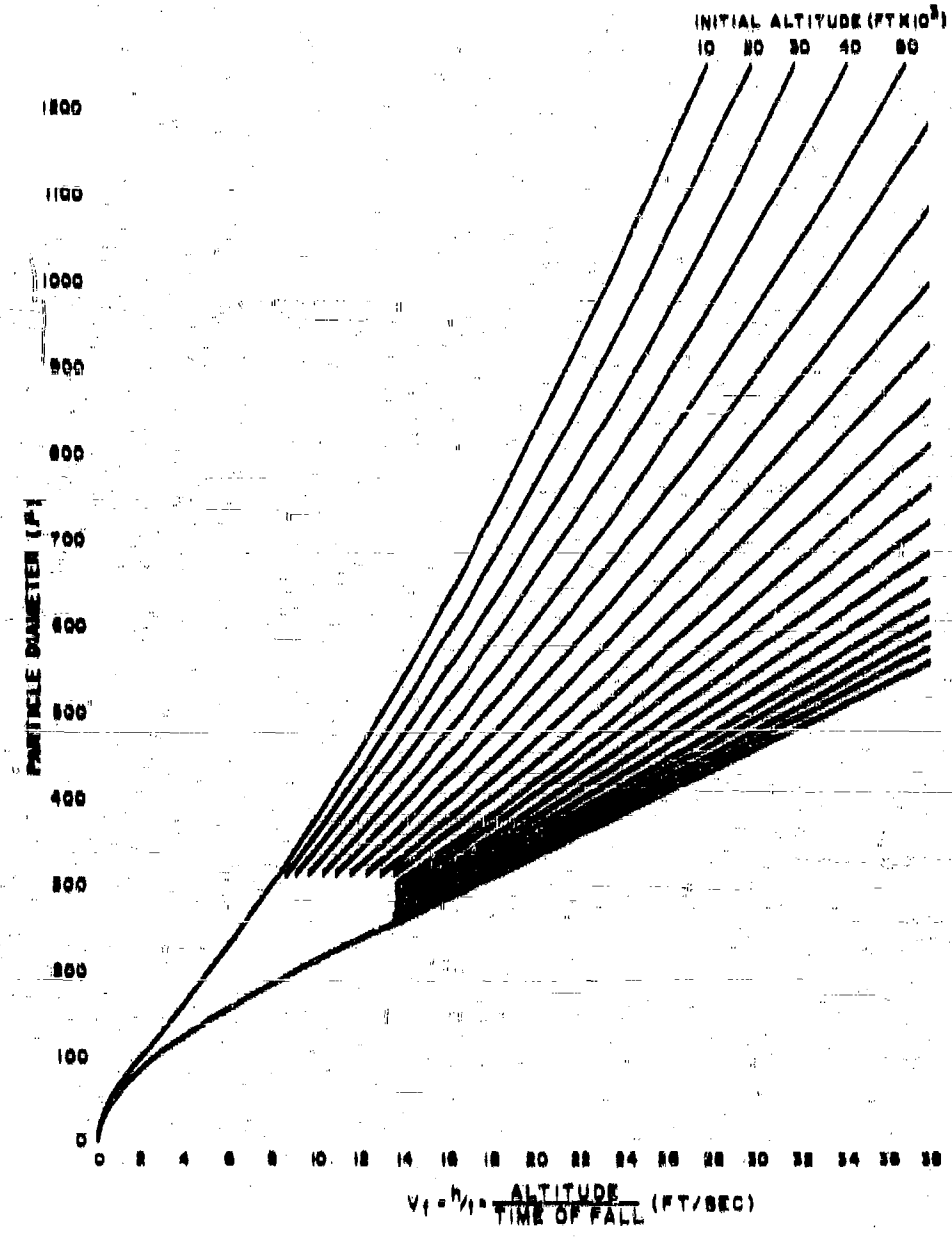

Figure 5.13 (continued)

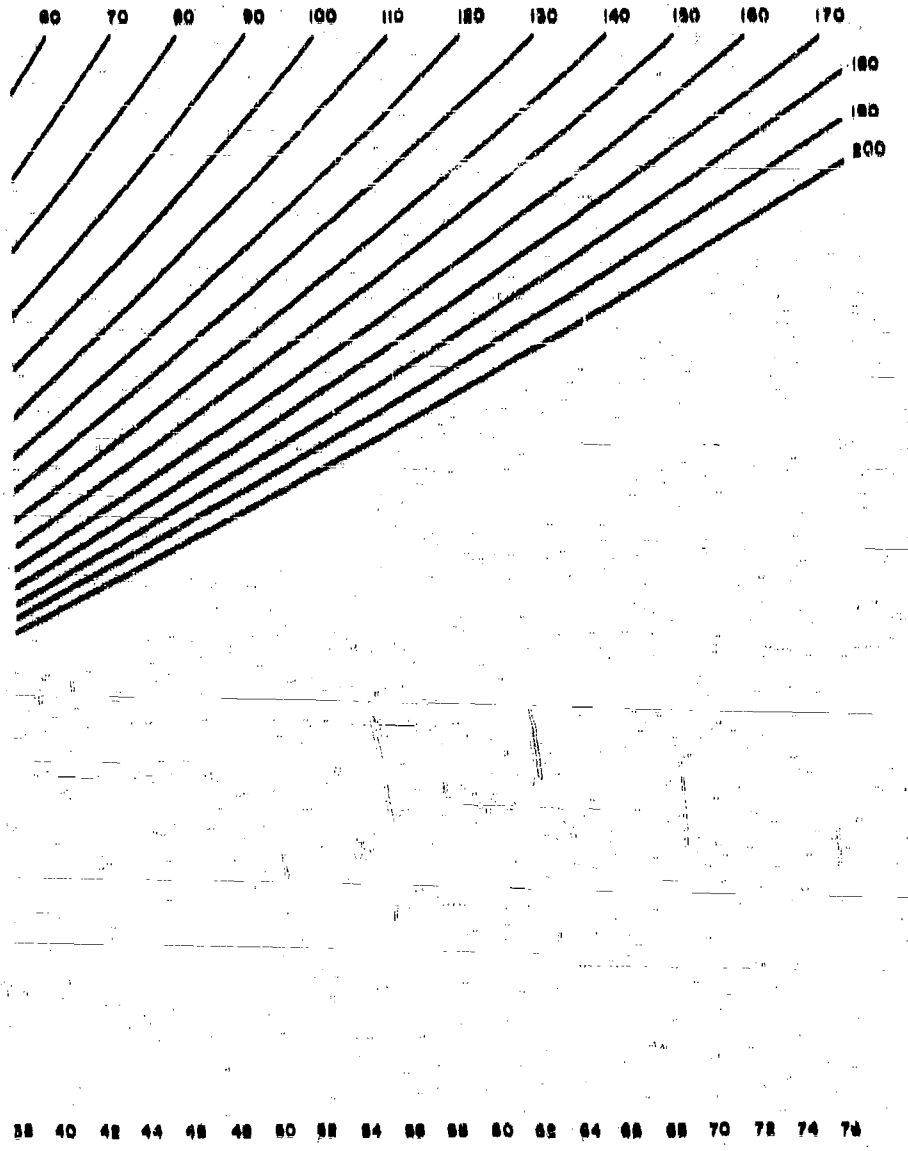

Figure 5.13 (continued)

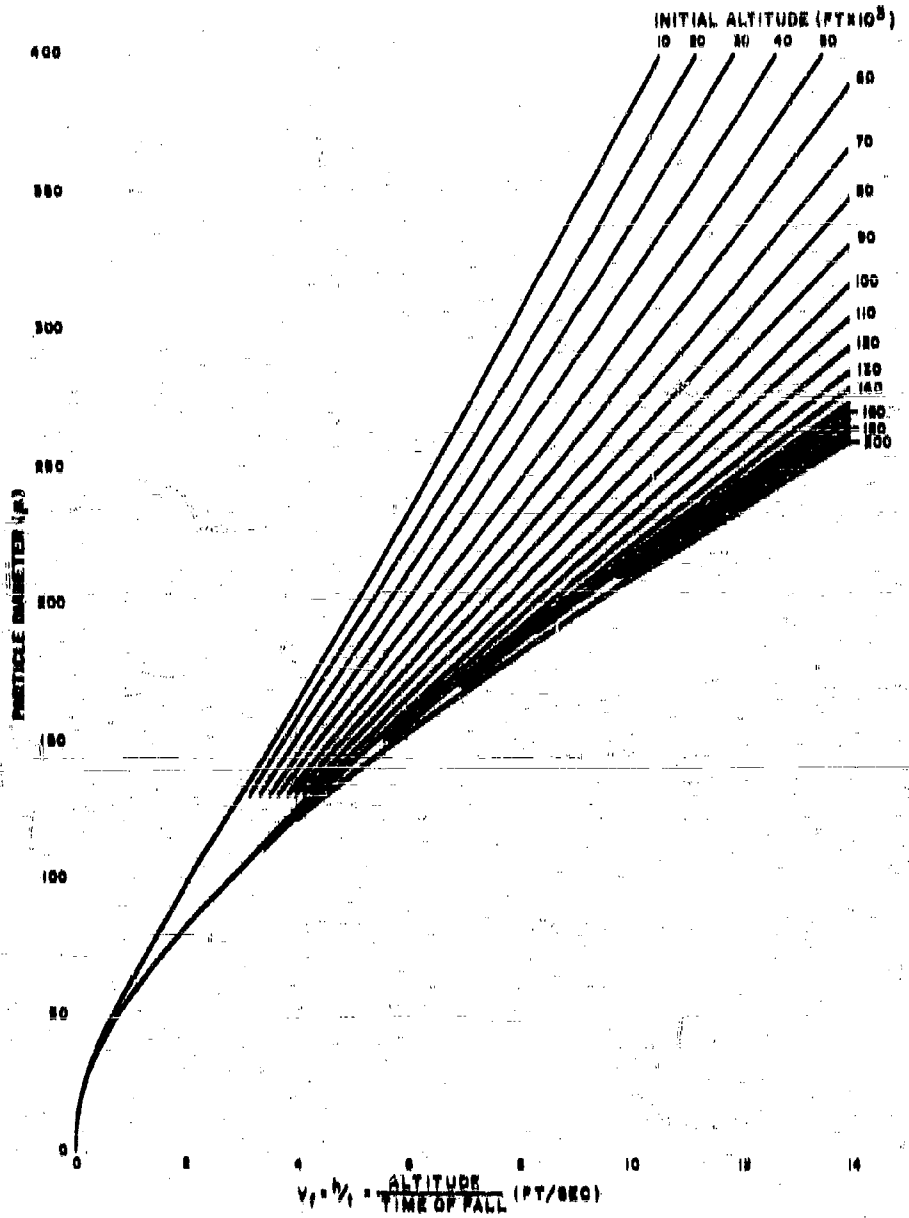

Figure 5.13 (concluded)

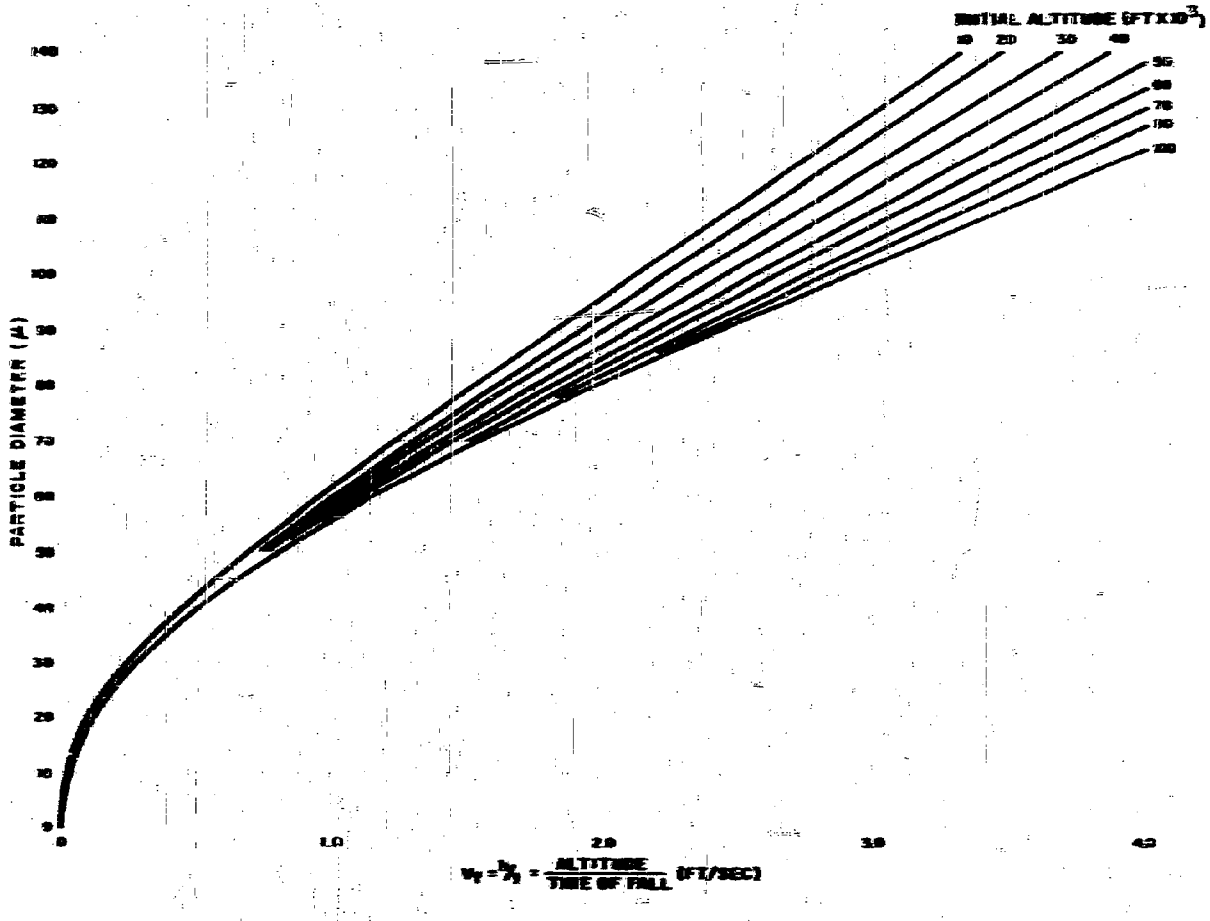

Table 5.0

DIAMETERS OF SPHERICAL PARTICLES FOR VARIOUS σ GROUPS FALLING AT 1.87×10^4 FT AND 3.55×10^6 FT DOWNWIND FROM A 1-MT YIELD SURFACE DETONATION ASSUMING A WIND SPEED OF 15 MPH

$X = 1.87 \times 10^6$ ft (y=o)							$X = 3.55 \times 10^6$ ft (y=o)			
σ	v_f ft/sec	h_1 10^5 ft	h_2 10^5 ft	d_1 (μ)	d_2 (μ)	Δd (μ)	σ	v_f ft/sec	z 10^5 ft	d (μ)
2.516	6.76	57.8	57.8	252	252	0	0.9	24.4	20.2	910
2.6	6.46	55.6	61.2	252	242	10	1.0	22.0	20.5	800
2.8	7.80	49.0	63.0	240	226	14	1.1	20.0	26.7	720
3.0	7.53	47.7	65.2	229	213	16	1.2	18.3	26.0	650
3.2	6.58	46.0	62.5	219	202	17	1.3	16.9	27.0	590
3.4	6.47	44.6	61.9	209	193	16	1.4	15.7	27.1	545
3.6	6.11	43.5	60.6	200	184	16	1.5	14.7	27.3	505
3.8	5.79	42.6	59.1	192	178	14	1.6	13.8	27.4	470
4.0	5.50	42.0	57.4	184	173	11				
4.2	5.24	41.4	55.5	177	167	10				
4.4	5.00	41.1	53.4	171	163	8				
4.6	4.78	41.0	51.0	165	158	7				
4.8	4.58	41.4	48.4	159	155	4				
4.905	4.40	43.7	43.7	153	153	0				

The spread in particle diameters for each α value for cloud fallout is seen to be quite small; at maximum cloud thickness the spread in diameter is only 17 microns. The spread should be somewhat larger at smaller distances and somewhat smaller at greater distances.

The stem fallout model, as formulated, gives no spread in the diameters of the particles falling from a given altitude. At the 1.87×10^5 foot distance, the over-all spread in particle diameters is about 100 microns; at the shorter distance it is 485 microns. The accumulated activity distributions (in r/hr at 1 hr) at the two locations are shown in Figure 5.14; these were obtained from the respective summations of $K_0(1)A_\alpha(\alpha)$ and $K_\pi(1)A'_\alpha$ over α.

The gross activity-particle size distribution for the 1-MT yield, calculated from the first approximation of $K_\alpha(1)A_\alpha$ for fallout from cloud altitudes, is shown in Figure 5.15 along with the distributions used in fallout models by Anderson[8] (NRDL distribution) and by Rapp (RAND distribution) as given by Pugh and Galiano[5]. If the stem fallout were included and additional approximations of the distribution were made, it is likely that the curve for the simplified fallout model presented here for the 1-MT yield would have slightly higher percentages of the activity on both the small and larger particles. Also, the distribution curve would change somewhat with weapon yield.

The NRDL distribution was obtained from data on sieved fallout sample fractions from a low-yield underground shot in Nevada. The amount of activity not accounted for in the fallout pattern consists of the fractions in the very small particles. Thus, if the NRDL distribution were readjusted to the distribution in the fallout on the ground, the high fractions in the small sizes would be reduced. The same would apply to the RAND distribution. These two distributions are generally used in terms of fraction of the weapon activity (fissions, d/s, etc.);but these units, during computation, are usually not directly proportional to roentgens per hour.

The RAND distribution was obtained from data on a few fallout sample fractions obtained from a high-yield detonation on coral. The absence of a significant amount of large particles in the distribution suggests either a high degree of particle breakage during shipment and sizing of the more fragile coral-based particles (as discussed in Chapter 2) and/or insufficient sampling for obtaining data on the larger particles. Also, even if the activity-size measurements were not subject to question because of bias and particle break-up, some question occurs regarding the use of activity distributions on coral particles in calculations for silicate-type fallout particles.

The noted discrepancies in the three activity-size distributions have not been satisfactorily resolved. The utility of the simplified fallout scaling system to predict shifting of the activity-size distributions with yield has not yet

Figure 5.14
ACCUMULATED ACTIVITY DISTRIBUTION AS A FUNCTION OF PARTICLE SIZE AT
$\bar{X}$ = 3.35 · 10^4 FT AND LAT · 10^5 FT DOWNWIND FROM THE 1-MT YIELD
SURFACE BURST FOR A WIND SPEED OF 15 MPH

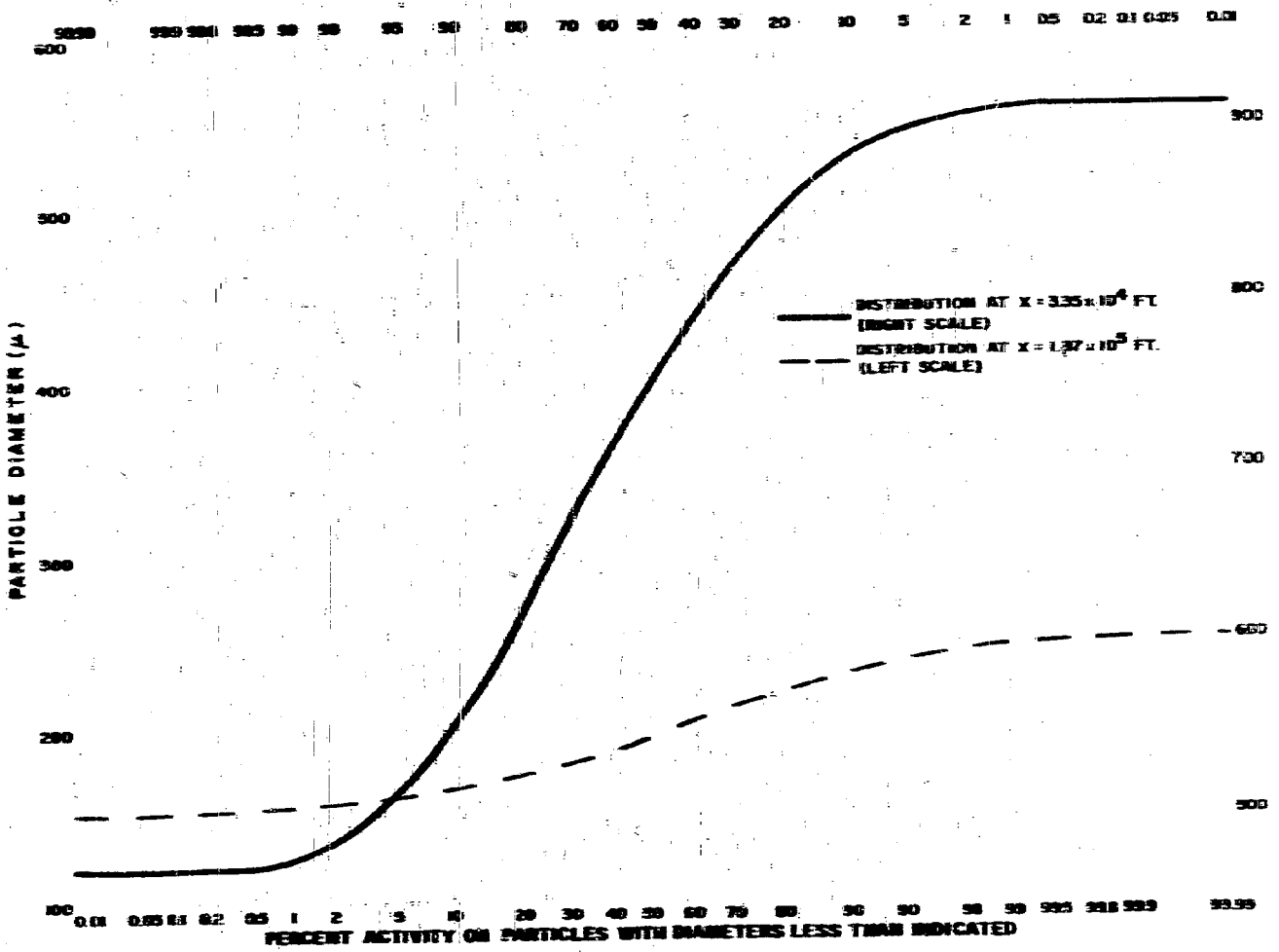

Figure 5.15
COMPARISON OF THE GROSS ACTIVITY DISTRIBUTION ON PARTICLES OF VARIOUS DIAMETERS DERIVED FROM THE SIMPLIFIED FALLOUT SCALING SYSTEM TO DISTRIBUTIONS USED IN OTHER MATHEMATICAL FALLOUT MODELS

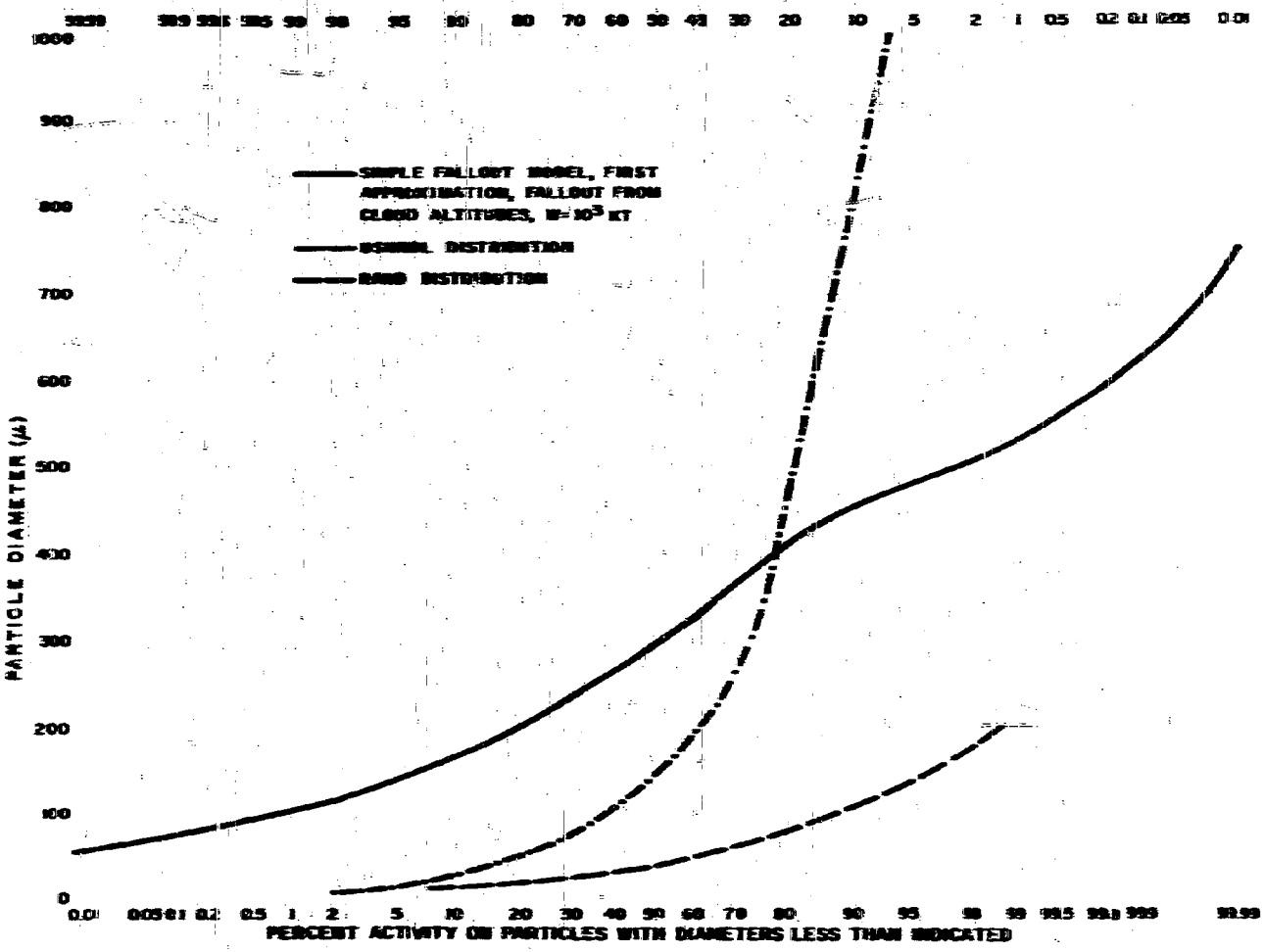

been used in the more refined models to determine whether the predicted change would result in any significant differences in the predicted fallout patterns. These discrepancies are of less importance when the results of the calculations are used to estimate the general magnitudes of the hazard from fallout and the extent of the area affected than when they are used to predict fallout effects at a given location with respect to a hypothetical burst point. Even in the more general use of the model, however, the maximum estimated hazard will still be sensitive to the shape of the activity-size distribution curve.

5.6 The Effect of Cross-Wind Shear on the Fallout Pattern Scaling System

The simple fallout scaling system contains the effects of some degree of wind shear because the original fallout patterns from which it was derived were formed under real wind conditions in which some shear occurred. The relative shear, or relative pattern spread, can be defined as $(Y_g-a)/Y_g$. This ratio is proportional to the tangent of the angle of the maximum lateral spread of particle trajectories falling from all altitudes to the ground.

For the 1-KT yield, the relative shear of the pattern from the simple fallout-model scaling method is 0.424. Since this scaling system was derived with use of the fallout data from the Jangle "S" shot whose yield was 1.2 KT, it is of interest to review the wind data for that shot with respect to the effect of the wind shear on the relative pattern spread. The wind data and particle fall trajectories are summarized in Table 5.10.

The lateral distance, Δd, traveled by a particle having a fall velocity, v_f, in a wind speed of v_w, while falling through the altitude increment, Δh, is:

$$\Delta d = v_w \Delta h / v_f \quad (5.70)$$

In Table 5.10, the quantity $v_f \Delta d$ is given since it is independent of particle size. The lateral distance component, Δy, is $\Delta d \sin \Delta\theta$ and the "downwind" distance, Δx, is $\Delta d \cos \Delta\theta$, where $\Delta\theta$ is the angle between the wind direction at the altitude of the top of the 10-minute cloud (12,000 feet) and the wind direction at any lower altitude. The summation of the component distances (starting at ground zero) assumes that v_f is constant from 4,000 to 12,000 feet. The reference direction of 200° was selected because it corresponds closely to the direction of the maximum pattern intensity, the "hot" line, in the fallout area from the Jangle "S" shot.

Table 5.10

WIND DATA AND PARTICLE FALL TRAJECTORY COMPONENTS FOR JANGLE "S" SHOT

Altitude Increment (10^3 ft)	Wind Direction (degrees)	Wind Speed (knots)	Δθ (degrees)	10^{-3} knot/ft				
				$v_t \Delta d$	$v_t \Delta y$	$v_t \Delta x$	$v_t \Sigma y$	$v_t \Sigma \Delta x$
11–12	200	37	0	37	0	37.00	22.33	186.04
10–11	200	34.5	0	34.5	0	34.50	22.33	149.04
9–10	200	32	0	32	0	32.00	22.33	114.54
8–9	200	28	0	28	0	28.00	22.33	82.54
7–8	190	26	20	26	8.89	24.44	22.33	54.54
6–7	190	20	20	20	6.84	18.80	13.34	30.06
5–6	170	13	30	13	6.50	11.26	6.50	11.26
4[a]–5	calm	calm	—	0	0	0	0	0

Note: Cloud base at ~ 10 minutes: h_b ~ 9,000 ft.
Cloud top at ~ 10 minutes: h_t ~ 12,000 ft.

a. Surface (4,200 ft).

The effective, or average, wind speed is:

$$\bar{v}_w = \frac{\sum_{i=1}^{i=n} t_i v_i}{\sum_{i=1}^{i=n} t_i} \qquad (5.77)$$

where t_i is the time a particle spends in the i^{th} altitude increment and v_i is the wind speed in that increment ($t_i = h/v_f$). For a constant fall velocity, $\bar{v}_w$ is equal to $\Sigma_i v_i/n$, where n is the number of altitude increments considered. The data of Table 5.10 give 23.8 knots (20.6 mph) for $\bar{v}_w$ for a constant v_f. The wind shear, S, between the altitude increments m and n is given by

$$S(m,n) = \left[\frac{\sum_{i=1}^{i=n} t_i v_i}{\sum_{i=1}^{i=n} t_i} - \frac{\sum_{i=1}^{i=m} t_i v_i}{\sum_{i=1}^{i=m} t_i} \right] \frac{1}{(h_n - h_m)} \qquad (5.78)$$

For the assumption of a constant v_f, the following values of S(m,n) are obtained from Table 5.10:

$$S(5,8) = 2.14 \text{ (knots/10}^3 \text{ ft)}$$
$$S(4,8) = 2.26 \text{ (knots/10}^3 \text{ ft)}$$
$$S(3,8) = 2.50 \text{ (knots/10}^3 \text{ ft)}$$
$$S(2,8) = 2.88 \text{ (knots/10}^3 \text{ ft)}$$

The notation S(5,8) is for the altitude range 9,000-12,000 feet, etc.

The value of wind shear of Eq. 5.78 (for a given particle size or fall velocity) gives the total wind shear rather than just the crosswind shear that spreads out the vertical distribution of particles laterally (from the downwind direction of the center of the pattern). Since Table 5.10 shows that the lateral shear for a given particle size originating from the cloud altitudes (9,000-12,000 feet) is negligible, the only cause of the relative pattern spread is the relative shear of particles of different sizes as they fall through the lower altitudes.

The lateral spread due to changes in v_f with particle size may be represented by the variation of $v_f \Sigma \Delta y$ with $v_f \Sigma \Delta x$. The deposition of particles (from

the center line of the source, say) starting from the lower altitudes nearest the origin (i.e., ground zero), proceeds in a lateral direction up to an altitude of 8,000 feet. And, since both coordinates are proportional to v_f, the variation of v_f (i.e., change of particle size) will result in the deposit of a continuous band of particles in the lateral direction bounded by the line (at low values of Δx) with a slope (tan $\Delta\theta$) of approximately 22.23/54.54 or 0.408. This ratio is very near the value of $(Y_n - a)/X_n$, 0.424, for the 1-KT yield that is obtained from the scaling functions.

The fallout pattern for the Castle Bravo shot pattern was also used to derive the scaling functions for the simple fallout-pattern scaling system. The particle fall trajectory components (in relative units), with respect to the estimated pattern center (or hot) line for Castle Bravo winds, and for a particle size of about 100 microns, is shown in Figure 5.10. (The effect of these winds on the lateral spread of the derived pattern for the 10-MT yield should be about the same as it was for the Castle Bravo shot pattern which was used to establish the scaling system.) The lateral shear in the Figure 5.10 plot is due to changes of both wind speed and direction over the range of altitudes containing the cloud (at 8-10 minutes after detonation).

It is seen that the maximum spread in particle deposition, for all from altitudes between 55,000 and 90,000 feet (heights of bottom and top of cloud), is equivalent to a shear angle of about 23°; the tangent of this angle is 0.39. This value of the tangent is reasonably close to $(Y_n - a)/X_n$ for the 1 r/hr at 1 hr contour at the 10-MT yield, which is 0.407.

If, for the Castle Bravo wind conditions, it is assumed that the smaller particles fell from altitudes as high as 100,000 feet, and that the fall trajectory components (for all the smaller particles) are proportional to those of Figure 5.10, then the maximum downwind distance at which the particles would have landed for a single wind direction would have been about 2.5 times greater than for the trajectories of Figure 5.10. Under such conditions, the value of X_n for the 1 r/hr at 1 hr contour would have been no more than 1,200 miles for the 10-MT yield.

The relative pattern spread and "equivalent" uniform wind shear, for the simple fallout scaling system patterns for several yields, are given in Table 5.11. It is interesting that the relative pattern spread (for the 1 r/hr at 1 hr contour) is about the same for both the Jangle "S" and the Castle Bravo fallout patterns, but the shear mechanism by which the spread occurred is very different. Of the two shots, the manner in which the shear occurred in the Bravo shot is more like the assumed uniform lateral shear used by Pugh and Gallano

Figure 5.16
PLOT OF PARTICLE FALL TRAJECTORY COMPONENTS RELATIVE TO ESTIMATED PATTERN CENTER LINE FOR CASTLE BRAVO WINDS

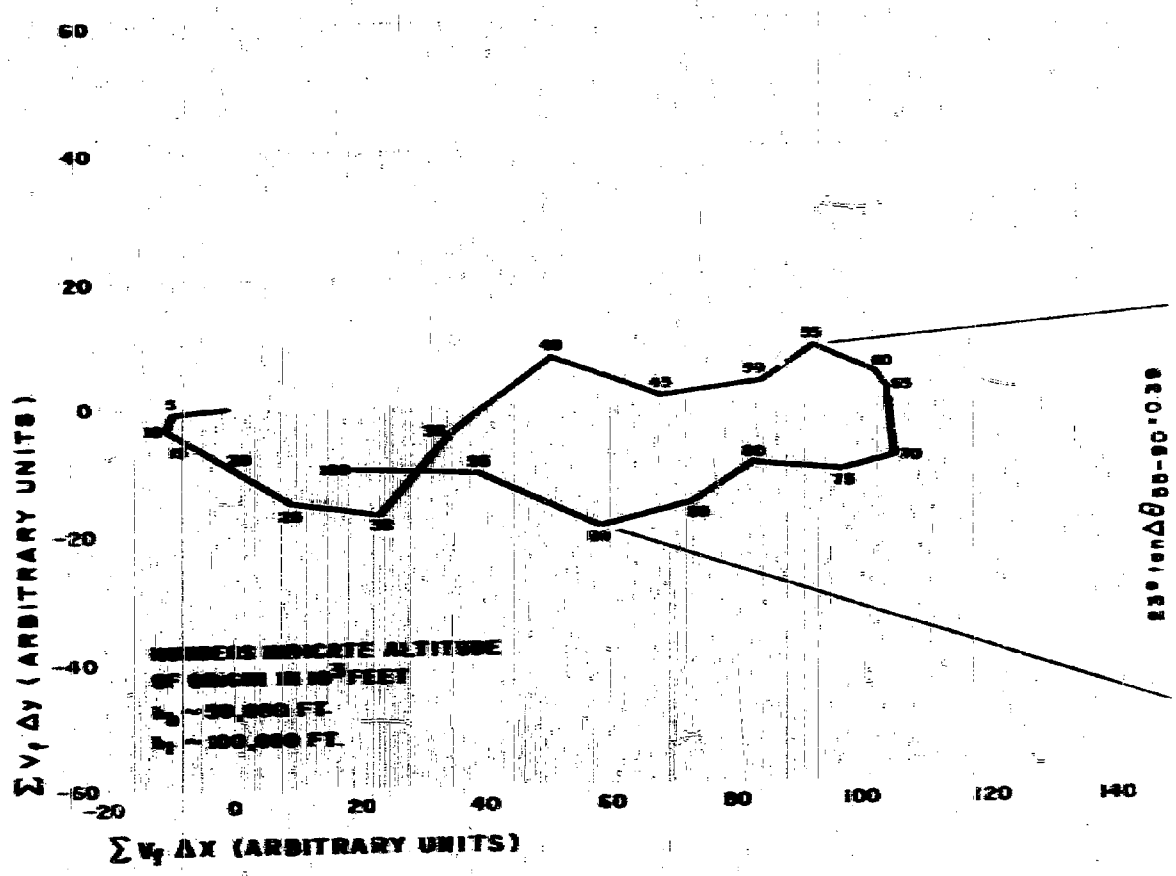

in their computations. Thus, for the larger yields, the included lateral shear for the simple fallout scaling system can be related roughly to a uniform wind shear through the cloud of 0.2 and 0.3 knots per 1000 feet when the average wind speed is about 15 mph.

Table 5.11

SUMMARY OF "EQUIVALENT" UNIFORM WIND SHEAR FROM RELATIVE PATTERN SPREAD FOR THE SIMPLE FALLOUT SCALING SYSTEM PATTERNS
(Wind Speed of 15 mph)

W(KT)	$(Y_n - n)/X_n$	S_y(knots/10^3 ft)
1.2	0.41[b]	2.88
10	0.14	0.98[a]
10^2	0.28	0.41[a]
10^3	0.53	0.40[a]
10^4	0.47	0.28[a]
1.5×10^4	0.80[b]	0.22[a]
10^5	0.88	0.15[a]

[a] From plots derived from the computations of Pugh and Gallano[6] for $(Y_n - n)/X_n$ as a function of S_y assuming a 15 mph wind and 100% fission yields; the standard intensities given by Pugh and Gallano were multiplied by 0.56 to account for terrain shielding and instrument response.

[b] From wind vector data.

5.7 Comparison of Several Fallout Pattern Computations

Methods of computing fallout patterns can be compared, in a gross way, by (1) the relative area that is enclosed within given standard intensity contours, and (2) the differences in the calculated variation with downwind distance of the standard intensity along the center line of the fallout pattern. Another way of gross comparison involves differences in the contour shapes.

A comparison has been made by Ferber and Hoffler[4] of several fallout models [5,6,7] considering wind effects. The fallout models compared were those developed by

1. Pugh and Galiano[8] (WSEG-RM10);
2. a revised but as yet unpublished version of the Pugh-Galiano model based on recommended changes by the National Academy of Science Working Group on Fallout Models in 1961 (WSEG-NAS);
3. a model developed by the weather bureau (WB);
4. a model developed by the Air Force Intelligence Center (AFCIN); and
5. a model developed by the RAND Corporation (RAND).

Comparing of fallout pattern computations by means of the areas enclosed within a given standard intensity contour is a fairly good method because the enclosed areas are not very sensitive to wind speed or wind shear. Because of this, it is possible also to compare the fallout patterns calculated for a 10-MT yield surface detonation and 15 mph wind speed based on the model given in ENW[5], the WSEG-RM10 model, the model developed by Anderson[6], and the simple fallout scaling system described here.

The wind shear for the ENW model is unspecified; for the WSEG-RM10 model it is taken at 0.1 knots/1,000 ft; for the Anderson model the wind shear is zero; and for the simple fallout scaling system it is about 0.8 knots/1,000 ft. The comparisons presented by Ferber and Hoffler[4] are for a 1-MT yield surface detonation, a 25 mph wind speed, and a vertical wind shear of 0.2 knots/100 ft. The areas within stated contours, for the two sets of calculations, are given in Table 5.12; the area ratios are relative to the WSEG-RM10 model since it is common to both sets.

Another factor of difference between the two sets of calculations which could have a small effect on the value of the ratios, is that the areas calculated by Ferber and Hoffler are, presumably, for the ionization rate at 0 feet above an ideal plane (except perhaps for the AFCIN model). The calculations presented here are for the observed ionization rate at 3 feet above a plane including a terrain attenuation factor of 0.75 and an instrument response factor of 0.75 for the WSEG-RM10 model and the simple fallout scaling system. It is not clear, from the referenced sources, what the value of these factors are for the ENW and Anderson models.

Table 5.12

RATIO OF AREAS WITHIN STATED STANDARD INTENSITY CONTOURS FOR FALLOUT PATTERNS COMPUTED FROM VARIOUS MODELS RELATIVE TO THOSE FROM THE WSEG-RM10 MODEL

Model Designation	Standard Intensity in r/hr at 1 hr			
	1	10	100	1000
A. 10-MT Yield, 15 mph Wind Speed (100% Fission)				
ENW	3.66	1.86	0.70	0.62
Anderson	1.40	1.14	1.00	0.96
Simple Fallout Scaling System	0.67	0.71	0.83	1.10
B. 1-MT Yield, 25 mph Wind Speed, 0.2 knots/10^3 ft Vertical Shear (100% Fission)				
AFCIN	0.15	0.18	0.26	0.57
WB	2.16	1.18	0.67	0.40
WSEG-NAS	1.00	1.00	0.87	0.60

Since most of the area within the stated contours is associated with the downwind distance, the ratio values in excess of unity for the lower-valued contours and the values that decrease to less than unity for the higher-valued contours correspond to a higher fraction of the total activity on smaller particles than the values used in the WSEG-RM10 model. This type of trend in the ratios is exhibited most clearly by the ENW and WB models and, to a lesser extent, by the WSEG-NAS and Anderson models. The reverse trend, representative of an activity-particle size distribution having a higher fraction of the total activity on the larger particles than is used in the WSEG-RM10 model, is exhibited by both the AFCIN model and the simple fallout scaling system.

The actual values of the area ratios are related, of course, to the assumed value of the yield-distribution contour ratio; this is given as $\overline{K(I)}$ or $\overline{K(I)}C(I)$ in r/hr at 1 hr per KT/mi^2 in Chapters 2 and 3. For the 10-MT yield patterns, the values of $\overline{K(I)}\,C\,(I)$ are computed, from pattern integrations, to be (in r/hr at 1 hr per KT/mi^2):

1,460 for the ENW model;
1,500 for the WSEG-RM10 model (corrected by 0.50);
1,550 for the Anderson model; and
1,130 for the simple fallout scaling system.

For the other patterns, according to Ferber and Hoffler,[1] the values of $\overline{K(I)}$ are:

2,500 for the WSEG-RM10 model;
2,400 for the WSEG-NAS model;
about 2,000 for the WB model; and
800 for the AFCIN model.

The low value of $\overline{K(I)}$ for the AFCIN model suggests that it applies to an observed ionization rate and that it includes terrain attenuation and instrument response factors. The higher values of $\overline{K(I)}$ for the other models apparently are for fallout deposited on an ideal smooth plane. If this is true, the comparable value of $\overline{K(I)}$ for the AFCIN model, on the ideal plane, would be about 1420 r/hr at 1 hour. The value of $\overline{K(I)}C(1)$ for the simple fallout model pattern, for the ideal smooth plane source and a 10-MT yield, would be about 2550 r/hr at 1 hour per KT/mi^2 at 3 feet.

The variation of the calculated infinite ideal plane standard intensity with downwind distance along the center line of the fallout pattern, for several of the fallout models, is plotted in Figure 5.17, for a 10-MT yield surface detonation assuming a 25 mph windspeed and 100 percent fission yield. The simple fallout scaling system and the RAND model are the only two methods that predict the observed downwind major peak.

A portion of the higher rate of decrease in the standard intensities with downwind distance, for the simple fallout scaling system, may be due to the higher degree of vertical shear. But most of the higher standard intensities in the first 500 miles downwind, and the high ratio of decrease with distance, is due to the higher fraction of the total activity implied as being associated with

Figure 5.17
VARIATION OF THE CALCULATED INFINITE IDEAL PLANE STANDARD INTENSITY WITH DOWNWIND DISTANCE (Center Line of Pattern) FOR A 10-MT YIELD SURFACE DETONATION (100% Fission)

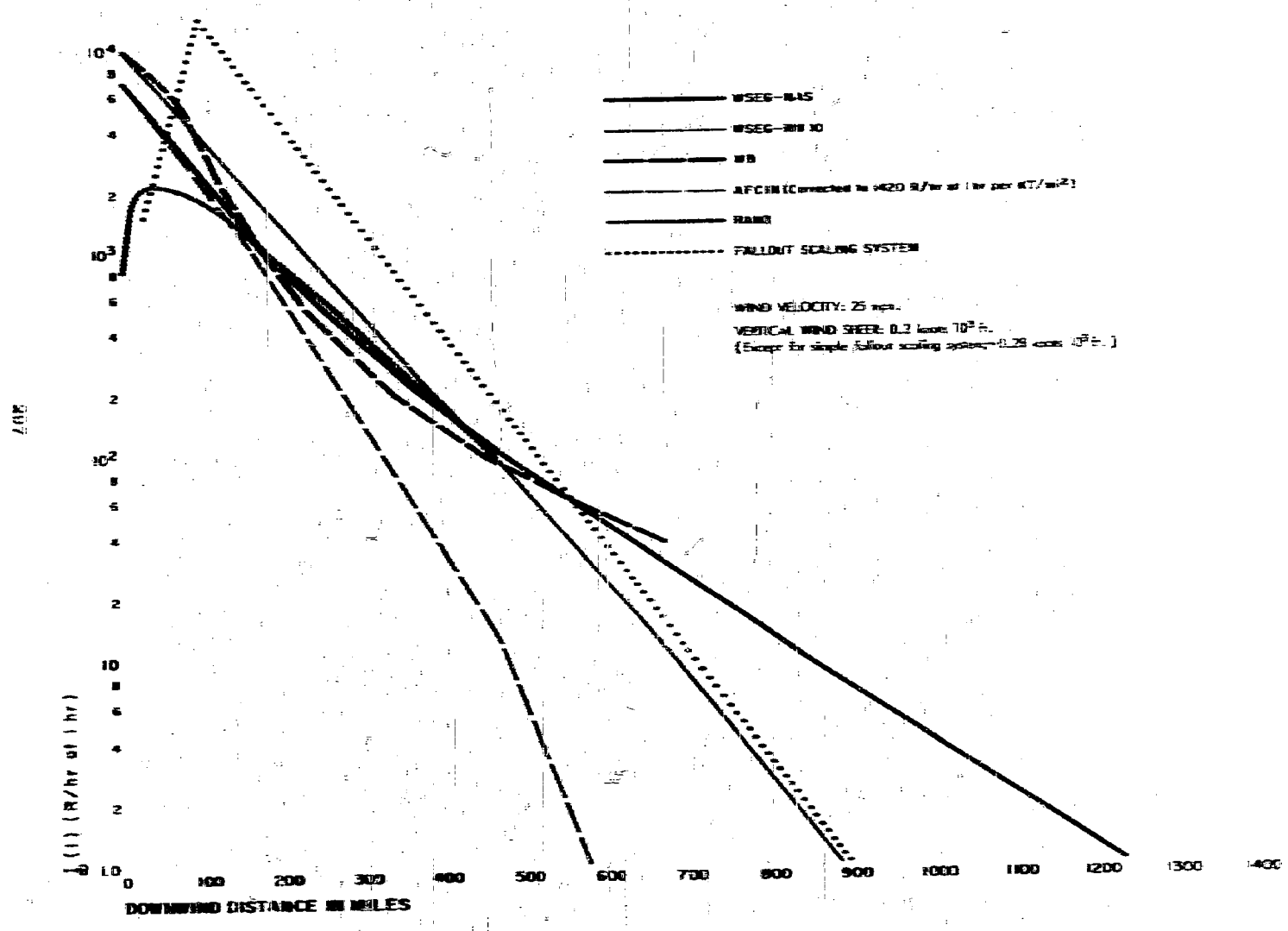

the larger particles. The curve for the AFCIN model implies an even sharper decrease in the fraction of activity with decreasing particle size.

The curve for the WB model implies an activity-particle size distribution in which the largest fractions of the activity are on the small particles. The development of fallout models for tower and balloon detonations[6] quite likely had an influence on the development of the WB surface-burst fallout model. The WSEG-NAS model curve also implies a larger fraction of the activity on the smaller particles.

Since the simple fallout scaling system is adjusted to the Castle Bravo fallout pattern, for which the yield and wind conditions were not very different from the conditions used in the calculations for the curves of Figure 5.17, it appears that the AFCIN model does not account for enough of the total activity, and that the WB and WSEG-NAS models give too much weight to the activity carried by the smaller particles. If factors for the type of soil at the point of detonation are taken into account, these factors could be responsible for some of the indicated differences. However, none of the models explicitly consider soil type; therefore, no explanation of the difference on this basis is possible.

Further work on the fallout distribution models and their connection with the fallout-formation process is discussed in Chapter 6. A thorough study of the early-time condensation and other dynamic processes that take place during the rise of the fireball is required before significant progress is possible in the development of improved fallout models. It is clear that, when differences of a factor of 10 to 50 occur in the calculated standard intensities, one or more of the models has been poorly calibrated to the available observed fallout data.

CHAPTER 6 REFERENCES

1. LaRiviere, P.D., Early-Time Gamma Ray Properties of U-235 Gross Fission Products, USNRDL-TM-80, 1958.

2. Clark, D.E., and A.D. Anderson, Private communication, USNRDL, July 1960.

3. Pugh, G.E., and R.J. Galiano, An Analytic Model of Close-In Deposition of Fallout for Use in Operational-Type Studies.

4. Research Memorandum No. 10, Weapons Systems Evaluations Group, 1959.

5. Forber, Gilbert J., and Jerome L. Hoffter, A Comparison of Fallout Model Predictions With a Consideration of Wind Effects, U.S. Weather Bureau, 1961.

6. Batton, E.S., D.L. Inglehart, and R.E. Rapp, Derivation of Two Simple Methods for the Computing of Radioactive Fallout, RM-2500, 1960.

7. Nagler, K.M., L. Machta, and F. Pooler, Jr., A Method of Fallout Prediction for Tower Bursts at the Nevada Test Site, TID-5489, OTS, Department of Commerce, Washington 25, D.C., 1955.

8. U.S. Government, Nuclear Weapons Employment Handbook, Air Force Manual 200-8, 1961 (Classified).

9. The Effects of Nuclear Weapons, U.S. Government Printing Office, Washington, D.C., 1957.

10. Anderson, A.D., Scaling Relations for Fallout Dose-Rate Patterns from Land Surface Nuclear Bursts, USNRDL-TR (in publication, 1961).

Chapter 6

IONIZATION RATE CONTOUR RATIOS AND COMPOSITION OF FALLOUT

6.1 Definition and Use of Ionization Rate Contour Ratios

These contour ratios are defined as the ratio of the surface density of some property of fallout to the ionization rate at 3 feet above an extended open area covered with fallout. The three fallout properties of most interest in radiological countermeasures are:

1. The mass of fallout per unit area,
2. The number of atoms or moles of fission products per unit area, and
3. The fraction of the weapon yield deposited per unit area.

At a given location in the fallout area, the contour ratios for these quantities are defined by

$$M_r(t) = \frac{m_s}{I_s(t)} \tag{6.1}$$

$$FP_r(t) = \frac{n_{fp}}{I_s(t)} \tag{6.2}$$

and

$$FD_r(t) = \frac{FD}{I_s(t)} \tag{6.3}$$

where $M_r(t)$ is the mass contour ratio, m_s is mass of fallout per unit area at the location, $FP_r(t)$ is the fission product or activity contour ratio, n_{fp} is the number of atoms or moles of fission products per unit area, $FD_r(t)$ is the fraction of device contour ratio, FD is the fraction of device per unit area, and $I_s(t)$ is the observed ionization rate.

Knowledge of the values of these contour ratios makes possible estimates of the amount of fallout particles, fission products, or other components of the weapon that are present, given the level of the ionization rate. These estimates are necessary in the design of realistic experiments using synthesized fallout materials, in the operational use of radiological counter measures, and in general evaluations of radiological hazards from fallout.

The reverse procedure is equally useful; knowledge of the chemical or physical behavior of particles or of the fission-product elements as a function of their surface density can, through the contour ratios, be associated with the level of the radiation hazard. For example, decontamination data based on the mass of particles can be readily converted into reduction in radiation hazard by means of the contour ratio. Use of the contour ratios and their scaling functions allows extrapolation of a modest amount of experimental data to innumerable operational cases because the contour ratios are not constants; they are point functions whose value depends on many variables. Thus a single value of m_R, for example, may be associated with many values of $I_R(t)$.

The final use of the contour ratios is to permit estimates of m_R, n_{1p}, and FD to be made, for use in radiological countermeasure operations, from observations of $I_R(t)$. In such estimates, additional information is required, along with the value of $I_R(t)$, before a reliable estimate of the quantity of interest can be made. This particular use of the contour ratio may be the only method available for estimating one of the desired quantities when fallout areas are monitored with portable survey instruments. The additional information needed for these estimates is discussed in the following paragraphs.

6.2 Dependence of the Mass Contour Ratio on Detonation Conditions and Other Parameters

6.2.1 Dependence on Weapon Type and Yield

Because the mass contour ratio is inversely proportional to the specific activity of fallout, its value or range of values must depend on the amount of radioactive materials produced in the detonation. The fission product yield is proportional to BW where B is the ratio of fission to total yield; hence, for the usual amount of induced activities, the total area activity from Eq. 4.74, is

$$I_R(t)A_{rea} = 5.46\times10^{10}\left[r_R(1) + 0.010\right]BW \text{ r/hr at 1 hr-sq ft} \qquad (6.4)$$

where $r_R(1)$ is the gross ionization rate fractionation number at H+1 and 0.010 is the ratio of the ionization rate from a nominal yield of induced activities to that of the fission products (both at H+1). The multiplier, 5.46×10^{10} r/hr at

1 hr per KT/sq ft, contains an instrument response and a terrain roughness attenuation factor. The value of r_x (1) will vary with downwind distance, or particle size, as well as with time after detonation. The value of the ratio, 0.010, for the induced activities will depend on the construction materials of the weapon, the environmental elements at the point of detonation, and, to some degree, on the height of burst and on the values of B. For example, if B is very small (the definition of the so-called "clean" bomb), then the relative induced activity yield could be much higher than is indicated by the 0.010 of Eq. 6.4. Except for the possible dependence of r_x (1) and induced activity ratio on yield, the total area activity of Eq. 6.4 is directly proportional to W.

If it is assumed that the total crater mass becomes uniformly mixed with the radioactive material in the fallout formation, then the expected maximum value of M_r (1) should be given by $M_s/(I_x$ (1)xArea) which (from Eqs. 3.166 and 6.4) is

$$\overline{M_r(1)_{max}} = \frac{93.6W^{-0.083}}{\left[B\ r_x(1) + 0.019\right]} \frac{\text{mg/sq ft}}{\text{r/hr at 1 hr}} \qquad (6.5)$$

If, on the other hand, it is assumed that only the soil that is melted at 1400°C, as in the case of the ideal surface burst, becomes uniformly mixed with the radioactive elements, then only the mass equivalent of the n(ℓ) moles of liquid soil would be considered. The yield dependence of this quantity, from Table 2.18, can be represented by

$$n(\ell) = 1.92\times10^{11}\ W^{1.018}\ \text{mg soil} \qquad (6.6)$$

On the average, the mass represented by n(ℓ) should result in an expected minimum value of M_r (1), which is

$$\overline{M_r(1)_{min}} = \frac{3.52W^{0.018}}{B\left[r_x(1) + 0.019\right]} \frac{\text{mg/sq ft}}{\text{r/hr at 1 hr}} \qquad (6.7)$$

The two limiting values of M_r (1) indicate that (1) the dependence on the total yield should be rather small, (2) the values are inversely proportional to the fraction of fission yield of the detonation, and (3) the real values are most likely to be in the range 1 to 100 (mg/sq ft)/(r/hr at 1 hr) for B=1. With respect to the fraction of fission yield, B, the type of weapon is apparently a more important parameter in determining the value of M_r (1) than is the yield itself. Because both melted and unmelted particles are found in fallout, more soil is involved in the fallout formation process than is indicated by n(ℓ), but the amount involved should certainly be less than that removed from the whole (apparent) crater -- even for the larger yield where essentially no crater lip remains.

Actually, the values of M_r (1) show a tendency to decrease with yield that is more or less proportional to the apparent crater mass. Therefore, the crater mass per KT associated with fallout formation, $m(\sigma,W)$, is assumed to have the form

$$m(\sigma,W) = f(\sigma)W^{-0.083} \text{ mg/KT} \qquad (6.8)$$

where $f(\sigma)$ is the mass per kiloton of yield for each particle group to be evaluated from available measurements of M_r (1). With the assumed dependence of $m(\sigma,W)$ on yield, the relative abundance of melted particles increases with yield, since $n(\ell)$ increases with yield, and the average value of M_r (1) decreases with yield.

6.2.2 Dependence on Downwind Distance from Shot Point

The variation of M_r (1) with downwind distance from shot point is best considered in terms of the particle group size parameter, σ. To represent this dependence r_x (1) is redesignated r_σ (1) for evaluation as a function of both σ and the yield. Appropriate values of $r_\sigma(1)$ along with observed values of M_r (1) are then used to evaluate $f(\sigma)$.

In estimating r_σ (1), the assumption is made that an abundance of solid surface (as particles) is present in the rising fireball and cloud at all times to facilitate the condensation of the gaseous radioactive species. With this condition, the amounts of each element condensed during the second period of condensation may be estimated by the method outlined in Chapter 2. In the simple process where all the particles are present at the end of the first period of condensation, differences in the radioactive composition on the various particles at a later time can occur only if some of the particles are removed from the volume before further condensation occurs. The particles that remain in the volume the longest time, providing a large number are always present, will then condense more of the volatile radioactive elements. In the fallout formation process, where the larger particles are falling out or leaving the gas volume at earlier times, the fraction of total available activity that is condensed on particles of various sizes should increase with decreasing particle size. Hence the fraction of the total activity condensed up to a given time after detonation should be described by an accumulative distribution curve that increases to a stated amount for a given particle size, or σ value for a group of particles. Such a representation cannot consider discrete values of the fraction condensed for a given particle size but may be given in terms of an average value for each of the particle groups.

In the real process, unmelted and melted particles become mixed during the second period of condensation. Since the unmelted particles have entered the fireball after it has cooled below their melting point, they can only condense radioactive materials not previously condensed. However, since these unmelted particles fall in the same areas as the melted particles of the same fall vector, the over-all radioactive composition of the group should not be changed. The main effect of the presence of the unmelted particles in condensing some of the remaining volatile radioactive materials is to reduce the specific activity of the whole group of smaller particles.

The fraction that each nuclide of a mass chain condensed in the second period of condensation, $r_n(A)$, is estimated from

$$r_n'(A) = \frac{\Sigma_j N_j(A,t)k_j^n/(1+k_j^n)}{\Sigma_j N_j(A,t)} - \frac{V}{0.23RTBW} \frac{\Sigma_j N_j'(A,t')p_j^n/y_j'(t')}{\Sigma_j N_j'(A,t')} \quad (6.9)$$

in which the first term contains the parameter values for the first period of condensation (see Eq. 3.40); V is the fireball or cloud volume at t'; 0.23 is the number of fission-moles per atom-KT; $y_j(t')$ is the number of atoms per fission of element j that are present at t'; p_j^n is the sublimation pressure of element j; and $N_j'(A,t')$ is the number of atoms of each element of mass chain A per 10^4 fissions not condensed in the first period of condensation, decay-corrected to t'.

In other words, $p_j^n V/RT$ is the number of moles of element j in the vapor phase and $0.2813Wy_j'(t')$ is the total number of moles of the element produced and in existence at t'. The first term gives the fraction not condensed in the liquid particles during their existence, and the second term gives the fraction in the vapor state, the difference being the fraction condensed to the solid state on or in the solid particles by the sublimation process.

In making the computations for $r_n(A)$: the yields of 84-KT and 14-MT were selected since the $r_n(A)$ values were already available (see Table 3.15). The times of the beginning of the second period of condensation are 0 seconds and 60 seconds, respectively. The later times selected are 238 seconds and 406 seconds for the 84-KT yield, and 174 seconds and 406 seconds for the 14-MT yield. The mid-time points were derived in previous estimates of the time when the top of the cloud is near h-b for the respective yields the longer time for when the cloud is near full expansion. These relatively late times were selected to simplify the computations of $r_n(A)$; in both cases, the temperatures at the indicated times should be less than 300 to 350°K, at which time the second term of Eq. 6.9 is essentially zero for most fission product elements.

However, there are two general cases where the vapor pressures are still significant with respect to $r_0(A)$ values at these temperatures. The first is for the rare gas elements which are normal gases at these temperatures, and the second is for elements in very low abundance having slight vapor pressures at normal temperatures. For both yields, $V/0.23RT\dot{m}W$ (R 1) is about 3×10^{11} at the second altitude point; thus $p_j^*/y_j(t')$ values less than about 10^{-10} make the term negligible with respect to unity. The only elements indicating relative pressures larger than this, except the rare gases, are the oxides of Se and As; for these $p_j^*/y_j(t')$ values of 10^{-8} to 10^{-9} are obtained, indicating that they would be entirely in the vapor state (since $r_0(A)$ cannot have values less than zero). With these exceptions, Eq. 6.9, for the temperature conditions of the computations reduces to

$$r_0'(A) = 1 - r_0(A). \qquad (6.10)$$

For the rare gases, $r_0(A)$ is taken to be zero, although some fraction of these gases would surely be absorbed on the surfaces of the particles. In this case, it is assumed that the fraction would be small and that the rare gas atoms formed from precursors previously condensed on the surface of the particle would evaporate (those formed inside the particle are assumed to remain in the particle). The $r_0(A)$ values calculated for the indicated times and described conditions are summarized in Table 6.1.

The independent nuclide yield data for the calculations were read from plots of the atom-yields for each nuclide calculated by Bolles and Ballou[1] based on the Glendenin postulate, and a set of calculations for both U-235 fission (thermal-neutrons) and U-238 fission (8-Mev neutrons) was made. For U-238 fission, the calculations were carried out as described in Chapter 2. For U-235 fission, the nuclide fractionation numbers were multiplied by the air ionization rates per fission/sq ft at 3 feet above a uniformly contaminated plane, as tabulated by Miller and Loeb[2] at 45.8 minutes and 1.12 hour after fission, and then summed. The sums obtained by use of the $r_0(A)$ fractionation numbers were then added to each of the sums for the later times obtained by the respective $r_0(A)$ sets. These were then used to evaluate the constants of

$$I = I_0 t^{-n} \qquad (6.11)$$

were I_0 is the air ionization rate at R=1, t is the time in hours, and n is a constant applicable from 45.8 minutes to 1.12 hour. The results of the computations are shown in Table 6.2 along with the fraction of the ionization rate condensed up to the indicated times defined by the ratio, I_0 (condensed mixture) /I_0 (normal mixture), for r_0 (1).

Table 6.1

SUMMARY OF FISSION PRODUCT NUCLIDE $r_{\frac{1}{2}}(A)$ VALUES FOR 84-KT AND 14-MT YIELD SURFACE DETONATIONS

Nuclide	84-KT		14-MT	
	288ft	400ft	174ft	400ft
Ge-75	0.058	0.058	0.395	0.395
Ge_g-77	0.320	0.320	0.854	0.854
Ge-78	0.570	0.576	0.925	0.925
As-77	0.105	0.133	0.383	0.340
As-78	0.552	0.540	0.890	0.872
As-79	0.00124	0	0.00000	0
Se_1-81	0	0	0	0
Se_g-81	0	0	0	0
Se_1-83	0	0	0	0
Br-83	0.047	0.018	0.479	0.012
Br-84	0.742	0.805	0.920	0.800
Kr-83	0	0	0	0
Kr_1-85	0	0	0	0
Kr_g-85	0	0	0	0
Kr-87	0	0	0	0
Kr-88	0	0	0	0
Rb-86	0.0208	0.0310	0.0200	0.0322
Rb-89	0.588	0.752	0.487	0.748
Rb_g-91	0.071	0.071	0.050	0.050
Sr-89	0.012	0.780	0.500	0.773
Sr-90	0.002	0.008	0.817	0.809
Sr-91	0.803	0.803	0.740	0.740
Sr-92	0.005	0.005	0.070	0.070
Sr-93	0.202	0.202	0.002	0.002
Y-90	0.002	0.008	0.817	0.809
Y_1-91	0.803	0.803	0.740	0.740
Y_g-91	0.803	0.803	0.740	0.740
Y-92	0.002	0.002	0.075	0.075
Y-93	0.270	0.270	0.002	0.002
Y-94	0.060	0.060	0	0

Table 6.1 (continued)

Nuclide	84-KT		14-MT	
	208m	400m	174m	400m
Zr-95	0.011	0.011	0	0
Nb_1-95	0.011	0.011	0	0
Nb_2-95	0.011	0.011	0	0
Mo-99	0.043	0.043	0.230	0.230
Mo-101	0.489	0.489	0.970	0.970
Mo-102	0.691	0.691	0.995	0.995
Tc-99	0.043	0.043	0.230	0.230
Tc-101	0.487	0.487	0.939	0.939
Tc-102	0.650	0.650	0.920	0.920
Ru-103	0.047	0.047	0.404	0.404
Ru-105	0.475	0.475	0.890	0.890
Ru-106	0.550	0.550	0.979	0.979
Rh-103	0.047	0.047	0.404	0.404
Rh_1-105	0.475	0.475	0.889	0.889
Rh-106	0.550	0.550	0.979	0.979
Rh-107	0.607	0.607	0.853	0.853
Pd-109	0.591	0.591	0.991	0.991
Pd-111	0.169	0.169	0.992	0.992
Pd-112	0.087	0.087	0	0
Ag-109	0.591	0.591	0.991	0.991
Ag-111	0.169	0.169	0.994	0.994
Ag-112	0.086	0.086	0	0
Ag-113	0.032	0.032	0.939	0.939
Ag-115	0.030	0.030	0.974	0.974
Cd_1-115	0.037	0.037	0.995	0.995
Cd_2-115	0.037	0.037	0.995	0.995
Cd-117	0.153	0.153	0.932	0.932
Cd-118	0.257	0.257	0.747	0.747
Cd-120	0.066	0.066	0.910	0.910

Table 6.1 (continued)

Nuclide	84-KT		14-MT	
	238m	400m	174m	406m
In_1-115	0.030	0.030	0.074	0.074
In-117	0.150	0.150	0.501	0.501
In-118	0.257	0.257	0.747	0.747
In-119	0.080	0.080	0.715	0.715
In-120	0.048	0.048	0.850	0.850
Sn-121	0.016	0.016	0.182	0.182
Sn-123	0.077	0.077	0.011	0.011
Sn-125	0.131	0.131	0.004	0.004
Sn-126	0.041	0.041	0.004	0.004
Sn-127	0.007	0.007	0.004	0.004
Sb-125	0.131	0.131	0.004	0.004
Sb-126	0.055	0.055	0.020	0.020
Sb-127	0.056	0.056	0.059	0.059
Sb-128	0.450	0.450	0.067	0.067
Sb-129	0.704	0.704	0.082	0.082
Sb-131	0.013	0.013	0.080	0.080
Te_1-125	0.131	0.131	0.004	0.004
Te_1-127	0.056	0.056	0.059	0.059
Te_2-127	0.056	0.056	0.059	0.059
Te_1-129	0.704	0.704	0.082	0.082
Te_2-129	0.708	0.708	0.082	0.082
Te_1-131	0.010	0.010	0.084	0.084
Te_2-131	0.025	0.025	0.084	0.084
Te-132	0.004	0.004	0.088	0.088
Te_1-133	0.087	0.087	0.080	0.080
Te_2-133	0.089	0.089	0.088	0.088
Te-134	0.002	0.002	0.093	0.093
I-131	0.025	0.025	0.084	0.084
I-132	0.005	0.005	0.088	0.088
I-133	0.080	0.080	0.080	0.080
I-134	0.001	0.001	0.093	0.093
I-135	0.000	0.000	0.086	0.086

Table 0.1 (concluded)

Nuclide	84-KT		14-MT	
	208m	406m	174m	406m
Xe_1-131	0	0	0	0
Xe_1-133	0	0	0	0
Xe_2-133	0	0	0	0
Xe_1-135	0	0	0	0
Xe_2-135	0	0	0	0
Xe-138	0	0	0	0
Cs-137	0.475	0.677	0.909	0.678
Cs-138	0.207	0.285	0.0102	0.285
Cs-139	0.988	0.988	0.988	0.980
Ba-137	0.475	0.677	0.909	0.678
Ba-139	0.908	0.908	0.908	0.908
Ba-140	0.862	0.865	0.555	0.558
Ba-141	0.424	0.424	0.000	0.000
Ba-142	0.144	0.144	0	0
La-140	0.862	0.865	0.555	0.558
La-141	0.418	0.418	0.000	0.000
La-142	0.130	0.100	0	0
La-143	0.015	0.015	0	0
Ce-141	0.418	0.418	0.000	0.000
Ce-147	0.014	0.014	0	0
Pr-143	0.014	0.014	0	0

For all Nuclides not listed, $r_0'(A) = 0$, $r_0(A) = 1.0$

Table 6.2

EQUATION CONSTANTS FOR AIR IONIZATION RATES FROM 0.70 TO 1.12 HOURS AFTER FISSION AND FRACTION OF THE TOTAL IONIZATION RATE AT H+1 FROM FISSION PRODUCTS CONDENSED ON PARTICLES AT GIVEN TIMES AFTER DETONATION OF AN 84-KT AND A 14-MT YIELD LAND SURFACE BURST

Source of Fission Product Mixture	I_0 $\left(\frac{\text{r/hr at 1 hr}}{\text{fission/sq ft}}\right)$	n	$F_0(1)$
1. U-235 (thermal neutrons)			
Normal Fission Product Mixture	7.10×10^{-16}	1.108	1.00
84-KT, 0 sec	2.47×10^{-16}	1.301	0.345
84-KT, 238 sec	5.48×10^{-16}	1.133	0.766
84-KT, 406 sec	5.61×10^{-16}	1.139	0.784
14-MT, 00 sec	2.50×10^{-16}	1.280	0.349
14-MT, 174 sec	5.20×10^{-16}	1.145	0.733
14-MT, 400 sec	5.61×10^{-16}	1.139	0.784
2. U-238 (8-Mev neutrons)			
Normal Fission Product Mixture	6.90×10^{-16}	1.084	1.00
84-KT, 0 sec	2.57×10^{-16}	1.307	0.360
84-KT, 238 sec	5.57×10^{-16}	1.157	0.800
84-KT, 406 sec	5.68×10^{-16}	1.163	0.816
14-MT, 00 sec	2.40×10^{-16}	1.301	0.349
14-MT, 174 sec	5.32×10^{-16}	1.161	0.764
14-MT, 406 sec	5.64×10^{-16}	1.169	0.810

Two rather significant conclusions about the radioactive compositions of fallout are indicated by the results of the computations (providing the assumptions used in setting up the calculation were not inappropriate). The first conclusion is that no large effect of yield is indicated, either for the gross fraction of the ionization rate (or of the number of fission product atoms) condensed in the liquid particles or for the total fraction condensed at a given later time. The second conclusion is that in local fallout the gross fraction of the ionization rate at 1 hour has a maximum value of about 0.8, since most of the particles falling in the local regions will have left the gas cloud by 400 seconds (6.8 minutes). The values of n vary from about 1.1 to 1.4; however, these n values apply only to the short time interval, 0.70 to 1.12 hours, without consideration of induced activities. The differences in the values in Table 6.2 between the two fissile nuclides are rather small.

The calculated ionization rates for the U-238 fission (8 Mev neutrons) are summarized in Table 6.3, and those for the 14-MT yield are plotted as a function of time after detonation in Figure 6.1. The values for the 0 second (84-KT) and 60 second (14-MT) condensations that were given in Chapter 2 are included for comparison. It may be noted that the mid-times selected (288 and 174 seconds) are not particularly good choices for obtaining differences in the decay curves as a function of condensation times. However, the differences shown between the mid-times and 400 seconds are mainly due to the net gain in condensed rare gas daughter products on the particle surfaces for the indicated time interval; this gain is rather small for both yields.

The fractionation numbers relative to the ionization rate from the normal fission-product mixture from thermal neutron fission of U-235 are given in Table 6.4 for the condensations at the end of the first period of condensation and at 400 seconds. The fractionation numbers in the table are not the ones applicable to $r_\alpha(t)$ because they include differences due to fission yields. The values of the fractionation numbers, however, do show that the fractionation number can vary by a factor or two or more during the second period of condensation (i.e., as a function of particle size) and can also vary with time after detonation, depending on the relative abundances of the condensed radionuclides.

In all cases, the computations of the particle sizes, or the a values, from the simple fallout scaling system based on the particle group fall-times, when compared with fractionation data of different particle groups of fallout from test devices of various yields, indicated that a time delay of considerable length must be taken into account before the computed $r_\alpha(1)$ values agree with the observed values. This time delay may be associated with the air circulation, presumably toroidal, in and about the rising cloud.

In this type of circulation (as discussed in Chapter 5), the particles entering the bottom of the cloud (or those within the volume when the circulation begins) apparently condense out gaseous radioactive elements and small previously condensed particles as they sweep through the gas volume. The larger particles circulate to the edge of the cloud, are accelerated downward and then continue to fall when the pull of gravity exceeds the upward force of the air circulating back into the bottom center of the fireball. In a circulation of this general type, the condensations that occurred at a given time in the central region of the circulation would be in evidence on particles whose apparent exit time, based on free fall from the bottom of the cloud, is much later.

From the few data of Chapter 2 and the tower shot data of Reference 5, the best agreement between the calculated and observed $r_\alpha(1)$ values and the observed time of arrival of a given particle size group is obtained by using a delay-time of about 180 seconds together with the apparent rate of rise scaling

Table 6.8

CALCULATED IONIZATION RATES OF CONDENSED FISSION PRODUCT MIXTURES FROM U-238 (8-Mev NEUTRONS) FISSION AT SELECTED CONDENSATION TIMES[a]

Time After Detonation			84-KT			14-MT		
Years	Days	Hours	0 sec	208 sec	400 sec	60 sec	174 sec	400 sec
		0.760	0.71	7.00	7.77	0.45	7.30	7.78
		1.12	2.30	4.05	5.00	2.10	4.65	4.94
		1.04	1.10	2.09	3.04	1.18	2.85	3.00
		2.40	0.642	1.79	1.81	0.807	1.72	1.79
		3.72	0.393	1.07	1.08	0.420	1.04	1.06
		5.10	0.274	0.753	0.754	0.313	0.742	0.745
		7.50	0.197	0.422	0.422	0.201	0.417	0.417
		11.1	0.107	0.280	0.280	0.101	0.282	0.283
		16.2	(1) 890[b]	0.180	0.180	0.102	0.180	0.180
		23.8	(1) 544	0.107	0.107	(1) 580	0.107	0.107
	1.45	34.8	(1) 333	(1) 930	(1) 930	(1) 307	(1) 920	(1) 920
	2.13	51.1	(1) 180	(1) 954	(1) 954	(1) 180	(1) 953	(1) 953
	3.12	74.9	(2) 965	(1) 920	(1) 920	(1) 103	(1) 220	(1) 221
	4.67	109.7	(2) 500	(1) 140	(1) 140	(2) 501	(1) 143	(1) 143
	6.70	161	(2) 200	(2) 940	(2) 949	(2) 958	(2) 947	(2) 948
	9.82	236	(2) 102	(2) 942	(2) 942	(2) 950	(2) 940	(2) 940
	14.4	346	(2) 110	(2) 427	(2) 427	(2) 101	(2) 427	(2) 427
	21.1	506	(3) 925	(2) 280	(2) 280	(2) 141	(2) 280	(2) 281
	30.9	742	(3) 630	(2) 178	(2) 178	(2) 100	(2) 177	(2) 177
	45.3	1087	(3) 408	(2) 106	(1) 106	(3) 978	(2) 105	(2) 105
	66.4	1594	(3) 267	(3) 611	(3) 611	(3) 455	(3) 610	(3) 611
	97.3	2335	(3) 200	(3) 378	(3) 378	(3) 311	(3) 378	(3) 378
	143	3430	(3) 198	(3) 230	(3) 231	(3) 200	(3) 230	(3) 230
	208	4990	(3) 110	(3) 135	(3) 135	(3) 107	(3) 135	(3) 135
	301	7230	(4) 470	(4) 805	(4) 805	(4) 408	(4) 802	(4) 800
1.20	438	10520	(4) 170	(4) 333	(4) 331	(4) 139	(4) 331	(4) 334
1.78	650	15600	(5) 977	(5) 559	(5) 560	(5) 810	(5) 548	(5) 550
2.60	940	22,780	(5) 370	(5) 518	(5) 520	(5) 138	(5) 508	(5) 540
3.80	1387	33,000	(5) 130	(5) 309	(5) 280	(6) 500	(5) 288	(5) 280
5.58	2027	48,000	(6) 575	(5) 154	(5) 154	(6) 284	(5) 120	(5) 150
8.18	2980	71,700	(6) 202	(6) 802	(5) 102	(6) 101	(5) 702	(5) 102
12.0			(6) 104	(6) 954	(6) 999	(6) 111	(6) 500	(6) 998
17.6			(6) 108	(6) 508	(6) 605	(7) 807	(6) 454	(6) 604
25.7			(7) 000	(6) 488	(6) 500	(7) 807	(6) 355	(6) 561

a. Values are for air ionization rates in 10^{-16} r/hr per fission/sq ft at 3 ft above a smooth ideal plane uniformly contaminated with the mixture.

b. Number in parentheses is the number of zeros between the decimal point and first digit.

Figure 6.1
CALCULATED IONIZATION RATE AS A FUNCTION OF TIME AFTER DETONATION FOR ASSUMED CONDENSATIONS UP TO 60, 174, AND 496 SECONDS AFTER FISSION OF FISSION PRODUCTS FROM 8-Mev NEUTRON FISSION OF U-238 AND AN ASSUMED SURFACE BURST TOTAL YIELD OF 14-MT

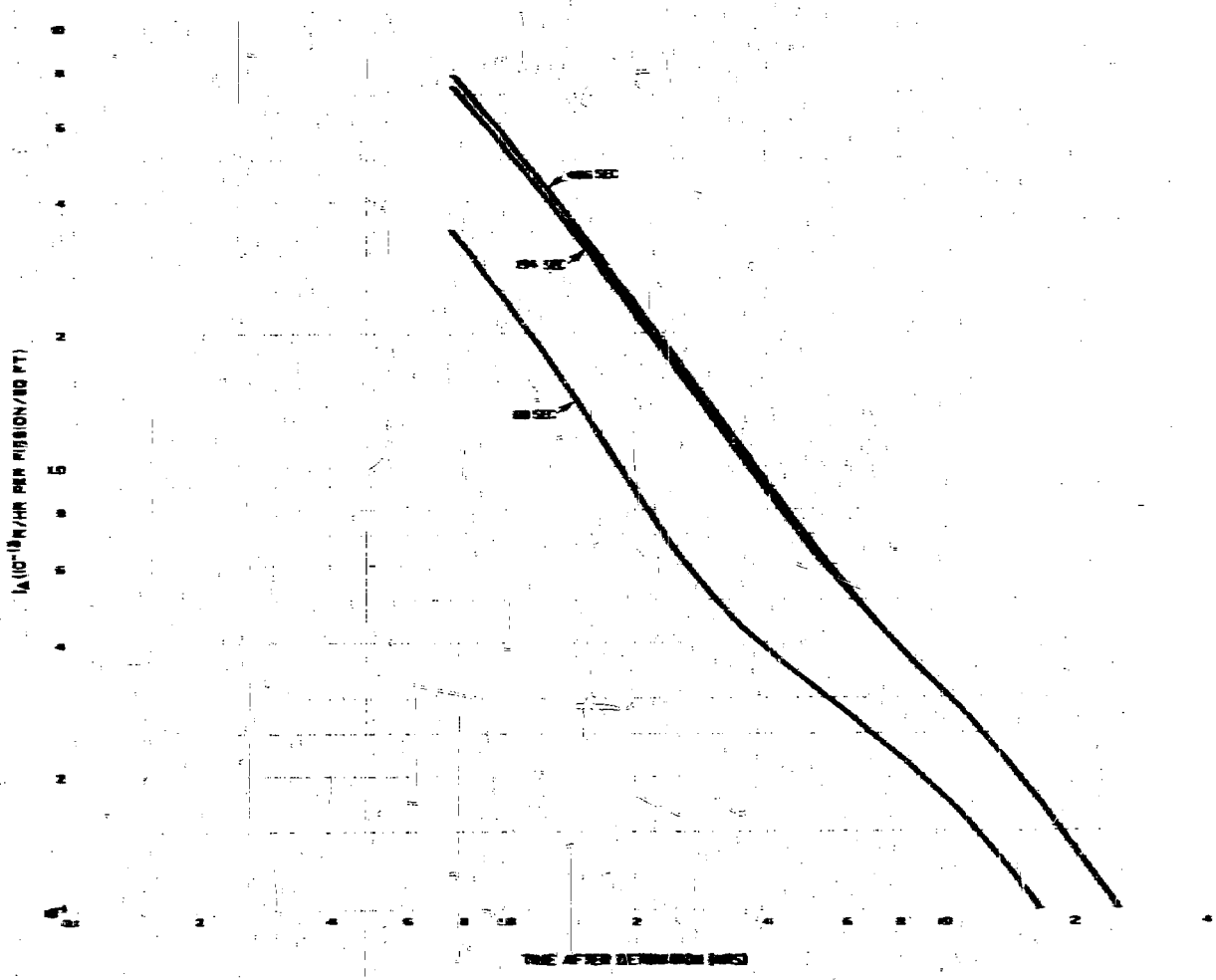

Figure 6.1 (continued)

Figure 6.1 (continued)

Figure 6.1 (concluded)

Table 6.4

FRACTIONATION NUMBERS FOR U-238 (8 Mev NEUTRONS) FISSION PRODUCTS RELATIVE TO THE NORMAL MIXTURE OF U-235 (THERMAL NEUTRONS) FISSION PRODUCTS AS CALCULATED FOR THE END OF THE FIRST PERIOD OF CONDENSATION AND AT 400 SEC AFTER DETONATION

Time After Detonation			84-KT		14-MT	
Years	Days	Hours	0 Sec	400 Sec	00 Sec	400 Sec
		0.703	0.372	0.778	0.040	0.774
		1.12	0.301	0.761	0.010	0.748
		1.64	0.287	0.750	0.284	0.740
		2.40	0.282	0.730	0.272	0.730
		3.52	0.279	0.705	0.304	0.752
		5.16	0.330	0.810	0.388	0.798
		7.56	0.412	0.882	0.486	0.872
		11.1	0.462	0.955	0.548	0.952
		16.2	0.400	1.00	0.505	1.00
		23.8	0.500	1.10	0.607	1.10
	1.45	34.8	0.512	0.984	0.535	0.984
	2.13	51.1	0.401	0.976	0.507	0.974
	3.12	74.9	0.424	0.956	0.453	0.971
	4.57	109.7	0.339	0.964	0.398	0.964
	6.70	161.	0.260	0.949	0.308	0.948
	9.82	236.	0.200	0.948	0.382	0.945
	14.4	346.	0.245	0.951	0.420	0.951
	21.1	506.	0.280	0.962	0.485	0.966
	30.9	742.	0.352	0.982	0.551	0.970
	45.3	1,087.	0.400	1.000	0.600	0.000
	66.4	1,594.	0.600	1.000	0.702	1.000
	97.3	2,335.	0.708	1.015	0.840	1.015
	143.	3,430.	0.910	1.000	0.922	1.000
	208.	4,990.	0.921	1.047	0.800	1.047
	301.	7,220.	0.962	1.150	0.808	1.101
1.20	438.	10,520.	1.215	1.052	0.922	1.001
1.78	650.	15,600.	1.480	2.522	0.821	2.522
2.60	940.	22,780.	1.075	2.655	0.630	2.660
3.80	1387.	33,300.	0.921	2.000	0.415	2.000
5.58	2037.	48,900.	0.498	1.334	0.240	1.325
8.18	2986.	71,700.	0.285	0.904	0.157	0.904
12.0			0.200	0.870	0.118	0.878
17.6			0.100	0.835	0.007	0.834
25.7			0.130	0.784	0.085	0.781

functions of the simple fallout scaling system. It might be expected that the delay-time should be dependent on both yield and particle-size (or on the true time after burst), but no reliable trends with these variables could be established with the few unclassified data available. Therefore, the same time-delay is used to estimate all the 15 mph σ values for each of the condensation times of Table 6.1. The calculations of the σ values corresponding to the particle groups leaving the fireball or cloud at the selected times, for the 180 second delay time, are shown in Table 6.5.

Table 6.5

COMPUTATION OF PARTICLE SIZE PARAMETERS FOR VARIOUS CONDENSATION TIMES OF THE 84-KT AND 14-MT YIELD LAND SURFACE DETONATIONS

Time (sec)	z (ft)	$\dot{z}$ (ft/sec)	v_t (ft/sec)	σ
1. 84-KT, $z_0 = 2.18 \times 10^4$ ft				
9	1.01×10^4	50.0	26.2	0.84
208	2.16×10^4	2.45	2.08	10.0
406	2.18×10^4	0.382	0.325	67.6
2. 14-MT, $z_0 = 4.09 \times 10^4$ ft				
60	3.80×10^4	32.1	24.3	0.92
174	4.01×10^4	0.18	0.75	5.26
406	4.00×10^4	0.710	0.524	42.0

The r_σ (1) values are plotted as an accumulated distribution curve, as a function of σ, in Figure 6.2; the dotted line applies to sea water fallout (see Subsection 6.2.4). The slope of the curve for σ values between 0.5 and 2.0 was determined with the aid of some observed fractionation data on several single nuclides relative to Zr-95 and Ce-144. A single curve was drawn through the points to indicate that, within the uncertainties in the calculations and data, no real differences in the function have been established to make certain that the small differences are due only to yield. As can be seen, the curve appears to approach a value of about 80 percent of the r/hr at 1 hr condensed, for σ values in excess of 100.

Figure 6.2
ESTIMATED PERCENT OF THE FISSION PRODUCT ACTIVITY IN 1 hr AT 1 HR FROM THE FISSION PRODUCTS CONDENSED ON PARTICLE GROUPS WITH α VALUES (15 MPH Wind Speed) LESS THAN A STATED VALUE

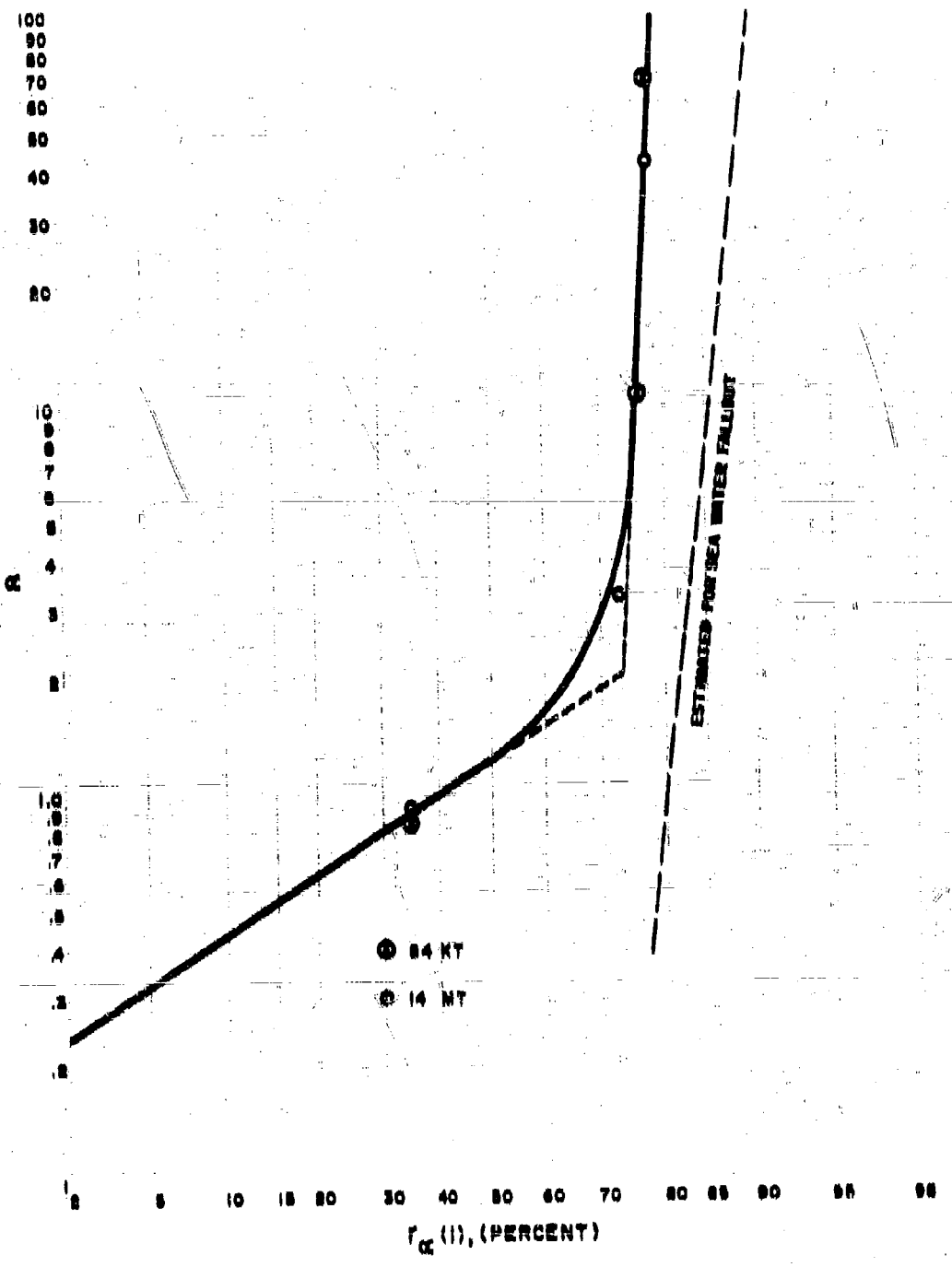

The concept of the accumulated distribution curve for the fraction of the total radionuclides condensed up to a given time as a function of the particle groups still present in the volume is a valid one, irrespective of the accuracy with which it can be calculated by using the thermodynamic data and the dynamic aspects of the fallout model. The use of the distribution curve in a precise way, however, requires information about the number distribution of the particles with respect to both their sizes and the fraction of the activity that is carried away by each size group. Details of this nature still need to be worked out before satisfactory estimates can be made; for example, of the fraction of I-131 or Sr-90 that is fused inside of particles of a given size and the fraction that is condensed on their exteriors. The amount or fraction of each nuclide on the smaller particles depends on the fraction of the chain in question that is carried away by the larger particles.

In the following treatments of the data in which the distribution curve is used, no account is made of the fraction of the activity (in terms of r/hr at 1 hr) that is carried away by the larger particles. The implied assumption is that the effect is small, due to the large abundance of smaller particles relative to the larger ones. For the gross ionization rates, this assumption may not involve very large errors, simply because the limit of the fraction condensed increases rapidly to about 70 percent and never increases beyond about 80 percent for the small-particle sizes of interest. But even if this is the case, and the effect is small, further study is needed of the relationships mentioned above, to estimate the fate of single radionuclides.

The curve of Figure 6.8 was used in conjunction with some observed M_r (1) values from Operation Jangle Shot "S"[4] to establish the dependence of $f(\alpha)$ on α. The calculation of the values of $f(\alpha)$ from the data is presented in Table 6.6; the values were obtained from

$$f(\alpha) = 5.46 \times 10^{10} \left| r_{\alpha}(1) + 0.019 \right| \quad M_r\,(1)\, W^{0.083} , \quad (6.12)$$

The fallout collectors nearest shot point collected considerable amounts of debris and dust from the desert, kicked up in the vicinity of the collectors by the blast wave. This extraneous dirt accounts for the exceedingly high observed $f(\alpha)$ values at those locations. Although it is likely that all the recovered samples contained some extraneous dust, the amount collected should have decreased with distance from shot point. Since this source of dust would not contribute to the fallout in other less desert-like regions, nor at the same relative distances from large yield detonations, it would be desirable to eliminate its contribution to $f(\alpha)$; unfortunately, there are no means for estimating the amounts of extraneous debris in the samples and for correcting the total mass to the mass of "pure" fallout.

Table 6.6

CALCULATION OF $f(\alpha)$ FROM $M_r(1)$ DATA FROM OPERATION JANGLE SHOT "S"

X (ft)	$M_r(1)$ $\left(\frac{\text{mg/sq ft}}{\text{r/hr at 1 hr}}\right)$	α_{min}	α_{max}	$\bar{\alpha}$	$r_\alpha(1)$	$(r_\alpha(1)+0.010)$	$f(\alpha)$ (mg/KT)
280	24,000	0.382	0.474	0.428	0.100	0.110	1.31×10^{14}
860	815	0.415	0.625	0.550	0.550	0.100	7.00×10^{12}
1,110	155	0.516	0.680	0.598	0.100	0.200	1.77×10^{12}
1,720	105	0.620	0.800	0.710	0.256	0.272	1.50×10^{12}
1,940	505	0.685	0.860	0.750	0.280	0.200	0.22×10^{12}
2,600	22.5	0.770	1.00	0.885	0.345	0.804	4.47×10^{11}
2,820	22.0	0.804	1.04	0.922	0.302	0.381	4.70×10^{11}
3,040	47.8	0.85	1.09	0.970	0.387	0.406	10.0×10^{11}
3,480	31.8	0.924	1.18	1.052	0.480	0.449	7.80×10^{11}
3,600	26.0	0.96	1.23	1.005	0.448	0.407	6.38×10^{11}
5,010	37.1	1.00	1.27	1.135	0.470	0.470	9.00×10^{11}
7,400	17.3	1.60	1.98	1.805	0.025	0.044	6.08×10^{11}
9,120	17.8	1.94	2.22	2.130	0.687	0.070	6.89×10^{11}
12,000	13.6	2.60	3.00	2.80	0.000	0.714	5.00×10^{11}

The variation of the function, $f(\alpha)$, with α can be indicated in a very general sort of way by making an analogy between what may occur in the fallout formation process to what should occur in an idealized condensing system. If the idealized system consists of a group of suspended drops in equilibrium with a dissolved gas, the concentration of the condensing gas should be the same in all particles whose diameter is larger than a few tenths of a micron. For these particles, the concentration is independent of the particle diameter and, therefore, independent of the parameter, α.

In a system where the particles are rapidly heated and cooled over a short period of time, only the surface of the particles having diameters larger than the same size will be melted; these larger particles should, in a given period of time, condense amounts of vapor that are proportional to their surface area or to the square of their diameters. The same result should occur for particles of all sizes that do not melt at all. If the particles are very large, only part of the surface may be melted (see discussion in Chapter 2); the amount that is condensed will not be proportional to their surface area.

Thus, in an ideal system where particles are exposed for the given period of time to a uniform concentration of condensing gas, the ratio of the particle mass to the amount condensed on each particle (m/a) should: (1) remain constant for smaller liquid particles; (2) be proportional to the particle diameter, d, for the larger surface-melted particles and for all solid particles, and (3) increase more rapidly than the particle diameter for very large partially-melted particles.

However, in the fallout formation process some of the smaller liquid particles can remain in the gas volume after they solidify, and condense material on their surfaces in addition to that contained in their volumes; these particles could carry more activity than would be indicated by (1) above. Smaller particles, with diameter less than about 80 microns, have terminal fall velocities proportional to the square of their diameter (Stokes' law). For These, the particle diameter is proportional to $\sqrt{v_w/\alpha}$. Hence, for a mixture of small spherical (previously melted) and irregular particles, the ratio, (m/a), should not decrease with α more rapidly than does $1/\sqrt{\alpha}$. If the amount of small unmelted particles that enter the cloud at late times is large, it would be possible for the average value of (m/a) actually to increase with α. For particles with diameters from about 80 to 1000 microns that have fall velocities roughly proportional to their diameter, their diameters are proportional to v_w/α. The dependence of the ratio, (m/a), for these particles on α should lie between being proportional to α and $1/\alpha$.

If $f(\alpha)$ roughly follows this admixture of behaviors, it should decrease very rapidly with α at low values of α; also, its rate of decrease with α should also decrease with the value of α. At high values of α, $f(\alpha)$ may decrease slowly with α, have a constant value, or even pass through a minimum and increase again.

In Figure 6.3 a proposed curve for the variation of $f(\alpha)$ with α is shown; it is based mainly on the Jangle "S" data. The slope of the curve from α=0.1 to 0.9 was determined with the aid of single-particle activity data of fallout from low tower detonations where the specific activity was roughly proportional to the diameter of the particles and, for larger sizes comparable to α values less than 0.1, increased less and less rapidly with size. The line from α= 0.9 to 20 was based on a geometric mean value of the plotted data in the range α= 0.88 to 2.8, and on several values of M_r (1) from higher yield detonations which, when corrected by use of Eq. 6.12, gave a mean value of $f(\alpha)$ of 1×10^{11} and an average α value of 20. No data were available for estimating $f(\alpha)$ at α values larger than 20; hence a constant value of 1×10^{11} was assumed for α values larger than 20.

The lack of available data for establishing more accurate values of $f(\alpha)$ at the higher α values is not of too much concern for many uses of $f(\alpha)$ because of the lower levels of fallout that are associated with the smaller particles. This lack of data is of much more concern in evaluating the longer-

Figure 6.3
PROPOSED CURVE FOR THE VARIATION OF f(x) WITH x FOR A 15-MPH WIND SPEED

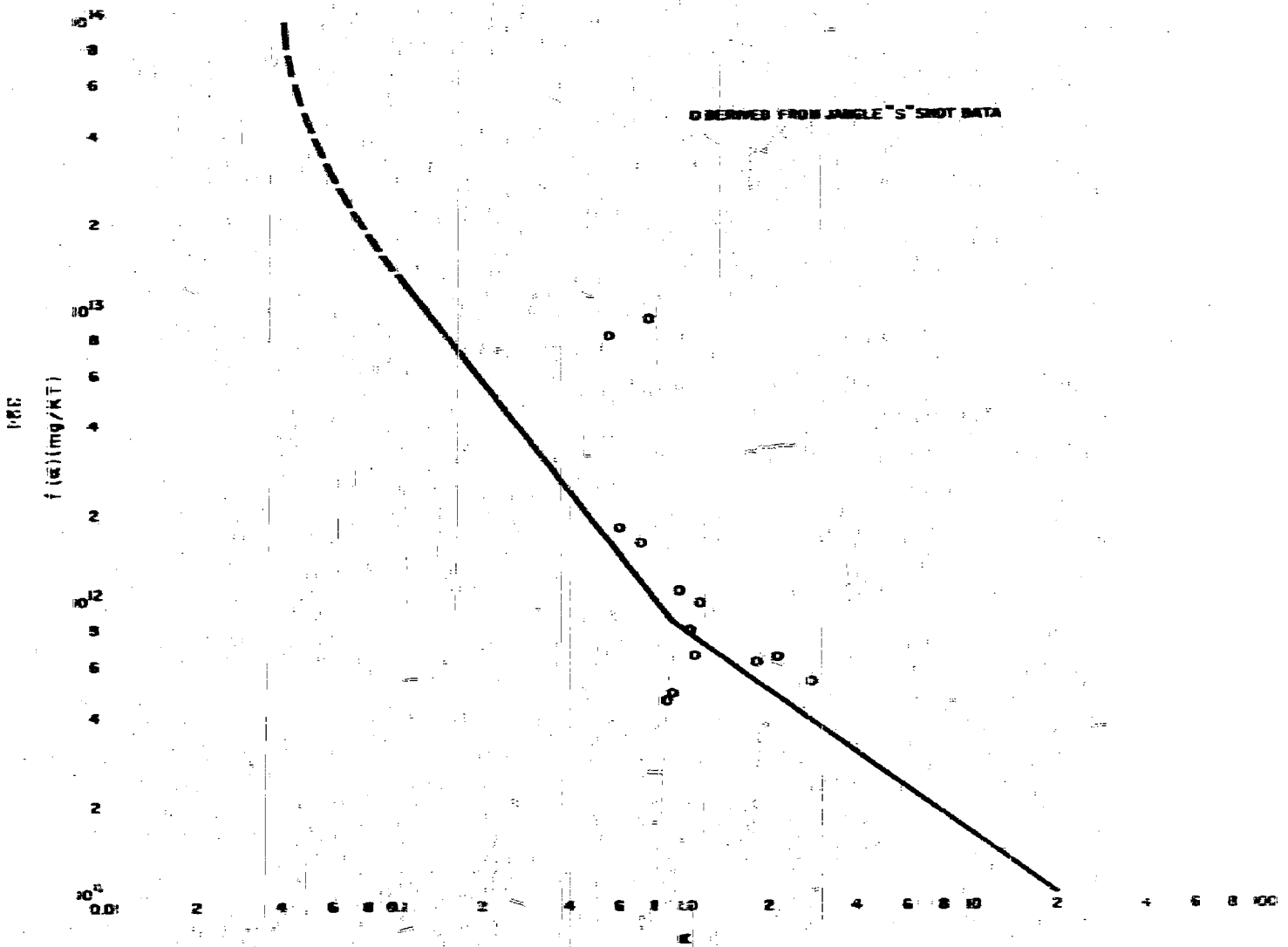

term hazards that are associated with the uptake of certain long-lived radioelements by plants and animals, since much of the surface-condensed, biologically available elements will be carried by the smaller particles.

The mathematical expressions for portions of the proposed function for $f(\alpha)$ are

$$f(\alpha) = 7.46\times10^{11}\ \alpha^{-1.25}\ \text{mg/KT, or} = 5.33\times10^{-19}\ \alpha^{-1.25}\ \text{mg/fission},\quad \alpha = 0.1 \text{ to } 0.9 \tag{6.13}$$

and

$$f(\alpha) = 7.90\times10^{11}\ \alpha^{-0.690}\ \text{mg/KT, or} = 5.64\times10^{-19}\alpha^{-0.690}\ \text{mg/fission},\quad \alpha = 0.9 \text{ to } 20 \tag{6.14}$$

$$f(\alpha) = 1.0\times10^{11}\ \text{mg/KT, or} = 7.14\times10^{-19}\ \text{mg/fission},\quad \alpha < 20 \tag{6.15}$$

in which the wind speed associated with the α values is approximately 15 mph.

The general equation for estimating $M_r(1)$ for a land surface burst, from the above treatment of the data, is

$$M_r(1) = \frac{f(\alpha)W^{-0.083}}{D(1)q_x B\left[r_\alpha(1)I_{fp}(1) + I_i(1)\right]} \tag{6.16}$$

in which $f(\alpha)$ is the ideal (or unfractioned) inverse specific activity in mg/fission, $D(1)$ is an instrument response factor, q_x is the terrain attenuation factor, B is the ratio of fission to total yield, $r_\alpha(1)$ is the gross fission-product ionization rate fractionation number at H+1, $I_{fp}(1)$ is the true air ionization rate at H+1 at 3 feet above an ideal plane uniformly contaminated with the radionuclides from a normal (unfractionated) mixture of fission products at a surface density equivalent to one fission per sq ft, and $I_i(1)$ is the true air ionization rate per fission contributed by induced activities.

By substituting 0.75 for $D(1)$, 0.75 for q_x, 0.04×10^{-13} (r/hr at 1 hr)/(fission/sq ft) for I_{fp} (1), and 0.13×10^{-13} (r/hr at 1 hr) (fission/sq ft) for I_i (1), the mass contour scaling function for the land surface burst is

$$M_r(1) = \frac{1.83\times10^{11}\ f(\alpha)W^{-0.083}}{B\left[r_\alpha(1) + 0.019\right]}\ \frac{\text{mg/sq ft}}{\text{r/hr at 1 hr}} \tag{6.17}$$

6.2.3 Dependence on Height or Depth of Burst

When an explosive charge is detonated below the surface of the ground, the apparent crater volume increases in size until a maximum amount of soil is thrown out. As the charge depth increases beyond this point, the amount of soil thrown out begins to diminish and, at some depth, the explosive force is no longer sufficient to break through the surface of the ground. When the height of burst is increased, the apparent crater from the explosion rapidly decreases until no crater is formed.

However, in nuclear explosions, the updraft of air following the rising fireball usually forms a column of loosened soil particles even when no real crater is formed. The height of burst at which the local fallout becomes insignificant occurs for detonations in which the rising dust column just fails to catch up with the rising cloud. Instead of specifying the requirement for entrainment of soil particles to form fallout, ENW gives a fireball radius of $180W^{0.4}$ feet as the minimum height of burst for negligible fallout; this height is supposedly associated with the height for contact of the fireball with the earth's surface.

Since the gross specific activity of the fallout for surface detonations has been found to be more or less proportional to the mass of soil removed from the crater, it seems that the same trend should occur with change of depth or height of burst. Thus, the value of $M_r(1)$ is expected to increase with depth of burst and decrease with height of burst, at least if the depths and/or heights of burst are not large. As the depth of burst becomes very large, only a small amount of activity should escape with most of the radioactivity remaining in or beneath the crater; that which does escape is on very small particles which could be dispersed over relatively large areas, so that no high levels of fallout would occur. However, the specific activity of those very small particles may still be higher than it is for the particles from detonations at intermediate depths.

As the height of burst is increased (by small distances) the smaller amounts of loosened (or melted) soil particles would result in increases in the specific activity of the fallout. However, as the height of burst becomes large, the size of the particles that can actually enter the cloud decreases. Since those that enter do so at later times (because of the height involved), and since, by this time, the concentration of the condensing radioactivity has decreased, due to both expansion of the cloud and depletion by vapor condensation to form very small solid particles, the amount of radioactivity collected by each soil particle that enters the fireball or rising cloud should be small. Therefore the specific activity of particles in the fallout should first increase and then decrease as the height of burst increases.

A proposed curve for a mass correction to M_r (1) is shown in Figure 6.4 in which the mass-correction factor, K_λ, is defined by

$$M_r^\lambda(1) = M_r(1)/K_\lambda \tag{6.18}$$

where $M_r^\lambda(1)$ is the mass contour ratio at the nuclear-scaled depth given by

$$\lambda_N = h/W^{1/3} \tag{6.19}$$

and h is the depth of burst (-h is the height of burst) and W is the total yield in KT rather than in pounds of TNT as usually defined.

The point at $K_\lambda = 0.3$ was obtained, from the M_r (1) data of Reference 4 for the Operation Jangle "U" shot, by comparing the measured values with those from the Jangle "S" shot at the same downwind distance. At the larger heights of burst one of the two points was derived from the specific activity and contour ratio data of fallout from a tower detonation; the other point was derived from the specific activity data of fallout from a balloon detonation. The values of K_λ are ratios of the average values of M_r^λ (1) in each case. The remainder of the curve was determined from high-explosive crater-volume data.

In using the proposed curve, the assumption is implied that the crater volume or mass that forms fallout varies as $W^{0.817}$ for all heights and depths of burst represented by the curve. This assumption is valid, within the accuracy of most crater data, for a fairly wide variation in soil type media, and for λ_N values between about -100 and +75. In estimating M_r^λ(1) for a low air-burst or shallow underground-burst, M_r (1) at selected values of the downwind distance is to be computed for the same yield surface burst and then corrected by use of Eq. 6.18. This procedure is indicated because K_λ was determined by comparison to the M_r (1) values at the same downwind distances. However, without methods for correcting the fallout contours themselves for height or depth of burst, the contour ratio M_r^λ (1), is of less immediate general use than M_r (1).

6.2.4 Mass Contour Ratio for Fallout from a Surface Detonation on Deep Sea Water

No unclassified data are available from which M_r (1) for sea water detonations can be computed; however, rough estimates may be made, using the data in ENW, if it is assumed that (1) the mass of water thrown up is proportional to the yield, (2) K_λ holds for a detonation in water as well as in soil, and (3) fractional mixing of the environmental materials and fission

Figure 6.4
PROPOSED MASS CORRECTION CURVE TO THE MASS CONTOUR RATIO AS A FUNCTION OF THE NUCLEAR SCALED DEPTH OF BURST

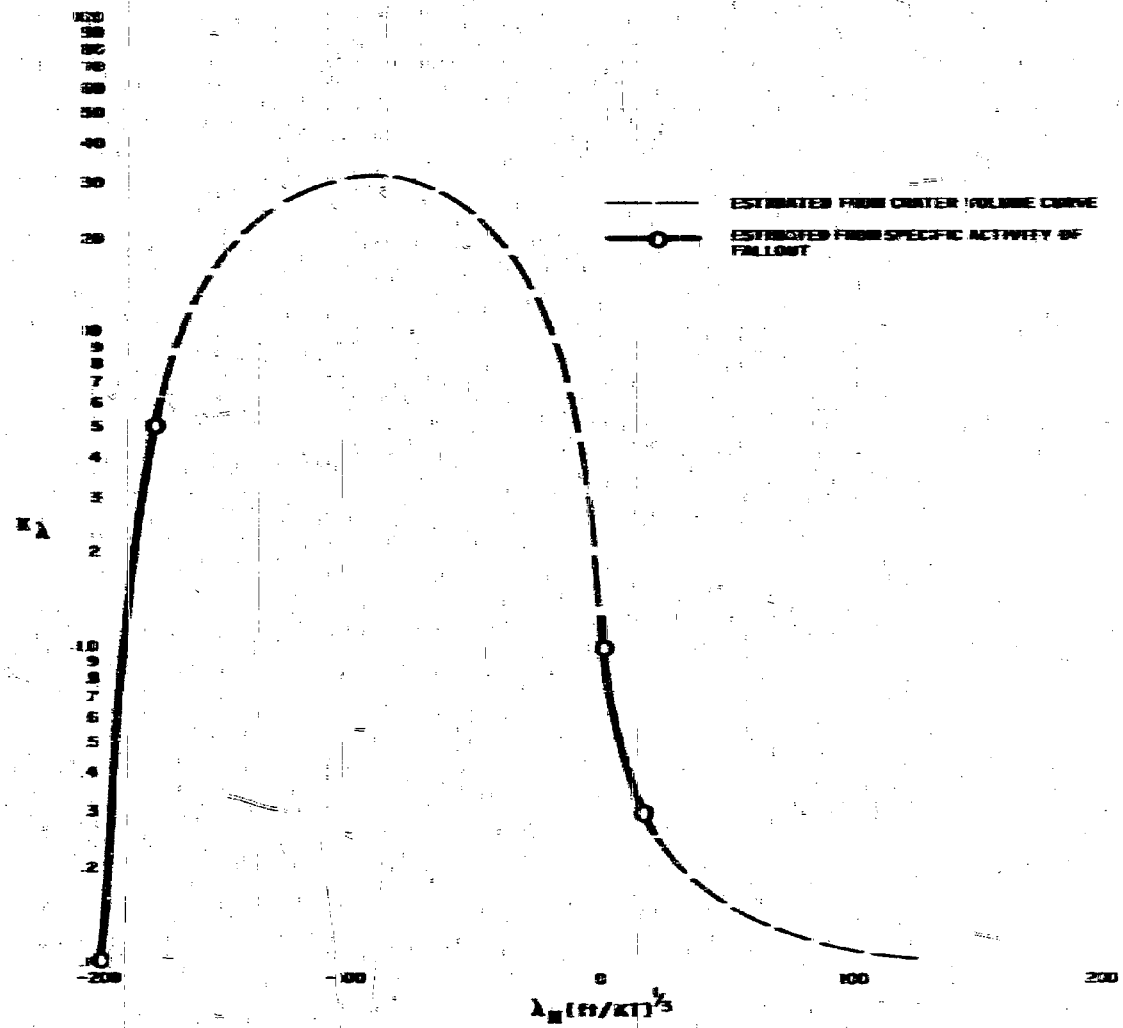

products is larger for a water shot. In ENW, p. 45, it is estimated that approximately 10^9 tons of water were ejected into the air by the 20-KT Bikini Baker detonation. This is equivalent to 4.5×10^{13} mg/KT. Taking the depth of burst as approximately half the depth of the lagoon, K_λ is about 0.21. Therefore, the amount of water thrown up for a sea water surface detonation may be approximated by

$$M_w = 9.6\times10^{12}\ W \text{ mg sea water.} \tag{0.20}$$

If α_γ is used to estimate an average value of $f(\alpha)$ for the fallout from a land-surface detonation, the fractional mixing of the soil can be estimated from $f(\alpha)/M_c$ which, from Figure 6.3 and Eq. 3.100, is found to be approximately given by $0.14W^{-0.014}$, or about 10 to 14 percent of the total soil thrown out of the crater. For the surface water burst, the fractional mixing was assumed to be about 50 percent of the water thrown up or about 3 to 5 times larger than that of the surface land detonations.

Because the end of the first period of condensation for a water shot occurs at about 0°C, very little fractionation of the fission products (with possible exception of the rare gas elements) should occur, especially for the larger yield detonations. This longer period of condensation for the water before the final sea water fallout particles are formed by vapor condensation should result in more thorough mixing of the water and the fission products, as well as in rather uniform concentrations of the radioactive elements in all fallout particles or drops. For these reasons, $f'(\alpha)$ for the water shots was taken to be independent of α, or droplet size, and equal to 4.5×10^{12} mg/KT or 8.4×10^{11} mg/fission. The mass contour ratio, in terms of the mass of original sea water, is then

$$M_r(1) = \frac{3.4\times10^{-11}}{D(1)q_{1k}\ B\left[t_{fp}(1)+t_i(1)\right]}\ \frac{\text{mg sea water/sq ft}}{\text{r/hr at 1 hr}} \tag{0.21}$$

where no fractionation of the radionuclides in the fallout is assumed.

The no-fractionation assumption is essentially valid for yields greater than about 5-MT. For lower yields than this, a gross estimate of the gross fractionation number for a surface water detonation, $r'_\alpha(1)$, can be made from a log-normal distribution curve of $r'_\alpha(1)$ in which the cumulative distribution curves passes through $r'_\alpha(1) = 0.8$ at $\alpha = 1$, and through $r'_\alpha(1) = 0.9$ at $\alpha = 100$ (see dotted line of Figure 6.2). The simple fallout scaling system for the land surface burst can be used to provide a gross estimate of the fallout areas from sea water detonations. No large or experimentally observed significant differences in the areas of heavy fallout at sea have been found between the land and sea types of detonations for large yields.

For sea water fallout that is deposited on land areas where the previous values of D(1) and q_s apply, the mass contour ratio for the fallout of a large yield detonation on the surface of the water reduces to

$$M_r(1) = \frac{88}{D} \frac{\text{mg salt water/sq ft}}{\text{r/hr at 1 hr}} \tag{6.28}$$

When completely dried, the sea water salt residue, at 3.5 percent of the initial sea-water mass, is only 2.8/D(mg/sq.ft.)/(r/hr at 1 hr).

Because the fallout drops apparently fall most of the distance from the high altitude in the solid state through temperatures where the sublimation pressure of the water is rather low, the change in droplet-size with time is probably rather slow. At the lower and warmer altitudes, where the particles exist in the liquid state, they either grow larger or decrease in size by evaporation, depending on the relative humidity of the surrounding air. Thus, the true value of M_r (1) for the arriving particles could be almost as low as the 2.8/D value or could be even larger than the 88/D value. In dry (warm) climates and over land areas where the M_r (1) value of the arriving material would be low, the fallout pattern would extend much farther downwind than would be estimated from use of the simple fallout scaling system for land surface detonations. This is simply because the droplets, decreasing in size and density as the water evaporates, would be carried to greater distances and dispersed over a larger area. Under these conditions, the deposit levels would all be decreased.

6.2.5 Mass Contour Ratio for Fallout from Detonations in Harbors

The mass contour ratio from detonations in shallow water should depend on (a) the height or depth of the burst point with respect to the water surface, (b) the depth of the water, and (c) the effective depth of the crater in the bottom of the harbor. Equations for estimating the contour ratio were derived from the assumption of proportional mixing of the soil and water contained in a set of assumed cone-shaped crater volumes.

For detonations in which the water depth, d_w, is small enough so that a significant amount of bottom material is removed, the crater depth, as measured from the surface of the water to the bottom of the crater in the harbor bottom, is assumed to approach the crater depth of a detonation in dry soil. Using the data of ENW (p.213) for a land surface detonation, the crater depth is given by

$$d_0 = \frac{25W^{0.25}}{\delta_A} \text{ ft} \tag{6.29}$$

where δ_λ is the ratio of the crater depth for a surface burst to the crater depth for a burst at the nuclear scaled depth, λ_N. An estimating curve for δ_λ, based on high-explosive data, is shown in Figure 6.6.

It is convenient to use the mass solid-to-liquid ratio, designated S, as a composition variable for the relative amounts of harbor bottom material and sea water as the two major constituents of this type of fallout. The same relative mixing ratios of the total material removed from the soil craters and the water volumes lifted up to form fallout are assumed to occur in the harbor detonation as occur for each type of shot separately; the ratios would then depend on the relative masses of water and soil that are drawn up. Accordingly, the ratios (of the masses of each constituent) would be roughly proportional to $f(\sigma)W^{-0.088}/f'(w)$; the proportionality factor itself must be related to the initial amounts of soil and water dislocated by the detonation. The initial amounts of each constituent involved must, in turn, depend on the depth of the water and the size of the crater in the harbor bottom.

Data are not available for establishing the proportionality factor on an empirical basis, so geometrical considerations were used to develop a model for estimating its values. The geometrical crater-shapes assumed were two inverted cones both having the same radius, R, at the water surface. The height of the cone involving the harbor bottom material is the depth of the water, d_w plus the depth of the crater in the harbor bottom, d_c^a. With this geometry, the volume of the harbor bottom material (solids) removed is

$$V_s = (\pi/3)R^2(d_c^a)^3/(d_c^a + d_w)^2 \qquad (6.24)$$

where R, for a land surface detonation, according to ENW, is $62W^{1/3}$ ft.

The depth (or height) of the cone for the water component, d_c', was taken to be equal to the depth of the water involved in the explosion for the case in which the water is sufficiently deep so that no crater is formed in the harbor bottom. For this geometry, the volume of water involved is

$$V_w = (\pi/3)R^2\left[d_c' - (d_c' - d_w)^3/(d_c')^2\right] \qquad (6.25)$$

By assuming the ratio of the bulk density of the bottom material to that of the sea water to be 2, the proportionality factor is given by

$$S_0 = \frac{2(d_c^a)^3}{d_c'(d_c^a + d_w)^2\left[1 - (d_c' - d_w)^3/(d_c')^3\right]} \qquad (6.26)$$

Figure 6.5
PROPOSED CRATER DEPTH CORRECTION CURVE FOR THE MASS CONTOUR RATIO AS A FUNCTION OF THE NUCLEAR SCALED DEPTH

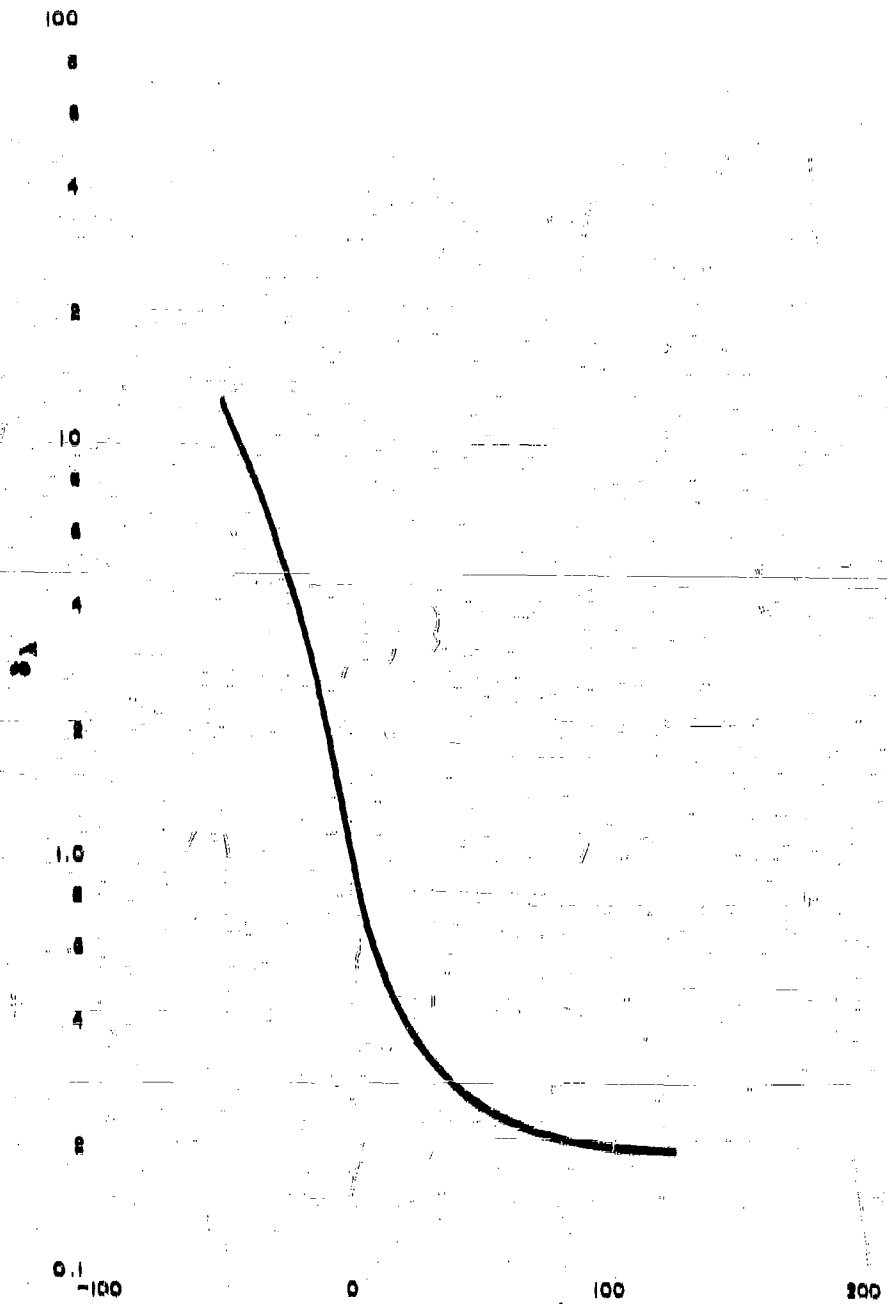

Since d_0'' should decrease with depth of water, a first-order approximation of d_0'' may be obtained from a function of the form

$$d_0'' \quad d_0^{\#} \left[1 - d_0(W) d_w\right] \tag{6.27}$$

where $d_0(W)$ is a yield dependent parameter that must be evaluated from available data. It was not possible to evaluate $d_0(W)$ from the data of ENW (pp.220 and 227) because, for yields of about 10-KT and greater, that data gives larger craters in a harbor bottom (clay mud) under water than for a land surface detonation. Because such results are not in accord with observations, the data in ENW are presumably extrapolated incorrectly from high explosive data; hence they are not directly applicable to the higher yield nuclear explosions. Correcting some of the ENW data to an equivalent nuclear yield (see Chapter 2 for fraction of energy in blast) gives

$$d_0(W) \approx 0.017 W^{-0.16} \text{ ft.} \tag{6.28}$$

The appropriate value of d_0' is obtained from Eq. 6.27 for the water depth at which d_0'' becomes zero; for a water surface detonation this is

$$d_w = d_0^{\#} \approx 59 W^{0.16} \text{ ft.} \tag{6.29}$$

From Eq. 6.29, the value of d_0' obtained by assuming the involvement of a hemispherical volume of water is $56W^{1/3}$ ft. On the other hand, if the shape of the water volume thrown up is assumed to be the same as that of a crater in soil, then d_0', from a linear increase in all the soil crater dimensions to the volume of the water removed, would be $38W^{0.270}$ ft. Thus the value of d_0' found for Eq. 6.29 suggests that the ratio of the radius to the depth for the water "crater" increases more rapidly with yield than it does for a crater in dry soil.

With S_0 defining the solid-to-liquid ratio weighting factor, the liquid mass fraction weighting factor is $1/(1 + S_0)$ and the solid mass fraction weighting factor is $S_0/(1 + S_0)$. With these weighting factors, the total mass of material for the mixture per unit of yield for the fallout from a harbor detonation on the surface of the water, is

$$f_{s,l}(\alpha) = \frac{f(\alpha) + S_0 f(\alpha) W^{-0.084}}{1 + S_0} \tag{6.30}$$

The solid-to-liquid mass ratio at a given location in the fallout area is, then,

$$S = \frac{S_0 f(\sigma) W^{-0.083}}{f(\sigma)} \tag{6.31}$$

and the mass contour ratio for this harbor detonation type of fallout may be estimated from

$$M_r(1) = \frac{7.1\times10^{-24} f_{sf}(\sigma)}{d(1) q_x K_\lambda D \left[r_\alpha^*(1) I_{fp}(1) + I_i(1)\right]}, \tag{6.32}$$

for $I_{fp}(1)$ and $I_i(1)$ in (r/hr at 1 hr)/(fission/sq ft), $f_{sf}(\sigma)$ in mg/KT, and in which $r_\alpha^*(1)$ is the gross fractionation number for the slurry.

For shot geometries where S_0 has values less than about one, a large amount of water and sea water salts are present in the fireball. Under such conditions the use of the $r_\alpha(1)$ values for fallout from a surface land detonation is not appropriate--even for the solid fraction--because of differences in vapor pressures between the oxides and hydroxides of many of the fission product elements. However, as the water content decreases (S_0 becomes larger) the use of $r_\alpha(1)$ for the solids becomes more applicable, and, as the S_0 values decrease, the $r'_\alpha(1)$ values for the water fallout apply. To account, in gross way, for these interactions, it is suggested that $r_\alpha^*(1)$ be estimated from

$$r_\alpha^*(1) \approx \frac{r_\alpha(1) + S_0 r'_\alpha(1)}{1 + S_0}, \quad S^0 > 1 \tag{6.33}$$

and

$$r_\alpha^*(1) \approx r'_\alpha(1), \quad S^0 < 1 \tag{6.34}$$

For large-yield detonations (W>1-MT) on the surface of the harbor water (where $r'_\alpha(1)$ is essentially unity for all α, S_0 is less than unity, and D(1), q_x, $I_{fp}(1)$, and $I_i(1)$ have the standard values), the mass contour ratio is

$$M_r(1) = \frac{1.8\times10^{-11}\,(4.8\times10^{18} + S_0 f(\sigma) W^{0.083})}{(1 + S_0)D} \frac{\text{mg slurry/sq. ft}}{\text{r/hr at 1 hr}} \tag{6.35}$$

and, for lower yields, the multiplier would be $1.88 \times 10^{-11} \cdot F_0^1(1) + 0.09$ instead of 1.88×10^{-11}.

Because the f(e)values were derived from data on fallout from land surface detonations, and because the simple fallout model applies only to land surface detonations, use of the scaling functions at other depths of burst will introduce errors among the distance, standard intensity, and particle size parameters. These errors should, of course, increase as the nuclear scaled depth (or height) shifts further away from zero.

For burst heights or depths that are a small deviation from a surface burst, the error in the extent of the fallout pattern itself should not be large since the cloud heights and size are not very sensitive to either height or depth of burst or type of media at the point of detonation. However, the value of the mass contour ratio is very sensitive to the depth of burst; this is indicated by the rapid change of K_λ and δ_λ with λ_N when λ_N is small. Considering the general trends and accuracy of the source data, the fallout model scaling functions for a surface detonation could be used, without significant increases in error for all types of detonations characterized by λ_N values up to 45, and it is likely that consistent errors would become increasingly large for λ_N values larger than 110. By use of K_λ and δ_λ, however, the scaling function for $M_r^\lambda(1)$ values appears to be as reliable as the original data up to λ_N values of 220.

6.2.6 Mass Contour Ratio for Fallout from a 1-MT Detonation at Several Detonation Geometries

To illustrate the use of the scaling functions for the mass contour ratio and how its value depends on the various parameters, computations for $M_r^\lambda(1)$ were made for: (1) a land surface detonation, (and detonations on the) (2) water surface, and (on the) (3) water bottom, for depths of 20, 50, and 100 feet. The calculation results for S_n are shown in Table 6.7.

The value of d_r^λ indicates that, for water depths in excess of about 180 feet, the fallout, from a surface detonation, would be a pure-sea water type of fallout. It may be noted that d_r^λ has been corrected for depth of burst by $1/\delta_\lambda$ in the same way as d_n and d_p^λ.

For computing $M_r(1)$, the parameters B, q_s, and D(1) were taken to be 1.0, 0.75 and 0.75, respectively. With those values, the mass contour ratio scaling function becomes

$$M_r^{\lambda}(1) = \frac{1.26\times10^{-33} f_{Rf}(a)}{K_{\lambda}\left[6.93\times10^{-13} r_{cr}^{4}(1) + 0.13\times10^{-13}\right]^{S_0 - 1}} \qquad (6.36)$$

and

$$M_r^{\lambda}(1) = \frac{1.83\times10^{-11} f_{Rf}(a)}{K_{\lambda}}, \quad S_0 < 1 \qquad (6.37)$$

Table 6.7

COMPUTATION OF S_0 FOR SEVERAL DETONATION CONDITIONS OF A 1-MT FISSION WEAPON

Depth of Burst (ft)	λ_N	d_w (ft)	δ_λ	K_λ	d_0 (ft)	d_0^s (ft)	d_0' (ft)	S_0
0	0	20	1.0	1.0	140	124	178	0.48
20	2.0	20	0.90	0.86	150	108	198	0.80
0	0	50	1.0	1.0	140	101	178	0.808
50	5.0	50	0.74	0.60	189	136	240	1.20
0	0	100	1.0	1.0	140	01	178	0.108
100	10.0	100	0.57	0.47	246	106	312	0.272

The $M_r^{\lambda}(1)$ values at various downwind distances are given in Table 6.8.

The values for $r_{cr}^{*}(1)$ were calculated by use of Eq. 6.33 for $S_0 = 0.40$, 0.80, and 1.20. At distances where both stem and cloud fallout occur, the overall $M_r^{\lambda}(1)$ values were calculated by multiplying the individual ratios by the respective I values, adding the masses obtained, and then dividing the total by the sum of the two I values.

Selection of the surface-water and bottom detonations was made so as to give the spread in $M_r^{\lambda}(1)$ values for detonations anywhere in the water layer; this spread is not large for 20 and 50 foot depths, but at 100 foot the spread is

Table 6.8

COMPUTATION OF M_x^{λ} (I) FOR SEVERAL DETONATION CONDITIONS OF A 1-MT YIELD FISSION WEAPON AT SELECTED DOWNWIND DISTANCES

X (10^5 ft)	$\bar{\sigma}$ or σ_m	r_m(I)	I (r/hr at 1 hr)	f(σ)$H^{-a_1 a_2}$ (10^{21} mg/KT)	M_x^{λ} (I) (mg slurry/sq ft) / (r/hr at 1 hr)						
					S_m = =	S_m = 1.83	S_m = 3.89	S_m = 0.808	S_m = 1.20	S_m = 0.105	S_m = 0.272
0.1	6.48	0.124	9000	*0.5	133	102	121	82.7	135	81.0	155
0.2	0.50	0.20	9000	5.56	31.7	57.3	65.4	76.8	102	80.1	151
0.3	1.15	0.48	3100	3.55	14.2	46.8	45.1	75.0	85.5	79.9	150
0.4	1.46	0.57	930	3.38	10.7	35.7	39.0	74.2	78.8	79.7	149
0.5	1.94	0.63	(280)	2.90							
0.5	0.96	0.36	(0.5)	4.37	8.32	32.9	35.8	73.6	75.6	79.7	149
0.6	2.19	0.66	(65)	2.69							
0.6	1.15	0.47	(68)	4.06	10.3	35.3	38.6	74.1	49.0	79.8	149
0.8	2.38	0.79	(7.5)	2.14							
0.8	1.54	0.58	(1000)	3.30	10.2	34.9	38.1	74.2	73.8	79.7	149
1.0	1.92	0.64	1220	2.84	7.83	32.0	35.6	73.6	75.3	79.7	149
1.52	2.92	0.70	2520	2.13	5.42	28.8	31.2	72.8	70.6	79.5	149
2	3.84	0.72	1840	1.76	4.45	27.4	29.3	72.4	69.1	79.5	148
3	5.76	0.74	570	1.34	3.22	26.4	28.5	72.8	67.5	79.4	148
4	7.67	0.75	580	1.09	2.58	25.7	27.7	71.5	67.1	79.4	147
5	9.58	0.76	265	0.942	2.21	25.5	27.9	71.5	66.1	79.4	147
6	11.5	0.76	140	0.835	1.95	25.2	26.8	71.2	66.1	79.4	147
7	13.4	0.76	72	0.744	1.74	24.7	26.5	71.2	65.8	79.4	147
8	15.4	0.77	38	0.677	1.58	24.7	26.2	71.0	65.8	79.4	147
9	17.3	0.77	20	0.632	1.47	24.5	26.0	71.0	65.6	79.4	147
10	19.2	0.77	10	0.581	1.35	24.5	26.0	71.6	65.5	79.4	147
11	21.1	0.77	5.4	0.564	1.31	24.5	26.0	71.0	64.8	79.4	147
12	23.0	0.77	2.8	0.564	1.30	24.5	26.0	71.0	64.8	79.4	147
13	24.9	0.77	1.5	0.564	1.30	24.5	26.0	71.0	64.8	79.4	147
13.6	26.1	0.77	1.0	0.564	1.30	24.5	26.0	71.0	64.8	79.4	147

about a factor of 3. The large change in $M_F(1)$ from dry-soil fallout to that for the fallout from a detonation on the surface of 20 feet of water is, of course, due to the larger amounts of water thrown up. No absolute accuracy can be stated for any of the numbers for the harbor-shot fallout; however, the values for the water-surface detonations are more accurate, taken relative to each other, than are the absolute values of the mass contour ratios.

6.3 Fission-Product and Fraction-of-Device Contour Ratios

Since two fission-product atoms are produced in each fission event, there are 3.32×10^{-24} moles of fission products formed per fission, or 0.466 moles of fission products produced per kiloton of yield. The distribution of these products over an extended area would result in an air ionization rate at 3 feet above the area given by I_{fp} (t) in r/hr per fission/sq ft. Thus the fission-product contour ratio for a fractionated mixture, including induced activities, from a land surface detonation, is given by

$$FP_F(1) = \frac{3.32 \times 10^{-24} \Sigma_{jA} r_{jA}(\alpha)}{D(1) q_x \left[r_\alpha(1) I_{fp}(1) + I_i(1) \right]} \quad \frac{\text{moles fp/sq ft}}{\text{r/hr at 1 hr}} \qquad (6.38)$$

where $r_{jA}(\alpha)$ is the fraction of each nuclide condensed on the particle group designated by α relative to the total number of fissions, and is defined by

$$r_{jA}(\alpha) = \frac{1}{2} \left[r_a(A) + r_b'(A) \right] y_A \qquad (6.39)$$

in which r_a (A) is the fraction of the mass chain for a given element (or chain mass number) condensed when the particles were in the liquid state, r_b' (A) is the fraction condensed on the surface of the particles of size α, y_A is the yield of the mass chain in atoms per fission, and the factor 2 is for the total yield of 2 atoms per fission. If no fractionation occurs the sum of the $r_{jA}(\alpha)$ for all α is unity.

Using the standard values of D(1), q_x, and I_i (1), FP_F (1) is given

$$FP_F(1) = \frac{8.51 \times 10^{-18} \Sigma_{jA} r_{jA}(\alpha)}{\left[r_\alpha(1) + 0.019 \right]} \qquad (6.40)$$

For non water or barob-type fallout, $r_\alpha(1)$ is replaced by r_{ii} (1) or $r_{ii}'(1)$; thus the value of FP_F (1) is dependent on the conditions of detonation only through the gross fractionation number.

The fraction-of-device contour ratio, in terms of the total number of fission events, is

$$FD_r(1) = \frac{7.1\times10^{-24}}{D(1)q_n BW\left[r_\alpha(1)f_{fp}(1)+i_i(1)\right]} \text{ (r/hr at 1 hr-sq ft)}^{-1} \qquad (6.41)$$

or, for the standard values of D(1), q_n, and $i_i(1)$,

$$FD_r(1) = \frac{1.83\times10^{-11}}{BW\left[r_\alpha(1)+0.019\right]} \qquad (6.42)$$

The fraction-of-device contour ratio has two uses. The first is that it is used to estimate the surface density of constituents that are assumed to mix uniformly with the more refractory fission products. The second is that it is used in conjunction with observed fallout patterns when the latter are integrated for the total fraction of the weapon contained within a stated ionization rate contour. The use of both contour ratios is illustrated in Chapter 7, Volume II.

For a land surface burst, the average concentration of the fission products is estimated from the ratio of FP_r (1) to M_r (1); this is

$$C_{fp} = \frac{1.12\times10^{-24}BW^{0.08}\Sigma_{jA}r_{jA}(\alpha)}{f(\alpha)} \quad \frac{\text{moles fp}}{\text{mg fallout}} \qquad (6.43)$$

6.4 Foliage-Contamination Factor Contour Ratio

In Chapter 2, the foliage contamination factor, a_L, was defined as the ratio of the number of fissions in the fallout on foliage per gram of dry plant (or foliage) to the number of fissions in the total deposited fallout, per sq ft of soil. Also, the foliage surface density, w_L, (subject to contamination) was defined as the grams of dry foliage per sq ft of soil. Therefore, the foliage-contamination factor contour ratio is defined by

$$FC_r(t) = \frac{a_L w_L}{K_\alpha(t)} \quad \frac{\text{fissions on foliage/ft}^2 \text{ of soil area}}{\text{r/hr}} \qquad (6.44)$$

The contour ratio, evaluated as of H + 1, is

$$FC_r(1) = \frac{a_L w_L}{K_\alpha(1)} \quad \frac{\text{fissions on foliage/ft}^2 \text{ of soil area}}{\text{r/hr at 1 hr}} \tag{6.45}$$

where

$$K_\alpha(1) = 3.90 \times 10^{-18} \left[r_\alpha(1) + 0.019\right] \quad \frac{\text{r/hr at 1 hr}}{\text{fission/ft}^2} \tag{6.46}$$

when the standard values of D(1) and q_α are used. It is seen that multiplication of FC_r (1) by I(1) gives the number of fissions on foliage per sq ft of soil area.

The "zero-time" number of atoms of a given radionuclide (at least for the end member of a mass chain) in the fallout is given by

$$N_A^0 = Y_A \, FC_r(1) I(1) \quad \frac{\text{atoms on foliage}}{\text{ft}^2 \text{ of soil area}} \tag{6.47}$$

in which Y_A is the mass chain yield in atoms per fission of mass number A.

The major interest in the contamination of foliage by fallout is related to the fact that the consumption of the foliage by animals and humans may produce an internal radiological hazard. Therefore, generalization and extensions of the foliage contamination factor data from tower- and balloon-detonation fallout are needed for making estimates of the potential biological availability of the radionuclides in the fallout from other types of nuclear explosions and for various foliage contamination conditions.

When contaminated foliage is consumed, some of the radionuclides or some fraction of each nuclide ingested is dissolved in the stomach fluids; the remainder stays with the particles and pass through the digestive tract. Many of the dissolved nuclides are assimilated into the blood and concentrate in specific body organs. The factors involved in this distribution and the methods for estimating the resulting internal doses are given by K.Z. Morgan and others.[7]

However, methods are needed for estimating the relative amount of each nuclide that is soluble in the stomach fluids. Evaluations of the internal hazard can be made (for fallout conditions in a nuclear war, for example) from the generalizations of the foliage contamination factor together with estimates of the solubilities of the radionuclides.

The amount of radionuclides that pass through the digestive tract may be considered separately because a large fraction of certain radionuclides in the fallout will be insoluble. For these radionuclides, only the gross amounts passing through need be considered. However, for the case of the assimilation of the soluble nuclides in other body organs, each radionuclide must be considered separately.

6.4.1 Insoluble-Nuclide Fractions

A gross estimate of the radioactivity of insoluble nuclides passing through the digestive tract from ingestion of contaminated foliage can be made if it is assumed that the gross solubility of the radioactivity is the same in the stomach as it is in 0.1N HCL. If the soluble fraction of the gross activity is defined as S(t), the number of moles of fission product atoms ingested that pass through the digestive tract with the particles is given by

$$FP_g = 3.32\times10^{-11}\left[1 - S(t)\right] A_F C_a(t) \quad \frac{\text{moles of fission products}}{\text{day}} \tag{6.48}$$

where A_F is $FC_F(t)f(t)$ in fissions on foliage/ft² of soil area, and $C_a(t)$ is in ft² of foliage consumed/day. Equation 6.48 can be written in terms of dis/sec, as

$$FP_g = \left[1 - S(t)\right] A_F C_a(t) a_{fp}(t) \quad \frac{\text{dis/sec}}{\text{day}} \tag{6.49}$$

where $a_{fp}(t)$ is in dis/sec per fission at the time, t, after detonation. It may be noted that if $C_a(t)$ is defined in terms of grams of dry foliage per day, w_f, may be eliminated from the definition of $FC_F(t)$ in Eqs. 6.44 and 6.45.

Theoretical estimates of the fractional amount of insoluble activities may be made from the data of Chapter 4 if it is assumed that all the fission-product nuclides on the exterior surface of the particles dissolve in the stomach fluids. The fraction not dissolved is then given by the $r_0(A)$ values for each of the fission-product nuclides. If these fractionation numbers are redefined as r_{jA}, where j designates the element and A the mass number (isotope), then Eqs. 6.48 and 6.49 can be written as

$$FP_g = A_F C_a(t) \Sigma_{jA} r_{jA} N_{jA}(t) \quad \frac{\text{moles of fission products}}{\text{day}} \tag{6.50}$$

and

$$FP_{\beta} = \Lambda_F C_{\beta}(t) N_{jA}(t) a_{jA}(t) \quad \frac{dis/sec}{day} \tag{6.51}$$

where N_{jA} (A) is the number of atoms of element j with the mass number A per fission at the time, t, after fission, and a_{jA} (t) is the activity in dis/sec per fission of the nuclide (the indices A and j define the nuclide in terms of its mass number and its atomic number, or elemental designation).

6.4.2 Soluble-Nuclide Fractions

The solubility in digestive fluids of each element, radionuclide, carried by the fallout particles deposited on edible foliage must be known before estimates of the amounts of each that concentrate in the tissue of (specific) body organs can be made. If the nuclide solubilities in 0.1 normal HCl solution are the same as in digestive fluids, then measurements of the solubilities in the acid can be used in such estimates. If the solubility in the 0.1 normal HCl solution is defined as S_j for the jth element, the amount and radioactivity of the ith radionuclide (of element j) dissolved is

$$N'_{jA} = 1.66\times10^{-24} \Lambda_F C_{\beta}(t) S_j N_{jA}(t) \quad \text{moles/day} \tag{6.52}$$

and

$$a'_{jA} = \Lambda_F C_{\beta}(t) S_j a_{jA}(t) \quad \frac{dis/sec}{day} \tag{6.53}$$

in which S_j is the fraction of element j that is soluble. Theoretical upper-limit values of N'_{jA} (t) and a'_{jA} can be estimated by substituting the appropriate values of r'_{β} (A), redefined as r'_{jA}, given by Eq. 6.9 for S_j.

It should be emphasized that, for general applicability, the values of S(t) and S_j must be known as a function of particle-diameter. For the smaller particles, the values of R_{β} (A), or r_{jA}, are independent of particle size but the values of r'_{β} (A), or r'_{jA}, are not.

6.4.3 Variation of the Foliage-Contamination Factor with Particle Size

The values of a_j and $K_{\alpha}(t)$ depend on particle size. The dependence of the latter on the particle-size designator, σ, is represented by Eq. 6.46. The dependence of a_j on σ was derived from the data of Romney and coworkers[6] presented in Chapter 2.

The values of σ that are applicable to the various measured values of a_L were calculated from

$$\sigma_a = X/h \qquad (6.54)$$

where X is the distance from ground zero and h is the mid-height of the cloud. The values of σ_a can be used to estimate the median particle-diameter of the particles deposited at the distance X by the methods described in Chapter 5. When v_f (the fall velocity) can be determined for the median particle diameter, as obtained from particle-size data, then the 15 mph value of σ_a can be determined from

$$\sigma_a = 22.0/v_f \qquad (6.55)$$

for v_f in feet per second. The values of h and other data, for the detonations for which values of a_L are available, are given in Table 6.9.

Table 6.9

SUMMARY OF SHOT CONDITIONS FOR ESTIMATING THE MEDIAN PARTICLE DIAMETER DESIGNATOR

Shot	Yield (KT)	Height of Burst (feet)	h (feet)	Type of Shot
Tesla	7	500	24,000	Tower
Apple I	14	500	27,000	Tower
Met	22	400	35,500	Tower
Apple II	29	500	38,500	Tower
Priscilla	37	700	34,500	Balloon
Diablo	17	500	30,000	Tower
Shasta	17	500	24,000	Tower
Smoky	44	700	32,000	Tower

The values of the median particle size, with respect to the distribution of activity on the particles, for two locations each on Shots Apple II and Smoky, along with the computations of σ_a are given in Table 6.10. The σ_a values calculated by the two methods are nearly the same.

Table 6.10

CALCULATION OF σ_0 FOR SOME FALLOUT LOCATIONS FROM SHOTS APPLE II AND SMOKY

Shot	X (miles)	d_m (micrograms)	v_f (ft/sec)	σ_0, X/h	σ_0, 22.0/v_f
Apple II	7	-	-	0.000	(0.000)
	48	120	3.24	0.68	0.59
	100	70	1.80	14.5	15.8
Smoky	182	50	0.94	21.8	20.4
	200	47	0.97	34.0	32.8
	259	-	-	42.8	(41.8)

The values of a_L given in Table 2.18 (see Chapter 2) are plotted in Figure 6.6 as a function of σ_0 values computed by use of Eq. 6.54. This set of data for the retention of fallout by native plants, is widely scattered; however, the general trend of the values of a_L from individual shots is to increase with increasing σ_0. Part of the difference in the observed variation of a_L with σ from one detonation to another is undoubtedly due to the fact that differences in wind speed occurred. Other causes of the differences in the variation with σ could be due to differences in humidity conditions and in the predominant types of foliage that were collected for analyses.

The values of a_L, calculated from the data of Table 2.16 (see Chapter 2) for the forage crops (clover, alfalfa, wheat, and mixed grasses) are plotted in Figure 6.6 as a function of the σ_0 values that were corrected to an average wind speed of 15 miles per hour (see Table 6.10). Since the absolute accuracy of the source data is probably not better than 50 percent, a single line was drawn through the plotted data, neglecting one point. The suggested representation of a_L for these four forage crops is therefore given by

$$a_L = 9.5 \times 10^{-6} (\sigma_0 - 0.34); \quad \sigma_0 \geq 0.34 \qquad (6.56)$$

The complete representation of the foliage contamination factor contour ratio for evaluation at 1 hour is then

$$FC_r(1) = \frac{2.44 \times 10^6 w_L (\sigma_0 - 0.34)}{(r_0(1) + 0.019)}; \quad \sigma_0 \geq 0.34 \qquad (6.57)$$

The value of $FC_r(1)$ for σ_0 values less than 0.34 is taken to be zero.

Figure 6.6
VARIATION OF a_1 WITH CALCULATED VALUES OF a_0

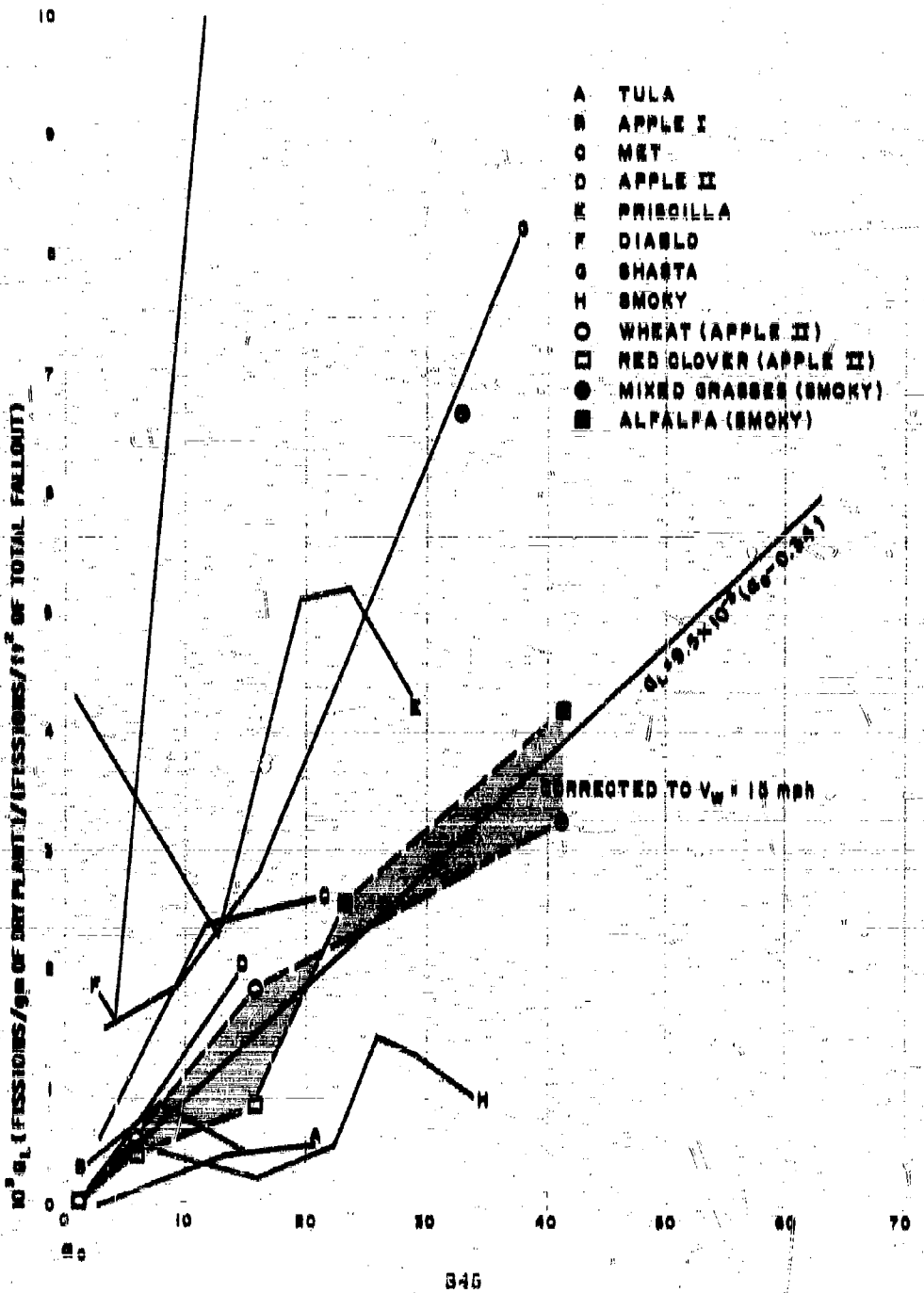

If it is assumed that the surface densities of the clover and wheat foliage in the flats used on Apple II detonation were higher than the average for such crops, then a range of values of w_L may be suggested. These are:

Red Clover	w_L = 5 to 25 gm. dry plant/ft^2 of soil surface
Wheat	w_L = 10 to 40 gm. dry plant/ft^2 of soil surface
Alfalfa	w_L = 10 to 30 gm. dry plant/ft^2 of soil surface
Mixed Grasses	w_L = 5 to 25 gm. dry plant/ft^2 of soil surface

Wide variations in w_L from these ranges might occur in various sections of the country.

The fraction of the total fallout that is retained on foliage can be estimated from the product $a_L w_L$. Thus, for a w_L value of 20, the fraction retained is 1.9×10^{-2} (α_0 = 0.84). In Table 6.8, the value of α_0 at the 1 r/hr at 1 hr contour farthest downwind from ground zero is 26.1; at this location, $a_L w_L$ is then 0.049, or about 5 percent, and the calculated value of $r_\alpha(1)$ is 0.77. Hence, from Eq. 6.57, the value of $FO_r(1)$, is 1.6×10^{11} (fissions on foliage/ft^2 of soil area)/(r/hr at 1 hr).

Estimates of the median size (or size-range) of particles retained on foliage may be made if the variation with α_0 of the median diameter of the particles in the deposited fallout is known. In Figure 6.7 the values of the median diameters of the fallout lodged on foliage, taken from Table 2.15, are plotted as a function of α_0. For these data, the median diameter of the fallout particles on the foliage increases with α_0; thus, the median diameter of the retained fallout increases as the median diameter of the deposited fallout decreases.

Clearly this trend in the median diameter of the retained particles with α_0 could not continue indefinitely since at some point, when the diameters of the deposited fallout particles become very small, all the particles could be retained by the foliage. To illustrate this aspect, calculated values of the median diameter (d_m) for the deposited fallout are also plotted as a function of α_0 in Figure 6.7. Extrapolation the linear representation of the data for d_m of the foliage-retained particles as a function of α_0 to the curve for d_m of the deposited fallout gives a maximum value of about 57 microns.

The various functional representations of the foliage contamination factor contour ratio, as derived from the data of Romney and coworkers[9], are based on information obtained from nuclear detonations of tower and balloon-mounted devices. However, in the treatment of that data the emphasis was placed on the particular mathematical functions that could be used in making estimates of internal hazard from fallout produced by land-surface detonations.

Figure 6.7
VARIATION OF THE MEDIAN PARTICLE DIAMETER OF FALLOUT ON FOLIAGE WITH σ_g OF THE DEPOSITED FALLOUT

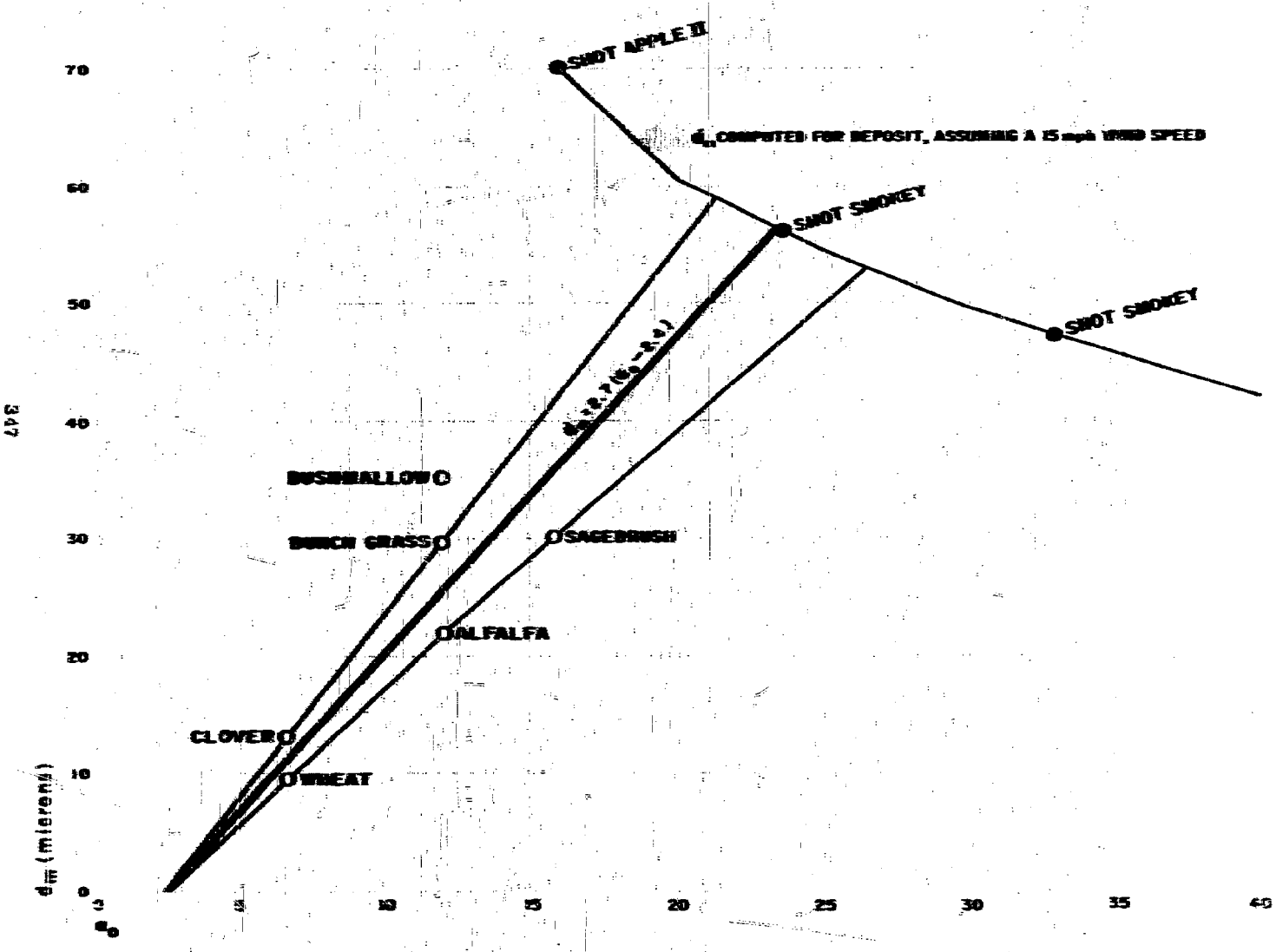

This application should be valid for any condition of detonation since the same physical phenomena must be involved in particle retention by foliage irrespective of the source of the depositing particles. When more data become available, the proposed representations of the processes can be altered to be either more specific for different types of foliage or otherwise more complicated depending on the observed variations in the data.

CHAPTER 6 REFERENCES

1. Bolles, R.C., and N.E. Ballou, Calculated Abundances of U-235 Fission Products, USNRDL-456, 1956.

2. Miller, C.F., and P. Loeb, Ionization Rate and Photon Pulse Decay of Fission Products From the Slow Neutron Fission of U-235, USNRDL-TR-247, 1958.

3. Strope, W.E., Evaluation of Countermeasure System Components and Operational Procedures, Operation Plumbbob WT-1404, 1958.

4. Miller, C.F., Analysis of Fallout Data, I. The Jangle "S" and "U" Shot Fallout Patterns, USNRDL-TR-220, Del. 1959.

5. Morgan, K.Z., et al., Report of ICRP Committee II on Permissible Dose For Internal Radiation (1959), Health Physics, Vol. 3 (1960).

6. Romney, E.M., R.G. Lindberg, H.A. Hawthorne, B.G. Bystrom, and K.H. Larson, Health Physics (to be published).

Symbol	Definition
	--A--
A	Mass number of a nuclide
A_b	Effective gross attenuation factor for decontamination equipment operator
A_F	Defined by $FC_F(t)I(t)$; in fissions on foliage per sq ft of soil area
A_h	Effective attenuation factor for streetsweeper operator from radiation sources in the hopper
A_s	Attenuation factor for streetsweeper operator from surrounding radiation sources
A_α	Cloud radioactivity concentration in fissions per cubic foot
A'_α	Stem radioactivity concentration in fissions per sq ft
a	Nuclear explosion cloud radius at 6 to 8 minutes after detonation
a, a_j, or a_{Fj}	Decontamination equation constant for absorption interaction (seawater and slurry type fallout)
a_L	Foliage contamination factor; fissions per gram of dry foliage divided by fissions per sq ft of soil area
a_s	Radius of stem or fireball at the altitude, z
$a_i(t)$	Radioactivity of the i^{th} nuclide at the time, t, after fission; in dis/sec per fission

Symbol	Definition
a_o	Stem or cloud radius at time of earliest fallout particle ejection
	— α —
α	Particle size parameter, defined as v_w/v_1
α_o	Size parameter for particles from cloud center, defined as X/h
	— B —
B	(1) Ratio of fission to total yield
	(2) Freundlich adsorption equation constant for elements in slurry type fallout
b	(1) Nuclear explosion cloud half-thickness at 6 to 8 minutes after detonation
	(2) Ratio of mass of solids to number of moles of radioactive element
	—C—
C(A)	Ratio of number of neutron captures to number of fissions (to form a nuclide of mass number A)
$C_o(t)$	Foliage croppage rate; in sq ft of foliage (dry) consumed per day
C_{fp}	Concentration of fission products in fallout, in moles of fission products per mg of fallout
C_l	Radioelement concentrations in liquid phase of slurry type fallout, in moles per mg of liquid
C_o	Radioelement concentrations in seawater fallout drops
$(ef)_j$	Radiation contribution factor of area j

Symbol	Definition
C_n	Concentration of radioelements entrained in the mass of solids in slurry type fallout, or, concentration of radioelements in the solid (melt) fallout particles, in moles per mg of solids
	D
DP	Planning dose or allowed dose; in roentgens
Dor D_{0x}	Potential exposure dose; usually defined for a location at 3 feet above an extended plane source of radioactivity
Dor $D_x(I)$	Instrument response factor
DRM	Dose-rate, or ionization rate, multiplier; defined as $D/I_x(I)$
d	(1) Particle diameter (2) Density of solids in seawater fallout
d_a	Crater depth (soils)
d'_a	Apparent crater depth (water)
d_m	Median diameter of fallout particles
d_w	Water depth (harbor detonation)
d''_a	Crater depth in harbor bottom
d(t,1)	Decay-correction factor (to standard time after detonation, H+1)
	Δ
Δ DRM	Difference in DRM
ΔE_D	Dissociation energy
ΔE_T	Change in internal energy
ΔF°	Change in standard free energy of chemical reactants

Symbol	Definition
ΔH_v	Heat of vaporization
δ_λ	Ratio of crater depth for surface detonation(s) to crater depth for detonation(s) at other depths or heights of burst
	--E--
E	(1) Energy, of photons, etc.
	(2) Decontamination method effort, or energy expended; in man- or equipment-hours per unit area
ϵ_n	Efficiency coefficient for (some) decontamination methods; in fraction of fallout mass removed per cycle
	--F--
F, F_j or F_{rj}	Decontamination ratio, or fraction of fallout, or of a radioelement in fallout, remaining after decontamination
$FC_r(t)$	Foliage-contamination factor contour ratio; in fissions on foliage/sq ft of soil area per r/hr at time, t, after detonation
FD	Fraction of device per unit area
$FD_r(t)$	Fraction of device contour ratio; in $(r/hr)^{-1}$
F_m	Fraction of mass of fallout remaining after decontamination
F_r	Fraction of ionization remaining after decontamination
FP_g	Amount of ingested nuclides on particles passing through digestive tract (gut); in moles of fission products per day or dis/sec per day
$FP_r(t)$	Fission product contour ratio; in moles of fission products/sq ft per r/hr at time, t, after detonation

Symbol	Definition
$f_{sl}(v)$	Total mass of solids and liquids per unit of yield for harbor-detonation fallout
$f(v)$	Ideal (or unfractionated) inverse specific activity of land-type fallout; in mg/fission
$f'(v)$	Ideal (or unfractionated) inverse specific activity of seawater fallout; in mg/fission
	--ϕ--
ϕ or ϕ'	Fallout model scaling parameter for computing standard intensities
	--G--
G^o	Constant for referenced free energy change
	--γ--
γ	Surface tension of drop of liquid
	--H--
h	(1) Altitude of center of cloud at 6 to 8 minutes after detonation
	(2) Depth or height of burst
	--I--
I (1)	Standard intensity; observed ionization rate decay-corrected to H+1; in r/hr at 1 hr, at 3 feet above an open, uniformly contaminated, field
$I_a(t)$	Air ionization rate; in r/hr at time, t, after detonation
I_l	The initially deposited amount of an element in the liquid phase of slurry fallout; in moles per sq ft
I_m	Initial mass level of fallout deposit; in gm/sq ft
I_o	Source intensity of a contaminated surface

Symbol	Definition
I, I_r, etc.	Ionization rate, radiation intensity, or other representation of the initial fallout deposit level
i	Number of moles of a given element in a drop of seawater fallout
	--K--
K or K_j	Decontamination equation parameter for seawater type fallout; in C-Level units
K_{aj}^{i}	Decontamination parameter for seawater fallout; in mg/sq ft
K_{rj}	Decontamination parameter for seawater fallout; in r/hr at 1 hr
K_a, K_s, K_s	Thermodynamic equilibria constants and/or solubility products
K_n	Various equation constants, for n = 1,2,3, etc.
$K(1), K_\alpha(t)$	Yield distribution contour ratio, same units as $K(1)C(1)$; in r/hr per fission/sq ft or in r/hr per K/sq mi
$K(E)$	Efficiency coefficient, wet decontamination methods
K_{AB}	Equilibrium constant for formation of compound designated AB
K_I	Equilibrium constant for exchange reaction of an element
K_p	Equilibrium, or dissociation, constant in terms of partial pressures
K_λ	Mass-correction factor (surface detonation)
$k_{s,w}$	Fallout model scaling system parameter
k_j	Henry's law constant
k_ℓ	Mixing coefficient for the insoluble elements with the soil particles in slurry type fallout

Symbol	Definition
k_s	Cloud or fireball rate-of-rise equation constant
	--L--
$\bar{L}_j^g$	Relative partial molar heat content of element in gas phase
$\bar{L}_j$	Relative partial molar heat content of element in liquid phase
	--λ--
λ_N	Nuclear-scaled depth; defined by $h/W^{1/3}$ where h is in feet and W is in kilotons
	--M--
M	(1) Molecular weight
	(2) Mass of fallout particles remaining after decontamination; in gm/sq ft
$M_T^{\lambda}(t)$	Mass contour ratio; in mg/sq ft per r/hr at time, t, after detonation (for the fallout from a detonation at a nuclear scaled depth of λ_N)
M^*	Mass of particles remaining after decontamination after expending an excess of energy (i.e., infinite effort)
	--μ--
μ_A	Klein-Nishina absorption coefficient for air
μ_l	Compton absorption or scattering coefficient
	--N--
N_A^o	"Zero time" number of atoms/sq ft of radionuclide of mass number A
N_j	Mole fraction of element j in liquid phase
N_j^g	Mole fraction of gaseous species of element j in vapor phase

Symbol	Definition
$N_j(A,t)$	Number of atoms of element j of mass chain A per 10^4 fissions
n_{fp}	Number of atoms or moles of fission products per unit area
n_j^g	Number of moles of element j in gas phase
n_j	Number of moles of element j condensed on or into liquid soil particle surfaces
$n(\ell,p)$	Number of moles of melted carrier in surface layer of particle
$n_o(p)$	Total number of moles of carrier in particle
$n(\ell)$	Moles of liquid carrier
n_α	Number of particles having size parameter α per unit volume of cloud
n_T	Total number of moles of gas molecules in fireball
	--P--
P	(1) Total pressure, in atmosphere (2) Kinetic power of a water stream
P_o	Initial pressure, in atmosphere
P_j	Ionization rate weighting factor for radionuclides of element j
PF_j	System protection factor
p	(1) Overpressure, in psi (2) Pressure, over the surface of a drop of liquid

Symbol	Definition
p_j	Partial pressure of element j over liquid phase
p_j^*	Sublimation pressure of element j
p_0	Vapor pressure of carrier material
	--Q--
Q	Water-flow rate through nozzle
Q_1	Energy in blast wave
Q_2	Energy in fireball
q_a	Terrain attenuation factor
	--R--
R	Molar Boltzman, or gas, constant
R_M	Remaining mass of fallout particles after decontamination, for infinite effort and a high initial level fallout deposit; in mg/sq ft
R_m	Remaining mass of fallout particles after decontamination, for infinite effort and a low or intermediate initial level fallout deposit; in mg/sq ft
RN	Residual number; ratio of exposure dose with a radiological countermeasure to the potential exposure dose (i.e., without a radiological countermeasure)
$R_\tau(\tau)$	Ionization rate remaining after decontamination, for a contact time of τ; in r/hr at 1 hr
$R_\tau(t)$	Ionization rate at time, t, after detonation (and after decontamination)
r	Fireball radius
$r_{fp}(1)$, $r_s(1)$, or $r_\alpha(1)$	Gross fission-product ionization-rate fractionation number at N+1
$r_{jA}(\alpha)$	Fraction of a nuclide of element j and mass number A that is condensed on particles, or particle groups, designated by α

Symbol	Definition
r_m	Maximum fireball radius
$r_o(A)$	Fraction of an element of mass chain A condensed into liquid particles at the time that they solidify; a fractionation number
$r_o'(A)$	Fraction of an element of mass chain A condensed on the surface of solid particles; a fractionation number
$r_i(A)$ or $r_i'(A)$	Same as $r_o(A)$ and $r_o'(A)$, respectively, for a radionuclide designated by i
	--ρ -- (rho)
ρ	Density of liquid (or solids)
	--S--
S	Solid-to-liquid mass ratio
S_i	Solubility of an element or nuclide in 0.1 normal HCl
S_o	Solid-to-liquid ratio weighting factor
S(t)	Fraction of gross amount of radioactivity that is soluble in 0.1 normal HCl at time, t, after detonation
	--T--
T	Absolute temperature in degrees Kelvin
t_a	Fallout arrival time; time after detonation
t_c	Fallout cessation time; time after detonation
t_e	Time of entry into a contaminated area; time after detonation
t_{dec}	Decontamination starting time; time after detonation

Symbol	Definition
t	Time, in days, of contact of fallout with a surface
	--V--
V	Fireball (or cloud) gas volume
V_0	(1) Original volume of heated air molecules (in fireball)
	(2) Initial liquid volume of a drop (seawater fallout)
V_2	Fireball volume at second temperature maximum
V_s	Volume of harbor-bottom crater
v_w	Wind velocity; a vector quantity for a particle group from its point of origin in the cloud to its location on the ground surface
v_f	Terminal fall-velocity vector of a particle or particle group
v_0	Particle fall-rate equation constant
	--W--
W	Total weapon explosive yield; in kilotons (of TNT)
w_L	Foliage surface density; in grams of dry foliage per sq ft of land area
w_0	Particle fall-rate equation constant

Symbol	Definition
	--X--
X	Downwind distance from ground zero
x	A distance or coordinate variable
x_h	Distance between sweeper operator and hopper
	--Y--
Y_A	Chain fission yield of mass number A; in atoms or moles per fission
Y_s	Half-width of stem fallout pattern to the 1 r/hr at 1 hr contour
y	Mass surface density of fallout particles (identical with I_m for land-type fallout); in mg per sq ft
$y_j'(t)$	Number of atoms per fission of element j (all mass numbers) at time, t', after fission
y_A	Fractional chain yield; in atoms per fission
	--Z--
z	Altitude coordinate; apparent altitude of fallout particle origins
z_0	Parameter defining cloud and particle rate-of-rise function; upper limit is h-b
z_s	Characteristic altitude at which first large particles fall away from rising fireball or cloud

INDEX

--A--

Abriam, J.O., 28
Absorption, energy, 5, 52, 114
Accumulated dosage, 357, 371, 547-549
Actions, defense, see Countermeasures
Active countermeasures, see Methods
Activity, see Radioactivity
  thermodynamic, 183, 400-407
Adams, C.E., 28, 31, 38, 41, 151, 488
Adsorption, particle
  chemisorption, see Chemical systems
  curves, 396
  equation variables, 423
  equilibrium, 394, 401
  interactions, see Surfaces
  isotherm, 394
  process, 52, 60, 114, 389; see also Methods reactions, see Chemical systems, fallout
AFOIN, 293, 294
Affected area,
  perimeter, 354
Agglomeration, see Particles
Agricultural area,
  decontamination, 508
Air
  burst, 4, 74, 114, 130, 360
  circulation, 312
  concentration, 222
  see Ionization
  velocity, 215
  ventilation, see Shelters
Air jets,
  high pressure, 484
Alfalfa, 87, 349
Allowed dose, see Planning factors
Alamogordo, N.M., 1
Albite, 135
Alcock, C.B., 169, 183
Alexander, L.T., 28
Alpha particles, 72, 84
Altitude, see Cloud
Ambrose clay, 496, 504
Anderson, A.D., 201, 208, 213, 214, 293, 299
Animals, see Hazard
Anorthoclase, 135
Apple Shot, 78, 84, 91, 340
Applicable countermeasures, see Planning factors
Applied effort, see Planning factors
Area(s),
  affected, 354, 547-549
  boundary, 351-354
  characteristic, 353
  clean, 368
  Damaged, 356
  decontamination, coverage rate, 353-471, 473, 476
  disposal, 475, 504
  exposed, 73-74, 327
  Free, 352
  gross, 365
  identification, 354-356
  land-, see Surfaces
  lawn-, 509
  major, 354
  paved, 486, 570
  perimeter, 351-356
  protective, 507

Area(s), (Cont.)
Radep, 353
residential, 554-590
roof, 490
rural, 367
source, 555
staging, 363-367
see Surfaces
target, 548
test, see Field tests
unaffected, 352
unpaved, 587
Asphalt, see Surfaces
Attack, nuclear war, 366-368
Attenuation, exposure
see Shelter, Shielding, Terrain

--B--

Backyard contributions, see Radioactivity
Badger, F.S., 465
Baker Shot, Bikini, 326, 405
Balloon-mounted devices, 72-77, 91, 297, 324-337
Ballou, N.E., 17, 23, 25, 50, 165, 176, 183, 226, 305, 347, 400
Band, Red, 356
Batten, D.R., 203
Batten, E.S., 298
Bellamy, A.W., 72
Belt, Gray, 356
Berkowitz, J., 183
Beta decay, 18, 50, 75, 81
Bigger, (Malumphy and), 465
Bikini Atoll, 45, 326, 405
Biological effects, see Hazard
Biological elimination period, 372, 375
Biological systems, see Hazard
Biosphere, 354
Birefringence, 71
Blackbody conditions, 125
Black Zone, 358, 362, 363
Blade angle, 506
Blast,
damage, 350
protection, 354
wave, 114, 316, 351, 358
Blume, J.M., 28
Boiling point, 164
Bolles, R.C., 17, 25, 50, 165, 176, 183, 223, 309, 347, 400, 405
Bomb
"clean", 27, 101
components, 407
structure, 3, 456
warhead, see Yield, weapon
Bone, effects on, 75
Bottom harbor, 324, 325
Bravo, Shot, see Shot
Breakaway time, 117, 118, 125
Brewer, L., 159, 163
Broom, rotary, 500
Broomed concrete, 489
Brushing, 382
Bucket scraper, 509
Building,
surface, 486, 495, 499
Buildings,
houses, 490
Buildings,
small, 490
Bulldozer, see Method(s)
Bunchgrass, see Foliage, 87
Bunney, L.R., 28
Burns, K.P., 159, 163
Burst
air, 4, 76, 329, 360
hypothetical, 290
land-surface, 328
multiple, 595
near-surface, 328
single, 595
yield, 362

Bushmallow, 87
Buster, Operation, 1
Bystrom, B.G., 73, 78, 81

--C--

Callahan, E.D., 203
Camp Parks, 80, 561, 573, 595, 597
Camp Stoneman, 470, 485, 486
Capabilities of Atomic Weapons, 202
Carr, W.J., 465
Carrier, fallout
  materials, 3, 15, 62, 96, 106-110
  matrix, 393
  properties, 380
  sea water, 405
  surface tension, 112
  total, 402-407
Castle, Operation, 1, 78
Chains, mass, 8-17, 63, 106-109, 146-165, 214, 305, 337, 380, 414-418, 490
Chandrasekharaiah, M.S., 159, 168
Charge-distribution curves, 25
Chemical systems, fallout
  additives, 382, 407
  see Adsorption
  assay, radiochemical, 17, 50
  chemisorption, 383, 401
  contact time, 407
  contamination process, 59, 73, 80, 417
  interactions, 10, 46, 52, 72, 80-85, 97-135, 159, 305, 349-351, 379-385, 393, 402, 417, 425, 429, 445, 460, 465; see also Methods, Surfaces
  oxide matrix, 393
  parameters, 383
  polymerization, 159
  radiochemical standards, 16
  reactions, 375-380, 392, 422-464
Chemical systems, fallout (Cont.)
  reference nuclide, 63
  slurry, 417-460
  solubility interactions, 76-99, 115, 340, 401-403
Chilton, A.B., 551, 599
Chupka, W.A., 159, 168
Civil defense,
  information, 373
  operations, 358, 368
  options, 356
  organization, 355, 362
  planning, see Planning
Clark, D.C., 511
Clark, D.E., 299
Clay soil, 496, 504
Clean area, 500, 507
Clean-up operations, 367
"Clean" weapon, 27, 101
Cleaning agent, Orvus, 426
C-Level unit, 400
Clothing, crew, 80, 356, 486
Cloud, fireball
  altitude, 154, 205, 215-216, 238-244, 294
  atmosphere effects, 117-121, 379-382
  chemistry, 10, 99, 305, 429, 464
  expansion, energy, 213
  formation, 10, 201-221, 304
  internal pressure, 155
  model parameters, 115, 150-152, 146-148, 297
  radius, 206, 239, 304
  rise rate, 213, 312
  size, 15, 205, 237, 301
  stem altitudes, 223, 235
  stem configuration, 205
  stem geometry, 215, 232, 237
  sublimation pressure, 98, 109, 305
  surface, 142, 152

Cloud, fireball (Cont.)
temperature(s), see model parameters
volume, 15, 95, 109, 134, 141, 208, 304
Clover, see Foliage
Coagulation process, 45
Cole, R., 222, 388, 391, 400, 408, 409, 411, 414, 420, 424, 428, 433
Collection, see Fallout
Colloidal particles, see Chemical system interactions
Complexing agent, EDTA, 407, 426
Compounds
chemical, 10, 99, 308
final, 429
Computations
computer, 202, 211
illustrative, 253, 303, 514
manual, 204, 210, 211, 218
see Planning factors
Concrete surfaces, 414, 426
Condensation equilibrium, 99, 102
Condensation process, see Particles
Contact time, 407
Contamination process, see Chemical systems, fallout
Contamination reduction, see Planning factors
Contour,
see Fallout
ground zero, 337
idealized, 253
isointensity, 9, 227, 241, 256, 297, 327, 349
mass, see Fallout
ratio, 10, 85, 109, 164, 207, 228, 241, 301, 315, 324, 332, 335, 349
ridge, 230, 243
standard, 235
Conventional flusher, 494, 498, 499
Coral, 31-98, 156, 284
Corrosion, 382
Coryell, C.D., 17
Cost-effectiveness, 470
Coughlin, J.P., 159, 163
Countermeasures
action options, 363, 550
actions, 365, 372, 520
active, 350, 364
applicable, 351
basic concepts, 513
communication, 365
composition, 351
cost-effectiveness, 470
crews, 364, 473, 486-490, 551-599
see Decontamination
defense actions, see Planning factors
design, 352
dispersal, 351, 362-368
distance effects, see Wind
distribution, 355
see Effectiveness
equipment, see Methods
evacuation, 351, 362, 368
see Fallout
feasibility, 204, 598
see Hazard
major, 353-366
objectives, 351, 371
operational use, 352
organization, 363
passive, see Shelters
see Planning factors
population distribution, 368
preventive, 300, 352, 548
priority, 356, 367-369
problems, 366
protective, 547-549
receptive, 351
recovery, 355-375, 529, 547-599
repair, 369

Countermeasures (Cont.)
rescue, 369
see Shelters
see Shielding
specification, 349-370
supplies, 361, 363, 365, 596
system analysis, 550
system development, 350
teams, 363
work times, see Time
Crater(s)
depth
materials, 14, 31, 114, 152, 303, 323
radius, 152
soil, 417
Crew, see Decontamination, see Methods
Criteria, planning dose, 470
Crooks, R.N., 195
Crossroads, Operation, 1
Crosswind
direction, 358
distance, 360
shear, see Wind shear
Crystals,
hydrated, 391
salt, 394, 396
Curie units, 61
Curtis, H.B., 470, 485, 511
Curve(s)
adsorption, 396
assumed decay, 3, 56, 60, 229, 318, 380, 386, 513
average decay, 514
calibration, 72, 486
charge distribution, 25
correction, 108-110, 167, 221, 324, 352
decay rate, 56, 229, 386, 416, 513, 524
delivery, 259, 355-366, 472, 547
Curve(s) (Cont.)
distribution, 324
DRM, 514
efficiency, 541
intensity, 277; see Radioactivity
ionization, see
rate-time, 513
reference, 183
temperature, 117, 121, 129, 148
yield, 16, 68, 142
Cycle, equipment,
area coverage, 503
crew exposure, 579
overlaps, 475
pass-width, 478, 504
ratio, decontamination, 474
speed, 475, 496, 500

--D--

Damage,
biological, 356
physical, 354, 358
property, 353, 365
Damaged area, 353, 356, 363, 370
Decay
correction, 108, 110, 167, 221, 352
curve, see Curves
see Ionization
radioactive, see Radioactivity
rate, see Curves
Debris, non-fallout, 69, 369
Decay, "normal", see Curves
Decontaminated area
as protection, 507
entry time, minimum, 537
Decontamination
active, 370
agents, 407-412
agricultural, 508
analysis, 500
area, 471-489, 498-504

Decontamination (Cont.)
building grounds, 509
building surfaces, 486
constants, 410
costs, 470
see Countermeasures
crew, 304, 473, 486, 532,535, 539, 551-599
critical parameters, 451-476
effectiveness, 382, 393, 410, 451, 471, 489, 508, 550, 572-599
efficiency, see Method
equation constants, 384, 405, 484, 494, 496, 535
see Equipment
equipment cycles, 472, 485, 500, see Pass
experiments, 451, 485, 486, 496, 577
feasibility, 204, 598
see Field tests
see Harbor
Hazard, see Dose, exposure
ion changes in, 385
land area, see Soil
manual, 494
mass fractions remaining, 430
see Methods
objectives, 10, 84, 371
paved area, see Surfaces
planning, see Planning factors
procedures, 382, 472, 489, 496
rates, see Method, Efficiency
removal, see Fallout
residential area, 564-590
see Residual number
scheduling, 489
see Seawater fallout
serial methods, use, 503
soil, coral, see Fallout
solubility, 401
start time, 535, 553
see Surfaces
times, see Method, Efficiency
vertical surfaces, 486
waste disposal, 375, 504, 508
water washing, see Method
wet method, 382, 472, 485
work times, 535, 553, 592
Decontamination solution, 401
Defense actions, see Countermeasures
Defense Planning, see Planning
Dehydration, 382
DeMaria, G., 159, 163
Density, see Particles
Density, liquid, 113, 305
Deposit level, see Fallout
Deposition, see Fallout
Desert surface, 485
Design, countermeasure system, 368
Designator, particle,
median diameter, 341
Desired dose, see Planning dose
Desorption rate, 391, 396
Detector, see Instruments
Detergents, 382
Detonation effects,
blast, 16, 114, 118, 312, 351-350, 360-368
cumulative, 354
see Crater
see Harbor
land-surface, see Soil
magnitude, 15, 56-72, 114, 227, 304-324, 337
materials, see Yield, weapon
multiple, 352, 360-365
overpressure, 118, 360, 368
point, 351, 417
see water surface, 45, 66-71, 320-380, 405
thermal, 356
underground, 485
see Yield

Dhein, E., 465
Diablo, Shot, see Shot, 86, 91
Diameter,
see Cloud,
Particle
Diesel equipment, 508
Differential coefficient, 473, 484
Differentiation of fallout 3
Diffraction, 31, 45, 71
Diffusion, 36, 113, 395
Diffusion process, 113
Digestive tract, 337
Dilution, 48, 99
Direct intake, see Fallout
Discs, see Particles
Discing, see Soil
Disintegration multipliers, see Radioactivity
Dispersal, 351, 362, 368
Disposal area, 375, 504
Dissociation, 116, 119, 120, 126, 135, 137, 159
Distance, effect on location, see Wind, Countermeasure
Distribution,
energy, 201, 350, 402
equilibrium, 120, 400
fractional mass, 203-205
NRDL, 337
population, 369
RAND, 337
relative, mud-sea water, 427
particle size, 384
smearing of, 385
Dolan, P.T., 170
Donovan, L.K., 551, 599
Dose, exposure
accumulated, 337, 372, 547-549, 578
allotted,"allowed", 356, 470, 489, 521, 528
Dose, exposure (Cont.)
biological, see Hazard, 15, 45, 73, 85-114, 164, 202, 337-354, 364 425, 469, 503, 532-534, 555, 571, 581
crew, 551, 579-599
criteria, see
critical, 308, 469, 513-515
decontamination crew, 364, 473, 480, 551-599
"desired", 350, 470, 489, 514, 522, 528, 532, 544
early, 356, 548
incremental, 357, 372, 548, 578
infinity, 356, 368, 529
lethal, 368, 469
levels, 355, 540
limit, 470
maximum, 364, 528
motor equipment operator, 585
observed, 357
planning, see Planning factors
potential, 6, 354, 350, 521, 528
property, 354
rate, see Curve, decay
ratio, RN, 514-544
reduction, 521
received, 99, 218, 591
Dose Rate Multiplier (DRM), 513-544
Downwind location, see Wind
Drainage systems, 370-393, 480
available, 530
pit, 480
storm, 530
surface, 475, 480
DRM, dose rate multiplier, 513-544
Drowart, J., 159, 163
Drop (droplet)
fireball, 14, 72, 112
interactions in, 304
see Radioactivity
see Seawater
volume, 395

Dry conditions
desert, 80, 330, 382
see Methods
see Soil
Drying period, see Particles
Dump truck, 508
Dumping area, 504, 508, 530
Dunning, G.M., 78
Dynamics, deposition, 218, 301
Dust, 318

--E--

Earth-cover, see Fallout
Earth-hauling, see Method
Ecological consequences,
nuclear war, 366
EDTA, complexing agent, 426
Edwards, R.R., 17
Effectiveness
cost, , 470
see Countermeasure
decontamination, 382, 393, 416, 451, 471-473, 489, 508, 550, 572-599
desired, 486
measure, 471, 476, 489, 503, 514
method, 480, 508, 520, 547
operational, 471, 502
over-all, 486, 507
parameters, 451-476
see Planning factors
recovery, 507
relative, 370, 407
removal, 10, 375, 380-386, 427, 507, 502
requirements, 470, 506
see Residual number
Shelter, 0, 81, 352, 366-368, 533
shielding, 520
variables, 451
variation, 451, 483

Efficiency
coefficient, 472, 477
concept, 469
curves, 541
decontamination, 480, 507-508, 544
differential coefficient, 473, 484
effectiveness, method, 382-393, 416, 451-471, 489, 508, 550, 572-599
man-hours per unit area, 473
parameters, 451-476
work-time, 470, 502
Effects of Nuclear Weapons (ENW), 15, 115, 125, 153, 186, 202, 215, 293, 323, 328, 330, 555
Effort, work
applied, 470, 508
expenditure, 485, 507
infinite-, 471
least, 503-508
rate, 471, 508, 535, 553
time parameter, 471, 508, 501-502
Electronic computers, 202-211
Elements,
see Ionization, Particles, Radioactivity
nonreactive, 425
refractory, 8-14, 48-74, 111-112, 164
scavenging, 253
trapped, 401
Elimination period, biological, 353
Emergency period,
centers 353-362
hospitals, 371-373, 540
see Shelters
Empirical data relationships, 204, 228
Emulsifier, 407
Energy, see Radioactivity
absorbed, -
balance, 74, 117, 144-148, 152
lost, 116
released, 13, 115-141

Enlwetok Proving Grounds, 56, 69, 78
Entry time, 532, 537, 593, 594
Environment effects, 36, 62, 349, 370, 481
ENW, see Effects of Nuclear Weapons
Equipment, countermeasure
availability, 530
capability, 361, 474, 486, 508
communication, 365
-crew, 364, 473, 551-599
design, 476
diesel, 508
firehosing, 486, 575
fuel requirements, 508
motorized, 366, 508, 570
requirements, 500
shovels, 489-491, 590
speed, 490
set-up, 508, 578, 582
work-time, 592
Estimates, see Planning factors
Evacuation, 351, 362, 368
Experimental decontamination, see Field Tests
Exposure, see Dose, Hazard
External
radiation hazard, 351, 364

--F--

Facilities,
protective, 349
recoverable, 353-366
Fallout,
aging, decay, see Curves, decay
areas, 297-304, 355-356, 361-370, 547
arrival rate, 299, 355-504, 398-356, 472
arrival time, 355, 364, 513
burying, 375, 504
cessation time, 513
chemistry, see Chemical system
Fallout (Cont.)
collection, 71, 81-84, 113, 318, see Field tests
colloidal, 393
composition, 71-97, 301-324, 392-393, 425-429, 514, 583, see Chemical systems
contributions, contamination, see Radioactivity
coral, 31-42, 53-63, 67-78, 98, 156, 284
coverage, area, 471
density, 38, 81, 113, 379, 380, 384, 386, 391, 496, 517
deposition rates, 80, 113, 156, 218, 235, 264, 324-340, 384
desert, 485
disposal, 375, 504
distribution, 7, 32, 73, 78, 104, 196 201, 251-272, 315, 324-341, 386, 427, 471, 489-490
earth-fill, cover, 500
formation, 111-114
fraction removed, see Decontamination
in body organs, see Hazard
initial mass, 386, 496
intake, direct, 75, 85, 425
pattern, 202-217, 227-241, 252-259, 300-321, 336, 464
precipitate, 401
properties, 379-380
removal, 275-280, 470-485, 504-508, 578-583, 592-596
removal effectiveness, 380, 507
residual mass, 471-496
retention, 340
scaling system, 125-139, 202-227, 295-301, 315-326, 513
solids, see Particles
see Surfaces
synthetic, 400, 471-485, 507

Fallout (Cont.)
types, see Harbor detonation, Land surface detonation, Sea water surface detonation
vaporization effects, 3-42, 76-98, 114-133, 199, 251, 306, 393
Fallout levels, see Particles, density
Farlow, N.H., 32, 45, 71, 151, 388
Farmers, 367
Fatalities, see Hazard, Planning factors, Dose, lethal
Feasibility, countermeasure, 204, 599,
Fer r, G.J., 293, 299
Field tests,
fallout collection, 71, 81-84, 113, 313-324
decontamination, 360, 469, 485-486, 489, 496, 504
Film, reagent, 45, 71
Filtration, 78
Fire(s)
control, 369
duration, 559
ignition, 352
large-scale, 356-360, 548
secondary, 351, 546
thermal, 547-549
Fireball, see Cloud
Fireball, formation process, 15, 30, 42
Firehose,
crew, 486
standard, 481, 486
Firehosing
automatic washdown, 491
concrete surfaces, 486, 489
crew arrangement, 486, 490
crew RN, 520, 575
distance, effect, 489
land surfaces, 382, 485, 498, 499
lobbing procedure, 490
nozzle team, 489
Firehosing (Cont.)
roof surfaces, 490, 567
runoff, 489
First aid, 362, 369
Fischer, E.M.R., 195
Fissile materials, see Materials
Fission(s)
chains, see Mass chains
concentration in seawater, 401
number of, 217, 245
tracer, 56, 414
Fission products, 8-31, 50-77, 97-102, 151-164, 186, 217, 245 251, 301-319, 379, 391-394, 414, 514
Flash,
thermal, 359
Flame, thermal, 359
Fluid stream energy, 456
Flushing method, 494-500
Foliage contamination
alfalfa, 87, 343
bushmallow, 87
clover, 79-84, 87, 343
rabbit brush, 89
sagebrush, 93, 97
wheat, 79, 84, 345
Food chain, see Hazard
Ford, M.R., 7
Fraction condensed, 164, 315
Fraction remaining, see Fallout, Particles, Radioactivity
Fractional yields, see Yields
Fractionated mixture, 155, 195, 221, 305, 317, 328, 392, 514
Fractionation, 8, 15, 50, 60, 69, 76, 81, 112, 120, 134, 189, 221, 251, 514
Fractionation number, 54, 60, 76, 108, 110, 221, 318, 341

"Free" area, 355, 363
Free energy
  equation, 402
  relationship, 399
Freiling, E.C., 62, 63, 195
Fukuryu Maru, 50
Fuller, R.K., 73, 408, 409, 414
Fuel consumption, 508
Fuel requirements,
  equipment, 508
  operation total, 508
Function, temperature-time, 139
  countermeasure, 352
  ENW scaling, 130, 226
  scaling, 134, 139, 141, 216, 332,
  step, 208
Fused particles, see Particles
Fusion,
  process, 13, 108
  see Thermonuclear reactions

--G--

Galiano, R.J., 203, 207, 284, 292
Gamma rays, see Hazard
Gas
  cooling, 146, 149, 319
  phase, 49, 97, 106, 111, 120, 304,
    311
Gaseous species, 392
Gasoline engines,
  fuel requirements, 508
Geometry, source, see Radioactivity
Gilfillan, E.S., 28
Glassy particles, see Particles,
  fused
Glendenin, L.E., 17, 25, 67, 165, 176,
  183, 306
Gloves,
  firehosing, 486
Gradient, 395
Graham, L.J., 408, 409, 414
Grass-cover soil, 504
Gravel, roof,
  removal, 490
Gravity, 201, 210, 383
  effect on fallout, 475
Greenfield, S.M., 201
Greenhouse, Operation, 1
Gray Belt, 358
  survivors, 362
  width, 362
Grimley, R.T., 159, 163
Ground, distribution on, 73
Grounds,
  near buildings, 509
Ground zero, see Wind direction

--H--

Habitability, shelter, 378
Harbor detonation, 327, 417
Haul distance, 509
Hawkins, M.E., 465
Hawthorne, H.A., 73, 78, 81
Hazard,
  beta, 5
  biological, 15, 45, 72-85, 114-164,
    202, 328, 337-354, 364, 425,
    469, 503, 532-534, 550, 571, 581
  contact, 5
  countermeasure, 471-489, 513-544,
    547-549
  critical dose, 368, 469, 513-515
  decontamination crew, 364, 478,
    486, 551-599
  degree, 73, 372, 470, 532
  external, 349-351, 364, 366
  fallout, see Radioactivity, Dose
  gamma, 5, 6-13, 56-70, 78, 182,
    366, 373, 389, 469, 547-549
  ingestion, 72-78, 85, 301, 328,
    345, 373, 549
  intensity, 10, 55, 109-115, 164-207,
    226-241, 304, 337, 341-349, 354,
    425, 485, 494, 534-544, 551-599

Hazard (Cont.)
internal, 85, 363-368, 375, 549
lethal, 368, 469, 548
potential, 5
protection, see Countermeasures, Planning factors
radiation sickness, 364, 469
residual radiation, 349, 351, 453
rural area, 368
thermal radiation, 351-360
x-ray, 4, 5, 8, 204
Health service centers, 361
Heffter, J.L., 293, 299
Height,
burst, 4, 76, 328
cloud, 211
optimum, 351
Helman, W.T., 78, 360, 382, 389, 391, 400, 411, 420, 424, 426, 433
Heinkell, R., 511
Henry's law, 99, 157, 159
Herrington, A.C., 25
Hiroshima, 361
Highway,
surface, 489
Holden, F.R., 511
Hooper, G.W., 159, 165
Hopper, fallout collecting, 500, 504
Horizontal surface, 494
Hose,
hook-up, 490
size, 490
Hosing,
see Firehosing
high-pressure, 484
Houses,
roofs of, 490, 555
Howell, J., 481, 511
Humans, see People
Humidity, 38, 85, 382, 387, 397
Humidity chamber, 387
Hydrants, availability, 539
Hydrous
oxides, 418
solids, 401, 428
Hygroscopic, see Particles
Hypothetical attack, 366

--I--

Ideal soil, see Soil
Identification methods, see Particles
Illustrative
analysis, 554-590
computations, 253, 305, 514-544
Impaction, see Particles
Impaction process, 46, 100
Impurity, see Particles
Improvised motor flusher, 494, 496, 499
Incandescence, 115, 117, 125
Incident neutrons, 16, 108
Independent yields, 17, 67, 107
Induced activity, see Radioactivity
Industry, national, 361
Inert materials, 15
Infinite effort, 471
Infinity dose,
criterion, 358
Initial
fallout level, 386, 414, 472, 488, 496
mass, 386, 414, 496
radiation, 351, 360, 362, 386, 414, 472, 488, 496
survival, 366, 371, see Planning factors
Ingestion hazard, 378
Inghram, M.G., 159, 165
Inglehart, D.L., 296, 299
Inhabited area, 486
Instrument(s)
NaI(T$_l$), 56, 70

Instruments(s) (Cont.)
portable, 9, 70, 189, 195, 196, 229, 232, 355
radiac AN/PDR/-39(TIB), 189, 195, 229
radiation detector, 355
response factor, 156, 171, 195, 229
scintillation counter, 56
Intensity
see Contour
contributions, see Radioactivity
gradient, 229, 339, 361-367
see Hazard
levels, 239-240
magnitude, 349-351
observed, 208, 357
pattern, 227, 241, 252, 259, 290-300, 321-326
radiation, 368
ridge, 230, 243
standard, 9, 227, 235, 247, 294
Intensity profile,
downwind, 241
standard, 247
upwind, 255
Interactions, see Chemical systems
Interface,
surface-liquid, 395
vapor-liquid, 395
Interference color, 71
Internal energy change, 117
Internal emitters, 375
Internal pressure, see Cloud
Ion chamber, 189, 418
Ion concentration, see Radioactivity
Ion current, 56-60
Ionization
air, 397, 400, 471
contribution, 494, 551-552
fraction remaining, see Particles, Radioactivity
gross fractionation, 464, 494
Ionization (Cont.)
maximum reduction, 391
rate, 5-14, 50-51, 116-126, 291-297, 304-314, 372, 391, 411, 464, 471, 485, 513-524, 552
ratio 183, 301-305, 471, 513
reduction, 471
weighting factor, 464
Irregular particles, see Particles
Isointensity
contour, 9
patterns, 349
Isotopes, 24, see Radioactivity
Ivy, Operation, 31

--J--

James, P.R., 508, 511
Jangle, Operation, 1, 28, 78, 156,
"S" Shot, 156, 288, 318
"U" Shot, 156, 324
Jeep, 509
Jefferson, M.E., 28
Jet, water, 114, 476
Jones, J.W., 56

--K--

Kaplan, J.D., 208
Katcoff, S., 17, 176
Kehrer, W.E., 511
Kelley, K.K., 120, 136, 159, 168
Kellogg, W.W., 201
Kimura, K., 50, 51, 78, 195
Kinetic energy, 118
Kinetic power,
water stream, 476
King, R.W., 31
Knapp, H.A., 60
Knothole, Operation, 38
Kaanda, C.F., 202

--L--

Land area, see Surface
Land area methods, see Decontamination, Soil
Land surface detonation, see Soil, Methods, Planning factors
Lane, W.B., 382, 408, 414, 418, 419, 425, 426
Lapp, R.E., 78
Lapple, C.E., 133
LaRiviere, P.D., 174, 228, 279, 511
Larson, K.H., 72, 73, 74, 75
Lateral distance, see Distance, Wind
Laughlin, R.A., 481, 511
Laumetz, E., 222
Laurino, R., 202, 470, 549
Lawn area,
  sod cutting, 509
Layer, soil, 504
Ledges, fallout on, 494
Lee, H., 470, 473, 478, 485, 500, 511, 532, 549
Lethality, see Hazard
Level, attack, 366
Level, ionization, see Radioactivity
Levels, fallout, see Particles, density
Lindberg, R.G., 72, 73, 74, 81
Liquid
  -condensation, 417
  -phase, 14, 45, 97, 106, 308, 392
  -surface interface, 395
  -vapor interface, 395
Loading, mass, see Fallout
Loam soil, 486, 504
Lobbing method, 485-491
Location, 84, 375, 514
Loeb, P., 6, 81, 167, 174, 189, 306, 347, 377, 437, 555
Love, D., 56, 195

--Mc--

McDonald, D., 56, 195

--M--

Machta, L., 293, 299
Mackin, J., 56, 60, 62, 189, 195, 382
Magnetic particles, 481
Maloney, J.C., 465
Manpower, trained, 365
Manual decontamination methods, 494
Margrave, J.L., 159, 165
Marshall Islanders, 2
Mass, see Fallout, Particles
Mass fraction remaining, see Particles
Materials, fallout
  balance of, 106, 164
  see Carrier
  colloidal, 395
  dense, 375, 552
  environmental, see Soil(s), Water
  handling of, 469
  inert, 15, 379-381
  released, 469
  structural, 391, 456
  -surface, 470
Mather, J.R., 80
Matrix, carrier, 395
Maxwell, R.D., 26
Medical service centers, 365
Menzel, R.G., 408, 511
Met Shot, 78, 85, 91
Meter response, see Instruments
Method(s), countermeasure
  analytical, 549
  application procedure, 476, 489, 533
  approximations, 206, 216, 547
  bulldozer, 485, 489, 506, 508, 533
  combination of, 506, 533, 547
  crew, 364, 473, 486, 551-599

Method(s) (Cont.)
decontamination, see Decontamination, Planning factors
distance effects, 469
dry, 382, 472, 484
earth-hauling, 504
effectiveness, 382, 393, 416, 451, 471, 489, 505, 520, 547
efficiency, 489, 507, 508, 544
efficiency coefficient, 472
efficiency differential coefficient, 473, 484
firehosing, 386, 486, 575
fuel requirements, 508
see Hazard
immersion stirrer, 387
land areas, 504
lobbing, 485, 491
manual, 459, 494
motor grader, 485
motorized sweeper, 485, 538, 574
operational effectiveness, 471, 585, 592
pick-up, 472
pile-up, 472, 475, 508
plowing, 500
procedural aspects, 486
recovery, 387
residual levels, 471, 489
residual number, 520
roof-washdown, 490
scraper, tractor, 489
scrubbing, 382
aerial use of, 505
set-up time, 503, 575, 582
simple washing, 482, 496
soil removing, 489, 507
spillage effects, 474
stirrer, 412
streets, 489
sweeping, 472, 538
water flushing, 472, 494
Method(s) (Cont.)
water spray, 387
water washing, 451, 491
wet, 382, 474, 485
work times, 592
Mike Shot, 31
Miller, C.F., 6, 78, 80, 81, 167, 174, 189, 306, 324, 348, 377, 382, 385, 391, 400, 405, 408, 413, 414, 417, 418, 420, 424, 426, 433, 437, 484, 485, 511, 514, 555
Miller, J.R., 80
Minvielle, L., 202
Missile, see Yield, weapon
Mixing coefficient, slurry, 447
Mixture, particle
fractionated, 8, 112, 186, 195, 221, 305, 317, 328, 392, 514
slurry, 425, 429
soil, 585
Model
air burst, 151, 189
condensation process, 157
mathematical, 202-210
scaling, see Scaling system
surface burst, 131-139, 147-149, 153-175, 187, 227
Moist soil, grass cover, 504
Molumphy and Bigger, 485
Morgan, K.Z., 7, 337
Moskin, A., 202
Motorgrader, 485, 508
Motorized methods, 481-510
Multiple detonations, 352, 360-365

--N--

Nagasaki, 361
Nagler, K M., 203, 209
Nakamura, J.K., 80
NAVDOCKS, 411, 416, 470, 514
Neel, J.W., 72, 74, 76, 78, 80
Neutron(s)
  activation, see Radioactivity
  capture, 3, 8, 15, 56
  emission, 6, 59, 114, 189
  excess, 26
  fission product, 3, 8, 13, 27, 56, 73, 97, 156, 164, 166, 251, 301, 319, 379-391, 514
  incident, 16, 26, 108
Nevada Test Site, 69, 73, 74, 77, 78, 80, 91, 213, 386, 466
New Mexico, 78
Nishita, H., 72, 73
Nozzle, firehosing
  bar, 491
  calibration data, 486, 500
  pressure, 476, 486, 489
  size, 476, 480
  team, 489, 490, 577
  tip, area of, 476, 488
NRDL, 28, 30, 41, 56, 284, 293
Nuckolls, M., 408, 412, 414, 417
Nuclear devices, see Yield, weapon
Nuclides, see Radioactivity

--O--

OCDM, National Plan Appendix Series, 551
O'Connor, J D., 41
Open area entry time, 594
Open field rate, see Ionization
Operation(s), test
  Buster-Jangle, 1
  Castle, 1, 78
  Crossroads, 1
Operation(s) (Cont.)
  Greenhouse, 1
  Ivy, 31
  Jangle, 48, 484
  Knothole, 35
  Plumbbob, 75, 485, 507, 551
  Redwing, 41
  Streetsweep, 481
  Teapot, 72, 73, 74, 78
  Upshot, 1, 28, 31, 38, 41, 151, 486
Organization, civil defense
  command and control structure, 384, 566
  countermeasure options, see Planning factors
  plans, 351, 366, 382, 550
  program, 553-566
Orvus, cleaning agent, 426
Outdoor surfaces, 491
Overman, R.T., 56
Overpressure, blast, 16, 115, 360, 368
Owen, W.L., 50, 440, 470, 475, 485, 486, 494, 500, 511, 561, 573, 586, 597

--P--

Pacific Proving Grounds, 440
Packing-fraction curves, 25
Painted surfaces, 491
Pappas, A.C., 25
Parameters, effectiveness, 451-476
Parks, Camp, 30, 501, 573, 595, 597
Particle(s), fallout
  adsorption, see Chemical systems
  agglomeration, 98, 380, 392
  albite, 135
  altitudes, source, see Cloud
  anorthoclase, 135
  collection, see Fallout, Field tests
  collisions, 30-49, 113

Particle(s), fallout (Cont.)
colloidal, 302, 407
condensation, 99-102, 310, 302, 417, 514
coral, 31-98, 150, 284
crystalline, 41-49, 71-98, 159, 382-391
density, 38, 81, 113, 218, 301, 370-386, 391, 414, 472, 483, 547
depth, surface layer, 115, 391
designator, 295
diameters, 238, 481
discs, 203
disposal, see Fallout removal
distribution, 204, 384, 427
drainage discharge, 489
drying, 445
fall time, 220-230, 337
fall trajectory, 191-201, 218-241, 288
see Fission products
flow lines, 38
fluffy, 36-38
form, 392
formation process, 111-114
fraction remaining, 386, 416-420, 474-489, 494
fraction removed, see Fallout
fused, 25-39, 56-60, 72-80, 95-111, 165, 379-388, 417
glassy-bead, grains in, 98, 223-251, 305, 380, 425
groups, 223, 251, 305, 380
hydrated crystal, 401, 425
hydrous oxide, 418
hydrous solid, 401, 426
hygroscopic, 388-397
identification methods, 70
impaction, 30, 48
initial deposit levels, 414, 471-472, 483, 496
insoluble hydroxide, 402
Particle(s), fallout (Cont.)
interactions in, see Chemical systems, Slurry
ionic, 393
irregular, 30-38, 41-62, 97, 157, 383
levels, see density
liquid, see Sea water, Slurry
magnetic, 481
median diameter, 238, 481
melted, 97, 114, 303
metal oxides, 112
see Mixture
molar concentration, 400
nonreactive, 425
prewetted, 387, 401, 496
purity, 40
remaining, 391, 471, 485-489, 496
removal, 380, 470-477, 481
removal methods, see Methods
residual, 471, 490
retention, 7, 81-88, 340, 391, 401, 471-491
saturation level, 489
silicates, 26, 38, 45, 60, 112, 153-159
sintered, see fused, glassy
size, 26, 35, 45, 48, 68, 76, 111, 195, 203, 288, 304, 380, 384, 471, 481
size distribution, 384
size effects, 480, 485
slurry, 429
smearing, 381-385
solid, 8, 14, 28, 30, 45, 72-78, 97-108, 150, 301, 320
solid phase, 98, 425
soluble crystal, 392, 401
source, see Radioactivity
spherical, 30-38, 59-60, 98-112, 283, 380
structure, 28, 48, 71
surface density, 384, 464, 472

Particle(s), fallout (Cont.)
tagged, 486
thin section analysis, 71
transport, 462, 475
travel distance, 401, 480
unmelted, 417
vaporization, 3-42, 76-98, 114-138, 199, 261, 306, 393
velocity, 40, 204, 216, 233, 238, 287, 296, 340
voids, 30, 98
volume, solid phase, 401
Pass, decontamination,
exposure, 570
method-, 472, 579, see Cycle
multiple, 486, 504
speed, 479, 481
Passive countermeasures, see Shelters, Planning factors
Pattern, isointensity
center, 217, 239
contour, 227-241, 252-259, 290-300, 321-336, 349
idealized, 247, 253
variation, 471
Paved surface decontamination, 486, 570
Pay-loader, 598
Perkins, J.F., 31
Pestaner, J.F., 409, 414
Petrography, 28, 31, 69, 71
Pettijohn, F.J., 31
Phase, attack, 368
Phenomena, detonation, 350-508
Pick-up method, 472
Pick-up truck, 508
Pile-up method, 472, 475, 583
Pit, drainage, 480, 504
Planning, countermeasure, see Planning factors
Planning dose, criteria, 470
Planning factors,
"acceptable" dose level, 470, 480
action options, 352-354, 363, 367-381, 513, 547, 570
affected areas, 353-363, 365
allotted dose, 356, 470, 480, 514, 521, 528, 532, 544
applied effort, 470-471
applicable countermeasures, 327, 354, 417, 532
attenuation, shielding, 81, 189-195 322-364, 372
burst altitude, 216-237
calculations, 26, 67, 117, 186, 202-211, 216, 258, 305, 356, 470, 489, 514, 522, 526, 532, 544
contamination, see Surfaces, Methods, Chemical systems
contamination reduction, 327, 354, 417, 470, 502
conversion data, 26, 67, 117, 186, 221
cost-effectiveness, 470
crew assembly, 539
crew, maximum exposure, 532-535, 551-579
criteria, 470
decay rate, fallout, 56, 80, 103, 107, 321, 329, 318, 350, 352, 360-386, 513
decontaminated area, 587, 598
decontamination method analysis, 566
"desired" dose, 470
dose rate, see Hazard
dose restriction, 470, 531, 534
see Effectiveness
see Efficiency
see Entry time
see Environmental effects
see Equipment
explosion phenomena, 15, 27, 65, 201, 324

Planning factors, (Cont.)
exposure dose, see Hazard
see Fallout; see also, Particles, Radioactivity
feasibility, countermeasure, 204, 598, see Chemical systems
harbor detonation, 327-417, see also Slurry
instrument response, 156, 195, 221, 324; see also Instruments
ionization rate, see Curves
land-area detonation, see Soil, Surfaces, Methods
location, see Wind
mass correction, 324
minimum shelter stay, 524; see also Shelters, Planning
meteorological effects, 79-84, 202 350-362; see also Wind
operational estimates, 489
operational parameters, 550
organization program, 566
preventive measures, 550
priority, action, 556, 567, 569
protection aspects, 356, 370, 486, 547-549
"R" factor, 16, 128, 138
recovery feasibility, 566, 567, 598
recoverable facilities, 353-366
repair operations, 567
requirements, 470-548-549, 596
schedules, 469, 547
shelter exit time, see Shelters
see Shielding
survival actions, 366, 371
target areas, 547
temperature effects, 117-121, 129, 148, 485
terrain, 156, 159, 195, 221, 322-329
training program, 566
Plowing method, 80, 508
Plumbbob, Operation, 75, 485, 507, 551
Point-location analysis, 548
Polymerization, 150
Population distribution, see Countermeasures
Pooler, F., Jr., 293, 299
Poppoff, I.G., 28, 31, 202
Portable survey meter, see Instruments
Porter, R.F., 183
Portland cement, 480
Potential dose, definition, 6, 354
Precipitate, fallout, 401
Present, R.D., 17, 188
Pressure, see Cloud, Ionization, Radioactivity
Preventive countermeasure, see Planning factors
Priscilla, Shot, 91
Properties, fallout, see Fallout
Property damage, 358, 366
Protection factor, system, 356, 370
Protection requirements, see Planning factors
Postattack period, 366; see also Planning factors
Pugh, G.E., 203, 207, 284, 292
Pump, firehosing, 456

--Q--

Quantity,
see Fallout
see Particles(s)
see Radioactivity

--R--

Rabbit brush, 89
Rabbits, 74
Radep areas, 355, 358, 361, 364
Radiac, see Instruments
Radiation, see Radioactivity
Radiation sickness, 354, 469
Radioactivity
  accumulated, 221, 351, 548
  amounts of elements, 15, 45, 72, 114, 164, 304-308, 341-355, 393, 401-405
  atoms, 2, 5
  back yard, 588
  colloid, 393, 400
  contributions, 195, 222, 351-357, 485-494, 534, 555-559, 571, 587
  decontamination effects, 354-366, 376-399
  deposition, 80, 113, 156, 218-285, 264, 324-340, 384
  detector, see Instruments
  disintegration multipliers, 168
  exposure, see Hazard
  fraction remaining, 393, 480, 471, 490
  fractional distribution, 205, 248, 301-311
  gamma ray, 5-13, 24, 50-75, 189 356-359, 469, 547-549
  induced, 8, 59, 195, 221, 308, 391
  ionic elements, 8, 48, 72, 97, 335, 393, 395, 400, 471, 485, 494
  insoluble elements, 425, 460
  intensity, 10, 95, 109-207, 226-241, 341-349, 554-544, 551-599
  long-lived elements, 371
  neutron capture, 3, 8, 15, 56
  neutron emission, 6, 59, 114, 189
  nuclides, 16-25, 50, 62-63, 106-110, 337
  point source, 350
Radioactivity (Cont.)
  radiation, 15, 45, 72, 114, 131-135, 164-207, 226-241, 304-337, 354, 425, 485, 494, 503, 534, 555, 571, 587
  refractory elements, 8, 14, 48, 55, 74, 111, 112, 154
  residual radiation, 471, 489-490
  scavenging elements, 253
  sources, 5, 10, 99, 201-243, 301-332, 503-513, 549, 552, 561
  source geometry, see Cloud, fireball
  specific, 337, 464, 471
  vaporization, 8-42, 76-95, 114-135, 169, 251, 306, 393
Radioelements, see Radioactivity
Radiography, 26, 31, 42, 69, 71
Radiological countermeasures, see Planning factors
Radionuclides, see Radioactivity
Radiotantalum particles, 451
Radishes, contaminated, 73
"Rad-safe" concept, 469
Rain, effects, 79-84, 350-352
Rainey, C.T., 72, 74
RAND distribution, 284
Raoult's law, 164, 165, 166
Rapp, R.R., 201, 205, 293, 299
Rate count, decay, 337
Rate, drying, 382
Rats, contaminated, 74
Reactions, see Chemical systems, fallout
Reagent film, 72
Recovery period, 351, 372, 548
  actions, 367, 529
  see Countermeasures
  crew, see Methods
  feasibility, see Planning factors
  of industries, 363
  Radep area, 365

Recovery period, (Cont.)
survival and, 368
teams, 364, 367
Red Band, 358–369
Redwing, Operation, 41
Rehabilitation centers, 393
Reitemeier, R.F., 80
Refractory elements, 8, 14, 48, 68, 74, 111, 112, 154
Relative effectiveness, 370, 407
Removal effectiveness, 10, 375–384, 420, 507, 592
Removal, fallout, see Methods
Removal, particle, see Decontamination
Repair operations, 367
Requirements, see Planning factors
Rescue operations, 362, 366
Residential area decontamination, 554–590
Residual mass, see Fallout
Residual number, RN
combination, 514
components, major, 514–521
maximum, 520, 589
minimum, 589
ratio, 416–427
requirements, 520
Residual radiation, see Radioactivity
Resources, nonhuman, 556
Response levels, 551
humans, 555
inanimate objects, 555
instruments, 150
Restriction, dose, see Planning factors
Roxepal, E., 465
Rich, intensity, 230, 248
Retention, particle, see Surfaces
RN, residual number, see Planning factors
Rise rate, cloud, 213, 312
Rodents, see Biological system, 74
Roentgen(s), see Dose, ionization
definition, 5
r/hr, 222
Rongelap Atoll, 2
Romney, E.M., 72, 75, 78, 81, 84
Rosenblum, L., 203
Roof decontamination, 80, 490–491; see also Surfaces, Methods
Roughness, surface, 480, 504
Runoff, firehosing, 480, 491
Rural area decontamination, 308

--S--

"S" Shot, 150
Safety procedures, see Countermeasures, Planning factors
Sagebrush, 83, 87
Salt crystals, 307
Sam, D., 50, 195, 400, 414
San Francisco Bay muds, 420
Sandbags, 375
Sandblasting, 382
Sartor, J.D., 80, 470, 476, 485, 486, 494, 500, 511, 561, 578, 580, 597
Saturation level, see Particles
Scadden, E.M., 20
Scaling system, model, 125–146, 202–208, 295–301, 315–326, 513–514, 530
Scheduling, see Planning factors
Schell, W.R., 151, 321, 385
Schorr, M.G., 28
Schubert, E.A., 201, 207, 218
Scintillation counter, see Instruments
Scraper method, motorized, 472–500
prime mover, 504
spillage, blade, 474, 485, 504
tractor, 480, 500
Scrubbing method, 382

Sea water fallout, 293, 301-307, 403-410
  characterization, 303
  C-Level unit, 405, 455
  components, 301-307
  concentration, 303
  contamination, 405
  decontamination, 410, 455
  residue, 72, 327
  salts, 72, 327, 396
  surface density, 402
  surface interactions, 307, 403-405
Serial use, see Method(s)
Service centers, survivor, 361-362
Set-up time, equipment, 508, 576, 582
Sewers, particle drainage, 489
Shallow water detonation, 417
Shasta, Shot, 85, 91
Shear effects, see Wind
Shelter
  adequate, 807
  blast, 352, 548-549
  buried, 308
  characteristics, 548
  communication, 365
  design, 308, 548
  effectiveness, 9, 81, 352, 366-368, 372, 520, 530
  exit time, 522
  "fallout", 308, 548
  fireproof, 370
  habitability, 365, 549
  inadequate, 307, 548
  requirements, 366, 549
  see Residual number
  sealing, 548
  see Shielding
  stay times, 522
  ventilation, 549
Shielding,
  attenuation, 81, 350, 366, 372, 552
  countermeasure, see Shelter
Shielding (Cont.)
  effectiveness, 520
  requirements, 304
  terrain, 150, 105, 221, 328, 552
Ships, target, 2, 50, 381, 397
Shock phenomena,
  effects, 14, 114, 124, 133, 351, 358
  wave energy, 115, 124, 340
  waves, 114-115
Shovels, see Equipment, counter-measure
Shot(s), test
  Apple, 78, 84, 91, 340
  Baker, 45, 320, 405
  Bravo, 1, 50, 290, 297
  Diablo, 85, 340
  Met, 78, 340
  Miko, 31
  Priscilla, 91, 340
  Jangle "S", 150, 288, 318
  Smoky, 75, 84, 340
  Tesla, 91, 340
  Trinity, 1, 78
  Jangle "U", 150, 324
Shrubs, in decontamination, 500
Sickness, radiation, 354, 469
Sidewalks, in decontamination, see Surfaces
Silicates, see Particles
Simulated fallout, 471, 485, 507
Single particle analysis, 70
Sinks, G.C., 130, 136, 159, 168
Sintered soil grains, see Particles
Simple washing method, 490
Skip loader, 480, 500
Slurry
  bulk solution, 432
  interactions, 417, 425, 460
  ionic species in, 410
  liquid phase, 422
  mixing coefficient, 447
  mixtures, 427, 460
  mud, 423

Slurry (Cont.)
phase concentrations, 425
solid phase, 420-429, 460
surface interactions, 366
volume-to-area ratio, 423
Smearing coefficient, 472, 496
Smoky, Shot, 75, 84, 97
Soaps, 382
Sod, lawn-cutting, 509
Soil(s)
characteristics, 486, 504-508
clay, 388, 496, 504
clean, 489, 500
cohesion, 474, 507
concentrations on, 146, 148
contaminated, 504
coral, see Surfaces
see Crater
decontamination, see Methods
desert, 485
-detonation, 363-383
dry, 504
excavated, 504
grass covered, 504
ideal, 185-188, 198, 474, 506
in fallout, see Particles
-layer, 504
liquid-, 147-151
loam, 496
loose, 506
-mixture, 496, 505
moist, 504
properties, 396, 475, 504
removal of, 474, 504-507, 585
-scraping, 585
shear strength, 504
shrubs on, 509
sod, 509
spilled, 474
subsoil drainage, 489
-surface layer, 473, 504
tagged, 485, 496, 507
Soil(s) (Cont.)
tilled, 504
-type, 504
uniform, 474
wet, 504
Solid particles in slurry, 429
Solid-to-liquid mass ratio, 429
Solution, decontaminating, 157, 401
Soulen, J.R., 159, 163
Source(s), fallout, see Cloud, Radioactivity
Special clothing, crews, 486
Speed(s), equipment, 496, 500, 506, 576
Spillage, fallout, 474, 485, 504
Spray, water, method
angle, 472, 486
chamber, 412, 496
high pressure, 472, 490
nozzle, 475
operating parameters, 475, 490-496
pattern, 490
Spreading coefficient, particle removal, 472, 484
Staging areas, survivor rescue, 361
Steinberg, E.P., 17
Stem, see Cloud
Stetson, R.L., 75
Stewart, K., 30, 99, 195
Sthapitanonda, P., 159, 163
Stirrer method, 412
Stokes' law, 320
Stoneman, Camp, 470, 485, 486, 496, 504, 511
Stream, water, method, 475, 476, 486-489, 496
Street sweeper, motorized, 481, 500, 508, 574
Stripping films, 71
Strope, W.E., 187, 470, 484, 485, 491, 511, 549, 551

Structure(s)
destruction of, 391
particle-, 28, 48, 71; see Particles
shielding effectiveness of, 520
surfaces of, 491; see Surfaces
test device, 36, 48
undamaged, 551
Stull, D.R., 120, 136, 159, 163
Sublimation pressure, see Cloud, fireball
Subsoil drainage, 489
Supplies, countermeasure, 361, 365, 590
Surface contributions, see Radioactivity
Surface(s)
Ambrose clay, 496, 504
asphaltic concrete, 414, 486
broomed, 489
building, 486, 490
-burst, 115, 133, 153, 380, 570, 585
carrier-, 99, 109
chemical interactions, 375
clay, 496, 504
concrete, 481-494
-condition, 489
contaminated, 65, 386, 416, 475
coral-, 91-98, 156, 234
decontaminated, 416
-density, 384, 471
desert, see Soil(s)
deterioration, 475
drainage, 475
earth-, 349, 509
exposed, 550
fractional coverage of, 384-385
galvanized iron, 414
highway, 469
horizontal, 400, 494
impervious, 418
land-type, 80, 485, 504, 585
Surface(s) (Cont.)
ledge, 494
-liquid interface, 395
macadam, 481
mass density, 384
microporosity of, 407
most difficult, 558
orientation of, 551
outdoor, 491
painted, 491
paved, 486, 570
Portland cement, 486, 494
reactions with, 375
removal of, 486, 585
road, 481
roof-, washdown, 490
roofing, 490
roughness of, 486, 489
saturation level of, 361, 385, 472
sidewalks, 486, 570
smoothness of, 489
-tension, 113
-types, 407
unpaved, 587
vertical, 491
water angle on, 486
window frame, 494
Surface-method combination, 472, 489, 568
Surface-removal methods, 486
Surprise attack, 360
Survival
initial, 366, 371
elements, 364
Gray Belt, 550
problems, 361-365, 368-371
population, 360
rate, 359-362
resources, 547
Sweeping method,
hand, 481
motorized, 382, 472, 484

Synthetic fallout, 400, 471-485, 507
System protection factor, 370

--T--

Tagged soil, 485, 496, 507
Tantalum particles, 481
Tar and gravel *roof*, 490, 491
Target
  analysis, 547, 566, 597
  complex, 351, 547, 589
  distribution, 355
  materials, 456
  prime-, 352
  -ship, 397
  spatial, 355
  -unit, 547, 566, 582
Team, hose, 490
Team, nozzle, 489, 490
Techniques, removal
  manual, 494
  motorized, 472-506
Temperature(s), see Ionization, Fallout
Tennant vacuum sweeper, 500, 503
Terrain shielding, 156, 195, 221, 328
Tesla, Shot, 91
Test series, see Field tests, Operation(s), Shot(s)
Thermodynamic equilibrium, 597
Thermodynamic model, 97, 100, 110, 124, 197, 210
Thermonuclear reactions, 26-27
Thin section analysis, 71
Thornthwaite, C.W., 80
Thyroid, 74
Tilled soil, 504
Time
  arrival, fallout, 74, 81, 153, 214, 311, 366, 370, 513
  breakaway, 117
  cessation, fallout, 218, 222, 513
Time, (Cont.)
  condensation, 67, 106, 305
  contact, 407
  critical, 514, 547-549
  entry, 522, 537, 535, 553
  decontamination start, 535, 553
  fall, particle, 220, 230, 337, 513
  ionization, 0, 13, 49, 62, 513
  measurement, 76, 81
  operating, 508
  reference, 115
  relative, 379
  rise, 232
  scale, 364
  set-up, 508, 578, 582
  shelter exit, 522
  shelter stay, 363, 365, 522, 548
  thermal balance, 116
  working, 385, 508
Tissue, 7, 75
Tower-mounted devices, 38-49, 72-84, 91-113, 151-156, 297, 324
Tracer, fission product, 56, 414
Toroid circulation in cloud, 215, 230, 312
Tractor,
  scraper, 489
  wheel, 509
Training,
  manpower, 395
  program, 566
Trajectory, particle-fall, 201, 241, 255, 491
Transattack period, 360, 364, 366
Transport, see Particles
Tripolyphosphate, 407, 412
Trinity Shot, 1, 78
Turbulence, 113
Truck,
  pay-loader, 508
  pick-up, 508

--U--

Unpaved area recovery, 587
"U" Shot, 156, 324
Underground,
  detonation, 77, 155, 485
  shelter, 361
Unit-average analysis, 549
Unmelted particles, 303
Unpaved surfaces, 80
Unshielded operations, 354
Updrafts, 154
Upshot, Operation, 72, 74
Uptake, see Hazard, Ingestion

--V--

Vacuum cleaning method, 382, 472, 484, 500
Van Horn, W.H., 470, 476, 485, 486, 494, 500, 511
Vapor-liquid interface, 395
Vaporization, 3-42, 76-98, 114-133, 169, 251, 306, 393
  process, 3-42, 76-98, 114-133, 158-169, 251, 306-393
Ventilation, 373
Vertical surfaces, 491
Volatile elements, 8, 40, 60, 76, 112
Volume, fallout drop, 72

--W--

Wahl, A.C., 25
Wallace, N.R., 28, 31
War, nuclear, 1, 540
Warhead, bomb
  missile, 4, 381, 391, 456
Warning, attack, 368
Washing method, 451, 490-491
Waste disposal, see Fallout removal
Water
  bulk, 330, 475
  countermeasure use, 392, 530, 595
  expenditure, 485
  -flow, volume, 451, 475
  -flushing, 472-494
  hydrants, available, 539
  jet, 114, 476
  -lobbing, 485-491
  pressure, 486
  sea water, synthetic, 392, 400
  shallow, 327, 417
  shelters, in, 355, 367
  source, availability, 539
  spray angle, 472, 486
  spray chamber, 494
  runoff, 490
  vapor, 392
  -washing, simple, 496
Water stream,
  kinetic power, 407, 476
  surface impingement, 475, 489
  volume, 330, 475
Wayne streetsweeper, 500, 539
Weapon, see Yield
Weapons tests, see Field tests, Operation(s), Shot(s)
Wet methods, 382, 472, 485
Weathering, 78, 381
Well-crystal (WC) counter, 56
Wheat, 70, 84-87, 343
Wheel barrow, 500, 590
Wheel tractor, 500
Width, equipment pass, 473
Width, Grey Belt, 360

Wind
  crosswind area, 244
  direction effects, 202, 237, 300, 382
  downwind location, 9, 63-91, 112, 195, 217, 227-245, 276-304, 362-370
  shear, 228, 242, 290, 301
  upwind location, 360
  vector, 81, 218
  velocity, 80, 202, 205, 218, 235, 242, 292
Wittman, J.P., 38
Work-effort, see Effort
World War II, 361
WSEG, 293, 294, 297

--X--

X-rays, 4, 8, 204

--Y--

Yield, weapon
  attack level, 366-367
  effects, 8, 27, 45, 56, 62, 67, 87, 101-115, 135-139, 157, 165, 183, 202-204, 230, 305, 327, 397, 355-366, 381, 392
  independent, 17, 67, 107

--Z--

Zone, Black, 356
Zigman, P., 56, 180, 195, 223

STANFORD RESEARCH INSTITUTE

MENLO PARK CALIFORNIA

Regional Offices and Laboratories

Southern California Laboratories
820 Mission Street
South Pasadena, California

Washington Office
808 17th Street, N.W.
Washington 6, D.C.

New York Office
270 Park Avenue, Room 1770
New York 17, New York

Detroit Office
The Stevens Building
1025 East Maple Road
Birmingham, Michigan

European Office
Pelikanstrasse 37
Zurich 1, Switzerland

Representatives

Honolulu, Hawaii
Finance Factors Building
195 South King Street
Honolulu, Hawaii

London, Ontario, Canada
85 Wychwood Park
London 14, Ontario, Canada

London, England
15 Abbotsbury Close
London W. 14, England

Milan, Italy
Via Macedonio Melloni 40
Milano, Italy

Tokyo, Japan
911 Iino Building
22, 2-chome, Uchisaiwai-cho, Chiyoda-ku
Tokyo, Japan